Examining the Decision-Relevance of Climate Model Information for the Insurance Industry

Joseph David Daron

Thesis submitted to the London School of Economics and Political Science for the degree of Doctor of Philosophy

Department of Geography and Environment

December 2011

Abstract

The insurance industry is becoming increasingly exposed to the adverse impacts of climate variability and climate change. In developing policies and adapting strategies to better manage climate risk, insurers and reinsurers are therefore engaging directly with the climate modelling community to further understand the predictive capabilities of climate models and to develop techniques to utilise climate model output. With an inherent interest in the present and future frequency and magnitude of extreme climate-related loss events, insurers rely on the climate modelling community to provide informative model projections at the relevant spatial and temporal scales for insurance decisions. Furthermore, given the high economic stakes associated with enacting strategies to address climate change, it is essential that climate model experiments are designed to thoroughly explore the multiple sources of uncertainty.

Determining the reliability of model based projections is a precursor to examining their relevance to the insurance industry and more widely to the climate change adaptation community. Designing experiments which adequately account for uncertainty therefore requires careful consideration of the nonlinear and chaotic properties of the climate system. Using the well developed concepts of dynamical systems theory, simple nonlinear chaotic systems are investigated to further understand what is meant by climate under climate change. The thesis questions the conventional paradigm in which long-term climate prediction is treated purely as a boundary value problem (predictability of the second kind). Using simple climate-like models to draw analogies to the climate system, results are presented which support the emerging view that climate prediction ought to be treated as both an initial value problem and a boundary condition problem on all time scales. The research also examines the application of the ergodic assumption in climate modelling and climate change adaptation decisions. By using idealised model experiments, situations in which the ergodic assumption breaks down are illustrated. Consideration is given to alternative model experimental designs which do not rely on the assumption of ergodicity. Experimental results are presented which support the view that large initial condition ensembles are required to detail the changing distribution of climate under altered forcing conditions. It is argued that the role of chaos and nonlinear dynamic behaviour ought to have more prominence in the discussion of the forecasting capabilities in climate prediction.

Acknowledgements

First and foremost I would like to thank my supervisor David Stainforth. Our many discussions, usually over a cup of coffee, have both challenged and motivated me to explore the many issues contained in this thesis. Special thanks also go to Lenny Smith, who was helpful in steering the research, and Trevor Maynard who's input regarding the nuanced world of insurance is greatly appreciated. I was also lucky enough to form friendships and collaborations during my PhD research with people both at the LSE and Exeter University. At the risk of missing someone out, I would simply like to thank all colleagues at the LSE Grantham Institute and the Centre for the Analysis of Time Series, particularly the folk in B717, as well as colleagues in the Geography department at Exeter University, especially those in the PhD office. I would also like to acknowledge members of the Climate Impacts Team at the UK Met Office where I spent six valuable months after the second year of my PhD. On a personal note I must express my deepest gratitude to my partner Gemma Ebsworth for her continued love and companionship. My mother, father, brother and extended family have also encouraged me throughout my research and I really value their support. Finally, although I was never fortunate enough to meet him, I owe much to Edward Lorenz, whose models I not only use but whose thoughts and insights have been inspirational to me throughout my PhD research. He died in April 2008 whilst I was in Vienna at the European Geosciences Union conference presenting some of my early work using the Lorenz-63 model. I can only hope that I have not done his pioneering work an injustice.

Declaration

I certify that the thesis I have presented for examination for the PhD degree from the London School of Economics and Political Science is solely my own work other than where I have clearly indicated that it is the work of others.

Contents

List of Figures

List of Tables

List Of Acronyms

AMO	Atlantic Multidecadal Oscillation
AOGCM	Atmosphere-Ocean General Circulation Model
AR4	Fourth Assessment Report
AR5	Fifth Assessment Report
BN	Bayesian Network
CDF	Cumulative Distribution Function
CMIP	Coupled Model Intercomparison Project
CPT	Conditional Probability Table
CRU	Climatic Research Unit
EC	European Commission
EMIC	Earth system Model of Intermediate Complexity
ENSO	El Niño Southern Oscillation
GCM	General Circulation Model (Global Climate Model)
GHG	Greenhouse Gas
IC	Initial Condition
IMS	Imperfect Model Scenario
IPCC	Intergovernmental Panel on Climate Change
KS	Kolmogorov-Smirnov
L63	Lorenz-63
L84	Lorenz-84
LS84	Lorenz-84 coupled to Stommel-61
LTI	Long-Term Insurance
NOAA	National Oceanic and Atmospheric Administration
ODE	Ordinary Differential Equation
PDF	Probability Distribution Function
PDO	Pacific Decadal Oscillation
PMS	Perfect Model Scenario
PNS	Post-Normal Science
PPE	Perturbed Parameter Ensemble
RCM	Regional Climate Model
RK	Runge-Kutta
S61	Stommel-61
SRES	Special Report on Emissions Scenarios
SST	Sea Surface Temperature
TAR	Third Assessment Report
UKCIP	United Kingdom Climate Impacts Programme
UKCP09	United Kingdom Climate Projections 2009
UNFCCC	United Nations Framework Convention on Climate Change
WMO	World Meteorological Organization

Chapter 1

Introduction

1.1 Understanding Climate Change

"The first step to dealing with your problem is knowing your problem"

Professor Ian Stewart[1]

In order for society to develop appropriate solutions to the emerging risks associated with climate change, individuals, businesses and governments need to make rational decisions utilising the available knowledge base. Effectively communicating what is known and what is unknown about the science of climate and climate change is therefore essential in providing guidance to decision-makers. Yet there is ambiguity within the climate change discourse about the most appropriate way to define climate. Father of chaos theory, Edward Lorenz, observed that questions regarding climate and climate change can be answered either affirmatively or negatively depending on the precise definition of climate (Lorenz (1997)). In order to adapt to possible future climate states, it is therefore important to find a suitable definition of climate which is tailored towards the needs of the climate change adaptation community. Furthermore, acknowledging both the rich complexity of the physical climate system and the intricacies of the policy-making process is imperative in establishing how to provide useful information from climate model experiments to inform decision makers. The purpose of this thesis is to develop a fundamental appreciation of the meaning of climate in the context of climate change given the dynamic, nonlinear and chaotic nature of the system. Ultimately, the research aims to provide guidance for the design of future climate model experiments to better respond to the needs of the adaptation community, with a particular focus on the (re)insurance industry.

The objective of this initial chapter is to provide a broad context for the research presented in this thesis. In section 1.2, the current state of knowledge regarding climate change is described with reference to international efforts to establish a global scientific consensus. Section 1.3

[1] In an address to The Royal Society in London at a meeting titled "Handling Uncertainty in Science" held on March 22nd 2010.

explores the role of climate models in providing output to inform climate change adaptation. The arguments for investigating the behaviour of simple models are introduced in section 1.4 whilst section 1.5 outlines the reasons for the engagement of the insurance industry in climate change research. Section 1.6 lists the main questions being addressed in this thesis and describes the aims of the research. Finally, section 1.7 provides a road-map for the thesis including a brief description of each chapter and how the chapters relate to one another.

1.2 Global Warming and Climate Change

The first decade of the twenty-first century was the warmest decade globally since record began in 1880 (NASA (2010)). Global warming over the past 50 years has been widely attributed to the increasing concentration of greenhouse gases (GHGs) in the atmosphere, primarily caused by anthropogenic emissions of carbon dioxide, methane and other trace GHGs (Hegerl et al. (2007)). Global warming, due to anthropogenic emissions of GHGs, has been recognised by climate scientists as a real and potentially dangerous global issue for more than thirty years. Wallace Broecker, a scientist from Columbia University, New York, first coined the term *global warming* in a study published in 1975 where he states, "it is possible that we are on the brink of a several-decade-long period of rapid warming" (Broecker (1975)). Over the subsequent decades the science of global warming, and more generally climate change, has evolved and the issue of how to respond to twenty-first century global warming has become an issue of great concern for international, national and local policymakers.

The Intergovernmental Panel on Climate Change (IPCC) was established in 1988 by the World Meteorological Organization (WMO) to compile research undertaken by the climate science community (IPCC (2011)). To date, the IPCC has produced four comprehensive assessment reports and the results provide the scientific basis for the policy debate regarding the implementation of the United Nations Framework Convention on Climate Change (UNFCCC). A vital component in each IPCC report is the presentation of climate model results. Modelling centres across the world have performed experiments to inform the analysis of past, current and future climate variability and climate change for inclusion in the IPCC assessment process. Combined with other sources of climate information, model results are used to illustrate potential future climate trajectories. The model experiments run for the Third Assessment Report (TAR) and Fourth Assessment Report (AR4) were conditioned on a set of specific emissions scenarios published in the Special Report on Emissions Scenarios (SRES). The SRES scenarios consist of alternative plausible future pathways based on assumptions about technological change and future economic development (IPCC (2000)). The AR4 report cited projections for an increase in the global mean temperature of between 1.1°C and 6.4°C by the end of the century (IPCC (2007b)). The UNFCCC relies upon the science contained within the IPCC reports to establish consensus agreements between nations which enact climate change policies and set international emissions targets.

Dessler and Parson (2006) divide the available responses to deal with climate change into three broad categories. Mitigation policies aim to address the rise in the concentration of GHGs through efforts to reduce GHG emissions or enhance GHG sinks. Geoengineering policies aim to actively manipulate the radiative balance of the climate system and offset the effects of the GHG forcing. Finally, adaptation policies are focussed on managing the physical impacts of climate change. This thesis is primarily concerned with the use of climate model output to inform adaptation policy but the implications of the research also have relevance for the design of model experiments to guide mitigation and geoengineering policy.

1.3 Model Guidance for Adaptation to Climate Change

Despite efforts to reduce the emissions of anthropogenic GHGs to mitigate against projected future warming, concentrations of GHGs in the atmosphere continue to rise and further warming of the planet is considered by many to be largely inevitable (IPCC (2007b)). As a result, policymakers are no longer concerned only with policies designed to reduce GHG emissions but also in enacting adaptation strategies to enable society to cope with the impacts of climate change. As the focus of climate change policy shifts from mitigation to adaptation, different forms of climate information will be required to guide policy decisions.

Climate models have been used extensively to inform the mitigation debate by providing estimates in the range of global and regional changes in climate variables, such as temperature and precipitation. However, policy responses have largely been centred on "best estimates" and mean values, particularly in relation to projected changes in the global mean temperature. For example, the European Commission (EC) has advocated a target of minimising the increase in global mean temperature to 2°C above the pre-industrial value (European Commission (2008)). The EC acknowledges that such a target will not avoid many of the adverse impacts of climate change but state that a higher rise in global mean temperature "will result in increasingly costly adaptation and considerable impacts that exceed the adaptive capacity of many systems". Conversely, when considering climate change adaptation, policy responses are likely to be dependent on the entire range of projected outcomes. As noted by Stainforth et al. (2007a), "most if not all decision support is sensitive to more than the mean". The distinction between what information is required for mitigation and adaptation decisions largely reflects the contrasting nature of the policy debates; the mitigation discourse primarily focuses on the global mean temperature because this variable is used to anchor negotiations on emissions reductions.

As the primary tool for assessing the future impacts of climate change, global circulation models (GCMs) enable scientists to test hypotheses and make predictions of future climate change subject to a number of assumptions. However, producing reliable and believable projections for informing adaptation decisions is fraught with uncertainty. Whilst climate models have been instrumental in attributing twentieth century global and regional warming to anthropogenic greenhouse gas forcing (Hegerl et al. (2007)), models show considerable disagreement when

predicting future climate changes at the spatial and temporal scales that interest decision makers. Oreskes et al. (2010) note that there is much less agreement between models regarding local changes in climate when compared to global mean changes, questioning the value of the current generation of climate model projections to guide adaptation. Presenting and communicating results which are subject to large uncertainty therefore poses a critical challenge to the climate modelling community. Similarly, interpreting highly uncertain model results which are conditional on a number of crude assumptions is problematic for decision makers.

Recently, modelling centres around the world have begun developing their capabilities in *Climate Services* to improve the communication and presentation of climate information, especially in aiding climate change adaptation. The emergence of Climate Services originates from a WMO meeting[2] held in 2009 where attendees discussed the need for suitable national-level provision of climate information relevant for adaptation decisions. The UK Met Office[3], the US National Oceanic and Atmospheric Administration[4] (NOAA) and the German Climate Service Center[5] (CSC) are all examples of institutions that have recently established a Climate Service to provide advice for customers, primarily within their respective nations. The central focus of each Climate Service is on translating climate model projections into usable formats to inform a wide range of decisions and applications.

In order to provide usable climate model information, many groups have advocated the use of higher spatial resolution modelling (both horizontal and vertical) to improve the realism of model results and produce more reliable information; especially in acknowledging the needs of the insurance sector (Strachan (2007b), HM Treasury (2009)). However, given the complexities of the system under investigation, there is no guarantee that higher resolution information will reduce uncertainty in climate model projections. As noted by Allen et al. (2000), it is possible that uncertainty may increase when resolving finer scale processes by reducing the number of modelling assumptions. Maintaining a dialogue between climate modellers and the user community is therefore essential to ensure that users understand how uncertainty arises and why future generations of climate models might increase, rather than decrease, the uncertainty. Moreover, any apparent reduction of uncertainty resulting from increased model resolution may be a consequence of limited computing capacity available to explore uncertainty.

The advance towards higher resolution models is driven, in part, by the belief that higher resolution models are able to better represent extreme weather. Given the relevance of information about extremes to many decision makers concerned with adaptation to climate change, improving the theory of how extreme weather will be affected in a changing climate is clearly a worthwhile endeavour. The IPCC has recognised the need to focus on extreme events and in a future special report[6], the IPCC will specifically address the management of

[2]World Climate Conference 3: Geneva, Switzerland, 31 August to 4 September 2009. Available at http://www.wmo.int/wcc3

[3]Available at http://www.metoffice.gov.uk/services/climate-services

[4]Available at http://www.climate.gov/#climateWatch

[5]Available at http://www.climate-service-center.de

[6]Further details available at http://www.ipcc-wg2.gov/AR5/sr.html

extreme risk with reference to the latest available science (IPCC (2009)). However, increasing model resolution to improve projections of extreme events inevitably leads to escalations in computational expense so a balance needs to be struck between resolving small scale processes and the need for large ensembles to explore uncertainty. This thesis aims to inform the debate regarding the tension between the need for increased model resolution and the need for a more rigorous exploration of uncertainty.

1.4 Modelling by Analogy

Key to aiding the communication process, not only between modellers and policymakers but also amongst climate scientists, is establishing a conceptual basis for understanding the meaning of climate under climate change. Given the complexity of GCMs, let alone the complexity of the real climate system, insights from simpler models may therefore help in illustrating the notion of climate in a model which exhibits climate change. In this thesis, low-dimensional models, which have features analogous to the climate system, are investigated to provide insights to inform the analysis of the more complex models that are used routinely to guide adaptation decisions.

Climate models will never include all of the physical processes that can influence the evolution of the climate system. Ultimately, there will never be a perfect model of the climate system and in reality, all models are wrong (Smith (2000)). The best climate modellers can do is select the dominant processes and model them at the relevant spatial and temporal scales to provide information which is fit for purpose. By doing this, it ought to be possible to determine for which phenomena and on which time scales climate models might reflect reality (Smith (2002)).

Climate model projections inherently provide imperfect and incomplete information but used appropriately, models can be an important tool to inform the decision making process. Understanding the ability of complex climate models to explore uncertainty is therefore crucial in establishing what constitutes the appropriate use of climate model projections. By understanding and interpreting the behaviour of the simple analogous models, one can begin to understand the capacity of complex, computationally expensive models to sample the different sources of uncertainty associated with climate change prediction. It follows that analysing low-dimensional nonlinear dynamic models makes it possible to develop hypotheses regarding the predictive capabilities of more complex climate models of much higher dimensionality. Smith (2002) states:

> "While it is unreasonable to expect solutions to low dimensional problems to generalise to million dimensional spaces, so too it is unlikely that problems identified in the simplified models will vanish in operational models."

The use of simple models in this thesis therefore has a dual purpose: providing a means to develop a conceptual understanding of climate under climate change and also to explore the

role of different types of uncertainty in the predictability of the climate system.

1.5 The Insurance Industry

Insurance provides a financial mechanism for individuals and businesses to protect themselves against risk. Policyholders pay a premium to an insurance company which indemnifies (compensates) the policyholder in the event of an incurred loss. The insurance industry is the world's largest industry worth an estimated $4.1 trillion in revenues in 2009 (TheCityUK (2010)). The success and sustainability of insurance therefore has significant implications for society and the global economy.

Mills (2005) stresses the importance of climate change to the sector, explaining that virtually all insurance business lines are vulnerable to the impacts of climate change. As the industry attempts to understand the consequences of climate change for specific business practices, insurers are becoming increasingly interested in the ability of climate science to provide information to estimate changes to weather- and climate-related perils. Given the large loss potential associated with insurance portfolios which cover extreme weather events, such as Atlantic Hurricanes, insurers and reinsurers (who effectively insure insurance companies) are particularly concerned with the trends in the frequency and magnitude of extremes and rare events. (Re)insurers are therefore beginning to develop partnerships with academic institutions and climate scientists to further understand the uncertainties and challenges associated with providing usable information to inform insurance decisions[7].

The research conducted in preparation of this thesis was supported by Lloyd's of London. In collaboration with the Emerging Risks team at Lloyd's, research was undertaken to understand the long-term strategic issues facing the industry which could be informed by the appropriate interpretation of climate model output. As a facilitator for the London insurance market, individual syndicates benefit from the impartial research conducted by Lloyd's, which is made available to the entire market.

1.6 Research Aims

In combining research into the fundamental principles associated with climate predictability, provided by the experiments on simple dynamic models, with research into the use of climate model information by the insurance industry, and more generally the adaptation community, this thesis attempts to contribute to the bridging of scientific endeavours with societal needs. Specifically, this thesis aims to address the following questions:

- What are the climate model information needs and desires for strategic decision-making

[7]Examples include the Willis Research Network (see http://www.willisresearchnetwork.com/) and the Lighthill Risk Network (see http://www.lighthillrisknetwork.org/).

within the insurance industry and are the current generation of climate model experiments capable of providing such information?

- How should climate be defined to best address the needs of the climate change adaptation community?
- Is the ergodic[8] assumption valid for a climate system subject to altered forcings?
- Is the future climate dependent on the pathway of the forcings?
- How should climate model experiments be designed to explore the full range of climate change uncertainties?

While exploring these specific research questions, this thesis investigates both the conventional paradigm in which long-term climate prediction is treated purely as a boundary value problem (as opposed to an initial condition problem) and the justification of the ergodic assumption inherent in the current design of climate model experiments. The analysis presented in later chapters is designed to provide insight regarding these two distinct notions. In the idealised model experiments, situations in which the ergodic assumption breaks down are illustrated and the relevance of these findings for understanding the validity of the ergodic assumption in climate prediction are discussed. Furthermore, by exploring the role of IC uncertainty in low-dimensional models, results support the view that climate prediction ought to be treated as both an initial value problem and a boundary condition problem for time scales relevant to climate change adaptation.

Given the broad scope of the research topic, this thesis does not attempt to provide answers which apply to all climate change adaptation applications and all business lines within the insurance sector. Nevertheless, it does represent an important step in re-focussing the attention of the climate modelling community in providing model output which is fit for purpose and addresses user needs.

1.7 Thesis Outline

This thesis consists of six further chapters. Chapter two provides background information and a literature review, related to the aims described and the themes outlined in this introductory chapter. In chapter three an analysis of the Lorenz-63 model is presented to generate insight regarding the meaning of climate under climate change. The experiments conducted explore the impact of fluctuating model parameters and initial condition (IC) specification. Chapter four extends the methodology to the Lorenz-84 model. Building on the concepts explored in the previous chapter, the analysis focuses on the impact of transitive[9] and intransitive[9] behaviour in the modelling of climate. Experiments using the Lorenz-84 model coupled to the Stommel

[8] Definition in section 2.1.4 and in the glossary.
[9] Definitions provided in relevant chapters and in the glossary.

ocean box model are presented in chapter five to further extend the analogy to the climate system, combining two dynamical systems operating on different time scales. The notions of ergodicity and transitivity are again explored in the context of climate predictability for climate defined as distribution of model states. Chapters three to five contain the body of results which are used in determining the necessity of exploring IC uncertainty in climate prediction. Chapter six however, focusses on the policy dimension of the research. The narrative attempts to address the needs of insurers, tasked with responding to climate change, with the insights gained from the exploration of climatic uncertainties using analogous simple dynamical models. The chapter includes a case study illustrating the potential application of Bayesian Networks (BNs) to translate climate model output into a usable format for addressing insurance decisions, specifically in relation to the emerging area of index-based microinsurance. Finally, chapter seven provides a discussion of the thesis results. The discussion centres on the appropriate design of climate model experiments to address user needs, particularly in the insurance sector, whilst acknowledging the multiple sources of climate change uncertainty explored in this thesis.

Chapter 2

Background and Literature Review

Following the signing of the United Nations Framework Convention on Climate Change (UNFCCC) in June 1992 (Dessler and Parson (2006)), climate change has become established as an issue of global importance. As a consequence, climate scientists have been urged by politicians and businesses to conduct policy-relevant science to inform decision makers. Inevitably, given the complexity of the system, the research community has continually modified theory and modelling methodologies to cope with the ever-changing science of climate and climate change. In striving to meet the needs of society, scientists have developed large computer simulation models of the climate system. To understand how the current (and future) generation of climate models can be used to inform decision makers requires a knowledge of the history of this rapidly evolving research area. In placing the research presented in this thesis into the wider scientific context, this chapter provides an analysis of the existing literature, relevant to the themes of the research.

Section 2.1 begins with a description of the alternative definitions of climate and then explores the development of dynamical systems theory to address climate and climate change. Section 2.2 presents a historical account for the development of models to inform climate change adaptation decisions. The section focuses on the methods and approaches adopted by various authors in the design and implementation of climate model experiments. In section 2.3, the impacts and responses of insurers to climate change are discussed in relation to the engagement of insurers with the climate research community and the use of climate model information within the insurance industry. Finally, section 2.4 documents the studies which have analysed the behaviour of the dynamical models explored in this thesis to provide insight into the treatment of uncertainty in climate modelling.

2.1 Climate as a Dynamical System

2.1.1 Defining climate and climate change

How an individual perceives the risks of climate change is fundamentally related to their understanding of the climate system. Appropriately defining climate and what constitutes a change in climate is therefore vital in enabling people to decide how to respond to climate model information. A number of years ago, Bostrom et al. (1994) presented evidence that the general public often confuses the notions of weather and climate and also misunderstands the causes of climatic change. More recently, Sterman and Sweeney (2007) described empirical evidence to suggest that low public support for mitigation policies (in the US) may have arisen due to misconceptions of how the climate evolves. Yet the contrasting perceptions of climate, and what constitutes a change in climate, within the public discourse are not well resolved even within the climate science community. After decades of research into the behaviour of the climate system, the many definitions of climate and climate change are not, and perhaps never will be, consistent across all domains of climate research.

Lorenz (1997) discusses the various working, often contradictory, definitions of climate and argues that the definition adopted for a particular application will impact the interpretation of climate variability and climate change. Many authors tend to favour a statistical temporal definition, similar to that adopted by Dymnikov and Gritsoun (2001) which states, "the climate is assumed to be the ensemble of states that the climate system (the system consisting of atmosphere, hydrosphere, cryosphere, land surface and biota) passes through during a sufficiently long time period". One therefore has to determine the modes of variability which ought to be associated with internal climate variability and infer a suitable time scale over which to define climate. For example, Lorenz (1997) states that one might decide that ENSO (El Niño Southern Oscillation) should be considered a regular feature of a stationary climate so the time-averaging period must be sufficient to account for positive and negative phases of the ENSO cycle. A climate change would then occur if ENSO events (El Niño and La Niña) became more regular and/or changed their magnitude. A typical period for analysing observations to derive climatological statistics is thirty years, consistent with the time scale advocated by the WMO (Burroughs (2003)). Thirty year datasets, representing the period 1961 to 1990, have been developed for use as a baseline for future climate projections (WMO (1996), New et al. (1999)). However climate variability is known to occur on all time scales (Schneider and Kinter III (1994), Pelletier (1997)) so the potential application for such a definition is limited. Given long-term internal variability, it is inevitable that the "climate" will be different from one thirty year period to the next, irrespective of any external forcings imposed on the climate system. Herein lies a major difficulty in using time-averaged statistics to represent the climate. The means and variances associated with a thirty year period, or indeed any other finite-time period, are dependent on the particular phases of long-term modes of climatic variability. Furthermore, in addressing the complexity of climate and investigating the methods used to provide climate

information, Lucarini (2002) states that there is an element of ambiguity in the definition of climate because "the time interval over which statistics are made is not determined a priori, but is operationally chosen depending on the goal of the research".

As explained by Peixoto et al. (1992), definitions of climate have evolved over the past decades and many disciplines now view the climate as a complex system which includes the biosphere, cryosphere and anthroposphere. An alternative definition to the broadly adopted statistical temporal definition, originates from dynamical systems theory in which the climate is considered as the set of states consistent with fixed forcings and boundary conditions (Fraedrich (1986), Smith (2002)). A change in climate is therefore given by the changing set of possible states to which the system evolves. The definition lends itself to considering the climate as an "attractor" for weather (Palmer (1999)) so that changes in the attractor represent a change in climate (discussed further in section 2.1.3). In the real climate system, past observations of weather variables simply represent one trajectory through the set of possible states associated with the climate attractor. However, given the high-dimensionality of the climate system and the inherently complex nonlinear interactions which occur on multiple time scales, this definition is perhaps conceptually more challenging.

The IPCC provides a non-specific definition of climate in the most recent AR4 report, which encompasses many competing definitions (IPCC (2007a)):

> "Climate in a narrow sense is usually defined as the average weather, or more rigorously, as the statistical description in terms of the mean and variability of relevant quantities over a period of time ranging from months to thousands or millions of years. These quantities are most often surface variables such as temperature, precipitation, and wind. Climate in a wider sense is the state, including a statistical description, of the climate system. The classical period of time is 30 years, as defined by the World Meteorological Organization."

Multiple time scales are acknowledged in the IPCC definition because of the varied interests and motives of researchers but the lack of specificity, regarding the time scale over which climate should be considered, leads to ambiguity regarding conclusions about detection of past climate changes and projections of future climate change. The IPCC definition alludes to the dynamical systems view of the climate with reference to the "state" of the climate system but the definition provides little clarity as to what that means in practice.

Understanding how the use of alternative definitions of climate can aid or hinder climate change adaptation decisions is a theme that runs throughout the work presented in this thesis. By adopting a dynamical systems approach to conceptualising the climate system, and using the notion of an attractor, this thesis investigates the most appropriate definition of climate for use by climate modellers and decision makers in the context of climate change adaptation.

2.1.2 Is climate chaotic?

The origin of chaos theory dates back to the 19th century, and to the work of Henri Poincaré. Stewart (2009) describes how Poincaré "gazed into the abyss of chaos" with his pioneering work on the theory of dynamical systems. However, it wasn't until the 1960s, and the work of meteorologist Edward Lorenz, that chaos was formally demonstrated using a simple numerical model (Lorenz (1963)). Ever since, scientists have been grappling with the implications of chaos in the modelling and prediction of a wide variety of complex systems (e.g. Scott (1989), Dettmer (1993) and Ditto (1996)). The definition of chaos has been adapted for the many disciplines to which it is applied but the first rigorous mathematical definition of chaos was provided by Li and Yorke (1975). For a system to be considered chaotic, the rate of divergence of model trajectories must be at least exponential-on-average. The Lyapunov exponent measures the rate of divergence (or convergence) of trajectories and a chaotic system is defined as having a positive first Lyapunov exponent (Wolf (1986)). In short, a chaotic system can be thought of as a dynamic system which displays sensitive dependence to ICs (Schuster and Just (2005)) but as noted by Smith (2007), two other properties of chaotic systems are equally important; they are nonlinear and deterministic. The climate system has been shown to exhibit both deterministic and nonlinear behaviour (Hasselmann (1976)) so the notion of chaos ought to be embedded in the way we view and model the climate system. As noted by James Gleick, "the world would be a different place - and science would not need chaos - if only the Navier-Stokes equation did not contain the demon of nonlinearity" (Gleick (1988)). However, the relevance of chaos for the large-scale climate (as opposed to weather) prediction is still an area of vigorous debate (Harrison (2007)).

Lorenz (1990) states that "the climate system is unquestionably chaotic". On a time scale of weeks, chaos prohibits the predictability of exact atmospheric states (predictability of the first kind) but certain features, such as the range and expected frequency of possible states, may be highly predictable (predictability of the second kind) (Sprott (2003)). Modern weather prediction centres account for the chaotic behaviour of the atmosphere by using IC ensemble forecasting techniques largely developed in the 1990s (Palmer (1993), Toth and Kalnay (1993), Houtekamer et al. (1996)). On weather forecasting time scales boundary conditions are assumed to be constant but in predicting the evolution of the climate we are faced with the problem of extrapolating the climate system into a region where boundary conditions are changing (Stainforth et al. (2007a)). Much of the focus of the climate science community has therefore been on understanding the uncertainty associated with altered boundary conditions in the prediction of future climate states. How chaotic behaviour, arising from uncertain ICs, in the atmosphere and ocean interacts with the deterministic dynamics of the climate system, forced by changes in the boundary conditions, is not well understood (Humble (2007)) but recent developments in the theory of *spatio-temporal* chaos applied to climate modelling may provide some new insights (Climate Etc. (2011)).

Rial et al. (2004) discuss the complexities of the climate system and suggest that certain climatic features such as ENSO and the NAO (North Atlantic Oscillation) show signatures of chaotic behaviour. In describing the climate system as a complex system, Rind (1999) asserts that the inherent complexity of the system may impact our ability to make long-term climate projections. However, Rind (1999) comments that whilst the atmosphere is not entirely stable, the variability of atmospheric states is not chaotic. Conversely, a study by Hansen et al. (1997) using ensembles of climate simulations found that most interannual climate variability in the period 1979 to 1996 at middle and high latitudes was chaotic. Shulka (1998) argues that chaos does not imply a lack of long-term predictability in the atmosphere if the ocean temperature can be predicted. The author lists examples of geographical areas where the boundary conditions dictate the variability of atmospheric modes. Rial (2004) presents a less optimistic view for the prospects of successful long-term climate prediction. The study analyses ice core time-series' and uses a simplified model to examine the question: "do the ice core records reflect a climate system operating between order and chaos?" The author concludes the study by speculating that the earth's climate may only be weakly driven by the external forcings (e.g. solar forcing) whereas features such as abrupt warming episodes may result from the nonlinear processing of the forcing.

From a palaeoclimate perspective, Harrison (2007) argues that reductionist attempts to model the climate system, such as the attempts to model the climate using high-resolution GCMs, may be inappropriate for the climate system which is highly nonlinear and displays *emergent* behaviour. With reference to emergence, Goldenfeld and Kadanoff (1999) suggest that "microscopic" scale processes do not necessarily influence the "macroscopic" scales, so whilst uncertainty at microscopic scales may be irreducible this may not be a barrier to successful climate prediction. Harrison (2007) however, concedes that "if the macroscopic behaviour of the system is sensitively dependent upon the microscopic, then the whole system may be expected to display non-linearity and may be chaotic".

2.1.3 The climate attractor

Fundamental disagreements about the precise role of chaos in the study of climate change can often stem from the precise definition of climate, discussed in section 2.1.1. To address the potential impacts of chaotic and nonlinear behaviour in the climate system, many scientists have referred to the tools of dynamical systems theory. From the viewpoint of climate as a nonlinear dynamic system, the climate can be considered in terms of an "attractor" (Palmer (1999)). The term attractor has many definitions and has been applied in many areas of research. Milnor (1985) reviews the various working definitions of the term *attractor* and Bhattacharya (1993) states that an attractor is a region in phase space to which trajectories from different ICs converge over time. Of more relevance to the climate system is the notion of a strange attractor, which is an attractor that displays sensitivity to ICs (Ruelle (1981)) and is therefore usually chaotic; though not all strange attractors strictly display chaos (Grebogi et al. (1984)).

In a climate context, Sahay and Sreenivasan (1996) comment that "strictly speaking, the

relevant phase space for weather and climate attractors would be the space of all global fields of atmospheric temperature, humidity and wind velocity and so forth." One of the first studies to investigate the existence of an attractor for the climate system was done by Nicolis and Nicolis (1984). Using isotope records from deep-sea cores the authors assessed the potential for a low-dimensional attractor by examining dynamic features of the climatic time-series and concluded that, based on their data and approaches, a low-dimensional attractor may indeed exist. In the years to follow, many studies used different methodologies to assess the potential for a low-dimensional climate attractor (Fraedrich (1986), Sahay and Sreenivasan (1996) and references therein). A number of the studies question the use of (relatively) short datasets to find approximations to a climate attractor and offer theoretical arguments to dismiss the claim that the climate can be represented by a low-dimensional attractor (Grassberger (1986); Lorenz (1991b); Zeng et al. (1992)). Whilst the characterisation of the climate as a low-dimensional climate attractor remains contested, Sahay and Sreenivasan (1996) note that one can differentiate climatic phenomena according to the spatial and temporal scales on which they display stationarity. The authors make the case for considering "local attractors", which can be dataset dependent and can be considered in the context of a large-scale "global attractor". In the work presented in this thesis, the notion of a climate attractor is not used to support either the presence of a low-dimensional or high-dimensional attractor on any particular length scale. Rather, the concept is utilised as a communication device to explore climate under climate change by analogy to simple nonlinear dynamic models. In determining the impact of altered parameters on the attractors of simple models, the assumption is that insight can be gained into the qualitative behaviour of the climate system in response to altered climate forcings.

2.1.4 Ergodic theory, intransitivity and climate

In the history of chaotic and nonlinear dynamic systems research, other concepts and tools have been key to developments in considering chaos in real-world problems. For climate research, ergodic theory has provided a conceptual basis for defining climate and interpreting the dynamics of the climate system. Ergodic theory stems from the study of statistical mechanics, dating back to the nineteenth century and the pioneering work of Ludwig Boltzmann on the development of the ergodic hypothesis (Boltzmann (1871), Boltzmann (1872)). Yet it wasn't until the late 1920s that George D. Birkhoff and John von Neumann established mathematical proofs of the "ergodic theorem" and "mean ergodic theorem" respectively (Birkhoff (1931), von Neumann (1929)). Research on the application of ergodic theory was subsequently extended to the discipline of nonlinear dynamics theory, notably in the work of Ruelle (1976). Eckmann and Ruelle (1985) describes ergodic theory in basic terms as the theory that for a dynamical system, "a time average equals a space average". There are a number ways of expressing ergodicity in relation to the climate system and climate modelling. Schneider et al. (2000) states that a system can be considered ergodic if an ensemble of "replicates" averaged at a point in time produces the same statistics as that produced from an infinite time average of one member

from the ensemble. The results presented in this thesis utilise the definition described by Sprott (2003):

> "The ergodic hypothesis (Ruelle (1976)) asserts that the probability distribution is the same for many iterations of a single orbit (time average) and for a high-order iteration of many orbits with a range of random initial conditions (ensemble average)"

The ergodic assumption has become an accepted, though rarely acknowledged, feature of many studies analysing past climates and projecting future climates with computer simulation models. In using past observations and forecast simulations to understand climate, von Storch and Zwiers (1999) consider climate as a realisation of a continuous stochastic process, stating that without the ergodic assumption, "the study of the climate would be all but impossible". Yet, by viewing the climate system as a cascade of hierarchical sub-systems, Peicai et al. (2003) conclude that climate processes are not ergodic.

Monin (1986) states that an ergodic system is one in which "during the course of time, the trajectory representing [the system's] evolution in the corresponding phase space goes around all points of this space". In this description, Monin (1986) is describing "transitive" behaviour, stating that an ergodic system displays transitivity. There is clearly disagreement regarding the extent to which the climate system can or cannot be considered ergodic and the relevant literature is dominated by the related concept of transitivity. A *transitive* system is one in which a trajectory can pass through all of the possible system states whilst an *intransitive* system is one in which a trajectory will only pass through a subset of all possible system states; the subset is determined by the initial state and once established, will persist forever (Lorenz (1968))[1]. Whether or not the climate system as a whole is ergodic may be important in developing a comprehensive theory of the climate system but in this thesis, the presence (or absence) of ergodicity is determined in relation to the time scales of interest for adaptation decision making; the precise mathematical definition of ergodicity and the axioms of proof are not studied in detail.

In 1968, Lorenz asked, "how about the real atmosphere? Is it transitive?" concluding "we do not know" (Lorenz (1968)). Lorenz (1990) explored this notion with the aid of a simple nonlinear model and he deduced that the climate system is unlikely to be intransitive due to seasonal forcing changes that move the system into chaotic (or near chaotic) regions of parameter space facilitating the transition to new climates; rendering the system transitive. A more refined concept, almost-intransitivity, describes a system which is transitive over an infinite time but appears intransitive on shorter finite time scales (Lorenz (1968)). Lorenz (1970) discusses this concept in relation to climate and sees it as an "attractive hypothesis" for a system which has processes operating on different time scales such as sea ice and continental snow cover. In a review of early climate modelling studies, Schneider and Dickinson (2000) comment on

[1] Detailed definitions of transitivity and intransitivity are provided in the glossary.

the difficulty of understanding the origin of climate changes in a system that may be almost intransitive. The authors state that the assumption of climate being transitive is unfounded, and the climate may change as a consequence of internal or external influences, or some combination of both. Schneider and Dickinson (2000) therefore conclude that in the absence of transitivity, a definition of climate as a time-mean, rather than an ensemble average, is beneficial. In the years to follow, various studies were unable to resolve the issue of whether or not the climate system is transitive of otherwise, leading to Lorenz' conclusion in 1976; "we have no means at present of determining whether the atmosphere-ocean-system is transitive or intransitive" (Lorenz (1976)). The possibility that climatic changes can be attributed not only to external forcing changes but also the integration of subsystems of the climate (i.e. internally induced changes) poses significant challenges for the climate modelling community and is still an area of contention as recognised more recently by McGuffie and Henderson-Sellers (2005) who state:

> "Should the climate turn out to be almost intransitive, successful climate modelling will be extremely difficult."

2.2 Developing Climate Models to Inform Policy

2.2.1 Historical context

Over the past few decades the capabilities of climate modelling centres has increased dramatically and the uptake in the use of climate model output to inform adaptation decisions has grown as a consequence. In the late 1960s the first GCM, which combined atmosphere, ocean and cryosphere processes, was developed by the NOAA Geophysical Fluid Dynamics Laboratory (Manabe and Bryan (1969)). However, it wasn't until the mid to late 1970s that modelling centres became sufficiently advanced to produce more realistic representations of the Earth's climate system (e.g. Manabe et al. (1975), Bourke et al. (1977)). The main focus of early numerical modelling efforts was to use GCMs to produce globally consistent weather forecasts. Long-term climate projections were rarely performed due to the computational demands and limited access to supercomputers.

Edwards (2010) describes how computer simulation models have evolved since their emergence in the 1960s and explains why initial experiments tended to focus on radiative transfer. The author describes the work of Svente Arrhenius, Guy Callendar, Gilbert Plass and other eminent scientists in estimating the climate sensitivity: the warming associated with a doubling of CO_2 concentrations from their pre-industrial levels. Whilst the variable remains uncertain, it has provided a foundation for experiments to investigate the impact of an increase in the atmospheric concentrations of CO_2 to inform policy in mitigating anthropogenic CO_2 emissions. Estimating the climate sensitivity became a central goal of the climate science community and has led to much disagreement amongst scientists. Arrhenius (1896) calculated the climate sensitivity using a 2-D radiative transfer model, and solved the model equations by hand, obtaining an estimate of $5 - 6°C$. The first GCM to simulate the effects of doubled CO_2 resulted in a $2.9°C$ warming (Manabe and Wetherald (1975)). More recently, a multi-thousand member perturbed parameter ensemble[2] (PPE) experiment utilising distributed computing, climate*prediction*.net, obtained a range between 1.9 and $11.5°C$ (Stainforth et al. (2005)); discussed further in section 2.2.3. The latest IPCC report judged that the most likely range for the climate sensitivity was between 2 to $4.5°C$ (Solomon et al. (2007)), informed from a number of modelling studies conducted in preparation for the IPCC report. Despite major advances in system understanding and computational capacity, the median estimate of climate sensitivity remains at approximately $3°C$ and the uncertainty has not been constrained.

Climate models have evolved from relatively simple energy balance, atmosphere only models (North et al. (1981)) to highly complex, fully coupled interactive climate system models (Karl and Trenberth (2003)). The development of climate modelling capabilities has been coupled to the developing political agenda and the increasing demands placed on modelling centres to address key policy questions. The first questions regarding the impacts of anthropogenic GHG emissions on the climate system were mostly scientific in nature until the 1980s when society and

[2] Also referred to as a perturbed-physics ensemble

politicians becamse increasingly concerned about the impacts of global warming, resulting in the foundation of the UNFCCC (Dessler and Parson (2006)). The political dialogue culminated in the formation of the IPCC in 1988 and complex numerical climate models became the primary tool for informing IPCC projections of the impacts of anthropogenic climate change. As the shift in policy focus has moved increasingly towards questions regarding impacts at regional and local scales rather than mitigation policy questions on global scales, the expectations placed on climate modelling centres has become evermore demanding. The next section discusses the efforts of climate modellers to address questions concerned with climate change adaptation.

2.2.2 Climate model information for adaptation

The term "adaptation" is widely used in many research fields and the relevant definition is dependent on the application of interest. For the purposes of this thesis, the definition used is that adopted by the IPCC and defined in Smit et al. (1999):

> "Adjustments in ecological-social-economic systems in response to actual or expected climatic stimuli, their effects or impacts."

A certain degree of adaptation to climate change is likely to be autonomous; spontaneous adaptation that will occur without direct intervention of a public agency (Smit et al. (2001)). The content of this thesis is relevant to autonomous adaptation where decisions require an appreciation of relevant climatic uncertainties but the primary focus is on the needs of policymakers in the insurance industry who are interested in planned adaptation to climate change.

Given the desire for reliable and accurate information on future climate states, there is an obvious role for climate models to be used as a tool for guiding advice to decision makers. However, the climate model projections used to address policy questions relating to climate change mitigation often lack the detail necessary to address policy questions related to climate change adaptation. Stainforth et al. (2007b) recognises the differences in the demands placed on climate modelling centres noting that mitigation decisions can be driven by global scale projections whilst adaptation decisions benefit from regional and local scale information. Burton et al. (2002) highlights the issue of a mismatch in the resolution of global climate model projections and adaptation measures which are usually local or site specific.

In an attempt to bridge the scale divide, a number of statistical and dynamical downscaling techniques have been developed. Giorgi and Mearns (1991) present an early review of the various approaches being adopted by modelling groups, identifying 'nested-models' as a promising methodology for exploring regional climate impacts. In the following years, statistical downscaling approaches were favoured and many studies implemented such techniques for a large number of applications (Heyen et al. (1996), Schubert and Henderson-Sellers (1997), New and Hulme (2000), Wilby et al. (2004)). Huth (1999) states that the essence

of statistical downscaling is to "seek statistical relationships between the variables simulated well by GCMs, which are treated as predictors, and those required by impacts researchers, treated as predictands". More recently, with the benefit of improved computational capacity, dynamical models representing sub-global domains have been employed in the hope of improving regional-scale predictions (Kundzewicz et al. (2006), Meier (2006), Christensen et al. (2007a)).

A number of studies have compared the benefits and limitations associated with statistical and dynamical approaches to modelling regional climates and the successes and failures of each approach depend strongly on the specific variables of interest, the geographical location and time scale (Mearns et al. (1999), Murphy (1999)). However, in many cases, the dominant source of disagreement between regional results is the driving GCM which leads to considerable uncertainty in the projections of regional impacts (Fowler et al. (2007)). A study by Kendon et al. (2010) concludes that in general, exploration of uncertainty using model ensembles should be focused on sampling GCM uncertainty rather than RCM uncertainty. Section 2.2.3 examines the methods which have been employed to explore uncertainty in the model projections of climate change.

2.2.3 Handling model uncertainties

Uncertainty can be separated into two broad categories; epistemic and aleatoric uncertainty. Aleatoric uncertainty arises due to "natural, unpredictable variation in the performance of the system under study" and epistemic uncertainty results from "a lack of knowledge about the behaviour of the system that is conceptually resolvable" (Daneshkhah (2004)). Climate change prediction has to cope with both types of uncertainty and considerable effort has been focussed on trying to reduce epistemic uncertainty by improving the ability of climate models to represent the climate system.

In order to provide model output to inform policy, Stainforth et al. (2007a) describes three distinct sources of uncertainty which must be considered: (1) forcing uncertainty from forcings considered external to the climate system; (2) IC uncertainty relating to the initialisation of a model run/ensemble; and (3) model imperfection resulting from insufficient and incomplete understanding and limited capability to model the climate system. Stainforth et al. (2007a) separates the third source of uncertainty into two types; (i) model uncertainty (or parametric uncertainty) describing the uncertainty about what parameter values and parameterisations to include; and (ii) model inadequacy (or structural uncertainty) which refers to the fact that no set of parameter values, parameterisation schemes and ICs would create a model which is "isomorphic" to the real system. Whilst a number of studies have stressed the need to consider IC uncertainty in long-term climate projections (Pielke (1998), Palmer (1999), Collins (2002), Giorgi (2005)), climate modelling experiments have tended to ignore IC uncertainty on longer time scales in favour of exploring forcing uncertainty and model imperfections (Meehl et al. (2007b)).

In a systematic attempt to explore model uncertainty, Murphy et al. (2004) created a 53 member PPE of the HadAM3 model coupled to a mixed-layer ocean to estimate a probability density function (PDF) for the climate sensitivity. Having identified 29 key parameters controlling sub-grid scale atmospheric and surface processes, the parameters were perturbed one at a time relative to the standard version of the GCM (Pope et al. (2000)). In a more comprehensive exploration of model parametric uncertainty, Stainforth et al. (2005) performed the first multi-thousand-member grand ensemble of GCM simulations, again using the HadAM3 model coupled to a mixed-layer ocean. The PPE utilised distributed computing technology available from the 'climate*prediction*.net' experiment (Allen (1999), Stainforth et al. (2002)). The results presented in the Stainforth et al. (2005) study show the range in climate sensitivity from an ensemble of 2,017 distinct independent simulations[3] in which just six parameters were varied. More recent experiments using the climate*prediction*.net infrastructure have included even larger PPEs (Knight et al. (2007)). A number of other studies have focussed on the potential application of PPEs in understanding and projecting climate change (Annan et al. (2005), Barnett et al. (2006), Knutti et al. (2006), Niehörster et al. (2006), Rougier et al. (2009)).

The Stainforth et al. (2005) approach does not attempt to provide an objective PDF of the climate sensitivity because of a "lack of an observational constraint combined with the sensitivity of the results to the way in which paramaters are perturbed". However, the Murphy et al. (2004) study introduced a Climate Prediction Index (CPI) to weight model runs according to their ability to represent "present-day climate variables". The effect of weighting increased the median from 2.9°C to 3.5°C and altered the 5-95% range from 1.9-5.3°C to 2.4-5.4°C. Allen et al. (2002) are critical of likelihood-weighted PPEs because observations "are almost certainly used twice, first in determining the perturbations made to the inputs and second in conditioning the ensemble". Piani et al. (2005) explain that by allowing the parameters to vary in the Murphy et al. (2004) study, the ensemble members are less well tuned to observations but the authors also note that the Murphy et al. (2004) results were sensitive to the ensemble design strategy, therefore preventing the output of objective probabilities.

Given the inability of any individual climate model to be isomorphic with the climate system, many studies have taken a multi-model approach to address structural model uncertainty (Palmer et al. (2004), Tebaldi et al. (2005), Tebaldi and Knutti (2007)). Tebaldi and Knutti (2007) state that the multi-model approach is required to fully explore model uncertainty in addition to a PPE, which explores uncertainty within a single model. The Coupled Model Intercomparison Project (CMIP) was first introduced by the World Climate Research Programme (WCRP)[4] in 1995 as a framework to allow scientists to analyse the results from atmosphere-ocean general circulation models (AOGCMs) from modelling centres across the world in a systematic fashion (PCMDI (2011). The initial phases of the project involved performing model runs for a set of consistent idealised experiments to explore current climate (CMIP-1) and simulations of climate change when subject to a 1% increase in CO_2 each year

[3]The analysis used 2,578 simulation but some were duplicates used to verify the model design.
[4]More details available at http://www.wcrp-climate.org/

(CMIP-2) (Meehl et al. (2000a)). CMIP-3 provided a more comprehensive analysis with a number of more 'realistic' scenarios developed to feed directly into the AR4 process (Meehl et al. (2007a)). In assessing the reliability of the CMIP-3 ensemble, Annan and Hargreaves (2010) state that the ensemble appears "fairly reliable when tested against recent observations" while the spread in results tends to be "over-broad". The authors advance the use of probabilistic interpretation based on the ensemble, a topic covered further in section 2.2.5. Knutti et al. (2010) analyse the use of multi-model ensembles, particularly the CMIP-3 ensemble, arguing that it is unclear how to combine model projections to provide useful output information and that multi-model comparisons often under-represent extreme behaviour. The next set of CMIP experiments[5] (CMIP-5) are now underway to provide multi-model information for the forthcoming IPCC Fifth Assessment Report (AR5).

Collins et al. (2010) compare the approaches of PPE experiments (using the HadCM3 model) with multi-model experiments in an attempt to identify their desirable characteristics to inform future modelling efforts which aim to produce improved probabilistic assessments of climate risk. The study deems the ability to control the design of the ensemble as a key strength of the PPE approach but lists a number of competing constraints which make the design process complicated. Collins et al. (2010) state that multi-model approaches suffer from not being able to represent an adequate sample of all possible models. The authors conclude that the process of model tuning (to observations) might result in an unrealistically narrow spread of future climate change responses. Allen and Ingram (2002) refer to a limited model sample as an 'ensemble of opportunity' and state that the range of uncertainty from such results are likely to underestimate the true range of uncertainty.

A number of studies have concluded that multi-model means provide improved forecast skill on climate time scales (Krishnamurti et al. (2000)), Hagedorn et al. (2005)). In the TAR report, the IPCC used multi-model means as 'best guess' results (IPCC (2001)). However, Du et al. (2011) show that the apparent skill of a multi-model mean is potentially misleading, and the use of route-mean-square error to determine the skill score is contentious. Furthermore, averaging multi-model ensembles can reduce the information content from an individual model. There is a danger in using multi-model means as a 'best-guess' forecast for the future behaviour of the climate system as all models are imperfect and the mean result is not necessarily the most likely outcome. The danger in using multi-model means is illustrated in the Dailey et al. (2009) study that analyses the financial risks of climate change to insurers, in which the authors state, "the multi-model mean suggests a weak shift towards the warm phase of the [ENSO] cycle". In the preceding lines, the authors state, "some models project greater variability of the ENSO cycle in response to global warming, others reduced variability, and others no change at all". The multi-model mean result therefore provides no information about the large uncertainty in the range of responses of ENSO under future warming scenarios.

[5]More details available at http://cmip-pcmdi.llnl.gov/cmip5/

2.2.4 Handling initial condition uncertainty

For the time scales of interest to weather forecasters, it is well acknowledged that uncertainty in the ICs prevents successful long-term weather prediction (Palmer (1993)). In the study of climate change, ICs are sampled to account for internal variability, which is the climate variability not forced by external agents (IPCC (2001)). Yet conventional wisdom in the climate science community is that internal variability, and thus IC uncertainty, becomes less important with lead-time and on the multi-decadal time scale the uncertainty associated with the radiative forcings and model imperfections are the dominant sources of uncertainty (Cox and Stephenson (2007), Hawkins and Sutton (2009)). However, there are a number of studies which challenge this line of reasoning (Lorenz (1976), Pielke and Zeng (1994), Rial (2004)). In an early modelling study using a simple idealised model, Lorenz (1976) shows that small disturbances in ICs can influence long-term variability. The nonlinear interaction between forcing trajectories and modes of internal variability have been examined and Pielke and Zeng (1994) show that long-term variability can be influenced by short-term natural variations in climate forcings. Rial (2004) focuses on abrupt shifts in climate explaining that the shifts are likely to be the result of nonlinear responses impacted by both internal and external forcings.

The tension between the relative contributions of uncertainty arising from imprecise and uncertain boundary conditions, compared to the uncertainty in the initial state of the system, fuels the debate about the extent to which IC uncertainty is important for decadal, multi-decadal and centennial scale climate change. In recent years, considerable attention has been focused on increasing the skill of climate model forecasts on decadal time scales (Collins et al. (2006), Smith et al. (2007), Keenlyside et al. (2008)). In the design of the CMIP-5 experiments, it has been recognised that initialising the ocean component of the coupled models, using observed ocean states, is key to improving the accuracy of model forecasts on a 10-year time scale "when the initial climate state may exert some influence" (Taylor et al. (2009)).

With a longer forecast time horizon, incorporating multi-decadal time scales, Collins and Allen (2002) develop a simple framework to perform a comparison between the two sources of uncertainty. The authors suggest that skilful lead times may be 'state dependent' and conclude that "both initial and boundary condition information will need to be considered when designing operational climate forecasting systems in the future" although their analysis was limited to assessing predictive skill on time scales shorter than 50 years. The experimental results presented in the main chapters of this thesis build on the work of those examining the nonlinear interaction of ICs and external climate forcings to further develop hypotheses regarding the role of IC uncertainty in the medium- and long-term prediction of future climate states.

2.2.5 Probabilistic climate model information

Schneider (2001) suggested that in the absence of subjective probabilistic information for specific

climate scenarios, decision makers would make implicit assumptions about the probability of a climatic event occurring. Whilst acknowledging the difficulties in providing such probabilistic information, Schneider argued that experts ought to be able to provide more trustworthy estimates than non-experts. Pittock et al. (2001) explains that probabilistic climate information allows decision makers to adopt risk-based climate change adaptation strategies. Over the past decade, methodologies to assign subjective probabilities, to quantities of interest, has driven much of the research conducted by the climate modelling community.

The UK Climate Impacts Project (UKCIP) has recently collaborated with UK Met Office to provide probabilistic projections (UKCP09) for twenty-first century climate change in the UK (Murphy et al. (2009)). The previous UKCIP02 projections simply provided four descriptions of how the climate in the UK may evolve consistent with four emissions scenarios (Hulme et al. (2002)). The lack of computing power, system understanding and availability of alternative RCM results meant that uncertainty was not comprehensively treated in the UKCIP02 projections (Jenkins and Lowe (2003)). Gawith et al. (2009) note that users responded to the projections by calling for better quantification of the likelihood of climate scenarios, including an improved assessment of the associated uncertainties. To address the lack of a formal uncertainty assessment, the UKCP09 projections provided probabilistic information in the form of conditional PDFs, at a 25km grid resolution over the UK, for three emissions scenarios. The projections are subjective probabilities "providing an estimate based on the available information and strength of evidence" (Defra (2009)).

Whilst many of the uncertainties associated with the UKCP09 approach are acknowledged (Defra (2009)), many scientists have been wary of how the model probabilities will be interpreted by non-specialists and caution that highly conditional PDFs may inadvertently lead to bad practice amongst users. Clark and Pulwarty (2003) argue that probabilistic climate projections can mislead decision makers by actually obscuring the real range of futures they face and by appearing to provide a greater degree of certainty about the future than is warranted. In relation to model-based PDFs, Smith et al. (2009) state that it is irrational to base decisions on a model-based PDF when known model inadequacy dominates the PDF. Furthermore, Smith et al. (2009) show that without an assessment of the lead-time over which probabilities can be considered robust, model-based PDFs are uninformative.

Dessai and Hulme (2004) presents a review of the studies for and against probabilistic approaches to climate prediction, demonstrating the existence of a bifurcation in the literature regarding the provision of model information for climate adaptation policy. The authors differentiate between a 'top-down' approach, where the initial focus is on global scales and large-scale drivers of change as inputs to more regional and local scale models (favoured by researchers studying the biophysical effects of climate change in the mid- to long-term), and a 'bottom-up' approach, where the focus is on the coping capacity of vulnerable groups regarding existing economic resources and infrastructure (favoured by scholars concerned with social vulnerability). The alternative approaches lead to different perceptions of the need for probabilistic information to

inform decisions. Proponents of the 'top-down' approach tend to favour probabilities and those adopting a 'bottom-up' approach consider the use of probabilistic information to be of limited value. More recently, Hall (2007) questioned the value of probabilistic forecasts stating that the incomplete exploration of uncertainty leads to probabilities highly conditional upon the model runs performed and the statistical method used to compute probability distributions. The author argues that without effectively communicating the limitations in probabilistic approaches, decision makers will not appreciate the ambiguous nature of the information being provided and bad adaptation decisions will be made.

In the context of adaptation decision making, Ranger et al. (2010) argue that continued research to refine probabilistic climate projections is costly and because of irreducible uncertainties the approach is unlikely to yield significant decreases in uncertainty in the short-term. The authors advocate the use of robust decision making in the face of large irreducible uncertainty; a methodological approach advanced by Dessai (2004). Wilby and Dessai (2010) assert that focussing on the adaptation options rather than climate change scenarios may yield significant benefits for the user community. Robust decision making strategies therefore aim to determine low-regret options and reversible measures which are robust to the range of climatic uncertainty. Hallegate (2009) discusses the approach advocating the consideration of 'soft' adaptation measures in addressing climate risk. The approach does not require a formal probabilistic assessment of climate risk and is therefore seen as advantageous for adaptation policy in the midst of considerable climatic uncertainties. Ranger and Garbett-Shiels (2011) outline a number of principles which are consistent with a robust approach to managing uncertainty and state that focussing on long-term adaptive capacity and avoiding inflexible decisions which 'lock in' future climate risk is a central principle in successfully managing uncertainties.

2.3 Use of Climate Information by the Insurance Industry

2.3.1 Climate change risks and insurance

The insurance industry is becoming increasingly susceptible to the risks associated with climate variability and climate change (Lloyd's (2006b)). In the IPCC AR4 report, authors highlighted the role of the insurance sector in providing means to spread losses and encourage adaptation practices, whilst stressing that the industry itself must also adapt to climate change to stay "financially healthy" (Wilbanks et al. (2007)). According to the global auditing company Ernst & Young the most pressing strategic risk facing insurers is climate change, ahead of demographic change, emerging markets and regulatory intervention (Ernst & Young (2008)). Climate change can directly impact insurance risk assessments by altering the nature of the hazards that are covered by insured policies. Hazards such as drought, flooding and windstorms can change in an altered climate by becoming more (or less) frequent or becoming more (or less) intense (Lloyd's (2006b)).

Vaughan and Vaughan (2003) define insurance as "an economic device whereby the individual substitutes a small certain cost (the premium) for a large uncertain financial loss (the contingency insured against) that would exist if it were not for the insurance contract". As stated by Bühlmann (2005), the calculation of insurance premiums is based on the assumption that "a contingent claims experience can be compensated by fixed payments; these fixed payments are known as premiums". Establishing an appropriate premium for an insurance policy requires an evaluation of the expected loss, $E[X] = \mu$ (where X is the loss of a random event), over a given coverage period. μ represents the *pure premium* and a *loading* is also added to provide for administration costs, the costs of holding capital[6] and profit margins (Bowers et al. (1986)). According to Bowers et al. (1986), a loaded premium, denoted by H, can be calculated according to equation 2.1:

$$H = (1 + a)\mu + c \qquad a > 0, c > 0 \tag{2.1}$$

where $a\mu$ represents the expenses that vary with expected losses and c is a constant for expected expenses that do not vary with losses.

At the core of a private insurer's business model is the calculation of the financial risk associated with a given peril. Actuaries assess the risk associated with insured perils to inform specific business lines, helping to design and price insurance products. The pricing process often utilises techniques developed in multiple disciplines, from finance and economics to computer science and statistics. Ultimately, it is insurance underwriters who determine the premium, level of coverage and specify the precise terms and conditions for insurance policies. It is also the responsibility of an underwriter to evaluate the level of risk in the context of other business pressures and issue policies accordingly. Of particular relevance to underwriting activity is the

[6]Insurers must hold a sufficient level of capital to cover payments in the event of a loss and this capital can be held in the form of cash, bonds, investments and other financial instruments.

dynamic state of the insurance market (Winter (1994)); in a "soft market" premiums are low, capital is high and competition is high whilst in a "hard market" (or "tight market") premiums are higher and the capital base is lower, usually as a result of a significant catastrophe affecting the market. While underwriters aim to derive premiums that are appropriate for the level of underlying risk, premiums also reflect business realities such as rules imposed within the regulatory environment. According to Lester (2009), "most classes of insurance are usually delivered through private markets and insurance regulation tends to reflect solvency concerns and information asymmetry between suppliers and policyholders".

Insurance can be divided into life (including pensions) and non-life (or general) insurance. In 2009, global insurance premiums were approximately $4.1 trillion with life insurance accounting for 57% of premiums and non-life insurance accounting for the remaining 43% (TheCityUK (2010)). Climate change undoubtedly has implications for the life insurance sector. Peara and Mills (1999) describe the potential effects on mortality from an increasing frequency and magnitude of natural disasters, heat waves and improved conditions for the spread of vector-borne diseases. The IPCC AR4 Working Group II chapter on health outlines the projected impacts of climate change on mortality, the spread of infectious diseases and other key health related issues such as malnutrition (Confalonieri et al. (2007)). The authors conclude that climate change will "bring some benefits to health, including fewer deaths from cold, although it is expected that these will be outweighed by the negative effects of rising temperatures worldwide, especially in developing countries". Nevertheless, the chapter highlights the complex interaction of other important health determinants (e.g HIV/AIDS) noting that areas in which there is a heavy burden of disease and disability are more likely to be severely impacted by the effects of climate change. Nissan and Williams (2009) state that quantitative assessments of climate risk for the life sector are complex and the associated costs are highly uncertain but the authors urge life insurers to conduct further research to understand the implications of climate change for their sector. However, the available literature and the apparent concern of insurers over the past decade has been predominantly focussed on the impacts of climate change on the non-life sector. With respect to non-life insurance, Maynard (2007) argues that insurers will be hit by a "quadruple whammy" of increased liability, falling asset values, increased capital requirements and potential risks to reputation.

For the purposes of this thesis, the use of the term *vulnerability* refers to the set of socio-economic conditions which determine the ability of people (or an institution) to cope with a stress or change (Allen (2003)). With respect to the insurance industry, insurers can be considered vulnerable to climate change if their business practices are unable to absorb or cope with the altered nature of loss events or return periods of hazards and catastrophes. For climate-related perils Füssel and Klein (2006) define *exposure* as "the nature and degree to which a system is exposed to significant climatic variations". An insurer is therefore exposed to climate change if insured policies are located in regions in which the hazard is expected to be affected by altered climatic conditions. Consequently, the risks faced by insurers are a combination of hazard, vulnerability and exposure. Whilst climate change acts to increase or decrease the

hazard component, an increase in either the exposure or vulnerability to climate-related perils will ultimately affect an insurer's profitability.

The industry initially became concerned about increasing losses from weather and climate-related perils following a series of costly loss events in the 1980s and 1990s (Munich Re (2003)). The most costly insured loss event of the last century was Hurricane Andrew in 1992, totaling $15.5 Billion USD in private insurance claims[7]. Following the hurricane, 11 insurance companies with insufficient reserves and/or reinsurance cover went bankrupt (Jametti and von Ungern-Sternberg (2009)). As a consequence, the remaining insurers dramatically increased premiums and there was a surge in interest in the use of catastrophe models to estimate the risk of large losses (mostly from Atlantic land-falling hurricanes). However, in assessing the contribution of climate change to the increase in weather-related losses, studies have suggested that the increased losses were caused primarily by enhanced exposure to hazards from the movement of populations to high-risk coastal and low-lying areas (Changnon et al. (2000)). Berz (1999) states, "there is absolutely no doubt that this increase in losses is due to a large, if not overwhelming, extent to mounting economic values and insured liabilities in heavily exposed metropolitan areas". A recent analysis by Barthel and Neumayer (2012) builds on a previous study (Neumayer and Barthel (2011)) to examine normalised trends of extreme weather and climate related perils, taking into account the increase in wealth accumulation over time. The authors conclude that there is no statistically significant increase in normalised insured losses globally, though they do find positive trends in the US and western Germany. Based on their findings, Barthel and Neumayer (2012) make the bold statement that "climate change neither is nor should be the main concern for the insurance industry". In addition, commentators such as Tol (1998) have argued that the impacts of climate change on hazards is unlikely to greatly affect the profitability of insurers and is more of an issue for policyholders. In any case, insurers are becoming increasingly aware of the possibility for climate change to impact their business lines and at the end of the twentieth century, insurers began to question the use of past data alone to guide the management of climate related risks (White and Etkin (1997)).

Over the course of the first decade of the twenty-first century, the science of global warming has become increasingly well understood (Solomon et al. (2007)) and as a consequence the insurance industry has become evermore engaged with climate scientists and the climate modelling community. Furthermore, the record losses of the 2004/2005 hurricane seasons (Swiss Re (2005), Swiss Re (2006)) prompted insurers to re-assess the contribution of climate change to the underlying risks to which insurers are exposed (Munich Re (2005), Lloyd's (2006a)). Mills (2005) provides an overview of the impacts of climate change on the insurance industry, stating, "virtually all segments of the industry have a degree of vulnerability to the likely impacts of climate change". The author explains how climate change might affect the availability and affordability of insurance and argues that if insurers manage the changing risks appropriately, the adverse impacts of climate change on society will be diminished.

[7]According to data compiled by the Insurance Information Institute from the ISO's Property Claim Services (PCS) unit. Available at http://www.iii.org/media/facts/statsbyissue/catastrophes/#households

Valverde and Andrews (2006) examine the role of uncertainty in the management of climate risk stating that the level of ambiguity and uncertainty associated with climate change "generates considerable anxiety for industry stakeholders". The study adopts an econometric approach to assess the impact of "worst-case" scenario extreme weather events on the insurance industry, concluding that the industry displays a high-level of macro-resilience to severe shocks that may be a more common occurrence under altered climate conditions. Yet the authors acknowledge the significant challenge faced by individual insurers in responding to the possibility of both gradual and abrupt changes in risk as a result of climate change. Ranger and Ward (2010) assert that the largest threat to insurers will likely be in the form of unanticipated changes in weather-related hazards and risks. The authors use the example of increased exposure to hurricane risk in the late twentieth century leading to largely unforeseen losses in the 1990s and 2000s. In reacting to future climate change Ranger and Ward (2010) advocate the incorporation of flexibility in long-term strategies to allow for rising ambiguity in hazards and risks on decadal time scales. Section 2.3.2 examines the ways in which the industry has responded to climate change highlighting the different initiatives and approaches to manage future climate risk.

2.3.2 Insurer responses

Mills (2007) provides a comprehensive list of the ways in which insurers can and are reacting to the threat of climate change. The review outlines a large number of examples where insurers are actively engaged in addressing the risks posed by climate change, including the promotion of risk management strategies, the development of new insurance products and sustainable, climate-sensitive investments (e.g. Dlugolecki and Lafeld (2005), AXA (2006), CEA (2007)). The majority of insurance initiatives highlighted focus on GHG emissions reductions but Mills (2007) does mention the role of insurance regulation in maintaining solvency and comments on recent efforts to include climate change in catastrophe modelling, discussed further in section 2.3.3.

The ABI (Association of British Insurers) produced a report in 2004 which stated that the part of an insurers' business which will be most directly affected by climate change is underwriting (ABI (2004)). Herweijer et al. (2009) examines the impacts of climate change on underwriting and investment performance highlighting the need for a forward-looking view of risk in assessing underwriting practices. The study also stresses the need for a long-term perspective to address the continued insurability of business lines and the potential dwindling returns on investments which are sensitive to climate change. Ward et al. (2008) suggest financial measures that individual insurers can use to incentivise policyholders to mitigate against climate risks, thereby rewarding the policyholder with lower premiums and decreasing the vulnerability of insurers covering the risk.

ClimateWise has been created as an initiative through which individual insurers and reinsurers can compare and disclose efforts to address climate change within their organisations

(ClimateWise (2011)). The initiative has 40 members[8] globally and each member signs up to a set of six principles committing insurers to action on climate change. The ABI has produced a report to underpin the ClimateWise initiative to address key areas such as changing customer requirements, barriers to implementing new policies and potential opportunities arising in relation to climate change (ABI (2007)).

In enabling policyholders to deal with the emerging threat of climate change, some authors have suggested that multi-year insurance policies ought to be made available. Kunreuther (2008) argues that long-term insurance (LTI) contracts (in the order of 10 to 20 years) will be attractive to policyholders who wish to protect their properties and assets against climate-related risks. Kunreuther (2008) states that LTI contracts "provide [policyholders] with stability and an assurance that their property is protected for as long as they own it". The argument in favour of LTI contracts was later developed by Jaffee et al. (2011) which addressed the interests of insurers. Using an example of a modification to the US National Flood Insurance Program (NFIP) for property cover, the authors state that the reduced administration costs of yearly renewals will offset the additional risk covered by the insurer; in this example, the federal government. Another related option for encouraging long-term protection from catastrophic risk is to link home insurance to mortgages; an option advocated in the study by Kunreuther et al. (2007).

However, Lloyd's (2008) address the possibility of multi-year contracts for properties liable to flooding in coastal locations, stating that the vast uncertainties associated with future climate change mean that offering multiple-year insurance policies would be inappropriate. A study by ABI (2010) highlight a number of potential practical problems with LTI. They comment that pricing would have to be guaranteed for the duration of the contract to be attractive to the consumer. In addition, the availability of reinsurance, the ambiguity in the administration costs, and the uncertainty in future conditions may lead to higher than expected premiums. Nonetheless, they do state that LTI may benefit the insurer in being able to manage larger investments and assert that LTI would incentivise the insurer to invest in adaptation measures to reduce the impact or probability of future loss events. Maynard and Ranger (2010) demonstrate that the high level of capital required to ensure solvency for LTI products would render the approach inappropriate for the non-life insurance market. The authors use a simple example to explore the claims, expenses and investment processes of a multi-year policy versus a single year policy and conclude that due to stakeholder expectations for increasing return on capital over the duration of the policy, premiums are likely to be unaffordable. Given that knowledge of the risk is likely to change over the duration of a policy and coupled with changing regulatory and environmental conditions, the premium estimates presented by Maynard and Ranger (2010) were also deemed to be an underestimate.

In recent years, insurers have become focussed on their role in aiding climate change adaptation in developing countries. IIASA (2008) suggests that "pro-poor" insurance should form part

[8] As of August 2010 - see http://www.climatewise.org.uk/member-signatories/

of the UN post-Kyoto international negotiations. Mills (2004) explains that insurance can act as an adaptation strategy augmenting international aid and improving the capacity of affected communities to cope with the impacts of natural disasters. The author also highlights the role of micro-insurance in developing markets. A form of micro-insurance that has received a considerable amount of attention in the past few years is index-based weather insurance, where a meteorological threshold is used to trigger payouts. Skees et al. (1999) examines the role of index-base insurance for agricultural applications in developing countries asserting that the lower administration costs of index-insurance make the insurance more affordable to farmers. The use of index insurance has been advocated as a potential soft form of climate change adaptation (UNDESA (2007)). Carriquiry and Osgood (2008) explore the potential of utilising seasonal climate forecasts in pricing. However, the use of climate model information to assess medium- to long-term insurance viability has not been thoroughly examined. The use of climate information in the emerging index insurance sector is explored in detail in Part B of chapter six.

Throughout the industry, there has been limited formal consideration of climate model output in the day-to-day decisions made by insurers regarding climate-related risks. Mills (2005) attributes this to disjointed modelling traditions, with insurance models being past-focused and climate models being future-focussed. However, one sector within the insurance industry, catastrophe modelling, is becoming increasingly involved in the direct use of climate models and this activity is described further in section in section 2.3.3.

2.3.3 Catastrophe modelling

An area of insurance activity which has recently forged strong links with the climate modelling community is catastrophe modelling. Insurers, and more notably reinsurers, rely on the output of catastrophe modelling companies to assess exposure in regions of the world which have a relatively high-risk of experiencing large losses from major natural and human-caused disasters (Grossi et al. (2005)). The current use of climate model output in the insurance industry is largely confined to the catastrophe modelling sector, where analysis is focussed on extreme hazards, such as land-falling Atlantic Hurricanes, in developed regions of the world.

There are currently three major commercial catastrophe modelling companies: Applied Insurance Research (AIR) Worldwide, EQECAT and Risk Management Solutions (RMS). In 2006, following the damaging hurricane season of 2005, each company updated their models to account for increased hurricane intensity in response to increased SSTs (Seo and Mahul (2009)). As discussed by Strachan (2007a), there are two aspects of climate-related catastrophes that insurers are concerned about; changes in exposure and changes in extremes. Whilst climate model results cannot inform insurers regarding the changes to exposure, they are being used to inform on the future frequency and magnitude of extremes. Strachan (2007a) notes that the modelling of catastrophe risk under altered climatic conditions often relies on the use of stochastic models, based on historical records of losses and meteorological variables. In

developing dynamical approaches, Strachan et al. (2010) used the HiGEM, high resolution, coupled AOGCM to output a 200 year time-series of dynamically created tropical cyclones in the Atlantic. The data was used to create an event-set as an input for the analysis of hurricane risk in catastrophe models. The 200 year period was chosen to account for the influence of internal climate variability on the strength and frequency of Atlantic hurricanes. Vitolo et al. (2010) extended the study to generate a stochastic event-set for tropical cyclone risk in the West Pacific.

The use of dynamic climate model data as input to the catastrophe models has only recently gained momentum. A recent report by the ABI, in collaboration with AIR and the UK Met Office, examined the implications of 2°C, 4°C and 6°C change in global mean temperature for inland flooding in Great Britain (Dailey et al. (2009)). The research assessed the insured losses associated with the 1 in 100 and 1 in 200 year return periods for flood events across regions of the UK, in addition to UK windstorm risk and Chinese Typhoon risk. The approach used scenario-based model information from a 17 member PPE of the HadCM3 model (Murphy et al. (2004)) and an 11 member PPE from the Hadley Centre regional model, HadRM3. The report provides a number of quantified projections for the changes to losses and premiums for the scenarios investigated.

Despite recent progress in aligning climate modelling and catastrophe modelling techniques, there is considerable uncertainty in the future impacts of climate change on extreme perils. Studies estimating the economic consequences of climate change for catastrophic risks are therefore largely reliant on scenario-based analyses which are highly conditional on model assumptions.

2.4 Experimenting with Simple Models

In attempting to use complex climate models to guide insurance decisions, it is important to understand their ability to represent the nonlinear dynamic nature of the climate system. Gaining a conceptual understanding of multi-million dimensional numerical models is challenging so simple analogous models are used in this thesis to develop hypotheses and explore the dynamics of chaotic nonlinear systems. As stated in chapter 1, the aim is to inform the design of climate model experiments to explore the full range of climate change uncertainties and provide relevant information for adaptation decisions.

Chapters three, four and five utilise two relatively simple models developed by Edward Lorenz (Lorenz (1963) and Lorenz (1984)) and a simplified ocean model developed by Henry Stommel (Stommel (1961)) to draw analogies to the climate system. Simple models such as those developed by Lorenz have been used extensively in the nonlinear dynamics community, partly due to their low computational demands, but also as the relative simplicity of low-dimensional models allows for a rigorous exploration of the system dynamics. Simple models also enable users to gain an appreciation for model intricacies and dependencies which can be difficult to ascertain in more complex models. The results presented in this thesis provide new insights based on original experiments investigating the behaviour of the model *climates* for time-varying (non-autonomous) parameters.

2.4.1 Lorenz-63 model

The Lorenz-63 model (hereafter L63) has been used extensively over the past half-century to draw analogies to complex systems which display nonlinear chaotic behaviour. Despite it's low dimensionality, the model contains non-trivial dynamics (Lorenz (1963)). In relation to the existence of "intermittency", Manneville and Pomeau (1979) suggested that, sixteen years after its introduction, the model had yet to be well understood. Many scientists have studied the system because certain regions of parameter space lead to interesting and insightful behaviour. Yorke and Yorke (1979) explore the existence of *metastable* chaos and note that below a certain threshold value in a particular model parameter, ρ, trajectories evolve towards stable states (fixed-points) but they exhibit chaotic behaviour for a period of time before "decaying" towards a fixed point. For values of ρ close to the threshold value, the authors show that the chaotic behaviour persists for longer. The transient chaotic behaviour was also observed to be dependent on the ICs.

In relation to weather and climate prediction, there have been attempts to relate the chaotic behaviour of the L63 model to numerical weather prediction and climate models. According to Palmer (1993):

> "While the Lorenz equations do not correspond directly to large-scale atmospheric equations of motion, there are striking qualitative similarities with the behaviour of

the large-scale atmosphere, notably the existence of regime structure, distinct time scales and variations in local predictability estimates around the Lorenz attractor."

Using the results of the experiments with the L63 model (and adapted versions of the model), Palmer (1993) was able to gain insight into the best ways to perturb ICs to create informative ensemble prediction methods for use in extended-range weather forecasts. The author also comments on the relevance of studying such systems for guiding the experimental design of climate time scale predictions; a topic that is central to the work presented in this thesis. However the L63 model has not just been used to explore error growth related to uncertain ICs and Chu (1999) uses the model to show that the impact of uncertain boundary conditions (uncertainty of the second kind) is of a comparable magnitude to that of ICs. The study advocates increased attention in preparing accurate boundary conditions for numerical weather prediction.

The rich dynamics of the L63 model is still being explored and Chekroun et al. (2010b) reveals the "amazing complexity" of the Lorenz-63 model when being driven with stochastic perturbations to the forcing parameters. Focusing on the topology of the system Chekroun et al. (2010b) attempt to combine stochasticity with the ergodic theory of dynamical systems to outline the relevance of 'random attractors' in the study of climate variability. Whilst there is clearly a tension in improving models of a physical deterministic system by including stochastic processes, a paradox noted by Palmer and Williams (2009), many climate scientists are supporting such a move because of the desire to provide improved predictions of climate change with limited computing capabilities (Lin and Neelin (2003), Teixeira and Carolyn (2008) and Yano et al. (2008)). In relation to the discussion on ergodicity provided in section 2.1.4, Ito (1984) demonstrates analytically that the L63 model is ergodic for any value of ρ. This result will be explored numerically in chapter three of this thesis and the relevance of the ergodicity of the L63 will be examined in the context of the climate system under climate change.

2.4.2 Lorenz-84 model

Similarly, the Lorenz-84 model (hereafter L84) has been used extensively to draw analogies to the climate system. Lorenz claims that the model "may serve principally in examining existing hypotheses and formulating new ones" (Lorenz (1984)). Roebber (1995) comment that quantitative information from studies using the Lorenz-84 model should be viewed in a fairly general way but such investigations have an important role to play in understanding the dynamics of the ocean-atmosphere system. Under certain parameter combinations, the model demonstrates the presence of intransitive behaviour; the existence of more than one long-term climate. A study by Freire et al. (2008) reveals the foliated structure of the model's basins of attraction and suggests that "the final climate scenario (attractor) crucially depends on subtle and minute tuning of parameters".

In using the L84 model to investigate climate predictability, some authors have introduced a

seasonal cycle in the model parameters; a seasonal cycle is also explored in this thesis and the initial model results are displayed in section 4.4. Lorenz (1990) analyses the model when subject to a seasonal cycle in the model parameter F (the equator-to-pole temperature difference) to show how chaotic behaviour in one of the seasons can lead to interannual variability in the model variables. Pielke and Zeng (1994) also used the model to investigate the hypothesis that short periodic variations can lead to long-term variability. The authors use the results to support a hypothesis that the combined effect of periodic variations (such as seasonal forcing variations) and the complex nonlinear interactions that occur in the climate system can lead to long-term variability. Investigations into the dynamics of the seasonally driven L84 model were also carried out by Broer et al. (2002) and Broer et al. (2003) to outline the routes to chaos for different parameter combinations and illustrate the associated attractors.

2.4.3 Stommel ocean-box model

The Stommel ocean-box model (hereafter S61) was first introduced by Henry Stommel in his 1961 paper examining the dynamics of the thermohaline circulation (THC) (Stommel (1961)). The dynamics of this highly simplified ocean model have been explored in great detail since its inception. Lohmann and Scheider (1998) provide a comprehensive analysis of the model dynamics, illustrating the phase diagrams associated with the model parameter space and linking the model to long-term climate variability. Like the Lorenz models, the S61 model is still actively being utilised in research projects to understand the dynamics of the climate system. A study by Prange et al. (2002) has analysed the S61 model response in relation to more complex AOGCMs to help develop hypotheses and test underlying theory.

In this thesis, the S61 model is not studied in isolation but is coupled to the L84 model to create a (highly idealised) atmosphere-ocean climate model. The method of coupling is provided in the analysis by Van Veen et al. (2001). The combination of two models allows for a closer analogy to the complex climate system which is subject to internal variability acting on multiple time scales.

Chapter 3

The L63 Model

3.1 Modelling by Analogy

In attempting to further understand the dynamics of the atmosphere, meteorologist Edward Lorenz discovered the existence of chaos in a simple numerical model simulating thermal convection (Lorenz (1963)). The notion of chaos is now ubiquitous across many scientific disciplines and is still highly relevant to the study of nonlinear dynamic systems today. In this chapter the Lorenz attractor, which has been explored in great detail since its inception in 1963, is examined to generate insight into the predictability of the more complex climate system under altered forcings.

In section 3.2 the Lorenz-63 (L63) model is described and the model attractor is illustrated for conventional parameter values. The climate of the L63 model is then determined using estimates of the model's probability distributions for each variable and the results are presented in section 3.3. The section begins with a visual analysis of the model climate distributions followed by a quantitative analysis exploring the ergodic hypothesis. The impact of IC ensemble location, in relation to climate prediction, is addressed in section 3.4 by investigating the rates of convergence for model ensembles originating from different regions of the model attractor state space. In section 3.5, the analysis focuses on the behaviour of the model in response to perturbations in the parameter ρ which can be considered analogous to an external forcing on the climate system. Section 3.6 and section 3.7 present the results of experiments exploring the impact of periodic and nonperiodic fluctuations in ρ respectively, on the model climate distributions. The notions of model resonance and hysteresis are examined in each of these sections. Section 3.8 describes the results of experiments in which trends in ρ are imposed on the L63 model to gain insight regarding climate under climate change. The section examines the behaviour of model climate distributions under transient parameter conditions when subject to both chaotic and non-chaotic regions of the parameter space. Finally, section 3.9 discusses the implications of the results for climate model experimental design and the interpretation of climate model output. Focusing on the fundamental issues of climate predictability for nonlinear chaotic systems, recommendations

are made for potential experiments using more complex climate models. The usefulness of the term 'attractor' in aiding the conceptual understanding of climate in the context of climate change is also reviewed.

3.2 The L63 Attractor

The L63 attractor was first introduced by Edward Lorenz in his seminal paper, Nonperiodic Deterministic Flow (Lorenz (1963)). The ordinary differential equations (ODEs) used to define the system (equations 3.1 to 3.3) are simplified forms of the equations describing thermal convection in a fluid:

$$\frac{dX}{dt} = \sigma(Y - X) \tag{3.1}$$

$$\frac{dY}{dt} = X(\rho - Z) - Y \tag{3.2}$$

$$\frac{dZ}{dt} = XY - \beta Z \tag{3.3}$$

where σ is the Prandtl number, ρ is the Rayleigh number and β is a geometric factor (Tabor (1989)). By convention, the parameters take the values $\sigma = 10$, $\rho = 28$ and $\beta = \frac{8}{3}$. X, Y and Z denote the variables of the model. Figure 3.1 shows a graphical representation of the three-dimensional attractor determined by a single simulation of the model integrated using a common fourth-order Runge-Kutta (RK) integration scheme[1] with a nondimensional time step, $\tau = 0.001$ Lorenz Time Units (LTUs). The integration method and time step used is important in approximating the climate of the L63 system numerically and is discussed further in section 3.3.5. The trajectory shown in figure 3.1 begins from an initial state near the model's attractor and over time the trajectory evolves ever closer towards the attractor. In order to produce figure 3.1, the model is run for 50 LTUs (equal to 50,000 time steps). The attractor is symmetric about the origin in the X and Y dimensions resulting in a two-lobed structure which has often been likened to "butterfly wings" (e.g. van den Berge et al. (2010)).

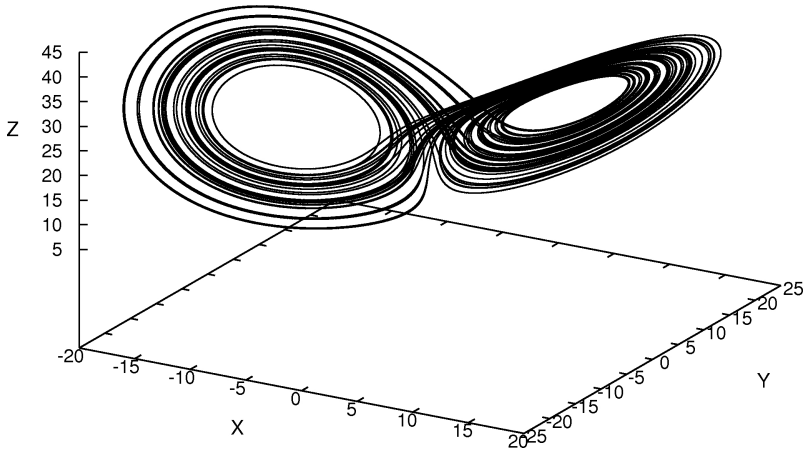

Figure 3.1: Single trajectory for a 50 LTU simulation of the L63 model with ICs $(X, Y, Z) = (1.0, 1.0, 25.0)$.

The L63 model evolves with two characteristic time scales; an oscillation time around the

[1] see http://en.wikipedia.org/wiki/Runge%E2%80%93Kutta_methods

regime centroid, and a residence time within a regime (Palmer (1993)). The oscillation time for a trajectory to orbit one of the lobes on the attractor (also referred to as model regimes in the literature) is typically slightly less than 1 LTU. Figure 3.2 shows the evolution of the model for each variable to illustrate the dynamic behaviour of the model and highlight the nature of the transitions of the trajectories from one regime to the other. The figure is extracted from the same model simulation data as used in figure 3.1 but shown only for the first 20 LTUs of the model run.

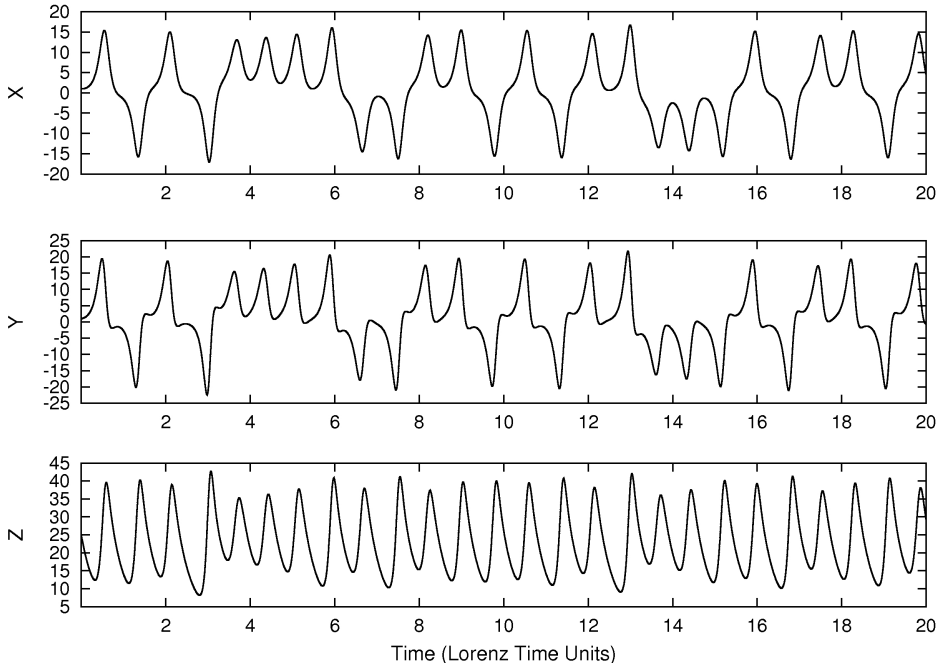

Figure 3.2: Evolution of three model variables for a 20 LTU simulation of a single trajectory from the L63 model, with ICs $(X, Y, Z) = (1.0, 1.0, 25.0)$.

The residence time spent in each of the attractor regimes (evident in the X and Y variables), before a transition to the alternate regime occurs, is variable. In figure 3.2 the trajectory initially transitions after every orbit but at $t = 4$, the trajectory resides in the same regime for four consecutive orbits. The transitions are subject to chaos so a small change in the ICs will ultimately lead to large differences in the evolution of the model trajectories (Lorenz (1963)). The predictability of the deterministic system is therefore limited by uncertainty in the initial state. Nevertheless, it is possible to estimate the likelihood of a trajectory being in a certain region within the model state space. One method to elucidate the likelihood of a trajectory being in a particular region of the model state space is to estimate the probability distributions for each of the three L63 variables for a given choice of parameter values. These distributions provide a measure of climate and represent projections of the possible system states onto each variable of the three-dimensional system. The resultant distributions therefore reveal the 'climate' of the system in relation to the three system variables, X, Y and Z.

3.3 The Climate of L63

To explore the climate of the L63 system, the Perfect Model Scenario (PMS) is adopted. The PMS arises when the model we are using admits the same mathematical structure as the system that generates the observations (Smith (2007)); in other words the system and the model are the same.

3.3.1 Defining the climate of the L63 system

Establishing a single definition of climate for the Earth system is non-trivial (see discussion in section 2.1.1) but the climate of the autonomous L63 model (with fixed parameters) can be well defined. The climate is given by the distribution of states, across all model variables, consistent with the model's attractor. For fixed parameters, the probability of a trajectory being in a particular region of the model state space is constant. For any given variable of the model, the climate is therefore manifest as a probability distribution over the range of possible variable states.

There are at least two methods for numerically estimating the probability distributions (which will hereafter also be referred to as the model climate distributions) for each of the L63 variables. Firstly, a single realisation of the model can be run for a long period of time and a frequency distribution for each model variable produced. If the distributions remain unchanged when running the model for a longer period of time, then the distributions have converged towards the model's climate distributions. Secondly, a large number of IC ensemble members can be run for a fixed length of time and the final states of each member used to generate a frequency distribution. If the length of the model simulation time is sufficient for the trajectories to adequately *explore* the attractor state space then the ensemble distributions will approximate the climate distributions for the model variables. According to the ergodic hypothesis, the distributions from each of the two methods should be equivalent.

To test the ergodic hypothesis for the L63 model, and provide estimates of the model's climate distributions, a number of model runs are performed. Initially, the single trajectory approach to estimating the climate distributions is tested and the length of time required for the frequency distributions to converge is investigated.

3.3.2 Convergence of single trajectory distributions

A single trajectory is initiated at a point close to (but not on) the attractor[2] and over the course of the model simulation, the trajectory moves towards the attractor. The frequency distributions of the model variables are determined for the single model realisation over increasing simulation periods, from 1 LTU to 10,000 LTUs. The frequency distributions for the X variable are given

[2]IC is $(X, Y, Z) = (1.0, 1.0, 25.0)$; a state that visually appears to be near the saddle point of the attractor shown in figure 3.1.

in figure 3.3 (the corresponding distributions for the Y and Z variables are given in Appendix A).

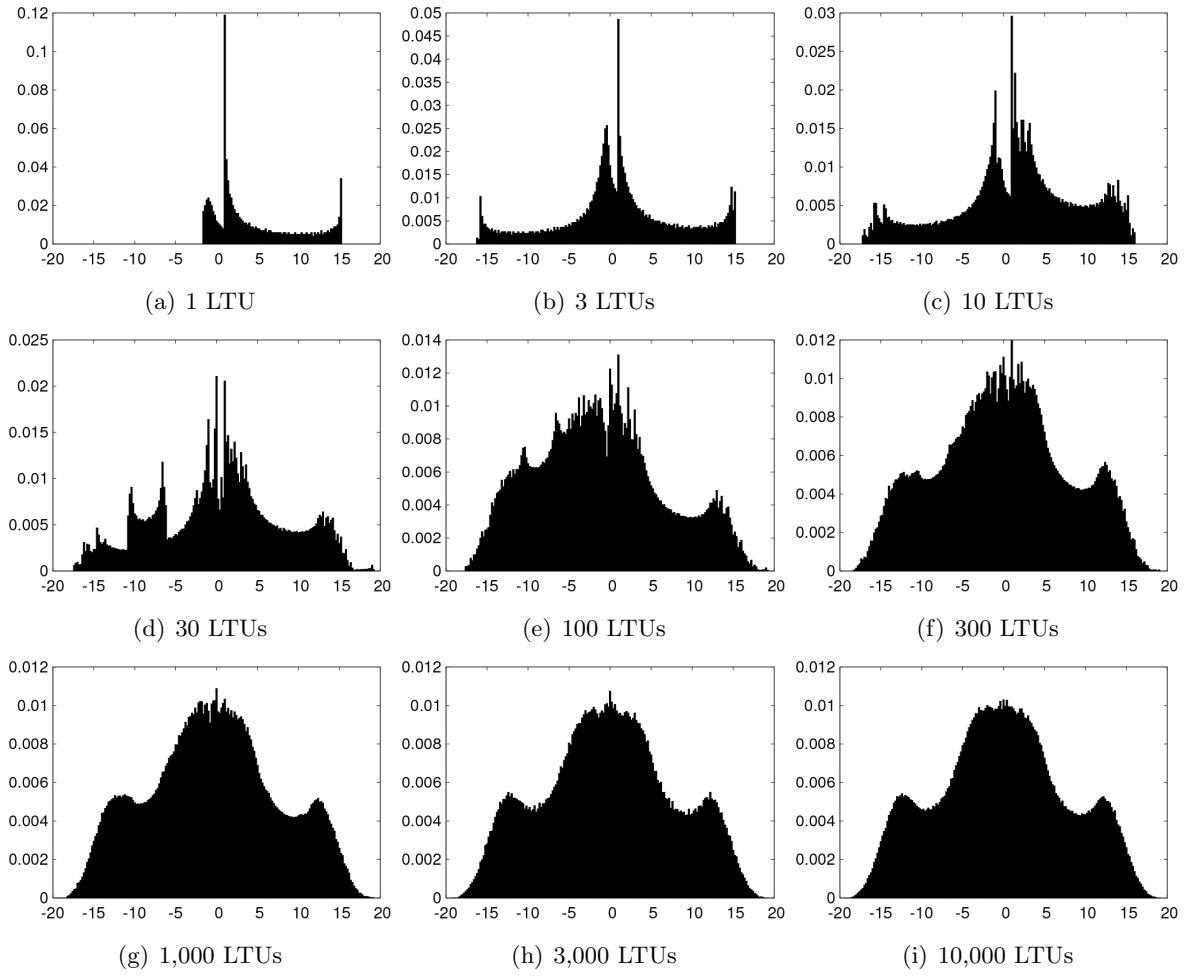

(a) 1 LTU (b) 3 LTUs (c) 10 LTUs

(d) 30 LTUs (e) 100 LTUs (f) 300 LTUs

(g) 1,000 LTUs (h) 3,000 LTUs (i) 10,000 LTUs

Figure 3.3: Normalised frequency distributions of the X variable from a single trajectory of the L63 model with ICs $(X, Y, Z) = (1.0, 1.0, 25.0)$, over increasing time periods. In each plot, the x-axis corresponds to the X variable and the y-axis corresponds to the frequency per occupied bin; bin width = 0.2.

The distribution depicted in figure 3.3(a) shows the distribution of model states over the first LTU of the model run. The distribution is highly asymmetrical as the trajectory only has sufficient time to propagate around one of the two model regimes. As the time period increases, the asymmetry becomes less pronounced because the trajectory spends approximately the same amount of time in each of the model regimes. The results illustrated in figure 3.3 show that the model distributions converge over time. The distribution that results after 10,000 LTUs, shown in figure 3.3(i), is a relatively smooth symmetric distribution with a primary peak at the origin and two secondary peaks at $X \approx \pm 13$. The distributions in the Y and Z variables similarly show convergence over time (see figures A-1(a) and A-2(a) in appendix A). In order to demonstrate the ergodicity of the L63 model for conventional parameters, the following sections explore the convergence of IC ensemble distributions and compare the rates of convergence to

that observed in the single trajectory distributions.

3.3.3 Convergence of initial condition ensemble distributions

In this section, results from large IC ensemble model runs are presented as an alternative approach to estimating the L63 model's climate distributions. Assuming a knowledge of the range of possible model state values but no prior knowledge of the model's climate distributions, a 100,000 member IC ensemble is selected with ICs that are evenly spaced along a transect from plausible low values, X_l, Y_l, Z_l $(-20, -25, 1)$, to plausible high values, X_h, Y_h, Z_h $(20, 25, 40)$. The ensemble is run for 1,000 LTUs and the distributions are shown at given time instants in the simulation period. The ensemble distributions displayed consist of a single state for each ensemble member. The distributions for the X variable are given in figure 3.4 (the corresponding distributions for the Y and Z variables are given in Appendix A).

In order to demonstrate the existence of ergodicity in the L63 model numerically, the distributions that result using long time interval integrations of a single trajectory, as explored in section 3.3.2, have to be shown to be equivalent to the distributions that result from an IC ensemble. Indeed, the ensemble distribution in figure 3.4(i) for the X variable closely resembles the distribution shown in figure 3.3(i), thus appearing to support the ergodic hypothesis for the L63 model. However, the distributions are not identical. One reason for this might be the size of the ensemble. Whilst a 100,000 member IC ensemble would be considered very large in a climate modelling context, the number of individual data points is two orders of magnitude smaller than the 10,000,000 data points that constitute the distribution given in figure 3.3(i). In addition, a 1,000 LTU integration time step may still be too short to guarantee that the ensemble members have spread around the attractor and can be considered independent of the IC ensemble design; an issue explored in the next section. Because of the chaotic nature of the L63 model and the fact that over time the trajectories move towards the attractor, a longer integration with more ensemble members would better approximate the model's climate distributions.

3.3.4 Time to converge to the model climate

In this section, the rates at which single trajectory distributions and IC ensemble distributions converge to the L63 model climate is presented. At any point in a model simulation a single trajectory may spend an unusually long time in one of the two regimes on the attractor. Consequently, the simulation time required for frequency distributions extracted from a single trajectory to approach the model's underlying climate distributions ought to be longer than the respective simulation time required for an IC ensemble. Given the chaotic nature of the L63 model, ensemble members initiating from different ICs will spread across the attractor independently from one another. Evidence that this occurs in the L63 model is apparent when comparing figure 3.3(e) to figure 3.4(g), both of which show frequency distributions after a 100

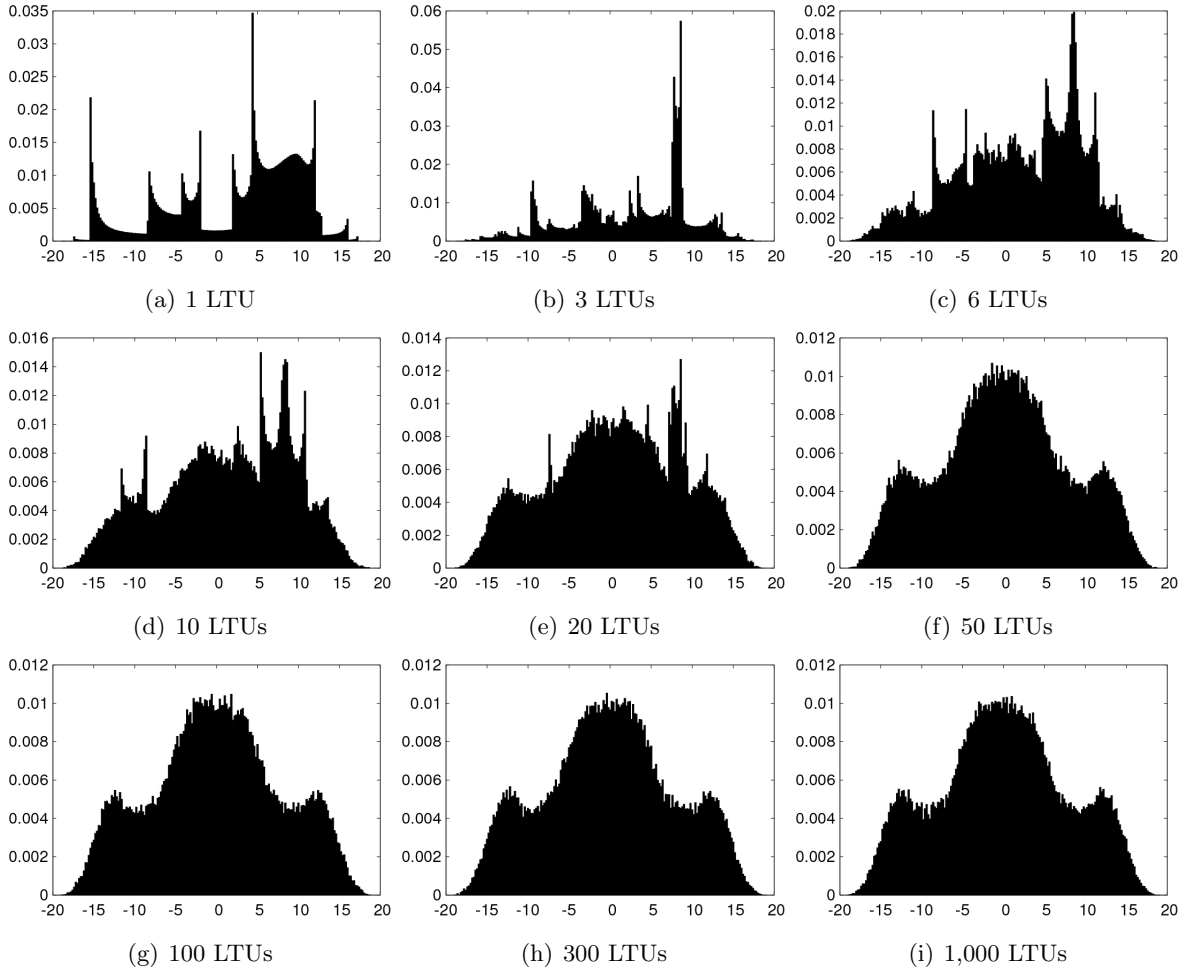

(a) 1 LTU (b) 3 LTUs (c) 6 LTUs

(d) 10 LTUs (e) 20 LTUs (f) 50 LTUs

(g) 100 LTUs (h) 300 LTUs (i) 1,000 LTUs

Figure 3.4: Normalised frequency distributions of the X variable for the L63 model, from a 100,000 member IC ensemble with ICs spread evenly along a transect from $(X_l, Y_l, Z_l) = (-20, -25, 1)$ to $(X_h, Y_h, Z_h) = (20, 25, 40)$. The distributions show the states of each ensemble member at the given time instant in the simulation period. In each plot, the x-axis corresponds to the X variable and the y-axis corresponds to the frequency of ensemble members per occupied bin; bin width = 0.2.

LTU run of the L63 model. The distribution from the single trajectory given in figure 3.3(e) is asymmetric and clearly different from the converged distribution that results over a longer simulation period. In figure 3.4(g), the distribution is largely symmetric and visually resembles the converged distribution shown in figure 3.3(i).

The distributions associated with the 100,000 member IC ensemble simulation at 1,000 LTUs (a long time with respect to the characteristic time scales of the system) provides benchmark "equilibrium" climate distributions, to which other distributions may be compared. Ideally, one would create distributions from an even larger ensemble and run the model for an even longer simulation period but practical considerations ensure restrictions. The 'equilibrium' climate distributions for each of the model variables are given in figure 3.5; where figure 3.5(a) is a reproduction of figure 3.4(i).

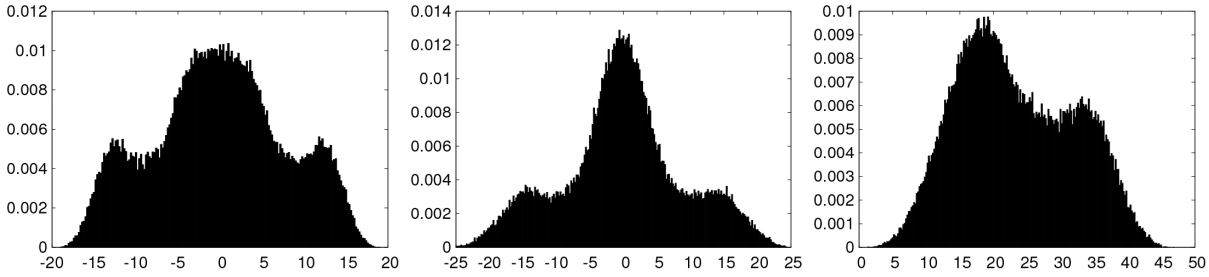

(a) X (b) Y (c) Z

Figure 3.5: Normalised frequency distributions for the three variables of the L63 model, from a 100,000 member IC ensemble with ICs spread evenly along a transect from $(X_l, Y_l, Z_l) = (-20, -25, 1)$ to $(X_h, Y_h, Z_h) = (20, 25, 40)$. The distributions show the states of each ensemble member at the 1,000 LTU time instant in the simulation period. In each plot, the x-axis is given in the panel title and the y-axis corresponds to the frequency of ensemble members per occupied bin; bin width = 0.2.

One method to quantitatively compare distributions is the Kolmogorov-Smirnov (KS) test. The KS statistic, D, is defined as the maximum value of the absolute difference between cumulative distribution functions (Press et al. (1992)). When comparing two cumulative distribution functions, $S_{N_1}(x)$ and $S_{N_2}(x)$, the KS statistic is given by equation 3.4:

$$D = \max_{x_{min} \leq x \leq x_{max}} \mid S_{N_1}(x) - S_{N_2}(x) \mid \tag{3.4}$$

When $D = 1$, the distributions are entirely different; the ranges of the data from which the distributions are derived do not crossover. As $D \to 0$ the distributions become more similar; when $D = 0$, the distributions are identical. To establish the significance of the test statistic, a critical value of D (K_α) can be determined according to equations 3.5 and 3.6 such that the null hypothesis[3] can be rejected at level α if:

$$\sqrt{\frac{nn'}{n+n'}} D_{n,n'} > K_\alpha. \tag{3.5}$$

$$Pr(D_{n,n'} \leq K_\alpha) = 1 - \alpha \tag{3.6}$$

where n and n' are the sample sizes of the two distributions. In a number of subsequent comparisons shown in this thesis, the KS statistic compares two ensemble distributions with 10,000 members each; when $n = 10000$ and $n' = 10000$, the critical KS value at the 95% confidence level is $K_\alpha = 0.019$. Whilst the significance of the D values presented in this chapter and the following chapters can therefore be easily obtained, the purpose of using this statistical measure is not to conclusively prove (or disprove) hypotheses at a given level of statistical significance. Rather the KS test is used to provide a simple quantitative measure with which distributions can be compared and the interest in this section, and subsequent sections, is predominantly in the *rate* of convergence between ensembles. The measure tends

[3]The null hypothesis asserts that the sample distributions come from the same population

to be more sensitive near the centre of the distribution (where the density is greater) than at the tails (NIST/SEMATECH (2008)) and in this analysis, it is clearly stated when results are impacted by this property. In addition, the KS test makes no assumptions about the shape of the distributions being compared (Gaussian, log-normal etc.) so it is therefore an appropriate measure to use in this study where the distributions are often irregular.

Using the KS test, the equilibrium distributions given in figure 3.5 are compared to the distributions resulting from both the single trajectory method (described in section 3.3.2) and the IC ensemble method (described in section 3.3.3). The distributions used are extracted from the same model runs that generated figures 3.3 and 3.4. The corresponding KS plots, for a period of 300 LTUs, are shown in figure 3.6.

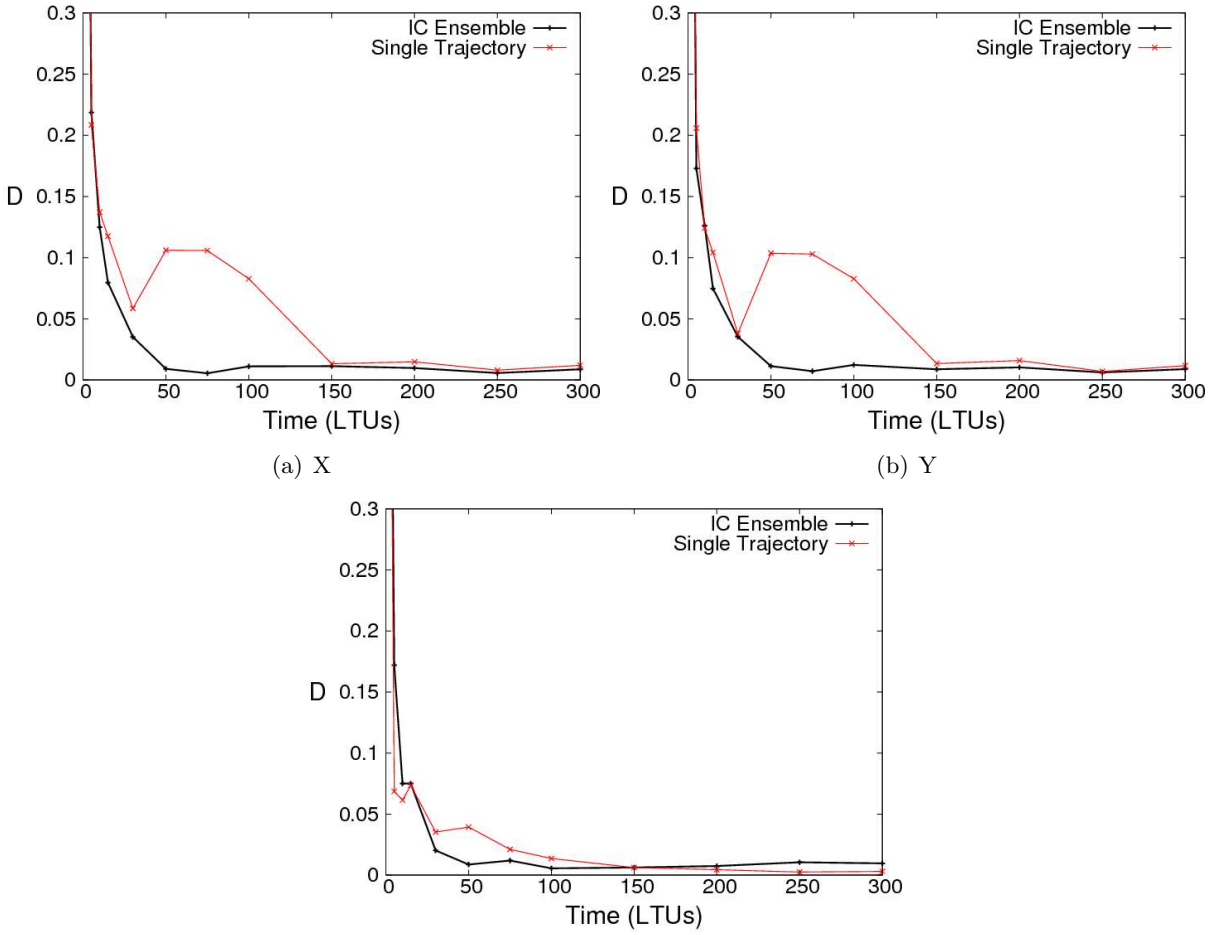

(a) X

(b) Y

(c) Z

Figure 3.6: KS results showing the comparisons between the equilibrium climate distributions (given in figure 3.5) and the distributions from single trajectory distributions and IC ensembles for each of the L63 model variables under fixed (conventional) parameter conditions.

The ensemble distributions converge towards the climate of the L63 model more rapidly than the single trajectory distributions. After 50 LTUs, the ensemble distributions appear to have converged towards the climate distributions given in figure 3.5. The single trajectory method

requires an additional 100 LTUs before the distributions display convergence towards the model climate distributions. The convergence is also less smooth using the single trajectory method because of the chaotic nature of the model which can lead to unusually long residence times within a particular regime. For example, at $t = 30$, D appears to be moving towards zero but at $t = 50$, D has increased. The convergence is faster in the Z dimension for both methods because the two attractor lobes (regimes) occupy broadly the same range in Z whilst the ranges in X and Y are limited to either positive or negative values for a single orbit around a model lobe.

One might question the value in running large IC ensembles which can consume a longer amount of computational time to arrive at the model climate distributions when compared to the single trajectory method. If the model in question is transitive[4] and the parameters of the model are fixed, the case for running large IC ensembles to fully explore the climate distributions may be weak given the additional computational capacity needed to run large IC ensembles. However, it is unknown whether the climate system is transitive, intransitive or almost-intransitive (McGuffie and Henderson-Sellers (2005)) and in the context of climate change, the system parameters (forcings) are certainly changing. This element is explored further in section 3.8 and considered again in later chapters with the insight from additional simple 'climate-like' models. However, there are other potential benefits of running IC ensembles as opposed to single realisations for nonlinear dynamic models and one such reason is outlined in section 3.4, which investigates the 'memory' of the climate system by analogy to the L63 model.

3.3.5 Sensitivity to integration method and time step

In the 1963 paper, Lorenz employs a simple Euler integration method with a time step, $\tau = 0.01$. Whilst sufficient for the model to exhibit chaos and produce a strange attractor, using a simple integration method with a relatively large time step introduces significant temporal truncation errors. Teixeira et al. (2007) investigate the sensitivity of the L63 model's climate to the choice of time step and conclude that the model's climate and model regimes show a complex sensitivity to the time step. The authors therefore suggest that climate statistics derived from climate model output may be affected by truncation errors in the temporal resolution in addition to truncation errors in model spatial resolution. Yao (2005) also examines the sensitivity of the numerical solutions in the L63 model to the time step and states that the numerical truncation errors can substantially alter the shape of the attractor. In order to ensure that the analysis presented in this chapter is robust to the choice of model time step, a number of model versions are run with different time steps for both Euler and RK integration methods.

[4]See glossary definitions.

The Euler Method

For an initial value problem of a given ODE, as expressed in equations 3.7 and 3.8 (where y is an independent variable and t denotes time), one may wish to estimate y at times, $t = t_0, t_1 ... t_n$.

$$y(t_0) = y_0 \tag{3.7}$$

$$y'(t) = f(t, y(t)) \tag{3.8}$$

Using the Euler method, given in equation 3.9 (where τ is the time step), one computes the tangent to the curve at each time step to approximate the model trajectory.

$$y_{n+1} = y_n + \tau f(t_n, y_n) \tag{3.9}$$

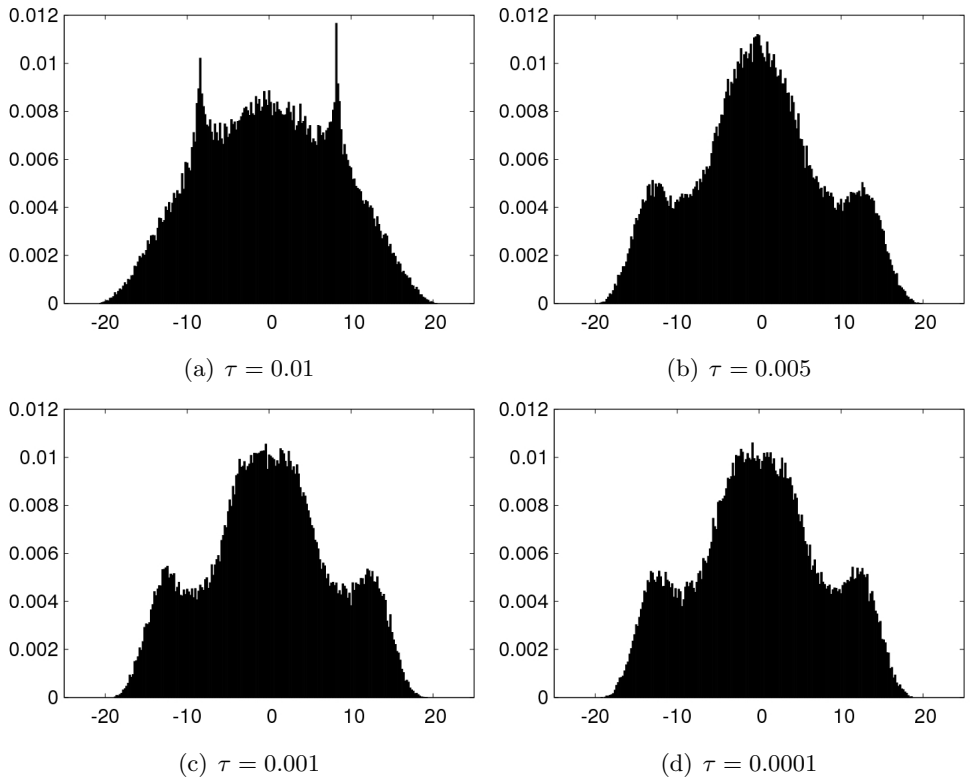

(a) $\tau = 0.01$ (b) $\tau = 0.005$

(c) $\tau = 0.001$ (d) $\tau = 0.0001$

Figure 3.7: Normalised frequency distributions for the X variable in the L63 model from a 100,000 member IC ensemble with ICs taken from the states used to generate figure 3.5. The distributions show the states of the ensemble members after a 100 LTU simulation period using the Euler integration method for given time steps, τ. In each plot, the x-axis corresponds to the X variable and the y-axis corresponds to the frequency of ensemble members per occupied bin; bin width = 0.2.

Figure 3.7 shows the frequency distributions (which approximate the model climate) for the X variable from a 100,000 member IC ensemble when using the Euler integration method for given time steps. Clearly, the time step employed has an impact on the distributions associated with the model attractor. For a time step of $\tau = 0.01$, the model displays a distribution with

two sharp peaks centred at $X \approx \pm 9$. By halving the time step to $\tau = 0.005$, a very different climate for the model results, showing a distribution which is more similar to the equilibrium climate distribution shown in 3.5(a) with a primary peak centred at $X = 0$ and two secondary peaks at $X \approx \pm 13$. Also, the range of the ensemble distribution is reduced for smaller time steps. Apparent in figure 3.7(a) but not in figures 3.7(b), 3.7(c) or 3.7(d), are a number of trajectories that occur at values of X close to $X = \pm 20$. For smaller time steps, the range in X is decreased. By reducing the time step to $\tau = 0.001$, and then again to $\tau = 0.0001$, it appears that the distributions have converged towards the model climate distributions. The results show that smaller time steps generate more accurate estimates of the model's climate distributions.

The Runge-Kutta Method

A higher order method of integration is the common fourth order RK method, expressed in equations 3.10 and 3.11:

$$y_{n+1} = y_n + \tfrac{1}{6}\tau\left(k_1 + 2k_2 + 2k_3 + k_4\right) \tag{3.10}$$

$$t_{n+1} = t_n + \tau \tag{3.11}$$

where k_1, k_2, k_3 and k_4 are four measures of the tangent to the model trajectory as given by equations 3.12 to 3.15, and τ is the model time step. The method calculates a weighted average for the slope of the curve which produces a more accurate approximation to the real solution than the Euler method.

$$k_1 = f(t_n, y_n) \tag{3.12}$$

$$k_2 = f(t_n + \tfrac{1}{2}\tau, y_n + \tfrac{1}{2}\tau k_1) \tag{3.13}$$

$$k_3 = f(t_n + \tfrac{1}{2}\tau, y_n + \tfrac{1}{2}\tau k_2) \tag{3.14}$$

$$k_4 = f(t_n + \tau, y_n + \tau k_3) \tag{3.15}$$

Figure 3.8 shows the resulting frequency distributions for the X variable, equivalent to figure 3.7, using the RK method. When $\tau = 0.01$ (figure 3.8(a)), the ensemble distribution is not too dissimilar from the equilibrium climate distribution shown in figure 3.5(a) but the primary peak is split into two peaks at $X \approx \pm 4$. Halving the time step (figure 3.8(b)) removes this anomalous feature but there is still an erroneous aspect to the distribution as the plot reveals a flattened primary peak. For $\tau = 0.001$ and $\tau = 0.0001$, the distribution converges towards the model climate distributions.

Both the Euler and RK methods seem to approach the "true" distributions for the model climate but the RK method appears to be less prone to distribution errors at relatively long time steps. For the analysis presented in this chapter, the higher-order RK method is adopted employing a time step, $\tau = 0.001$. As commented on by Teixeira et al. (2007) and Yao (2005), the impact

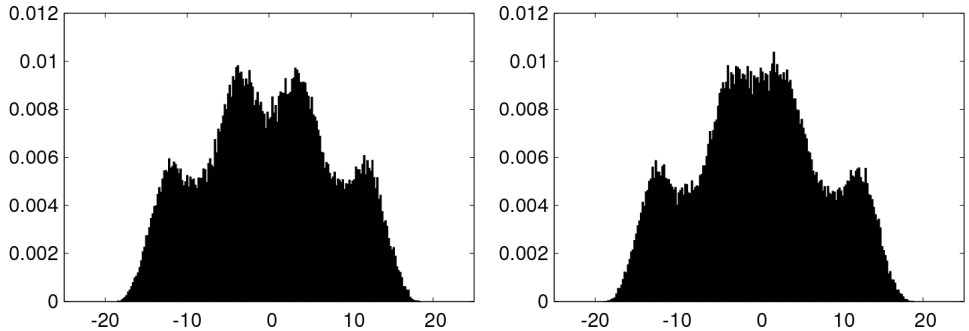

(a) $t = 0.01$ (b) $t = 0.005$

(c) $t = 0.001$ (d) $t = 0.0001$

Figure 3.8: Normalised frequency distributions for the X variable in the L63 model from a 100,000 member IC ensemble with ICs taken from the states used to generate figure 3.5. The distributions show the states of the ensemble members after a 100 LTU simulation period using the Runge-Kutta integration method for given time steps, τ. In each plot, the x-axis corresponds to the X variable and the y-axis corresponds to the frequency of ensemble members per occupied bin; bin width = 0.2.

of temporal truncation error introduced by crude integration methods and time steps is clearly an aspect of climate modelling which needs to be considered more routinely. Whilst the impact may not be seemingly apparent in the results from single realisations, exploring model climate distributions can highlight the sensitivities of particular models to such a class of errors.

3.4 Convergence of Model Ensembles

As discussed in the opening chapters, a primary focus of the research conducted in preparation of this thesis is to further understand the role of IC uncertainty for climate prediction on time scales relevant to climate change adaptation. Determining the time scales over which IC uncertainty is important for the dynamic evolution of the atmosphere-ocean system is therefore of central concern in developing the analogy to the climate system using simple idealised models. The L63 model has been used by a number of authors, in relation to weather forecasting, to develop theory regarding the temporal limits of predictability for single trajectories attributable to IC uncertainty. It has been observed that the deterministic predictability of an individual model trajectory in the L63 model can vary considerably depending on the initial location of the trajectory on the model attractor (Palmer (1993)). The implications of this sensitivity to the location of the initial state on the attractor have been acknowledged in the development of short- and medium-term weather prediction (Palmer (1993), Palmer (1999) and Lea et al. (2000)). However, in this section and in the following sections the L63 model is utilised to extend the analogy in understanding the limits of predictability, attributable to IC uncertainty, for model ensemble "climate" distributions.

In this study, the term *memory* is introduced to refer to the traceability of IC uncertainty in the model climate distributions. On long time scales, relative to the characteristic dynamic time scales of the system, it becomes pertinent to consider whether or not the region of state space in which an IC ensemble originates affects the system's *memory* and thus affects the time scales of predictability for the model climate distributions. The time it takes for IC ensemble distributions, originating in different regions of model state space, to converge provides a measure of the range in the time scales associated with the model memory (for the region of parameter space under investigation). When the ensemble distributions converge to the equilibrium climate distributions (approximated in figure 3.5), the memory of ICs is judged to have been lost.

As the L63 model has been shown to be ergodic (for conventional parameter values) and the model is known to display chaotic behaviour (Lorenz (1963)), the presumption is that ensembles originating from different regions of the model state space would converge to the same distribution and do so at approximately the same rate, thus exhibiting a narrow range in the model memory. Here, the memory of the L63 model is investigated for fixed parameters whilst in section 3.7.5 experiments are conducted to investigate the memory of the L63 model under altered parameter conditions.

Figure 3.9 shows the starting locations of four different 10,000 member IC ensembles superimposed onto the model attractor as depicted in figure 3.1. An ensemble size of 10,000 members is chosen as opposed to 100,000 members (used in earlier plots) in order to decrease the computational time required for model simulations. The locations are chosen from regions spread across the L63 attractor in order to investigate the impact of ensemble location on the

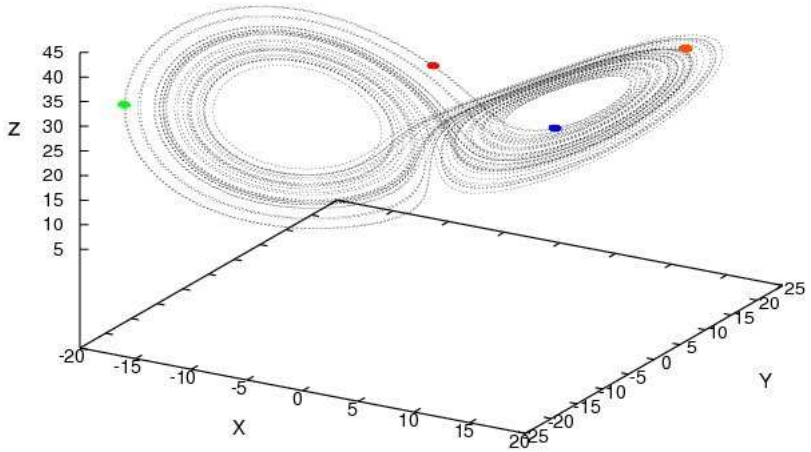

Figure 3.9: Single trajectory from figure 3.1 (dashed line) with four 10,000 member IC ensembles each with members normally distributed about a sphere with diameter, $d = 1$ in each of three dimensions. IC ensembles centred on (from left to right): **1** green points $(-17.228, -22.383, 34.031)$; **2** red points $(-2.520, 5.867, 31.340)$; **3** blue points $(6.683, 9.593, 20.451)$; and **4** orange points $(15.668, 15.564, 36.882)$.

model memory. The ICs within each ensemble are normally distributed within a sphere of diameter, $d = 1.0$. Because of the way the ICs are selected, very few (if any) of the IC states lie precisely on the attractor. However in the analogy to climate prediction, given that the initial state of the climate system is highly uncertain, because of observational uncertainty and sparse data sets, one cannot expect to initiate an ensemble with ICs precisely on any particular climate "attractor".

The four IC ensembles shown in figure 3.9 are run for 100 LTUs and the resulting frequency distributions for each ensemble are compared to the equilibrium climate distributions (shown in figure 3.5) using the KS test as a measure of comparison. The results for each variable are displayed in figure 3.10. The results show that over time the IC ensemble distributions converge towards the equilibrium climate distributions, as expected for a transitive system. After 5 LTUs, there is a large difference between the values of D observed for the different ensembles, with values ranging between $D = 0.21$ (for IC 4 in Y) and $D = 0.58$ (for IC 3 in Z). Over the first 20 LTUs of the model simulation, the values of D decrease rapidly but even after 30 LTUs, the values of D have not reached their minimum, suggesting that the ensemble distributions still retain memory of the ICs. The decrease in D is slower in the Z dimension than in the X and Y dimensions which may be a result of the asymmetry in the distribution and the tendency of the KS statistic to be more sensitive in the high density regions of the distribution (NIST/SEMATECH (2008)). After 40 LTUs in X and Y and 50 LTUs in Z, the KS values converge to a minimum (where $D \to 0$) and the ensemble distributions appear to have converged to the equilibrium climate distributions. Whilst there are differences in the rates of convergence between the IC ensembles, when viewing all three variables together it does not appear that any particular ensemble converges more quickly than the others. The results described here therefore suggest that the memory of ICs in the L63 model is largely

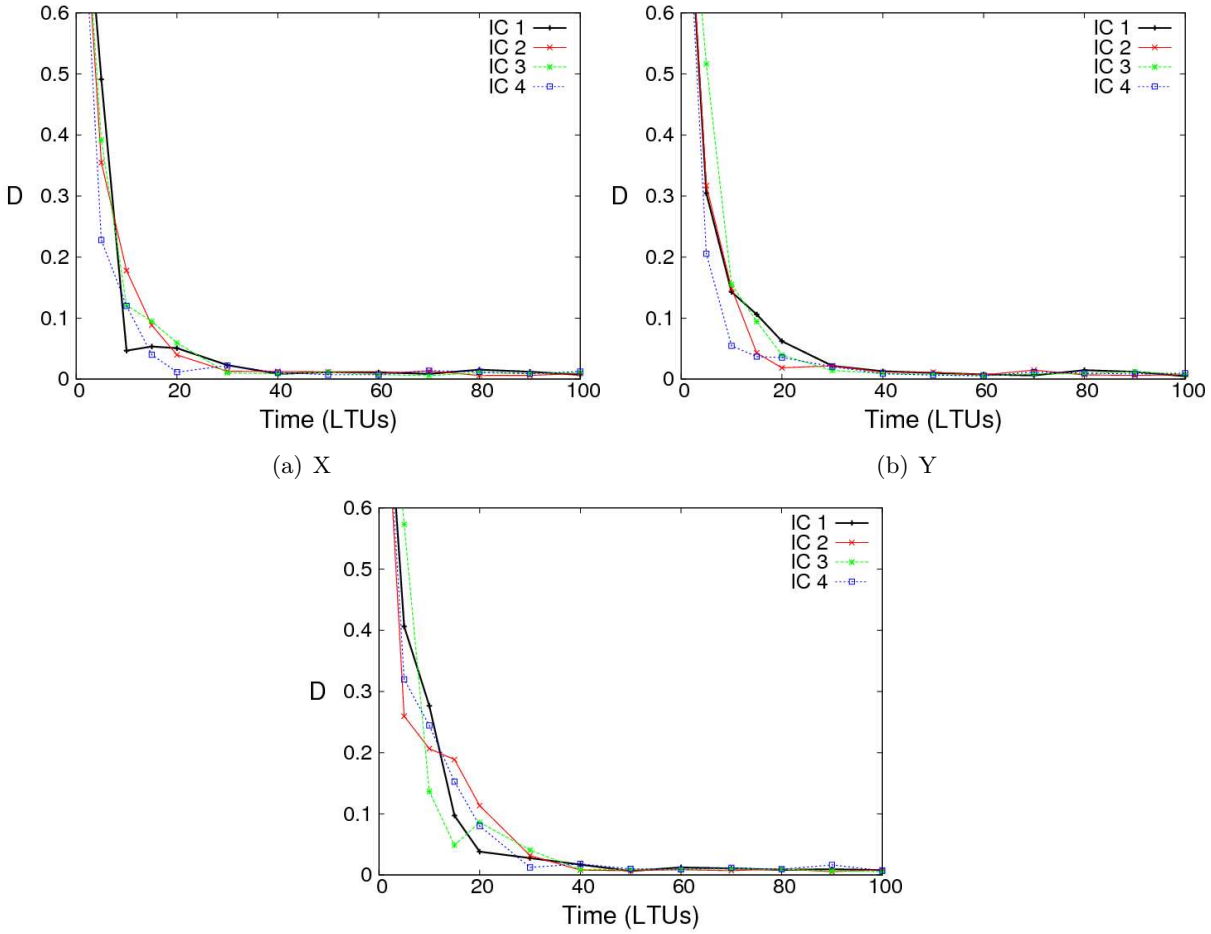

(a) X

(b) Y

(c) Z

Figure 3.10: KS results showing the comparisons between IC ensemble distributions from IC locations shown in figure 3.9, to the distributions resulting from an IC ensemble with ICs spread proportionally across the attractor for $\rho = 28$, at given time intervals for fixed parameter values.

independent of the initial location of the IC ensemble in the model state space and the memory of ICs is lost on a typical time scale of approximately 40 to 50 LTUs. In section 3.7.5, the impact of nonperiodic variations in ρ on the memory of the L63 model is investigated.

3.5 Varying the Parameter ρ

3.5.1 Motivation for varying ρ

Typically the nonlinear dynamics research community is concerned with *autonomous* dynamical systems whose equations have no explicit dependence on time (Lakshmanan and Rajasekar (2003)). Increasingly however, particularly in relation to climate research, attention is being given to *non-autonomous* dynamical systems whose equations are time-dependent (e.g. Chekroun et al. (2010a)). Unlike global weather prediction models, global climate models are used to determine the evolution of the atmosphere-ocean system under changing boundary conditions and altered radiative forcings. Such changes in the system's forcings are inherently time-dependent and consequently the climate system is a non-autonomous dynamical system. In developing the analogy to the climate system and utilising the notion of a climate attractor, the L63 model is used to explore the impact of climate variability and climate change (i.e. altered forcing conditions) on the probability distributions associated with the model attractor.

Recall that in the L63 system, the forcings are represented by the parameters σ, ρ and β. In the Rayleigh-Benard system, an increase in the temperature difference between the horizontal plates (ρ) leads to an increase in the heat flux (Z). Whilst one must be cautious in using the analogy of the L63 system to the far more complex climate system, the impact of altering ρ can be likened to the impact of changes in the meridional temperature gradient on the equator to pole heat flux (Lea et al. (2000)). More generally, introducing a time-dependence to one of the L63 model parameters can provide useful insight into the possible behaviour of a system's attractor when subject to altered forcings. Consequently, one can loosely relate changes to ρ in the L63 model to changes to the climate forcings in the climate system, such as the impact of GHG concentrations on the radiative forcing of the climate. By exploring the behaviour of a low-order model, when subject to time-dependent parameter changes, insight might be gained about how a more complex nonlinear dynamic system responds. Furthermore, analysis of simple models can help in establishing a theoretical framework to underpin the design of experiments to explore the sensitivity of model climate distributions to scenarios in which the forcing parameters are changing.

3.5.2 L63 attractor for alternative values of ρ

Before imposing a time-varying component in ρ, it is considered necessary to investigate the properties of the L63 model for alternative fixed values of ρ. Rothmayer and Black (1993) provide a concise explanation of the impact of different values of ρ on the model's attractor. When $\rho < 1$, all trajectories propagate towards the origin $(0, 0, 0)$ which is globally attracting. For $\rho \geq 1$ the origin becomes unstable and two new stable fixed points emerge at values $C^{\pm} = (\pm\sqrt{\beta(\rho-1)}, \pm\sqrt{\beta(\rho-1)}, \rho-1)$. At the value $\rho = 24.74$, a Hopf bifurcation occurs (denoted by ρ_H). For values of $\rho > \rho_H$, the fixed points located at $C^{\pm}$ become unstable and

chaos ensues (Sparrow (1982)). Therefore ensuring the attractor maintains its chaotic nature, a feature which is an inherent part of the climate system, the following analysis focuses on the climate of the L63 model when $\rho > \rho_H$.

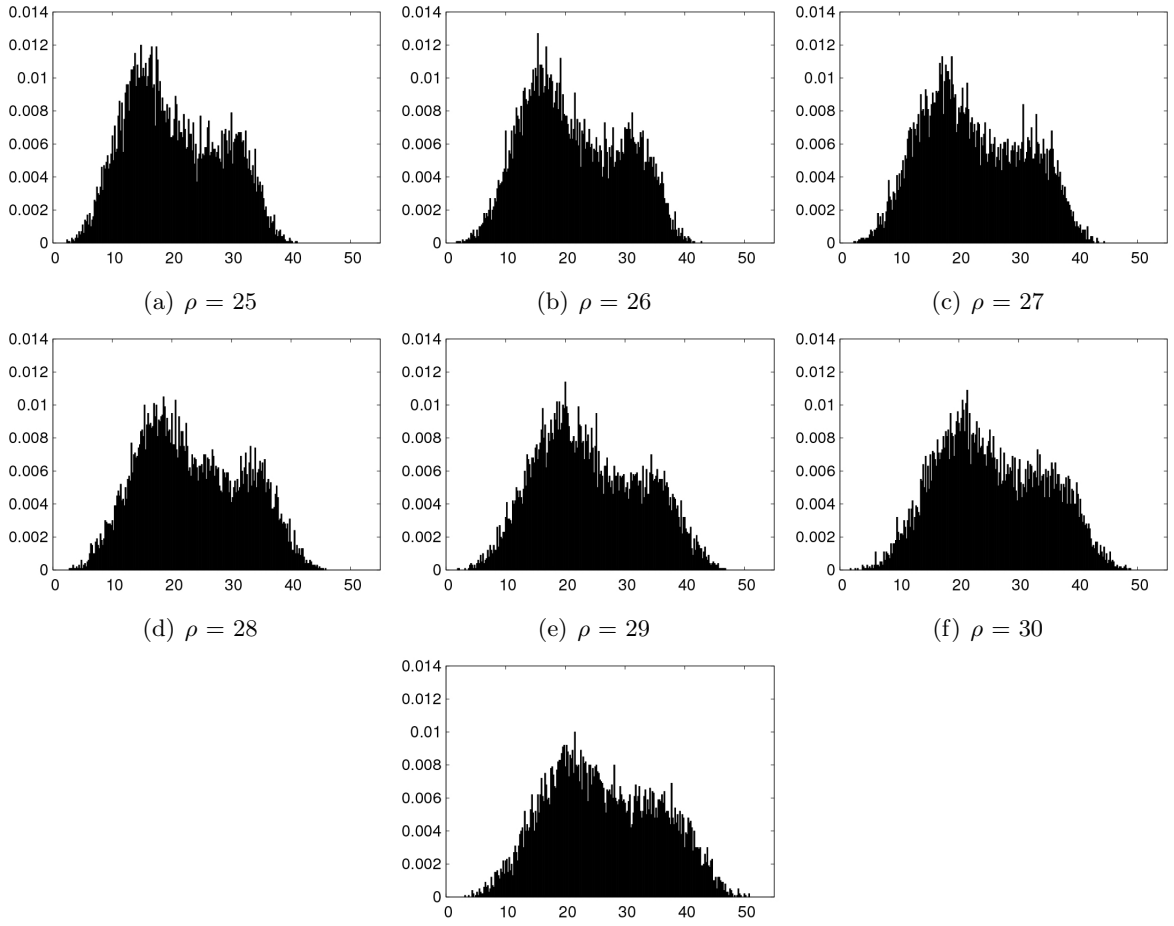

(a) $\rho = 25$ (b) $\rho = 26$ (c) $\rho = 27$

(d) $\rho = 28$ (e) $\rho = 29$ (f) $\rho = 30$

(g) $\rho = 31$

Figure 3.11: Normalised frequency distributions for the Z variable from a 10,000 member IC ensemble after 100 LTUs, for different values of ρ. The IC ensembles are initiated with ICs taken from the first 10,000 members of the equilibrium climate distributions for $\rho = 28$, shown in figure 3.5. In each plot, the x-axis corresponds to the variable Z and the y-axis corresponds to the frequency of ensemble members per occupied bin; bin width = 0.2.

Figure 3.11 shows frequency distributions, from a 10,000 member IC ensemble, for the Z variable after a simulation period of 100 LTUs having evolved with different values of ρ. The Z variable distributions are shown here rather than the X or Y variable distributions (which are shown in figures A-5 and A-6 in Appendix A) because the effect of increasing the parameter ρ on Z forms an interesting analogy to the climate system as described in section 3.5.1. The plots demonstrate that as ρ increases from $\rho = 25$ to $\rho = 31$, the range in the location of the trajectories increases with a notable shift towards higher values of Z. The maximum value of Z increases from $Z_{max} = 41.0$ to $Z_{max} = 50.9$, the mean value increases from $\bar{Z} = 20.5$ to $\bar{Z} = 26.4$ and the minimum value shows relatively little change, moving from $Z_{min} = 2.5$

to $Z_{min} = 3.4$. Consequently, as the parameter ρ increases, the range in Z increases and the peaks become less pronounced (whilst shifting to higher values) but the general shape of the distribution is preserved. The climate of the model is, in a general sense, similar for the range of ρ values chosen whilst the impact of increasing the parameter is most significant in the tails of the distribution. The likelihood of a model trajectory passing through areas of the state space where Z is high is greatly increased for higher values of ρ; the percentage of trajectories above $Z = 40$ increases from 0.04% when $\rho = 25$ to 8.56% when $\rho = 31$. Such a large relative change in the exceedance probabilities at the tails of the distributions, compared to the relative change in the mean, is a common feature of climate model projections (Meehl et al. (2000b)).

The climate distributions for the X and Y variables also remain relatively unchanged for the values of ρ explored here (see figures A-5 and A-6). However, as ρ increases, the number of trajectories moving to the tails of the distributions increases and the range becomes wider whilst maintaining the inherent symmetry about the origin; the maximum/minimum values of X and Y increase/decrease from $X = \pm 17$ and $Y = \pm 22$ when $\rho = 25$ to $X = \pm 20$ and $Y = \pm 28$ when $\rho = 31$. Therefore the signatures of a change in model climate, whilst evident in the shift in the mean for the Z variable, are most prevalent at the tails of the distributions in all model variables.

3.6 Periodic Fluctuations in ρ

The climate system is subject to modes of variability on a number of temporal and spatial scales (Ghil (2002)). Such variability can sometimes be attributed to fluctuations in the forcings on the climate system (Petit et al. (1999), Rind (2002)). In order to examine the potential influence of continuously varying forcings on the climate, using the analogous behaviour of the L63 model, a number of experiments are conducted in which the L63 model is subject to smoothly varying fluctuations in ρ. Adopting the range of ρ values explored in section 3.5.2, perturbations are added to a reference value, ρ_0, in the form of a sinusoidal time series according to the equation:

$$\rho(t) = \rho_0 + A(\sin 2\pi f t) \tag{3.16}$$

where A is the wave amplitude, t represents time and f denotes a controlling factor to adjust the frequency of the wave (with units LTU^{-1}); when $f = 1$ the wavelength is 1 LTU.

To investigate the impact of a non-stationary ρ parameter, a range of f values between $0.1 < f < 10$ are selected and ρ_0 is set to $\rho_0 = 28$ with $A = 3$ so that ρ oscillates between $25 < \rho < 31$. The L63 model is then run with an IC ensemble using initial values from the states of the first 10,000 members of the equilibrium distributions shown in figure 3.5. The resulting distributions for the ensemble simulations are displayed in figure 3.12 at 40 LTUs into the model simulation, as a 40 LTU time scale has been determined broadly sufficient to allow the ensembles to converge to the model climate distributions (see section 3.4).

When the model is subject to a stationary value of ρ, unsurprisingly the ensemble distributions do not change and the plots shown in figures 3.12(b) to 3.12(d) are very similar to the equilibrium climate distributions shown in figure 3.5; albeit less smooth because of a reduced number of ensemble members. Similarly, for a low frequency fluctuation in ρ ($f = 0.1$), as illustrated in figure 3.12(e), the ensemble distributions that occur after a simulation period of 40 LTUs are similar to the equilibrium climate distributions. The slow modulations between $\rho = 25$ and $\rho = 31$ lead to a relatively smooth response in the distributions and as seen in the fixed ρ plots given in figure 3.11 (for the Z variable), the distributions do not vary considerably in this parameter space.

However, when $f = 1$ the distributions that occur after a 40 LTU simulation period are very different from the model climate distributions for $\rho = 28$. When $f = 3$, and to a lesser extent when $f = 5$, the distributions are also dissimilar to the model climate distributions. By design, the frequency with which ρ is varying when $f = 1$ is of a similar time scale to the time it takes for a trajectory to orbit one of the attractor regimes. The model trajectories appear to be resonating with the fluctuations in ρ. This apparent resonance leads to dramatic changes in the distributions of the model variables and significantly alters the model climate. Further discussion of the impact of model resonance in the L63 model and its potential significance for climate change prediction is given in section 3.9.2.

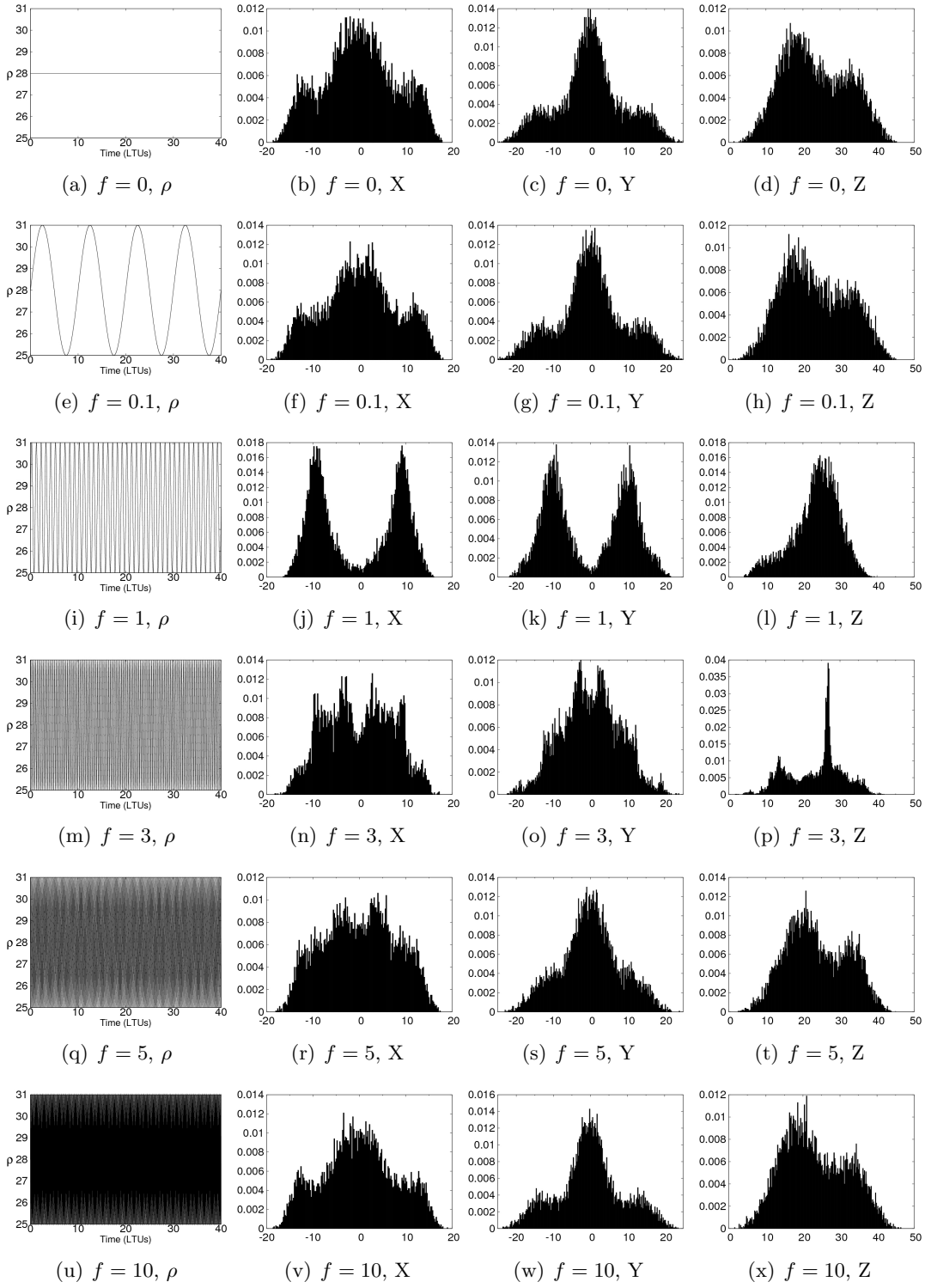

(a) $f = 0$, ρ (b) $f = 0$, X (c) $f = 0$, Y (d) $f = 0$, Z

(e) $f = 0.1$, ρ (f) $f = 0.1$, X (g) $f = 0.1$, Y (h) $f = 0.1$, Z

(i) $f = 1$, ρ (j) $f = 1$, X (k) $f = 1$, Y (l) $f = 1$, Z

(m) $f = 3$, ρ (n) $f = 3$, X (o) $f = 3$, Y (p) $f = 3$, Z

(q) $f = 5$, ρ (r) $f = 5$, X (s) $f = 5$, Y (t) $f = 5$, Z

(u) $f = 10$, ρ (v) $f = 10$, X (w) $f = 10$, Y (x) $f = 10$, Z

Figure 3.12: Normalised frequency distributions for a 10,000 member IC ensemble after a 40 LTU model run for given values of f. ICs are taken from the first 10,000 members of the climate distributions shown in figure 3.5. The left column shows the time series' in ρ, the distributions for X, Y and Z are shown in the centre-left, centre-right and right columns respectively. In the L63 variable plots, the y-axis corresponds to the frequency of ensemble members per occupied bin; bin width = 0.2.

For relatively high frequency fluctuations of $f = 10$, the ensemble distributions shown in figure 3.12(v) to 3.12(x) appear similar to the climate distributions. It is postulated that the rapid perturbations to ρ act as stochastic *noise* in the model and the consequence is that model trajectories evolve in a manner consistent with the model attractor at the mean reference value, $\rho_0 = 28$.

To further elucidate the impact of a sinusoidal variation in the model parameter ρ, the KS test is utilised to reveal the temporal evolution of the ensemble distributions for different values of f, relative to the ensemble climate distributions when ρ is fixed at $\rho = 28$. Figure 3.13 shows the time series' of the KS comparisons for each model variable. The ensembles are all initiated with the same ICs so $D = 0$ at time $t = 0$. The highest values of D are observed when $f = 1$, consistent with the significantly altered distributions shown in figures 3.12(j) to 3.12(l). D is also high when $f = 3$ in the Z variable largely due to a peak in the ensemble distributions at $Z \approx 27$ (see figure 3.12(p)). In the X and Y variables, the lowest KS values are observed when $f = 0.1$ and $f = 10$. When $f = 0.1$, there is an element of periodicity in the X and Y variables but the periodicity is most evident in the Z variable. The periodicity has a wavelength of 5 LTUs which is half the wavelength of the time series in ρ. This is no coincidence and occurs because the model distributions are continuously being altered in response to the changing value of ρ. Every 5 LTUs, ρ returns to $\rho = 28$ and this corresponds to a minimum in the value of D shown in figure 3.13(c). The periodicity in D is most evident in the Z dimension because the response of Z distributions to different values of ρ is larger than in the X and Y dimensions, particularly towards the upper tail of the distributions (as shown in figure 3.11). It is interesting to note that the value of D appears to reach a lower minimum every 10 LTUs (at 10, 20, 30 LTUs etc.), corresponding to the recurrence in $\rho = 28$ on the positive gradient of the sinusoid. This result demonstrates a memory of the forcing pathway, providing circumstantial evidence of hysteresis in the L63 model.

3.6.1 Implications for ergodicity

The ergodic assumption is shown to be valid for the L63 model under fixed parameter conditions (see section 3.3.3) but in this section, the ergodic assumption is tested when ρ varies periodically. A single realisation of the model is run with $f = 1$. The single trajectory is illustrated in figure 3.14 after a 40 LTU model simulation. Unlike the evolution of the single trajectory under fixed ρ, shown in figure 3.2, when the model is subject to periodic changes in ρ the trajectory evolves with some orbits passing much closer towards the centre of the two attractor lobes identified in section 3.2. The orbits also lose an element of regularity; in figure 3.2 the orbits are largely concentric (away from the saddle point) but in figure 3.14 the concentric behaviour is no longer observed.

In order to test the ergodic assumption, frequency distributions from the single model trajectory are compared to the IC ensemble distributions described in section 3.6. Because the value of ρ is varying in time, it is necessary to determine the ensemble distributions over an entire cycle

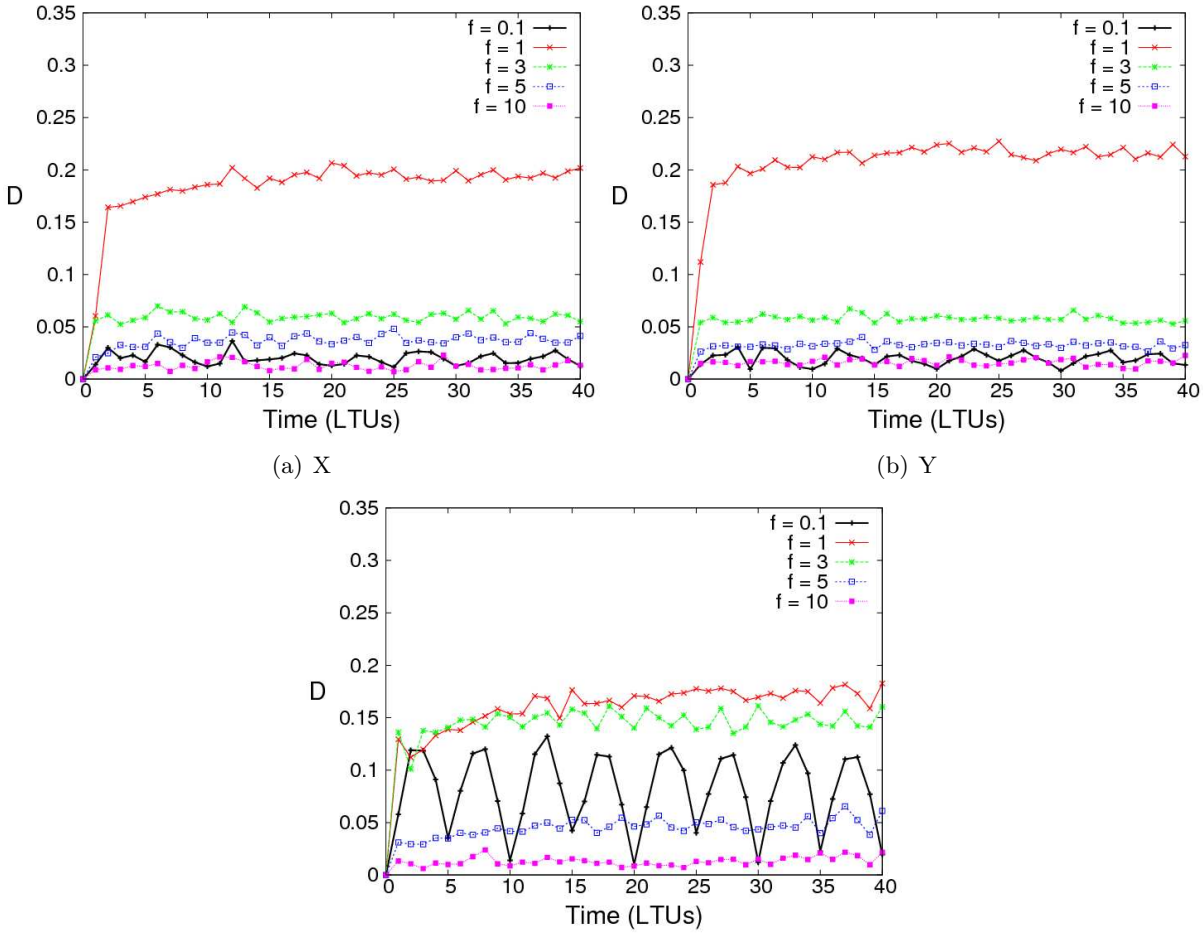

(a) X

(b) Y

(c) Z

Figure 3.13: KS results showing comparisons between the ensemble distributions when $f = 0$ (such that ρ is fixed at $\rho = 28$) and the ensemble distributions for other values of f for each of the L63 model variables subject to periodic variations in ρ.

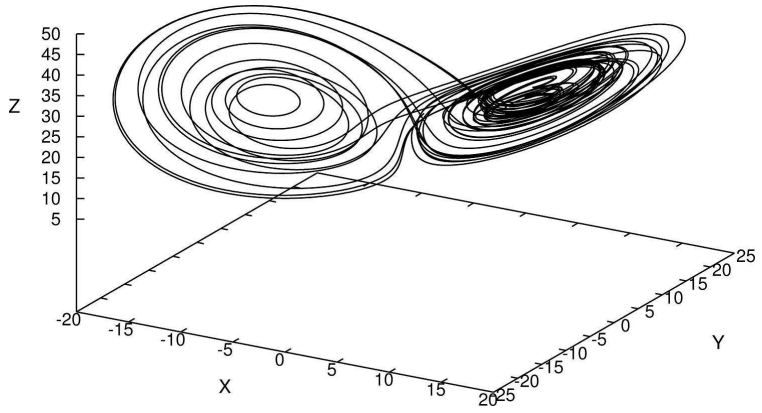

Figure 3.14: Evolution of model "attractor" for a 40 LTU simulation of a single trajectory from the L63 model with $f = 1$ and ICs $(X, Y, Z) = (2.12, -0.72, 25.08)$.

in ρ rather than a specific instant in time. A cycle in ρ is equivalent to 1 LTU when $f = 1$ (see figure 3.12(i)). The time step used in the model simulations is $\tau = 0.001$ so extracting 10,000 ensemble states at each time step over an interval of 1 LTU means that the ensemble variable distributions consist of 10 million values $(10,000/0.001)$. The ensemble distributions are extracted for the last whole ρ cycle in the 40 LTU model simulation used to construct figure 3.12; from 39 to 40 LTUs. To produce equivalent variable distributions from a single trajectory, the model is run over 10,000 LTUs and states are extracted at each time step so the single trajectory plots also consist of 10 million values. The resulting single trajectory and IC ensemble distributions are shown in figure 3.15.

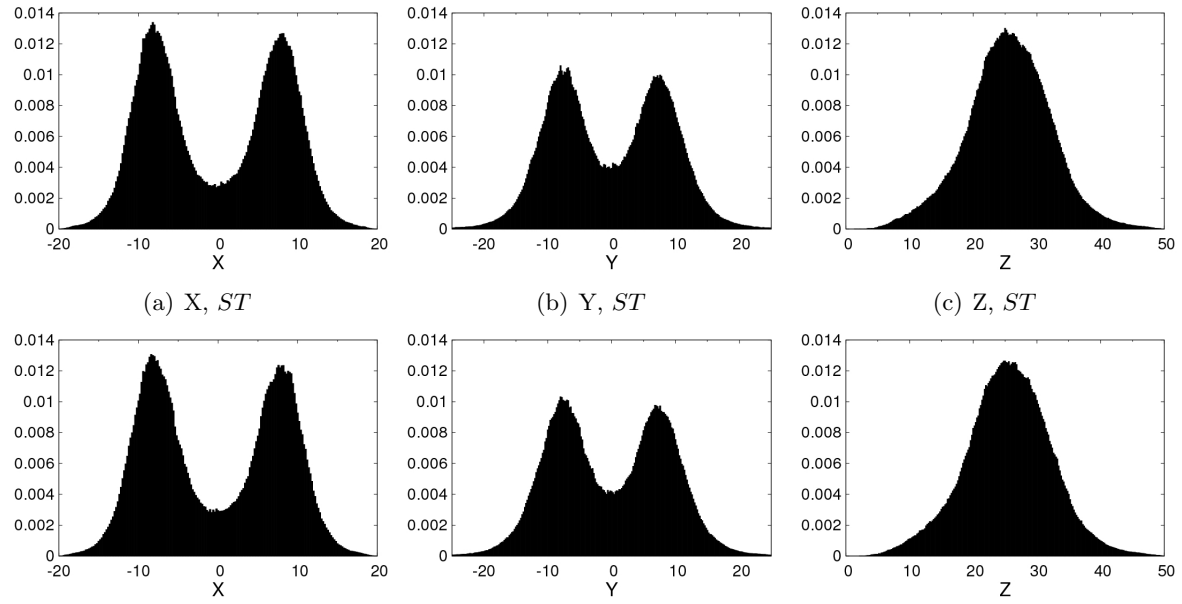

(a) X, ST (b) Y, ST (c) Z, ST

(d) X, Ens (e) Y, Ens (f) Z, Ens

Figure 3.15: Normalised frequency distributions for the L63 model when $f = 1$. Panels (a) to (c) correspond to single trajectory distributions (ST) for a 10,000 LTU model simulation and panels (d) to (f) correspond to IC ensemble distributions (Ens) extracted from all time steps in the last LTU of a 40 LTU model simulation (with ICs taken from the model states of the equilibrium climate distributions shown in figure 3.5). In each plot, the y-axis corresponds to the frequency of ensemble members per occupied bin; bin width = 0.2.

The distributions in figure 3.15 show that a single trajectory over 10,000 LTUs approximates the same model climate as a 10,000 member IC ensemble over 1 LTU. Therefore the introduction of a smooth (sinusoidal) time-varying parameter (ρ), which induces model resonance, does not mean that the ergodic assumption is invalid. The KS statistics which provide a quantitative comparison of the respective variable distributions are given in table 3.1. All values are very close to $D = 0$ indicating the strength of the similarities in the distributions. However, the value of D for the Z variable comparison is almost double the values of D deduced for X and Y. This is possibly attributable to the unimodal nature of the distribution in Z accentuating the differences in the high density areas towards the centre of the distribution. In the next section, the ergodic hypothesis is examined when the variations in ρ are no longer smooth in

time but are nonperiodic and non-repeating.

	X	Y	Z
D	2.72×10^{-03}	2.76×10^{-03}	5.24×10^{-03}

Table 3.1: KS comparison values between single trajectory distributions and IC ensemble distributions shown in figure 3.15.

3.7 Nonperiodic Fluctuations in ρ

3.7.1 Creating a nonperiodic time series in ρ

As described in section 3.5.2 the climate distributions do not vary considerably for fixed values of ρ between $\rho = 25$ and $\rho = 31$. When the model is subject to smooth fluctuations in ρ, as examined in section 3.6, the model displays very different behaviour. The climate distributions are highly sensitive to the frequency of the fluctuations in the parameter ρ and the model exhibits resonance at wave frequencies in phase with the orbiting time scale for model trajectories. Yet for smooth variations in ρ, the application of the ergodic assumption is valid, as shown in section 3.6.1.

In the climate system, there are multiple internal and external forcings which exert an influence on the dynamic evolution of the climate system. External factors which alter the radiative forcings on the climate system, such as solar variability, volcanic eruptions and anthropogenic emissions of GHGs, have differing degrees of periodicity. The cumulative effects of these individual components will likely lead to a highly aperiodic forcing time series on the climate system. In extending the analogy to the climate system, it therefore becomes interesting to consider how the L63 model behaves when subject to irregular fluctuations in ρ.

In order to investigate the impact of irregular fluctuations on the climate distributions of the L63 model, three sine waves of different frequencies are added together to create a nonperiodic time series $\psi(t)$, as shown in equation 3.17:

$$\psi(t) = A\Big(\frac{1}{3}\sin(2\pi)f_i t + \frac{1}{3}\sin(\sqrt{3})f_i t + \frac{1}{3}\sin(\sqrt{17})f_i t\Big) \tag{3.17}$$

$$\rho(t) = \rho_0 + \psi(t) \tag{3.18}$$

where A and t assume the definitions used in equation 3.16 and f_i is a controlling factor to simultaneously adjust the frequencies of the three component waves (with units LTU^{-1}). The three frequency multipliers are chosen as 2π, $\sqrt{3}$ and $\sqrt{17}$ so that the wave is both nonperiodic and also non-repeating on long time scale integrations, relative to the time scales being considered. $\psi(t)$ is added to ρ_0, which denotes the reference (mean) value of ρ, as shown in equation 3.18.

Figure 3.16 shows the time series of ρ over 20 LTUs, when $A = 3$ and $f_i = 1$. The time series is clearly aperiodic and the fluctuations, although entirely deterministic, appear random. The first of the three component sinusoid waves has a frequency exactly the same as the sine wave used in section 3.6 but the second and third component sine waves have slower frequencies ($\sqrt{3}$ and $\sqrt{17}$) which are approximately 3.6 and 1.5 times slower respectively. Therefore, the average wavelength of the combined wave is increased and the results for different values of f_i do not exactly correspond to different values of f explored in section 3.6.

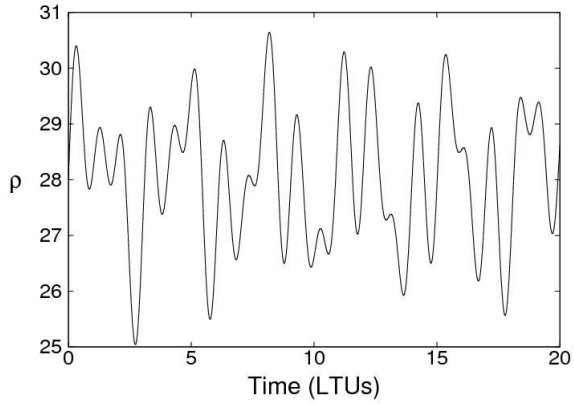

Figure 3.16: Time series of fluctuations in ρ over 20 LTUs; $A = 3$, $f_i = 1$ according to equation 3.18.

3.7.2 IC ensemble results

Model experiments are run over a 40 LTU simulation period with 10,000 member IC ensembles (ICs same as used in figure 3.12). The frequency distributions for each model variable for different values of f_i are given in figure 3.17. The plots are displayed using the same format as that used in figure 3.12. The time series' of ρ over the 40 LTUs of the model simulation, shown in the left column, demonstrate the irregular nature of the parameter fluctuations for different value of f_i because of the irregular nature of the parameter time series'. The corresponding frequency distribution plots illustrate the impact of the parameter fluctuations on the climate distributions of the L63 model for the three model variables after a 40 LTU simulation. It is important to note that the value of ρ is different after 40 LTUs for each different value of f_i. Therefore, in the comparison to the equilibrium climate distributions for $\rho = 28$, one would not expect the distributions to be exactly the same at the 40 LTU time instant; the larger the departure from $\rho = 28$, the greater the difference ought to be. Figure 3.17 doesn't include the distributions when $f_i = 0$ as they are identical to the equilibrium climate distributions given in figures 3.12(b) to 3.12(d).

The fluctuations in ρ clearly affects the climate distributions of the model when varying at intermediate frequencies. When the fluctuations are relatively slow, as demonstrated in figures 3.17(b) to 3.17(d) (where $f_i = 0.1$), the frequency distributions closely resemble the equilibrium climate distributions shown in figures 3.12(b) to 3.12(d). It is important to note that at 40 LTUs ρ approaches the reference value $\rho_0 = 28$ for $f_i = 0.1$. The distributions would be less similar to the fixed $\rho = 28$ climate distributions if observed after 28 LTUs where $\rho \approx 25$. Further analysis to quantify the differences between distributions over time is presented later in section 3.7.3 using the KS test. When the fluctuations are relatively fast, as shown in figures 3.17(v) to 3.17(x), the climate distributions remain largely unchanged. This result is consistent with the outcome observed for fast periodic fluctuations in ρ, shown in section 3.6, where the ρ perturbations are believed to act simply as noise about ρ_0. When the time scale of the parameter fluctuations approaches the orbiting time scale of the L63 model trajectories about the attractor lobes, the distributions become very different to the equilibrium distributions. The differences

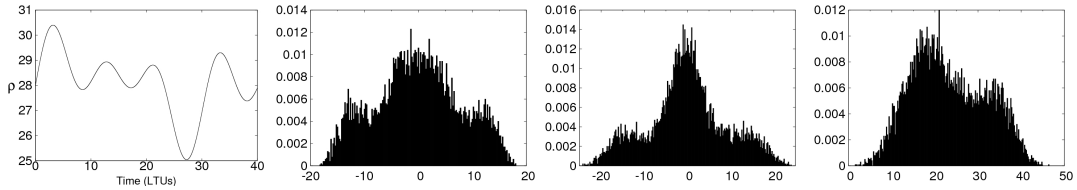

(a) $f_i = 0.1$, ρ (b) $f_i = 0.1$, X (c) $f_i = 0.1$, Y (d) $f_i = 0.1$, Z

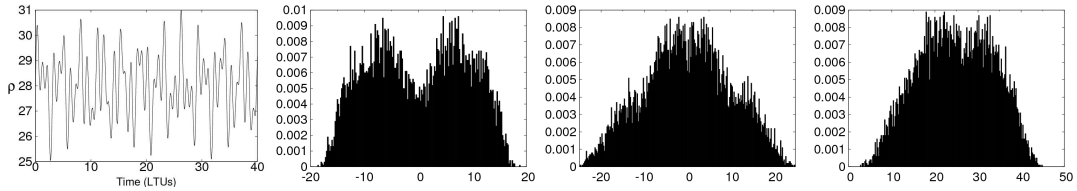

(e) $f_i = 1$, ρ (f) $f_i = 1$, X (g) $f_i = 1$, Y (h) $f_i = 1$, Z

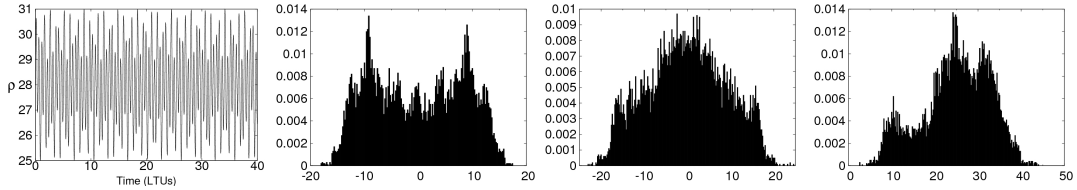

(i) $f_i = 3$, ρ (j) $f_i = 3$, X (k) $f_i = 3$, Y (l) $f_i = 3$, Z

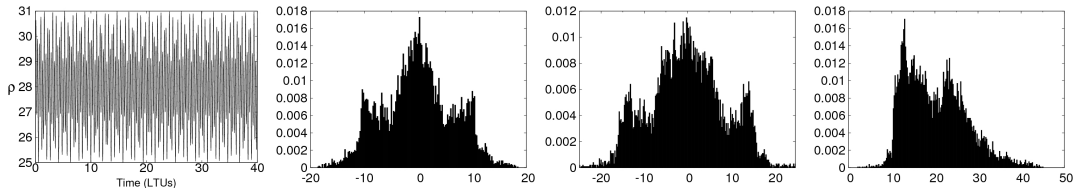

(m) $f_i = 5$, ρ (n) $f_i = 5$, X (o) $f_i = 5$, Y (p) $f_i = 5$, Z

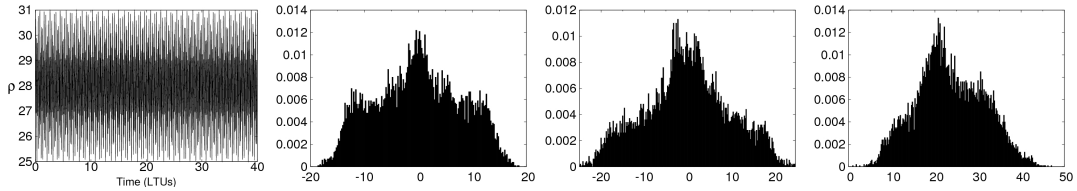

(q) $f_i = 10$, ρ (r) $f_i = 10$, X (s) $f_i = 10$, Y (t) $f_i = 10$, Z

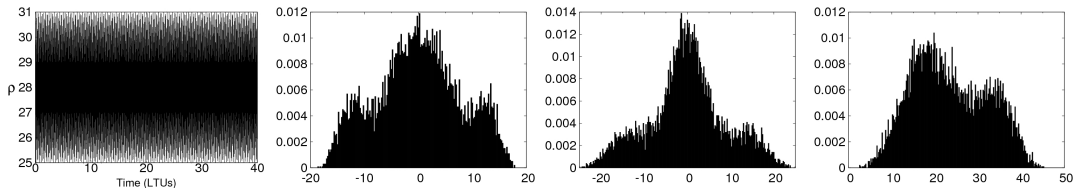

(u) $f_i = 30$, ρ (v) $f_i = 30$, X (w) $f_i = 30$, Y (x) $f_i = 30$, Z

Figure 3.17: Normalised frequency distributions for a 10,000 member IC ensemble after a 40 LTU model run for given values of f_i. ICs are taken from the first 10,000 members of the climate distributions shown in figure 3.5. The left column shows the time series' in ρ, the distributions for X, Y and Z are shown in the centre-left, centre-right and right columns respectively. In the L63 variable plots, the y-axis corresponds to the frequency of ensemble members per occupied bin; bin width = 0.2.

in the distributions are apparent in all variables when $f_i = 1, 3$ and 5. Also, unlike in the case where ρ varies periodically in time, the distributions at $f_i = 10$ are noticeably different from the equilibrium climate distributions shown in figures 3.12(b) to 3.12(d). This is caused by the addition of waves with slower frequencies described in section 3.7.1 which act to increase the overall wavelength of the fluctuations in ρ. Consequently, the effect of resonance is observed for higher values of f_i than f which controls the periodic variations in ρ.

3.7.3 KS comparison for nonperiodic variations in ρ

Following the same approach used in section 3.6, the temporal changes in the climate distributions for different values of f_i are determined using a KS comparison to the equilibrium climate distributions for $\rho = 28$. Crucially however, because the time series' in ρ are irregular, choosing to compare the IC ensemble frequency distributions to the equilibrium climate distributions at regular intervals ensures that comparisons occur at time instants when $\rho \neq 28$. Nonetheless, the comparison provides an interesting insight into the behaviour of the ensemble frequency (climate) distributions over time.

Figure 3.18 shows the time series' in the KS statistic (D) over the 40 LTU simulation period for the three model variables. The differences between the distributions are more significant in the Z variable than in the X and Y variable (note the different scale on the y-axis for the Z variable). This is likely to be caused by symmetry in the response of the climate distributions for X and Y which is not present in Z meaning that the shifts in the distribution densities can be accentuated in the Z dimension. For periodic fluctuations in ρ, the highest values of D are observed when $f = 1$ but in the experiments conducted in this section, the highest values of D occur at $f_i = 3$ and $f_i = 5$, consistent with the reasoning that the wavelengths of the nonperiodic fluctuating waves are longer so f and f_i are not exactly equivalent. The differences are also large when $f_i = 1$ and $f_i = 10$ because the distributions are affected by the interaction of waves with different frequencies. One of the most interesting features that emerges from figure 3.18, is the time series in D for the Z variable when $f_i = 0.1$. The time series illustrates that the climate distributions have a strong dependence on the value of ρ. The equivalent time series in ρ is given in figure 3.17(a) and the peaks in D correspond exactly to the peaks and troughs in ρ, with the greatest value of D occurring after 28 LTUs which corresponds to a minimum in the value of ρ.

It appears that resonance is once again a crucial factor in determining the climate distributions of the L63 model under nonperiodic fluctuating parameters. However, with a nonperiodic variation in ρ, it is unclear what the relative contributions of hysteresis and resonance are in the overall distortions to the climate distributions. The interaction of hysteresis and resonance on the L63 model climate distributions is certainly worthy of further investigation. The analysis presented in this thesis only partly addresses this intricate relationship. In the next section, analysis is focussed on exploring the impact of hysteresis in the L63 model. The results are related to the response of the climate system to the precise trajectory of the system forcings.

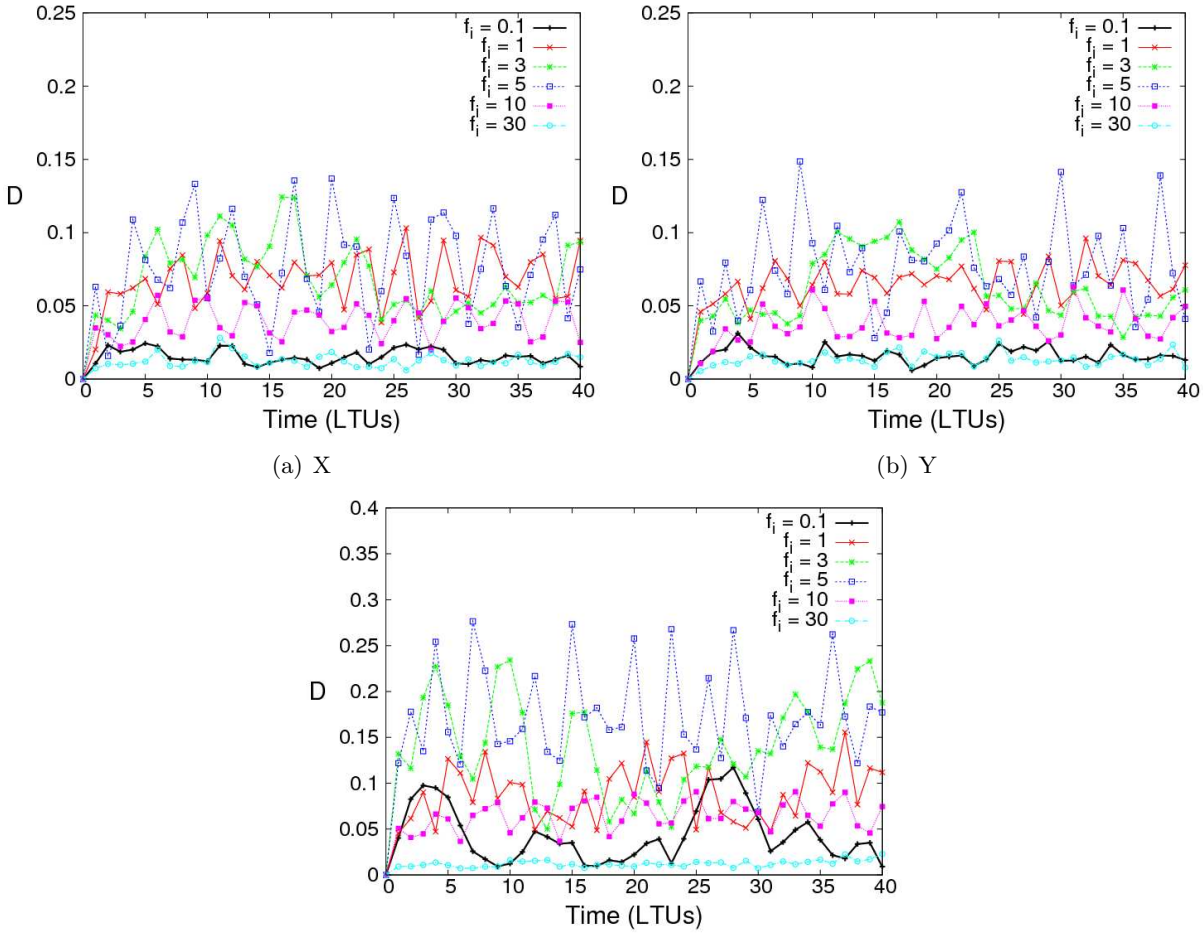

(a) X

(b) Y

(c) Z

Figure 3.18: KS results showing comparisons between the ensemble distributions when $f_i = 0$ (such that ρ is fixed at $\rho = 28$) and the ensemble distributions for other values of f_i for each of the L63 model variables subject to nonperiodic variations in ρ.

3.7.4 Hysteresis in the L63 model with nonperiodic fluctuations in ρ

To examine the extent to which the L63 model exhibits hysteresis (path dependence), the model climate distributions are extracted at time instants when the fluctuating parameter ρ returns to the reference value $\rho = \rho_0 = 28$. As the fluctuations in ρ used in this section are irregular, the instants at which $\rho = \rho_0$ are not evenly spaced throughout the time series'. Using the results of the model run when $f_i = 5$, figure 3.19 shows the distributions in X at specific time instants when $\rho = \rho_0$. Even though $\rho = 28$ at each time instant shown in figure 3.19, the corresponding IC ensemble distributions are clearly very different. In figure 3.19(a), there is a primary peak at the origin but there are defined secondary and tertiary peaks which are not observed in any of the other plots. Figures 3.19(b) and 3.19(d) are both unimodal about the origin but the density is constrained closer to the origin in figure 3.19(d). The distributions in figure 3.19(c) is more uniform across the model state space but there are two peaks located at $X \approx \pm 2$.

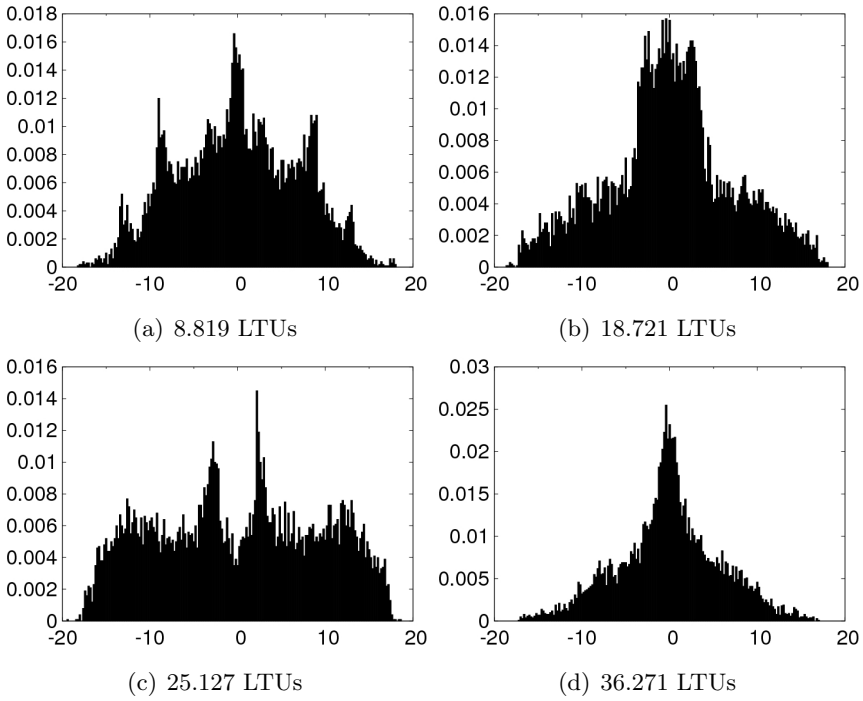

(a) 8.819 LTUs (b) 18.721 LTUs

(c) 25.127 LTUs (d) 36.271 LTUs

Figure 3.19: Normalised frequency distributions for a 10,000 member IC ensemble at given time instants when $f_i = 5$. In each plot, the x-axis corresponds to the X variable and the y-axis corresponds to the frequency per occupied bin; bin width = 0.2.

The differences in the distributions shown in figure 3.19 imply that the L63 model climate is not only sensitive to the frequency of fluctuations in ρ but also displays hysteresis; the climate distributions are a function of the pathway of ρ. A simple and elegant way to confirm the presence of hysteresis in the L63 model is to invert the time series in ρ when $f_i = 5$ and determine the climate distributions at exactly the same time instants as those illustrated in figure 3.19. If the corresponding distributions are different, then the differences must be attributed to the sensitive dependence of the model to the pathway in the parameter ρ. The time series for ρ in equation 3.18 is inverted (by multiplying $\psi(t)$ by (-1)) and the model ensemble simulation is repeated. Figure 3.20 shows the resulting distributions at the same time instants as those depicted in figure 3.19.

The distributions in figure 3.20 are entirely different to those shown in figure 3.19. Figures 3.20(b) and 3.20(d) no longer display unimodal peaks at the origin but rather show a high density of ensemble members towards the tails of the distributions. Figure 3.20(a) now appears similar to figure 3.19(c) whilst figure 3.20(c) appears similar to figure 3.19(a). The differences confirm the presence of hysteresis in the climate of the L63 model.

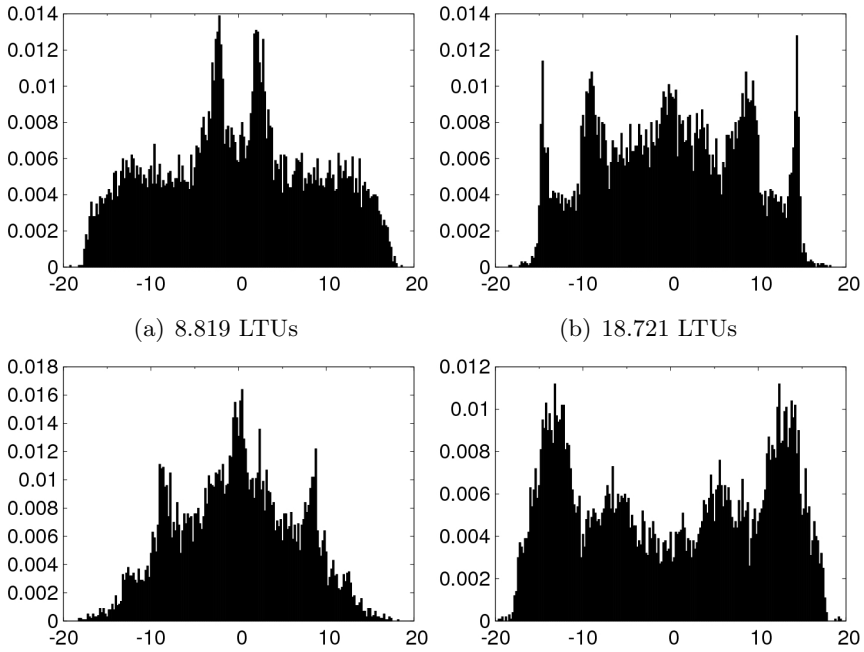

(a) 8.819 LTUs (b) 18.721 LTUs

(c) 25.127 LTUs (d) 36.271 LTUs

Figure 3.20: Normalised frequency distributions for a 10,000 member IC ensemble at given time instants when $f_i = 5$ and the time series in ρ is inverted. In each plot, the x-axis corresponds to the X variable and the y-axis corresponds to the frequency per occupied bin; bin width = 0.2.

Implications for ergodicity

The path-dependence of the IC ensemble distributions implies non-ergodic behaviour in this non-autonomous (time-dependent) version of the L63 model; the IC ensemble frequency distributions at an instant in time are different from the frequency distributions over a *long* time interval of a single model trajectory. To confirm this numerically the model configuration used to produce figure 3.19 is run for a single model realisation and the frequency distributions for time intervals centred on the time instants displayed in figure 3.19 are extracted. As the time step $\tau = 0.001$, after 10 LTUs a single trajectory will include 10,000 model states and the distribution of these states can be compared to the ensemble distributions shown in figure 3.19. For example, the first time interval centred on 8.819 LTUs includes the single trajectory states from 3.820 to 13.819 LTUs.

The initial state of the single trajectory is chosen to be the first member of the IC ensemble used to generate figure 3.19: $(X_0, Y_0, Z_0) = (0.62, -0.98, 21.93)$. Figure 3.21 shows four frequency distributions from the single trajectory, subject to nonperiodic fluctuations in ρ at the frequency $f_i = 5LTU^{-1}$, over 10 LTU intervals centred on the time instants considered in figure 3.19. The single trajectory distributions do not resemble the IC ensemble climate distributions at the time instants where $\rho = \rho_0$. The plots show that the ergodic hypothesis is therefore no longer valid for the L63 model when subject to nonperiodic time-dependent fluctuations in the parameter ρ, at least at frequencies which are sensitive to model resonance. Using longer intervals cannot

compensate for the differences as the ensemble distributions are time-dependent. The possibility of non-ergodic behaviour in the real climate system as a result of nonperiodic forcing variations has potentially profound implications for climate prediction given the way climate models are currently used to generate future projections. A more detailed discussion of the potential issues for climate prediction is given in section 3.9.

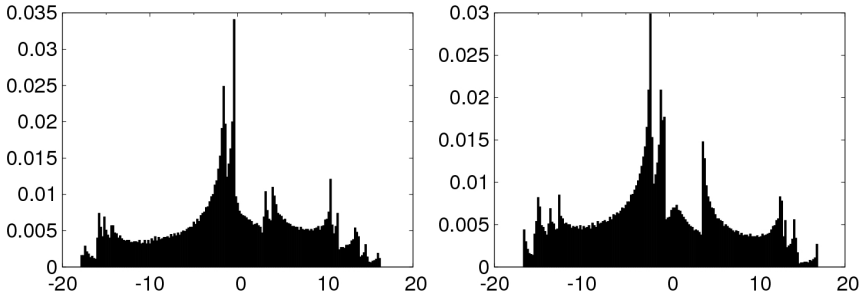

(a) 3.820 to 13.819 LTUs (b) 13.722 to 23.721 LTUs

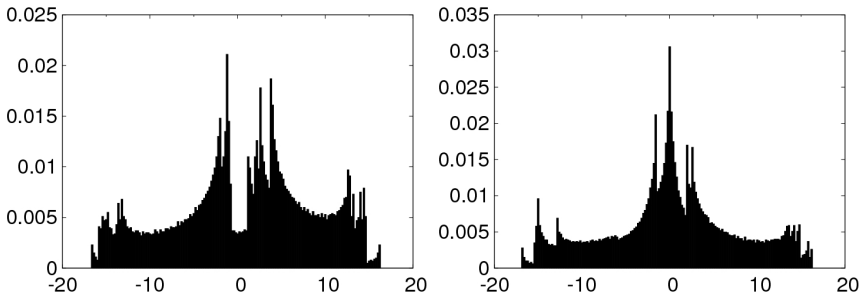

(c) 20.128 to 30.127 LTUs (d) 31.272 to 41.271 LTUs

Figure 3.21: Normalised frequency distributions for a single trajectory with ICs $(X_0, Y_0, Z_0) = (0.62, -0.98, 21.93)$, when $f_i = 5$ over 10 LTU intervals centred on: (a) $t = 8.819$ LTUs; (b) $t = 18.721$ LTUs; (c) $t = 25.127$ LTUs; (d) $t = 36.271$ LTUs. In each plot, the x-axis corresponds to the X variable and the y-axis corresponds to the frequency per occupied bin; bin width = 0.2.

3.7.5 Convergence of model ensembles for nonperiodic forcing in ρ

In section 3.4, it is shown that the IC ensemble location is not important in determining the equilibrium climate distributions for the L63 model with fixed parameters. Additionally, the memory of the model is investigated and shown to exist for a time period of up to approximately 40 LTUs in X and Y and 50 LTUs in Z. It is not obvious however, whether or not IC ensembles from different regions of model state space will converge when ρ is fluctuating periodically or non-periodically. Furthermore, if the ensembles do converge, the rate at which they do so may be different and/or a function of the initial IC ensemble location when subject to fluctuations in the parameter ρ.

The experiment conducted in the previous section, when $f_i = 5$, is used as the reference experiment in this section. Using the same four IC ensembles depicted in figure 3.9, the memory of the L63 model is investigated when subject to nonperiodic fluctuations in ρ. The KS test is

once again employed but rather than comparing the distributions from the four ensembles to the equilibrium climate distributions, they are compared to *reference* distributions (which are shown at specific time instants in figure 3.19) resulting from the integration of a 10,000 member IC ensemble, when $f_i = 5$. The IC ensemble has ICs extracted from the first 10,000 members of the 100,000 member equilibrium ensemble distributions illustrated in figure 3.5. The four IC ensemble distributions are compared to the reference distributions at specific time instants over a time period of 100 LTUs and the results are given in figure 3.22.

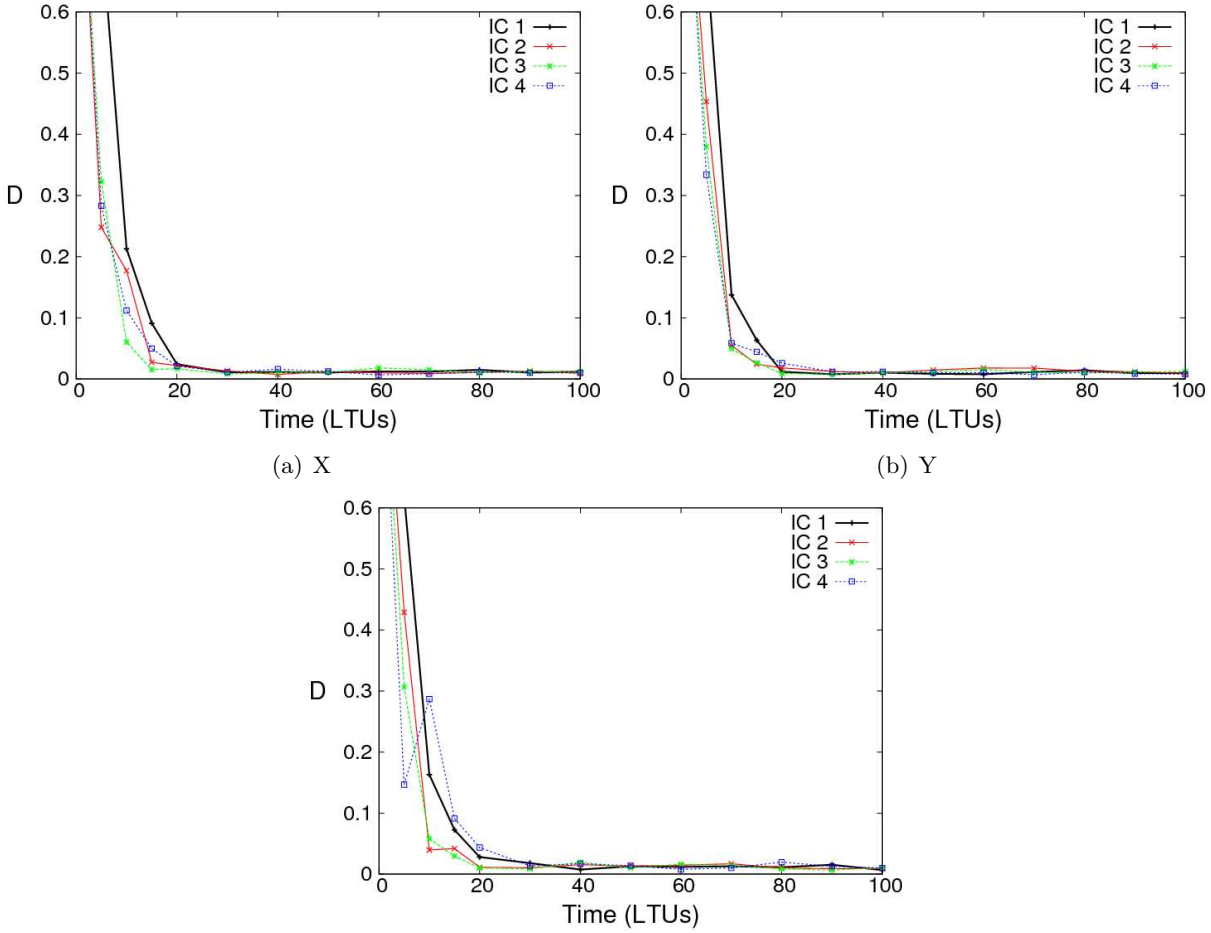

(a) X

(b) Y

(c) Z

Figure 3.22: KS results showing the comparisons between IC ensemble distributions, from IC locations shown in figure 3.9, to the distributions resulting from an IC ensemble, with ICs extracted from the first 10,000 members of the equilibrium climate distributions illustrated in figure 3.5, at given time instants. In all model runs, ρ varies according to equation 3.18 with a wave frequency, $f_i = 5LTU^{-1}$.

The KS results show that the ensembles converge to the same distributions, irrespective of the initial location for the IC ensemble. The IC uncertainty, encapsulated in the IC ensembles, does not appear to limit the long-term predictability of the climate distributions in the L63 model when subject to nonperiodic fluctuations in ρ. Moreover, the time scale for convergence is actually faster than that observed when ρ is constant (illustrated in figure 3.10). For constant

values of ρ, the ensembles retain memory of the ICs after 30 LTUs and even after 40 LTUs in the Z variable. With nonperiodic fluctuations in ρ, the ensembles show no evidence of retaining memory of ICs after 30 LTUs and after 20 LTUs the values of D are only higher than the converged minimum values for IC ensembles 1 and 4 (most evident in the Z variable). The ensembles therefore appear to converge between 20 and 30 LTUs, 20 LTUs faster than when ρ is constant. The interpretation of this result is necessarily speculative given only four IC ensembles but it appears that for the model version considered here, the introduction of a time-dependent parameter fluctuation causes trajectories to spread about the model state space more rapidly than for a fixed value of ρ. This could be due to the changing nature of the underlying model attractor enabling the ensemble members to diverge more rapidly.

There is also a discernible discrepancy between IC ensembles in the first 15 LTUs of the simulation period. In figure 3.22, ensemble *IC 1* appears to converge more slowly than the other ensembles. For the first 15 LTUs, D is much larger for ensemble *IC 1* than it is for the other IC ensembles in the X and Y dimensions. In the Z dimension, ensemble *IC 4* also converges more slowly than ensemble *IC 2* and *IC 3*. Without further experimentation, it is difficult to generalise about the discrepancy between different IC ensembles at the early stages of the model simulation period but the difference in the model memory for different IC ensembles appears to be non-negligible.

The impact of a *time-dependent modulating attractor* on the model climate distributions, and the associated memory of ICs, is of interest in the analogy to the climate system which is subject to time-varying forcings. In chapters four and five, the notion of a *time-dependent modulating attractor* is explored further and the terminology used to describe this concept is refined. For the L63 model, further research with alternative perturbations to the parameter ρ might illuminate the dynamic features which control the evolution of the model climate distributions. In the next section, the work is extended to explore the changes to the model climate distributions when subject to trends in ρ.

3.8 Trends in ρ

An important uncertainty in climate change predictions is how internal climate variability will be affected under altered climate forcings. Cox and Stephenson (2007) assert that the fractional proportion of the total uncertainty in the future climate state attributable to uncertainty in the initial state of the climate system decreases smoothly over time. The underlying assumption is that the internal variability of the climate system is not dependent on the system forcings implying that internal climate variability will be the same under any forcing scenario. However, palaeoclimate evidence suggests that the internal variability of the climate system changes under altered forcing conditions (Overpeck and Webb (2000)). Using the L63 model to further extend the experiments conducted in this chapter, this section focuses on the internal variability of the model when subject to different trends in ρ, considered analogous to a climate forcing. The discussion relates the findings to the system *memory* (traceability of IC uncertainty). Understanding the relationship between internal climate variability, the forcing scenario and the memory of the system's ICs in a nonlinear system becomes highly relevant in guiding the design of climate model experiments to inform predictions relevant on adaptation time scales.

The experiments conducted in previous sections have focussed on the memory of the model for fixed, periodic and nonperiodic fluctuations in the forcing parameter ρ in the absence of any trends. The results show the impacts of fluctuations in ρ on the internal *climate* variability in the L63 model under fixed mean parameter conditions. The convergence of IC ensembles from different locations on the model attractor is shown to occur on a time scale of 40 to 50 LTUs for fixed values of ρ (section 3.4) and 20 to 30 LTUs for nonperiodic fluctuations in ρ (section 3.7.5). The extent to which IC ensembles from different initial locations on the L63 model attractor converge when subject to trends in the model parameters has not yet been considered. By introducing trends in the parameter ρ, the impact of transient parameter changes on the climate distributions of the L63 model is investigated.

3.8.1 L63 attractor for alternative values of ρ

In this section, the behaviour of the L63 model is investigated for a doubled value of ρ ($\rho = 56$) and a halved value of ρ ($\rho = 14$). As observed in section 3.5.2, increasing the parameter ρ leads to an increase in the ranges of the climate distributions for all model variables. Figure 3.23 shows the L63 attractor for a single model simulation when $\rho = 28$ (as in figure 3.1) and $\rho = 56$. Doubling the parameter ρ results in a shift of the attractor to increased values of Z and greater variability in the X and Y dimensions. The attractor retains a symmetry about the origin in the X and Y dimensions preserving the two-lobed structure. When ρ is decreased, the range of behaviour in all three dimensions decreases. For values of $\rho < \rho_H$ (associated with a Hopf bifurcation), the model is no longer chaotic over an infinite time scale. The regime structure of the L63 attractor is no longer observed and all trajectories propagate towards the model fixed points at $C^{\pm}$.

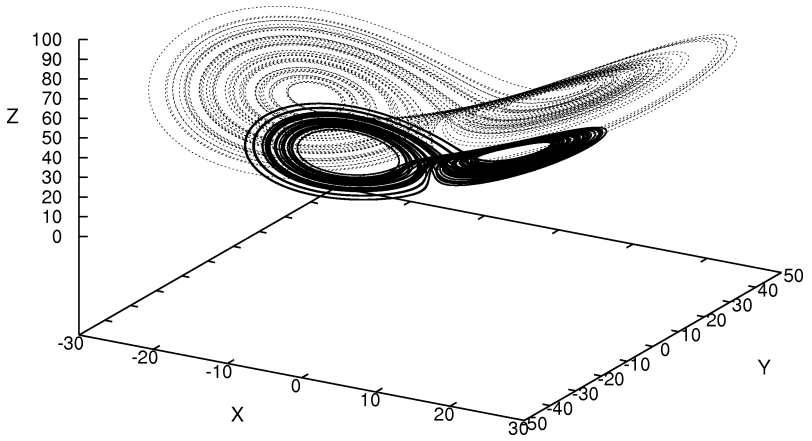

Figure 3.23: Single trajectory for a 50 LTU simulation of the L63 model with ICs $(X, Y, Z) = (1.0, 1.0, 25.0)$: $\rho = 28$ shown in solid line and $\rho = 56$ shown in dashed line.

Using the same approach adopted to determine the climate of the L63 model when $\rho = 28$, a 10,000 member IC ensemble is run (using ICs extracted from the first 10,000 members of the equilibrium climate distributions illustrated in figure 3.5) over a period of 1,000 LTUs for doubled and halved values of ρ. The final distribution of states for each variable are shown for $\rho = 56$ in figures 3.24(a) to 3.24(c) and for $\rho = 14$ in figures 3.24(d) to 3.24(f). When $\rho = 56$ the ensemble distributions appear unimodal and the secondary peaks found in the climate distributions when $\rho = 28$ are no longer apparent. The ranges in each dimension are increased, consistent with the attractor illustrated in figure 3.23. When $\rho = 14$ the ensemble distributions reveal that all trajectories have transitioned to the model fixed points located at $C^{\pm}$. In the X and Y distributions (figures 3.24(d) and 3.24(e)), the ensemble members are evenly split between the two fixed points. In fact, there are slightly more members located at C^{+} than C^{-} which highlights the sensitivity of the ensemble distributions to choice of ICs. In the Z dimension, all members are found at the fixed point located at $Z = 13$ $(\rho - 1)$.

3.8.2 System memory for fixed ρ

The IC ensemble distributions in figure 3.24 are used to represent the climate distributions of the L63 model when $\rho = 56$ and $\rho = 14$. The memory of the model is investigated for each value of ρ using the same four IC ensembles utilised in section 3.4 (displayed in figure 3.9). The four IC ensembles are run over a 200 LTU simulation period for the L63 model when $\rho = 56$ and $\rho = 14$. The KS test is used to compare the four ensemble distributions to the climate distributions at regular intervals: every 5 LTUs for the first 20 LTUs and every 10 LTUs for the remainder of the simulation period. The KS results for all three variables in each experiment are shown in figure 3.25.

Figures 3.25(a) to 3.25(c) show the KS comparisons when $\rho = 56$. The IC ensembles appear to converge to the model climate distributions over time but the convergence is slower than that observed in section 3.4 when $\rho = 28$. The memory of the model is therefore observed to

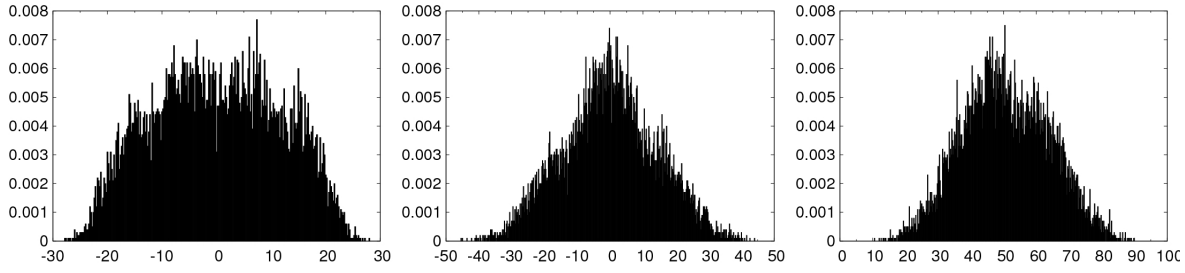

(a) X, $\rho = 56$ (b) Y, $\rho = 56$ (c) Z, $\rho = 56$

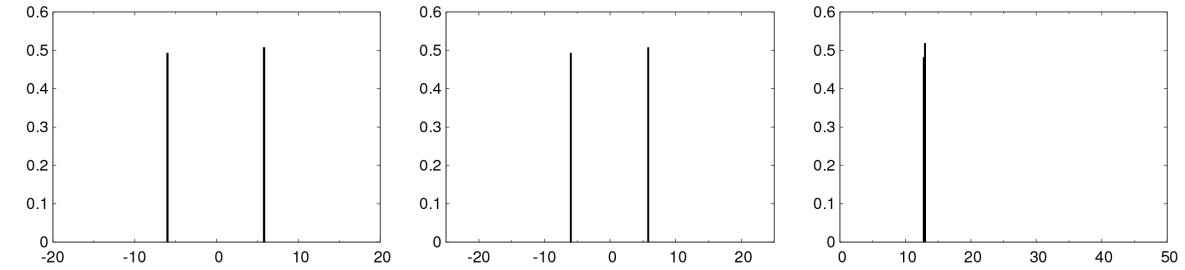

(d) X, $\rho = 14$ (e) Y, $\rho = 14$ (f) Z, $\rho = 14$

Figure 3.24: Normalised frequency distributions for the three L63 model variables when $\rho = 56$ (panels (a) to (c)) and when $\rho = 14$ (panels (d) to (f)), from a 10,000 member IC ensemble with ICs extracted from the first 10,000 members of the equilibrium climate distributions illustrated in figure 3.5. The distributions show the states of each ensemble member after a 1,000 LTU simulation period. In each plot, the x-axis is given by the panel title and the y-axis corresponds to the frequency of ensemble members per occupied bin; bin width = 0.2.

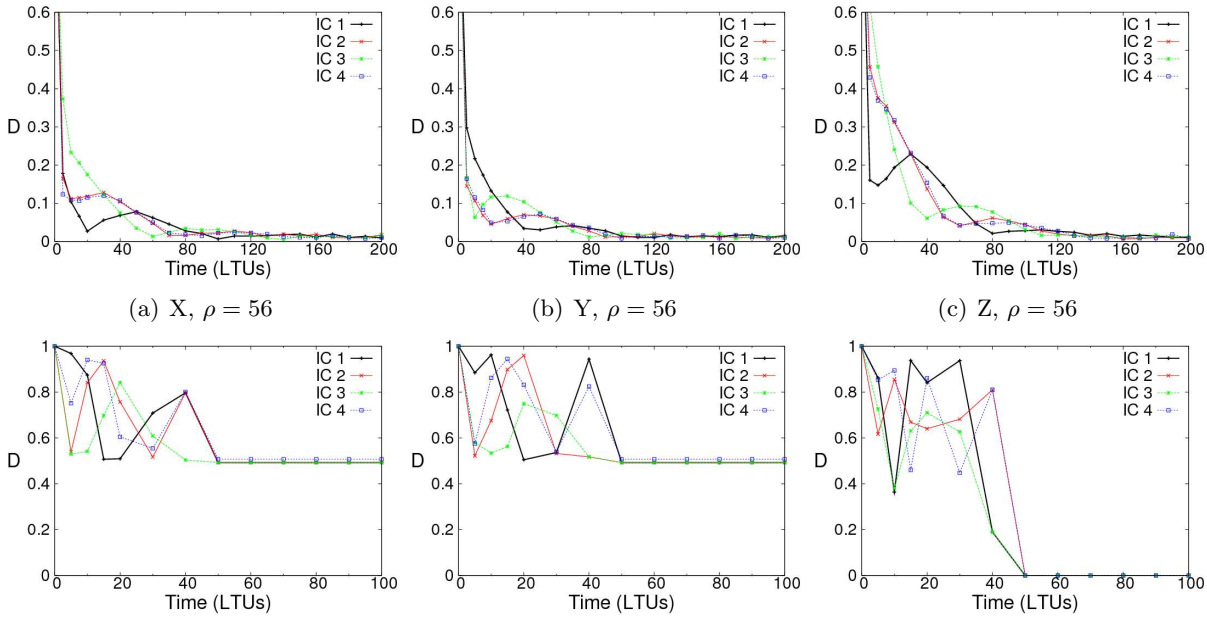

(a) X, $\rho = 56$ (b) Y, $\rho = 56$ (c) Z, $\rho = 56$

(d) X, $\rho = 14$ (e) Y, $\rho = 14$ (f) Z, $\rho = 14$

Figure 3.25: KS comparisons over time between the four different IC ensembles introduced in section 3.4 and the ensemble climate distributions given in figure 3.24, for each model variable, at given values of ρ.

increase when ρ is doubled. This is likely to occur because the range of state space occupied by the attractor at $\rho = 56$ is considerably larger than the range at $\rho = 28$ and therefore more time is required before trajectories can fully explore the attractor state space. There are some differences in the KS comparisons for each ensemble but the convergence times are fairly similar for all ensembles, occurring on a time scale of $t \approx 100$ LTUs. The convergence in the Z dimension is slower than in the X and Y dimensions and this is believed to be due to the asymmetry in the Z climate distribution as Z occupies only positive values. Ensembles 2 and 4 (labelled *IC 2* and *IC 4*) converge at broadly the same rate in all variables but this result is not observed when $\rho = 28$ indicating that convergence between individual ensembles is not consistent for different values of ρ.

Figures 3.25(d) to 3.25(f) reveal that the four IC ensembles fail to converge to the climate distributions in the X and Y dimensions when $\rho = 14$. Ensembles 1, 2 and 3 (labelled *IC 1*, *IC 2* and *IC 3*) converge to a minimum of $D = 0.49$ and ensemble 4 converges to $D = 0.51$. The memory of the ICs is therefore permanent as trajectories are unable to spread across the attractor state space before evolving to the fixed points. The ensembles converge in the Z dimension because there is only one fixed point in Z to which all trajectories evolve. All of the trajectories from the ensembles 1, 2 and 3 move to the fixed point at C^+ whilst the trajectories from ensemble 4 move to the fixed point at C^-. The plots reveal that memory of the individual ensembles is evident for 40 LTUs in each dimension before all ensemble members evolve to either of the two fixed points. This time scale is similar to that observed when $\rho = 28$.

3.8.3 System memory for increasing ρ

In this section and the next section, the memory of the model is investigated when subject to linear trends in ρ. Trends in ρ are introduced to examine the rates of convergence of ensembles originating in different locations of the model state space according to equation 3.19:

$$\rho(t) = \rho_0 + (\rho_f - \rho_0)\lambda^{-1}t \tag{3.19}$$

where ρ_0 is the initial value, ρ_f is the final value, t denotes time (LTU) and λ^{-1} is the gradient of the trend (LTU^{-1}). In the following experiments, when $\rho(t) = \rho_f$ the trend is stopped and ρ remains at ρ_f for the remainder of the simulation.

Initially, trends to the doubled value of ρ are investigated. The parameter values are therefore set to $\rho_0 = 28$ and $\rho_f = 56$. Three different gradients are explored to determine whether or not convergence of IC ensembles is a function of the trend/pathway of the parameter (forcing) in the L63 model. Figure 3.26 shows the different time-series' in ρ over a 100 LTU simulation period for positive trends with different values of λ.

The four IC ensembles introduced in section 3.4 and used in section 3.8.2 are utilised again in this section. The four ensembles are run with three different trends in ρ, shown in figure 3.26, and are compared to the evolution of a 10,000 member IC ensemble (with ICs extracted from

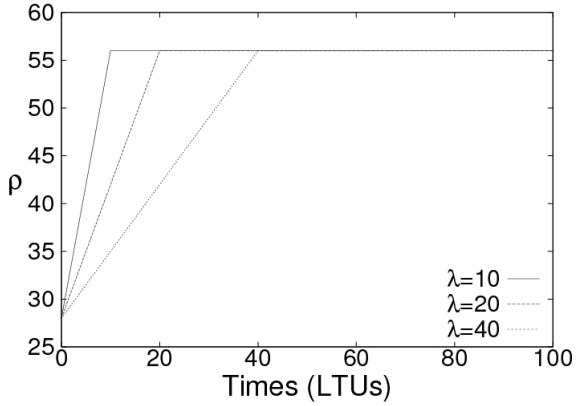

Figure 3.26: Time series' in ρ for different positive trends from $\rho_0 = 28$ to $\rho_f = 56$.

the first 10,000 members of the equilibrium climate distributions illustrated in figure 3.5) using the KS test at specific instants in the model simulations. The reference ensemble also evolves according to the time series' in ρ shown in figure 3.26. The KS comparisons for each variable and each trend in ρ are given in figure 3.27 for 200 LTU simulation periods.

The results in figure 3.27 show that the four IC ensembles from different locations on the initial attractor converge to the reference ensemble with ICs spread across the initial attractor. The results differ in detail for each of the four ensembles but there is no clear evidence that any of the ensembles converge more quickly than the others for all three variables under each trend in ρ. The key result from this experiment is that when the trend in ρ is more rapid, the convergence between the ensembles is slower. When $\lambda = 10$, the value of ρ increases from $\rho_0 = 28$ to $\rho_f = 56$ over a 10 LTU period and memory of the ICs is evident for at least 100 LTUs in the X and Y dimensions and possibly up to 150 LTUs in the Z dimension, as the value of D have still not converged towards a minimum. When $\lambda = 40$, the value of ρ increases from $\rho_0 = 28$ to $\rho_f = 56$ over 40 LTUs and memory of the ICs is evident for about 50 to 60 LTUs in the X and Y dimensions and 100 LTUs in the Z dimension. The attractor becomes larger in each dimension for higher values of ρ and the geometric properties of the attractor change more quickly when the trend in ρ has a high gradient (for low values of λ). Consequently, ensemble trajectories take longer to explore the attractor state space and converge towards the same distributions when the value of ρ increases rapidly.

In the analogy to climate prediction, the results suggest that it is worth considering the time scales at which uncertainty in the ICs is lost. In the L63 model, it has been shown that memory is dependent on the pathway of the parameter change; the more rapid the increase in ρ (to a new value ρ_f), the longer the memory in the model. The result implies that the memory of IC uncertainty in nonlinear systems might be forcing scenario dependent. It would be worth investigating this result to see if it is observed in more complex climate models.

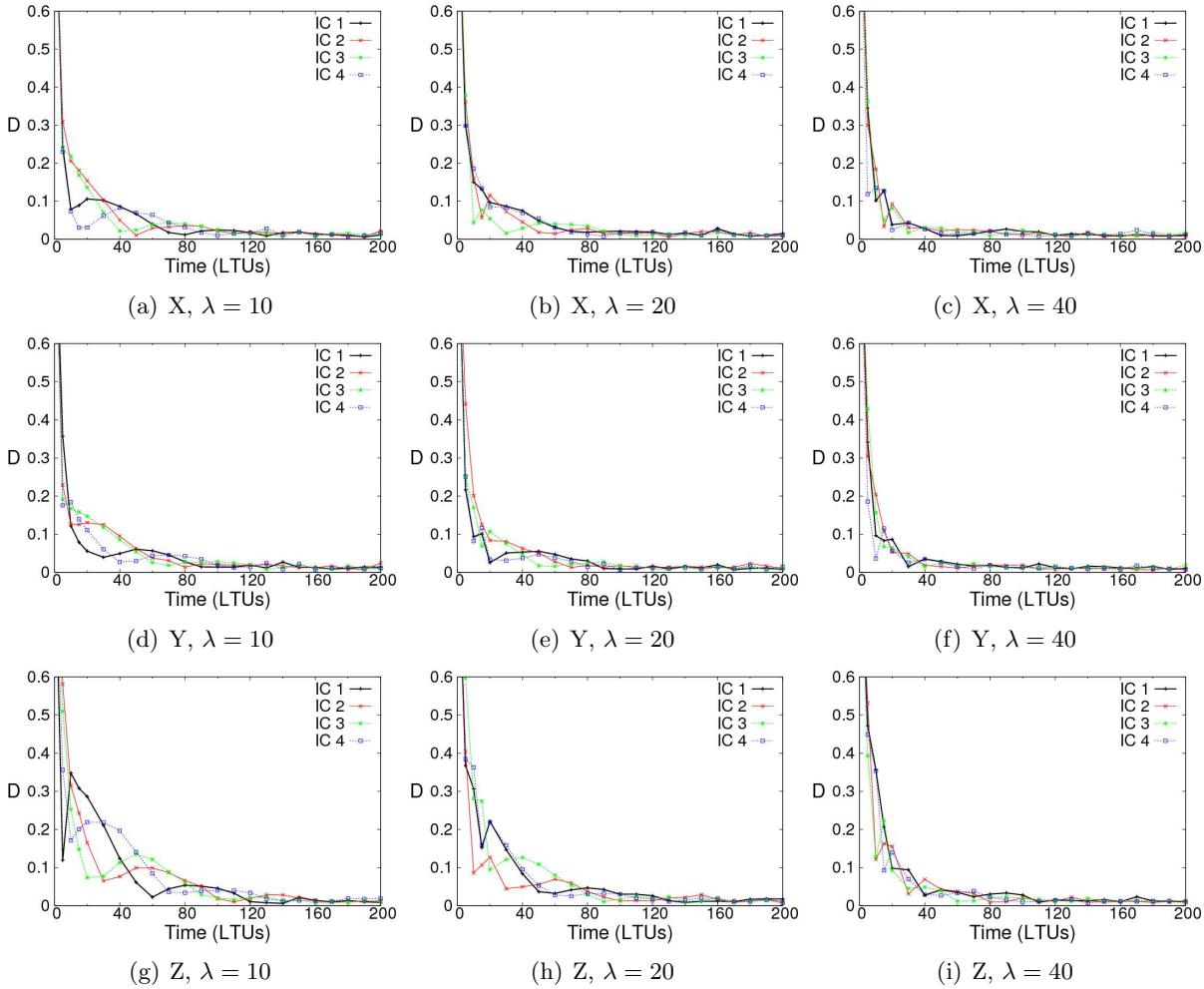

(a) X, $\lambda = 10$ (b) X, $\lambda = 20$ (c) X, $\lambda = 40$

(d) Y, $\lambda = 10$ (e) Y, $\lambda = 20$ (f) Y, $\lambda = 40$

(g) Z, $\lambda = 10$ (h) Z, $\lambda = 20$ (i) Z, $\lambda = 40$

Figure 3.27: KS comparisons over time between the four different IC ensembles introduced in section 3.4 and the IC ensemble with ICs extracted from the first 10,000 members of the equilibrium climate distributions illustrated in figure 3.5, for each model variable at given values of λ.

3.8.4 System memory for decreasing ρ

In the experiments conducted using the L63 model, the model simulations have been confined to chaotic regions of parameter space where the model is known to display transitive behaviour. In this section, the model is exposed to regions of parameter space that lead to non-chaotic behaviour. The same approach used in section 3.8.3 is adopted here for decreasing trends in ρ. The parameter values are set to $\rho_0 = 28$ and $\rho_f = 14$. Three negative gradients are explored to determine whether or not the convergence is a function of the trend/pathway in the parameter (forcing) when the model is moved into non-chaotic regions of parameter space. Figure 3.26 shows the different time-series' in ρ over a 100 LTU simulation period for negative trends with different values of λ.

The same four IC ensembles used throughout the analysis in this section are used once again and run with the three decreasing trends in ρ shown in figure 3.28. The distributions are compared

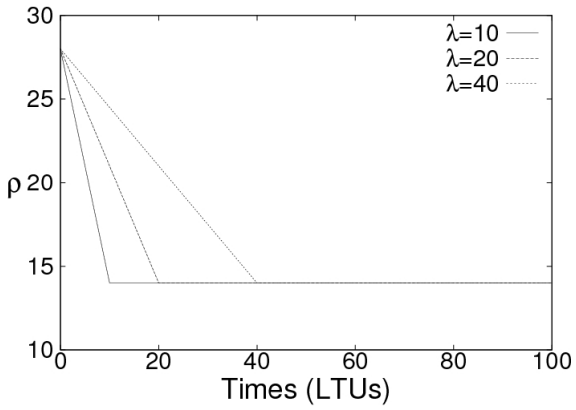

Figure 3.28: Time series' in ρ for different negative trends from $\rho_0 = 28$ to $\rho_f = 14$.

to the distributions resulting from the reference ensemble (used in the previous section), using the KS test. Figure 3.29 shows the KS results for negative trends in ρ. The KS comparisons reveal that the convergence between the four ensembles (with ICs from different locations on the initial attractor) to the reference ensemble (with ICs spread across the attractor) is dependent on the gradient of the trend. When $\lambda = -40$, convergence is observed in all variables. The decrease in the value of ρ is sufficiently slow to allow ensemble members to diverge across the attractor state space before they move to one of the fixed points ($C^{\pm}$) consistent with $\rho = 14$. When $\lambda = -20$, the ensembles converge in the Z dimension but only partially converge in the X and Y dimensions. At this rate of change in ρ, the ensemble trajectories are able to partially diverge but the resulting distributions of members between the two model fixed points are biased and therefore retain memory of the ICs. When $\lambda = -10$, the ensembles once again converge in the Z dimension but the convergence is slower than that observed when $\lambda = -20$ and $\lambda = -40$. In the X and Y dimensions, three of the ensembles converge to values of $D = 0.51$ whilst ensemble 4 converges to a value of $D = 0.05$. The result suggests that only ensemble members contained within ensemble 4 are able to diverge across the attractor state space before being attracted to one of the model's fixed points. This result is significant as it shows that not only is the trend in ρ important for the rate of convergence but also that when the model moves from a transitive region of parameter space to an intransitive region of parameter space, the exploration of the states consistent with the parameter conditions is dependent on the initial location of the IC ensemble.

The experimental results presented in this section are extended in the following chapter using a model which can be considered a closer analogy to the climate system. In chapter four, the dynamic behaviour of the Lorenz-84 model is investigated to elucidate the issue of moving between transitive and intransitive regions of parameter space which contain co-existing attractors.

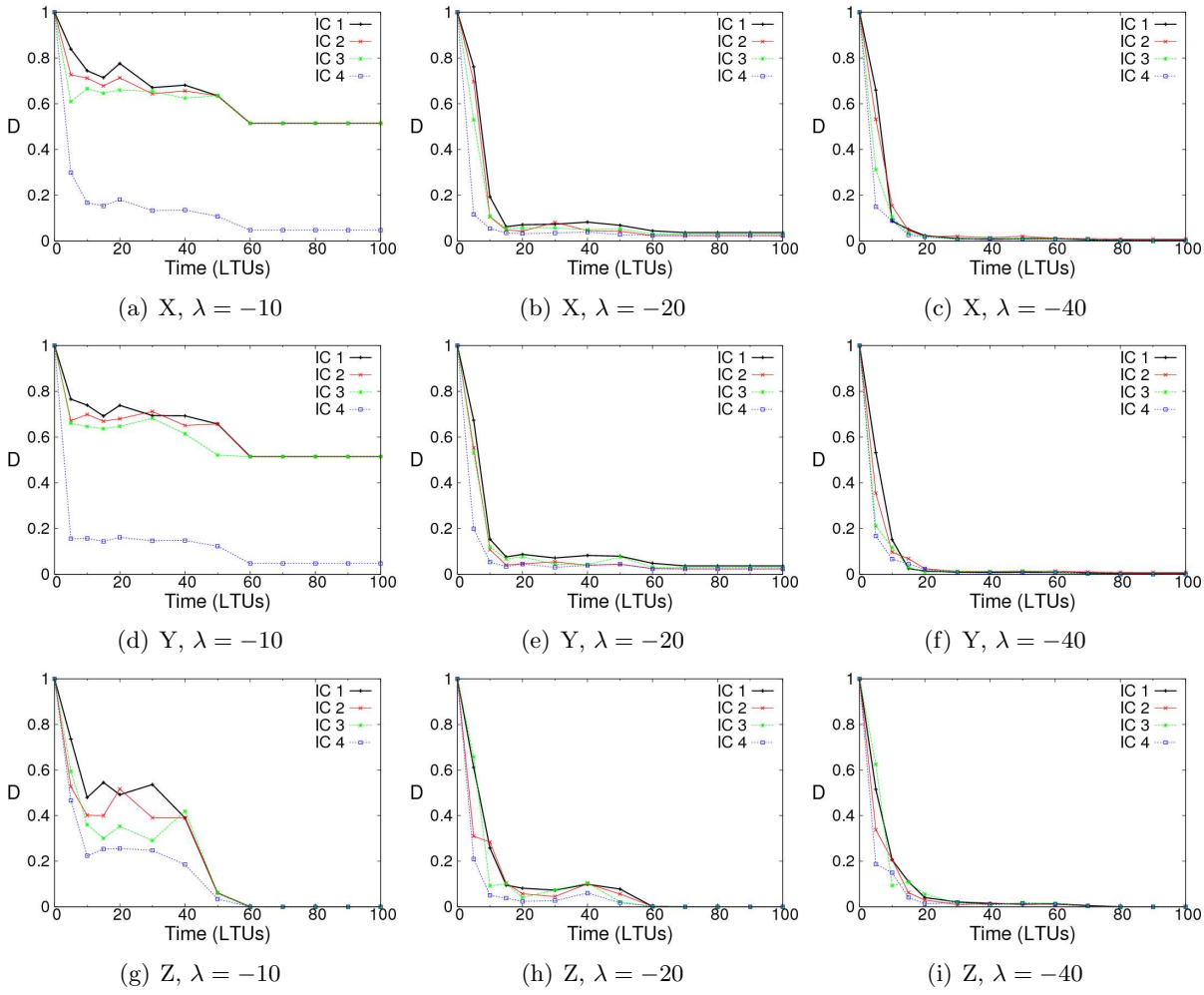

(a) X, $\lambda = -10$ (b) X, $\lambda = -20$ (c) X, $\lambda = -40$

(d) Y, $\lambda = -10$ (e) Y, $\lambda = -20$ (f) Y, $\lambda = -40$

(g) Z, $\lambda = -10$ (h) Z, $\lambda = -20$ (i) Z, $\lambda = -40$

Figure 3.29: KS comparisons over time between the four different IC ensembles introduced in section 3.4 and the IC ensemble with ICs extracted from the first 10,000 members of the equilibrium climate distributions illustrated in figure 3.5, for each model variable at given values of λ.

3.9 Discussion of L63 Results

3.9.1 Conceptual understanding of the climate system

Results from experiments conducted on simple models, such as the L63 model, are inevitably limited in their relevance to higher dimensional systems. Consequently, one cannot expect the results described in this chapter to generalise to higher-order climate models, let alone the real climate system. However, in exploring the rich dynamics of the L63 model, a better conceptual understanding of variability and change in complex nonlinear systems, such as the climate system, can emerge to inform the way climate model experiments are designed and to guide the interpretation of the output from complex climate models.

The motivation for the experiments conducted on the L63 model is to understand potential areas of uncertainty that may be poorly explored using conventional climate modelling methodologies. The emphasis is strongly on the implications of IC uncertainty and its impacts on system memory. In the following chapters, this theme continues to be addressed and the results of further experiments are described to illustrate potential limitations of existing climate model experimental designs.

In addressing the needs of the adaptation community, it is essential that *climate* and *climate change* are appropriately defined by the climate modelling community. The results presented in this chapter suggest that a statistical description of climate under climate change, which relies on the ergodic assumption, is insufficient to account for the potential effects of nonlinearities in the system's dynamics. In section 3.3.1, it is argued that the climate of the L63 model can be expressed as the distribution of possible system states consistent with the system's attractor. However, when the L63 model is subject to nonperiodic fluctuations in ρ, as shown in section 3.7, the ensemble distributions are observed to continuously change in accordance with the changing nature of the model's attractor. Both resonance and hysteresis effects are shown to be active factors in determining the climate model ensemble distributions. In refining the definition of climate to be suitable for climate change adaptation applications, climate ought to be defined as some future distribution of states consistent with the system's forcings, conditioned on the uncertainty in the initial state.

In section 3.7.4 the ergodic assumption is shown to fail when the model is subject to the nonperiodic parameter fluctuations. Whilst the model remains transitive, such that all possible model states can eventually be visited, the impact of varying the parameter ρ means that frequency distributions associated with a single trajectory do not represent the IC ensemble distributions at any instant in time. The results therefore show that for the non-autonomous L63 model, transitivity does not always imply ergodicity. If similar behaviour were to be observed in more complex climate models then the output of climate statistics based on single model realisations would be flawed.

The final section analysed the behaviour of the model when subject to trends in ρ. The results

show that when the parameter values change, the dynamic behaviour of the model changes. The convergence time of IC ensembles from different locations on an attractor is slower when the parameter ρ increases and in the analogy to climate it might be the case that the memory of ICs becomes extended when the system's forcings are altered. Furthermore, experiments with the L63 model reveal that IC memory is permanent when moving from a chaotic region of parameter space to a non-chaotic region. Understanding the changes in dynamic behaviour of the climate system is therefore important in determining the relevance of different sources of prediction uncertainty.

3.9.2 Implications of resonance for climate model predictions

Resonant behaviour has previously been explored in the analysis of dynamical systems and is more commonly referred to as *stochastic* resonance for systems which undergo resonant-type behaviour as a function of the noise level (Gammaitoni et al. (1998)). The phenomena has been observed in the L63 model and related to the predictability of dynamic systems (Benzi et al. (1981), Crisanti et al. (1994), Sutera (1980)). Furthermore, the L63 model has been studied to understand the impact of stochastic resonance from variations in climate forcings on climatic change (Benzi et al. (1982), Tobias and Weiss (2000)). However, these studies have not explicitly acknowledged the potential effects of resonance on ensemble climate distributions. More recently, in relation to the potential of stochastic resonance to cause transitions between climatic regimes, Benzi (2010) stressed that fast variables should not be ignored in the study of long-term climate change.

The connection between the potential existence of resonant-type behaviour in the climate system and the way climate model experiments are designed to explore uncertainty is rarely made by scientists within the climate modelling community. Part of the reason for this may be attributable to the time scales on which the phenomena are deemed to be relevant. The focus of previous studies has predominantly been on the transitions between climate regimes on palaeoclimate time scales, which may be deemed largely irrelevant for decadal and multi-decadal climate predictions. However, in linking the design of climate model experiments to the information needs of decision makers, the potential of resonance to alter the shape of climate variable distributions ought to be evaluated. As argued by Stainforth et al. (2007a), and explored further in chapter 6, decisions regarding climate change adaptation are more often sensitive to the tails of climate distributions rather than shifts in the mean. Therefore, if there is a chance that the distribution of climate may be sensitive to resonance, at relevant spatial or temporal scales, then such a phenomenon ought to be accounted for in the exploration of uncertainty in climate model experiments. Furthermore, it is also important to distinguish between the impact of resonance and hysteresis on the climate. Even in the absence of any resonance effects, hysteresis can affect the climate distributions and such a possibility must also be recognised in the design of climate model experiments.

Given the results described in this chapter, particularly those illustrated in sections 3.6 and 3.7,

it seems appropriate to hypothesize that if there is a mode of internal variability within the climate system that operates on a similar time scale to planetary scale forcings which impact the climate system, then the distribution of climate for certain variables at particular spatial scales may be highly sensitive to the phase and pathway of such forcings. Unfortunately, it is not possible to test such a hypothesis using the observational record, as there is only one observed trajectory for the evolution of the atmosphere-ocean system.

From a nonlinear dynamics perspective, the occurrence of erratic behaviour in the climate distributions of the L63 model, associated with temporal fluctuations in the parameter ρ, may indicate that the use of the term "attractor" is no longer suitable in the analysis of the system's behaviour. In dynamical systems research, other terms such as "stochastic", "pullback" and "random" have been used as a prefixes for the word attractor to extend the applicability of the term attractor into a non-autonomous context (Chekroun et al. (2010a), Chekroun et al. (2010b)). However, as a conceptual tool, the term attractor may still be valuable in understanding the implications of uncertain ICs and uncertain forcing scenarios on the ultimate evolution of the climate system.

3.9.3 Implications for climate model experimental design

Because of computational limitations, climate model simulations are rarely run with more than a handful of IC members. Therefore, when utilising climate model information to inform impacts models, the ergodic assumption is pervasive. The ergodic assumption has been shown to be invalid for the L63 model when subject to nonperiodic fluctuations in the parameter ρ, as outlined in section 3.7, and when ρ is forced into the non-chaotic region of parameter space, as shown in section 3.8. Therefore accurate estimates of the climate (as defined in section 3.3.1) of the L63 model cannot be achieved by single model realisations for certain parameter conditions. In making the case for considering large IC ensembles in climate model predictions, if the climate system exhibits hysteresis, then the absence of ergodicity suggests that the use of large IC ensembles is necessary to estimate the plausible distribution of climate states consistent with a particular climate forcing scenario.

In the transitive, chaotic regions of parameter space in the L63 model, convergence of IC ensembles is observed irrespective of the response to fluctuations in ρ. In extending the experiments conducted with L63 model to the Imperfect Model Scenario (IMS), any differences observed between IC ensemble distributions, after a period sufficient for convergence to occur, must be attributed to model error. By comparing the IC ensemble distributions which arise in the IMS to the IC ensemble distributions in the PMS, an estimate of the model discrepancy could be achieved. Such work would be a natural extension from the work presented in this chapter. For an ensemble of different models, assuming they are sufficiently independent from one another, comparisons between IC ensemble distributions from each model (under the same forcing scenario) at a given point in time and space could provide a valuable measure of model diversity and inform assessments of model reliability. Comparing single trajectory results only

could not distinguish between errors caused by model inadequacy from anomalous features induced by internal climate variability.

In section 3.4, memory of ensemble IC location is shown to exist for a time scale of approximately 20 to 40 LTUs. However, the time scales in the L63 model are not directly comparable to those in the climate system so it is not possible to make any direct assertions regarding the time scale at which memory of ICs is lost in the climate system. However, understanding the time scale at which the initial state of the system is traceable will have important implications for decadal and longer time scale climate predictions. Using GCMs in a research mode to better estimate this time scale, by comparing the convergence rates of large IC model ensembles, is therefore potentially valuable in constraining the uncertainty in future climate projections. However, the climate system consists of many sub-systems operating on disparate time scales (e.g. ice sheets, oceans) which may blur any distinct time scale for memory of the initial state. In chapter five, the L84 model is coupled to the S61 model in order to address the issue of competing dynamic time scales.

Chapter 4

The L84 Model

4.1 From Lorenz-63 to Lorenz-84

Results from the experiments conducted with the L63 model offered insight into the potential value of IC ensemble based experiments to explore uncertainty in the behaviour of the climate system. It was argued that sufficiently accounting for IC uncertainty not only benefits short- to medium-term weather forecasting but might also aid long time scale climate change prediction. The results highlighted the possible impacts of forcing variations on the climate system and the associated climate distributions. Going beyond the L63 model experiments, the primary aim of the work presented in this chapter is to gain additional insight by analysing the behaviour of a nonlinear chaotic system which can be more directly related to the climate system.

The Lorenz-84 (hereafter L84) model was described by Edward Lorenz as "the simplest possible model capable of representing an unmodified or modified Hadley circulation" (Lorenz (1984)). The model has subsequently been used by many researchers to make inferences about the behaviour of the climate system (e.g. Van Veen et al. (2001), Broer et al. (2002), Freire et al. (2008), Broer and Vitolo (2008)). Here, the model is examined to further understand how sensitive the climate of a nonlinear dynamic system is to changes in the system's forcing parameters. The experiments outlined in this chapter have been designed to determine the extent to which the predictability of the model's climate distributions is a function of the model's initial state. The ultimate goal of performing experiments with the L84 model is to develop hypotheses to inform the design of experiments to be conducted on more complex climate models.

In the L63 model, for $\rho > \rho_H$, the model displays *transitive* behaviour[1]. One of the primary reasons for performing additional experiments with the L84 model is that, at certain parameter values, the model contains coexisting attractors which display *intransitive* behaviour[1] (Lorenz (1984), Freire et al. (2008)). The conceptual challenge of understanding what constitutes climate and climate change in a system which displays intransitivity is examined using the L84 model.

[1]Definitions provided in the glossary.

It is demonstrated that the definition of climate in a system with coexisting attractors is not trivial and therefore interpreting climate under climate change is as much a communication problem as it is a simulation problem.

Adopting the methodology used for analysing the L63 model, this chapter first illustrates the climate of the L84 model for fixed parameter values. The plots focus on the distributions in the X variable, though the results for the Y and Z variables are qualitatively consistent and appear in Appendix B where relevant. In section 4.2, the attractor of the L84 model is illustrated for both chaotic and non-chaotic regions of parameter space. Section 4.3 displays the climate distributions resulting from single model trajectories and IC ensembles. This section begins with a visual analysis of the model climates followed by a quantitative analysis exploring the ergodic hypothesis. A seasonal cycle in one of the key parameters, F (the equator-to-pole temperature difference) is then introduced in section 4.4 and the impacts on the model climate distributions are presented. Maintaining the seasonal variations in F, in section 4.5 trends are imposed on F to further the analogy to modelling climate change. In section 4.6, the implications of the model results are discussed in relation to the design of experiments on more complex climate models.

4.2 The L84 System

4.2.1 The L84 model

Consistent with the approach used in chapter three, in the analysis of the L84 system the PMS is adopted so that the L84 model is equivalent to the L84 system. The model, used in this chapter to draw analogies to the climate system, is a simplified representation of the quasi-geostrophic equations and is defined by the three ODEs:

$$\frac{dX}{dt} = -Y^2 - Z^2 - aX + aF \tag{4.1}$$

$$\frac{dY}{dt} = XY - bXZ - Y + G \tag{4.2}$$

$$\frac{dZ}{dt} = bXY + XZ - Z \tag{4.3}$$

where X denotes the strength of the large-scale westerly wind current, assumed to be in equilibrium with the poleward temperature gradient, and Y and Z are the strength of cosine and sine phases of a chain of superposed waves transporting heat polewards. The term b represents the displacement of the waves due to interaction with the westerly wind and the term a is a coefficient which, if less than 1, allows the westerly wind current to damp less rapidly than the waves. F and G are thermal forcings: F represents the cross-latitude heating contrast (equator-to-pole temperature difference) and G accounts for the heating contrast between oceans and continents. A time unit in the L84 model is considered in relation to the damping time of the waves, which Lorenz equated to 5 days in the atmosphere (Lorenz (1984)). The time step used in Lorenz' original paper is $\tau = \frac{1}{30}$, equivalent to 4 hours, but for the following experiments a smaller time step, $\tau = 0.01$ (equivalent to 1.2 hours), is chosen with a common fourth order Runge-Kutta (RK) integration scheme as applied in chapter 3. The sensitivity of the model climate to the time step is investigated in section 4.3.2.

Lorenz (1990) imposed a seasonal variation in the parameter F to demonstrate that chaos and/or irregular dynamic behaviour can lead to interannual variability, manifest in the "random" onset of alternative periodic summer circulations. Adapting the seasonal variations introduced by Lorenz (1990), the impact of IC uncertainty is investigated in relation to the ergodicity of the L84 model and the memory of the system's climate distributions in the PMS. The following analysis examines the behaviour of the L84 model in what Lorenz termed "winter" and "summer" parameter conditions. Initially the idealised cases of permanent winter and permanent summer are investigated. In section 4.4, a seasonal cycle in F is introduced and the impact on the model's climate distributions is explored.

4.2.2 L84 in winter

In L84 winter, $F = 8$ and the other parameters are given their conventional values: $a = \frac{1}{4}$, $b = 4$ and $G = 1$. Figure 4.1 shows the three-dimensional evolution of a single trajectory orbiting the L84 attractor for permanent winter conditions over a period of 1 year. Figure 4.2 shows the same model run illustrated in two dimensions for the X-Y, X-Z and Y-Z planes. At first the trajectory orbits the primary 'lobe' (or regime) of the attractor, where $X > 0$, and subsequently spirals out away from the origin; the spiralling is most evident in the Y-Z plane shown in figure 4.2(c). The majority of the time the flow is westerly ($X > 0$) but occasionally the trajectory moves across to the secondary 'lobe', where $X < 0$. Physically, the transition to negative values of X represents a shift from westerly to easterly circulation. In the winter configuration the system is chaotic so small differences in the initial model states ultimately lead to large differences in the timing of transitions for individual model trajectories.

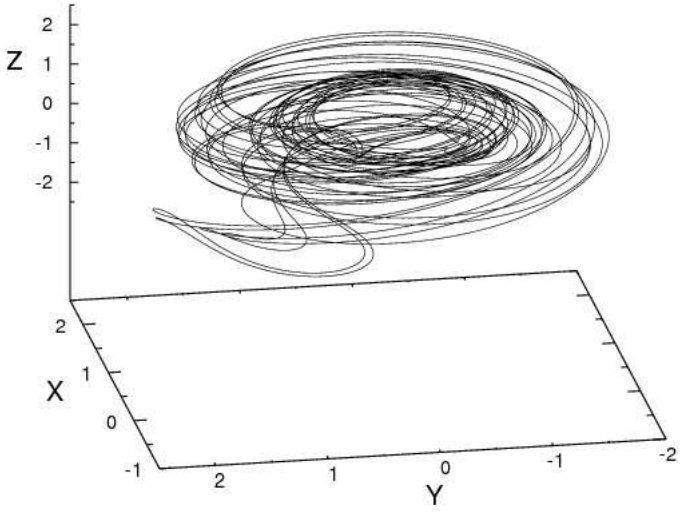

Figure 4.1: The L84 model attractor when $F = 8$ illustrated using a single trajectory over a simulation period of 1 year with ICs: $(X, Y, Z) = (1.0, 1.0, 1.0)$.

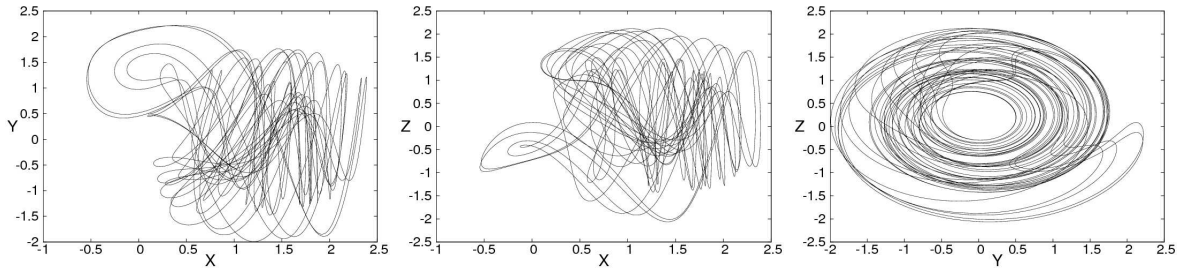

(a) X-Y Plane (b) X-Z Plane (c) Y-Z Plane

Figure 4.2: The L84 model attractor in the X-Y, X-Z and Y-Z planes when $F = 8$, illustrated using a single trajectory over a simulation period of 1 year with ICs: $(X, Y, Z) = (1.0, 1.0, 1.0)$.

4.2.3 L84 in summer

In the atmosphere, the meridional temperature difference between the pole and the equator is decreased during the summer months as the pole heats up, due to increased solar insolation, while the heating of the equator remains largely constant throughout the year. Lorenz (1990) encapsulates this change in the L84 model by suggesting a value of $F = 6$ for the summer configuration while keeping the other parameters constant. It is worth noting that one could decrease or even change the sign of G during the summer months where the land-sea temperature contrast is typically reversed. However, Lorenz (1990) keeps G constant and focuses his analysis on altered values of F only. In order to be consistent with the Lorenz (1990) study, the value of G is left unchanged in the following analysis.

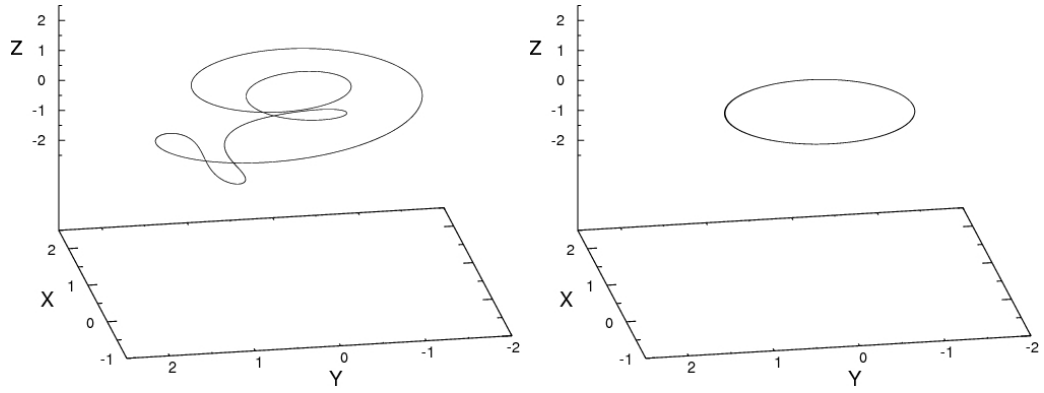

(a) IC 1 (b) IC 2

Figure 4.3: The L84 model attractor when $F = 6$, illustrated using a single model realisation over a simulation period of 1 year with ICs: (a) $(X, Y, Z) = (0.12, 0.95, -0.26)$ and (b) $(X, Y, Z) = (0.93, -1.04, 0.58)$.

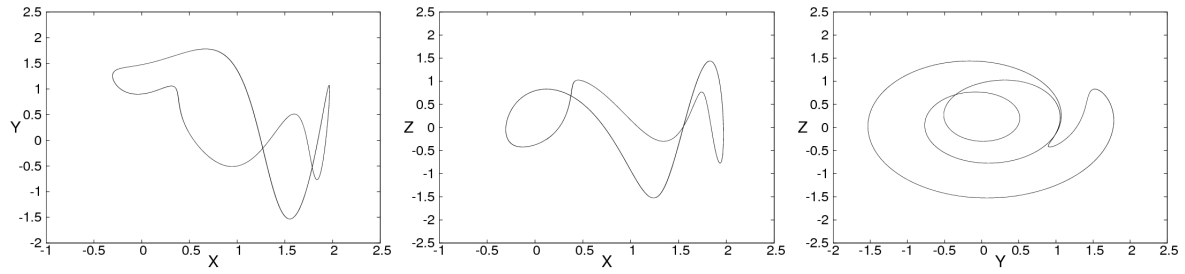

(a) X-Y Plane, IC 1 (b) X-Z Plane, IC 1 (c) Y-Z Plane, IC 1

Figure 4.4: The L84 model attractor in the X-Y, X-Z and Y-Z planes when $F = 6$, illustrated using a single model realisation over a simulation period of 1 year with ICs: $(X, Y, Z) = (0.12, 0.95, -0.26)$.

Figures 4.3(a) and 4.3(b) show the evolution of two single model trajectories orbiting the L84 attractor with summer parameter values ($F = 6$) from two different initial states: *IC 1* $(0.12, 0.95, -0.26)$ and *IC 2* $(0.93, -1.04, 0.58)$. The two initial states were specifically chosen to depict the two coexisting attractors, referred to as $A1$ for figure 4.3(a) and $A2$ for figure

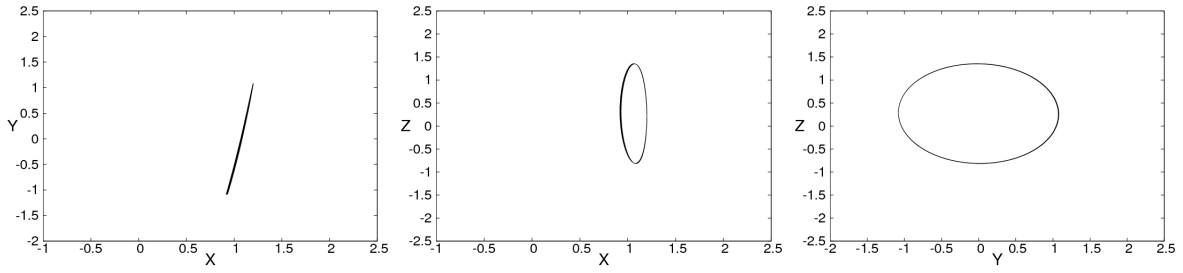

(a) X-Y Plane, IC 2 (b) X-Z Plane, IC 2 (c) Y-Z Plane, IC 2

Figure 4.5: The L84 model attractor in the X-Y, X-Z and Y-Z planes when $F = 6$, illustrated using a single model realisation over a simulation period of 1 year with ICs: $(X, Y, Z) = (0.93, -1.04, 0.58)$.

4.3(b). In both examples the attractors no longer exhibit chaotic behaviour but rather display periodicity. Attractor $A1$ (associated with *IC 1*) is shown in three dimensions in figure 4.3(a) and in two dimensions in figures 4.4(a) to 4.4(c). The plots reveal that the attractor occupies similar ranges in each model variable to those observed when $F = 8$. The attractor is composed of predominantly westerly winds which spiral away from the origin with a regular transition to easterly flow.

The alternative attractor $A2$ (associated with *IC 2*), shown in three dimensions in figure 4.3(b) and in two dimensions in figures 4.5(a) to 4.5(c), reveals a much simpler geometric shape; an ellipse which is almost parallel to the Y-Z plane. The strength of the westerly winds are constrained to values between $0.9 < X < 1.2$ and the periodicity is highly regular.

The coexistence of two attractors for the same parameter values indicates sensitivity of the attractor itself to the initial model state; not to be confused with chaotic sensitivity to the initial state when $F = 8$. As stated by Lorenz (1990), the attractors in the summer configuration display intransitive behaviour where the climates, once established, will persist forever. The presence of intransitivity and coexisting attractors has implications when considering the predictability of the climate from an uncertain initial state. Clearly IC uncertainty is a primary concern when predicting the evolution of any dynamical system which does not have a unique attractor.

A basin of attraction can be defined as the set of ICs in the model/system state space for which trajectories evolve towards a certain attractor (Aguirre et al. (2003)). To illustrate the nature of the basins of attraction in the summer configuration of the L84 model, a large IC ensemble is run and the attractors to which the model trajectories evolve over time are identified for each ensemble member. The plot in figure 4.6 shows the results of a 1,000,000 member ensemble run (1,000 by 1,000 grid resolution), for an array of ICs spread evenly from $(-1.0, -2.5, 0)$ to $(2.5, 2.5, 0)$, after a 20 year model simulation (a lower resolution version is provided in the Lorenz (1990) study). The results show the basins of attraction in the X-Y plane, where $Z = 0$.

Figure 4.6 shows that for the IC ensemble selected, the majority of ensemble members propagate

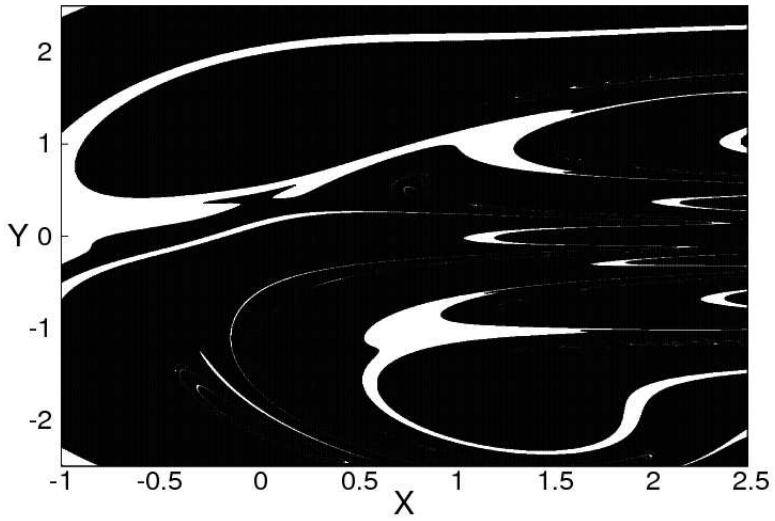

Figure 4.6: The basins of attraction in the X-Y plane where $Z = 0$ for ICs in the L84 model when $F = 6$. The black area denotes the basin of attraction for $A1$ and the white area the basin of attraction for $A2$. The image resolution is 1,000 by 1,000 points equivalent to 1 mega-pixel.

towards $A1$. The regions of model state space in which ICs propagate towards the alternative attractor $A2$ are relatively narrow and meander within the basin of attraction for $A1$. The boundaries between the basins of attraction are smooth and the separations appear distinct. However the limited resolution may obscure regions of model state space which are more intricate on finer resolutions. The overall image reveals a complicated terrain with fine structure and narrow separation between basin's of attraction in certain regions of the model state space where the attractor to which a trajectory propagates is highly sensitive to the precision of the initial model state.

It is suggested in the paper by Freire et al. (2008) that for certain parameter values the basins of attraction for the L84 model display evidence of the "Wada" property. The existence of such a property means that the attractor to which a model trajectory evolves is not only highly sensitive to the initial state but that, when there exist at least three basins, an individual basin's boundary belongs simultaneously to the boundary of the other two (or more) basins (Aguirre et al. (2003)). In permanent summer, when $F = 6$, only two attractors have been found to coexist so the Wada property cannot exist. However, a seasonal cycle is introduced in section 4.4 and the model becomes exposed to regions of parameter space that exhibit the Wada property. The implications of the exposure of model trajectories to such regions are discussed further in section 4.6.

4.3 L84 Climates

4.3.1 Single trajectory results

Adopting the same approach as that applied to the analysis of the L63 model, the climate of the L84 model is first investigated by running a single model realisation and determining the time scale over which the frequency distributions converge. The model is initialised at the three different states used to generate the figures in section 4.2 and each model realisation is integrated for a period of 100 years. The frequency distributions for the X variable of the model trajectories are given in figures 4.7 to 4.9 (Y and Z variable distributions given in figures B-1 to B-6 in Appendix B). The bin width used to generate the frequency distribution plots in this chapter is 0.01, unless stated otherwise. Each single trajectory distribution consists of every model state through which the trajectory passes during the simulation period. For longer simulation periods, the number of points included in the frequency distributions therefore increases.

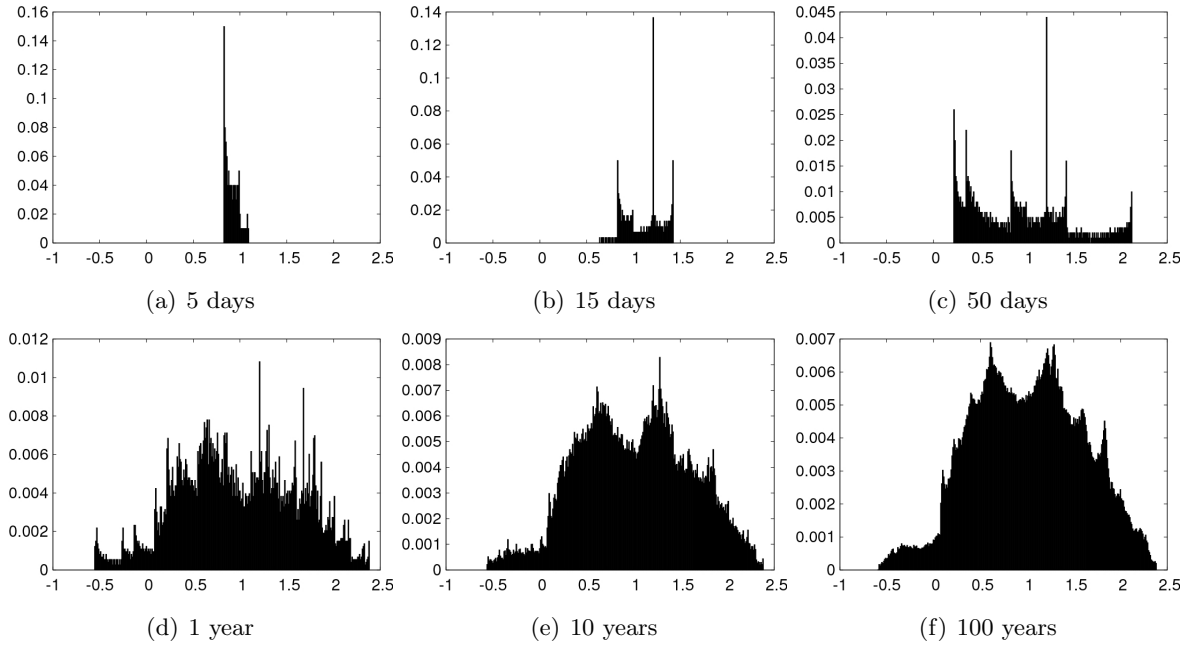

(a) 5 days (b) 15 days (c) 50 days

(d) 1 year (e) 10 years (f) 100 years

Figure 4.7: Normalised frequency distributions of the X variable for a single trajectory in the L84 model when $F = 8$ after given simulation periods, with ICs: $(X, Y, Z) = (1.0, 1.0, 1.0)$. In each plot, the x-axis denotes the X variable and the y-axis corresponds to the frequency per occupied bin; bin width = 0.01. Y and Z variable distributions given in Appendix B: figures B-1 and B-2.

The plots in figure 4.7 show the normalised frequency distributions when $F = 8$ (permanent winter conditions) for simulation periods of 5 days up to 100 years. The results show that a number of orbits are required before the range of the attractor is fully explored. Even after 50 days, the negative X (easterly) regime is not visited for the model trajectory shown. In figures 4.7(d) to 4.7(f), the majority of the distribution's density is in the positive X (westerly) regime. The 10 and 100 year distributions reveal two peaks at approximately $X = 0.6$ and $X = 1.3$ and

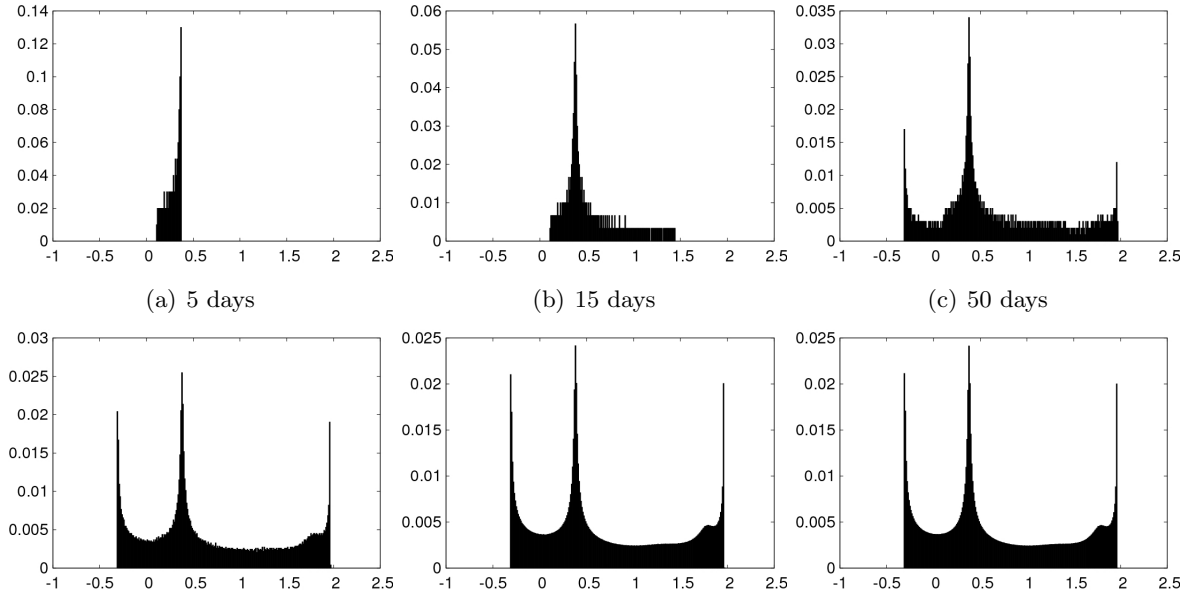

(a) 5 days (b) 15 days (c) 50 days

(d) 1 year (e) 10 years (f) 100 years

Figure 4.8: Normalised frequency distributions of the X variable for a single trajectory in the L84 model when $F = 6$ after given simulation periods, for *IC 1*: $(0.12, 0.95, -0.26)$. In each plot, the x-axis denotes the X variable and the y-axis corresponds to the frequency per occupied bin; bin width = 0.01. Y and Z variable distributions given in Appendix B: figures B-3 and B-4.

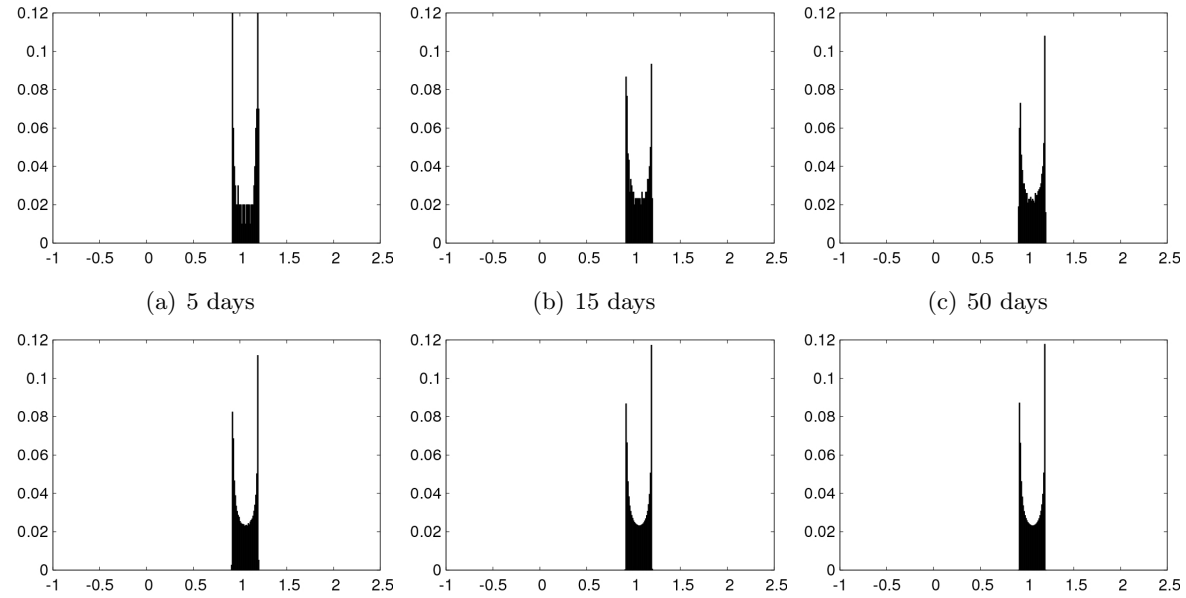

(a) 5 days (b) 15 days (c) 50 days

(d) 1 year (e) 10 years (f) 100 years

Figure 4.9: Normalised frequency distributions of the X variable for a single trajectory in the L84 model when $F = 6$ after given simulation periods, for *IC 2*: $(0.93, -1.04, 0.58)$. In each plot, the x-axis denotes the X variable and the y-axis corresponds to the frequency per occupied bin; bin width = 0.01. Y and Z variable distributions given in Appendix B: figures B-5 and B-6.

a range of X values that extends between $-0.6 < X < 2.4$.

Figure 4.8 and 4.9 show the normalised frequency distributions for two single trajectories, initialised at *IC 1* and *IC 2* respectively, for permanent summer conditions over simulation periods of 5 days up to 100 years. The results show that the time required for a trajectory to explore the range of model states on attractor $A2$ is longer than the time it takes to visit the complete range of states on attractor $A1$. In figure 4.9, the full range of X values is sampled after only 5 days (see fig. 4.9(a)), largely as a result of the simple geometric nature of the attractor $A2$; an ellipse consisting of periodic orbits on the time scale of approximately one time unit (equivalent to 5 days). However, as shown in figure 4.8(c), it takes 50 days before the frequency distribution begins to visually resemble the distributions associated with longer model simulations. In general, the model climate distributions are much smoother under summer parameter conditions for both ICs because of the periodic nature of the model attractors.

4.3.2 Ensemble results

The climate distributions of the L84 model with fixed parameter values are also estimated for permanent summer and permanent winter conditions using an IC ensemble approach. Large IC ensembles (10,000 members) are run for simulation periods of up to 100 years with ICs spread along a transect in the model state space; from $(-1.0, -2.5, -2.5)$ to $(2.5, 2.5, 2.5)$. Figure 4.10 shows the evolution of the IC ensemble frequency distributions for the X variable at particular time instants during permanent winter conditions. The distributions appear to converge after approximately one year; after 50 days the distribution retains significant memory of the ICs with some members still located outside of the range of X values consistent with the model attractor.

As expected, from experience with the L63 model, convergence of the distributions is more rapid using the IC ensemble approach. Visual inspection suggests that the ergodic assumption is valid in the winter configuration, as the converged distribution resembles the single trajectory distribution shown in figure 4.7(f); a quantitative analysis is employed in section 4.3.3 using the KS test.

The equivalent plots for permanent summer conditions are displayed in figure 4.11. After one year, the range of X values becomes well constrained and matches the range associated with the single trajectory distributions shown in figure 4.8, associated with attractor $A1$. The location of the peaks in the distributions shown in figures 4.11(d) to 4.11(f) are broadly consistent with the five peaks identified in figures 4.8 and 4.9 indicating that the two coexisting attractors illustrated in section 4.2.3 are both prevalent in the ensemble frequency distributions. However, because the ensemble distributions do not match the single trajectory distributions for both *IC 1* and *IC 2*, the ergodic assumption does not appear to be valid in permanent summer conditions. Furthermore, at the time instants chosen, the ensemble distributions have not converged as some of the peaks are inconsistent in magnitude. In permanent summer conditions, the model is not

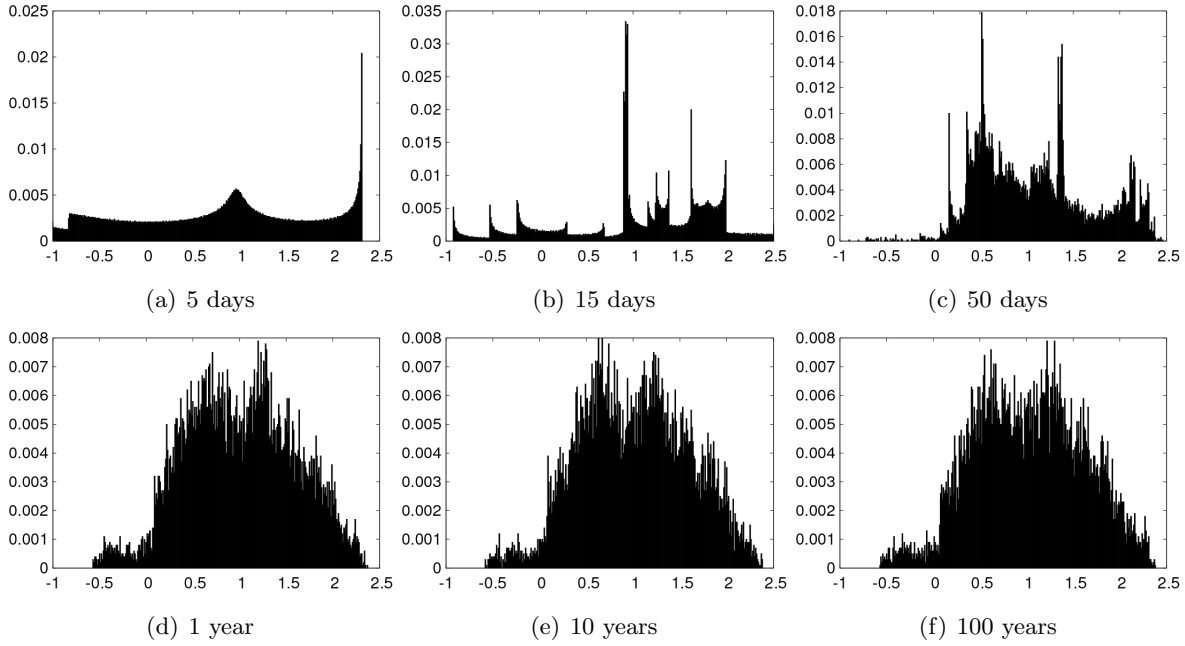

(a) 5 days (b) 15 days (c) 50 days

(d) 1 year (e) 10 years (f) 100 years

Figure 4.10: Normalised frequency distributions for a 10,000 member IC ensemble of the L84 model when $F = 8$ after given simulation periods with ICs spread along a transect from $(-1.0, -2.5, -2.5)$ to $(2.5, 2.5, 2.5)$. In each plot, the x-axis denotes the X variable and the y-axis corresponds to the frequency per occupied bin; bin width = 0.01. Y and Z variable distributions given in Appendix B: figures B-7 and B-8.

chaotic and the model trajectories display periodicity. As a result the ensemble distributions (at a specific instant in time) show the distribution of model states at a specific phase of each trajectory's periodic cycle so the distribution is, and always will be, conditioned on the ICs in the ensemble.

Analysis of four different IC ensemble distributions evolving over a 80 year simulation period shows that under permanent summer conditions IC ensemble distributions are different at every instant in the model simulation and that the distributions are conditioned on the IC uncertainty encapsulated in the IC ensemble. Figure 4.12 shows frequency distributions from four different ensembles (labelled $E1$, $E2$, $E3$ and $E4$) at regular intervals over a 80 year simulation period. The ICs for the ensembles are chosen with reference to the basins of attraction (shown in figure 4.6) in the X-Y plane, where $Z = 0$, and the ranges are listed in table 4.1. For each ensemble, the ICs are uniformly distributed within the specified ranges. Ensembles $E1$ and $E2$ are selected for regions in which all trajectories evolve to attractor $A1$ and attractor $A2$ respectively. Ensembles $E3$ and $E4$ are selected in other regions of the model state space which span both basins of attraction.

Figures 4.12(a) to 4.12(d) show the initial uniform spread of the IC ensembles in the X variable for each ensemble. The plots in the first two columns of figure 4.12 show the $E1$ and $E2$ distributions at 20 year intervals over the 80 year simulation period. The distributions are constrained to the ranges in the model variables associated with their respective attractors.

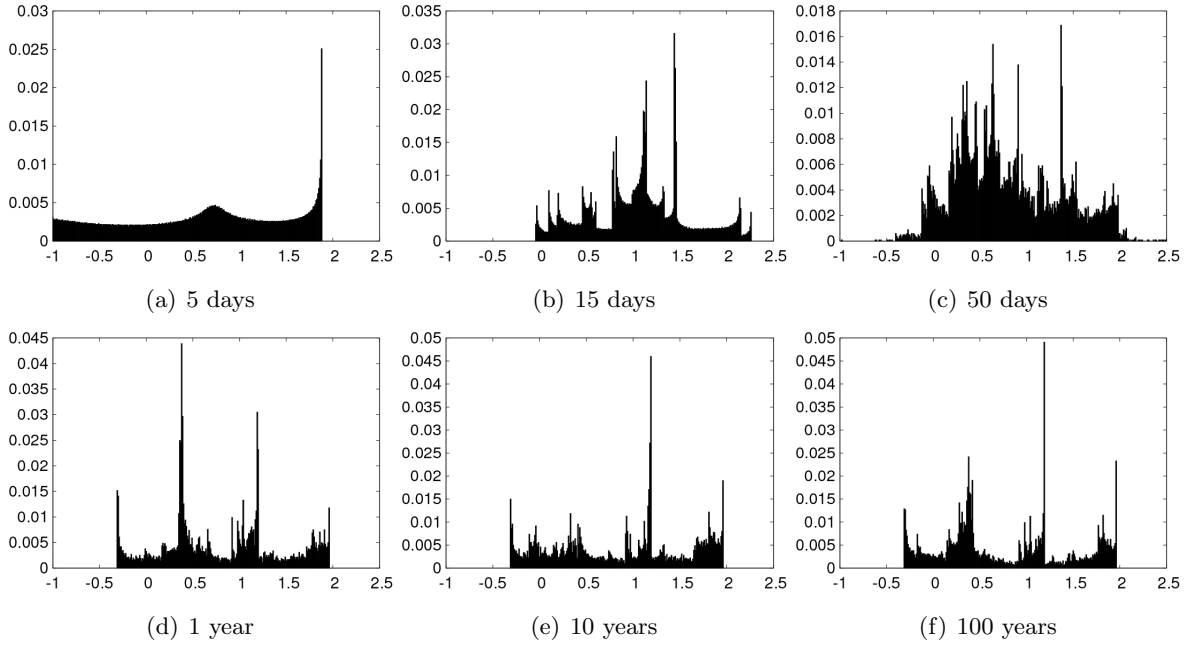

(a) 5 days (b) 15 days (c) 50 days

(d) 1 year (e) 10 years (f) 100 years

Figure 4.11: Normalised frequency distributions for a 10,000 member IC ensemble of the L84 model when $F = 6$ after given simulation periods with ICs spread along a transect from $(-1.0, -2.5, -2.5)$ to $(2.5, 2.5, 2.5)$. In each plot, the x-axis denotes the X variable and the y-axis corresponds to the frequency per occupied bin; bin width = 0.01. Y and Z variable distributions given in Appendix B: figures B-9 and B-10.

Ensemble	X_{min}	X_{max}	Y_{min}	Y_{max}
$E1$	-1.0	-0.5	-1.5	-1.0
$E2$	-1.0	-0.8	0.0	0.3
$E3$	1.0	1.5	1.0	1.5
$E4$	-0.5	0.0	0.0	0.5

Table 4.1: IC ranges for four different ensembles used to investigate memory in the L84 model for permanent summer conditions, when $F = 6$.

The plots in columns three and four show the distributions associated with $E3$ and $E4$. The results show that when the IC ensemble crosses the boundaries in the basins of attraction, some members evolve on attractor $A1$ and others evolve on attractor $A2$, as evident in the locations of the primary peaks consistent with $A2$ and the location of other members in the state space consistent with $A1$. The distributions are also different at each time instant for each ensemble supporting the inference that periodicity controls the evolution of the model trajectories. Because the model is not chaotic, trajectories do not separate from each other so the distributions continue to exhibit memory of the ICs and do not converge. In section 4.3.3, the convergence of both single trajectory and IC ensemble distributions is quantitatively assessed using the KS test and the results support the notion that IC memory is apparent in the ensemble distributions under permanent summer conditions.

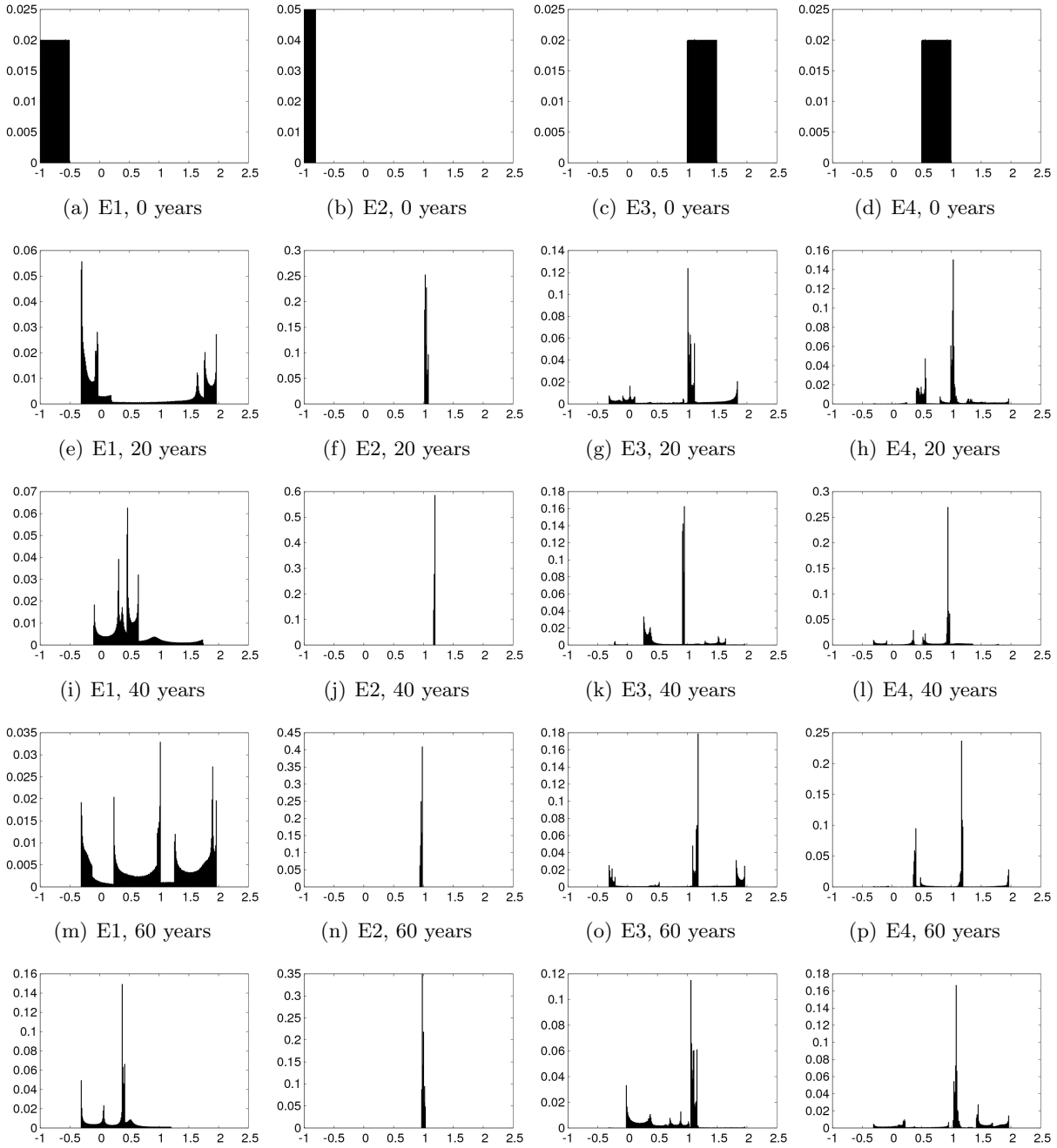

(a) E1, 0 years (b) E2, 0 years (c) E3, 0 years (d) E4, 0 years

(e) E1, 20 years (f) E2, 20 years (g) E3, 20 years (h) E4, 20 years

(i) E1, 40 years (j) E2, 40 years (k) E3, 40 years (l) E4, 40 years

(m) E1, 60 years (n) E2, 60 years (o) E3, 60 years (p) E4, 60 years

(q) E1, 80 years (r) E2, 80 years (s) E3, 80 years (t) E4, 80 years

Figure 4.12: Normalised frequency distributions of four different 10,000 member IC ensembles for the X variable in L84 model in permanent summer conditions ($F = 6$). The first column shows the distributions for ensemble E1, the second column shows the distributions for ensemble E2, the third column shows the distributions for ensemble E3 and the fourth column shows the distributions for ensemble E4. In each plot, the x-axis denotes the X variable and the y-axis corresponds to the frequency per occupied bin; bin width = 0.01.

Sensitivity to model time step

In section 3.3.5, the L63 model climate distributions are shown to be sensitive to the model

time step. To test the sensitivity of the L84 model to the chosen time step, a series of model runs are performed. Lorenz (1984) used a time step $\tau = \frac{1}{30}$, albeit with a fourth order Taylor-series integration procedure, whilst in this study a smaller time step $\tau = 0.01$ is implemented using a fourth order RK integration method. Figure 4.13 shows the distribution in X from a 100 year run of a 10,000 member IC ensemble for four different time steps of decreasing size. The ICs used are the same as those used to generate figures 4.10 and 4.11; a transect from $(-1.0, -2.5, -2.5)$ to $(2.5, 2.5, 2.5)$. The results indicate that the time step used is an important consideration in determining the climate distributions of the L84 model. For time steps of $\tau \leq 0.01$, the distributions are very similar but when $\tau = \frac{1}{30}$ the climate distribution is significantly altered. Over reasonably short times scales (years to decades), when $\tau = \frac{1}{30}$ the L84 model displays chaotic behaviour but over longer time scales (multi-decadal to centennial) model trajectories become periodic and affect the ensemble climate distributions. Figure 4.14 illustrates the transition from chaotic to periodic behaviour, shown for the X variable for a 50 year simulation of the L84 model with a time step, $\tau = \frac{1}{30}$. Whilst the truncation effect resulting from the time step choice on model climates has been observed in the L63 model (Teixeira et al. (2007)), at the time of writing (to the author's knowledge) no such acknowledgement regarding the sensitivity of the L84 model climate to the time step has been published in the formal literature. Based on these results, a time step of $\tau = 0.01$ using the fourth order RK method was deemed appropriate for the L84 experiments presented in this thesis.

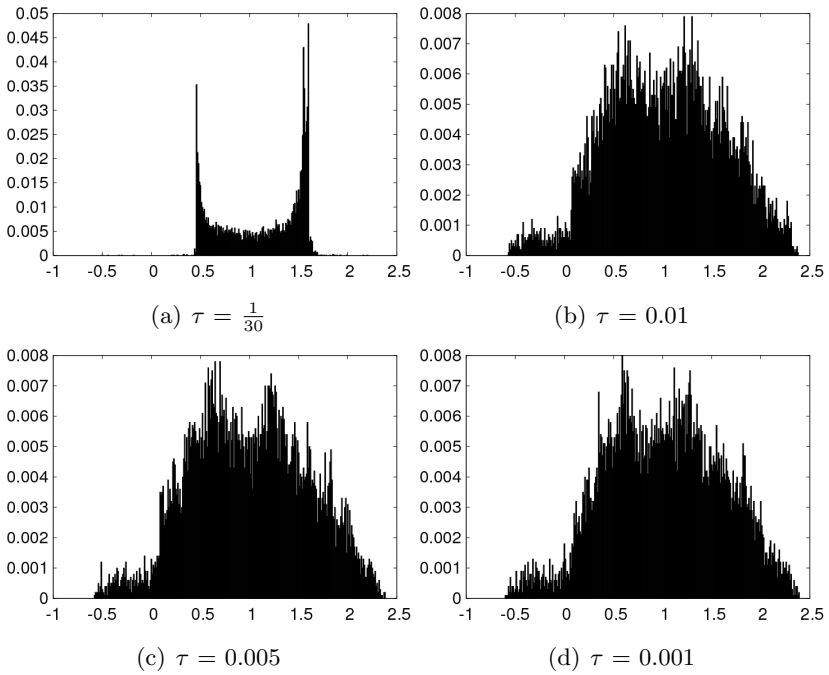

(a) $\tau = \frac{1}{30}$ (b) $\tau = 0.01$

(c) $\tau = 0.005$ (d) $\tau = 0.001$

Figure 4.13: 10,000 member IC ensemble normalised frequency distributions for the L84 model when $F = 8$ after an integration period of 100 years for given time steps, using a fourth order RK integration scheme and ICs spread along a transect from $(-1.0, -2.5, -2.5)$ to $(2.5, 2.5, 2.5)$. In each plot, the x-axis denotes the X variable and the y-axis corresponds to the frequency per occupied bin; bin width = 0.01.

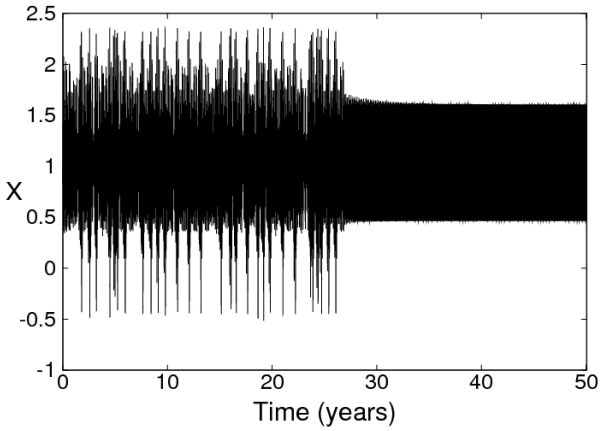

Figure 4.14: Single model trajectory for the variable X in the L84 model after a 50 year simulation with $\tau = \frac{1}{30}$ and IC: $(X, Y, Z) = (1.0, 1.0, 1.0)$.

4.3.3 Rates of convergence for model climate distributions in the L84 model

In order to estimate the time scales at which the distributions from single model trajectories and IC ensembles converge to the climate distributions of the L84 model, a very large IC ensemble (100,000 members) is run to provide benchmark ensemble climate distributions for the L84 model in permanent winter and permanent summer parameter conditions. The ensemble is run for a period of 200 years with ICs spread along a transect from $(-1.0, -2.5, 2.5)$ to $(2.5, 2.5, 2.5)$. A period of 200 years is chosen to ensure that model trajectories evolve many times around the model's attractor(s).

Using the KS test, the corresponding benchmark ensemble distributions (shown in figure 4.15) are compared to the single trajectory distributions from section 4.3.1 and the 10,000 member IC ensemble distributions described in section 4.3.2. The corresponding KS plots for permanent winter and permanent summer parameter conditions are shown in figures 4.16 and 4.17 respectively.

When $F = 8$ (permanent winter), the L84 model displays chaotic transitive behaviour and over time the trajectories spread out across the attractor state space. The KS plots in figure 4.16 reveal the rate at which memory of the initial state(s), of a single trajectory and an IC ensemble, are lost as the distributions converge towards the benchmark ensemble distributions. After only one and a half months, D decreases to values close to $D = 0.1$ in both the single trajectory and ensemble distributions. After one year the IC ensemble appears to have largely converged towards the model climate distributions whereas the single trajectory distributions retain some memory of the initial state for approximately ten years.

The KS plots in figure 4.17 show that the initial rates of convergence for permanent summer conditions are similar to those for permanent winter conditions but crucially, both of the single trajectory distributions and the ensemble distributions do not entirely converge towards the benchmark ensemble distributions (consistent with the results in section 4.3.2). Given the

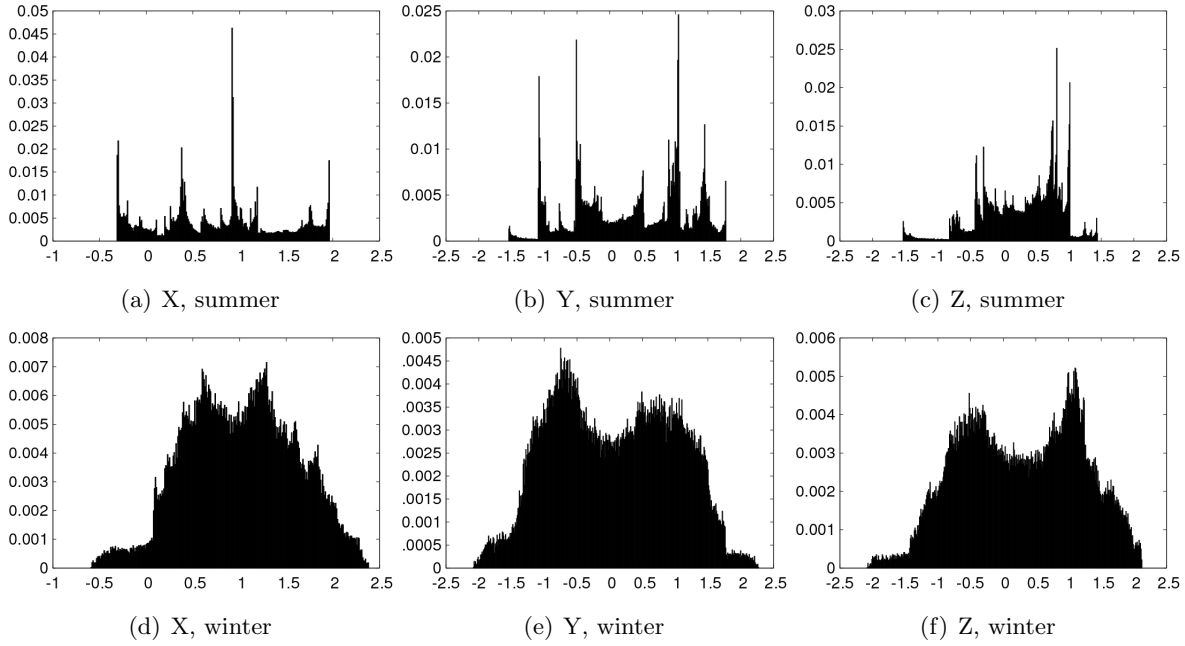

(a) X, summer (b) Y, summer (c) Z, summer

(d) X, winter (e) Y, winter (f) Z, winter

Figure 4.15: Normalised frequency distributions for given variables in permanent summer, (a) to (c), and permanent winter, (d) to (f), after a 200 year simulation of the L84 model from a 100,000 member IC ensemble with ICs spread along a transect from $(-1.0, -2.5, 2.5)$ to $(2.5, 2.5, 2.5)$. In each plot, the y-axis corresponds to the frequency per occupied bin; bin width = 0.01.

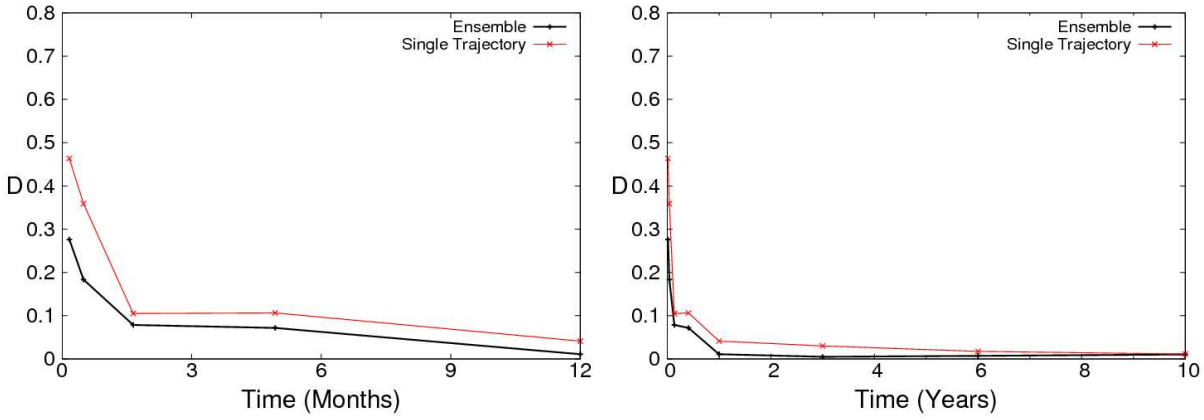

(a) 1 year (b) 10 years

Figure 4.16: KS comparisons for the X variable in the L84 model when $F = 8$ between the 100,000 member IC ensemble distributions shown in figure 4.15 and: (i) the 10,000 member IC ensemble distributions shown in figure 4.10; and (ii) the single trajectory distributions shown in figure 4.7. Y and Z variable KS comparisons shown in Appendix B, figures B-11 and B-12.

intransitive nature of the model when $F = 6$, it is not surprising that the single trajectory distributions do not converge to the benchmark ensemble distributions. The distributions from the trajectory associated with $A1$ converge more than those associated with $A2$, as the range of behaviour of model trajectories evolving on $A1$ is consistent with the range of the ensemble

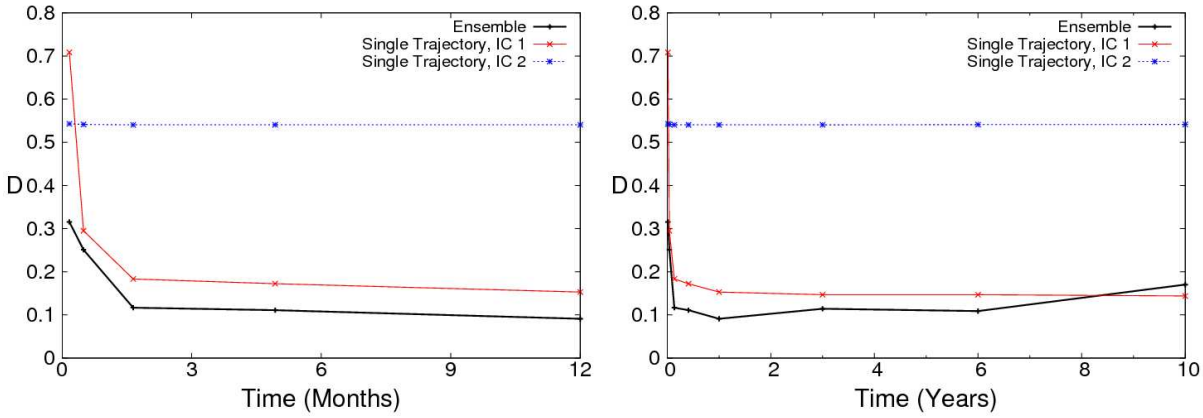

(a) 1 year (b) 10 years

Figure 4.17: KS comparisons for the X variable in the L84 model when $F = 6$ between the 100,000 member IC ensemble distributions shown in figure 4.15 and: (i) the 10,000 member IC ensemble distributions shown in figure 4.11; (ii) the single trajectory distributions shown in figure 4.8 from $IC1$ (associated with attractor $A1$); and (iii) the single trajectory distributions shown in figure 4.9 from $IC2$ (associated with attractor $A2$). Y and Z variable KS comparisons shown in Appendix B, figures B-13 and B-14.

distributions, and more ensemble members are likely to evolve on $A1$ based on evidence from their basins of attraction (see figure 4.6).

The KS results confirm that over the 10 year period shown in figure 4.17(b) the ensembles also retain memory of their ICs as the ensemble distributions do not fully converge. Figure B-15 in appendix B shows that the distributions similarly fail to converge over a much longer simulation period of 160 years. The ergodic assumption is therefore invalid for permanent summer conditions, where the model behaviour is intransitive. In the L84 model, when $F = 6$, two climates coexist and the long-term climate which is realised is dictated entirely by the model's initial state. If this initial state is uncertain then an IC ensemble will generate the PDFs of the model variables for some future time conditioned on the IC uncertainty.

In the analogy to climate prediction under IC uncertainty, if the uncertainty in the initial state of the climate system crosses the boundaries of the basins of attraction of at least two coexisting attractors then using an IC ensemble is essential to determine what states are possible in the future. If two (or more) climates coexisted and the uncertainty in the initial state of the climate system encompasses more than one basin of attraction then running an IC ensemble to determine possible future states would be vitally important in guiding robust adaptation strategies. Deriving the distribution of climate using a single model trajectory from a single initial state would be misleading.

4.4 Seasonally Driven L84 Model

A number of studies have explored the dynamics of the seasonally driven L84 model documenting the associated phenomenology and linking the results to interannual climate variability (Lorenz (1990), Kock (1998), Broer et al. (2002) and Broer et al. (2003)). The seasonality has usually been introduced into the modelling studies by imposing a periodic (sinusoidal) variation in the equator-to-pole temperature difference, F. Broer et al. (2002) also impose a seasonal cycle on the land-ocean temperature contrast, G, but for the purposes of this study G shall be held constant, consistent with the methodology adopted by Lorenz (1990). The focus of the work presented in this section and the following section is to investigate how a seasonal cycle in F can impact the L84 model climate distributions, with and without a trend in the model parameter, and to relate the L84 model results to the real climate system in terms of understanding the potential predictability of climate under climate change.

4.4.1 Single trajectory under seasonal variations in F

To implement a seasonal cycle in the L84 model, the value of F in equation 4.1 is replaced by the sinusoidal function given in equation 4.4:

$$F \rightarrow F_m + M\cos\left((2\pi\frac{i}{K\tau^{-1}}) - \frac{\pi}{12}\right) \tag{4.4}$$

where F_m is the mean value of F, τ is the model time step, i is the iteration step number, K denotes the number of time units per year and the term $\frac{\pi}{12}$ is introduced to ensure that the time series in F begins each phase on January 1st, half a month before the maximum value of F is reached (to align a model year with a calendar year). M represents the magnitude of the wave so that in the case where $M = 1$, and $F_m = 7$, the seasonal fluctuations are contained in the range: $6 < F < 8$. The parameter space contains a diverse set of chaotic and non-chaotic attractors (Freire et al. (2008)) exhibiting both transitive and intransitive behaviour. Lorenz (1990) states "intransitive behaviour occurs nearly everywhere between $F = 5.2$ and 6.9 while transitive chaotic behaviour occupies the interval from 7.9 to 8.8. Between 6.9 and 7.6, transitivity prevails, with only weak periodic fluctuations, while between 7.6 and 7.9 intransitivity reappears, with weak periodic or strong chaotic variations." Crucially, Lorenz notes that these findings only correspond to fixed value of F.

Figure 4.18 shows the evolution of a single model trajectory for each model variable over a 10 year simulation of the seasonally driven L84 model where $F_m = 7$ and $M = 1$. The plots show interannual variability in the summer and winter circulation patterns. In the third, fourth, fifth, seventh and final year of the simulation, periodicity which spans the range of the model state space is apparent during the summer months. The remaining summers are associated with constrained periodic oscillations, particularly evident in the X variable. Lorenz (1990) refers to these summers as strong and weak respectively. In the winter months, the trajectory appears to

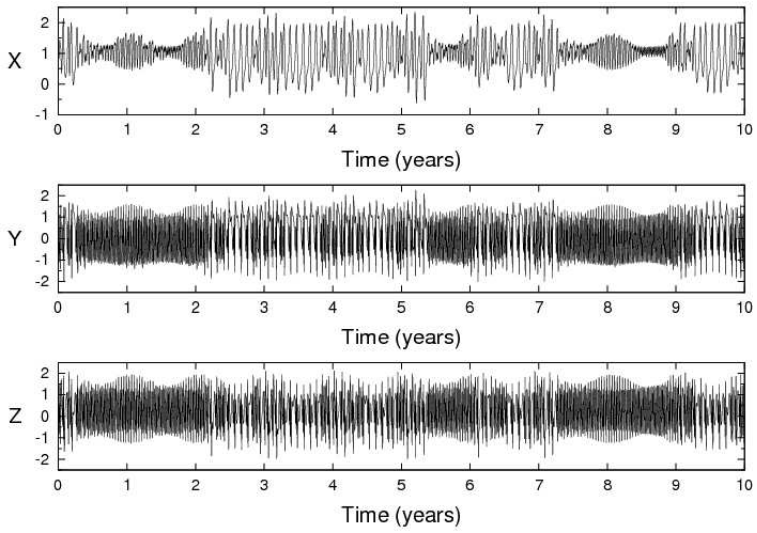

Figure 4.18: Time series' for model variables from a single trajectory simulation of the seasonally driven L84 model over a 10 year interval initiated on January 1st with ICs: $(X, Y, Z) = (1.0, 1.0, 1.0)$. $F_m = 7$, $M = 1$.

be less regular but at $t = 1$ year and $t = 8$ years there is evidence of periodicity in the months leading to mid-winter. The dynamics of the seasonally driven L84 model has been relatively well studied for single model trajectories (Lorenz (1990), Broer et al. (2002)). In the analogy to the climate system and climate prediction the focus of the remainder of this chapter is on the model climate distributions which haven't (to the author's knowledge) been researched in any detail. In the next section, the climate distributions of the seasonally driven L84 model are determined.

Although model trajectories strictly evolve according to different attractors at different fixed values of F, the effect of a seasonal cycle is to create a new "pseudo-attractor" on which trajectories propagate. Whilst the term has been used for other purposes elsewhere in the literature (e.g. Burns et al. (1993)), here the term *pseudo-attractor* (PA) is used to describe the geometric nature of the attractor as it evolves in time in accordance with the periodic variations in F. The term pseudo-attractor is subsequently used throughout the remainder of this chapter to distinguish it from an autonomous attractor at fixed parameter values.

4.4.2 Seasonally driven L84 model climate distributions

The conventional approach to assessing climate variability using a single model realisation is compared to the IC ensemble approach in the seasonally driven L84 model. A 100,000 member IC ensemble, with ICs spread along a transect from $(-1.0, -2.5, 2.5)$ to $(2.5, 2.5, 2.5)$, is run for a period of 200 years to estimate the equilibrium climate distributions of the seasonally driven L84 model for mid-winter (when F returns to $F = 8$) and mid-summer (when F returns to $F = 6$). The frequency distributions for the three model variables at mid-winter and mid-summer (in

the 200th simulation year) are shown in figure 4.19.

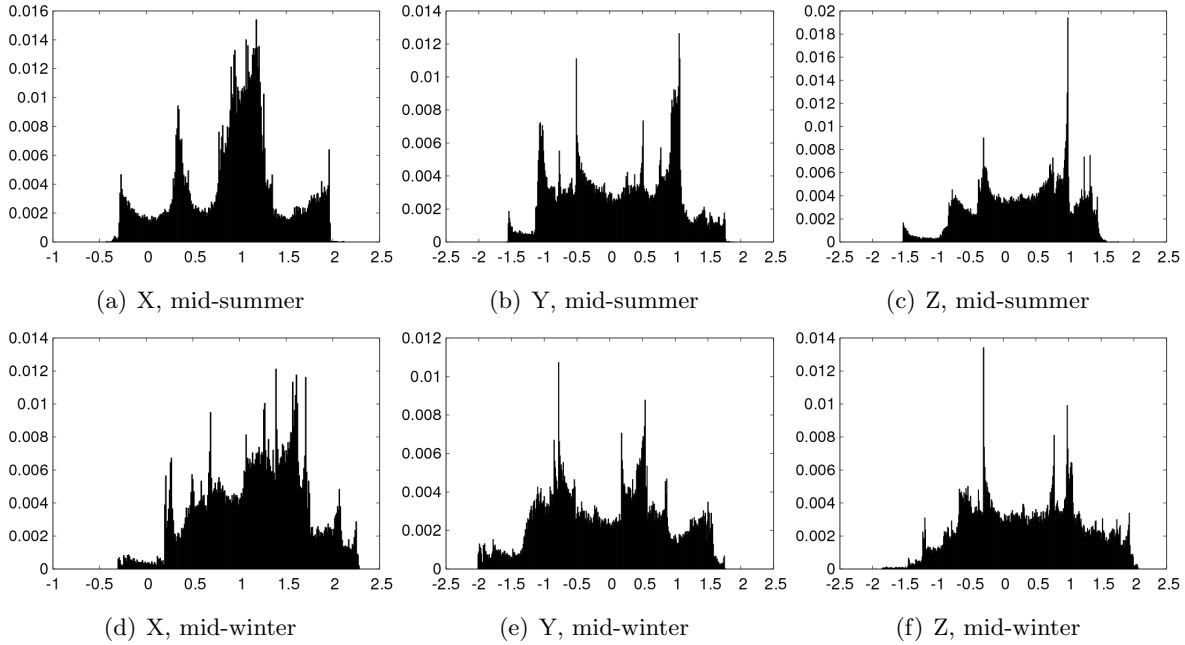

(a) X, mid-summer (b) Y, mid-summer (c) Z, mid-summer

(d) X, mid-winter (e) Y, mid-winter (f) Z, mid-winter

Figure 4.19: Normalised frequency distributions for given variables in mid-summer, (a) to (c), and mid-winter, (d) to (f), after a 200 year simulation of the seasonally driven L84 model with $F_m = 7$ and $M = 1$ from a 100,000 member IC ensemble with ICs spread along a transect from $(-1.0, -2.5, 2.5)$ to $(2.5, 2.5, 2.5)$. In each plot, the y-axis corresponds to the frequency per occupied bin; bin width = 0.01.

The distributions in figure 4.19 are different to the equivalent plots in the non-seasonally driven L84 model, shown in figure 4.15. Whilst the range in model behaviour remains consistent across all variables, the density of the trajectories in given regions of the PA state space is altered. For example, during permanent summer in the non-seasonally driven model (figure 4.15(a)), there is a narrow peak at $X \approx 0.9$. Yet in the seasonally driven model (figure 4.19(a)), the summer distribution shows a much wider peak in this region of state space, with a more uniform modal range of trajectories occurring between $0.8 < X < 1.2$. Similarly, during permanent winter in the non-seasonally driven model (figure 4.15(d)), there is a high density of values in the range $0.5 < X < 1.5$. In the seasonally driven model during mid-winter (figure 4.19(d)), there remains a high density of trajectories where $1.0 < X < 1.5$ but there is a smaller density in the range $0.5 < X < 1.0$.

The seasonal cycle in F significantly influences the probabilities of trajectories passing through certain regions of the model state space. The seasonal cycle imposes transitions from regions of parameter space with chaotic attractors, associated with transitive behaviour, to regions with multiple periodic attractors, associated with intransitive behaviour. Model trajectories are constantly adjusting to the changing geometry of the underlying model attractor(s). Trajectories retain memory of previous states associated with different regions of parameter space which exhibit alternative long-term dynamic behaviour. The ensemble 'climate' distributions shown

in figure 4.19 therefore seem to be exhibiting hysteresis; a memory of the pathway in F.

4.4.3 Testing the ergodic assumption

The ergodicity of the seasonally driven L84 model is explored for both mid-summer and mid-winter forcing conditions. Given the inference that the seasonally driven L84 model displays transitive behaviour, one would expect the ergodic assumption to be valid for a sufficiently long single model realisation. However, determining the length of time required for single model distributions to converge towards the ensemble distributions at specific times in the year (e.g. mid-winter/mid-summer) is not a trivial calculation.

A single model realisation is run for 10,000 years with ICs $(1.0, 1.0, 1.0)$ initiated on January 1st. The single trajectory distributions are then derived from the distribution of yearly recurring values for mid-winter (when F returns to $F = 8$) and mid-summer (when F returns to $F = 6$). Only one model state is extracted per year for both mid-winter and mid-summer; hence a 10 year sample includes 10 data points. Each value can be considered independent from the previous years value as chaotic conditions in the preceding winter lead to rapid deviations of model trajectories[2]; as discussed in section 4.2.1, Lorenz (1990) demonstrated that the summertime circulation is effectively randomly selected due to chaotic conditions in the previous winter circulation.

Figure 4.20 shows the distribution for mid-summer values of X from a single trajectory integrated over increasing time periods. As the model simulation period increases, the frequency distributions appear to be converging towards the ensemble distribution displayed in figure 4.19(a); a quantitative comparison is provided in figure 4.22. For shorter simulation periods, the distributions are inevitably less detailed given that only one state is selected per year. After 30 years, a time scale typically associated with climate definitions (Burroughs (2003)), the range of possible states is reasonably well captured but the density of values is not sufficient to provide reliable estimates of the model probabilities. After 100 years and certainly by 300 years, some important features of the distributions become more apparent but quantitative estimates of the entire model PDF are likely to contain inaccuracies.

The equivalent distributions for the mid-winter values of X are shown in figure 4.21. The 10,000 year distribution, shown in figure 4.21(h), visually appears to closely resemble the ensemble distribution for mid-winter X given in figure 4.19(a). Consistent with figure 4.20, shorter time intervals provide less representative estimates of the model climate distributions. Unlike in figure 4.20(c), the 30 year distribution shown in figure 4.21(c) does not fully capture the range of X values associated with the mid-winter ensemble distribution. Crucially the distribution does not include any values of X that are negative, which represent transitions to easterly flow. The density of points is also different with a primary cluster of points close to $X = 0.6$; a region with a relatively lower probability of occurring in larger samples.

[2]For a comparative analysis of the error growth in both the L63 and L84 models, see Anderson and Hubeny (1997).

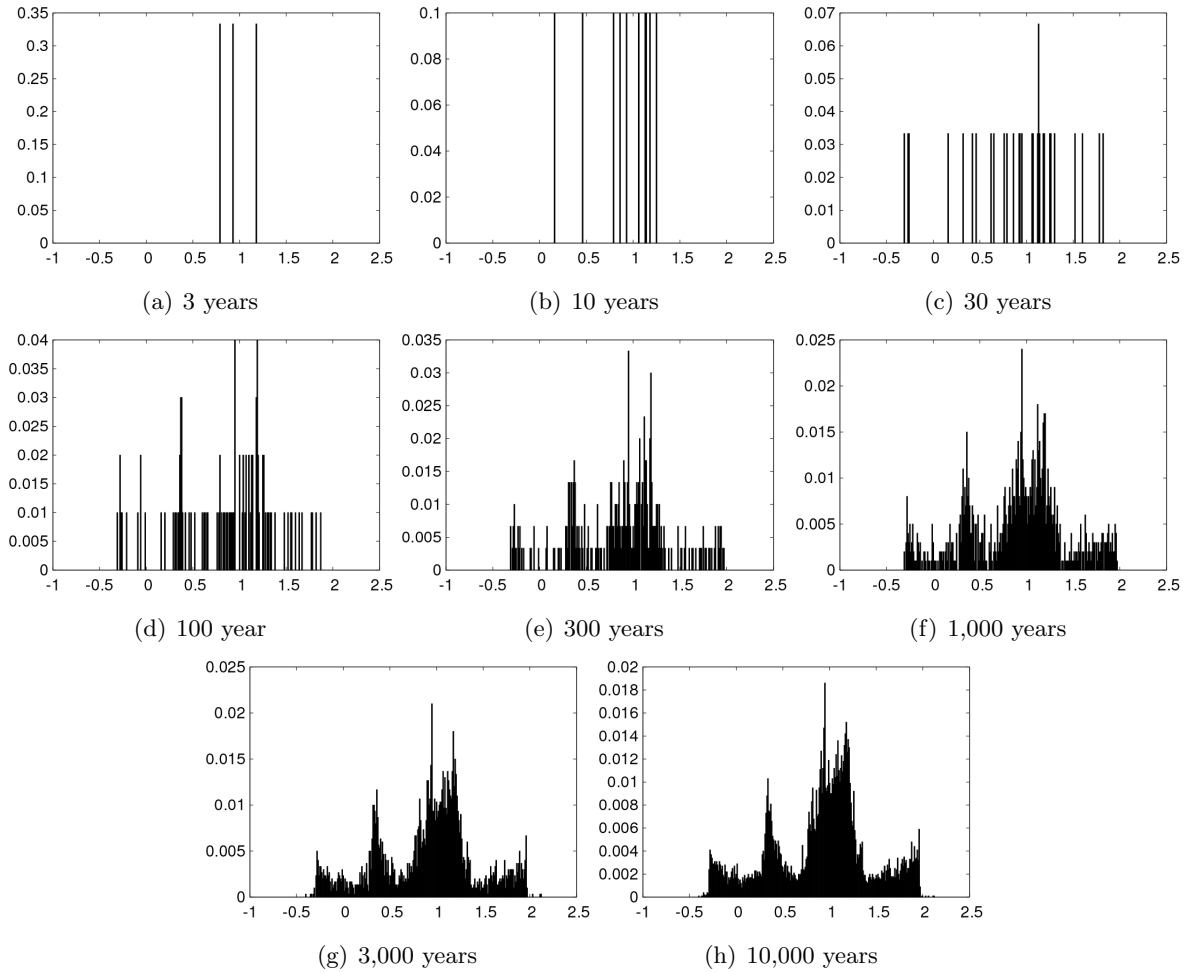

(a) 3 years (b) 10 years (c) 30 years

(d) 100 year (e) 300 years (f) 1,000 years

(g) 3,000 years (h) 10,000 years

Figure 4.20: Normalised frequency distributions of the X variable for a single trajectory in the L84 model in mid-summer after given simulation periods with seasonal F variations between $6 < F < 8$ and ICs: $(X, Y, Z) = (1.0, 1.0, 1.0)$. In each plot, the x-axis denotes the X variable and the y-axis corresponds to the frequency per occupied bin; bin width = 0.01.

Using the KS test, the large IC ensemble distributions, representing the climate of the seasonally driven L84 model (shown in figure 4.19), are compared to the single trajectory distributions of increasing simulation periods (shown in figures 4.20 and 4.21). Time series' of D comparing the single trajectory distributions to the ensemble distributions are displayed in figure 4.22. The x-axis has a logarithmic scale from 1 to 10,000 years. The results reveal, unsurprisingly, that the longer the integration period for a single model realisation the lower the value of D (corresponding to a better fit).

The convergence illustrated in figure 4.22 is simply a function of an increasing number of data-points in the single trajectory distributions. Increasing the number of data-points, by including data at time steps close to mid-summer or mid-winter, might therefore appear to be a possible solution to estimating the model climate in a more computationally efficient manner. However, this approach is problematic. The parameter F and the associated model attractor(s)

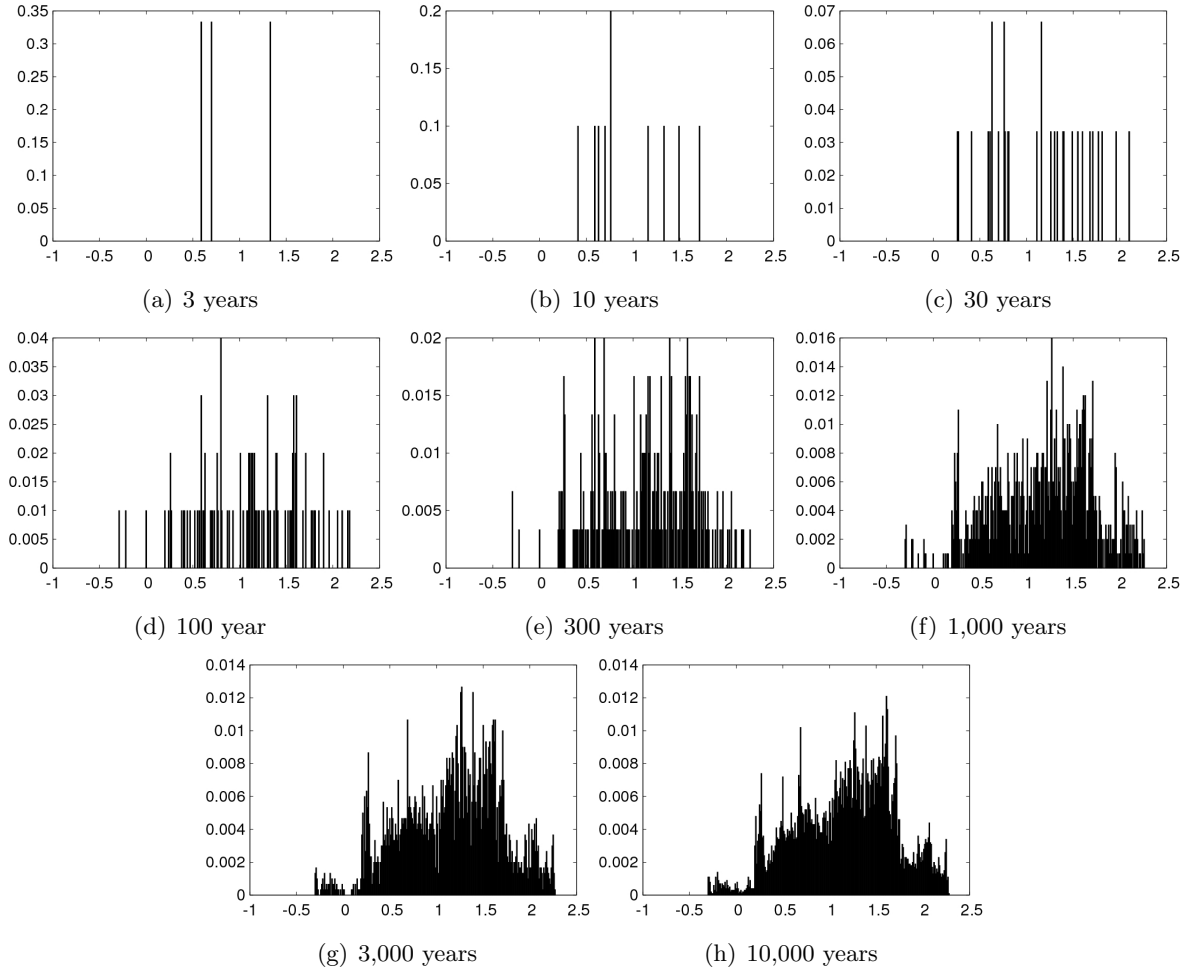

(a) 3 years (b) 10 years (c) 30 years

(d) 100 year (e) 300 years (f) 1,000 years

(g) 3,000 years (h) 10,000 years

Figure 4.21: Normalised frequency distributions of the X variable for a single trajectory in the L84 model in mid-winter after given simulation periods with seasonal F variations between $6 < F < 8$ and ICs: $(X, Y, Z) = (1.0, 1.0, 1.0)$. In each plot, the x-axis denotes the X variable and the y-axis corresponds to the frequency per occupied bin; bin width = 0.01.

is continuously changing throughout the year so using data points from time steps close to but not at the time of interest risks including data points that are potentially associated with a different attractor. The impact of increasing the sample size is investigated and the results are described in the following section.

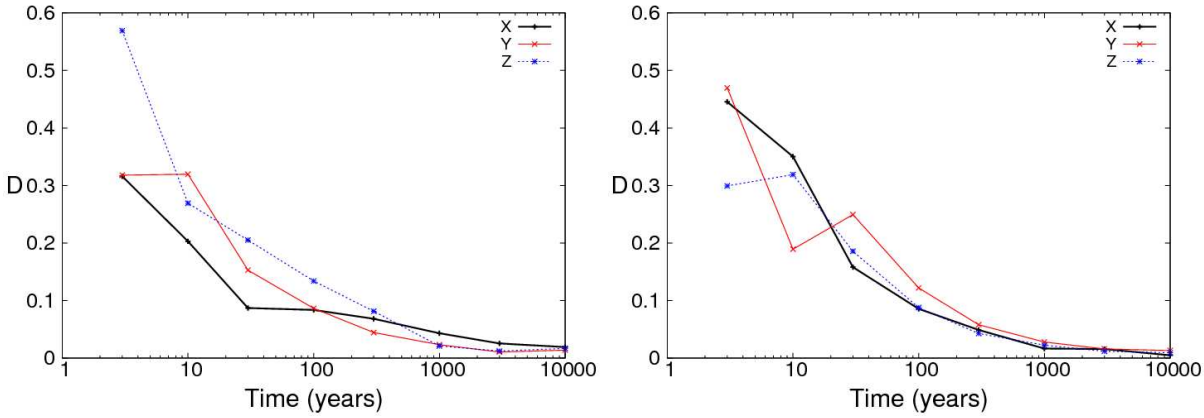

(a) Summer

(b) Winter

Figure 4.22: KS comparison between single trajectory distributions and 100,000 member IC ensemble climate distributions for the seasonally driven L84 model. The single trajectory distributions consist of one model state per year extracted at mid-winter and mid-summer. The ensemble distributions are also extracted at mid-winter and mid-summer.

4.4.4 Increasing the sample size

With a time scale of 5 days and a time step, $\tau = 0.01$, the number of data-points in the L84 model year is 7300 (equivalent to the number of time-units per year ($\frac{365}{5}$) divided by the time step). Rather than selecting a single data point for each consecutive mid-winter/mid-summer, all of the January/July data points are selected, thus increasing the number of data points per year for a single model realisation by a factor of 608[3]. The value of F at the beginning and end of January is $F = 7.966$; only 0.034 K less than the mid-winter value of $F = 8$. Similarly, the value of F at the beginning and end of July is $F = 6.034$; only 0.034 K greater than the mid-summer value of $F = 6$. One might therefore expect that by including all of the January/July data points, the frequency distributions of mid-winter/mid-summer resulting from a single model trajectory should converge towards the IC ensemble distributions more rapidly.

Figure 4.23 show the KS comparison of the single trajectory distributions with monthly data to the IC ensemble distributions shown in figure 4.19. The KS plots show that the single trajectory distributions do indeed converge to the ensemble distributions more rapidly when including all of the monthly data points (note the y-axis is the same scale as that used in figure 4.22). Even after the first year, the KS result conveys a moderate level of agreement. However the distributions never converge entirely and the values of D remain significantly larger than zero, even over a long simulation period of 1,000 years (which includes 608,000 data points). D does not decrease any further after a time interval of approximately 10 years in both mid-winter and mid-summer, suggesting that longer simulation periods do not necessarily lead to better agreement in the distributions.

The most significant differences between the single trajectory distributions and the ensemble

[3]The number of data points in an individual month is therefore 608.

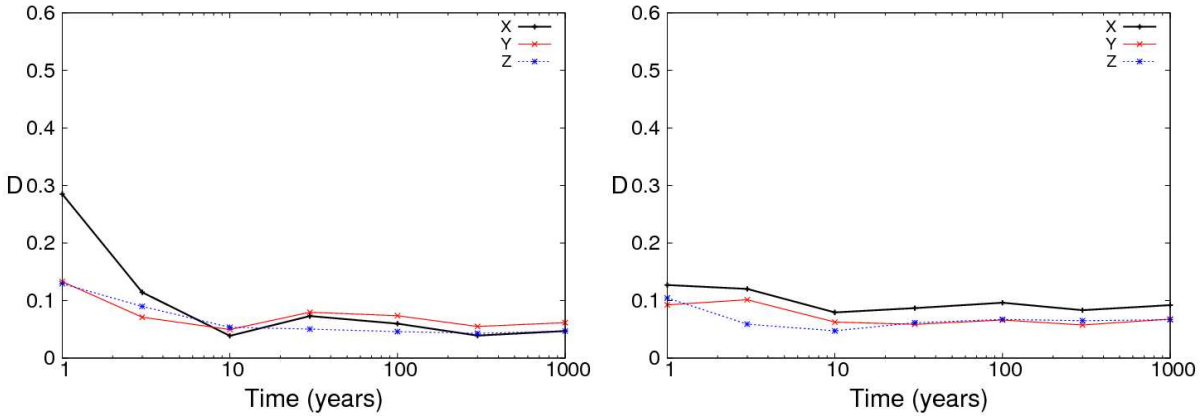

(a) Mid-summer

(b) Mid-winter

Figure 4.23: KS comparison between single trajectory distributions and IC ensemble climate distributions for the seasonally driven L84 model. Data taken from the entirety of January and July for the single trajectory distributions whilst ensemble distributions are extracted at mid-winter and mid-summer respectively.

distributions appears in the X variable in winter, where the KS statistic converges to $D \approx 0.1$. Figures 4.24(a) to 4.24(c) show the frequency distributions associated with consecutive January values of X from 100, 300 and 1,000 year simulation periods and figure 4.24(d) shows the 200 year ensemble distribution of mid-January X values, also illustrated in figure 4.19(d). The distributions from the single model trajectory shown in figures 4.24(a) to 4.24(c) appear to have converged toward a stable distribution that is different from the ensemble distribution shown in figure 4.24(d). There is a small difference in the range of X values; the mid-winter ensemble distribution suggests a slightly narrower range, $-0.3 < X < 2.3$, as opposed to the single trajectory approach using data from the whole of January which suggests a range of $-0.4 < X < 2.4$. However the most significant difference is in the density of values in the region close to $X = 0.6$. The single model realisations show distributions with high densities of values in the regions close to $X = 0.6$ and $X = 1.3$. The ensemble result reveals a comparatively less dense region near $X = 0.6$ with more ensemble members in the region close to $X = 1.3$.

Using data which is not consistent with the underlying forcings, as a pragmatic solution to limited computational capacity, is potentially misleading. Utilising model data points that are close in time to the interval of interest can yield inaccurate information about the statistical properties of a particular variable's climate distributions. Such discrepancies may be less obvious for a system which is not subject to complex changes in the behaviour of attractors associated with the system forcings but high-dimensional systems, such as the climate system, are unlikely to exhibit less complex behaviour than the highly idealised model considered here. The results demonstrated using the L84 model have implications for climate modelling relating to the interpretation of probabilistic estimates based on temporally averaged data in addition to those already discussed in relation to the ergodic assumption. These potential implications are discussed further in section 4.6.

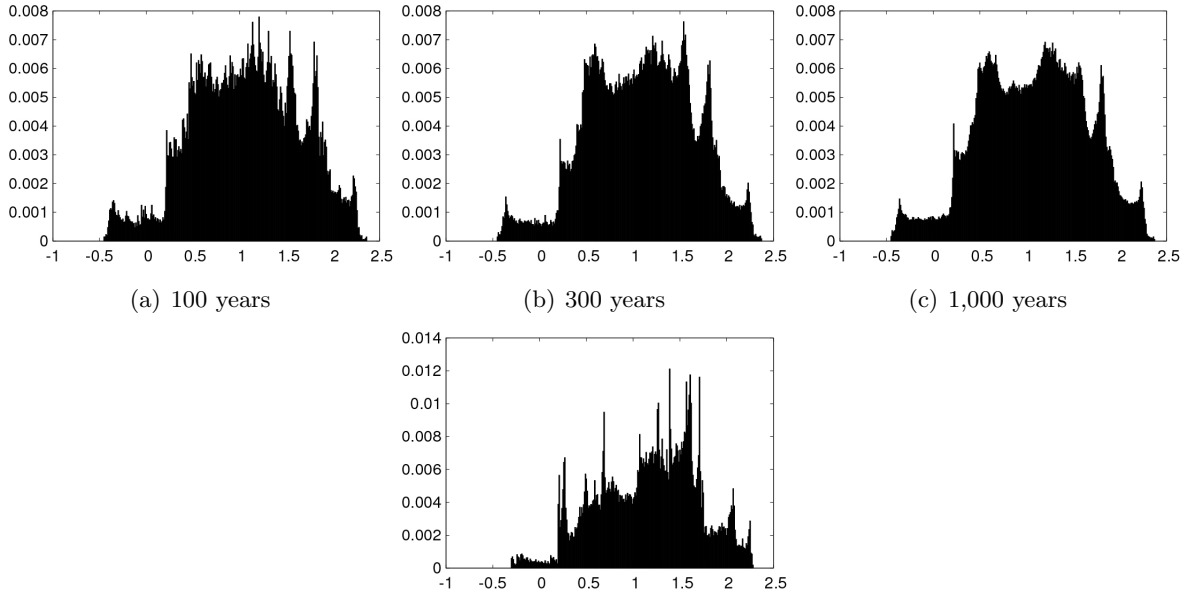

(a) 100 years (b) 300 years (c) 1,000 years

(d) Ensemble from fig. 4.19(d)

Figure 4.24: Normalised frequency distributions of the X variable for a single trajectory of the L84 model for consecutive month's of January after given simulation periods, (a) to (c), and a 100,000 member ensemble after 200 years (d), with seasonal F variations between $6 < F < 8$ and ICs: $(X, Y, Z) = (1.0, 1.0, 1.0)$. In each plot, the x-axis denotes the X variable and the y-axis corresponds to the frequency per occupied bin; bin width = 0.01.

The results presented in this section suggest that long multi-centennial simulations of a single model trajectory are required to establish a distribution of model states that accurately represents the climate distribution at a specific time of the year, given a seasonal variation in a key model parameter. Short sampling periods of a single model trajectory are unable to capture some of the large scale features of the IC ensemble distributions. Over longer simulation periods the number of sample points increases to provide improved estimates of the model's climate in both of the seasons investigated and the use of the ergodic assumption becomes less problematic.

For a number of variables in the climate system, even in the absence of long-term trends in the climate forcings, it seems likely that the distribution of system states will have irregular properties due to the numerous modes of internal variability which can affect atmospheric and oceanic circulation patterns on all spatial scales. Therefore, even if ergodicity is considered to be a valid assumption for the system over very long time scales, experiments with the L84 model suggest that a short sampling period of observations or model projection data may provide misleading estimates of the climate variable distributions associated with a particular forcing scenario.

When using climate models to investigate climate variability at a given spatial scale for decadal and multi-decadal predictions, long-term global and regional trends need to be acknowledged in both the design phase of modelling experiments and in communicating the model output

to the user community. In extending the analogy, the next section presents an analysis of the behaviour of the seasonally driven L84 model when subject to trends in the parameter F.

4.5 Introducing Trends into the L84 Model

Climate model projections support theoretical reasoning that as the world warms in response to anthropogenic emissions of GHGs, high latitude regions will warm at a faster rate than equatorial regions (Collins and Senior (2002), Masson-Delmotte et al. (2006)). As a consequence the average equator-to-pole temperature difference will decrease. In the L84 model, F represents the meridional temperature difference and in the seasonally driven L84 model, the value of F decreases in the summer. Consequently, introducing a trend towards lower values of F, as an analogy to the impact of global warming on the equator-to-pole temperature difference, will manifest itself in a change towards a more "summer-like" parameter configuration. Whilst no direct quantitative comparison can be made between the behaviour of the L84 model and the real climate system, understanding the impact of trends in the L84 model may yield qualitative insight into the predictability of the climate under climate change. Hence there is no *correct* specification for the magnitude and pathway of a trend in F to represent the GHG-induced radiative forcing. A number of different trends were therefore considered but the results of the L84 experiments presented here focus on a linearly decreasing trend in F.

4.5.1 Linear decrease in F

To introduce a linear trend in the parameter F, in the seasonally driven L84 model, another term is added to equation 4.4 so that F varies according to equation 4.5:

$$F \rightarrow F_m + M\cos\left((2\pi\frac{i}{K\tau^{-1}}) - \frac{\pi}{12}\right) + H\frac{i}{K\tau^{-1}} \tag{4.5}$$

where H is the average increase (or decrease when negative) in F per year and the other variables take the values given in section 4.4.

The time series of F, shown in figure 4.25, is applied to the L84 model. The oscillations during the first 30 years of the period remain unchanged but after 30 years, a linear decreasing trend is imposed where $H = -0.0\dot{2}$ (a decrease in F of 1 unit every 45 years) so that the mean value of F decreases from $F_m = 7$ to $F_m = 6$ at 75 years into the model simulation. The magnitude of the seasonal cycle is kept constant throughout the simulation period.

The ergodic assumption is examined for the L84 model with a linear trend in F. A large IC ensemble is run subject to the trend in F illustrated in figure 4.25. The 10,000 ensemble members are selected at the end of a 100 year ensemble run of the seasonally driven L84 model; the original 10,000 ensemble members were initiated from points along the transect described in section 4.3.2. The ICs generated span the range of the ensemble distributions that occur on January 1^{st}, where $F = 7.966$. The ICs that are used for the ensemble runs are displayed in figure 4.26.

Maintaining the focus on the mid-summer and mid-winter climates, the states of the IC ensemble members are examined in both mid-summer and mid-winter every 15 years over the 90 year

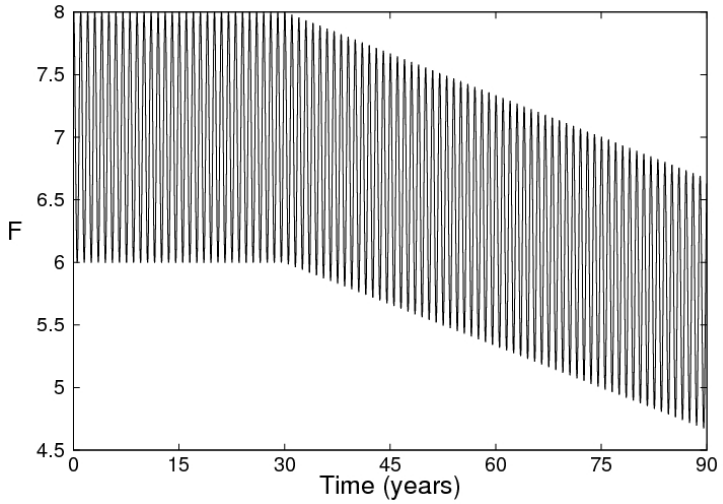

Figure 4.25: Time series in F over 90 year period with a linear decrease in F beginning after 30 years with a rate $H = -0.0\dot{2}$.

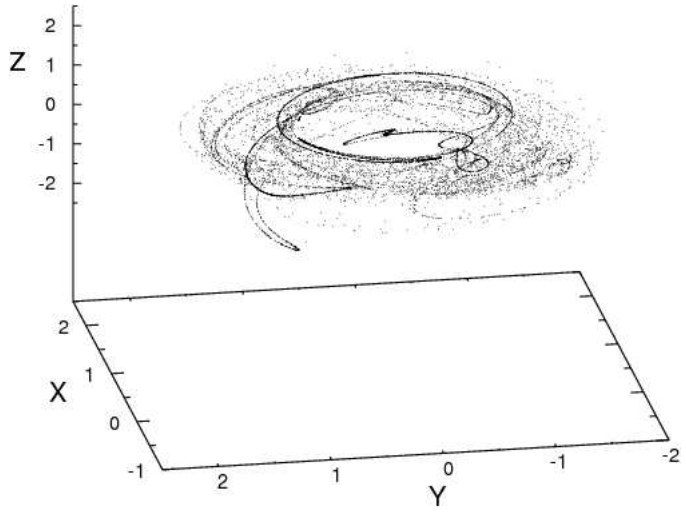

Figure 4.26: 10,000 ICs used for the ensemble model runs in section 4.5. Extracted from the output of a 100 year run of the seasonally driven L84 model with ICs originating from points spread evenly along a transect in the model state space from $(-1.0, -2.5, -2.5)$ to $(2.5, 2.5, 2.5)$

period (i.e. ensemble distributions observed at 15, 30...90 years). A single model trajectory is also run for the 90 year period and the state of the trajectory at each consecutive mid-summer and mid-winter time step is extracted. The IC ensemble frequency distributions taken at 15 yearly intervals are compared to the distribution of states from a 30 year sample of the single model trajectory, centred on the 15 yearly time instants. The results reveal the extent to which single model trajectory distributions capture the statistics of the IC ensemble distributions and support (or oppose) the ergodic hypothesis under a changing climate. Figure 4.27 shows the temporal evolution of the IC ensembles and the single trajectory distributions.

The left column of figure 4.27 shows the IC ensemble distributions at given years in the

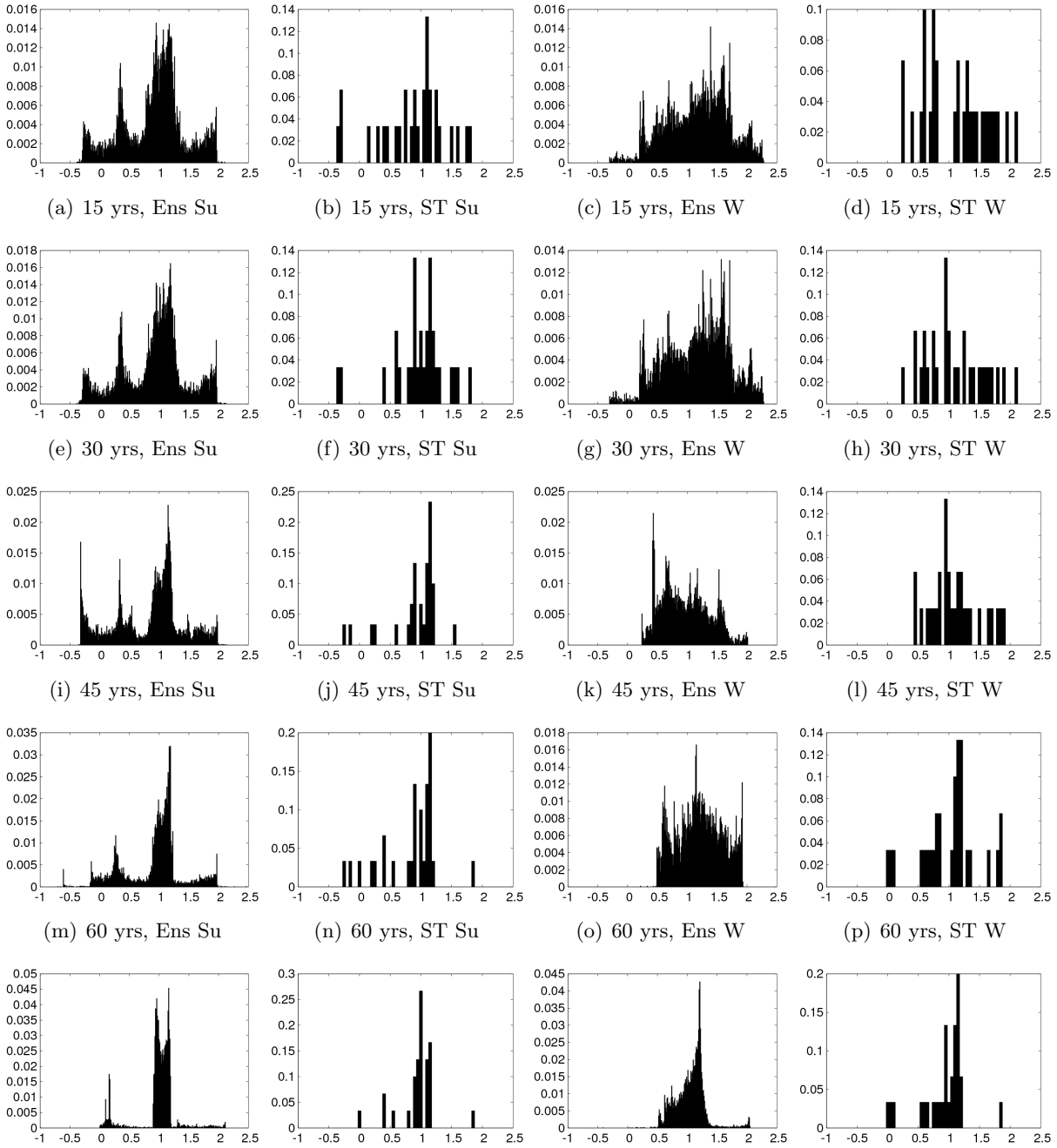

(a) 15 yrs, Ens Su (b) 15 yrs, ST Su (c) 15 yrs, Ens W (d) 15 yrs, ST W

(e) 30 yrs, Ens Su (f) 30 yrs, ST Su (g) 30 yrs, Ens W (h) 30 yrs, ST W

(i) 45 yrs, Ens Su (j) 45 yrs, ST Su (k) 45 yrs, Ens W (l) 45 yrs, ST W

(m) 60 yrs, Ens Su (n) 60 yrs, ST Su (o) 60 yrs, Ens W (p) 60 yrs, ST W

(q) 75 yrs, Ens Su (r) 75 yrs, ST Su (s) 75 yrs, Ens W (t) 75 yrs, ST W

Figure 4.27: IC ensemble and single trajectory normalised frequency distributions for the X variable in the seasonally driven L84 model when subject to a decreasing trend in F with $H = -0.0\dot{2}$. The first and third columns show the 10,000 member IC ensemble frequency distributions (Ens) after given time instants for mid-summer (Su) and mid-winter (W) respectively. The second and fourth columns show the equivalent distributions from 30 year samples centred on given time instants of a single model realisation (ST) initiating from $(1.0, 1.0, 1.0)$ in mid-summer and mid-winter respectively. In each plot, the x-axis denotes the X variable and the y-axis corresponds to the frequency per occupied bin; bin width = 0.01 for the ensemble distributions; bin width = 0.05 for the single trajectory distributions.

simulation period at mid-summer. In panels (a) and (e), the distributions are similar, which is unsurprising given that there is no trend in F during the first 30 years of the model simulation; the distributions therefore approximate the climate distribution of the seasonally driven L84 model in the X variable in mid-summer. Over time the value of F decreases, as shown in figure 4.25, and the ensemble distributions respond. The density of trajectories in the region close to $X = 1$ increases at the expense of the other regions illustrated in the subsequent plots shown in panels (i), (m) and (q). The second column shows the equivalent climate distribution estimates from 30 year samples of a single model trajectory centred on the given time instants. The distribution in panel (b) captures the range of X values reasonably well and shows a greater density in the modal region at $X = 1$, apparent in panel (a). However, due to the irregular nature of the climate distribution, a sample of 30 data points is too small to capture many of the key features of the ensemble distributions such as the secondary modal peaks. In panel (f), the single trajectory distribution suggests an increase in the probability of moving to the region close to $X = 1$. Whilst this is observed to occur in the ensemble distributions for decreased values of F, after 30 years the parameter values remain unchanged; the change observed in the single trajectory is presumably influenced by the inclusion of points in years 30 to 45 of the model integration. The distribution in panel (m) shows a non-negligible probability (0.6%) of a trajectory occurring at a value $X < -0.5$; a region which has previously not been visited. The corresponding single trajectory distribution in panel (n) does not have any density in this region and therefore using a single model trajectory, with a limited number of data points, to estimate the entire PDF and associated exceedance probabilities is potentially misleading.

The mid-winter comparison demonstrates additional pitfalls in using a single model realisation, as opposed to an IC ensemble distribution, to understand the climate of the L84 model. The (c) and (g) panels in the third column show the ensemble distributions for X after 15 and 30 years respectively when there is no trend in the seasonal cycle of F. Whilst the corresponding single trajectory distributions in panels (d) and (h) are fairly similar and do not change markedly, neither of the distributions resemble the ensemble distributions sufficiently to justify using a single model trajectory to provide reliable quantitative probabilistic information. After 60 and 75 years, the single trajectory distributions in panels (p) and (t) show density in the region close to $X = 0$ whilst in the ensemble distributions in panels (o) and (s) there is very little density below $X = 0.5$. Again, this is likely due to the inclusion of earlier years in the single trajectory distributions but could equally be due to a limited sample size. Being unable to distinguish without further analysis is an unhelpful feature of using single trajectory distributions to investigate the model climate.

The changes in the statistics of the climate distributions over time, which map the evolving geometry of the pseudo-attractor, are not smooth. The irregular nature of the distributions means that comparing the single trajectory approach to the IC ensemble approach using traditional statistical measures such as means and variances can produce misleading information. The KS test is employed once again and the corresponding ensemble and single trajectory distributions in figure 4.27 are compared over the 75 year period. The results for mid-summer

and mid-winter are given in figures 4.28(a) and 4.28(b) respectively. In general, the values of D are greater in the mid-winter comparisons than in the mid-summer comparisons. The values range from just below $D = 0.1$ to just below $D = 0.3$. This range is similar to that observed for the sample size of 30 points shown in figure 4.22 where the model evolves in the absence of a trend in F. It is not possible to conclude that the ergodic assumption becomes weaker in a climate change scenario based on these results alone. However, it is reasonable to conclude that a 30 year sample is insufficient to provide credible probabilistic information about the pseudo-attractor climate distributions.

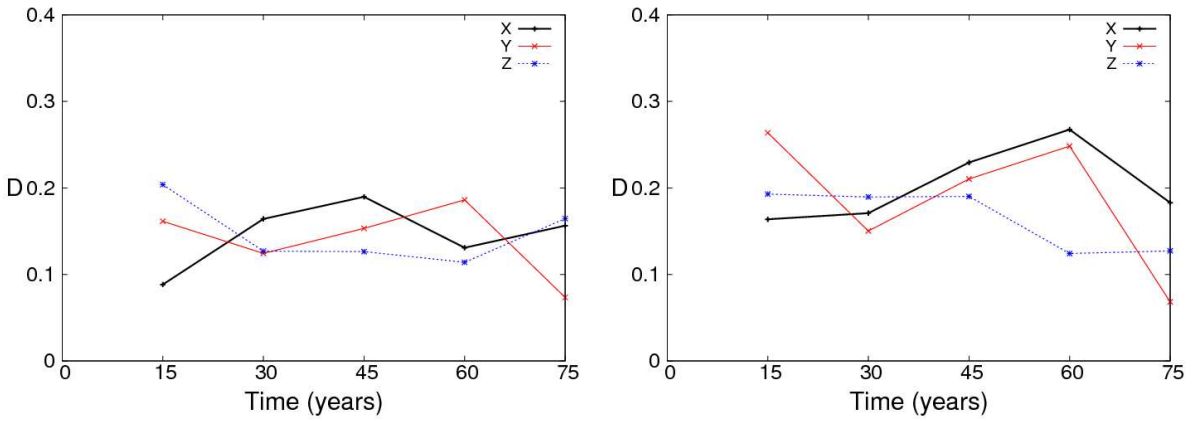

(a) Mid-summer

(b) Mid-winter

Figure 4.28: KS comparison between single trajectory distributions and respective IC ensemble distributions for the seasonally driven L84 model when subject to a trend in F (as shown in figure 4.25).

A major limitation of using a single model trajectory and invoking the ergodic assumption is that in creating a climatology, the data points used can span two or more very different underlying climates; effectively sampling different pseudo-attractors. Therefore the estimated probability distributions risk being misleading, even in the PMS. The implications of this for climate change impacts assessments are potentially important and are further discussed in section 4.6.

4.5.2 Influence of intransitivity on the L84 model under climate change

It is shown in section 4.4.3 that in the absence of a trend in the model's forcing, a 30 year sample is unlikely to be a long enough period to sample the irregular climate distributions associated with the seasonally driven L84 model. Furthermore, when a trend in the parameter F is introduced, section 4.5.1 demonstrates that relying on the statistics of a single model trajectory distribution is unsatisfactory as the changes in the geometry of the pseudo-attractor are not smooth, even with a linear trend in F. Additional experimental results with the L84 model reveal another reason why it is necessary to consider an ensemble of initial states, as opposed to a single model trajectory, when assessing the impact of climate change on the dynamic behaviour of the L84 model.

As the variation in F shifts towards lower values, model trajectories become exposed to qualitatively different regions of parameter space that are associated with intransitive behaviour (for fixed values of F). In an extension of the experiment outlined in section 4.5.1, the value of F is subject to a linear decreasing trend between 30 and 75 years but is then held constant at $F_m = 6$ for the following 75 years. The associated time series in F is illustrated in figure 4.29.

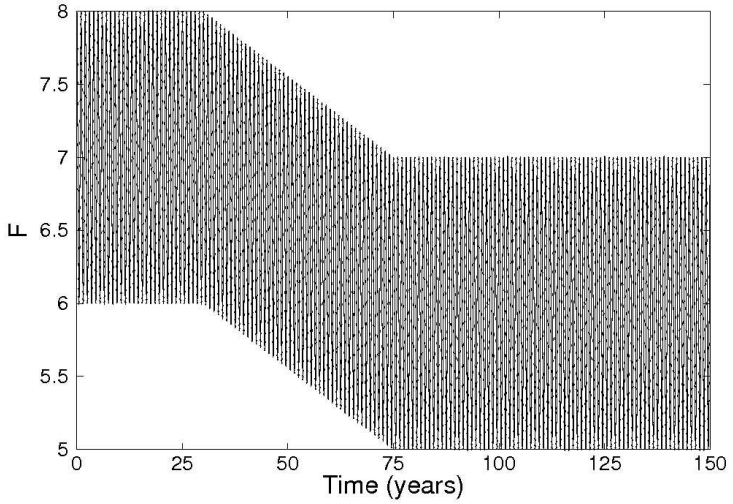

Figure 4.29: Time series in F over a 150 year period with a linear decrease between 30 and 75 years ($H = -0.0\dot{2}$) from $F_m = 7$ to $F_m = 6$.

When the IC ensemble illustrated in figure 4.26 evolves according to the changing parameter F shown in figure 4.29, after 75 years the vast majority of the IC members display constrained periodic oscillations associated with a pseudo-attractor (hereafter PA1, illustrated in figure 4.31) at the altered parameter setting, where $F_m = 6$ (with $M = 1$). However, there are a number of IC members that appear to be outliers in the decades after the trend in F has ceased. Figure 4.30 shows the evolution of three individual model trajectories over the 150 year simulation period. The time series in figure 4.30(a) shows the trajectory associated with the first member of the 10,000 member IC ensemble which displays behaviour that is typical of the majority of ensemble members. Initially, the trajectory demonstrates intermittency transitioning between periodic and aperiodic cycles spanning the range $-0.6 < X < 2.4$. This behaviour continues for the first 65 years of the model integration. During the latter part of the time series, when F_m is held constant, the trajectory displays dampened periodic oscillatory behaviour propagating in the range $0.5 < X < 1.5$ with the highest density of values in the range $0.9 < X < 1.2$. The time series' shown in figures 4.30(b) and 4.30(c) illustrate alternative model responses that are observed. At approximately 70 years into the model integration, as the trend in F approaches the new value of F_m, the two trajectories appear to develop according to a different, seemingly coexistent pseudo-attractor (hereafter PA2). The range of values is predominantly confined to the region $-0.3 < X < 1.9$ with occasional departures that extend to values close to $X = -0.5$ and $X = 2.5$. The results suggest that the model has two coexisting pseudo-attractors when

$F_m = 6$ and the model trajectories exhibit long-term memory of the initial state dictating the pseudo-attractor to which each trajectory evolves. PA1 appears to be a stable pseudo-attractor of the seasonally driven L84 model for $F_m = 6$ whilst PA2 is an unstable pseudo-attractor as all trajectories are observed to transition to PA1 over time (quantitative analysis presented in section 4.5.3).

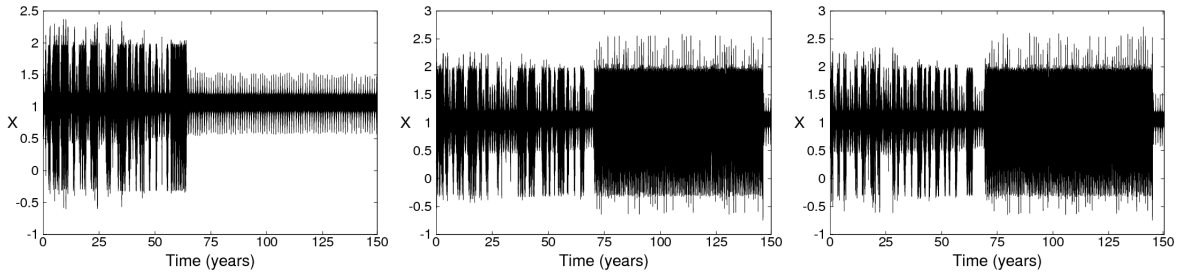

(a) IC member 1 (b) IC member 1099 (c) IC member 2054

Figure 4.30: Single trajectory results for the seasonally driven L84 model when subject to a parameter change given in figure 4.29, for given members of the IC ensemble.

The geometric properties of PA1, associated with the seasonally driven L84 model in the new climate regime where $F_m = 6$, are illustrated in figure 4.31. A single model realisation is run for one year starting from an IC on PA1. The resulting trajectory is shown in the X-Y, X-Z and Y-Z planes. The trajectory consists of a collection of ellipses which are reasonably well constrained in the X dimension and lie approximately parallel to the Y-Z plane. The plots are very similar to those shown for permanent summer conditions in figure 4.5 implying that PA1 consists of solutions which are modulations of the ellipse-like attractor, $A2$, observed when F is held constant at $F = 6$.

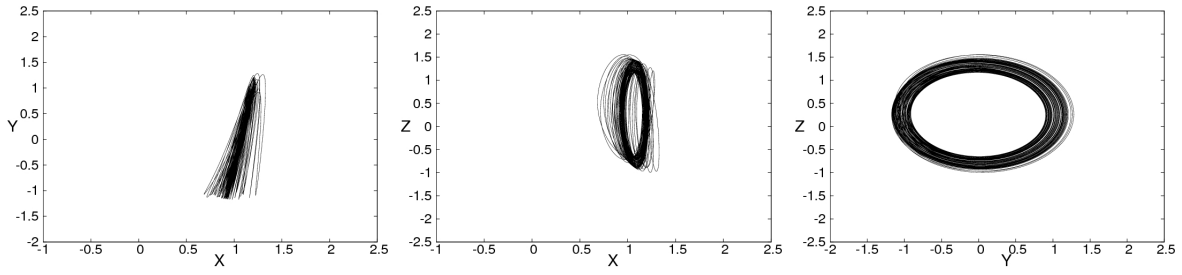

(a) X-Y Plane (b) X-Z Plane (c) Y-Z Plane

Figure 4.31: Pseudo-attractor, PA1, for the seasonally driven L84 model (with $M = 1$ and $F_m = 6$) for the X-Y, X-Z and Y-Z planes. The trajectory is run for one year beginning on January 1st with ICs $(0.90, -0.75, -1.19)$.

4.5.3 Memory of IC location

In this section the time scale at which trajectories evolving on PA2 transition to PA1 is investigated. A large IC ensemble is run for a 500 year simulation period under permanent summer conditions. The IC ensemble consists of 10,000 members spread evenly along a transect in the model state space, from $(-1.0, -2.5, -2.5)$ to $(2.5, 2.5, 2.5)$. The frequency distributions at the end of the 500 year simulation are given in figure 4.32 for each of the model variables in mid-summer and mid-winter. The range of X values in mid-summer and mid-winter is $0.64 < X < 1.35$ and $0.90 < X < 1.21$ respectively. The ranges of model states are therefore consistent with the ranges displayed in figure 4.31 suggesting that after a period of 500 years all 10,000 trajectories have transitioned towards PA1, which is intransitive and non-chaotic.

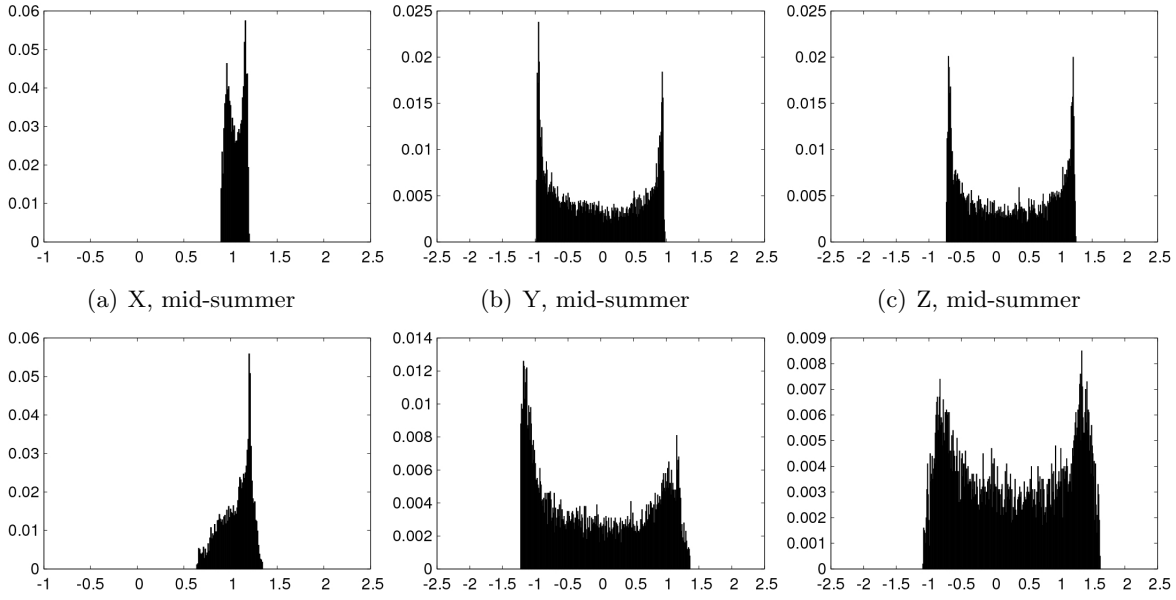

(a) X, mid-summer (b) Y, mid-summer (c) Z, mid-summer

(d) X, mid-winter (e) Y, mid-winter (f) Z, mid-winter

Figure 4.32: Normalised frequency distributions of a 10,000 member IC ensemble for the seasonally driven L84 model in mid-summer, (a) to (c), and mid-winter, (d) to (f), after a 500 year simulation with $M = 1$ and $F_m = 6$. In each plot, the x-axis denotes the X variable and the y-axis corresponds to the frequency per occupied bin; bin width = 0.01.

An extension of the experiment outlined in section 4.5.2 is performed to determine the rate at which the IC ensemble converges towards the distribution of model states consistent with PA1. When subject to the trend in F implemented in section 4.5.2, the percentage of trajectories originating from the IC ensemble (shown in figure 4.26) that fall outside the identified ranges in X for mid-summer and mid-winter consistent with PA1 (as shown in figure 4.32) are determined over the period from 75 years to 125 years. After the instant at 75 years in which the trend in F stops, if a trajectory from the ensemble lies outside the identified ranges for the X, it is assumed that the trajectory is evolving on PA2. Of course, at any given time a trajectory evolving on PA2 may pass through the range associated with PA1 so the estimated percentage

of trajectories on PA2 is an underestimate. However, the rate at which trajectories converge to PA1 can still be estimated given the rate of change in the relative number of trajectories inside and outside the ranges.

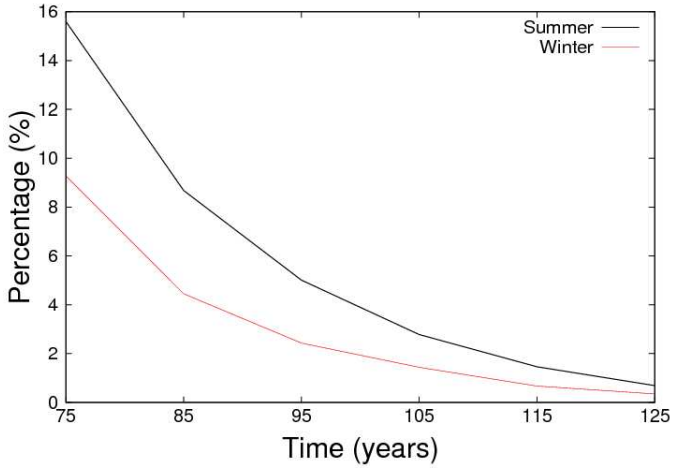

Figure 4.33: Percentage of trajectories from the IC ensemble shown in figure 4.26 not yet evolving on PA1 following the stabilisation of F at $F_m = 6$, consistent with the trend in figure 4.29.

Figure 4.33 shows the combined percentage of trajectories above and below the specified ranges in X identified for PA1 over a 50 year period following stabilisation of the trend in F at $F_m = 6$. Typically more ensemble members are found below the minimum values of $X = 0.9$ in mid-summer and $X = 0.64$ in mid-winter than above the upper thresholds of $X = 1.21$ and $X = 1.35$ respectively. The percentages are systematically greater during mid-summer, largely because the range of values associated with PA1 during mid-summer is smaller than the range associated with PA1 during mid-winter. The plots show exponential-like decreases in the percentage of ensemble members continuing to evolve on PA2. However, even 50 years after the altered parameter configuration has become established, not all trajectories have transitioned to PA1 suggesting multi-decadal memory in the L84 model under altered parameter conditions.

In the analogy to modelling of the climate system, it is pertinent to ask what relevance such results have for predicting climate change. In addition to the arguments previously set out for invalidating the ergodic assumption, the results suggest that the behaviour of single model trajectories from different initial states can differ considerably when the system is forced into a region of parameter space containing coexisting stable (and unstable) pseudo-attractors. The frequency distributions associated with the single trajectories can therefore only sample a subset of the possible climate states consistent with the forcing under a particular climate change forcing scenario. In the seasonally driven L84 model under transient parameter changes, the emergence of alternative model trajectory responses only became evident when running large IC ensembles. It is therefore important to account for the potential long-term memory of the initial state of the system when predicting climate change by implementing large IC ensemble experiments.

4.6 Implications for Climate Prediction

In analysing the experiments conducted with the L84 model, it is immediately apparent that despite the model's low dimensionality, the model displays enormously rich and interesting dynamic behaviour. The analysis presented in this chapter suggests that understanding and ultimately predicting the evolution of a nonlinear system's climate becomes more challenging when dealing with time-varying parameters. The following discussion relates the issues identified using the L84 model to the predictability of the climate system under climate change. The discussion focusses on three themes which are addressed in this chapter; the coexistence of attractors, the ergodic assumption and the long-term memory of the initial state.

4.6.1 Coexisting attractors

The coexistence of attractors presents significant problems for prediction in nonlinear dynamic systems. If the climate system has coexisting attractors then it is pertinent to ask whether or not IC uncertainty, which has previously been considered relatively unimportant for long-term climate prediction (Cox and Stephenson (2007), Hawkins and Sutton (2009)), impedes the accurate prediction of future climate states using existing climate model experimental designs. Whilst a definitive answer regarding the potential of the climate system to have two or more coexisting attractors is currently elusive, scientists have inferred the possibility of coexisting climate regimes using insights from palaeoclimatology. Over four decades ago, Budyko (1969) stated:

> "With the present distribution of continents and oceans the existence of two climatic regimes is possible: one of which is characterised by the presence of polar ice and large thermal contrast between the pole and equator, and the other by the absence of glaciation and small meridional mean gradient of temperature."

To link the possibility of the coexisting regimes identified by Budyko (1969) to the coexistence of climate attractors is speculative. However in considering the potential for the climate system to exhibit multistability on a number of spatial and temporal scales, the notion of coexisting attractors is a relevant and useful concept. The experiments with the L84 model have highlighted some of the nuanced behaviour that can exist in a system displaying both transitive and intransitive behaviour associated with a single attractor and multiple coexisting attractors respectively.

In section 4.2.3, two coexisting attractors are illustrated for permanent summer parameter forcings and figure 4.6 shows the complicated structure of the basins of attraction. Given uncertainty in the initial model state, the results show that estimating the probability of a trajectory propagating to one of the two attractors, requires a detailed exploration of the model state space.

Recently, Freire et al. (2008) used bifurcation analysis to report phase diagrams of the L84 model which reveal highly complex behaviour and unlike the basins of attraction shown in figure 4.6, the Freire et al. (2008) study shows regions of parameter space where the basins of attraction contain up to *four* coexisting attractors. The authors conclude that the precise tuning of parameters is paramount in establishing the number of coexisting attractors in the L84 model. In addition, both Lorenz (1990) and Freire et al. (2008) suggest that the basins of attraction are complicated with the latter study referring to "foliated" structures, suggesting the presence of the Wada property. Whilst the L84 model does not strictly possess the Wada property in permanent summer conditions (when $F = 6$), the basins of attraction have a complicated structure inevitably influencing the convergence of IC ensemble distributions and single trajectory distributions. The Wada property is similar to an even more daunting concept for climate modellers, "riddled basins", which refer to basins of attraction which are "so densely intertwined that it may be virtually impossible to determine the final state" (Viana et al. (2009)). The combination of coexisting attractors, the number of which can be highly sensitive to parameter choice, and the prospect of riddled basins, or the Wada property, which ensures that the attractor to which a trajectory evolves is sensitively dependent on the initial state, presents a problematic situation for the climate modelling community.

Pseudo-attractors

In section 4.4, the L84 model is subject to smooth variations in the forcing parameter F. The consequence is to impose regular transitions between chaotic and non-chaotic regions of parameter space. The seasonal cycle investigated ($6 < F < 8$), effectively created a "pseudo-attractor" which is ultimately transitive, as all points in the pseudo-attractor state space are visited over a long integration period (see section 4.4.2). The ensemble distributions for mid-summer and mid-winter, with a seasonal cycle in F, are shown to be different to the permanent summer and permanent winter ensemble distributions. In the climate system, we may expect chaos to be a permanent feature of the atmospheric circulation throughout the year but the impact of a continuously changing forcing may well alter the geometric properties of any climate attractor. Therefore the concept of a pseudo-attractor may be more apt in the analogy to climate change; a significant change in the geometry of the system's pseudo-attractor would indicate a change in climate.

An extension of the possibility for coexisting attractors would be the coexistence of pseudo-attractors. It is observed that multiple pseudo-attractors coexist (albeit temporarily) following the transient phase of the experiment in section 4.5.1. Once the final parameter conditions are established, and the F parameter oscillated between $5 < F < 7$, there is evidence of two coexisting pseudo-attractors (PA1 and PA2), which initially appeared intransitive over the following decades for certain ensemble members. The observation of long-term memory in the forced L84 model stresses the importance of adequately representing IC uncertainty to generate robust distributions for model variables under altered forcings. Further discussion of

the memory in the L84 model is given in section 4.6.3.

4.6.2 The ergodic assumption: lessons from L84

For a chaotic transitive system the ergodic assumption is valid, as shown in the L63 model with conventional fixed parameter values and demonstrated in section 4.3.2 for the L84 model evolving under permanent winter parameter conditions. The convergence of the single trajectory distributions to the IC ensemble distributions is fairly rapid and only requires a simulation period of a few months (see section 4.3.3). In permanent summer conditions however, the ergodic assumption is inappropriate. As the system is non-chaotic and two periodic attractors coexist, the intransitive behaviour of the model means that the ensemble distributions incorporate regions of state space that are not observed for individual single trajectories.

Further experiments with the L84 model demonstrated that ergodicity is not observed when using data that is inconsistent with the underlying parameter conditions. In section 4.4.3, the seasonally driven L84 model is investigated and the time scale at which the frequency distributions of a single model trajectory converged to the IC ensemble distributions is estimated to be on the order of a few hundred years under fixed parameter conditions (with one data point used per year). Distributions from shorter simulation periods do not converge to the ensemble distributions. In an attempt to speed up the convergence time, additional data from all time steps in January and July are included in the single trajectory distributions for winter and summer respectively. The distributions, given in section 4.4.4, do not fully converge to the IC ensemble distributions centred on mid-winter and mid-summer. The reason for the discrepancies is that the single trajectory distributions include data points which are never observed at mid-winter and mid-summer. Incorporating data from time instants in which the parameter fluctuations differ to those at the time of interest risks producing misleading PDFs of the model climate.

The active use of the ergodic assumption, as an alternative to running large IC ensembles, may be founded in a belief that climate variability, at a particular scale of interest, is insensitive to the forcing scenario and any change in the distribution of a particular variable is likely to be smooth in time. In section 4.5.1, a linear trend in F is imposed on the seasonal cycle in F. The IC ensemble distributions illustrated in figure 4.27 change dramatically over the 45 years in which the trend is present. Whilst the single trajectory distributions also change over the period, the changes are not always consistent with the ensemble distributions. This is partly caused by a limited sample of data points but is also a consequence of including data from instances when the model trajectory is evolving towards different attractors. The former point is simply a statistical problem pervasive across all domains of science but the latter point has specific significance to climate modelling. If the attractor (or pseudo-attractor) associated with the climate system changes in an irregular fashion, then any PDF that is derived from a time-averaged distribution of a single model trajectory will be fundamentally flawed. The resulting probabilities will therefore be misleading and estimates of threshold exceedance will be

incorrect; an important consideration for the adaptation user community (particularly insurers) when utilising climate model output.

As described in section 4.5.1, the ergodic assumption is invalid when simulating a change in climate from transitive to intransitive model behaviour. If the future climate scenario consists of a pseudo-attractor that is transitive and varies smoothly in response to a trend in a climate forcing, then the ergodic hypothesis would not necessarily fail. The ergodic assumption would remain valid for a time series in which variability about some mean value is stationary over time but in the context of a changing climate, particularly at regional scales where changes are often nonlinear and abrupt, the stationarity of climate variability under climate change is unlikely. In relating the concepts explored in this chapter to climate prediction, an important question that arises is whether or not we expect the distribution of climate (inexorably linked to climate variability) to vary smoothly and predictability over time in response to an external forcing. If not, then the results in this chapter suggest that climate model experiments must take account of IC uncertainty to explore the changing geometry of climate distributions consistent with the climate's pseudo-attractor(s).

4.6.3 Memory of ICs

There is inevitable uncertainty in the observable initial state of the atmosphere-ocean system. In developing climate change adaptation strategies, it is advantageous to know the full range of possible future states of the climate. Therefore, even if different model trajectory ICs evolve towards different attractors consistent with a future forcing scenario, it is important to know the range of plausible future states conditioned on the current uncertainty in the initial state. In examining the sensitivity of the climate to the uncertainty in the initial state, the notion of system memory therefore becomes a relevant consideration. In seeking predictive skill, knowing the time scale over which uncertainty in the initial state is lost can provide climate modellers with a time horizon for the extent of successful climate prediction, over and above considering all states which are plausible given certain forcing scenarios.

By initially considering intransitive behaviour with the L84 model in parameter regions not exposed to chaos, it was demonstrated that knowledge of the initial state is crucial in estimating the model climate. If the climate system, or sub-systems of the climate system, are exposed to the possibility of intransitive coexisting (pseudo-)attractors, then single model realisations will only ever sample one (pseudo-)attractor. In section 4.3.3, it is shown that during permanent summer conditions, the convergence of ensembles is affected by memory of the ICs. The future distribution of states associated with a single model trajectory is entirely determined by the initial state of the model. An IC ensemble approach to predicting the model's climate would therefore generate distributions that span more than one coexisting climate, provided the ICs cross the boundaries of the basins of attraction. Therefore, if there is uncertainty in the initial state, there is a danger in relying on the variability of a single model realisation to inform on the range of future possible model states.

In creating an analogy to climate change, the analysis presented in section 4.5 focusses on the impact of a linear trend in F that moves the model into a more summer-like configuration. As referred to in section 4.6.1, in the new climate where $F_m = 6$ the model shows memory of the ICs which extended over many decades. Over time all trajectories evolve towards PA1 but temporarily some trajectories evolve on PA2. The existence of long-term memory exhibited by certain trajectories in the L84 model suggests that in transitioning to a new climate, trajectories can become trapped in an apparently anomalous pattern. In estimating the probabilities associated with the model, it would therefore be misleading to consider only one (or a few) model realisations. Clearly, unanticipated behaviour can result when model parameters or system forcings vary in time. In modelling the climate system, using IC ensembles might help to elicit possible dynamic behaviour that results from different ICs and guide the suitable extraction of quantitative probabilistic information from climate model output.

The parameter space explored in section 4.5 is subject to intransitive, non-chaotic behaviour. It is therefore sensible to determine what relevance such an exercise can have for the real climate system which is known to display chaotic behaviour. As an example, one could consider the potential for regional climates to display intransitivity. Certain feedbacks in the climate system have the potential to lead to intransitive behaviour and one could argue that certain feedbacks are highly sensitive to the initial state of the atmosphere-ocean system. For example, in certain regions of the world which are highly sensitive to the hydrological cycle, rainforest conditions are potentially coexistent with savannah conditions. An example where much research has recently been focussed is the destabilisation of regions of the Amazon rainforest in response to future climate change and deforestation (Betts et al. (2008)). Therefore when projecting the impacts of climate change as a response to altered forcings, it is not irrelevant to consider the potential consequences of intransitive behaviour. A related concept which is explored in the following chapter is almost-intransitivity; a feature of a dynamical system which is ultimately transitive but displays long-term IC-dependent behaviour. The relation of almost-intransitivity to memory and climate predictability is considered in the analysis presented in chapter 5 using the L84 model coupled to the Stommel ocean box model (Van Veen et al. (2001)).

4.6.4 Conclusions from the L84 experiments

So what do the results of the L84 experiments reveal about the predictability of the climate system and what lessons are there for the climate modelling and adaptation communities? Ultimately, the L84 model results suggest that no climate change modelling exercise is complete without fully taking into account uncertain ICs. The experiments conducted with L84 model suggest that ignoring the impact of nonlinearities in the climate system, and their interaction with time-varying parameters, could lead to a distorted view of climate change. The concept of a pseudo-attractor can help to conceptualise the dynamic behaviour of a time-dependent system undergoing change in response to changes in external forcings.

The results in the L84 model have focussed on the PMS. In the IMS, ensemble methods

sometimes account for uncertainty by perturbing parameters. However, an ensemble modelling approach based on sampling parameter uncertainty without accounting for IC uncertainty, and relying on the data from single model realisations, risks providing misleading information which doesn't take into account the potential memory of the initial model state. Results with the L84 model suggest that without fully assessing the consequences of uncertainty in the initial state, it is difficult to generate relevant quantitative information about the future state of the climate system for decision makers.

Chapter 5

The LS84 Model

5.1 Understanding Climate in a Simple Atmosphere-Ocean Model

As described by Palmer (1993), and highlighted in chapter three, the L63 model evolves with two characteristic time scales: the oscillation time around the regime (or lobe) centroids, and a residence time within each regime (or lobe) of the model attractor. Similarly, the L84 model is characterised by the time spent orbiting the primary lobe of the attractor (denoting westerly motion) and the frequency of transitions to the secondary lobe (denoting easterly motion). For conventional parameter values, both systems have been shown to display transitive behaviour with regular transitions between attractor lobes. In addition, the L84 model exhibits intransitive behaviour for particular values of F (e.g. when $F = 6$). In the L63 and L84 models, the regularity of regime and lobe transitions occurring in transitive regions of parameter space ensures that the model attractors are reasonably well explored by observing single model trajectories over relatively short time scales (see sections 3.3.2 and 4.3.1). Ergodicity is therefore observed in the L63 and L84 models (in the absence of climate change and nonlinear parameter fluctuations) using relatively short single trajectory simulations, as demonstrated in the numerical experiments presented in section 3.3.3 for the L63 model and section 4.3.3 for the non-seasonally driven L84 model.

In developing the analogy to the climate system and considering the time scales of interest for climate change adaptation, it is important to acknowledge the existence of internal climate variability which can occur on long as well as short time scales. Long-term internal climate variability occurs because the climate system is sensitive to changes in subsystems (such as the ocean, cryosphere and biosphere) which evolve on very different time scales to the atmosphere. Consequently, investigation of a coupled system consisting of two components evolving on different time scales is a valuable and necessary endeavour to further develop understanding of the role of IC uncertainty in climate change prediction.

On the time scales of interest for climate change adaptation (primarily decadal to multi-decadal) one of the dominant sources of internal climate variability is the ocean (Manabe and Stouffer (1996)). Modes of variability such as El Niño Southern Oscillation (ENSO), the Pacific Decadal Oscillation (PDO) and the Atlantic Multidecadal Oscillation (AMO) are driven by the nonlinear dynamic interactions of the ocean and atmosphere which affects global and regional weather patterns (Anderson and Willebrand (1996), Ghil (2002) and Delworth et al. (2007)). Furthermore, the heat content and thermal inertia of the ocean is a key factor in determining the rate and extent of climate change. Accounting for the impact of the oceans (in addition to other slowly evolving climate drivers) on present and future climate is therefore key to the success of climate model experiments designed to aid climate change adaptation.

In this chapter, the role of IC uncertainty in climate prediction is investigated in relation to internal climate variability induced by the interaction of subsystems operating on different dynamic time scales. The obvious limitation of investigating this issue with operational GCMs, aside from model inadequacy and lack of process understanding for key modes of variability (Huang et al. (2004)), is the expense and computational demands of running large IC ensembles. Therefore, this chapter will present the theoretical case for adequately sampling IC uncertainty using a simple system considered analogous to the climate system, in the perfect model scenario (PMS).

The experiments presented in this chapter are conducted with a simple coupled model developed by Van Veen et al. (2001) (referred to as the LS84 model) combining the L84 model with the much studied Stommel-61 (S61) ocean box model. The L84 component of the coupled model evolves on a relatively fast time scale compared to the S61 model. Consequently, the L84 model is considered analogous to the atmospheric component, and the S61 model represents the more slowly evolving ocean component. The dynamic evolution of the model variables are described further in section 5.2.

In section 5.2, the LS84 model is described and the parameter transformations from the uncoupled L84 model are outlined. This section also shows the geometry of the LS84 model pseudo-attractor by illustrating a single model trajectory in the atmosphere (L84) and ocean (S61) variables. Section 5.3 details the evolution of the LS84 model climate distributions from both a single trajectory and IC ensembles for two types of atmosphere-ocean coupling referred to as "active" and "passive" coupling (described in section 5.2). The ergodic hypothesis is investigated by comparing single trajectory distributions to ensemble distributions and the time scale of convergence for model distributions is elicited. Section 5.4 investigates the use of IC ensembles to inform probabilistic assessments of the model climate. The almost intransitive[1] nature of the model (under passive coupling) is exploited to estimate the probability of transitions between model regimes. The memory of ICs is explored in section 5.5 by comparing convergence rates of model distributions for IC ensembles initiating from different regions in the pseudo-attractor state space. In section 5.6, the LS84 model is investigated when subject

[1]See definition provided in section 2.1.4 and in the glossary.

to forced transient changes in key model parameters. The behaviour of both single model trajectories and IC ensembles are explored and the results are linked to the use of the ergodic assumption in climate change projections. Finally, the results of the experiments conducted with the LS84 model are discussed in section 5.7 and are related to the issues of climate prediction, under altered forcing conditions, for a system which displays dynamic behaviour dependent on the boundary conditions.

5.2 The LS84 Model

5.2.1 Coupling L84 to the S61 model

In extending the use of simple models as analogies to the climate system, the S61 model is utilised to represent the ocean component in a simple coupled atmosphere-ocean model. As described in section 2.4.3, the S61 model was developed by Henry Stommel in 1961 to demonstrate the impact of two important ocean variables which influence sea-water density and drive the circulation of ocean currents; namely temperature and salinity (Stommel (1961)). In essence, the two-box model is a simple representation of the thermohaline circulation (THC) showing the direction and intensity of the flow governed by the temperature and density differences between two ocean "vessels". Despite its simplicity, oceanographers and climate researchers continue to study versions of the S61 model to gain insight into the THC and the dynamics of the ocean-atmosphere system (Hearn (1998), Lohmann and Scheider (1998) and Wunsch (2005)). The presence of multiple equilibria, stable (and unstable) model states and the existence of hysteresis in the S61 model have led scientists to examine the results from the model in relation to more complex GCMs (Prange et al. (2002)). Of course, in such an idealised model, there are a number of assumptions which limit the model's realism. For example, the assumption that each ocean box (or vessel) is well mixed is particularly crude as the vertical gradient in ocean temperature can be considerable, especially in the tropics (Pacanowski and Philander (1981)).

The S61 model equations used by Van Veen et al. (2001) are given in equations 5.1 to 5.3:

$$\dot{T} = k_a(T_a - T) - |f(T,S)|T - k_w T \tag{5.1}$$

$$\dot{S} = \delta - |f(T,S)|S - k_w S \tag{5.2}$$

$$f = \omega T - \epsilon S \tag{5.3}$$

where T is the equator-to-pole temperature difference ($T_e - T_p$), S is the equator-to-pole salinity difference ($S_e - S_p$) and f is the strength of the THC in sverdrups (Sv). The units for T are in degrees Kelvin (K) and the units for S are in practical salinity units (psu). When f is positive (temperature driven), the surface flow is poleward and the return (deep) flow is equatorward. When f is negative (salinity driven) the situation is reversed and the surface flow is equatorward whilst the return (deep) flow is poleward. For certain parameters, both possibilities occur as stable solutions in the S61 model (Stommel (1961)). T_a is the inhomogeneous forcing by solar heating and δ is the coefficient of atmospheric water transport. k_a is the coefficient of heat exchange between the ocean and atmosphere, k_w is the coefficient of internal diffusion and ω and ϵ derive from the linearised equation of state.

In coupling the L84 model equations (given in equations 4.1 to 4.3) to the S61 model, Van Veen

et al. (2001) introduced a number of transformations, which are shown in equations 5.4 to 5.7:

$$F \rightarrow F_0 + F_1 T \tag{5.4}$$
$$G \rightarrow G_0 + G_1(T_{av} - T) \tag{5.5}$$
$$T_a \rightarrow \gamma X \tag{5.6}$$
$$\delta \rightarrow \delta_0 + \delta_1(Y^2 + Z^2) \tag{5.7}$$

where F_0 is a reference value for the equator-to-pole temperature difference in the atmosphere, G_0 is a reference value for the land-sea temperature difference, F_1 and G_1 are the coupling parameters to the ocean and T_{av} is the mean surface temperature difference between the equatorial and polar boxes. γ is the proportionality constant between the westerly wind strength and inhomogeneous forcing by solar heating (T_a). The parameter δ_0 is the reference coefficient of the atmospheric water transport and δ_1 is a measure for the rate of water transport through the atmosphere.

The coupled LS84 model is therefore given by the following equations:

$$\dot{X} = -Y^2 - Z^2 - aX + a(F_0 + F_1 T) \tag{5.8}$$
$$\dot{Y} = XY - bXZ - Y + G_0 + G_1(T_{av} - T) \tag{5.9}$$
$$\dot{Z} = bXY - XZ - Z \tag{5.10}$$
$$\dot{T} = k_a(\gamma X - T) - |f(T,S)|T - k_w T \tag{5.11}$$
$$\dot{S} = \delta_0 + \delta_1(Y^2 + Z^2) - |f(T,S)|S - k_w S \tag{5.12}$$
$$f = \omega T - \epsilon S \tag{5.13}$$

where X, Y, Z, a and b assume their definitions given in section 4.2.1. Table 5.1 shows the values of the constants used in the Van Veen et al. (2001) study, which have been adopted for the experiments conducted in this thesis. For these values, the atmosphere evolves on a time scale approximately one thousand times faster than the ocean (Roebber (1995)).

Constants	Value
G_0	1
a	0.25
b	4
T_{av}	30
γ	30
k_w	$1.8 \cdot 10^{-5}$
k_a	$1.8 \cdot 10^{-4}$
ω	$1.3 \cdot 10^{-4}$
ϵ	$1.1 \cdot 10^{-3}$
δ_0	$7.8 \cdot 10^{-7}$
δ_1	$9.6 \cdot 10^{-8}$

Table 5.1: Constants used in the LS84 model (Roebber (1995), Van Veen et al. (2001)).

In the L84 model, the seasonal variation in F is given as a sinusoid over one model year, according to equation 4.4, with a maximum in mid-winter (where the equator-to-pole temperature difference is greatest) and a minimum in mid-summer. In order to maintain the analogy to the climate system and provide continuity from the previous chapter, the version of the L84 model used in the coupled system also includes a seasonal variation in F. However, in the LS84 model F is replaced by $F_0 + F_1 T$, as shown in equation 5.4. The sinusoidal variation given by equation 4.4 is therefore imposed on the reference value F_0. Because of the continuous perturbation to F_0 by the addition of the term $F_1 T$, the behaviour of the L84 component in the coupled model is always different to the uncoupled model, for non-zero values of T.

The quantitative results and subsequent model interpretation presented in this thesis are an extension of the results presented by Van Veen et al. (2001) which focusses investigation on the system with a constant equator-to-pole temperature difference, $F_0 = 8$. Van Veen et al. (2001) demonstrate that when $F_0 = 8$ the "fast variables" (L84 variables) show intermittent behaviour which is a result of the slow-varying ocean variables continually moving the system through a series of bifurcations. It is shown in section 4.2 that intermittent behaviour is also present in the uncoupled seasonally driven L84 model, where the seasonal cycle in F induces transitions from chaotic behaviour in mid-winter to alternative types of non-chaotic behaviour in mid-summer. In this chapter, the presence of a slowly-varying ocean component which modulates the seasonal cycle in F_0 is explored to investigate the quantitative and qualitative impacts on the model behaviour and crucially, the model climate distributions.

The rationale underlying the mechanisms by which the S61 and L84 models are coupled was provided by Van Veen et al. (2001). The authors note that the LS84 model can be likened to a perturbation to the L84 model. In the study, the authors differentiate between two modes of ocean coupling referred to as "passive" and "active". The prevalent mode is controlled by the coupling parameters, F_1 and G_1. Table 5.2 provides the values for the coupling parameters used by Van Veen et al. (2001). When the passive coupling parameters are used, the ocean is observed to have little effect on the evolution of the atmospheric variables, which continues to exhibit chaotic behaviour. There is not much variability in the ocean variables and Van Veen et al. (2001) state that "the ocean basically integrates the atmospheric forcing". However, when the active coupling is used, the atmospheric variables display intermittent behaviour and the ocean is found to have a significant impact on the model dynamics. Van Veen et al. (2001) show power spectra that reveal important modes of variability, likely caused by the emergence of periodicity. The relative merits of studying each coupling regime for the purposes of this thesis are examined in sections 5.2.2 and 5.3. Crucially, the coupling parameters lead to very different model behaviour for the seasonally driven LS84 model compared to the non-seasonally driven model explored by Van Veen et al. (2001).

The rich dynamics that result from the coupling of the two models are documented in the Van Veen et al. (2001) study and this knowledge is used in the design of the experiments presented in this chapter. In a later study, Van Veen uses the Maas (1994) model to act

Parameter	Ocean State	Value
F_1	Active	0.021685
	Passive	0.02
G_1	Active	0.01
	Passive	0.01

Table 5.2: Coupling parameters used in the LS84 model (Van Veen et al. (2001)).

as the ocean component of a low-order climate model while retaining the L84 model as the atmospheric component (Van Veen (2003)). This is because the Maas (1994) model is directly formulated from the governing fluid dynamical equations; the S61 model is not based on such equations. However, the S61 model is chosen for this analysis because of the existence of transitive/intransitive behaviour when coupled to the L84 model (discussed in section 5.2.3) and the familiarity of the climate modelling community with this well studied and relatively well understood model (Pagaran (2010)).

In the next section, the pseudo-attractor (PA) of the seasonally driven LS84 model is described and illustrated. The term *pseudo-attractor* (introduced in section 4.4.2) is used rather than the term *attractor* in this chapter because the parameter F_0 is a function of time.

5.2.2 The LS84 model pseudo-attractor

Coupling the S61 model to the L84 model increases the number of dimensions from three (X, Y, Z) to five (X, Y, Z, T, S) so visualising the LS84 model's pseudo-attractor for a given set of forcings becomes more difficult. Therefore, for practical reasons, the plots in figures 5.1 and 5.2 show the atmosphere and ocean variables separately to illustrate the geometric character of the model's PA for the parameter values given in table 5.1 in both the active and passive ocean coupling regimes. The regions of state space in which the model trajectories propagate are dependent on the coupling regime. In order to determine suitable ICs to help illustrate the model PA for each coupling regime, a single model simulation is performed with initial state values informed by the results of the Van Veen et al. (2001) study.

A one hundred year model simulation is conducted with ICs $(X, Y, Z, T, S) = (1.0, 1.0, 1.0, 5.5, 1.3 \times 10^{-3})$ under both passive and active coupling conditions (beginning on January 1st in the first year). The final states of the model, given in table 5.3, are assumed to be on (or very close to) the model PA under each coupling regime so these states are used as the ICs for subsequent single model trajectory plots. As in chapter four, the fourth-order Runge-Kutta integration method is employed with a time step of $\tau = 0.01$, which is equivalent to 1.2 hours (72 minutes) given the assertion that one time unit (the damping time for the waves) is approximately five days (Lorenz (1984)).

The three-dimensional plots in figure 5.1 show the evolution of the atmospheric variables from

Variable	Active	Passive
X	1.554	1.087
Y	0.778	1.129
Z	0.459	0.635
T	4.453	3.949
S	$1.605 \cdot 10^{-3}$	$1.693 \cdot 10^{-3}$

Table 5.3: ICs used for single model simulations of the LS84 model for each coupling regime.

a single realisation of the LS84 model for both active and passive coupling parameters. Whilst the behaviour of the atmosphere is altered by the presence of the ocean, the general geometric character of the model's PA in the X, Y and Z variables is similar to that of the uncoupled L84 model when $F = 8$ (see figure 4.1, section 4.2.2). The dominant flow is still westerly with occasional chaotic transitions to easterly flow denoted by the secondary lobe. The modulated behaviour induced by the presence of the ocean is difficult to detect in figure 5.1 but the impact of the ocean on the atmosphere is further elaborated in section 5.2.5. Analysis of the model behaviour is more insightful when focusing on the behaviour of the model trajectories for each individual model variable, along with the associated climate distributions.

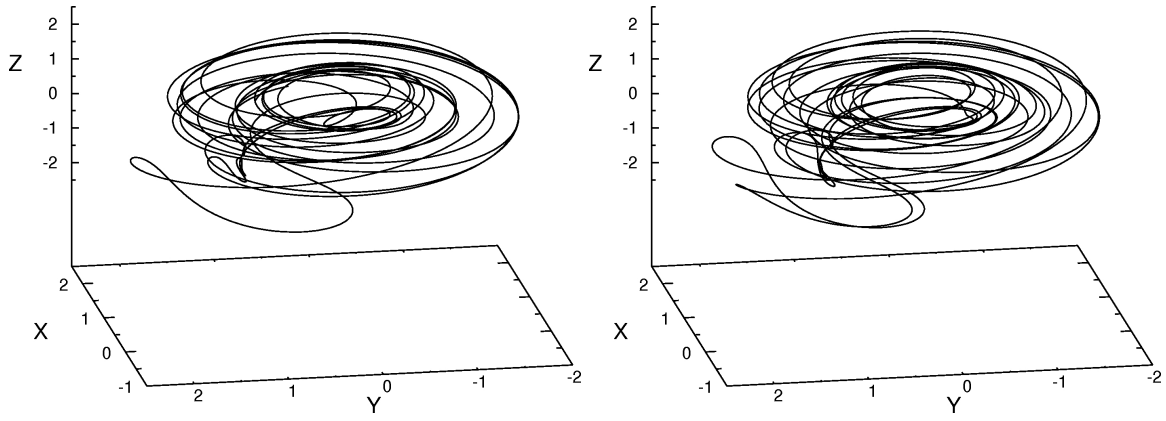

(a) Active (b) Passive

Figure 5.1: Single trajectory of the atmosphere variables from a one year simulation of the LS84 model for (a) active and (b) passive coupling parameter values. ICs given in table 5.3.

Figure 5.2 shows the evolution of the same model trajectory for the two ocean variables T and S. As the dynamic time scale of the ocean component is approximately one thousand times slower than that of the atmospheric component (Roebber (1995)), the plots show the model behaviour for considerably longer time scales, from 100 to 10,000 years. The plots in the left column of figure 5.2 show the model trajectory when subject to active coupling parameters and the plots in the right column show the model trajectory when subject to passive coupling parameters. The scale of the axes are the same for all six plots so it is therefore apparent that when the ocean is "actively" coupled to the atmosphere, the ranges in the ocean variables are more constrained in comparison to the range of behaviour in the passive coupling regime. In

both regimes, it is evident that higher values of T are typically associated with lower values of S. The Pearson correlation coefficient for the data shown in figure 5.2(e) (active coupling) is $r = -0.573$ and the Pearson correlation coefficient for the data shown in figure 5.2(f) (passive coupling) is $r = -0.733$ indicating that the correlation is more significant under passive coupling.

Clearly, the PA state space is not well sampled after only 100 years of the model simulations for both coupling regimes. Even after 1,000 years, there are areas of the PA state space that have not been visited by the model trajectory. After 10,000 years, certain regions of the model state space have been visited regularly by the model trajectory but it remains unclear whether or not the PA state space has been fully explored. In section 5.3.1, the frequency distributions of the single trajectory are shown for increasing time periods for each of the ocean variables and the rates of convergence are discussed.

Of relevance to the climate analogy presented in this chapter is the emergence of two dominant regions of state space in which model trajectories oscillate, when subject to passive coupling. In figures 5.2(d) and 5.2(f), there appears to be two identifiable areas of model state space where there is a high density of data points, located at approximately $T = 4.0$ and $T = 4.4$. The emergence of *regime* behaviour suggests that the model is more stable in these regions of state space. For active coupling, regime behaviour is not evident in the plots shown in figure 5.2. Further analysis of the regime structure of the LS84 model with passive coupling is provided throughout the chapter and the implications for climate are considered in relation to known regime behaviour occurring in the climate system.

5.2.3 Single trajectory results

Van Veen et al. (2001) show that for active coupling parameters, the slow time scale of the ocean plays an important role in the ocean-atmosphere dynamics. When the model is subject to passive coupling parameters, the effect of the ocean on the coupled model dynamics is determined to be less important. However, the research presented here shows that when there is a seasonal cycle in the parameter F_0, considerable long-term internal variability can be observed in the system for passive coupling parameters while for active coupling parameters the system shows rather less variability on longer time scales. As evident in the analysis presented in this section, the coupling parameters referred to "active" and "passive" lose their previous meanings when a seasonal cycle in F_0 is introduced into the model but for continuity from the Van Veen et al. (2001) study, these terms will continue to be used throughout the analysis to denote the values of F_1 and G_1.

Figure 5.3 shows the evolution of the atmospheric variables for a period of 10 years beginning in mid-winter for both active and passive coupling. Under both modes of coupling, the behaviour of the atmospheric variables is intermittent (alternating periodic, chaotic behaviour). In the winter, when F returns to the chaotic regions of parameter space, the trajectories exhibit transitive behaviour which span the range of the model PA. In the summer, the model behaviour

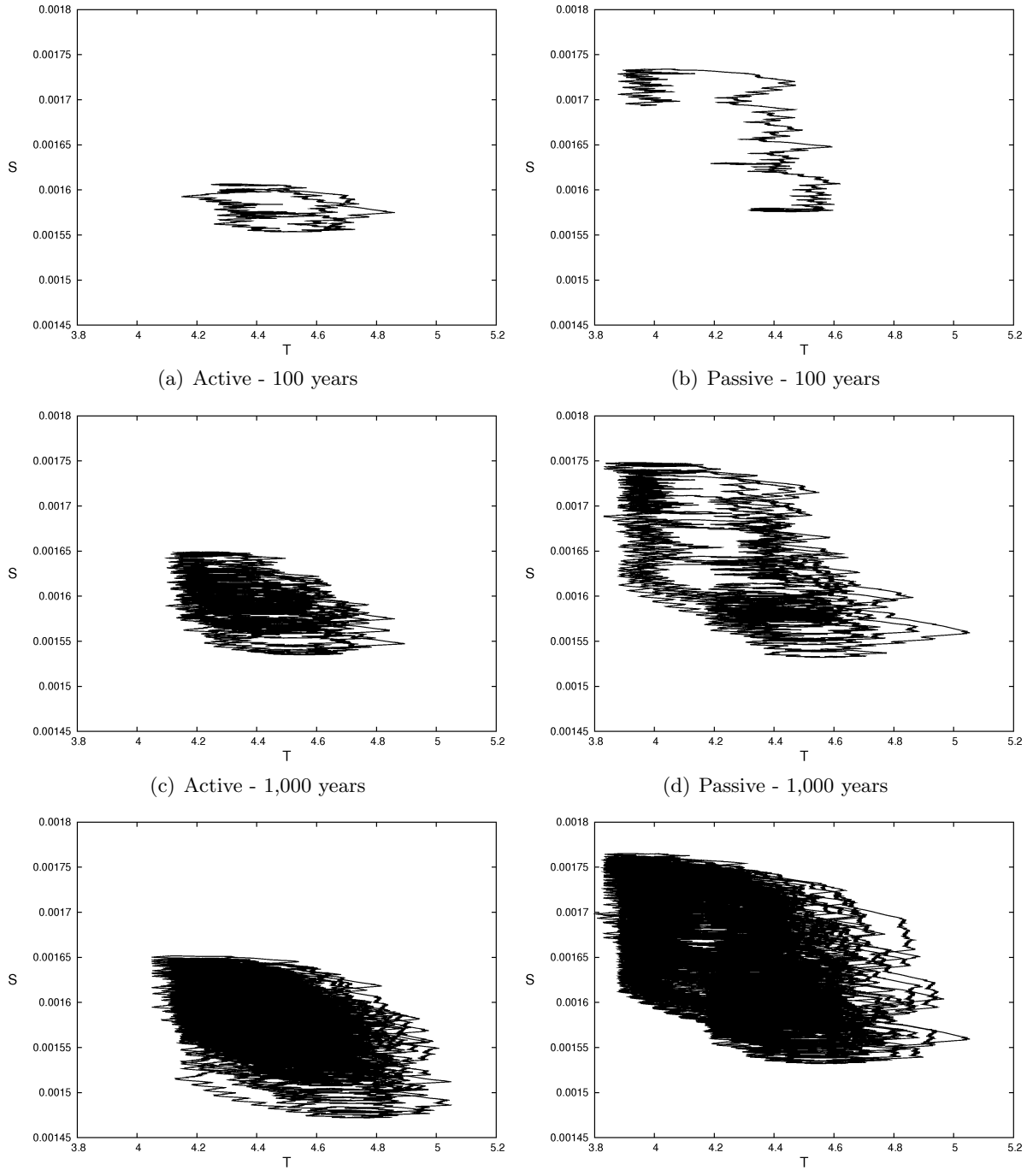

(a) Active - 100 years

(b) Passive - 100 years

(c) Active - 1,000 years

(d) Passive - 1,000 years

(e) Active - 10,000 years

(f) Passive - 10,000 years

Figure 5.2: Single trajectories of the ocean variables for simulations of the LS84 model over given time intervals. The plots in panels (a), (c) and (e) result from active coupling and (b), (d) and (f) result from passive coupling with associated ICs given in table 5.3.

is strongly influenced by the values of the coupling parameters. For passive coupling, shown in figure 5.3(b), in most (but not all) summers the trajectories move towards a model fixed point, before entering another phase of chaotic behaviour in the subsequent winter. However,

in years two and six the trajectories display periodic behaviour in summer rather than moving towards a fixed point. For active coupling, the summer behaviour is more variable with four of the ten years displaying transitions towards a fixed point, two years displaying a mode of dense periodic behaviour and the remaining four years displaying an alternative mode of periodic behaviour. Lorenz (1990) comments on transitions between "active" and "inactive" summer circulation patterns in the L84 model stating that the resulting summer behaviour is dictated by the chaotic behaviour which occurs during the previous winter. It is therefore postulated that the recurrence of periodic and fixed-point summers in the seasonally driven LS84 model are determined by the chaotic transitions which occur in the preceding winter. On the evidence provided in figure 5.3 alone, the model atmospheric component's response to ocean coupling appears to be more variable under active coupling with at least three modes of summer behaviour evident.

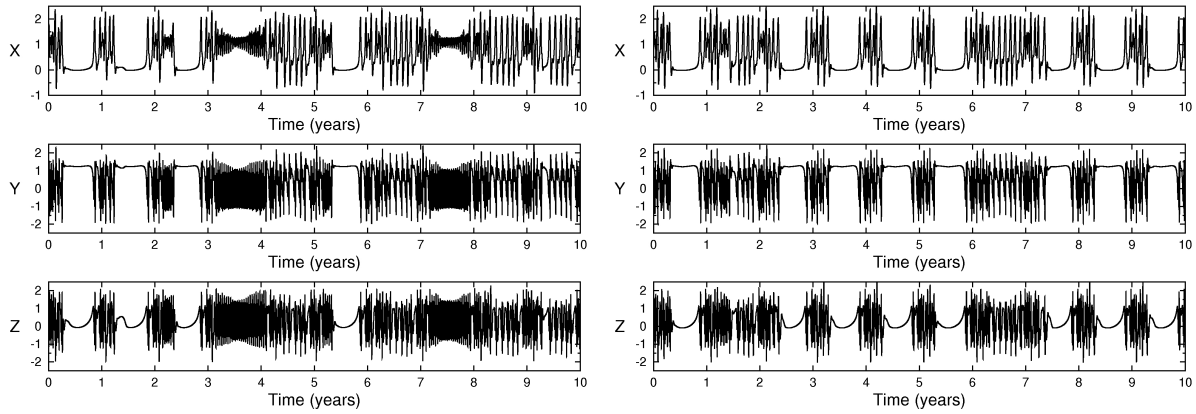

(a) Active (b) Passive

Figure 5.3: Atmospheric variables from single trajectory simulations of the LS84 model over a 10 year interval with (a) active coupling parameters and (b) passive coupling parameters using ICs given in table 5.3.

Figure 5.4 shows the evolution of the ocean variables T and S and the THC represented by f under active and passive coupling for the same model run depicted in figure 5.3 but for an extended period of 1,000 years. These figures reveal that various modes of variability are present in the ocean with considerable fluctuations occurring on decadal, multi-decadal and centennial time scales. As described in the previous section, in both coupling regimes, the inverse correlation between T and S is relatively clear with peaks in T broadly corresponding to troughs in S and vice versa. The time series shown in figure 5.4(b) displays two previously identified regimes centred at approximately $T = 4.0K$ and $T = 4.4K$ corresponding to high and low values of S respectively (consistent with figure 5.2(f)). The transitions between the high T, low S values (hereafter referred to as the HT regime) and the low T, high S values (hereafter referred to as the LT regime) occur at irregular intervals. Once a trajectory moves into one of these two regimes, the trajectory persists in the regime for many years before transitioning to the other regime. For example, at $t \approx 390$ years the trajectory spends approximately 100

years in the LT regime before transitioning to the HT regime for the following 80 years. The existence of regime behaviour suggests that under passive coupling, the model exhibits almost intransitive behaviour; assuming centennial time scales are considered 'long'. If the system was observed for relatively short time intervals (e.g. 100 years in this realisation), then it would be possible to observe only one of the two climate regimes; the implication being that a false interpretation of the model's climate would result. Furthermore, without an adequate understanding of the model's internal climate variability in the absence of trends in the model parameters, a transition to another regime may be misinterpreted as a change in climate. The transitions in T are more abrupt than the transitions in S suggesting a strong inertia in the response of the ocean salinity which is not as apparent in the ocean temperature.

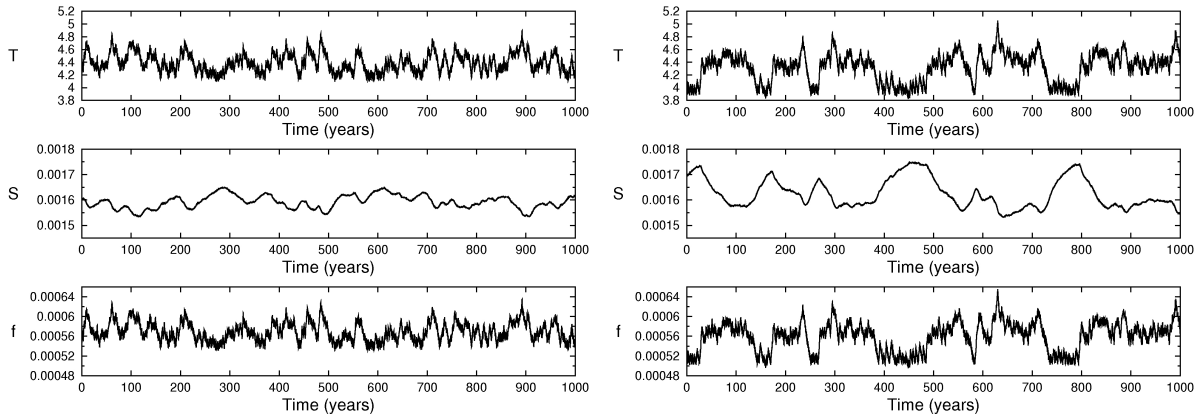

(a) Active (b) Passive

Figure 5.4: Ocean variables from single trajectory simulations of the LS84 model over a 1,000 year interval with (a) active coupling parameters and (b) passive coupling parameters using ICs given in table 5.3.

When the model is subject to active coupling parameters, as shown in figure 5.4(a), there is considerable variability in the ocean on decadal and multi-decadal time scales but the time series does not reveal distinct regime behaviour on a centennial time scale. Abrupt changes in T are still observed and the time series in S similarly displays relatively slow changes in ocean salinity circulation. The trajectories propagate in different regions of state space under each mode of coupling, as shown by the different spread in the values of T and S.

For the parameter values and constants used in the experiments presented in this thesis, the ocean circulation (THC) is strongly driven by the ocean temperature difference, T. Therefore, changes in T dominate the response in f and this can clearly be seen in figure 5.4 as the time series for f closely resembles the time series in T. As the focus of this study is not on the behaviour of the THC per-se, subsequent plots of the ocean variables will be limited to T and S.

In order to further explore the differences between the two modes of coupling and provide a basis for running experiments to draw analogies to the climate system, the climate distributions

of the model are determined using both the single trajectory model runs illustrated in figures 5.3 and 5.4, and by running large IC ensemble model simulations. The results are presented in section 5.3.

5.2.4 Almost intransitivity for passive coupling

In the analogy to the real climate system, one can consider the existence of regime behaviour in relation to the many modes of natural internal variability that are described in section 5.1. In the seasonally driven LS84 model, under passive coupling parameters, a long-term (multi-decadal to centennial) mode of internal variability is evident in the ocean variables from a single trajectory. Figure 5.4(b) shows the presence of two regimes which are most clearly seen in the T variable, referred to as the LT and HT regimes. Under active coupling parameters, variability exists on a number of time scales, as evidenced by the time series shown in figure 5.4(a), but it is more difficult to identify specific regions of the model state space which possess regime characteristics.

The occurrence of long-term internal variability relates to the transitivity of the model. Recall from section 2.1.4 that a transitive system is one in which a trajectory can pass through all of the possible system states and an intransitive system is one in which a trajectory will only pass through a subset of all possible system states; the subset is determined by the initial state and once established, will persist forever. According to Lorenz (1968):

> "In an almost intransitive system, statistics taken over infinitely long time intervals are independent of initial conditions, but statistics taken over very long but finite intervals depend very much upon initial conditions."

The definition of "very long" should be considered in relation to the system being studied. In the context of anthropogenic climate change, *very long* may therefore refer to behaviour which persists for many years, decades or perhaps even centuries.

When subject to active coupling parameters, the LS84 model appears to exhibit behaviour which can be considered transitive on multi-decadal to centennial time scales. However, over such time scales, almost intransitivity is apparent in the ocean variables under passive coupling parameters. The almost intransitive behaviour of the ocean in the LS84 model under passive coupling is of particular interest in the analogy to the climate system. Lorenz (1970) and Lorenz (1990) note that the climate system consists of subsystems operating on different time scales and explore the hypothesis that as a result the climate may be subject to almost intransitive behaviour. This is primarily because regime behaviour has been observed in the climate system on a number of temporal and spatial scales (from long-term global changes in glacial-interglacial cycles to shorter-term regional modes of variability such as the AMO). In addition, the capacity of a relatively simple nonlinear system to display regime behaviour with occasional abrupt transitions provides a valuable platform to develop a conceptual understanding of the role of internal climate variability in climate change prediction.

5.2.5 Impact of the ocean on the atmosphere

In this thesis, the focus is on determining the relevant experiments to run in order to produce climate model output which is usable and useful for the insurance sector and the wider adaptation community. Decisions regarding climate change adaptation, particularly within the insurance sector (described further in chapter six), are primarily concerned with changing atmospheric conditions (such as wind storms and precipitation events) but as the climate is a complex coupled system, the changing dynamics of subsystems such as the ocean have the potential to dominate future changes in atmospheric circulation. Whilst the intuitive response to producing more reliable model forecasts for atmospheric phenomena might be to better represent the atmosphere in a particular model, over increasing time scales the contributions of more slowly evolving components of the climate system, which ultimately constrain and control the atmospheric circulation, are likely to become increasingly important to accurate prediction. By analysing the behaviour of the LS84 model, the aim is to understand how sensitive a model's climate distributions are to uncertainty in the initial state of the ocean as well as the uncertainty in the atmosphere.

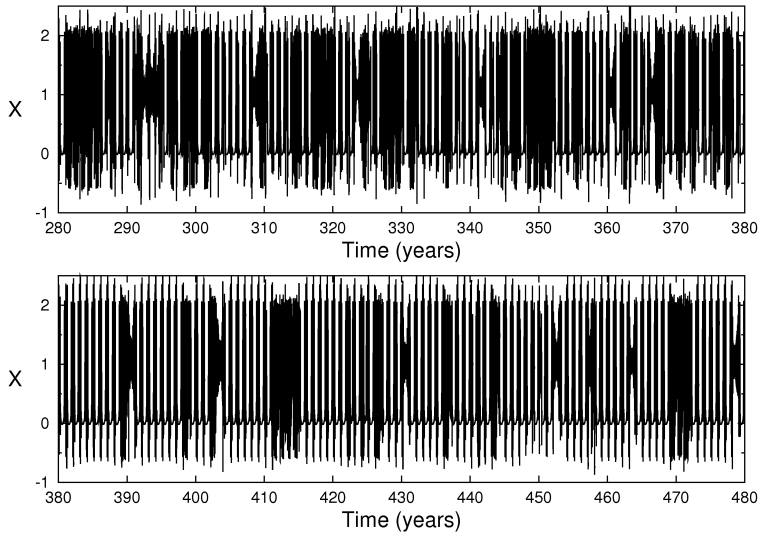

Figure 5.5: Time series of the X variable for a single LS84 model trajectory under passive coupling, initiated with ICs given in table 5.3. The top panel shows the time series for the interval between 280 and 380 years and the bottom panel shows the time series for the subsequent interval between 380 and 480 years.

To demonstrate the influence of the ocean on the atmospheric component of the LS84 model, figure 5.5 shows the evolution of the X variable over the interval from 280 to 480 years for the same model simulation used to generate figures 5.3(b) and 5.4(b). The top panel shows the trajectory from 280 to 380 years corresponding to the HT regime in figure 5.4(b) and the bottom panel shows the trajectory from 380 to 480 years which corresponds to the LT regime. When evolving in the LT regime, during the majority of summers (about 75%) the model trajectory evolves towards a model fixed point (at $X \approx 0.017$). However, in the HT regime the behaviour

of X appears more erratic with only half of the summers showing the model moving towards the fixed point and the remainder exhibiting periodic oscillations. Figure 5.5 therefore serves to demonstrate that the state of the ocean has a discernible impact on the annual variability of the atmosphere. Appropriately accounting for uncertainty in the ocean state is therefore crucial in forecasting the evolution of the atmospheric variables. The following analysis is therefore focussed on predicting the behaviour of the ocean variables and investigating the implications of almost intransitivity for climate modelling.

5.3 The LS84 Model Climate Distributions

In this section, the climate of the seasonally driven LS84 model is determined for both active and passive coupling using single model trajectory distributions and IC ensembles distributions. The LS84 model has been shown to be chaotic when F_0 is fixed at $F_0 = 8$ and G_0 is fixed at $G_0 = 1$ (Van Veen et al. (2001)). If the model continues to exhibit chaotic behaviour and the model is shown to be transitive, then the single trajectory distributions will converge to the IC ensemble distributions over time demonstrating the ergodicity of the coupled model.

5.3.1 Single trajectory frequency distributions

Using the LS84 model runs for passive and active coupling described in section 5.2, with ICs listed in table 5.3, single trajectory frequency distributions are plotted for each model variable over increasing time periods. As in section 4.4.3, only one value per year is selected for each season (mid-winter/mid-summer) to ensure that the value of F_0 is identical at the instant each model state is extracted. Hence, a 100 year simulation includes 100 points.

Figures 5.6 and 5.7 show the frequency distributions for the S and T ocean variables respectively. The first column in each figure shows the distribution of states in mid-summer (when F_0 return to $F_0 = 6$) for active coupling; the second column shows the distribution of states in mid-winter (when F_0 return to $F_0 = 8$) for active coupling; the third column shows the distribution of states in mid-summer for passive coupling; and finally, the fourth column shows the distribution of states in mid-winter for passive coupling. Because the time scale of the ocean dynamics is approximately three orders of magnitude slower than that of the atmosphere in the LS84 model, the distributions for mid-winter and mid-summer are nearly identical for both active and passive coupling. Therefore, the plots shown in later sections of this chapter for the ocean variables are only given for mid-winter.

Under active coupling, figure 5.6 shows that the 100, 300 and 1,000 year distributions fail to span the entire range of possible values of S that are observed over longer simulation periods. Notably, after 1,000 years the trajectory has not visited the region in which $S < 1.53 \times 10^{-3}$, consistent with the plot shown for the T-S plane in figure 5.2(c). After 3,000 years, the trajectory has visited this region and the plots shown for 10,000 and 30,000 years do not vary considerably from the 3,000 year plot (see section 5.3.3 for a quantitative comparison) indicating that the distributions are converging. The converged distribution is a negatively skewed unimodal distribution with a peak at $S \approx 1.59 \times 10^{-3}$.

When the model is subject to passive coupling, the range of possible values of S is explored after 1,000 years, as shown in panels (o) and (p) but the 100 and 300 year distributions do not incorporate the region in which $S < 1.57 \times 10^{-3}$. The distribution after 3,000 years suggests a bimodal shape but the 10,000 and 30,000 year plots have more density in the higher of the two modal regions. Therefore, the distributions cannot be said to have converged until a period

greater than 3,000 years. The converged distribution is bimodal with the lower modal region centred on $S \approx 1.59 \times 10^{-3}$ (as observed for active coupling) and the higher modal region revealing a peak at $S \approx 1.74 \times 10^{-3}$. In general, passive coupling leads to approximately half of the distribution density occurring where $S > 1.65 \times 10^{-3}$, associated with the LT regime and half occurring where $S < 1.65 \times 10^{-3}$, associated with the HT regime. The distributions for active coupling are limited to density only in the region in which $S < 1.65 \times 10^{-3}$. Therefore, under active coupling the equilibrium model behaviour is constrained to the HT regime, at least according to analysis based on the S variable.

The results plotted in figure 5.7 show the equivalent distributions for the T variable. Again, the mid-summer and mid-winter results are very similar but there are some differences in the exact location of the distribution peaks. The T distributions are also different under active and passive coupling. When the model is subject to active coupling, the behaviour is limited to the HT regime as all observed states occur at $T > 4.1K$. The general shape of the distribution is well approximated by the century-long simulations but the states in the tails of the distributions are only observed for longer simulation periods of at least 3,000 years.

Under passive coupling, figure 5.7 shows the bimodal nature of the distributions apparent in figure 5.6. The largely converged distributions for active coupling appear very similar to the upper model region of the T distributions (the HT regime) under passive coupling. In the 100, 300, 1,000 year plots (in panels c, d, g, h, k and l) and to a lesser extent in the 3,000 year plots (panels o and p), there is a disproportionately large area of density in the HT regime when compared to the distributions associated with longer periods. This shows that memory of the initial model sate is apparent in the single trajectory distributions for thousands of years. The implication is that a multi-thousand year single model simulation is required to approach the climate distributions for the ocean variables in the LS84 model. Without analysing the IC ensemble distributions, it is not possible to determine whether the eventual converged distributions associated with a single trajectory do in fact represent the full set of states consistent with the model parameters.

As discussed in section 5.2.5, the focus of the analysis presented in this chapter is on the predictability of the ocean variables because the evolution of the ocean controls the behaviour of the atmosphere and is of greater interest in the analogy to climate change. The frequency distributions for the atmospheric variables are shown in Appendix C, figures C-1 to **??**. The distributions show considerable differences between mid-winter and mid-summer because of the impact of the value of F ($F_0 + F_1 T$) on the model's underlying attractor. These differences are greater than those which arise because of the different coupling regimes.

5.3.2 IC ensemble distributions

A 10,000 member ensemble was initiated with ICs spread evenly along a transect spanning the range from $(X_1, Y_1, Z_1, T_1, S_1) = (-1.0, -2.5, -2.5, 3.8, 1.45 \times 10^{-3})$ to

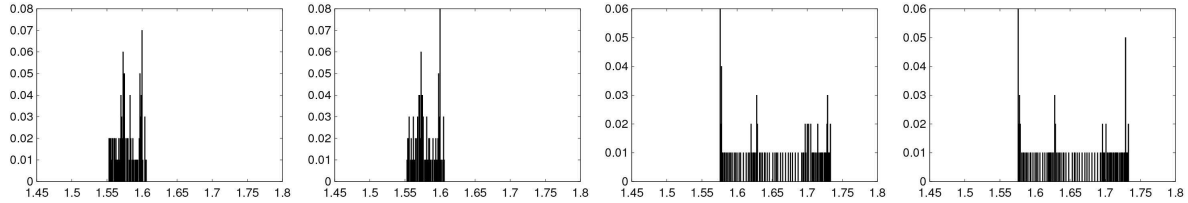

(a) 100 yrs, Active, Su (b) 100 yrs, Active, W (c) 100 yrs, Passive, Su (d) 100 yrs, Passive, W

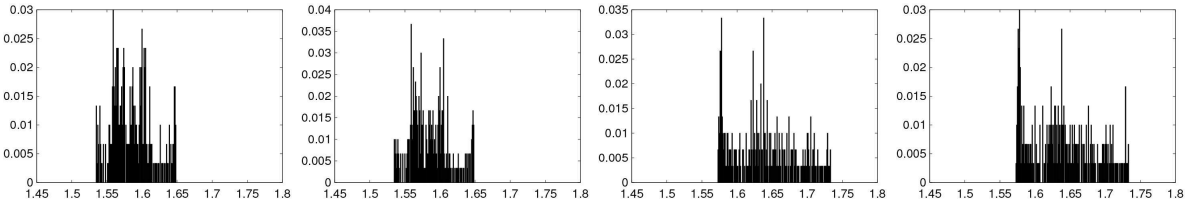

(e) 300 yrs, Active, Su (f) 300 yrs, Active, W (g) 300 yrs, Passive, Su (h) 300 yrs, Passive, W

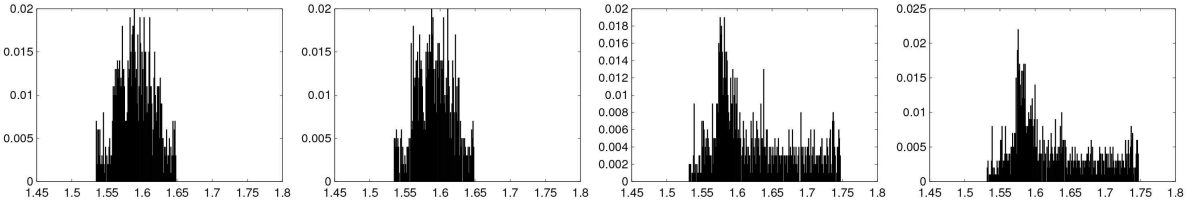

(i) 1,000 yrs, Active, Su (j) 1,000 yrs, Active, W (k) 1,000 yrs, Passive, Su (l) 1,000 yrs, Passive, W

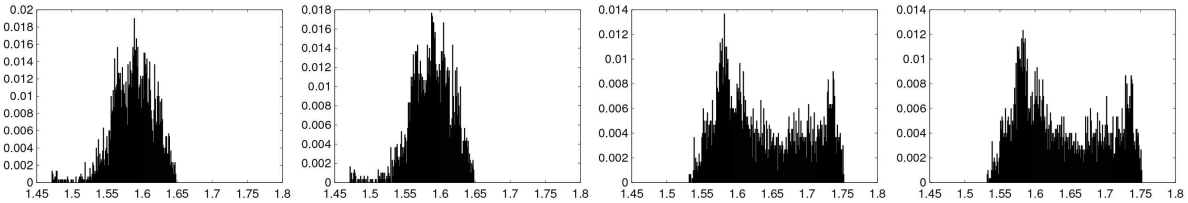

(m) 3,000 yrs, Active, Su (n) 3,000 yrs, Active, W (o) 3,000 yrs, Passive, Su (p) 3,000 yrs, Passive, W

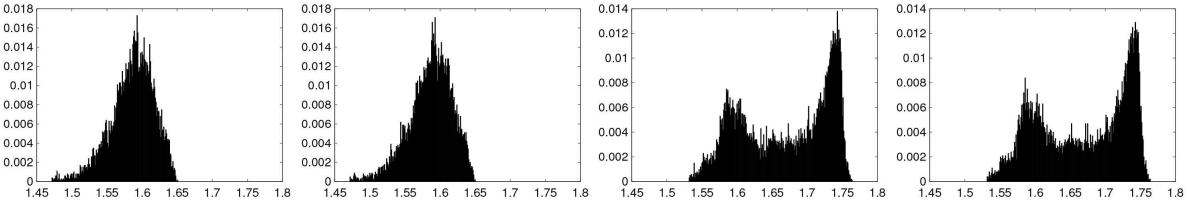

(q) 10,000 yrs, Active, Su (r) 10,000 yrs, Active, W (s) 10,000 yrs, Passive, Su (t) 10,000 yrs, Passive, W

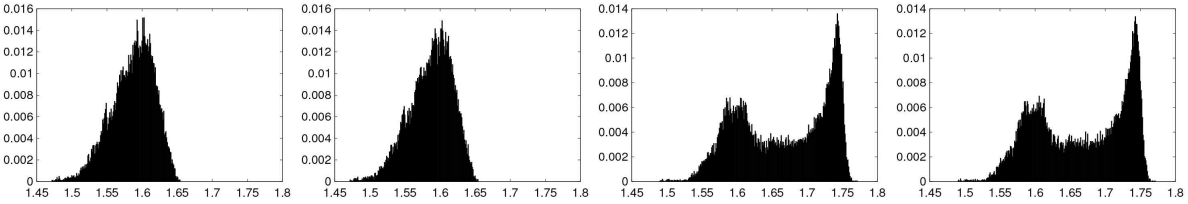

(u) 30,000 yrs, Active, Su (v) 30,000 yrs, Active, W (w) 30,000 yrs, Passive, Su (x) 30,000 yrs, Passive, W

Figure 5.6: Normalised frequency distributions for a single trajectory of the LS84 model variable S over increasing time periods. The method of coupling is given as active or passive and the respective ICs are given in table 5.7. *Su* denotes mid-summer and *W* denotes mid-winter. In each plot, the x-axis corresponds to ocean variable S ($\times 10^{-3}$) (psu) and the y-axis corresponds to the frequency per occupied bin; bin width $= 1 \times 10^{-6}$.

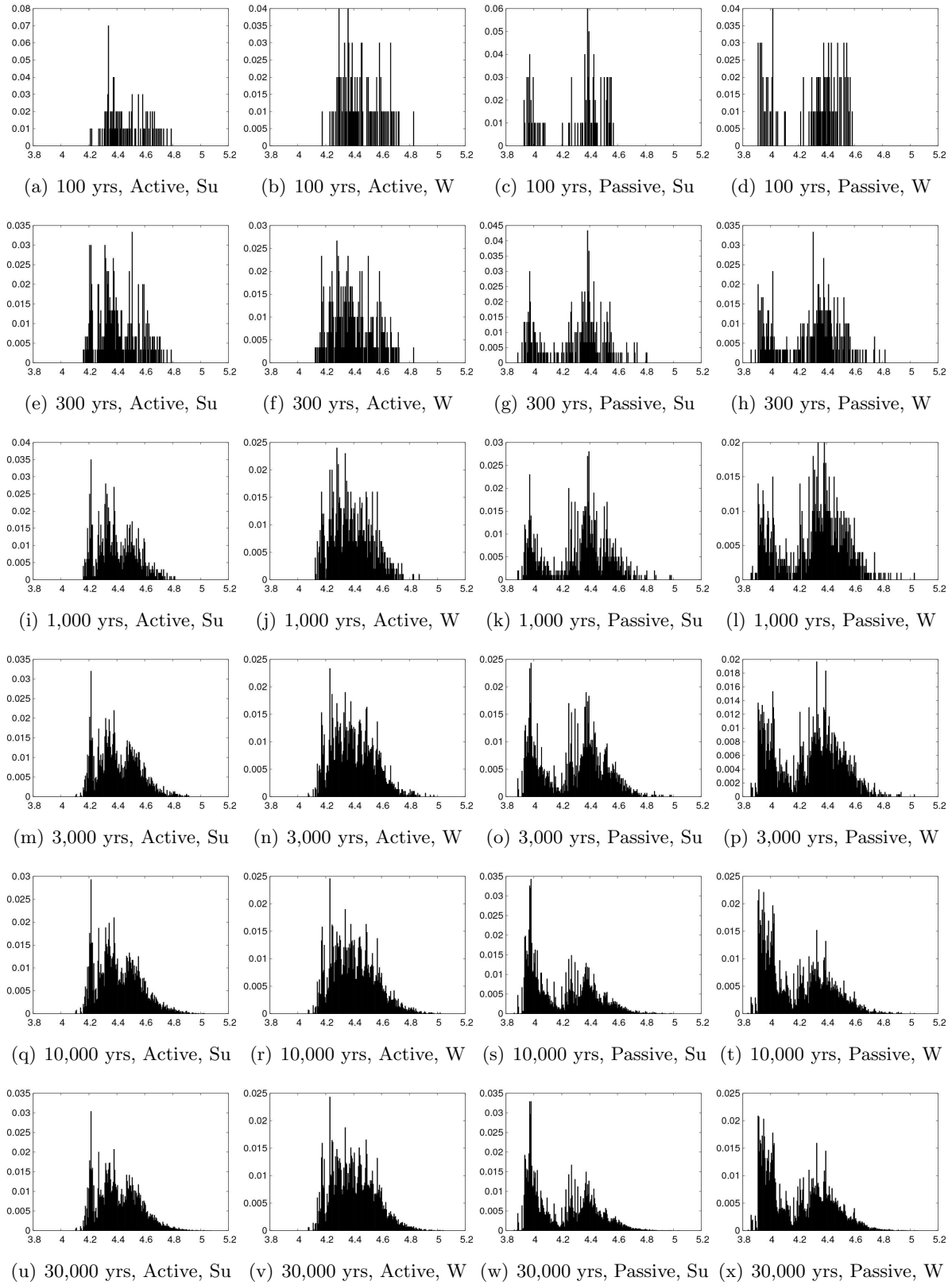

(a) 100 yrs, Active, Su (b) 100 yrs, Active, W (c) 100 yrs, Passive, Su (d) 100 yrs, Passive, W

(e) 300 yrs, Active, Su (f) 300 yrs, Active, W (g) 300 yrs, Passive, Su (h) 300 yrs, Passive, W

(i) 1,000 yrs, Active, Su (j) 1,000 yrs, Active, W (k) 1,000 yrs, Passive, Su (l) 1,000 yrs, Passive, W

(m) 3,000 yrs, Active, Su (n) 3,000 yrs, Active, W (o) 3,000 yrs, Passive, Su (p) 3,000 yrs, Passive, W

(q) 10,000 yrs, Active, Su (r) 10,000 yrs, Active, W (s) 10,000 yrs, Passive, Su (t) 10,000 yrs, Passive, W

(u) 30,000 yrs, Active, Su (v) 30,000 yrs, Active, W (w) 30,000 yrs, Passive, Su (x) 30,000 yrs, Passive, W

Figure 5.7: Normalised frequency distributions for a single trajectory of the LS84 model variable T over increasing time periods. The method of coupling is given as active or passive and the respective ICs are given in table 5.7. *Su* denotes mid-summer and *W* denotes mid-winter. In each plot, the x-axis corresponds to the ocean variable T (K) and the y-axis corresponds to the frequency per occupied bin; bin width = 0.005.

$(X_{10000}, Y_{10000}, Z_{10000}, T_{10000}, S_{10000}) = (2.5, 2.5, 2.5, 5.0, 1.8 \times 10^{-3})$. A transect between these values was selected assuming a knowledge of the range of model values but no information about the shape of the distributions. The ensemble is run for a period of 10,000 years. Figures 5.8 and 5.9 show the evolution of the ensemble at mid-winter at given time instants for the S and T variables respectively, under both active and passive coupling. Only mid-winter distributions are shown because the mid-summer distributions are very similar (as illustrated in section 5.3.1) due to the relatively slow evolution of the ocean variables. As previously stated, the long-term variability in the atmospheric variables (X, Y and Z) of the LS84 model is largely dominated by the dynamic behaviour of the ocean so analysis of the ocean variable distributions is most beneficial in extending the analogy to the climate system. The ensemble distributions for the atmospheric model variables are given in Appendix C, figures C-2 to C-4.

After three years of the model simulation with active coupling (see fig. 5.8(a)), the ensemble members remain fairly uniformly spread across the PA state space in the S dimension. After 30 years, the ensemble begins to converge to a smooth unimodal, negatively skewed distribution centred on $S = 1.6 \times 10^{-3}$. The general shape of the distribution remains unchanged for much longer simulation periods up to 10,000 years. The corresponding plots in T are less smooth, particularly at the lower range of the distribution, yet display a similar unimodal character centred on $T = 4.4$ with a positive skew.

When subject to passive coupling, the ensemble distributions appear to converge more slowly in the S variable. After 30 years (see fig. 5.8(k)), a bimodal distribution becomes apparent but the location of the upper modal region is lower than that observed after longer simulation periods. The converged distribution is bimodal with a primary peak at $S \approx 1.74 \times 10^{-3}$ and a secondary peak at $S \approx 1.59 \times 10^{-3}$ consistent with the converged single trajectory distribution after 10,000 years. The converged ensemble distributions for T also suggest a bimodal distribution consistent with converged single trajectory distributions but the convergence does not appear to be as slow as that observed in the S variable. The results support the observation made previously that a greater inertia is present in the ocean salinity as it responds slowly to changes in T.

The converged ensemble distributions are visually very similar to the distributions associated with long multi-thousand year single trajectory simulations. In the following section, the KS test is used to to investigate the ergodicity of the coupled model and provide quantitative estimates of the rates at which single trajectory frequency distributions converge to the reference climate distributions. In section 5.5, different IC ensembles from across the PA state space are run to explore how IC ensemble location affects the memory of the LS84 model.

5.3.3 Ergodicity in the LS84 model

In experiments with the L63 and L84 models, the ergodic assumption is shown to be valid when the parameters are fixed at values which lead to transitive behaviour. The versions of the LS84 model explored here are ultimately transitive but, as described in the previous section, when

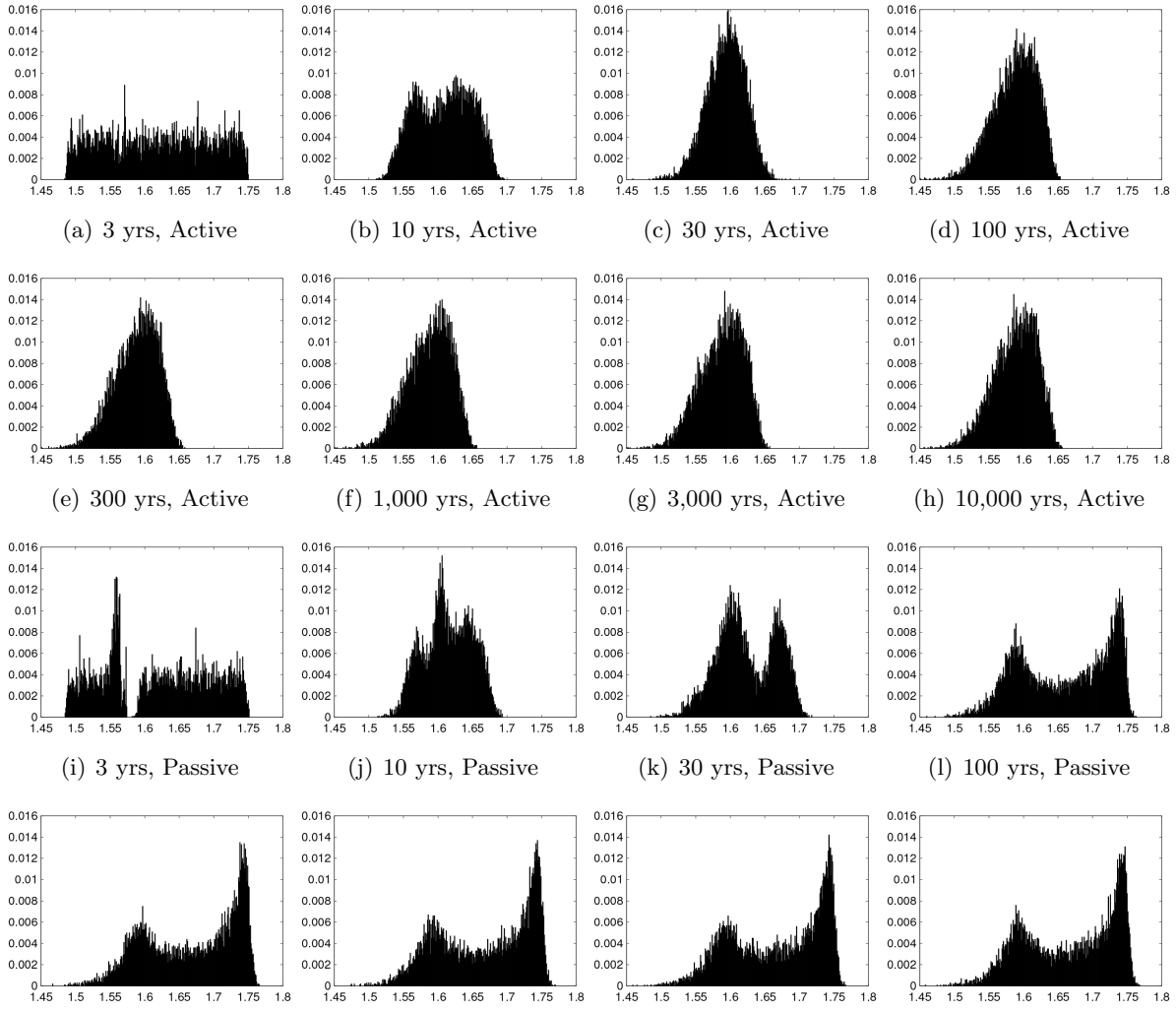

(a) 3 yrs, Active (b) 10 yrs, Active (c) 30 yrs, Active (d) 100 yrs, Active

(e) 300 yrs, Active (f) 1,000 yrs, Active (g) 3,000 yrs, Active (h) 10,000 yrs, Active

(i) 3 yrs, Passive (j) 10 yrs, Passive (k) 30 yrs, Passive (l) 100 yrs, Passive

(m) 300 yrs, Passive (n) 1,000 yrs, Passive (o) 3,000 yrs, Passive (p) 10,000 yrs, Passive

Figure 5.8: Normalised frequency distributions for the ocean variable S from a 10,000 member IC ensemble of the LS84 model in mid-winter at given instants in time. The method of coupling is given as active or passive and ICs are spread evenly along a transect spanning the range from $(X_1, Y_1, Z_1, T_1, S_1) = (-1.0, -2.5, -2.5, 3.8, 1.45 \times 10^{-3})$ to $(X_{10000}, Y_{10000}, Z_{10000}, T_{10000}, S_{10000}) = (2.5, 2.5, 2.5, 5.0, 1.8 \times 10^{-3})$. In each plots the x-axis corresponds to S ($psu \times 10^{-3}$) and the y-axis corresponds to the frequency of ensemble members per occupied bin; bin width $= 1 \times 10^{-6}$.

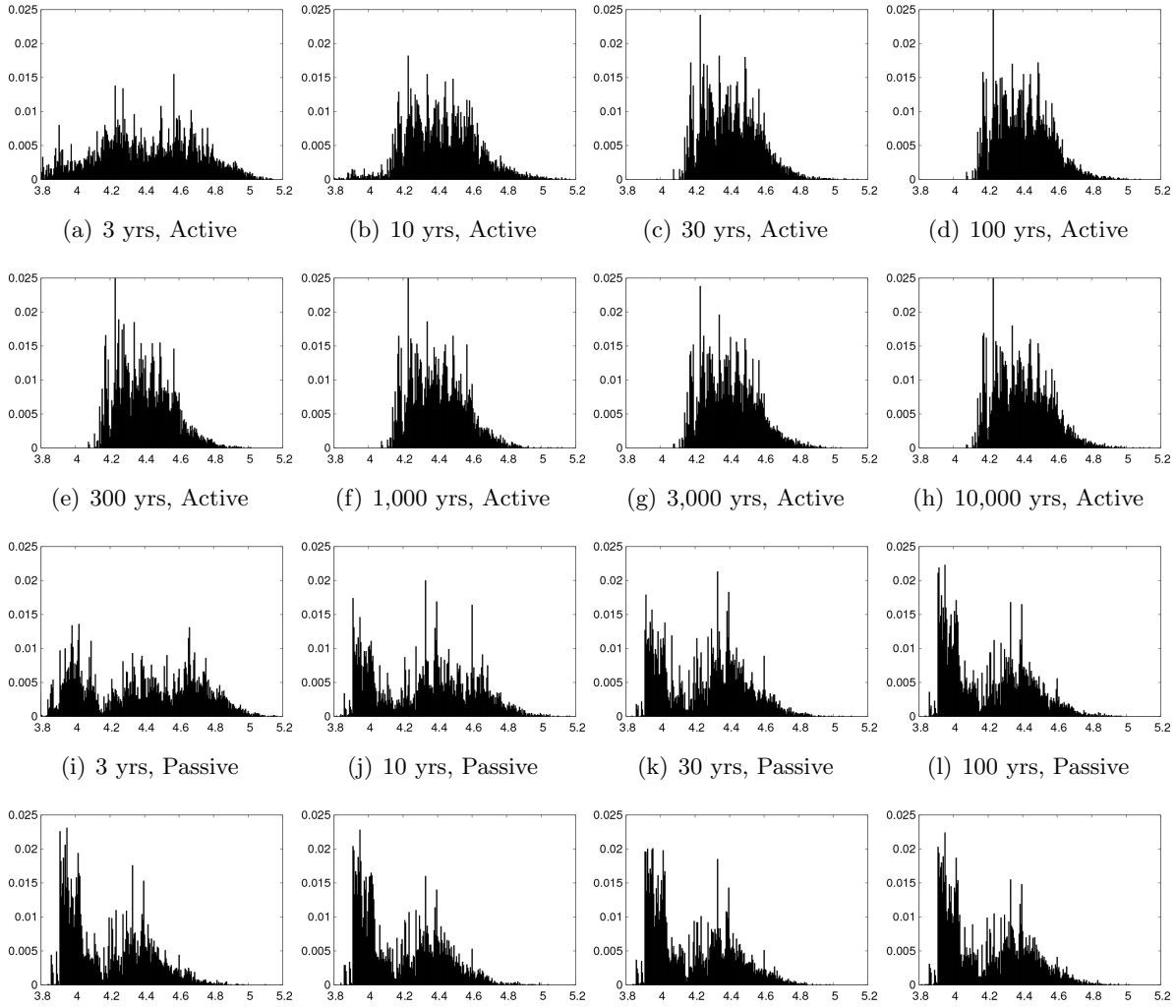

(a) 3 yrs, Active (b) 10 yrs, Active (c) 30 yrs, Active (d) 100 yrs, Active

(e) 300 yrs, Active (f) 1,000 yrs, Active (g) 3,000 yrs, Active (h) 10,000 yrs, Active

(i) 3 yrs, Passive (j) 10 yrs, Passive (k) 30 yrs, Passive (l) 100 yrs, Passive

(m) 300 yrs, Passive (n) 1,000 yrs, Passive (o) 3,000 yrs, Passive (p) 10,000 yrs, Passive

Figure 5.9: Normalised frequency distributions for the ocean variable T from a 10,000 member IC ensemble of the LS84 model in mid-winter at given instants in time. The method of coupling is given as active or passive and ICs are spread evenly along a transect spanning the range from $(X_1, Y_1, Z_1, T_1, S_1) = (-1.0, -2.5, -2.5, 3.8, 1.45 \times 10^{-3})$ to $(X_{10000}, Y_{10000}, Z_{10000}, T_{10000}, S_{10000}) = (2.5, 2.5, 2.5, 5.0, 1.8 \times 10^{-3})$. In each plot, the x-axis corresponds to T (K) and the y-axis corresponds to the frequency of ensemble members per occupied bin; bin width = 0.005.

the model is passively coupled trajectories display almost intransitive behaviour. The length of time over which the model must be run to ensure that a single model realisation produces 'climate' statistics representative of the underlying PA is investigated for both passive and active coupling parameters. The analysis in this section again focusses on the ocean variables.

The 10,000 member IC ensemble and single trajectory distributions are compared to reference "climate" distributions shown in figure 5.10. These ensemble distributions consist of 100,000 members, with ICs spread evenly along a transect spanning the range from $(X_1, Y_1, Z_1, T_1, S_1)$ $= (-1.0, -2.5, -2.5, 3.8, 1.45 \times 10^{-3})$ to $(X_{100000}, Y_{100000}, Z_{100000}, T_{100000}, S_{100000})$ $= (2.5, 2.5, 2.5, 5.0, 1.8 \times 10^{-3})$, after a simulation period of 1,000 years. Running a 100,000 member ensemble generates more precise estimates of the model climate distributions than a 10,000 member ensemble. A period of 1,000 years is chosen based on the ensemble results in section 5.3.2 which suggest that memory of the original IC ensemble location is lost on the order of hundreds of years.

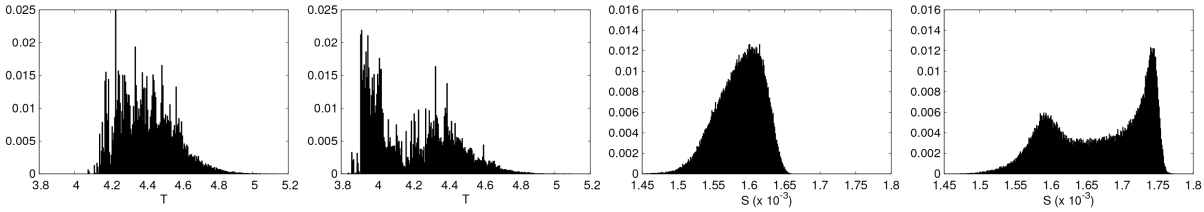

(a) T, Active (b) T, Passive (c) S, Active (d) S, Passive

Figure 5.10: Normalised frequency distributions for the ocean variables after a 1,000 year simulation from a 100,000 member IC ensemble of the LS84 model in mid-winter. The method of coupling is given as active or passive and ICs are spread evenly along a transect spanning the range from $(X_1, Y_1, Z_1, T_1, S_1) = (-1.0, -2.5, -2.5, 3.8, 1.45 \times 10^{-3})$ to $(X_{10000}, Y_{10000}, Z_{10000}, T_{10000}, S_{10000}) = (2.5, 2.5, 2.5, 5.0, 1.8 \times 10^{-3})$. In each plot, the y-axis corresponds to the frequency of ensemble members per occupied bin; bin width = 0.005 for T and 1×10^{-6} for S.

The frequency distributions associated with single trajectory simulations of increasing periods, some of which are illustrated in figures 5.6 and 5.7, are compared to the IC ensemble distributions shown in figure 5.10 which represent the model climate distributions under each coupling regime. The KS test is used to compare the distributions and the results are shown in figure 5.11.

The plots in figure 5.11 show the KS comparisons for the T and S variables over the 100,000 year time period for both active and passive coupling parameters. In both coupling regimes the single trajectory distributions eventually converge towards the ensemble climate distributions, indicated by the decrease in D over time towards $D = 0$. The ergodic assumption is therefore valid provided the model is run for a *sufficiently* long simulation period. In the LS84 model versions explored here, a *sufficient* simulation period is dependent on the values of the coupling parameters.

The results show that convergence is slower under passive coupling (fig. 5.11(b)) because of

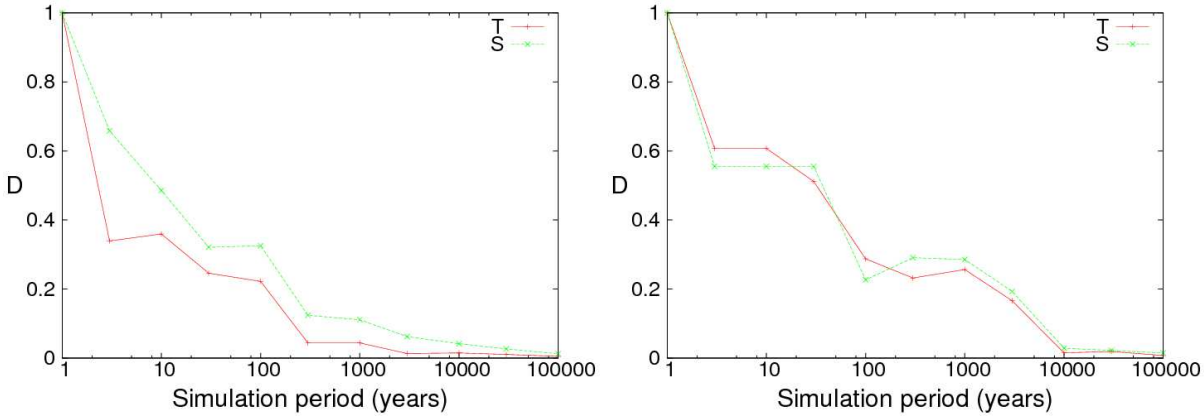

(a) Active (b) Passive

Figure 5.11: KS comparisons between single model trajectories of increasing simulation periods (using ICs given in table 5.3) and the 100,000 member IC ensemble "climate" distributions (shown in figure 5.10) for both active and passive coupling parameters.

the long-term internal variability between the HT and LT regimes causing the model to display almost intransitive behaviour. A 10,000 year single trajectory simulation is required before D approaches $D = 0$ for both ocean variables. Under active coupling (fig. 5.11(a)), the convergence is more rapid but a simulation period of hundreds and perhaps even thousands of years is still required before the ergodic assumption can be considered valid. Also, because of the slow response of the salinity component of the ocean model, the convergence is slower in the S variable than in the T variable. This result is clear under active coupling but the convergence appears to occur at a similar rate for both T and S under passive coupling. However, as the simulation period increases, the inertia in S is once again evident. The appropriate use of the ergodic assumption therefore appears to be not only time scale dependent but also variable dependent.

As the duration of the sample from a single trajectory increases one would expect the 'climate' statistics of the trajectory to converge towards those of the ensemble climate distributions. Whilst this is broadly what is observed, the trends in D are not smooth. As evident in figure 5.11(b), increasing the simulation period from 100 to 3,000 years does not lead to sizeable decreases in the magnitude of D in either of the ocean variables. In the S variable, the value of D actually increases after a 1,000 year simulation compared to a 100 year simulation which suggests that increasing the simulation length, for a system which displays almost intransitivity, will not necessarily render the ergodic assumption valid. The internal variability in the system means that a single trajectory may spend a disproportionate period of time in a particular regime of the PA causing the frequency distributions to diverge from the ensemble climate distributions.

If the climate system is almost intransitive on spatial scales and temporal scales relevant to climate change adaptation, then using a single simulation to estimate the PDF of a particular

climate variable to estimate exceedance probabilities will be misleading. The results shown using the LS84 model suggest that even if there are no trends in the forcings, increasing the simulation period doesn't always improve the viability of the ergodic assumption. Large IC ensembles are therefore required to estimate the climate distributions of the model. The obvious question that follows is how big IC ensembles need to be in order to provide reliable quantitative estimates of climate variable distributions. This question has so far been side-stepped in this thesis but the next section provides some guidance using the LS84 model.

5.4 Using IC Ensembles to Inform Probabilities

5.4.1 IC ensemble size

Throughout the thesis it is argued that in the analogy to climate, the model results support the case for running large IC ensembles to establish the range of behaviour consistent with the climate system's forcings. However, the issue of an appropriate ensemble size has not been addressed. This is largely due to the abstract relationship between the experiments conducted on the L63, L84 and LS84 models and experiments performed using complex GCMs but also because the primary focus has been on establishing the need (if any) for IC ensembles in climate change prediction rather than in optimising the design of IC ensemble experiments. Furthermore, the link between IC ensemble based forecasts and probabilistic information of climate and climate change has not been discussed thus far in the results. Experiments analysing the L63 and L84 model behaviour were directed towards developing a conceptual understanding of climate under altered forcing conditions and therefore focussed primarily on the concepts of transitivity, ergodicity and IC memory. Here, the LS84 model allows analysis of a system with two different time scales and the distinct regime behaviour in the ocean variables under passive coupling presents an opportunity to investigate the impact of IC uncertainty (and IC ensemble size) on the probability of transitioning between defined regimes. Having developed a conceptual framework and the appropriate language for understanding climate in a nonlinear chaotic system in previous chapters, the analysis shown here attempts to provide further guidance for climate model experimental design in order address decisions which can be informed by characterisation of uncertainties in relation to probabilities. This section explores the issue of ensemble size using the LS84 model under passive coupling, in the absence of any trends in the forcing parameters. The aim is to determine the minimum IC ensemble size necessary to provide robust quantitative estimates of the probabilities associated with the climate distributions of the LS84 model.

5.4.2 Experimental design

Utilising the previously identified HT and LT regimes evident in the ocean variables under passive coupling, an experiment is performed to estimate the probability of a trajectory being in a particular regime as a function of lead time. Ensembles of increasing size are investigated to understand how many ensemble members are required to give a reliable assessment of the model PDFs after a given simulation period. The HT and LT regimes are therefore given explicit quantitative ranges. A trajectory is determined to be in either of the two regimes based on the value of T. If $T > 4.25$, the state is in the HT regime and if $T < 4.1$ the state is in the LT regime. If T is in the range $4.1 < T < 4.25$ then the state is considered to be *ambiguous*. For example, in the time series of T shown in figure 5.4(b), the model trajectory initially evolved in the LT regime for 20 years before transitioning to the HT regime.

The ICs of the ensemble members are determined by generating coordinates close to an initial

state $(X_{IC}, Y_{IC}, Z_{IC}, T_{IC}, S_{IC}) = (1.087, 1.129, 0.635, 3.949, 1.693 \times 10^{-3})$. For an ensemble of size N (in this example $N = 10,000$) each ensemble member, i for $i = 1, 2, ..., N$, is assigned an initial state according to the coordinates:

$$(X_i, Y_i, Z_i, T_i, S_i) = (X_{IC} + r_{xi}, Y_{IC} + r_{yi}, Z_{IC} + r_{zi}, T_{IC} + r_{Ti}, S_{IC} + r_{Si})$$

where r_{xi}, r_{yi} and r_{zi} are randomly generated numbers from a three-dimensional uniform distribution in a sphere with a radius, $rad = 0.1$, centred on $(0, 0, 0)$; and r_{Ti} and r_{Si} are random numbers from one-dimensional uniform distributions in the ranges $-0.02 < r_{Ti} < 0.02$ and $-2 \times 10^{-5} < r_{Si} < 2 \times 10^{-5}$ respectively.

Initially all ensemble members are in the LT regime. For a selection of lead times, the percentage of ensemble members in the LT regime and the percentage in the HT regime are calculated. Those trajectories which are in the region where $4.1 < T < 4.25$ are labelled ambiguous. 17 ensembles of increasing sizes are investigated, with the number of ensemble members (E) given by $E = 2^{n-1}$, where $n = 1, 2...17$. The minimum ensemble size is therefore 1 member and the maximum size is 65,536 members.

5.4.3 Ensemble size results

The percentage of ensemble members in each regime is plotted against E for lead times of 3, 10, 30 and 100 years. One would expect that the probability of a transition to the HT regime would increase with lead time. This is indeed what is observed in the results illustrated in figure 5.12. After three years the ensemble results display convergence to a result where approximately 81% of members are in the LT regime, 3% are now located in the HT regime and the other 16% are classed as ambiguous. When the lead time is extended to 100 years, the probability of the trajectory being in the HT regime increases to nearly 40% while the number of ensemble members in the LT regime decreases to less than 50%.

The results of the experiment show that the probability estimates converge as the ensemble size increases for each lead time investigated. Furthermore, increasing the ensemble size beyond a certain threshold does not lead to significant improvements in the estimates of the regime probabilities. In all of the plots shown in figure 5.12, an ensemble size of approximately 2,000 to 4,000 members appears sufficient to provide a reliable estimate of the percentage of trajectories in the LT regime, the HT regime and those which are ambiguous. When the LS84 model is subject to almost intransitive behaviour and there is no trend in the model parameters, an ensemble size of approximately 2,000 to 4,000 is therefore sufficient to estimate the broad statistical properties of the model climate distributions. However, in estimating the probabilities of more extreme events, such as the probability of a trajectory where $T > 5$, increasing the size of the ensemble further still is expected to generate more reliable probability estimates. Further experiments with the LS84 model could be performed to establish the necessary ensemble sizes to determine robust estimates of the probabilities of rare/tail events.

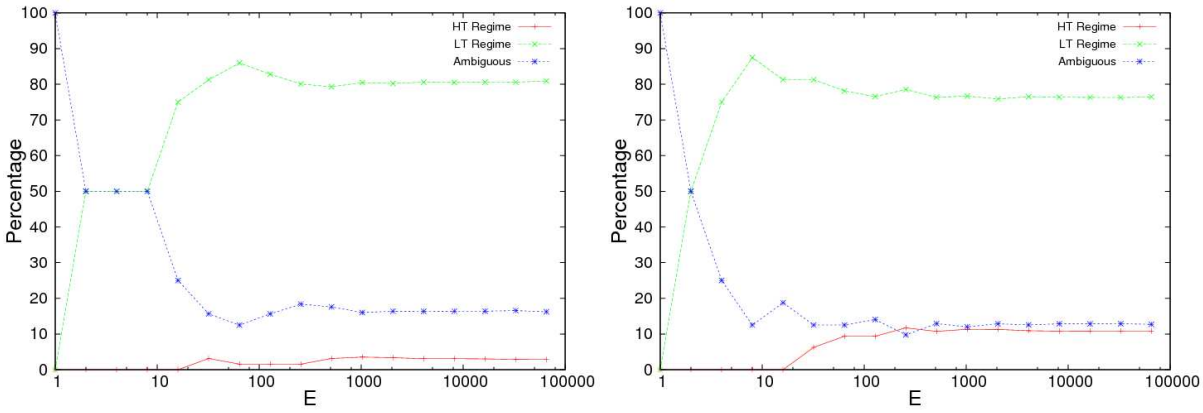

(a) 3 years

(b) 10 years

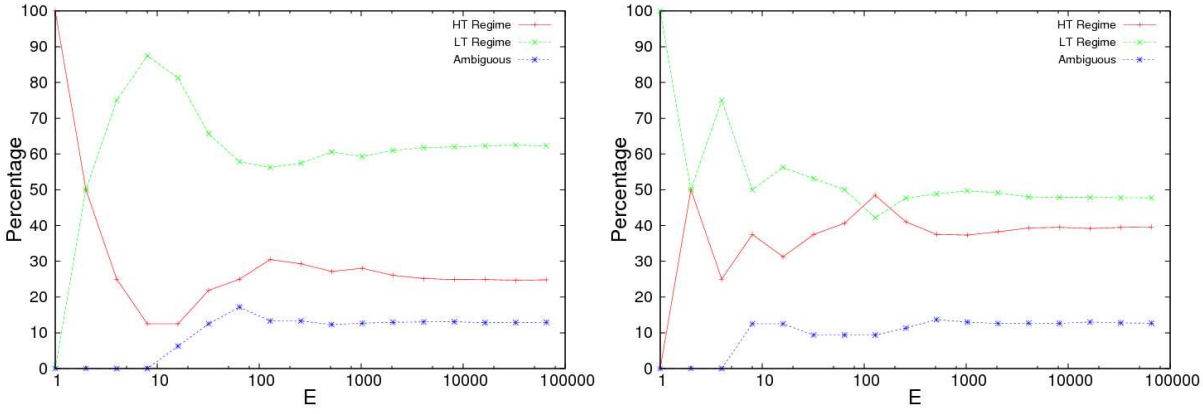

(c) 30 years

(d) 100 years

Figure 5.12: The percentage of ensemble members remaining in the LT ($T < 4.1$), having transitioned to the HT regime ($T > 4.25$) and those which are ambiguous ($4.1 < T < 4.25$) as a function of ensemble size for simulation periods of (a) 3 (b) 10 (c) 30 and (d) 100 years in the LS84 model under passive coupling. The ensembles members are initiated with ICs close to a reference state $(X_i, Y_i, Z_i, T_i, S_i) = (1.087, 1.129, 0.635, 3.949, 1.693 \times 10^{-3})$.

5.4.4 Convergence of prediction lead times

The experiment designed to explore ensemble size can be adapted to study the lead time at which memory of the IC ensemble location is lost. Previously, the probability of a trajectory being located in a particular regime is determined for increasing ensemble sizes. In this section, the experimental design is inverted so that rather than focussing on a specific lead time and varying the ensemble size, the ensemble size is fixed and the lead time is varied. Ensemble simulations are performed for increasing lead times (up to 1,000 years) using three ensemble sizes, where $E = 2^4$, 2^8 and 2^{12}. The aim is to establish the lead time at which the percentages stabilise, providing a measure of the memory of ICs in the model. Figure 5.13 shows the convergence in the percentage of members in the LT and HT regimes as a function of the model simulation lead time.

When $E = 2^4$ (see fig. 5.13(a)) the percentage of trajectories in each of the regimes changes

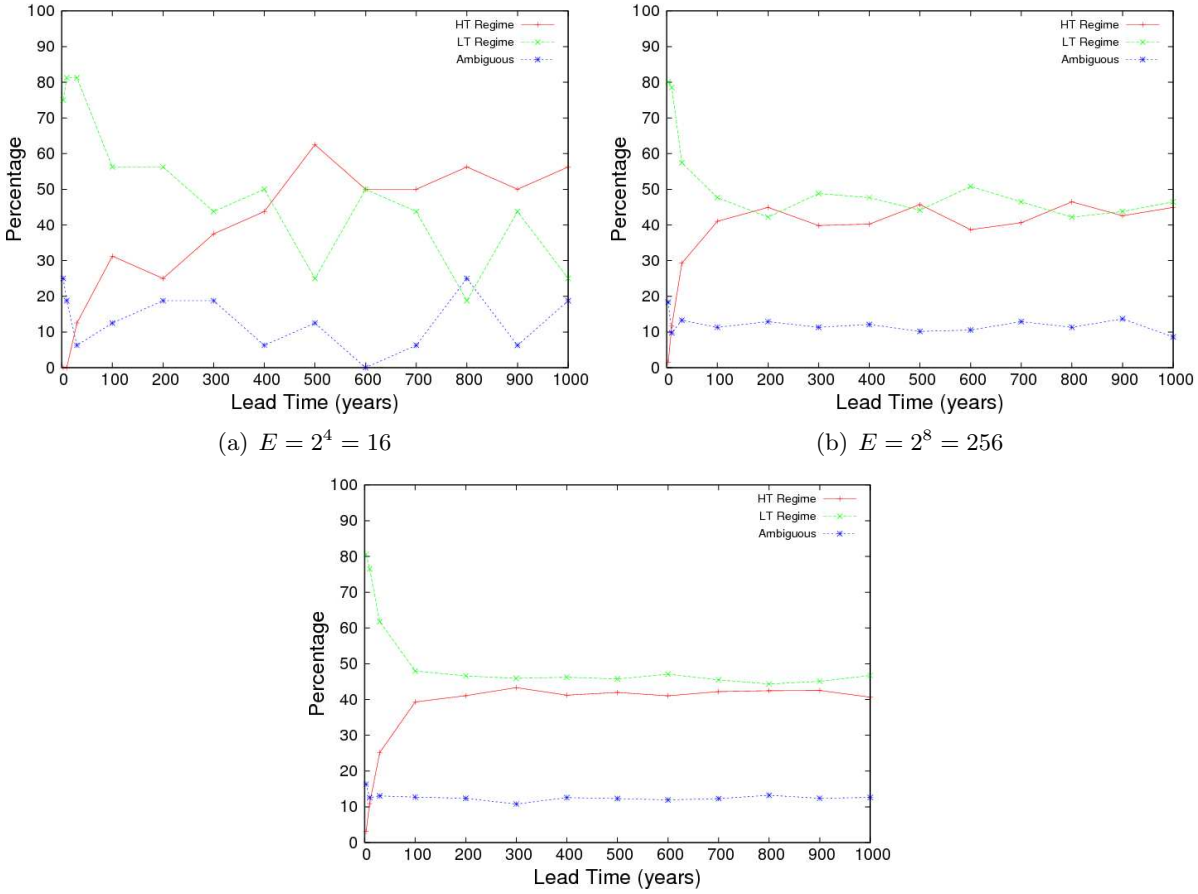

(a) $E = 2^4 = 16$

(b) $E = 2^8 = 256$

(c) $E = 2^{12} = 4096$

Figure 5.13: The proportion of ensemble members in the LT ($T < 4.1$), HT ($T > 4.25$) and ambiguous ($4.1 < T < 4.25$) regimes as a function of lead time for ensemble sizes of (a) 16 (b) 256 and (c) 4096 in the LS84 model under passive coupling. The ensembles members are initiated with ICs close to a reference state $(X_i, Y_i, Z_i, T_i, S_i) = (1.087, 1.129, 0.635, 3.949, 1.693 \times 10^{-3})$.

considerably at each time instant. As a consequence of a limited number of ensemble members, the experiment is relatively uninformative regarding the memory of ICs in the LS84 model. For a larger ensemble, when $E = 2^8$ (see fig. 5.13(b)), the experimental results are more informative. The percentage of trajectories in the LT regime decreases over the first 200 to 300 years of the model simulation. For lead times of 200 to 1,000 years, the percentage of trajectories in either the LT or HT regime oscillates between 40 to 50%. The result suggests that for at least 100 years and perhaps even 200 or 300 years, the PDFs of the LS84 model variables are a function of the IC ensemble location. In figure 5.13(c), when the ensemble size is increased to $E = 2^{12}$, convergence of the percentages occurs after 200 years. The percentages are also more constrained and for lead times of 200 to 1,000 years the percentage of ensemble members in the HT regime converges to approximately 42%, the percentage in the LT regime converges to approximately 46% and the remaining 12% are considered ambiguous.

In this section, the memory of ICs in the LS84 model has been investigated but the analysis

has been limited to a single IC ensemble originating in the LT regime. In the next section, the sensitivity of the IC ensemble distributions to the initial location of the ensemble on the model's PA is investigated to determine whether or not the model memory is a function of IC location.

5.5 Memory in the LS84 Model

5.5.1 Experimental design

The time it takes for the distributions associated with two different IC ensembles to converge provides a measure of the memory in the LS84 model. For a system which has coexisting attractors and displays intransitivity, the ensembles will never fully converge (assuming the ensembles span more than one basin of attraction). If the system is transitive, the ensembles will eventually converge but if that time is long relative to the dynamic time scale of the system then the system can be considered almost intransitive. In this section, the rates of convergence between the distributions associated with four different IC ensembles are compared when the LS84 model is subject to passive coupling. As explained in section 5.2.4, analysing the model under passive coupling can provide useful insights into the predictability of the climate system which displays regime behaviour and therefore may also be subject to almost intransitive behaviour.

Variable	IC 1	IC 2	IC 3	IC 4
X	1.087	0.439	0.625	0.303
Y	1.129	0.470	1.084	0.790
Z	0.635	1.133	-0.844	0.979
T	3.949	3.993	4.343	4.300
S ($\times 10^{-3}$)	1.693	1.723	1.686	1.628

Table 5.4: ICs used as the centre of the four IC ensembles investigated in section 5.5.

The four IC ensembles are centred on observed states from the single trajectory plots shown in section 5.2. The ICs are given in table 5.4. The IC state referred to as *IC 1* is the initial state used for the single trajectory simulation under passive coupling. *IC 2* is the state observed after 20 years of that particular model run, *IC 3* is the state observed after 40 years of the model run and *IC 4* is the state observed after 60 years of the model run. These four IC states are chosen because the first two states are located in the LT regime and the second two are located in the HT regime. The aim is to establish and compare the rates at which IC ensembles converge when originating in the same regimes and in different regimes.

Using the four states listed in table 5.4 as the central coordinates of the IC ensembles, the 10,000 individual members for each ensemble are given slightly different ICs according to the coordinates given in section 5.4.2 where $(X_{IC}, Y_{IC}, Z_{IC}, T_{IC}, S_{IC})$ is the reference state from table 5.4 and the other variables are the same as those defined in section 5.4.2. The ICs for each ensemble are illustrated in figures 5.14(a) and 5.14(b) for the atmosphere and ocean variables respectively. The figures are reproductions of figure 5.1(b) and figure 5.2(b) with the locations of the IC ensembles superimposed.

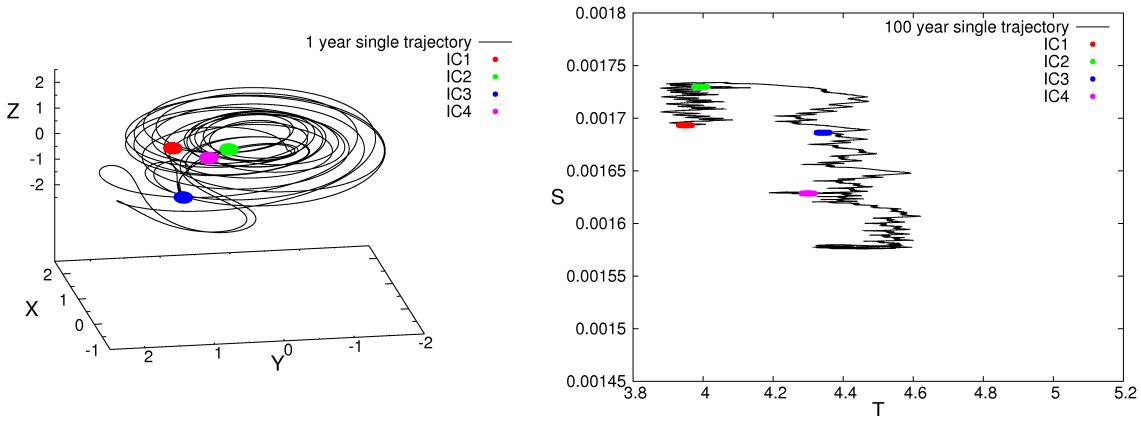

(a) Atmosphere (b) Ocean

Figure 5.14: Four 10,000 member IC ensembles superimposed on the model pseudo-attractor of the LS84 model under passive coupling parameters in: (a) the atmospheric variables, X, Y and Z; and (b) the ocean variables, T and S.

5.5.2 IC ensemble distributions

Plotting using a 3D colour-map

Throughout the thesis, frequency distributions have been presented in the form of two-dimensional histograms. The KS test has also been employed to provide statistical comparisons between distribution results over time. To reduce the number of plots shown in this section and subsequent sections, an alternative plot-type is used. A 3-dimensional colour-map is utilised to show how frequency distributions vary in time. The colour-map consists of two axes for the variable and time dimensions while the third dimension, the frequency within each variable bin, is expressed using a colour scale with a gradient between two colours (white and blue) where the darker the shade, the higher the frequency. In the 3D colour-map plots, the values given to the right of each figure correspond to the frequency of states per bin. The temporal resolution of the data dictates the width of each distribution plotted. In the following plots, data is extracted every ten years so the first ten years of the time series' in the 3D plots denotes the distribution at time $t = 0$ years (mid-winter), the next ten years denotes the distribution at $t = 10$ years (mid-winter) and so on.

IC ensemble results

The results presented in figures 5.15 and 5.16 show the evolution of the different IC ensembles over a 250 year period at 10 yearly intervals. Figures 5.15(a) and 5.15(b) show the response in the T variable of the IC ensembles originating in the LT regime and figures 5.15(c) and 5.15(d) show the response in the T variable of the IC ensembles originating in the HT regime. Over the first few decades of the model simulation, the ensemble members remain in their original

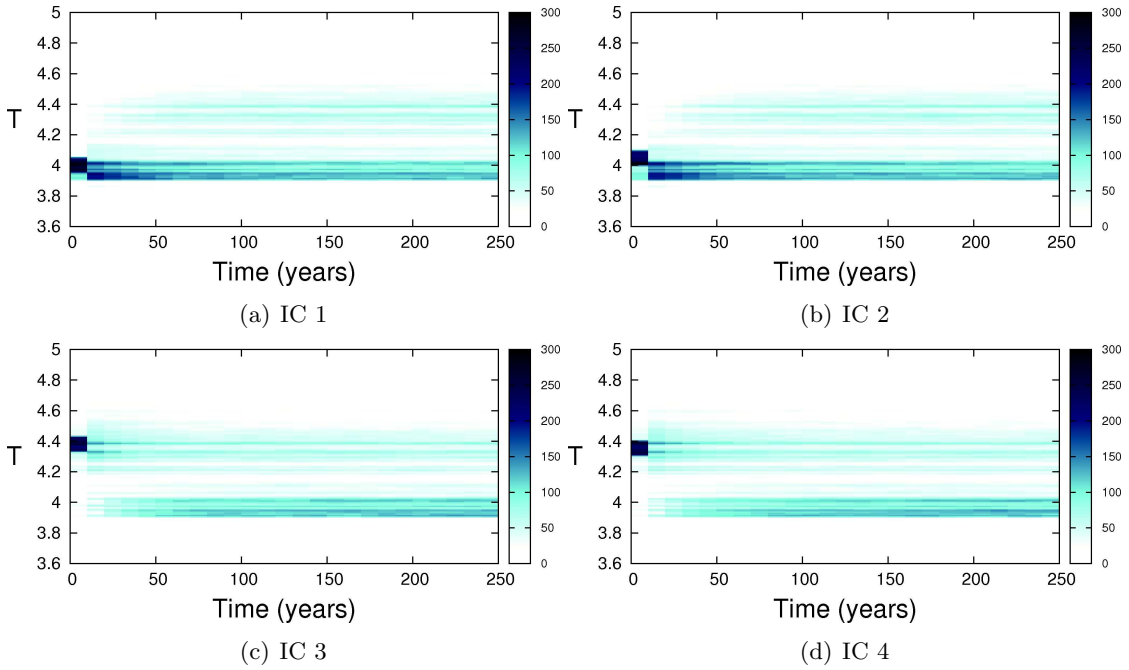

(a) IC 1 (b) IC 2

(c) IC 3 (d) IC 4

Figure 5.15: 3D colour-map showing the evolution of the four ensembles illustrated in figure 5.14 for the T variable.

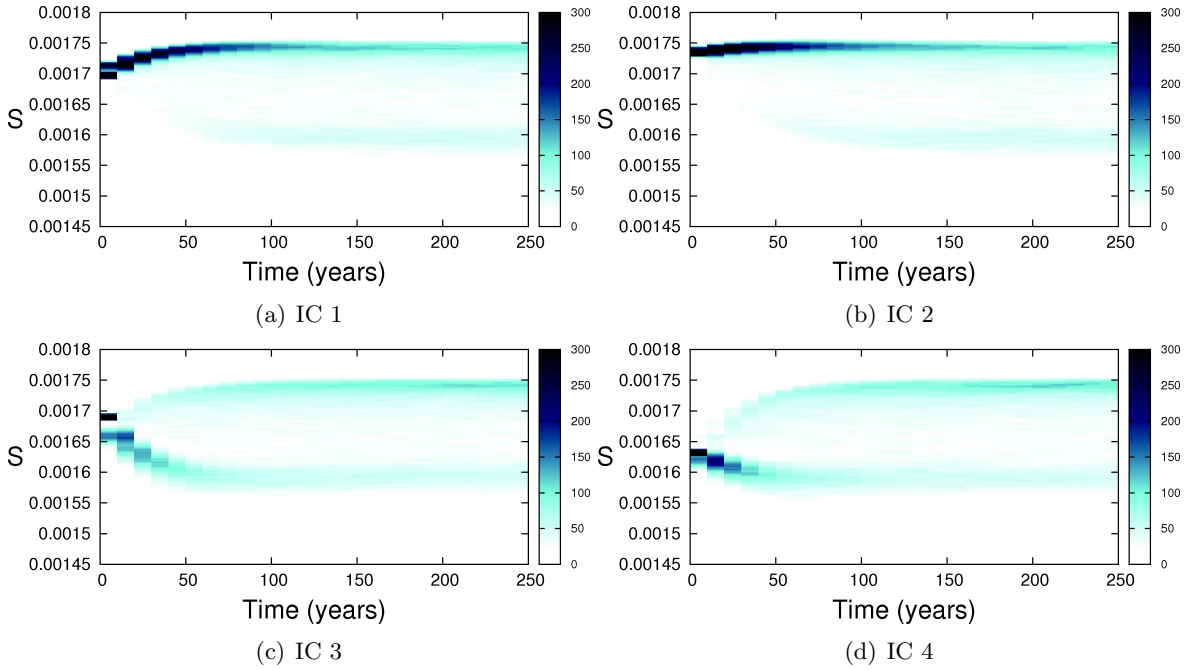

(a) IC 1 (b) IC 2

(c) IC 3 (d) IC 4

Figure 5.16: 3D colour-map showing the evolution of the four ensembles illustrated in figure 5.14 for the S variable.

regimes but over time the ensemble members spread across the PA state space and the ensemble distributions from both regimes appear to converge. The results for the S variable show that

the ensembles from *IC 1* and *IC 2* evolve in a similar way with the majority of members moving initially towards high values of S. Conversely, the majority of ensemble members from the ensembles labelled *IC 3* and *IC 4* initially move towards low values of S. Although ensembles *IC 1* and *IC 3* initiate from regions of state space with very similar values in S, because the behaviour of the model is temperature driven (see section 5.2.3), the evolution of model trajectories is dominated by the initial values of T. Therefore, irrespective of the initial value of S, the model trajectories are likely to remain in their original regime (LT or HT) for a number of years. This is an important result in the analogy to the climate system as it shows that reducing uncertainty in the measurement of a particular variable is only of value in climate prediction if the variable has an active role in the dynamic evolution of the system.

5.5.3 Convergence of IC ensembles

To quantify the memory of IC ensemble location in the LS84 model under passive coupling, KS comparisons between each pair of ensembles are presented for both ocean variables. Figure 5.17 shows the values of D over time for each of the six ensemble pairings. Focussing initially on T in figure 5.17(a), the results show that the ensemble pairing of *IC 1*/*IC 2* and the ensemble pairing of *IC 3*/*IC 4* converge more rapidly than the other ensemble pairings. This is because the ensembles originate in the same regime; ensembles *IC 1* and *IC 2* originate in the LT regime and ensembles *IC 3* and *IC 4* originate in the HT regime. The ensemble members spread initially in their regime of origin before transitioning to the other regime and spreading across the PA state space. After only 20 years the values of D approach a minimum for these two pairings.

The other KS comparisons show the rates of convergence in the ensemble distributions when the ensembles originate in different regimes. The rate of decline in D shows an exponential-like decay towards $D = 0$. The ensembles appear visually indistinguishable after approximately 180 years of the model simulation. The rates of convergence are nearly identical for the ensembles originating in different T regimes suggesting that the initial values of T strongly control the evolution of trajectories. Ensembles *IC 1* and *IC 3* are initially in different T regimes but their initial values of S are very similar. Nonetheless, these ensembles converge at the same rate as those ensembles with very different initial values in S.

The KS comparisons for the S variable in figure 5.17(b) support the conclusion that the rate of convergence is predominantly a function of the initial T values. Again, the two ensemble pairings that converge the fastest are ensembles *IC 1*/*IC 2*, and ensembles *IC 3*/*IC 4*. However, the rate of convergence is much slower because of the inertia of the system evident in the S variable. The values of D don't reach a minimum until at least 100 years of the model simulation have passed. The ensembles originating in different regimes converge even more slowly and D finally converges to a minimum after approximately 220 years. The initial decrease in D after 10 years for ensembles *IC 1*/*IC 3* occurs because the ensembles initiate with similar values of S but this decrease is premature as the values of T dominate the subsequent convergence.

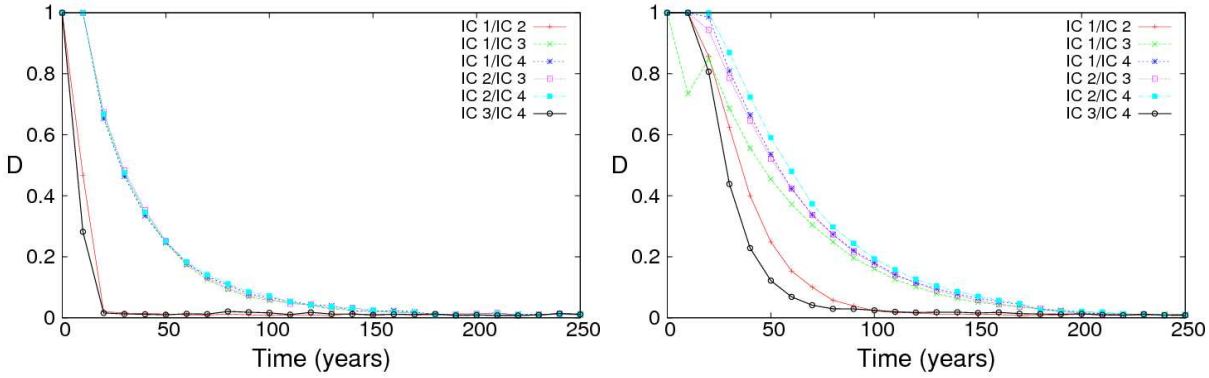

(a) T

(b) S

Figure 5.17: KS comparisons of the four IC ensembles shown in figure 5.14 for the T and S variables. Each line corresponds to the KS comparison for a different ensemble pair given in the figure key.

As described in section 5.2.3, the THC is temperature driven for the parameter values chosen. Under passive coupling, the initial values of T also strongly dictate the behaviour of the trajectories and the initial values of S appear to be unimportant in the evolution of the IC ensembles. In relating this work to the climate system, the results suggest that in order to improve predictions regarding the future evolution of variable climate distributions, it is important to constrain uncertainty in the dominant variables which control the system dynamics.

5.6 Climate Change in the LS84 Model

5.6.1 Rationale for experiments

In chapter four, the L84 model is used to investigate climate predictability when the model is forced from a region of parameter space associated with transitive behaviour to a region of parameter space associated with intransitive behaviour. In this section, the concept of climate under climate change is considered in the LS84 model which exhibits regime behaviour and almost intransitivity. Before proceeding it is important to re-examine the reasons for investigating climate change in this highly idealised coupled model. Given an increase in global atmospheric CO_2 concentrations, climate model projections largely agree about the direction and, to a lesser extent, magnitude of global and indeed regional changes in *mean* temperature (IPCC (2007b)). Yet there remains significant uncertainty in the nature of climatic changes at the regional scale with respect to extremes and tail events, in part due to the possibility of changing atmospheric and ocean dynamics. Circulation patterns which prevail under current forcing conditions may be very different under altered forcing conditions because of nonlinear responses in the climate system (Clegg et al. (2011)). Therefore, under changing global radiative forcing conditions, not only might we expect the mean of climate variable distributions to change at regional scales but also the shape of the variable distributions, reflecting altered dynamic behaviour of the climate system. Moreover, smooth transient changes in the radiative forcings do not imply that changes to climate distributions will also be smooth. Given the complexity of the climate system and the known existence of nonlinear system interactions, in the design-phase of climate model experiments it is therefore pertinent to consider the possibility of irregular and abrupt changes to the system's distributions. Given an appreciation of the complex nonlinear responses of the climate system to altered forcings, this section proceeds to explore the LS84 model under climate change.

In section 4.5 it is argued that the meridional temperature difference, represented by F, will decrease as the polar regions warm more rapidly than equatorial regions in response to anthropogenic radiative forcing. A trend towards lower values in F_0 is therefore imposed on the LS84 model to develop the analogy of the climate system under climate change. The focus of the LS84 model analogy is primarily on understanding the impact of almost-intransitivity on climate predictability and the memory of IC uncertainty in a system that evolves on more than one dynamic time scale. By introducing climate change into the LS84 model, the intention is to force the model between regions of parameter space which lead to alternative dynamic behaviour.

Considering the LS84 model under passive coupling is of more interest in the analogy to climate because of the existence of distinct regime behaviour (see section 5.2.4). However, Palmer (1999) asserts that the existence of regimes on decadal or longer time scales remains to be established. Suppose that the current climate is in fact largely transitive (i.e. regime behaviour, if present, is only found on short time scales). Now suppose that under a certain forcing scenario the climate

is subject to almost intransitivity, leading to the onset of regime behaviour with relatively long residence periods. Such a change in the dynamic behaviour of the climate system under climate change may be possible at a regional and perhaps even a global scale but single climate model realisations are unlikely to be able to confirm or dismiss such conjecture. By performing experiments with the LS84 model subject to trends in the model parameters, the implications of such a change in the climate system dynamics for climate change prediction can be investigated.

5.6.2 Single trajectory results

In an idealised example, the LS84 model is forced from a region of parameter space associated with transitive behaviour to a region associated with almost intransitive behaviour (relative to the dynamic time scales of the system). Almost intransitive model behaviour representing a possible future climate scenario is given by the model under passive coupling parameters and a meridional temperature difference oscillating in the range $6 < F_0 < 8$ so that F_{0m} (mean F_0) is $F_{0m} = 7$. To establish an initial climate scenario which displays transitive behaviour, the LS84 model is run with a number of different values of F_{0m} under passive coupling and the resulting time series' in the ocean variables are analysed.

Figure 5.18 shows five single model trajectories of the model variable T for 1,000 year simulations of the LS84 model where F_{0m} takes values between $F_{0m} = 7$ and $F_{0m} = 9$. The model version used to generate figure 5.18(a) is therefore identical to that used to generate figure 5.4(b), albeit with a different initial state. Figure 5.18(a) therefore displays a similar trajectory evolution with abrupt transitions between the LT and HT regimes and relatively long residence times (decades to centuries) in each of the regimes. As F_{0m} is increased to $F_{0m} = 7.5$ (see fig. 5.18(b)), the distinct regimes disappear but a mode of long-term variability is still apparent in the time series, particularly evident between $t = 400$ and $t = 600$ years. In figures 5.18(c) to 5.18(e) the model trajectories show little evidence of centennial variability and appear to be dominated by more constrained short-term variability on annual, decadal and perhaps multi-decadal time scales. Relative to the model behaviour when $F_{0m} = 7$, the model appears largely transitive for values of $F_{0m} \geq 8$ shown in figures 5.18(c) to 5.18(e). Based on this evidence, a value of $F_{0m} = 8$ (where F_0 oscillates seasonally between $7 < F_0 < 9$) is chosen to represent the initial climate forcing.

In section 5.3.3 it is observed that when $F_{0m} = 7$ a single trajectory needs to be run a period of approximately 10,000 years before the ergodic assumption can be considered valid. The long simulation period is required because of the almost intransitive nature of the model in this region of parameter space dictated by the slow time scale in the model's ocean component. In the extended analogy presented in this section, the model is initially in a (relatively) transitive region of parameter space. The frequency distributions associated with three single trajectories, with slightly altered ICs, when $F_{0m} = 8$ are shown for the T variable in figure 5.19 after a 1,000 year simulation period (the distributions for S are given in Appendix C, figure C-5). The distribution listed as *IC 2* is associated with a trajectory initiated using the final state of the

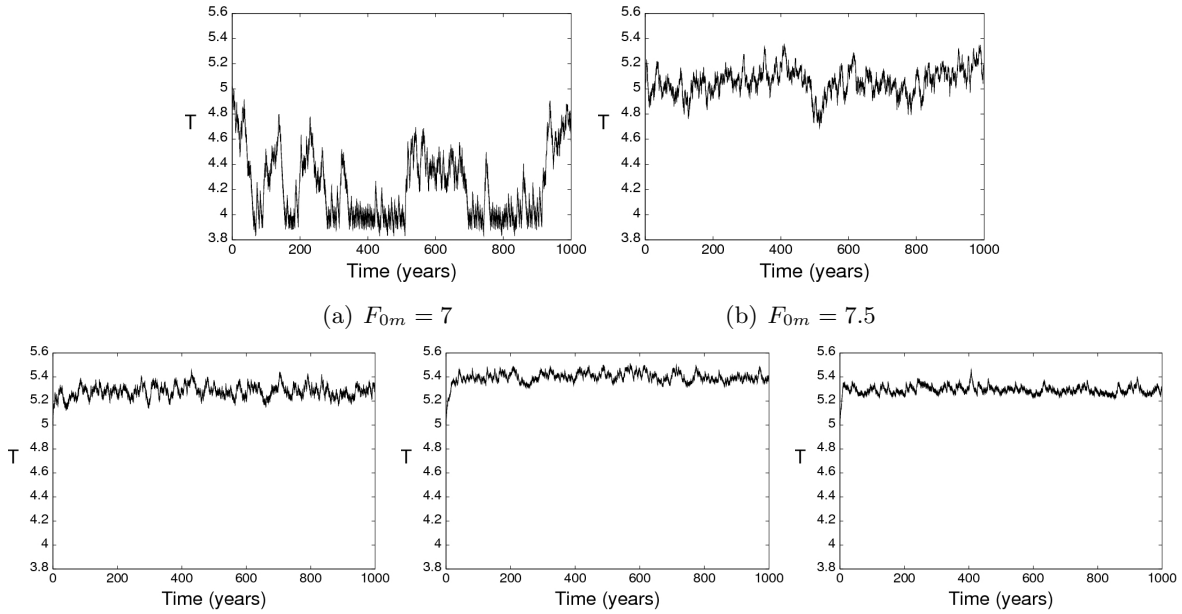

(a) $F_{0m} = 7$ (b) $F_{0m} = 7.5$

(c) $F_{0m} = 8$ (d) $F_{0m} = 8.5$ (e) $F_{0m} = 9$

Figure 5.18: Evolution of the LS84 model variable T with passive coupling for alternative values of F_{0m}. Each model simulation is initiated from the state $(X, Y, Z, T, S) = (1, 1, 1, 5, 1.5 \times 10^{-3})$.

trajectory shown in figure 5.18(c): $(0.167, 1.045, -0.547, 5.348, 1.352 \times 10^{-3})$. The other two single trajectory distributions are derived from model realisations initiated with ICs that are the same in all of the variables except T where the initial state is perturbed to $T = 5.248$ for *IC 1* and $T = 5.448$ for *IC 3*. There are some differences in the three distributions but they are all unimodal with peaks close to $T = 5.3$. The distribution for *IC 3* shows greater density in the high tail of the distribution. Each distribution serves as an approximation to the model climate for T when invoking the ergodic assumption. KS comparisons with a large IC ensemble climate distribution are provided later in this section.

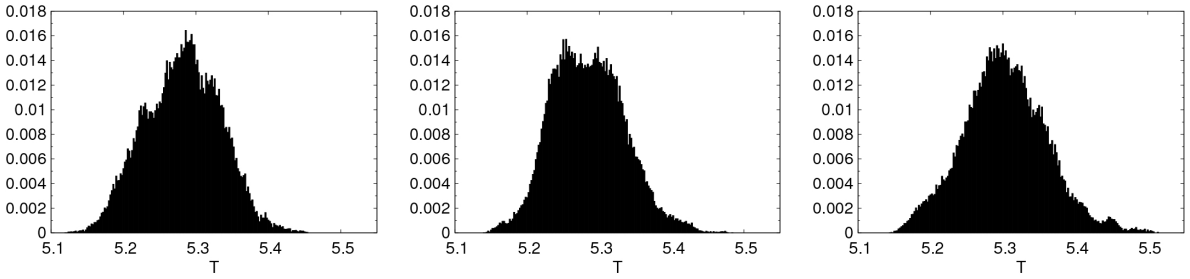

(a) IC 1 (b) IC 2 (c) IC 3

Figure 5.19: Normalised frequency distributions from three single trajectories of T from the LS84 model with passive coupling and a fixed value of $F_m = 8$, with different initial values in T. The three ICs correspond to: *IC 1* $= (0.167, 1.045, -0.547, 5.248, 1.352 \times 10^{-3})$; *IC 2* $= (0.167, 1.045, -0.547, 5.348, 1.352 \times 10^{-3})$; *IC 3* $= (0.167, 1.045, -0.547, 5.448, 1.352 \times 10^{-3})$. In each plot, the y-axis corresponds to the frequency of ensemble members per occupied bin; bin width = 0.002.

5.6.3 Single trajectory results under climate change

In the main experiment presented in this section, the model evolves according to a climate change scenario. The value of F_{0m} decreases linearly from $F_{0m} = 8$ to $F_{0m} = 7$ over the first 1,000 years of the simulation period according to equation 5.14 so that the rate of change in F_{0m} is equal to $\mu = -1 \times 10^{-3}$ (Kyr^{-1}). After 1,000 years, F_{0m} is then held constant at $F_{0m} = 7$ for the subsequent 1,000 years.

$$\frac{dF_{0m}}{dt} = \mu \tag{5.14}$$

Figure 5.20 shows the evolution of the T variable from three single trajectories with ICs used to generate the frequency distributions in figure 5.19 (for the S variable results, see Appendix C, fig. C-6). Even though the three trajectories are initiated with very similar ICs, the results show that the evolution of the trajectories over the 2,000 year simulation period are noticeably different. The divergence is not a particularly surprising result as the LS84 model displays chaotic behaviour in the parameter space explored in this experiment. More interestingly, the results show that the variability exhibited by the model trajectories is apparently dependent on the initial state. Focusing on figure 5.20(c), one might conclude by visual analysis of the time series that the final climate of the model is dominated by oscillations in the LT regime with occasional brief transitions to the HT regime. However, the responses of the model shown in figure 5.20(a) and in figure 5.20(b) display more transitions and longer residence periods in the HT regime. The underlying parameter conditions are exactly the same in each simulation so the differences in the variability that are observed are attributable to the initial state.

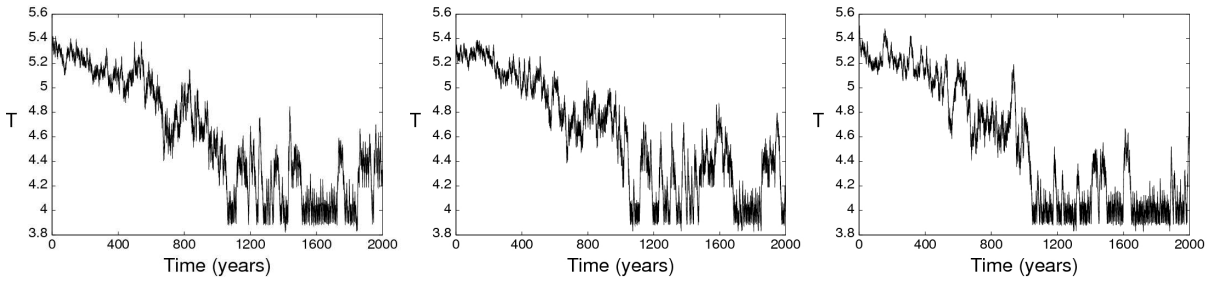

(a) IC 1 (b) IC 2 (c) IC 3

Figure 5.20: Evolution of three single trajectories of T from the LS84 model with passive coupling under climate change, with different initial values in T. The mean value of F decreases from $F_m = 8$ to $F_m = 7$ over the first 1,000 years and then remains constant at $F_m = 7$ for the following 1,000 years. The three ICs correspond to: *IC 1* $= (0.167, 1.045, -0.547, 5.248, 1.352 \times 10^{-3})$; *IC 2* $= (0.167, 1.045, -0.547, 5.348, 1.352 \times 10^{-3})$; *IC 3* $= (0.167, 1.045, -0.547, 5.448, 1.352 \times 10^{-3})$.

Figure 5.21 shows the frequency distributions associated with the last 1,000 years of the three model simulations illustrated in figure 5.20 (the corresponding distributions for S are shown in Appendix C, fig. C-7). The distributions highlight the differences observed in the single trajectory time series'. Figures 5.21(a) and 5.21(b) are visually similar with a small discrepancy in the density where $T \geq 4.6$. However, figure 5.21(c) shows considerably more density in the LT

regime with a peak just below $T = 4.0$ that is almost double the magnitude of the corresponding peaks in figures 5.21(a) and 5.21(b). The increased residence time in the LT regime over the 1,000 year period is simply a consequence of the altered initial state. In the next section, IC ensemble distributions are determined and a quantitative comparison of the single trajectory distributions and the ensemble climate distributions is made using the KS test.

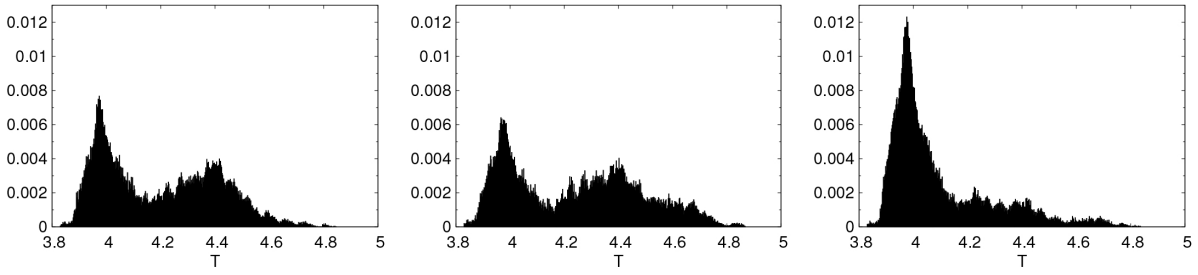

(a) IC 1 (b) IC 2 (c) IC 3

Figure 5.21: Normalised frequency distributions from three single trajectories of T from the LS84 model over a 1,000 year period following a linear change in F_{0m} from $F_m = 8$ to $F_m = 7$ over the previous 1,000 years (as in fig. 5.20). The three ICs correspond to: *IC 1* $= (0.167, 1.045, -0.547, 5.248, 1.352 \times 10^{-3})$; *IC 2* $= (0.167, 1.045, -0.547, 5.348, 1.352 \times 10^{-3})$; *IC 3* $= (0.167, 1.045, -0.547, 5.448, 1.352 \times 10^{-3})$. In each plot, the y-axis corresponds to the frequency of ensemble members per occupied bin; bin width = 0.002.

5.6.4 Ensemble results

A 10,000 member IC ensemble is used to estimate the climate distributions of the LS84 model for passive coupling when F_{0m} is initially fixed at $F_{0m} = 8$, and when F_{0m} decreases linearly toward $F_{0m} = 7$ as described in sections 5.6.2 and 5.6.3 respectively. The IC ensemble consists of 10,000 members, each of which have the same initial value of X, Y, Z and S whilst the initial value of T is given for evenly spaced increments in the range $5.248 < T < 5.448$ to match the range explored for the three individual model realisations.

The 3D colour-maps in figure 5.22 show the evolution of the ensemble over a 1,000 year simulation period when $F_{0m} = 8$. Figure 5.22(a) shows that the range in T is well explored after 100 years with the majority of ensemble members located in the region $5.2 < T < 5.4$. The specific details of the distribution changes subtly at each time instant but the broad characteristics remain consistent over the duration of the model simulation. Similarly figure 5.22(b) shows that the distributions in the S variable are well explored after 100 years with the majority of members in the range $1.34 < S < 1.37 \times 10^{-3}$.

Figure 5.23 shows the KS comparison between the ensemble distributions at each 100 year interval (at mid-winter every 100 years) and the ensemble after the 1,000 year simulation period for the T and S variables; hence $D = 0$ at $t = 1,000$. The value of D approaches $D = 0$ in both variables for all time instants where $t > 0$ years indicating that the ensemble has converged.

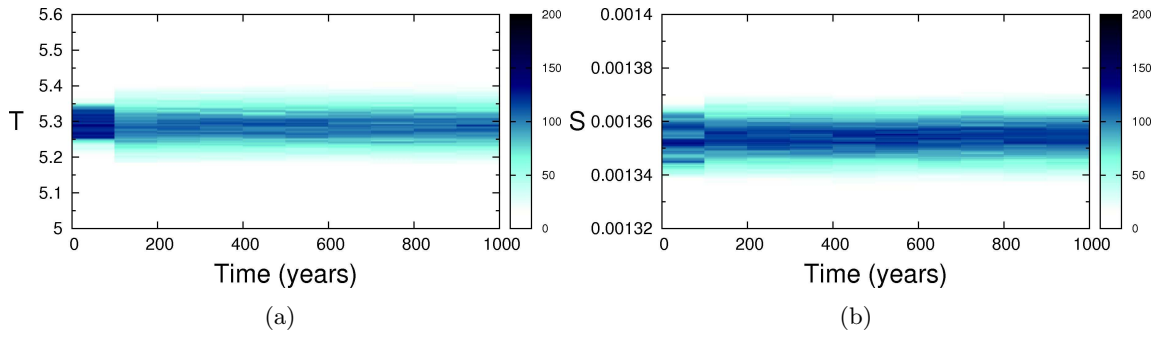

Figure 5.22: 3D colour-map showing the evolution of a 10,000 member IC ensemble in the passively coupled LS84 model when $F_{0m} = 8$ for the variables T and S. The ensemble members have ICs: $(0.167, 1.045, -0.547, T, 1.352 \times 10^{-3})$ where T is uniformly distributed in the range $5.248 < T < 5.448$.

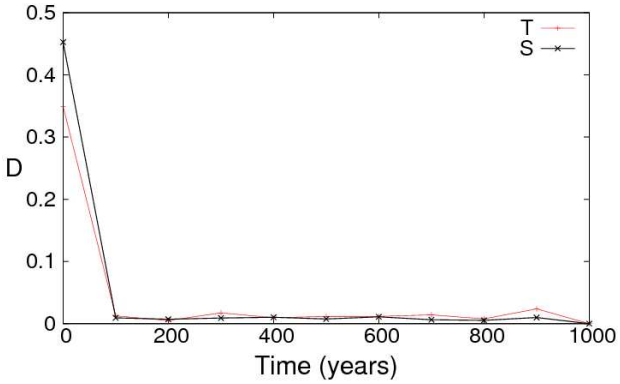

Figure 5.23: KS comparison for the T and S variables between the IC ensemble distributions after a 1,000 year simulation and the evolving ensemble distributions at 100 yearly intervals over the 1,000 year simulation period.

The values of D are between $0.005 < D < 0.024$ for both T and S where $t \geq 100$ years.

The KS test is also used to compare the single trajectory frequency distributions shown in section 5.6.2 to the ensemble distributions after the 1,000 year simulation period. The values of D are given in table 5.5. In both variables, the values of D are higher than the values associated with IC ensemble distributions. This shows that a 1,000 year simulation period of a single trajectory is insufficient to assume ergodicity in the LS84 model when $F_{0m} = 8$. Furthermore, the distributions are less similar in the S variable than in the T variable where the values of D are closer to $D = 0$ due to the inertia in the ocean salinity noted previously. The KS comparison therefore provides a measure of reliability for the ergodic assumption quantifying the ability of single trajectories to produce climate statistics that approximate the climate statistics of the ensemble climate distributions associated with the underlying PA.

Figure 5.24 shows the evolution of the same 10,000 member ensemble when subject to a decreasing trend in F_{0m}, described in section 5.6.3. The ensemble distribution is initially well

Variable	*IC 1*	*IC 2*	*IC 3*
T	0.0579	0.0577	0.0908
S	0.1553	0.1181	0.1137

Table 5.5: KS comparison for the T and S variables between the IC ensemble distributions illustrated in figure 5.22 after a 1,000 year simulation and the single trajectory distributions given in figures 5.19 and C-5 when $F_{0m} = 8$.

constrained in both the T and the S variables and over time the values of T decrease and the values of S increase whilst the range in the distribution expands. After 600 years, there appears to be a small step-change present where trajectories temporarily evolve on a PA where $T \approx 4.8$ and $S \approx 1.5 \times 10^{-3}$. After 1,000 years the trend in the F_{0m} ceases and a larger step-change is evident as the ensemble distributions move rapidly towards the climate distributions associated with the model PA at $F_{0m} = 7$. The ensemble distributions provide the range and relative likelihood of possible states conditioned on the IC uncertainty (embedded in the ensemble design).

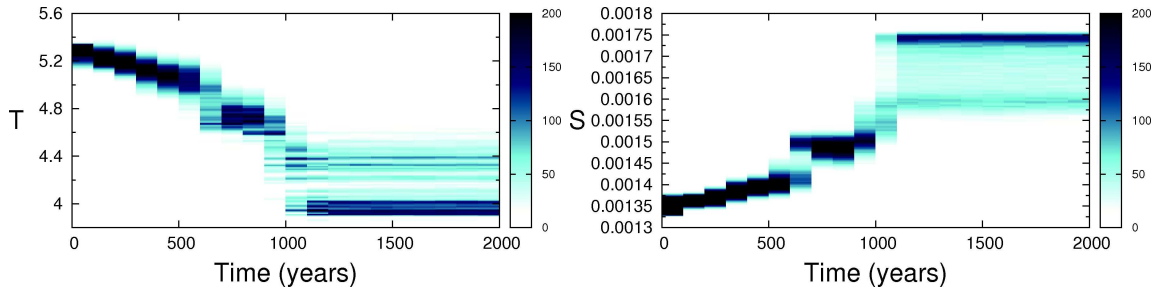

(a) (b)

Figure 5.24: 3D colour-map showing the evolution of a 10,000 member IC ensemble in the passively coupled LS84 model for the variables T and S when $F_{0m} = 8$ initially and then linearly decreases to $F_{0m} = 7$ after 1,000 years and is then held constant. The ensemble members have ICs: $(0.167, 1.045, -0.547, T, 1.352 \times 10^{-3})$ where T is uniformly distributed in the range $5.248 < T < 5.448$.

The single trajectory distributions shown in figure 5.21 are compared to the IC ensemble distributions after the 2,000 year simulation period using the KS test. The results are presented in table 5.6. For *IC 1* and *IC 2*, the values of D increase slightly in the T variable compared to the values derived when $F_{0m} = 8$, given in table 5.5. For *IC 3*, the value of D increases dramatically. A similar result is also observed in the S variable. The results show that the use of the ergodic assumption for a 1,000 year simulation period becomes slightly less reliable for *IC 1* in the T variable and for both T and S in *IC 2* under transient parameter conditions. The ergodic assumption appears to be significantly less reliable for *IC 3* in the climate change scenario presented. In this experiment only three single model realisations are investigated so any conclusion regarding the applicability of the ergodic assumption under climate change in the LS84 model is necessarily tentative. Nonetheless, the results imply that confidence in the ability of a single model realisation to provide reliable quantitative information regarding the climate

distributions of the LS84 model under one set of parameter conditions need not necessarily lead to confidence under altered parameter conditions; further single model runs would be beneficial in refining the conclusion for the LS84 model. More importantly the experiment provides a methodological approach for assessing the reliability of the ergodic assumption for the studies of the climate system involving more complex climate models.

Variable	*IC 1*	*IC 2*	*IC 3*
T	0.0683	0.0884	0.2458
S	0.1242	0.1643	0.3040

Table 5.6: KS comparison for the T and S variables between the IC ensemble distributions illustrated in figure 5.24 after a 2,000 year simulation and the single trajectory distributions given in figures 5.21 and 5.21 when F_{0m} is stabilised at $F_{0m} = 7$ after a 1,000 year linear trend from $F_{0m} = 8$ to $F_{0m} = 7$.

In section 5.3.3 it is shown that a single trajectory frequency distribution, derived from a simulation period of hundreds or even thousands of years (under passive coupling), provides misleading information about the PDFs associated with the PA of the LS84 model under passive coupling, even in the absence of trends in the parameters. In this section, the methodology developed could help to explore whether or not the level of confidence in the ergodic assumption resulting from analysis under particular parameter/forcing conditions is misplaced when extrapolating to the behaviour of the model under altered parameter/forcing conditions. Increasing the scope and scale of the experiment presented here would help to refine the conclusions in the context of the LS84 model. However, potentially more value could be gained by following the methodology to study a range of more complex climate models which exhibit variability on a number of time scales due to the inclusion of more climatic processes. Further discussion of the implications for model experimental design is given in section 5.7.

5.7 Discussion of LS84 Results

5.7.1 Climate variability in a simple coupled model

The climate system includes many subsystems for which the initial state is poorly known. In using simple nonlinear models to inform the design of GCM experiments, it is sensible to focus on the interaction of the primary components which control the variables of interest, on the time scales of interest. The ocean and the atmosphere operate on different time scales and the ocean plays a critical role in determining atmospheric circulation patterns. The ocean also affects the timing and magnitude of extreme events, such as the development of hurricanes and tropical storms which are of particular interest to insurers, so understanding modes of variability in the ocean is a crucial element of the climate change prediction problem.

In section 5.2.5 it is shown that the dynamics of the ocean component of the LS84 model play a significant role in determining the behaviour of the atmosphere. The state of the ocean influences the annual variability in the atmosphere and appears to control the number of summers in which atmospheric variables evolve towards a fixed point solution. The chapter therefore focuses on the role of IC uncertainty in the ocean.

To develop an understanding of climate under climate change and improve predictive capabilities on the time scales of interest to policymakers, it is essential to account for internal climate variability. In the LS84 model, long-term internal variability is manifest in regime behaviour present in the ocean variables, when the model is subject to passive coupling. The internal variability occurs on centennial time scales and the regimes are distinct (in the T variable) leading to almost intransitivity. Lorenz (1997) states that it is difficult to establish whether or not the climate system is indeed almost intransitive but Lorenz explains that "almost intransitivity implies the existence of two or more time scales, which the climate system certainly possesses".

5.7.2 Utilising IC ensembles

Because of the presence of long-term variability in the LS84 model, the use of single model realisations to estimate the model climate PDFs is limited. The ergodicity of the LS84 model is investigated in section 5.3.3 and the results show that almost intransitive behaviour restricts the applicability of the ergodic assumption, even in the absence of trends in the model parameters. The possible existence of almost intransitive behaviour in the climate system (on any relevant spatial and temporal scale) means that an externally driven climate change may be indistinguishable from an internally driven climate change given only one time series of observations. This not only has important implications for the attribution of past climatic changes (as noted by Lorenz (1991a)) but also for how climate models are used to project future climate change and how model output is interpreted by users.

In section 5.4, the LS84 model is used to help determine an appropriate IC ensemble size to

provide robust quantitative probabilistic information about the model climate distributions. An experiment is conducted to determine the minimum ensemble size required to produce a reliable estimate of the probability of a trajectory being in a given regime after a specified simulation period. The results suggest that an ensemble size of 2,000 to 4,000 members is sufficient but any fewer isn't. The experiment is also inverted to determine the memory (traceability of IC uncertainty) in the LS84 model by plotting the percentage of ensemble members (from an IC ensemble originating in the LT regime) in each regime at various time instants, for fixed ensemble sizes. The results show that memory of the IC ensemble is present for a period of up to 200 years. The implication is that multi-decadal and/or centennial variability in the climate system might cause the distributions of climate variables to be IC dependent for many decades or even hundreds of years.

5.7.3 Memory of ICs in the LS84 model

Whilst the memory of ICs in the atmosphere may be lost over a number of weeks, the memory that resides in the oceans and other subsystems of the Earth's climate system (such as the cryosphere, biosphere or stratosphere) is relevant on much longer time scales. As noted by Ghil (2001), "the interactions between the subsystems give rise to climate variability on all time scales". How the memory of ICs in the slowly evolving subsystems influence the evolution of the climate system under altered forcings is highly uncertain. How internal variability reacts under transient forcing is complicated further still (Epstein and McCarthy (2004)).

The time it takes for an ensemble to converge to the model climate distributions provides a measure of the memory of ICs in the model. The evolution of IC ensembles from a transect across the PA state space is presented in section 5.3.2 and the rate at which the ensembles explore the range of model states consistent with the models PA is found to be different for active and passive coupling. Because the model exhibits long-term centennial variability under passive coupling, there is a greater memory of the ensemble ICs and a longer model simulation is required before the IC ensemble approaches the model climate distributions.

Experiments relating to the convergence of model ensembles from different locations on the PA under passive coupling are presented in section 5.5. The convergence between IC ensembles is shown to be dominated by the initial values of T. IC ensembles from the same initial regime converge rapidly but IC ensembles from different regimes converge more slowly. This is an important result in the analogy to the climate system as it means that long-term modes of variability affect the spread of IC uncertainty. Moreover, the results show that reducing uncertainty in the measurement of a particular system variable may reduce the spread in uncertainty for future climate states but only if the variable has an active role in the dynamic evolution of the system.

5.7.4 LS84 with climate change

In section 5.6, the behaviour of LS84 model is investigated when subject to a trend in F_{0m} moving the model between a region of parameter space considered largely transitive to a region which is almost intransitive under passive coupling. The results of single model trajectories are displayed, showing that the evolution of the model is sensitive to ICs. Observing the model behaviour over a simulation period of 2,000 years reveals that the variability exhibited by the model trajectories under altered parameter conditions is dependent on the initial state of the model. The methodology used in the main experiment examines the reliability of the ergodic assumption and in the LS84 model, albeit with a limited sample of single model realisations, the tentative conclusion is that changes in the dynamic behaviour associated with the model parameter conditions limit the reliability of the ergodic assumption. Confidence in estimating the distribution of past climates from a single trajectory need not necessarily lead to confidence in the ability of single trajectories to capture the range of states consistent with some future forcing scenario. Further experiments with more model runs analysing the behaviour of the model in different regions of parameter space would be valuable to understand how the dynamic interactions affect the validity of the ergodic assumption. Furthermore, the methodology could be applied to more complex climate models to understand the implications for assuming ergodicity in the climate system which displays variability on a number of different time scales.

5.7.5 Value of the LS84 model experiments

In the next chapter, the focus is directed towards the use of climate model information in the insurance industry. Addressing the needs of the user community whilst ensuring that scientific uncertainties are well explored is a significant challenge given limited computational capacity. Nonetheless, the results and discussion presented in chapter six suggest that user demands and scientific rigour can be consolidated by the appropriate design of climate model experiments. The objective of the experiments conducted with the LS84 model, and indeed the L63 and L84 models, has therefore been to gain insight into the complex dynamic behaviour of a nonlinear system analogous to the climate system, to guide the design of climate model experiments.

The results presented in this chapter have implications for the way climate modellers explore and interpret uncertainty using GCMs. The seasonally driven LS84 model has been explored to highlight the dangers of relying on the ergodic assumption for a system which displays long-term variability and almost intransitive behaviour. Large IC ensembles are necessary to estimate the climate of the model under fixed and altered parameter conditions and to explore the range of possible states consistent with the IC uncertainty. Ultimately, for climate model experiments to be useful to the user community, they ought to explore all possible future scenarios. This requires a thorough exploration of epistemic and aleatoric uncertainty. Establishing what is possible is a precursor to determining what is likely.

Chapter 6

Climate Model Output and the Insurance Industry

6.1 From Complex Models to Complex Decisions

In the analysis of nonlinear and chaotic low-dimensional models, the focus has so far been on understanding the role of IC uncertainty in the predictability of climate under climate change. The results in chapters three, four and five convey the need for large IC ensemble experiments to detail the changing variable distributions associated with evolving model attractors and pseudo-attractors in response to altered parameter conditions. Throughout these chapters, the experiments have been contextualised by the interests of the climate change adaptation community and specifically the needs of the insurance industry. Here the messages relating to climate predictability amidst uncertainty explored in previous chapters are considered in the context of insurance decisions which are sensitive to climate change. The objective is to present an analysis outlining the needs of insurers, concerning the uptake and use of climate model information in the decision making process, and to expose the challenges in using existing climate model output to inform decisions.

In this chapter, the use and interpretation of climate model information is explored with respect to strategic decisions faced by the insurance industry. The initial part of the chapter focuses on the specific interests of insurers and highlights the relevance of the previous chapters in the interpretation of model-based projections. In section 6.2, the time horizons over which climate information might be deemed relevant for informing decisions linked to specific strategic insurance issues are identified. The rest of the chapter presents the results of a case study analysing the use of Bayesian Networks (BNs) to inform the viability of index-based crop microinsurance (a sector of strategic interest to insurers) for a region in India sensitive to changing climate patterns. Section 6.3 provides an overview of BNs and explains how they have previously been used to tackle climate change decision problems. The scope of the case study is introduced in section 6.4, detailing the geography of the focus area and highlighting

the recent development of index-based microinsurance for climate-related perils. Section 6.5 documents the methodology adopted and provides a preliminary analysis of the data which is used in the BN analysis. The BN results are presented in section 6.6, illustrating different ways to combine model information with past observations of climate to inform decisions using the BN framework. Section 6.7 concludes the chapter with a discussion of the case study results, an appraisal of the methodology and ideas for future work to extend the research.

6.2 The Use of Climate Model Information for Strategic Decision-Making in the Insurance Industry

6.2.1 Interpretation of model output for assessing insurance risks

This thesis aims to combine the insights from simple model experiments with research regarding the relevance of model output for insurance industry decisions to guide the future design of climate model experiments. The previous three chapters present the results for a wide ranging set of experiments conducted with low-dimensional nonlinear models considered analogous to the climate system. The analysis serves a dual purpose in providing a conceptual basis for understanding climate under climate change and in underpinning the design of future experiments on more complex climate models. Although the models used in chapters three, four and five are much less complex than GCMs, the results highlight a number of issues which are relevant to insurers tasked with interpreting the output from climate model projections to guide insurance decisions.

Insurers are ultimately interested in return periods of loss events. Utilising climate science to estimate the frequency and magnitude of damaging meteorological events is therefore an important element in the process of designing insurance products. The analysis presented in chapter three shows that estimating frequency distributions of variables in nonlinear systems using a single trajectory can be problematic; even if it displays transitive behaviour. The results in section 3.7 reveal that a transitive system does not always display ergodicity. The combined effects of resonance and hysteresis in the L63 model climate distributions limit the use of single model realisations to understand the climate of the model. Even in the absence of climate change the results suggest that utilising past observations to estimate frequency distributions of climate variables can be misleading.

Under transient climate change, the predictability of climate variable frequency distributions becomes further complicated by the potential for the underlying dynamic behaviour of the climate system to be forcing dependent. Analysis of the L84 and LS84 models in chapters four and five respectively reveals the impact of altering key parameters on the predictability of the model climate distributions. The shift from transitive regions of parameter space to intransitive or almost-intransitive regions of parameter space, in response to fluctuations in the model parameters, leads to nonlinear responses in the model pseudo-attractor evident in the properties of the IC ensemble distributions. By analogy, the irregularity of the variable frequency distributions imply that estimating recurrence probabilities for climate variables under climate change requires an acknowledgement of the potential for nonlinear shifts in variable distributions and the possibility of abrupt changes in the system's dynamic behaviour.

The use of return periods to estimate insurance risks becomes somewhat confusing in the context of climate change. The notion of a 1 in 200 year loss event implies stationarity, or at least an element of periodicity in the system. Dailey et al. (2009) state that "the 200-year loss has a

0.5% probability of occurring in any given year; that is, it is the loss that can be expected to occur or be exceeded on average once every 200 years". However, as explained in previous chapters, the climate attractor (or pseudo-attractor) is continuously changing in response to altered forcings and boundary conditions so the probability of a 1 in 200 year event, for a system which is undergoing systematic change, is ill-defined. Even in the absence of climate change the magnitude of a hazard with 0.5% probability of occurring is continuously being altered from year to year. Under climate change, the problem of identifying hazard probabilities is exacerbated.

6.2.2 The ergodic assumption in insurance

Part of the motivation for studying the dynamics of the L63, L84 and LS84 models is to establish the limitations of the ergodic assumption in understanding climate under climate change. Insurers also invoke the ergodic assumption when pricing risk based on observational data. For weather and climate-related perils, historical meteorological datasets are utilised to assess the hazard component of the insured risk. Implicit in the use of such data is the notion that the past is a good guide to the future. In estimating the hazard component of the risk, insurers usually assume that the PDF estimated from observed records of meteorological data at a given location is equivalent to the PDF of a meteorological event occurring in the next insurance period.

It is well acknowledged that nonstationarity poses a significant challenge to the insurance industry (Herweijer et al. (2009), Lloyd's (2011a)). For nonlinear dynamical systems, the ergodic assumption has been shown to be misleading in the presence of internal modes of climate variability and forced climate change. To better understand the impact of the ergodic assumption on insurance decisions, it is important to establish how sensitive decisions are to the use of climatology and time series data as opposed to forecast model information in the form of ensemble distributions conditioned on IC uncertainty. Yet until large IC ensembles are run routinely, climate scientists and insurers will not be able to distinguish model uncertainty from errors related to the ergodic assumption. This inevitably hampers the efforts of climate modellers to appropriately communicate model uncertainty to decision makers within the insurance industry. The case study presented in this chapter provides a possible method for evaluating the impact of the ergodic assumption on insurance decisions. As a precursor to the development of the case study, the next section outlines the main strategic issues which would benefit from the appropriate interpretation of climate model output.

6.2.3 Identifying the relevant strategic issues

Climate change is one of a number of strategic issues facing policymakers within the (re)insurance industry. Mills (2009) presents climate change as an issue "bound up in the very fabric of the [insurance] industry and its business environment". The insurance industry

is generally better placed than other societal sectors to cope with the changing nature of risks associated with climate change and can have an important role to play in communicating climate risks to society (Dlugolecki et al. (2009)). However, the insurance industry is vulnerable to an increase in losses associated with the changing frequency and magnitude of climate-related perils. In examining the hazard component of climate-related insurance risks for specific business lines, insurers inevitably turn to the climate modelling community to provide quantitative and qualitative guidance to inform the decision-making process.

Within the elaborate and complex trading structures of the insurance industry, the decision-making process can become convoluted with actions taken at a variety of organisational levels. Decisions are often multifaceted and are seldom made by one individual. In relation to the use of climate model projections, decisions are likely to be mainly strategic rather than operational. In section 6.3, the results of a case study exploring the use of climate model output in the emerging microinsurance sector is presented. The decision to focus on microinsurance was informed by the identification of strategic issues in this field that may benefit from climate model information.

Establishing the planning time horizons for strategic insurance issues is important in determining how model information can best be incorporated into the decision making process. Preliminary research involved analysis of the existing literature relating to long-term insurance interests and the extent to which climate affects the planning process (documented in section 2.3). In addition, informal discussions were held with insurance practitioners from a number of insurance institutions. Structured interviews were not deemed appropriate due to the exploratory nature of the research. The practitioners involved were selected based on their expertise in the application of climate information to insurance decision making. The preparatory questions used to facilitate discussion are given in Appendix D.

The relevant literature and discussion outcomes were used to construct the planning time scale diagram in figure 6.1. Ten strategic issues were identified (see table 6.1) and subjective estimates for their respective planning time horizons assessed. The information contained in figure 6.1 illustrates the time scales over which climate model predictions may be used to inform policy decisions.

Because of the lack of formal guidance in the use of model information for insurers on the longer time scales associated with anthropogenic climate change, this chapter is focused on strategic issues which have "long" planning horizons. The issues considered to have a long planning horizon in figure 6.1 are those which extend to 10 years or more. Nevertheless, the definition of climate as the distribution of states conditioned on IC uncertainty is as relevant for short term risk analysis as it is for long-term climate change impacts assessments. In determining the forecast distribution of a particular climate variable, a large IC ensemble is required because of the absence of stationarity and potential lack of ergodicity in the climate system. In the PMS, the climate-related risks could be exactly calculated but given imperfect models, IC ensemble distributions are best used to highlight areas of agreement (or disagreement) between different model forecasts.

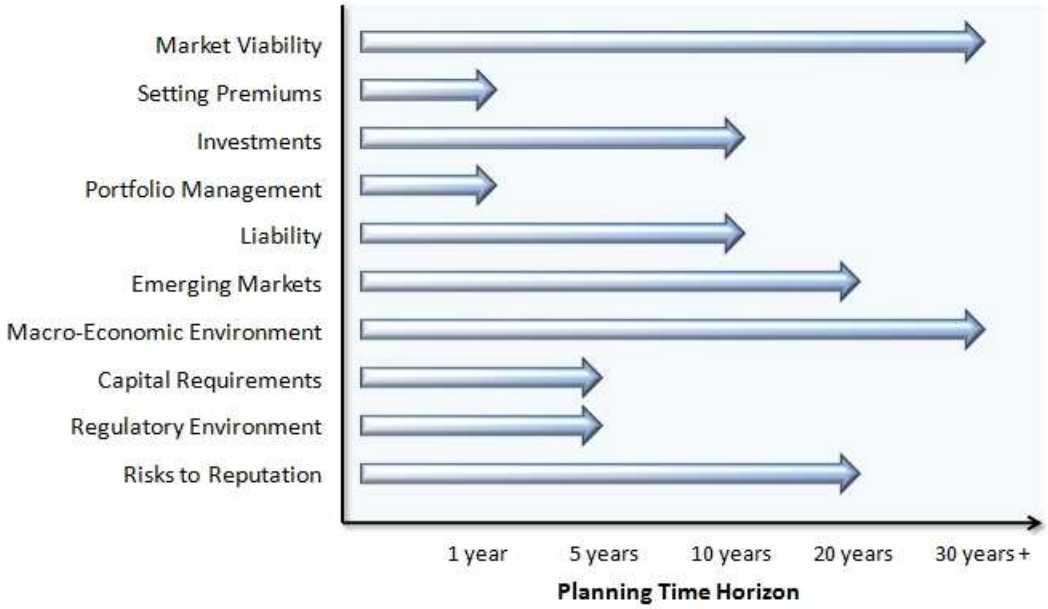

Figure 6.1: Subjective assessment of planning time horizons for strategic non-life insurance issues which could be directly or indirectly impacted by climate change.

For strategic planning climate risk becomes entangled with many other pressures facing the industry. The relative importance of climate variability and climate change compared to other strategic considerations will depend on an insurer's specific exposures and lines of business. Nevertheless, as mentioned in section 2.3.1, the global auditing company Ernst & Young have stated that for insurers, climate change is a more pressing concern than demographic change, emerging markets and regulatory intervention (Ernst & Young (2008)). However, such concerns are not necessarily mirrored in the views of insurance company board executives. Lloyd's of London and the Economist Intelligence Unit (EIU) have published a joint report assessing corporate risk priorities and attitudes around the world (Lloyd's (2011b)). Of the 50 identified strategic risks, climate change was ranked 32nd behind "Strikes and industrial action" and just ahead of "pandemics". However, as shown in figure 6.1, knowledge of the impacts of climate change can influence other strategic concerns. Notably in the Lloyd's (2011b) report, "reputational risk" was identified as the third most important strategic risk, behind "loss of customers" and "talent and skills shortages" yet climate change has the potential to affect the reputation of an insurance company. For example, if an insurer fails to acknowledge changes in the risk of a loss event of a climate-related peril and suffers increased losses as a result, this can affect the confidence of policyholders and shareholders. These issues are highlighted in the Lloyd's (2011b) report which states, "as the impacts of climate change accumulate, [insurers] may be failing to grasp the very real threats that natural catastrophes pose to business continuity".

As described in this section, when considering future loss events it is essential for insurers to understand climate risk in the context of other socio-economic factors. In sections 6.3 to 6.6, a

Strategic Issue	Description
Market Viability	The capacity for a given business line or insurance activity to remain profitable.
Setting Premiums	Determining the price or percentage of the maximum indemnity to be charged to the policyholder.
Investments	Allocation of capital in externally managed assets, funds or other financial products.
Portfolio Management	Assessing the collective performance of a number of insurance products.
Liability	The legal responsibility of the insurer to account and communicate the risks covered for a particular line of business.
Emerging Markets	New lines of business in established markets and/or existing lines of business in burgeoning economies.
Macro-Economic Environment	The large scale external drivers of societal and economic change which affect business performance and influence decisions.
Capital Requirements	The level of capital required to underwrite insurance policies and cover payouts in the event of a loss.
Regulatory Environment	Political, financial, environmental and social obligations by which insurers must operate.
Risk to Reputation	Negative implications for a particular insurance company as result of unpopular business activities and/or behaviour before, during or following loss events.

Table 6.1: Description of the strategic issues identified in figure 6.1.

case study is presented to address two strategic insurance issues identified in figure 6.1; market viability and emerging markets. Climate model output is used directly to explore the viability of microinsurance[1] in relation to the use of climate information and other important decision factors in an emerging economy, India.

[1]Microinsurance refers to insurance characterised by low premiums and low coverage limits.

6.3 Case Study: Using Climate Model Output to Inform the Pricing of Weather Index Microinsurance

In order to exemplify the issues related to the use of climate model output for decision making within the insurance industry, a case study is developed. A Bayesian Network (BN) is constructed to explore the viability of index-based microinsurance (defined in section 6.4.1) in providing crop coverage against drought and excess rainfall in Kolhapur, western India. The following analysis outlines the methodology adopted and presents the results in relation to the key themes of the thesis; model uncertainty, the use of the ergodic assumption and decision making under uncertainty and ambiguity. A key objective is to establish whether or not climate model output in it's current format is useful and usable by insurance practitioners.

6.3.1 The Bayesian Network approach

A number of techniques can be applied by insurers and practitioners in using climate model output to inform the pricing of weather index insurance. Fitting statistical distributions to model output data is one such method to estimate tail probabilities. The *Poisson* distribution is often used in risk analysis within the insurance sector to generate estimates of the expected frequency of claims (Embrechts et al. (2003)). With specific regard to rainfall data, other statistical distributions with positive "fat tails", such as the Weibull distribution, can be fitted to climate data to determine the probability of exceeding defined thresholds. Yet fitting statistical distributions requires assumptions to be made about the nature of the data which may be unrepresentative. Furthermore, when combining different types of quantitative information to inform pricing decisions, it is useful to consider techniques that can handle and propagate multiple sources of data. A number of decision tools are available to combine multiple sources of data. Decision trees have been used to propagate probabilistic information to inform climate sensitive decisions (e.g. Hobbs et al. (1997)). However, there is only a one-way flow of information in a decision tree and it can be useful to consider a two-way flow of information to make inferences. Hall et al. (2005) shows how different types of inference diagrams can be used in climate impacts analysis stating that "influence diagrams can communicate knowledge in a formal but accessible manner". BNs are simply one form of inference diagram that can be used to propagate probability distributions combining continuous and discrete data. Given the uncertainties associated with climate change, it is not always appropriate to characterise climate uncertainties in probabilistic terms (see section 2.2.5). However, a BN analysis can be used to highlight sensitivities and in this section, the BN approach is adopted to explore the sensitivity of pricing assumptions to different sources of climate information to assess the viability of weather index insurance under climate change.

A BN is a graphical model with an underlying probabilistic framework, which characterises and quantifies an outcome of interest, the relevant variables and the causative interactions (Donald et al. (2009)). BNs update probabilities throughout the network according to Bayes Theorem

given in equation 6.1:

$$P(A\,|B) = \frac{P(B\,|A)\,P(A)}{P(B)} \tag{6.1}$$

The BN constructed here is a decision tool which provides a means for quantifying and communicating the output from complex computer models in relation to other factors and pressures facing decision makers. The approach benefits from the input of experts across disciplines and, more importantly, direct communication with the end user. Unlike traditional sector-based climate impact assessments, the tool is designed to be tailored to a specific decision for a particular user. BNs allow for the explicit quantification of risk and uncertainty combining evidence from diverse sources incorporating subjective beliefs and objective data (Fenton and Neil (2004)). Cain (2001) distinguishes between two potential uses of a BN:

1. BNs can be developed to provide a mathematically optimal decision on the basis of the information provided to the BN.

2. BNs can be used in a way that promotes the improved understanding of the system, leaving the decision makers to reach their own conclusions on the basis of that knowledge.

Given the large number of inherent uncertainties associated with climate prediction, it is more appropriate to use BNs to promote improved understanding rather than attempting to provide optimal decisions based on incomplete information. Indeed, although the network developed here aims to be exhaustive with regards to the factors included, the network doesn't have to be complete in order for the BN to act as an instrument for consultation (Ouerdane and Tsoukias (2009)).

The BN approach has been used extensively in a wide range of research fields and industrial sectors as a tool for structuring and informing the decision-making process (Heckerman et al. (1995), Fenton (2007)). Advances in research over the past few decades, led by Pearl (1986) and Lauritzen and Spiegelhalter (1988), have enabled a transition from a computationally inefficient and time-consuming process towards the development of a powerful tool which can be employed in many real-world applications (Fenton and Neil (2007)). The tool has been applied to a small number of climate-related studies which each address specific decision problems (Kuikka and Varis (1997), Wooldridge et al. (2005), Musango and Peter (2007)). However, in these studies BNs are not used to test the sensitivity of decisions to multiple climate information sources. Here the approach is developed to investigate whether or not the BN tool is useful in providing a framework to inform insurance decisions using data from multiple climate models in combination with observed data.

6.3.2 Example Bayesian Network: winter forecasts for salt stocks

In this section, an example BN is described to demonstrate how a BN can be used to inform a decision. A hypothetical example, depicted in figure 6.2, shows how the decision of whether

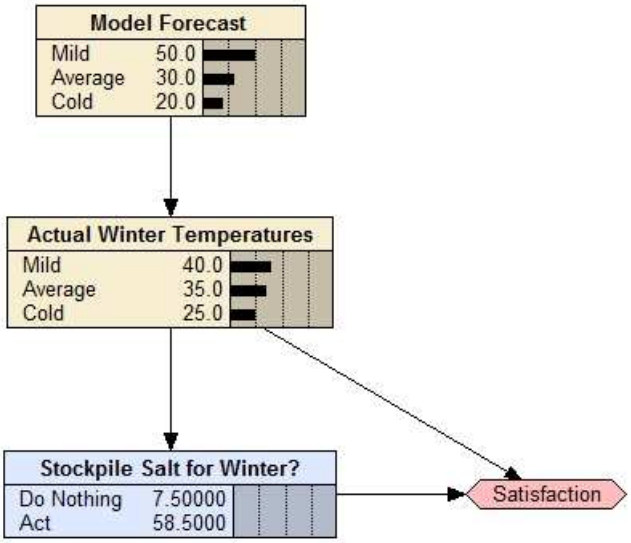

Figure 6.2: BN for an example decision problem; whether or not to stockpile extra salt for the coming winter.

or not to stockpile extra salt for the forthcoming winter might be aided by a seasonal forecast of mean temperature. The software used to create the eBN is Netica (Software Corp. (1998)); this software is also used to develop the microinsurance case study. The two yellow nodes denote the variables (*Model Forecast* and *Actual Winter Temperatures*) and the linking arrow represents a relationship between the two variables; *Model Forecast* is called the *parent* node and *Actual Winter Temperature* is the *child* node. The horizontal bars show the probabilities associated with each state and in each variable node the probabilities must sum to 100. Arrows typically denote a causative relationship but in this example the actual winter temperatures are clearly not conditional on the model forecast. Rather, the arrow represents a relationship between the actual winter temperatures and the model forecast based on verification statistics of past forecasts. The conditional probability table (CPT) associated with the *Actual Winter Temperatures* node is given in table 6.2. The values in the table are illustrative but they could be derived from observations and verification statistics of the seasonal forecast. Based on the information in the CPT and the probabilistic model forecast, the probabilities given in the *Actual Winter Temperatures* node show that mild conditions is the most likely outcome (40%), average conditions is the second most likely outcome (35%) and cold conditions is the least likely outcome (20%).

Model Forecast	**Actual Winter Temperatures**		
	Mild	Average	Cold
Mild	67	20	13
Average	15	70	15
Cold	10	20	70

Table 6.2: Conditional probability table for the *Model Forecast* node in figure 6.2.

The blue decision node (*Stockpile Salt for Winter?*) shows two possible decisions that can be made: do nothing or act (where acting means to stockpile salt). The pink *Satisfaction* node calculates the utility for each decision in the decision node based on the input data from the *Actual Winter Temperatures* node. The numbers given in table 6.3 are also illustrative but show the plausible utility values associated with the six potential outcomes. The values would be defined by the user to represent objective economic measures or subjective preferences. The values are relative to each other so they do not need to add up to a specific total. The scale is linear and values can be negative to convey dissatisfaction; here a value of *-200* is used to highlight a deeply unsatisfactory outcome.

Actual Winter Temperatures	**Stockpile Salt for Winter?**	**Satisfaction**
Mild	do nothing	100
Mild	act	0
Average	do nothing	50
Average	act	60
Cold	do nothing	-200
Cold	act	150

Table 6.3: Utility node outlining the satisfaction of the user based on the information in figure 6.2.

The numbers displayed in the decision node, next to the two options (*act* and *do nothing*), show the expected utility of each decision based on the information in the network; the higher the value the more favourable the option. Unlike in the variable nodes, the values are not probabilistic and need not add up to 100. In the example BN in figure 6.2, the optimal decision would be to "act". Based on the model forecast, the relationship with actual temperatures and the values in the utility node, the risk of a cold winter is sufficient to warrant stockpiling salt.

In this simple example, the probabilities are well known and the utility of options are assumed to be representative so taking the optimal decision is sensible. However, when using the BN tool with imperfect and incomplete information the network is more appropriate for challenging the user's preconceptions regarding the relative utility of the available options. The chapter now proceeds to introduce the focus and scope of the BN case study.

6.4 Case Study Description: Weather Index Insurance for Drought and Excess Rainfall cover in Kolhapur, India

6.4.1 Index-based microinsurance

Traditional forms of crop insurance cover multiple perils, including weather-related perils such as hail and drought as well as non-weather-related perils such as pest and disease outbreaks. However, as explained by Skees et al. (1999), many of the risks covered by private and public insurance schemes in the developed world are considered infeasible in developing countries. The costs of administering traditional claims-based insurance products to low-income farmers in developing countries becomes prohibitively expensive for private insurers. Skees et al. (1999) state that index-based insurance provides an attractive alternative for developing countries. For a weather index insurance scheme, "loss estimates are based on an index, or proxy for loss rather than upon the individual loss of each policyholder" (Skees et al. (2007)). This means that once a proxy is triggered (e.g. rainfall accumulation falls below a certain threshold) all policyholders in the affected area receive a payout. The administration costs of index insurance schemes are significantly lower as the claims-handling process is bypassed. Consequently, over the past decade there has been a huge increase in the research and deployment of crop index-based microinsurance for weather-related perils such as drought, excess rainfall and wildfire.

For weather-related perils, traditional claims-based insurance and reinsurance premiums are typically derived from available loss data-sets as well as established relationships between meteorological events and accumulated losses. However, it is challenging to disentangle the climatic and socio-economic components of claims-based insurance losses because damages are non-trivially related to the magnitude of the hazard (i.e. weather event), exposure to the hazard and vulnerability of insured assets. For index insurance schemes, the uncertainties associated with the response of the physical climate system are disaggregated from socio-economic considerations so a direct sensitivity analysis of a given insurance pricing structure to climate input data can be achieved. Yet from an insurance perspective, setting the thresholds at which payouts for a given peril are triggered is often problematic, given the need for robust relationships between meteorological conditions and insured losses. Index insurance is therefore associated with significant "basis risk" which represents the chance that the payment a policyholder receives when the proxy measure is triggered does not match the actual loss experienced. A study prepared by GlobalAgRisk states that basis risk can deter consumers because individuals may not have sufficient confidence that payouts will reflect the losses that occur in reality (USAID (2006)). Skees (2008) therefore states that index-based schemes are not replacements for traditional insurance but rather they serve as a foundation for developing financial mechanisms in new markets.

The United Nations has advocated the use of index insurance as a "soft" climate change adaptation measure[2] within developing countries but it is important that the index insurance

[2]See UNDP best practice project, available at http://unfccc.int/adaptation/nairobi_work_programme/

policies are themselves resilient to climate change. There is a need to ensure that pricing mechanisms are fair and utilise the available climate information. Alderman and Haque (2007) note that in order for index insurance to be effective, indices ought to be easily measured, objective, transparent, independently verifiable, and available in a timely manner. They also comment that the probability distributions ought to be reliably estimated implying the need for a stable time series' of information. Yet in the context of climate change, meteorological variable time series' are unlikely to be stationary so index-based insurance policies, derived from past data alone, may be at risk of over or underestimating the probabilities of triggering payments. Nonetheless, current weather index insurance products are priced according to past times series of ground-based observations. A report by the World Bank (2011) states that in order to derive an appropriate premium for a weather index insurance product, 30 years of continuous daily data are ideally required meaning that weather index insurance products are typically contingent on the availability of long time series' of observations. The BN analysis presented here, which incorporates climate model forecast information, therefore represents a step beyond the reality of how index insurance pricing decisions are currently made.

Hochrainer et al. (2008) state that the viability of microinsurance schemes can be viewed from two perspectives: from the view of insurers (or supply-side perspective) or from the view of the clients (the demand-side perspective). This study investigates whether climate model information can inform the supply-side in guiding the appropriate pricing of index insurance and determining the viability of weather index insurance under altered climatic conditions.

6.4.2 Focus region: Kolhapur, India

The focus region for the case study is Kolhapur district, in western India. The region was chosen for a number of reasons. Initially, India was chosen because a large volume of high resolution RCM data has recently been made available by the HighNoon project; a project exploring the future water resource of the Ganges river basin (Wiltshire et al. (2010)). It is therefore advantageous to choose India as the focus developing country, given data is available to demonstrate the use of climate model output within a BN framework in guiding index-based microinsurance policy design. Kolhapur was specifically chosen as it is located at the edge of the core monsoon region (see figure 6.3) so the region's climate is highly influenced by the variability associated with the summer monsoon rains. Changes in the timing and/or magnitude of the monsoon would therefore have a significant impact on the region's crop yields. In addition, the microinsurance company MicroEnsure have recently begun a pilot project for farmers in the area (Hazell et al. (2010)). There is evidently a market and a need for appropriately designed microinsurance in this region of India[3].

Kolhapur district has a population of approximately 3.5 million people, with almost 30% living

knowledge_resources_and_publications/items/4748.php.

[3]The results are not being directly used by MicroEnsure or any other microinsurance companies.

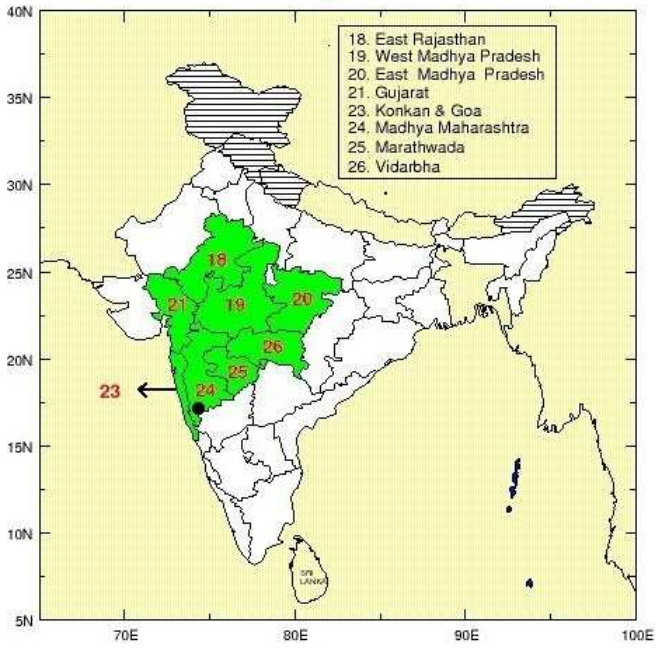

Figure 6.3: Indian Core Monsoon Region (highlighted in green). The black circle denotes the location of Kolhapur City in Madhya Maharashtra, India (IITM (2011)).

in urban areas, most of whom live in the district's main city also named Kolhapur[4]. The district has a total land area of 768,500 hectares, of which 104,000 hectares (13.5%) are devoted to rice production, making it the main crop for local farmers and the regions main commercial crop. The rice crop is a Kharif crop which means the main growing period occurs in summer during the monsoon period. The BN developed for this study focuses on the meteorological triggers at which payouts might occur for losses associated with rice yields in Kolhapur.

[4]Data correct for 2001 - available from Collector Office, Kolhapur (2009).

6.5 Methodology

6.5.1 Constructing the Bayesian Network

An approach developed by Ames et al. (2005) in relation to watershed management, and adapted by Daron and McNeall (*in preparation*) for climate change impacts assessments, is used in this study. The approach consists of seven key steps (given below) to guide the construction of the BN. Implementation of the seven steps is described in this section with each step taken in turn.

1. Identify management endpoints
2. Identify alternative decision pathways
3. Identify critical intermediate and exogenous variables
4. Establish discretization states for network variables
5. Decide on the causalities in the network
6. Identify data sources
7. Interpret the meaning of the probabilistic results

As the initial step aims to identify user objectives, the approach is decision-oriented and therefore consistent with an "assess-risk-of-policy" framing rather than a "predict-then-act" approach (Dessai and Wilby (2011)). Consequently, the BN is tailored to the needs and interests of the user and inherently excludes irrelevant and superfluous information.

Implementing the methodology

To address the first step in the BN construction methodology, informal discussions were held with insurance experts from Lloyd's of London and Willis Reinsurance to determine possible management endpoints for the case study being developed. The discussions were centred on the current use of climate information in designing crop microinsurance products in emerging markets. It became apparent that strategic decisions and pricing decisions, related to index-based microinsurance policies, are challenging for a number of reasons. From an actuarial perspective, the primary concern results from the lack of reliable and detailed historical loss data and meteorological data within many developing countries meaning that the estimation of return periods for crop loss events is difficult. Additionally, minimising basis risk and building trust between the policyholders and the insurers was expressed to be of paramount importance. Discussants also highlighted the issue of price volatility in yields which can hinder the development of successful insurance products[5]. Discussants agreed that the objective of

[5]Battisti and Naylor (2009) argue that whilst food price volatility presents a daunting short-term challenge for the markets, the long-term impact of climate change on food production is far more serious.

the BN approach should be to demonstrate the sensitivity and viability of various pricing assumptions to different sources of climate information, including model projections and observational data. The management endpoint was therefore established as a determination of the viability of insurance premium/payout structures under the current climate and plausible future climates.

In addressing the second step in the methodology, the possibility of alternative decision pathways was considered but only one decision pathway was identified. The management endpoint of establishing the viability of the product is a function of the threshold exceedance probabilities, utilising different climate information sources, and the pricing structure. The decision options are therefore constrained to adjusting the pricing structure or withdrawing the product. If the study were to be broadened in future research, to analyse the development of index insurance across different perils and regions, the number of possible decision pathways may increase.

A number of possible variables were considered in step three of the methodology. The agricultural sector in India is dependent on the timing and magnitude of the summer monsoon rains. The risk of drought is most acute for rain-fed agriculture where crops can suffer from water stress leading to low crop yields (Gadgil and Kumar (2006)). Using data from 306 rain gauges across India from 1871 to 1978, Mooley and Parthasarathy (1984) show that historically about 75 to 90% of annual rainfall occurred during the summer monsoon months, June to September. The primary variable nodes were therefore identified as the cumulative precipitation totals for key periods in the monsoon season. This information would feed into threshold exceedance estimates for the perils under consideration; excess rainfall and rainfall deficit. In addition, the sources of climate information (model/observations) are key to the objectives of the BN study and accordingly a variable which can weight/select the climate information sources is necessary. Given the focus on past and future climate the time scale of interest becomes a variable node. Finally assumptions about premium prices and policy expenses are included in the network.

Step four involved establishing the states to which the data is discretised. For the rainfall data, the states of interest correspond to the thresholds at which payouts occur. Whilst the thresholds change according to the crop-type, location, soil-type and actuarial judgements, typical values are selected for drought and excess rainfall conditions for the rice-crop. Rajagopalan (2009) states that the rice crop requires about 1200 mm of rain over the monsoon season and Veeramani et al. (2005) uses similar figures whilst citing a monthly requirement of between 250 and 350 mm. Another study by Bhuiyan (1992) gives a suitable range for rice crop production between 700 and 1500 mm over the monsoon season. Veeramani et al. (2005) states that the rice crop is more sensitive to drought than flooding. Threshold values for rainfall deficit and rainfall excess are therefore chosen with reference to the available literature as well as exercising an inevitable element of subjective preference. Maximum indemnity payouts for drought are assumed to be issued for precipitation totals below 150mm per month and maximum payout for excess rainfall is assumed to be issued for precipitation totals above 600mm per month. As illustrated in section 6.6.1, intermediary thresholds are also selected for partial payouts related to decreased

but not failed yields.

The causalities are determined in step five of the methodology. The input data is determined by the climate time scale of interest and by the choice of observational data, model data or a weighted combination. The combined or individually selected data determines the expected distribution of precipitation for the period of interest. This data then translates into threshold exceedance values for rainfall deficit and rainfall excess. The losses are determined from the threshold exceedance probabilities and the expected utility is a function of the losses, the premiums and the expenses.

The sixth step involves identifying the data on which the BN is conditioned. A recent project funded by the European Commission, "HighNoon", aims to assess the impact of Himalayan glacier retreat and possible changes in the Indian summer monsoon on the water availability in northern India (HighNoon (2009)). With help from the UK Meteorological Office, data was made available for use in this study. The model output covers the Kolhapur region and a detailed explanation of the model runs and model output is included in sections 6.5.2 and 6.5.3. Observational data was also available for the period 1961 to 2004 from the APHRODITE project which has developed high resolution (0.25° x 0.25°) gridded daily precipitation datasets for Asia (Yatagai et al. (2008), Yatagai et al. (2009)). The project predominantly used data from rain-gauge observations across Asia, including India, and refined algorithms in collaboration with climate modellers and data users.

The final step of the methodology refers to the use of probabilistic information for informing decisions. The objective of the insurer is to ensure that the index insurance provided to farmers is fair, representative and profitable. To maintain profitability, the insurer has various options. The most simple option is to adjust the premium to reflect the underlying risk. However, the insurer can also change the thresholds at which payouts occur, the value of the payouts at each threshold and target decreases in the expenses (per policy) to make the premiums more affordable. The probabilities in the BN can therefore be used to stress-test pricing assumptions to enable insurers to find suitable policy structures which are profitable but ultimately appealing and affordable to the policyholders. In the results section of this chapter (section 6.6), a number of different BNs are presented to show how the methodology can be used to contrast different network assumptions and climate model choices.

6.5.2 Description of the climate model and observational data

The HighNoon project utilises data from the UK Hadley Centre regional model, HadRM3 (Jones et al. (2004)). The configuration of HadRM3 used in the model simulations has a horizontal resolution of 25km, with 19 vertical levels in the atmosphere and includes MOSES II (Met Office Surface Exchange Scheme), a tiled land surface scheme (Essery et al. (2001)). Whilst the study is focussed on the Ganges river basin, RCM runs have been performed for a domain which covers India and a broad area of southern Asia, as shown in figure 6.4.

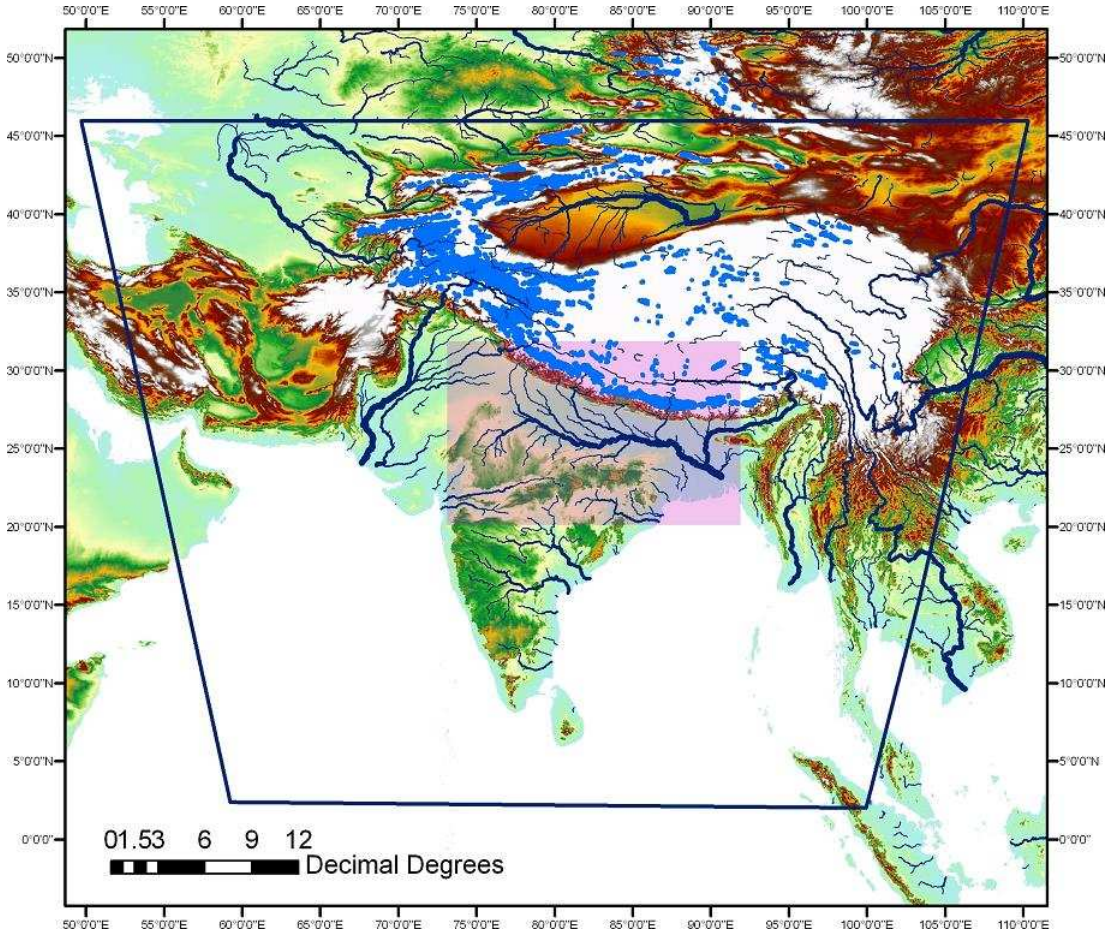

Figure 6.4: HighNoon model domain used for the HadRM3 RCM runs (blue box) where the pink shaded area is the Ganges sub-region considered in the HighNoon project (reproduced from Wiltshire et al. (2010)).

The HadRM3 model was run using boundary conditions from two GCMs, ECHAM5 (Roeckner et al. (2003), Hagemann et al. (2006)) and HadCM3 (Gordon et al. (2000), Pope et al. (2000), Collins et al. (2001)). The GCM climate change simulations are based on a single emissions scenario; the SRES A1B scenario which assumes rapid economic growth, a convergent world and a balanced emphasis on all energy sources (Nakićenović et al. (2000)). Consequently, the projections do not account for forcing uncertainty from alternative future anthropogenic emissions trajectories. However, the simulations do provide an opportunity to test the sensitivity of RCM results to the driving GCM. In addition, the HadRM3 model was run using boundary conditions from ERA-Interim data (Simmons et al. (2010)) and the reanalysis climate time series data is included in this study.

With a focus on drought and excess rainfall risk in Kolhapur, precipitation data for the 25km grid cell which encapsulates the latitude and longitude values of Kolhapur city (16°70'N, 74°23'E) was extracted from the HighNoon data archive with help from the UK Met Office Hadley Centre. The data consists of monthly precipitation totals. The ERA-Interim model

reanalysis data used in this study is given for the period 1990 to 2008 whilst the time series' from the two driving GCMs consists of monthly data for the period 1960 to 2099.

6.5.3 Preliminary data analysis

The model data extracted from the HadRM3 runs driven by HadCM3, ECHAM5 and ERA-Interim is compared to the observational data from the APHRODITE project. The precipitation data from the RCM runs was available as raw model output so does not include any bias corrections. Figure 6.5 shows cumulative precipitation data for the monsoon months (June to September) for the period 1960 to 2099. The figure includes observational data (black) for the period 1961 to 2004 and the output of the RCM driven by ERA-Interim reanalysis data (purple) for the period 1990 to 2004. The blue short dashed line shows the output from the RCM driven by the HadCM3 GCM and the long dashed red line shows the output from the RCM driven by the ECHAM5 GCM.

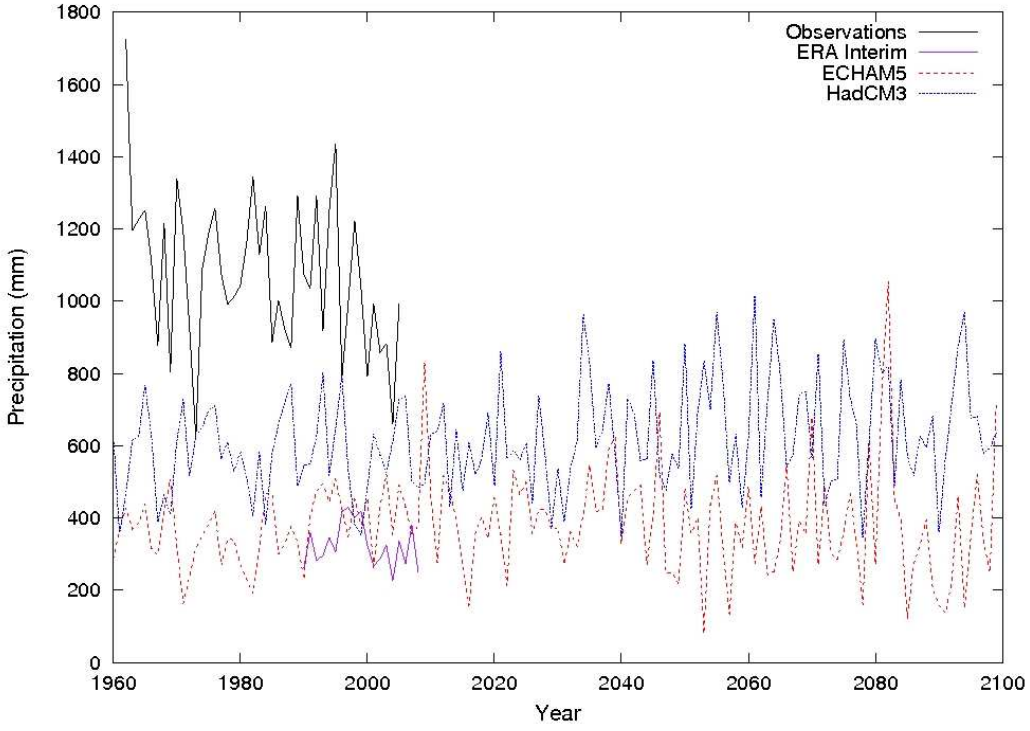

Figure 6.5: Model and observational cumulative precipitation data for Kolhapur, India for the monsoon months June to September. Observational data from APHRODITE is shown for the period 1961 to 2004, ERA-Interim data is shown for the period 1990 to 2008 and the HadRM3 data driven by HadCM3 and ECHAM5 is shown for the entire period, 1960 to 2099.

The data shown in figure 6.5 reveals large systematic biases between the model output and the observational data. Summary statistics of the data are provided in the table in figure 6.6. The summary statistics for the model projections are given for 1961 to 2004 (to provide a comparison to the observed results); for 2020 to 2049 (the extent of the planning time scale

for developing insurance products in emerging markets); and for 2070 to 2099 (to highlight the long-term changes in rainfall projections). There is a large difference in the mean of the observations and the RCM output for both GCMs and the ERA-Interim reanalysis data. The HadCM3 driven output for the period 1961 to 2004 produces a mean rainfall value almost half the observed value of $1073.64mm$ whilst the ECHAM5 and ERA-Interim driven output produce roughly three times less mean rainfall than the observations. The annual variability in the observations also appears greater than the RCM output. The ERA-Interim data produces a relatively low standard deviation ($61.87mm$) in the precipitation values. The relatively high annual variability in the observed data suggests that the ERA-Interim reanalysis does not capture the annual rainfall patterns accurately. Both sets of GCM driven data suggests that the variability increases under future climate conditions, indicated by the increased standard deviations and ranges in precipitation values in columns four and eight of figure 6.6 respectively.

Data Source	Time Interval	Mean	Standard Deviation	Trend	Min	Max	Range
Observations	1961 to 2004	1073.64	213.93	-5.78	621.60	1725.68	1104.08
ERA-Interim	1990 to 2008	325.82	61.87	-1.93	225.62	429.13	203.51
HadCM3	1961 to 2004	573.89	119.13	0.28	353.46	800.66	447.20
HadCM3	2020 to 2049	603.10	145.91	0.30	351.26	962.78	611.53
HadCM3	2070 to 2099	651.45	159.59	1.43	347.37	969.45	622.08
HadCM3	1961 to 2099	617.13	147.36	0.92	347.37	1016.73	669.36
ECHAM5	1961 to 2004	367.23	88.47	1.69	163.62	522.17	358.54
ECHAM5	2020 to 2049	409.07	119.23	-0.54	212.35	693.63	481.28
ECHAM5	2070 to 2099	383.31	212.33	-3.40	121.70	1054.98	933.28
ECHAM5	1961 to 2099	381.84	140.38	0.04	80.57	1054.98	974.41

Figure 6.6: Summary statistics for cumulative precipitation in Kolhapur for the monsoon season (June to September) from observations and the HadRM3 output driven by ERA-Interim, HadCM3 and ECHAM5 for given time intervals. The units of the precipitation values in columns 3, 4, 6, 7, and 8 are mm while the units for the trend values in column 5 is $mmyear^{-1}$.

Given discrepancies in the data, either the observations are overestimating the rainfall in the Kolhapur region or the model results are providing an underestimate. There are a number of reasons why the RCM runs might underestimate the rainfall totals. Firstly, systematic errors in the GCM precipitation fields are not uncommon (Schmidli et al. (2006)). Figure 6.5 reveals large differences between the precipitation totals from HadCM3 compared to ECHAM5, despite using the same regional model. In the latest IPCC report, the individual model projections of precipitation over India show large differences in the accumulations over the region. The mechanisms that lead to precipitation are often challenging to model in GCMs and therefore RCM output associated with imperfect GCM driving data produces precipitation values that are subject to large errors. The regional model results from the IPCC AR4 report show a multi-model mean change in summer precipitation over western India of between 5 and 10% for the 2080 to 2099 period, using 1980 to 1999 as a base period (Christensen et al. (2007b)).

However, approximately half of the AR4 GCMs show a mean increase in rainfall in central western India while the other half GCMs show a mean decrease in rainfall. The disagreement between the ECHAM5 model and HadCM3 model is therefore indicative of wider disagreement amongst GCMs.

Furthermore, whilst the HadRM3 model provides a much better representation of the land surface and the local orography when compared to GCMs, many of the small scale orographic features are still not adequately represented by a 25km $\times$ 25km gridbox. Enhancing horizontal model resolution further ought to reduce biases resulting from errors in the specification of orography and the land surface. The resolution of the observational grid is $0.25^\circ \times 0.25^\circ$, approximately equal to a 28km $\times$ 28km gridbox, which is slightly larger than RCM horizontal resolution (25km $\times$ 25km). Perhaps more importantly, the model grids may not be representing exactly the same area and may therefore account for areas with different orography and rainfall characteristics. Situated to the west of Kolhapur is the southern extent of the Sahyadri hills. The enhanced orography is typically associated with increased rainfall and as the dominant wind direction during the monsoon is south-westerly, eastern parts of Kolhapur district often receive significantly less rainfall than the western parts. A detailed analysis of the gridbox formulation would elucidate the discrepancies in coverage and help to attribute the systematic biases evident in the model precipitation data.

In addition to the possible discrepancies from systematic GCM errors and poor RCM gridbox representation, the differences between the time series data may be partly caused by uncertainties associated with the observations and the use of rain-gauge stations. Wiltshire et al. (2010) states, "the uncertainties associated with observed precipitation are potentially large primarily due to known gauge undercatch errors (which are often corrected in post-processing) as well as the high spatial variability of precipitation which is often statistically undersampled".

To further understand the trends and discrepancies associated with the data, it is useful to analyse the separate monthly rainfall totals for June, July, August and September. Figure 6.7 displays a breakdown of the observational data and the RCM data for each of the individual months in the summer monsoon period (note different scales on y-axis). The observations show higher precipitation values than the model projections and the reanalysis data for all months but there are periods when the observed data falls within the range of variability associated with the model projections. During the first ten years of the time series for June, shown in figure 6.7(a), interannual variability in the observations is broadly consistent with the RCM projections driven by HadCM3 and ECHAM5 but from the 1970s onwards the observations shift to higher values than those associated with model projection data. The monthly plots highlight the differences between the HadCM3 and ECHAM5 model responses. In July and August, the HadCM3 results show precipitation totals that are approximately a factor of two greater than the totals given by the ECHAM5 model. Over this period, the ECHAM5 model results are in close agreement with the ERA-Interim results. In the absence of observational data, one might therefore be inclined to conclude that results should be weighted more strongly in favour of the ECHAM5 model.

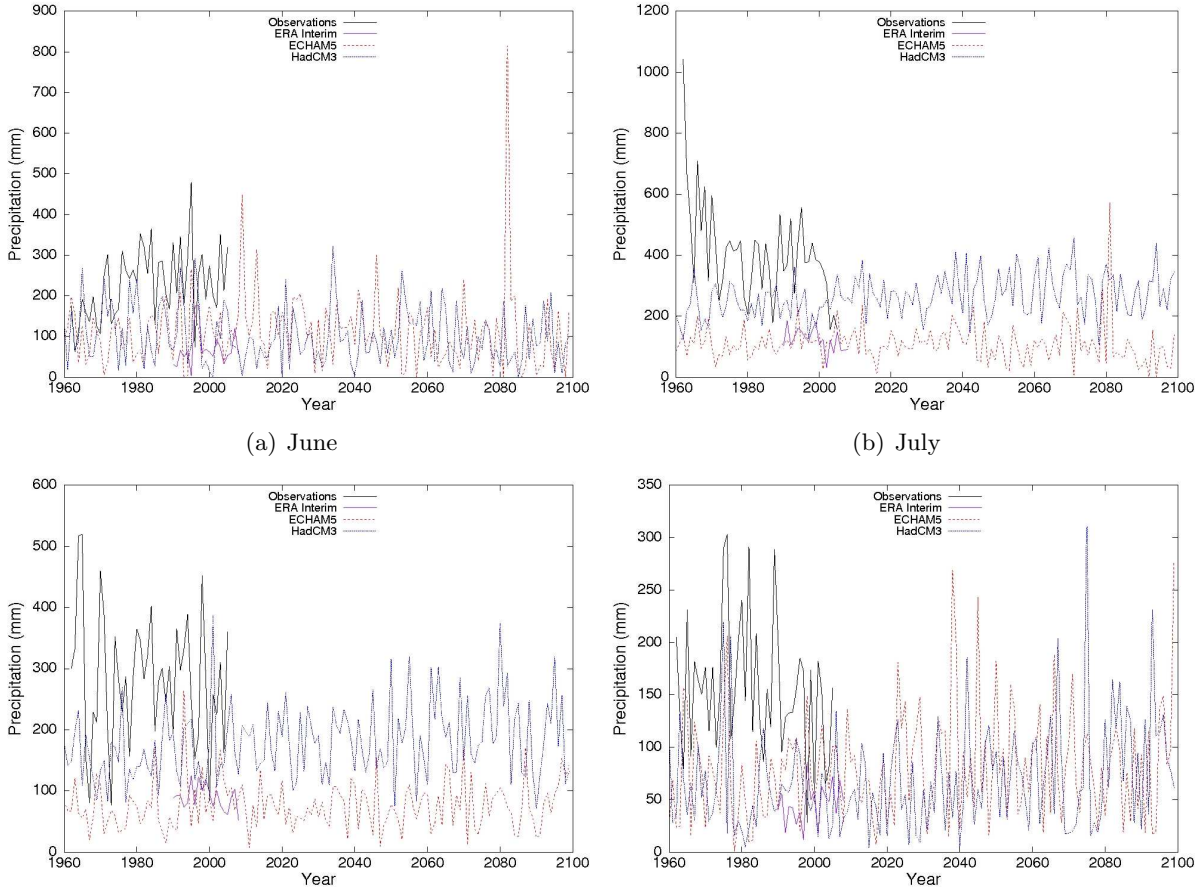

(a) June

(b) July

(c) August

(d) September

Figure 6.7: Model and observational cumulative precipitation data for Kolhapur, India for individual months in the summer monsoon. Observational data from APHRODITE is shown for the period 1961 to 2004, ERA-Interim data is shown for the period 1990 to 2008 and the model data driven by HadCM3 and ECHAM5 is shown for the entire period 1960 to 2099.

However, the HadCM3 model results, although still significantly lower, appear to be much closer to the observational data than the ECHAM5 results. On this evidence, one might conclude that the HadCM3 data should be weighted more favourably. Certainly the model trajectory appears to capture the increase in rainfall observed during July, which impacts the peak monsoon rains. Yet the lack of IC runs needed to elucidate the complete model distributions, and the large discrepancy between all RCM output and the observations suggests that weighting of model results isn't appropriate.

July has the highest observed monthly precipitation values. Rainfall during this month is particularly important for the success of the rice crop in the Kolhapur region (Bhuiyan (1992)). If the rainfall is significantly delayed, the season's crop risks failure. Therefore the BN analysis presented in the following sections is centred on the use of observations and model estimates of July precipitation under past and future climates. Focusing on the month of July is both sufficient to illustrate the issues in using model data and also clarifies those issues by excluding

Data Source	Time Interval	Mean	Standard Deviation	Trend	Min	Max	Range
Observations	1961 to 2004	405.06	162.36	-6.42	155.99	1043.76	887.77
ERA-Interim	1990 to 2008	120.90	37.93	-3.00	31.31	185.80	154.50
HadCM3	1961 to 2004	234.01	54.72	0.27	121.82	361.96	240.14
HadCM3	2020 to 2049	269.00	66.89	0.45	146.59	409.41	262.83
HadCM3	2070 to 2099	284.66	76.61	-0.22	106.22	456.50	350.28
HadCM3	1961 to 2099	266.68	69.15	0.52	106.22	456.50	350.28
ECHAM5	1961 to 2004	111.57	40.57	0.12	27.07	229.69	202.63
ECHAM5	2020 to 2049	119.27	46.44	-0.36	31.64	229.68	198.05
ECHAM5	2070 to 2099	103.85	108.86	-2.97	1.00	572.70	571.70
ECHAM5	1961 to 2099	110.38	64.94	-0.11	1.00	572.70	571.70

Figure 6.8: Summary statistics for cumulative precipitation in Kolhapur for July from observations and the HadRM3 output driven by ERA-Interim, HadCM3 and ECHAM5 for given time intervals. The units of the precipitation values in columns 3, 4, 6, 7, and 8 are mm while the units for the trend values in column 5 is $mm\ year^{-1}$.

unnecessary complexity.

The summary statistics for the July precipitation data are provided in the table in figure 6.8. There are large differences in the mean of the observations and the model output data which is likely to be attributable to systematic errors in the representation of precipitation in the driving GCMs. The systematic biases and model anomaly information is utilised in sections 6.6.3 and 6.6.4 to assess the impact of corrective adjustments in the model output on the losses associated with the index insurance pricing structure. The linear trends shown in column 5 show that there has been a decrease in total July rainfall ($-6.42\ mm\ year^{-1}$) over the observed period. The magnitude of the trend is influenced by the anomalously high value in the first year but there is still a decrease of $-4.75\ mm\ year^{-1}$ even if this value is omitted. The ERA-Interim reanalysis data also shows a decreasing trend over the period, 1990 to 2008, but the HadCM3 and ECHAM5 driven output do not show decreasing trends over the observed period. The HadCM3 output for July rainfall over the entire period (1961 to 2099) reveals an upward trend with an increase in annual variability shown in the increasing standard deviation values and the ranges for future periods. Conversely, the ECHAM5 output shows a weak decreasing trend over this period but the annual variability increases and notably a very significant event occurs in 2081 where the rainfall reaches a value of 572.7 mm. The occurrence of this event shows the ability of the model to produce an extreme event.

The systematic biases in the model output suggest that caution must be applied when interpreting the impact of climate change on the future precipitation patterns in the Kolhapur region. Given the multiple sources of uncertainty, and without further investigation, it is not clear which data should be considered more or less reliable. However, the aim of this chapter is not to provide definitive results regarding the optimum pricing strategy for index insurance in

Kolhapur but rather to demonstrate a methodology one could use to investigate the sensitivity of pricing assumptions to input climate information. The preliminary analysis of the raw model output suggests that decision makers, and particularly insurers interested in designing weather index products, should be cautious in relying on one source of climate information to form policy. Using multiple sources of climate information in the design phase of insurance products may increase the uncertainty but, used appropriately, could lead to a more robust analysis of the appropriate meteorological triggers for payouts. The BN approach, introduced in the following section, is designed to understand how this data could be used to determine weather index insurance viability under climate change.

6.6 Bayesian Network Results

The software Netica (Software Corp. (1998)) is used here to develop the BN. Netica provides an interactive graphical interface to allow users to switch between nodes and select options to develop an understanding of the variable dependencies. The images included in this section are extracted from the Netica user interface. The methodology outlined in section 6.5.1 is implemented here to derive a range of BNs with different levels of complexity. Section 6.6.1 focusses on BNs which utilise the July precipitation observational data only. The BNs presented in section 6.6.2 combine observations with climate model forecast data. Results presented in section 6.6.3 show BNs with bias corrected model output. Finally, section 6.6.4 presents BNs which are driven by observational data adjusted using anomaly information identified in the analysis presented in the previous section.

6.6.1 BNs using observational data

The BNs listed in this section assess pricing structure using observational data only to illustrate how premiums might be determined if reliant solely on a single observed time series. A payment structure, shown in figure 6.9, is adopted using a payout profile with three tiers, each corresponding to a fixed proportion of the maximum indemnity (total insured sum) per policy. Rainfall thresholds are chosen to correspond to each tier and although the threshold triggers are only illustrative they are considered plausible given the evidence presented in section 6.5.1. In this payment structure, the maximum payout equates to a *Tier 3* payment and this sum would be paid to policyholders if the observed July precipitation was below 150mm or above 600mm. If the precipitation was between 150 and 180mm or between 570 and 600mm, then a specified fraction of the maximum indemnity (*Tier 2*) would be paid to each policyholder. Similarly, if the precipitation was between 180 and 210mm or between 540 and 570mm, then a smaller specified fraction of the maximum indemnity (*Tier 1*) would be paid to each policyholder. No payout would be given for precipitation totals between 210 and 540mm.

For many index insurance products, the payout increases linearly to the maximum payout but a step-wise function (similar to a collar graph) is chosen in this study for two reasons. Firstly, existing weather index products for rainfall deficit are often structured using a step-wise function in the payouts (MicroEnsure (2010)) and secondly if payouts increased linearly then there would have to be many more states within the *rainfall deficit* and *excess rainfall* nodes to incorporate probabilities effectively. Later in this section, a BN using a seven tiered structure is illustrated (see figure 6.12) to demonstrate an alternative payout structure and highlight the problems associated with using more tiers.

The BN shown in figure 6.10 utilises the three tiered payout structure and consists of four nodes linking observed July precipitation to losses. As discussed in section 6.5.3, July is chosen as the time period of interest as the month is typically associated with the highest rainfall totals during the monsoon season (see figure 6.7(b)). In practice, the period for which individual

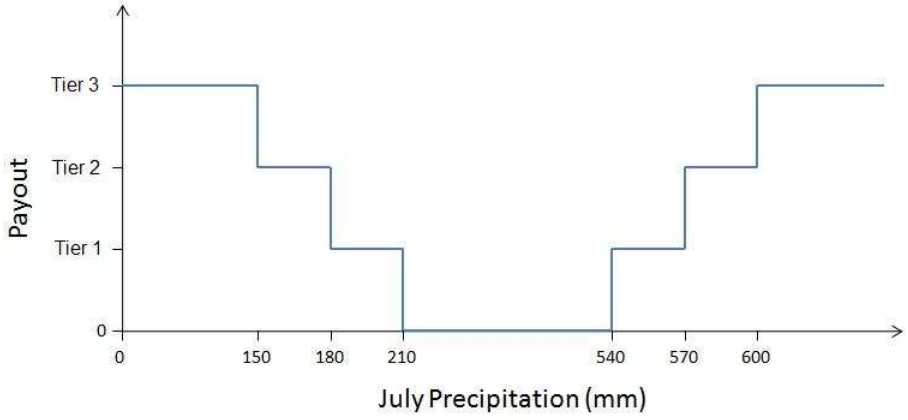

Figure 6.9: Example payout profile for for an idealised index insurance policy covering rainfall deficit and excess rainfall.

index insurance providers offer coverage will vary according to specific crop requirements and user demands.

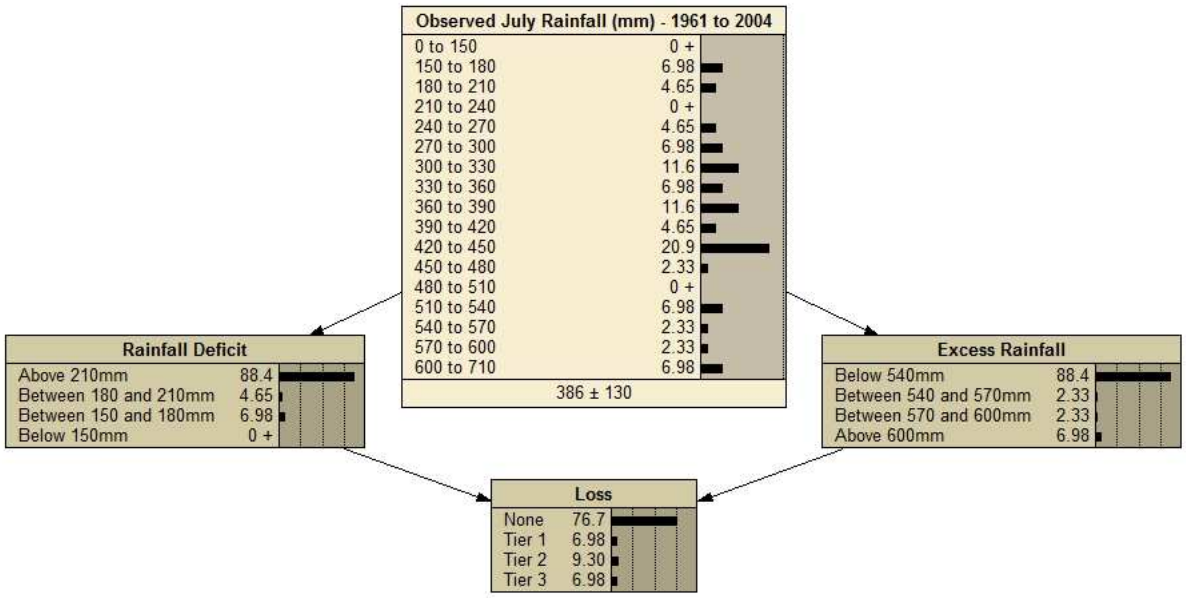

Figure 6.10: BN for rice crop index insurance in the Kolhapur region with a three tiered payout structure, using observational data from the APHRODITE project (Yatagai et al. (2009)).

The parent node in figure 6.10 incorporates observational data from the APHRODITE project for the period 1961 to 2004[6]. The two child nodes simply propagate the probabilities in the parent node to present the probability of rainfall exceeding specific thresholds. The *rainfall deficit* and *excess rainfall* nodes in figure 6.10 are the parent nodes for a final variable node.

[6]The node therefore includes 44 data points so a probability of 2.33% for a particular bin indicates that one year in the 44 year time series has a July precipitation value that falls within the bin range.

The *Loss* node combines the probabilities in the parent nodes to generate a combined probability of paying out on an individual policy. The BN shows that 76.7% of the observed years would have been associated with no losses meaning the insurer would not have been required to payout on any of the policies. The remaining years would have resulted in losses with 6.98% of years resulting in a maximum payout to each policyholder.

Figure 6.10 demonstrates the capability of a BN to handle and propagate continuous data, albeit with relatively few nodes. Figure 6.11 includes four additional nodes; a decision node, a utility node and two constant nodes. The *Premium* and *Expenses* nodes are given constant values which can be adjusted to influence the viability of the pricing structure based on information in the *Loss* node. Their values are represented as percentages of the total insured value.

The *Loss* node combines the values in the parent nodes to produce probabilities for the different tiers of loss. It then multiplies these by the payout values for each tier, shown in table 6.4, to produce an expected loss value (E). The example values in table 6.4 represent possible proportions of the total insured value (maximum indemnity) that could be paid out if the relevant threshold is surpassed. The first value at the bottom of the *Loss* node denotes E and the second value is the standard deviation (σ) in E (assuming a normal distribution about the expected loss). In figure 6.11, $E = 11.7$ and $\sigma = 27$ based on the three tiered payout structure contained in the BN.

Loss	Payout (% of total insured value)
None	0
Tier 1	15
Tier 2	40
Tier 3	100

Table 6.4: Payout values assigned to individual states in a three tiered payout structure embedded in the *Loss* node.

The utility node (U) incorporates equation 6.2 to calculate the expected utility for each decision state in the decision node; in this context there is only one state (*Yes*). The value of the state in the decision node conveys the viability of the policy pricing structure. If the value is positive, then the premium is sufficient to cover the expected loss and expenses thus declaring the insurance viable. If the value is negative, then the premium is not sufficient to cover the expected loss and expenses, thus declaring the insurance not viable (i.e. negative *yes* means *no*).

$$Utility = Premium - Loss - Expenses \tag{6.2}$$

Expenses are assumed to be 3% of the total insured value which means that a premium value of 15% is necessary in order for the policy to be profitable for the insurer (i.e. to yield an expected utility of greater than zero).

One of the ways to increase the expected utility without adjusting the premium or expenses values is to create a different payout structure. Figure 6.12 shows the same BN illustrated in

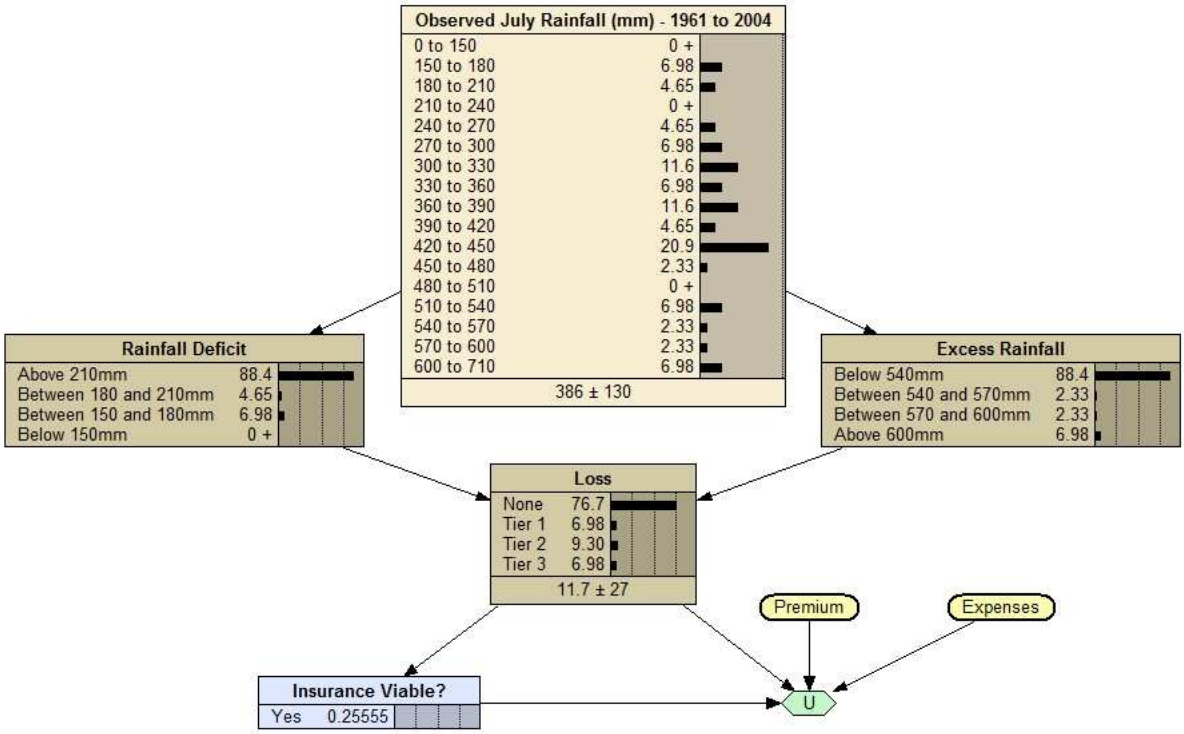

Figure 6.11: BN for rice crop index insurance in the Kolhapur region with a three tiered payout structure, including a decision node to assess the viability of insurance given APHRODITE observational data and assumptions about premium and expenses values; premium = 15% of maximum indemnity and expenses = 3% of maximum indemnity.

figure 6.11 but with a seven tiered payout structure; the payout percentage values assigned to each tier are given in table 6.5. The payout values were selected so that E is approximately the same in the three-tiered and seven-tiered policy structure.

Loss	Payout (% of total insured value)
None	0
Tier 1	5
Tier 2	10
Tier 3	15
Tier 4	25
Tier 5	35
Tier 6	50
Tier 7	100

Table 6.5: Payout values assigned to individual states in a seven tiered payout structure embedded in the *Loss* node.

Increasing the number of tiers should mean that the level of payment can be more closely correlated to the actual losses thus reducing the basis risk and making the policy more attractive to both the insurer and the policyholder. However, as evident in figure 6.12 even when assuming a stationary climate, a limited observational data set means that the probabilities within each

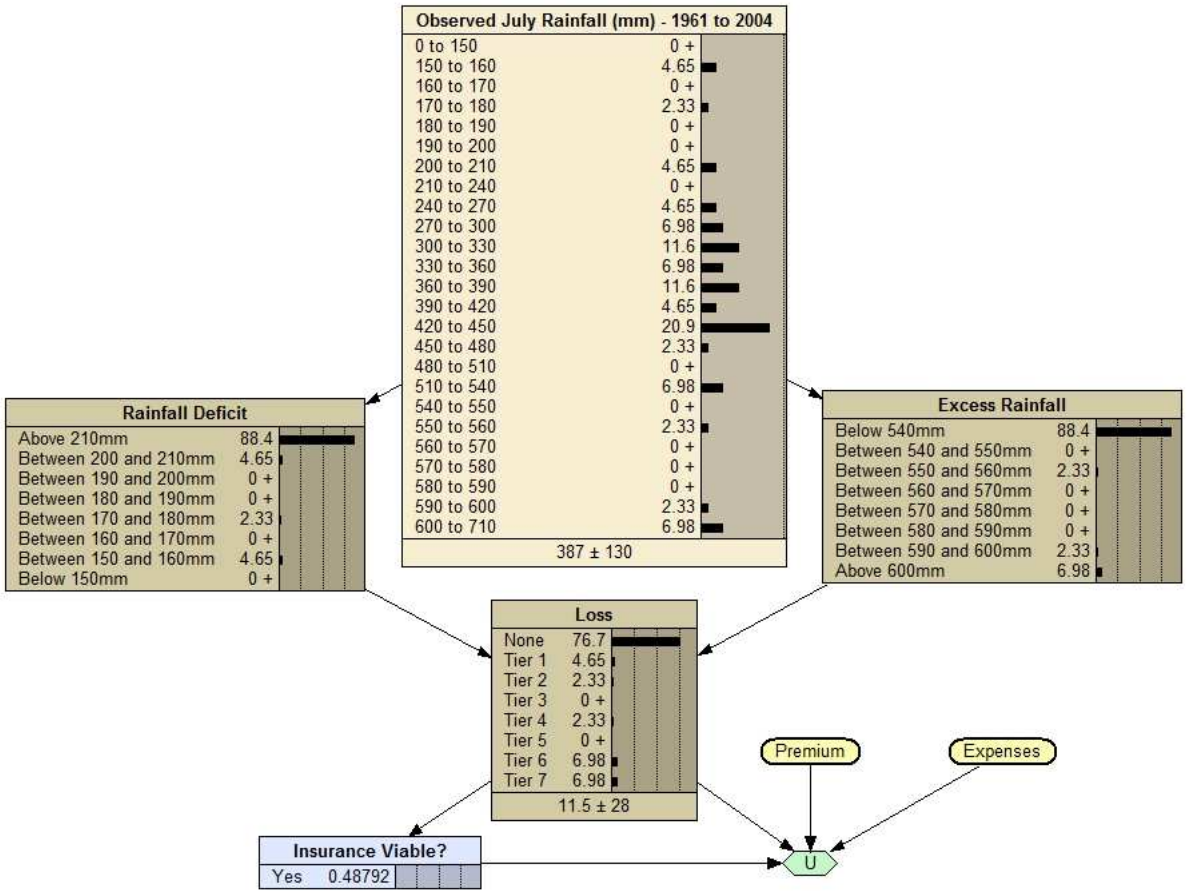

Figure 6.12: BN for rice crop index insurance in the Kolhapur region with a seven tiered payout structure, including a decision node to assess the viability of insurance given APHRODITE observational data and assumptions about premium and expenses values; premium = 15% of maximum indemnity and expenses = 3% of maximum indemnity.

payment tier are not well defined. In tier 3 and tier 5, the probability is zero according to the data in the BN. Of course the real probability is very likely to be non-zero. Insurers may typically choose to fit a distribution to the data to make the estimated losses smoother but this approach is problematic. Firstly, the choice of distribution can significantly impact the probability of tail events and the losses are highly sensitive to assumptions about tail probabilities, though this is a well known problem amongst insurers and risk modellers (Haimes (2009)). Secondly, the climate is nonlinear and non-stationary. In previous chapters experiments with simpler models reveal that assuming stationarity and invoking the ergodic assumption is problematic in nonlinear systems subject to altered forcings. In the observational data set used here, it is likely that the temporal distribution of events does not fully represent the probability distribution of expected losses for the present climate. Indeed, figure 6.7(b) shows that there has been a downward trend in precipitation values for July suggesting that the probability of a year with rainfall deficit may have increased in recent years whilst the probability of a year with excess rainfall may have decreased. Alternative sources of climate information may help to improve

the probability estimates and in the next section, BNs which combine observational data with climate model data are presented.

6.6.2 BNs combining observational and model data

The BN illustrated in figure 6.13 provides a simple view (node names only) of a BN which incorporates multiple sources of data. The parent node, *Climate Timescale*, listed in the first row determines the period for which model data is used. The second row displays the four sources of data used in this case study; the APHRODITE observations and the three HadRM3 runs driven by HadCM3 and ECHAM5 for hindcasts and future projections and ERA-Interim reanalysis data. The information contained in each data node (listed in the second row) can be individually selected or combined, using the *Model Choice* node. With the exception of the *Model Choice* node, rows three, four, five and six are identical to figure 6.11.

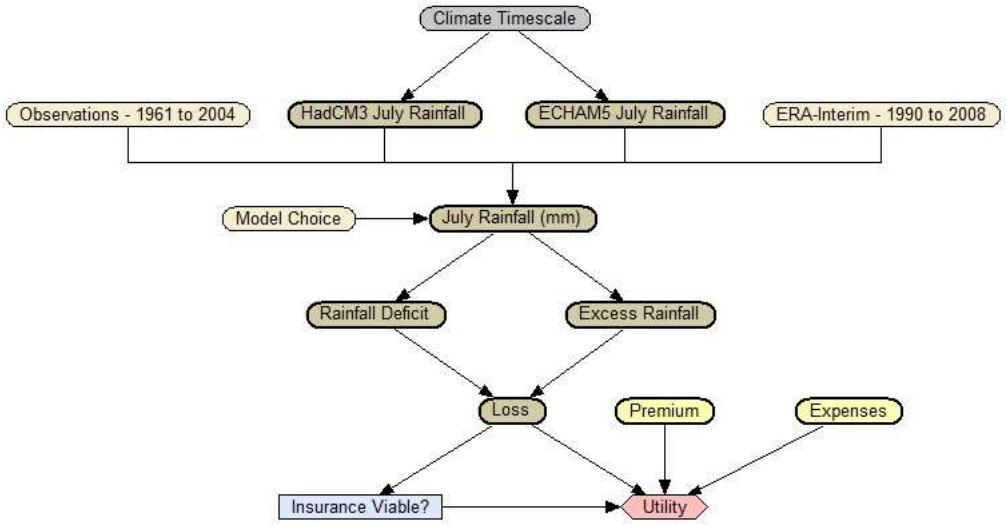

Figure 6.13: BN developed for weather index insurance in the Kolhapur region, including multiple sources of climate information using node names only.

Following exactly the same approach as that utilised in the UKCP09 projections (UKCP09 (2011)), 30 year time intervals are selected from the available data and centred on the decade of interest; for example, the 2030s are represented using the data from 2020 to 2049. To derive probability distributions from the model projections to inform the threshold exceedance probabilities in the future, it is therefore necessary to apply the ergodic assumption. As expressed in section 6.2.2 and discussed extensively throughout the previous chapters, the ergodic assumption can be misleading and potentially undermine robust climate change adaptation decisions. By employing the ergodic assumption, the BN analysis here simply serves to illustrate how current climate model data might be used to explore possible future climates. This BN framework could be improved if large IC ensemble distributions were available.

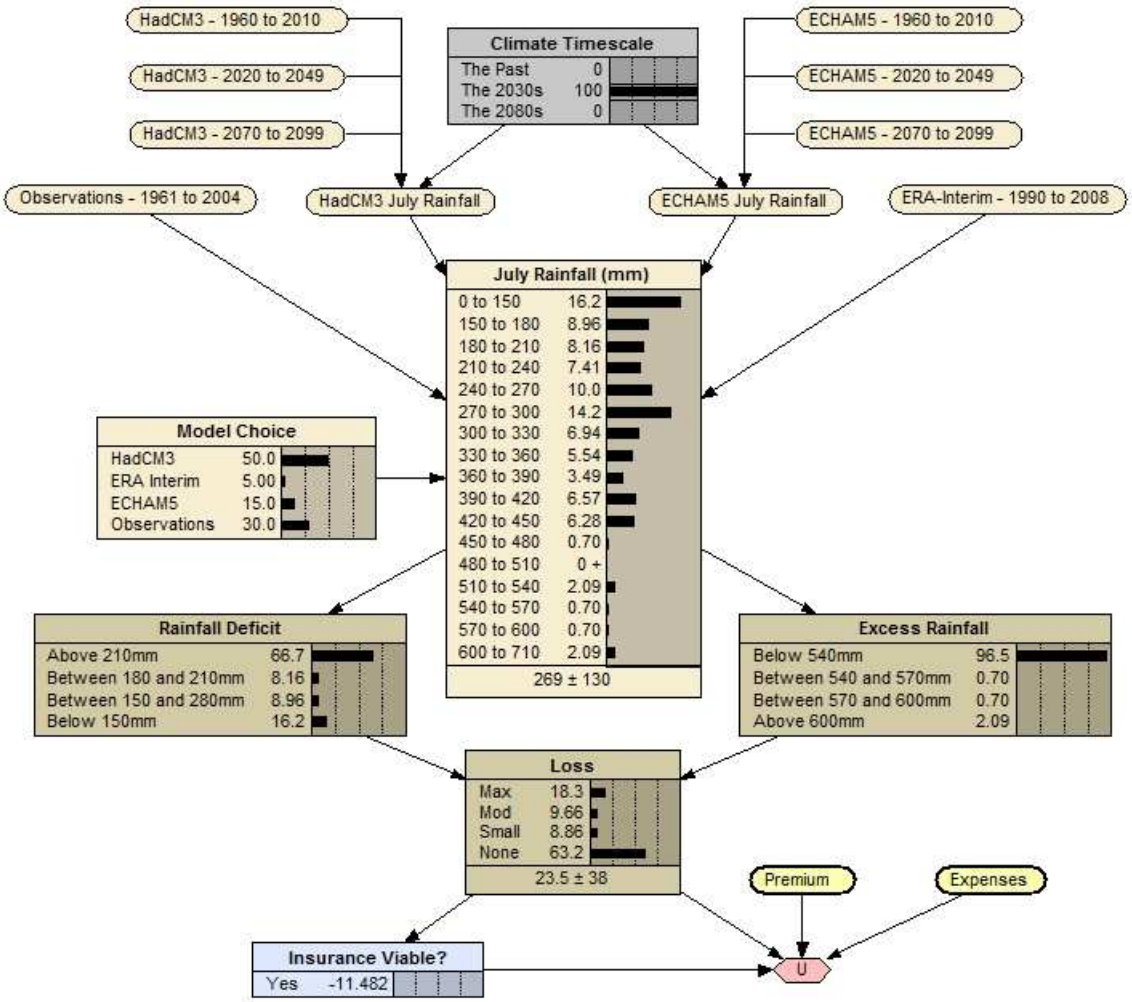

Figure 6.14: BN to inform viability of weather index insurance for rice production in Kolhapur, India. The relative weights of the states in the *Model Choice* node have been arbitrarily selected and the *Climate Timescale* set to the 2030s. Constants are given the values: premium = 15% of maximum indemnity and expenses = 3% of maximum indemnity.

Figure 6.14 shows an expanded version of the BN depicted in figure 6.13. The BN utilises the three tiered payout structure (see fig. 6.9) and consists of 20 nodes: 16 variable nodes, 2 constant nodes, 1 decision node and 1 utility node. Of the 16 variables nodes, only two (*Climate Timescale* and *Model Choice*) consist of discrete states, the remaining 14 incorporate continuous data. The three parent nodes for the *HadCM3 July Rainfall* node and the three parent nodes for the *ECHAM5 July Rainfall* include frequency distributions for the model precipitation data over Kolhapur for the given time intervals. The propagation of the probabilities is controlled by selecting one of three different states in the *Climate Timescale* node. In this BN the combination of model data, reanalysis data and observational data is determined by the probabilities (weights) dictated by the *Model Choice* node. The configuration shown in figure 6.14 gives a 50% weighting to the HadCM3 model, 35% to the APHRODITE observations, 15% to the ECHAM5 model and 5% to the ERA-Interim data; these values are arbitrarily chosen.

Weighting the data is problematic (see discussion in section 6.7) but is illustrated in figure 6.14 for demonstration purposes; further examples are given where individual models are selected. The time scale in the BN shown in figure 6.14 is set to the 2030s (for the same versions of the *weighted* BN in the past and 2080s, see Appendix D, figures D-1 and D-2). The climate risks in the 2030s are of particular interest to insurers developing products in emerging markets (see figure 6.1). The resulting probabilities show that a premium of 15% of the maximum insured value (assuming expenses of 3%) is not viable given the probabilities and assumptions in the BN for any time period. According to the BN, there is a 16.2% chance that rainfall during July in the 2030s will be below 150mm. The chance of a maximum payout is therefore too large to deem the premium and policy structure viable; indicated by a negative utility of -11.482 in the decision node. Increasing the premium to 27% would make the expected utility positive but this premium is likely to be less acceptable to policyholders. Further work on the demand-side could establish thresholds at which the premiums become unaffordable for a particular community. Combining supply-side and demand-side studies should enable progress to be made in understanding the viability of index-based insurance mechanisms in a changing climate.

In the BN developed, the user can select each state in the *Model Choice* node exclusively to see how each source of information alters the probabilities in the network. Figure 6.15 shows the BN when the HadCM3 model is selected in the *Model Choice* node. The time scale is set to 2080s (for the past and 2030s see Appendix D, figures D-3 and D-4). Recall from figure 6.7 that the precipitation totals from the HadCM3 model are significantly lower than the observational data during the monsoon season. During July the HadCM3 data increases markedly from the June values but still does not approach the observed totals. The *July Rainfall* node in figure 6.15 shows the spread of precipitation values and despite an average increase in precipitation values compared to the past and 2030s (figs. D-3 and D-4), all of the probability density remains below the 540mm threshold for excess rainfall payout. There is density below the rainfall deficit threshold values with 3.45% (one year out of the 30 year sample) below 150mm. With a premium of 15% of the total insured sum, the expected utility is 5.619. A premium value of 10% would therefore be sufficient to ensure the profitability of the product based on the network assumptions and the use of the expected utility value as a measure of profitability.

If one believed the precipitation values associated with the raw HadCM3 model output, climate change would therefore appear to pose no real threat to the long-term sustainability of index-based insurance in the Kolhapur region (at least on the supply side). However the raw model output from the RCM driven by the ECHAM5 model suggests that the pricing structure is wholly inadequate under past and future climate conditions. Figure 6.16 shows the impact of selecting the ECHAM5 model as the driving GCM on the threshold exceedance probabilities for rainfall deficit and excess rainfall in the 2080s. 86.2% of the data falls below the 150mm threshold associated with the maximum rainfall deficit payout. Clearly, if this data were credible, then the index insurance would not be viable based on the thresholds selected. By considering the ECHAM5 raw output data in the policy design, insurers would therefore need to be prepared to

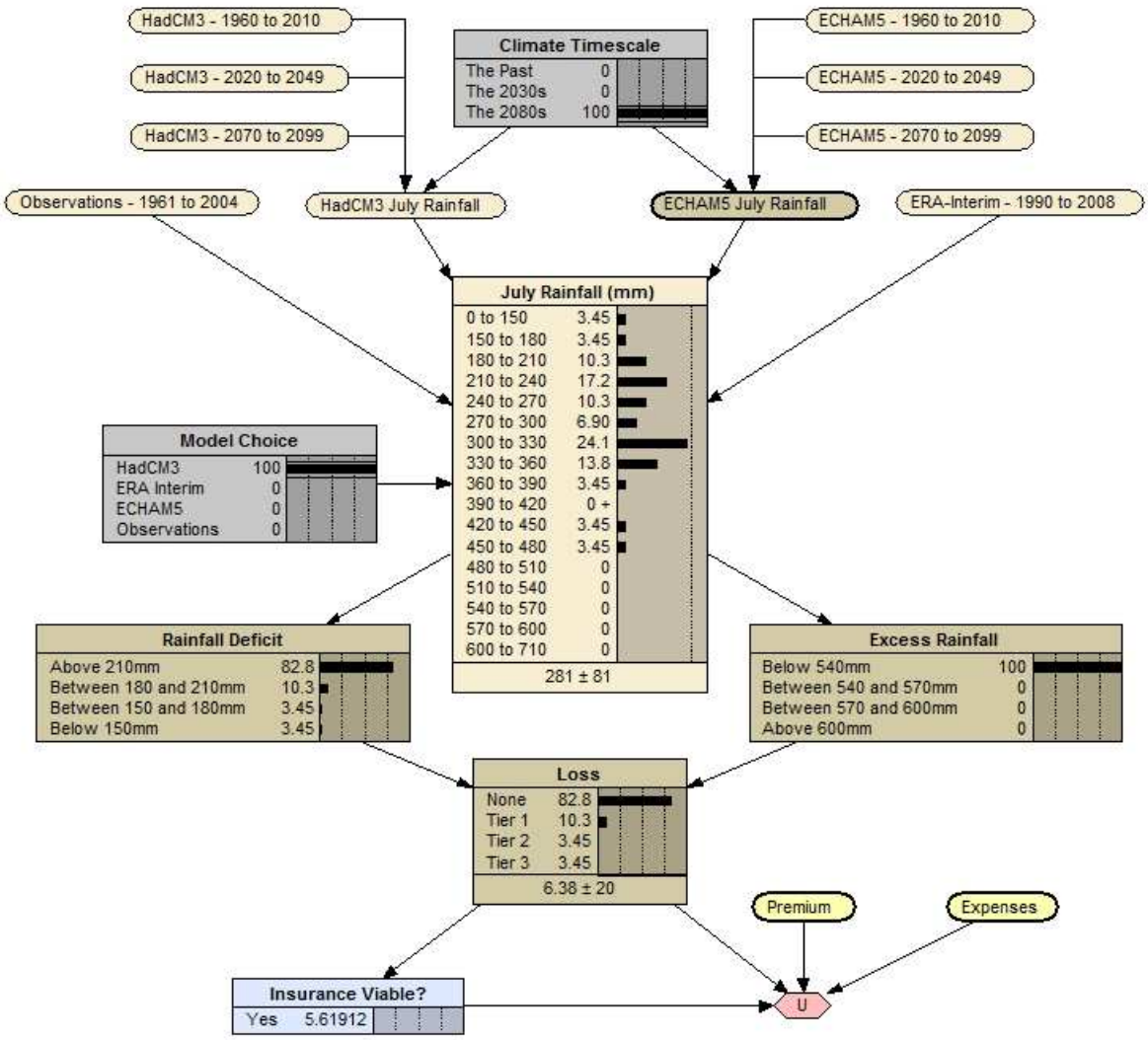

Figure 6.15: BN to inform viability of weather index insurance for rice production in Kolhapur, India. The HadCM3 model has been selected in the *Model Choice* node and the *Climate Timescale* set to the 2080s. Constants are given the values: premium = 15% of maximum indemnity and expenses = 3% of maximum indemnity.

eventually decrease the thresholds at which payouts for rainfall deficit occur and/or dramatically increase premiums. Of course the reliance of the rice crop on rainfall totals greater than 150mm per month would mean that a significant decrease in the thresholds would render the product unfit for purpose. Moreover, analysis of the hindcast ECHAM5 data (shown in Appendix D, figure D-5) shows that the probability of rainfall being below the 150mm value in July does not change considerably throughout the time series. Clearly, if the actual precipitation accumulations are this low, farmers would not be able to harvest the rice crop using rain-fed irrigation methods. The use of the ECHAM5 model data is therefore brought into question; the HadRM3 model driven by output from ECHAM5 does not appear to adequately reproduce the correct precipitation patterns over the Indian subcontinent.

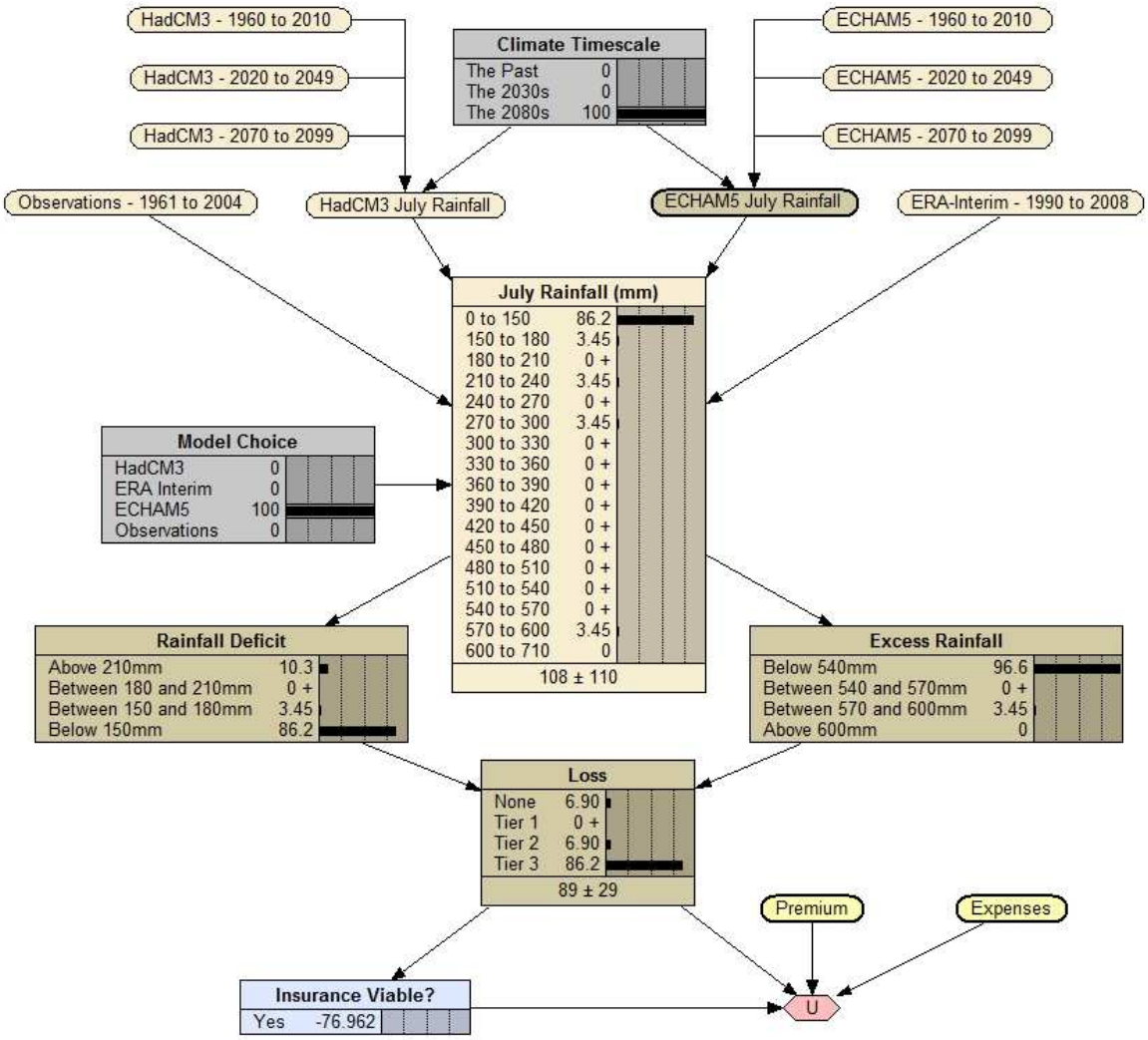

Figure 6.16: BN to inform viability of weather index insurance for rice production in Kolhapur, India. The ECHAM5 model has been selected in the *Model Choice* node and the *Climate Timescale* set to the 2080s. Constants are given the values: premium = 15% of maximum indemnity and expenses = 3% of maximum indemnity.

The choice of driving GCM is clearly a crucial factor in determining the viability of an index-based product under climate change, at least in the case study explored here. However, given the evidence of systematic model errors described in the analysis of the raw model output in section 6.5.3, an obvious next step is to examine the effects of introducing bias corrections to the model output. In the next section, simple bias corrections are made to the model data and the impact on the BN probabilities is analysed.

6.6.3 BNs incorporating bias corrected model data

The preliminary data analysis in section 6.5.3 and the BN results presented in section 6.6.2 reveal large systematic errors in the raw model output. Accounting for these biases is possible

in the BN framework. Yet whilst the process of bias correction is common in climate science, the introduction of statistical bias corrections requires careful consideration so as not to create misleading information which can lead to maladaptation. Statistical bias corrections to precipitation data from a GCM with a closed hydrological cycle has questionable physical implications. Artificially decreasing or increasing the precipitation data with reference to observed data means that the total moisture content in the model is altered. The reasoning behind statistical bias corrections therefore needs to be clear and justifiable. Additionally, in the context of climate change, bias corrections assume that the past is an appropriate guide for the future. Haerter et al. (2011) note that all bias correction methods make assumptions about the applicability of statistical transfer functions from observed climate to future climate and caution that the extent of the impact on the climate signals of model projections is uncertain. Furthermore, Haerter et al. (2011) claim that existing bias correction methods do not take into account that oscillations occur on different time scales caused by disparate physical mechanisms. The authors suggest a "cascade of bias corrections" to address this problem. However, in projecting climate change, it is not obvious whether the oscillatory patterns observed in the past will continue or change their behaviour under future forcing conditions. Certainly the evidence from simple nonlinear systems explored in previous chapters, particularly in the experiments on the LS84 model, suggests that the internal climate variability can be forcing scenario dependent.

In section 5.6, it is shown that the dynamic behaviour of the LS84 model is qualitatively different as the parameter F is decreased from a transitive region of parameter space to an almost-intransitive region of parameter space. In the climate system it is possible (and perhaps even likely) that the dynamics of the climate system will be altered under future forcing conditions, at least on regional scales. The use of a bias correction for future climate model projections explored here is therefore purely demonstrative of the approach one could adopt if there was sufficient reason to believe that biases and systematic errors identified using past observed data might apply under altered climate conditions. A bias correction could include high order moments, adjusting for variance, skewness and other statistical properties of the observed precipitation distribution. However, given the errors in the model results described in section 6.5.3, it is inappropriate to introduce a complicated bias correction method. Therefore, the simplest form of bias correction is used where distributions are simply shifted according to a mean change[7]. This is sufficient to show how one may incorporate bias corrected data in a BN framework.

In this section, the BNs presented show the sensitivity of the insurance viability to bias corrected model output. The summary statistics presented in section 6.5.3 are used to bias correct the model projections. The difference between the mean of the observed precipitation data and the means of both the ECHAM5 and the HadCM3 driven RCM data, over the same period (1961 to 2004), is added to the time series data in each forecast period. Table 6.6 shows the biases of the model output fom different sources.

[7] A bias correction using the first moment.

Data Source	Mean Bias (mm)
HadCM3	-171.05
ECHAM5	-293.49
ERA-Interim	-284.16

Table 6.6: Mean biases of model output data using the observed July Rainfall over Kolhapur from 1961 to 2004.

Figure 6.17 shows how a mean bias correction to the HadCM3 output data for the 1961 to 2004 period affects the threshold exceedance probabilities and the viability of the index insurance product. The consequence of the bias correction is that there is no density in the lower range of precipitation values so there are no rainfall deficit losses. As the variability in the HadCM3 precipitation values (standard deviation of 54.72) is less than the observed variability (standard deviation of 162.36), a shift in the mean does not lead to large probabilities of exceeding excess rainfall thresholds. The expected loss is $E = 0.213$ (% of the maximum insured value) so a very low premium would render the product financially viable for an insurer. However the policyholder may be reluctant to purchase insurance if the bias corrected model probabilities were accurate given the very low probability of any thresholds being exceeded.

Figure 6.18 shows the effect of the bias correction on the HadCM3 driven output in the 2080s. The bias corrected distribution shows increased density in the higher range of the precipitation values when compared to the output shown in figure 6.17. There remains a 90.7% probability of no loss with a 5.77% probability of the maximum payout being triggered for excess rainfall. Given no probability of a loss from rainfall deficit, the policy structure is viable, conditioned on a 10% (or higher) premium.

The effect of the bias correction when applied to the ECHAM5 driven output for the past and 2080s is shown in the results provided in appendix D, figures D-7 and D-8. Because of the narrow range of the precipitation values from the RCM driven by ECHAM5 model for the period 1961 to 2004 (see figure 6.8), the effect of a mean bias correction shifts all precipitation values to the range between 270 and 540 mm so no losses are triggered. In the 2080s, there is a small amount of density in region associated with rainfall excess but 93% of the distribution does not trigger a payout so the insurance pricing structure appears viable on the supply-side.

Another approach is to measure the anomalies between model forecast periods and add these anomalies to the observed data. Section 6.6.4 presents BNs which incorporate observational data which is adjusted according to the anomalies in the model output.

6.6.4 BNs with observational data altered using model output anomalies

In assessing the impacts of climate change, it is common to use anomaly data from climate model simulations instead of the raw model output because of large systematic biases (e.g. Hudson and Jones (2002)). The reasoning is that whilst the absolute values extracted from

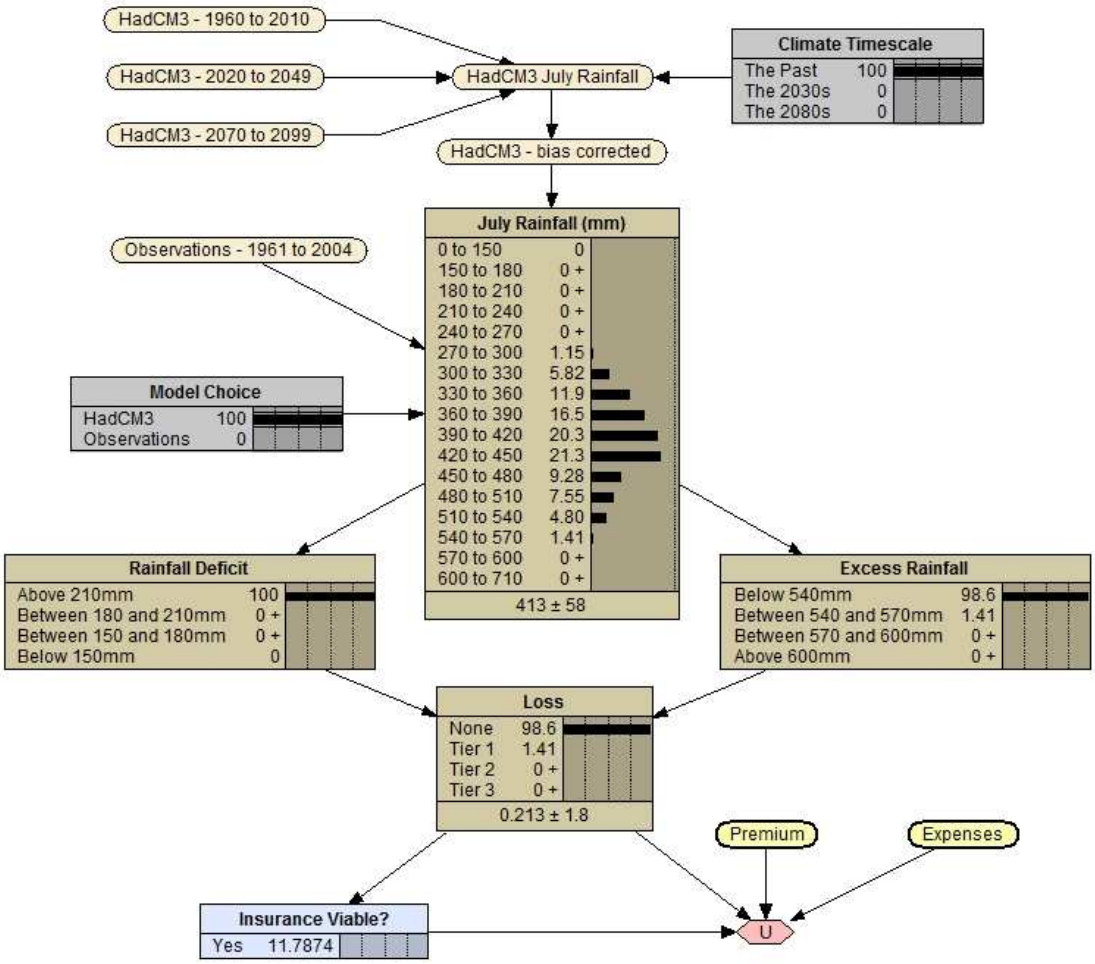

Figure 6.17: BN to inform viability of weather index insurance for rice production in Kolhapur, India. The HadCM3 model has been selected in the *Model Choice* node and a bias correction has been applied according to table 6.6. The *Climate Timescale* is set to the past. Constants are given the values: premium = 15% of maximum indemnity and expenses = 3% of maximum indemnity.

the raw model output may be subject to systematic errors, the relative change in the statistics of climate from one period to another provide useful information regarding the direction and magnitude of possible changes. In this section, the RCM anomalies (changes in the mean) are used to adjust the observational data for future climate periods to assess the impact on the losses associated with the weather index-based insurance product. Table 6.7 shows the change in the means of the future precipitation time series' relative to the observational period, 1961 to 2004, for the RCM output driven by the HadCM3 and ECHAM5 GCMs. These values are added to the mean of the observational data for July precipitation from 1961 to 2004.

Here the ECHAM5 BN results are presented to demonstrate the effect of incorporating anomalies with different signs in the 2030s and 2080s. Figure 6.19 illustrates the effect of adding the mean change in the ECHAM5 output in the 2030s to the observational time series data. The change in the mean is only 7.7 *mm* so the effect on the losses is small. Compared to the losses associated with observational data shown in figure 6.11, there is a slight decrease in the chance of a deficit

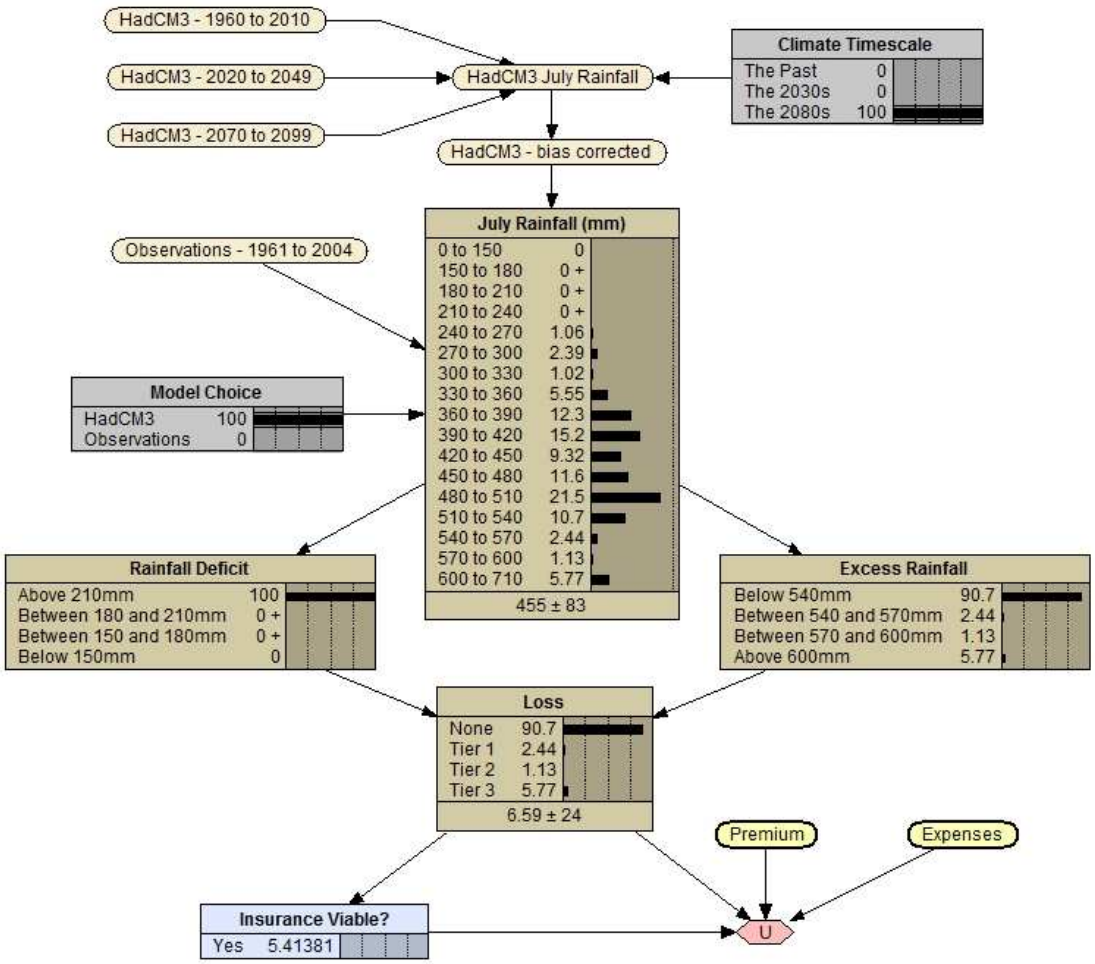

Figure 6.18: BN to inform viability of weather index insurance for rice production in Kolhapur, India. The HadCM3 model has been selected in the *Model Choice* node and a bias correction has been applied according to table 6.6. The *Climate Timescale* is set to the 2080s. Constants are given the values: premium = 15% of maximum indemnity and expenses = 3% of maximum indemnity.

rainfall and a small increase in the chance of rainfall excess but the changes are not significant enough to affect the viability of the pricing structure. In the 2080s, the ECHAM5 model shows a decrease in the mean precipitation; the high precipitation event in 2081 prevents the decrease in the mean being more significant. Figure 6.20 shows that the perturbed observational data is shifted to lower precipitation values and an increase in the risk of rainfall deficit below 150 mm means the existing pricing structure is no longer viable (as shown by the negative expected utility value in the decision node). The change in the mean precipitation is only $-7.72mm$ but because the pricing structure is sensitive to changes in the tails of the distribution, a small shift in the mean can result in significant changes in the estimates of product viability.

The anomalies associated with the HadCM3 output are larger in magnitude than the ECHAM5 output and this causes the observed time series data to be shifted to higher precipitation values. Figures D-9 and D-10 in appendix D show the results when the HadCM3 anomalies are used.

Data Source	Time Period	Mean Change from Past (mm)
HadCM3	2030s	34.99
HadCM3	2080s	50.65
ECHAM5	2030s	7.70
ECHAM5	2080s	-7.72

Table 6.7: Anomaly data showing the change in the means of the RCM precipitation output driven by HadCM3 and ECHAM5 for given future time period relative to the observational time period 1961 to 2004.

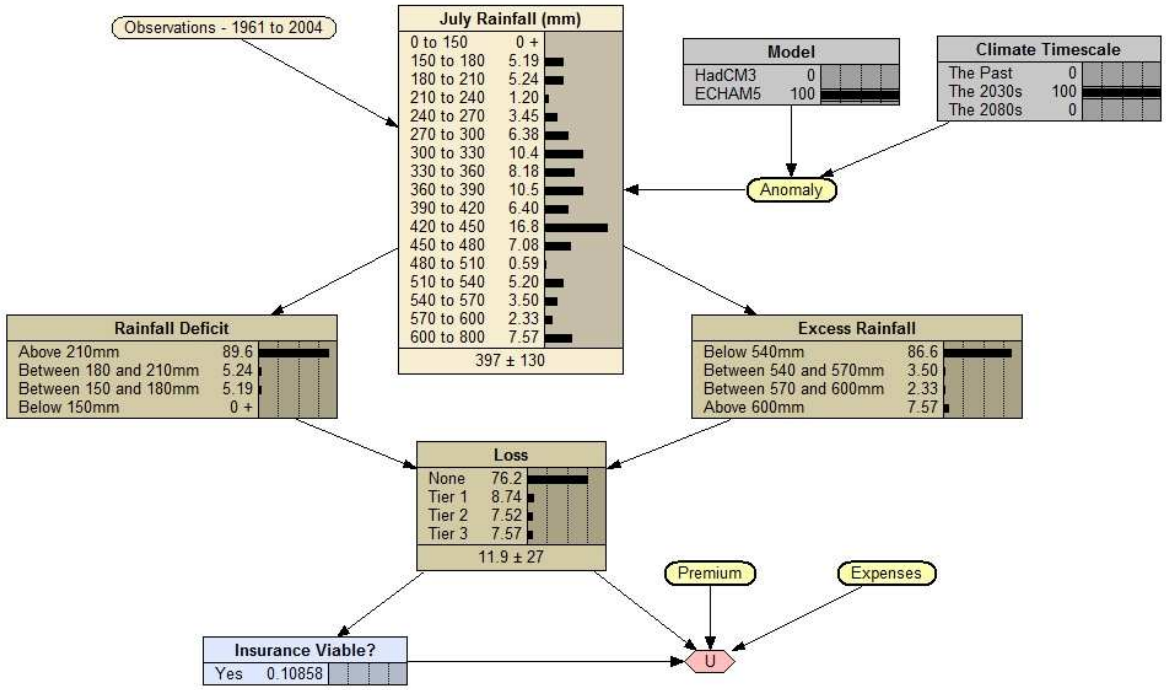

Figure 6.19: BN to inform viability of weather index insurance for rice production in Kolhapur, India. Observational data is altered using anomaly information from the ECHAM5 model projections according to table 6.7. The *Climate Timescale* is set to the 2030s. Constants are given the values: premium = 15% of maximum indemnity and expenses = 3% of maximum indemnity.

The BN pricing structure isn't viable in either the 2030s or 2080s and a higher premium would be required to offset the increased expected losses and render the product viable for the insurer.

6.6.5 Acknowledging model error

Perhaps the main barrier to the formal uptake and use of the BN approach to assess future climate risk in index based insurance products is the existence of large errors in climate model projections. The HadRM3 model output data, driven by the HadCM3 and ECHAM5 GCMs and the ERA-Interim reanalysis data, significantly underestimates the observed precipitation occurring in Kolhapur in the monsoon season. Capturing the complex interactions which control the monsoon rains and the corresponding flood/drought risk is challenging given a lack of

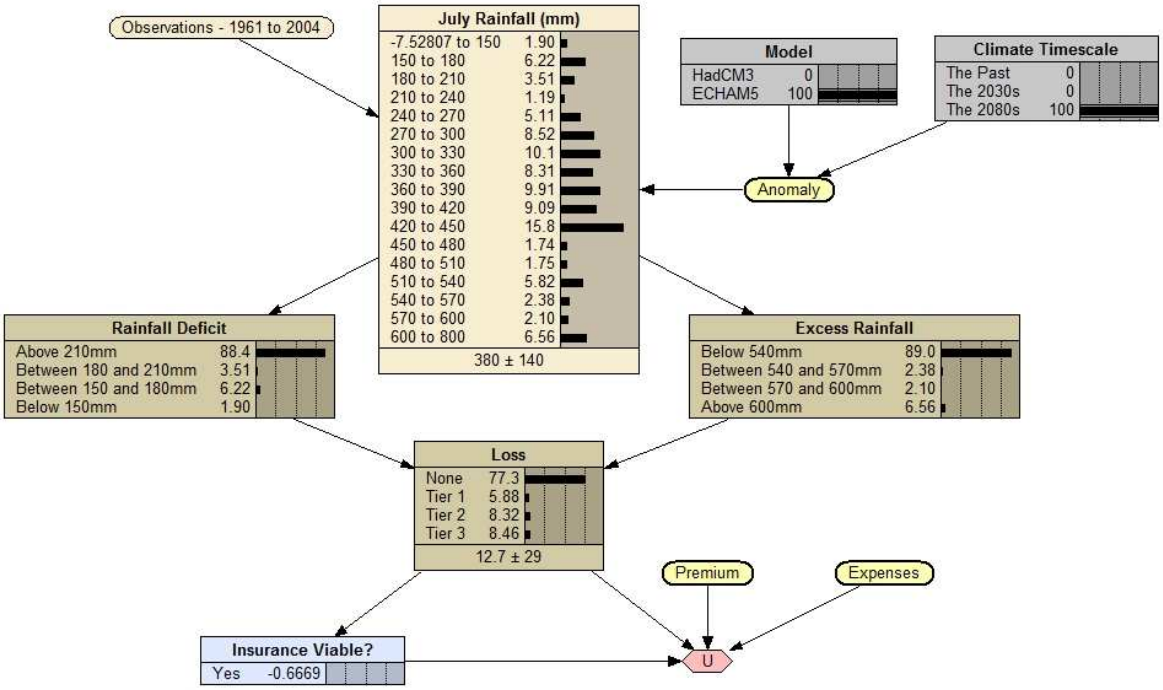

Figure 6.20: BN to inform viability of weather index insurance for rice production in Kolhapur, India. Observational data is altered using anomaly information from the ECHAM5 model projections according to table 6.7. The *Climate Timescale* is set to the 2080s. Constants are given the values: premium = 15% of maximum indemnity and expenses = 3% of maximum indemnity.

computing capacity and limited process understanding. A number of studies have attempted to model the monsoon rainfall under altered climate forcings. Recently, Lucas-Picher et al. (2011) examined the ability of a four RCMs to simulate the Indian monsoon concluding that the timing of the monsoon onset was broadly consistent across the models and reanalysis data but that the monsoon withdrawal was less well simulated. Meehl et al. (2000c) refer to the modelling results of Meehl and Washington (1993) and Kitoh et al. (1997) to suggest that under a range of future climate scenarios, increasing year-to-year monsoon precipitation variability will increase the likelihood of drought and flood during the monsoon season. However, Lal et al. (2001) use a coupled AOGCM to study the climate of India under GHG warming and the model results suggest no significant change in the year-to-year variability in rainfall in central India during the monsoon season. The inconsistencies in the conclusions from different modelling approaches suggest that a consensus regarding the future trends and magnitudes of the monsoon rainfall in RCMs and GCMs for specific emissions scenarios is unlikely to be achieved in the near future. In the absence of reliable model projections, subjective expert judgements concerning the trend and magnitude of change for precipitation in the Monsoon region could be elicited and incorporated into the BN.

The BN presented in this chapter could be updated with improved model information if and when it becomes available. However, in guiding decisions made now the BN approach can be used to assess system sensitivities and provide an analysis tool to develop pricing structures

which are robust to uncertainty. Incorporating results from additional models, both GCMs and RCMs, would allow for a greater exploration of the model uncertainty. Yet given the large biases in the model data, it may be some time before model forecasts can replace observational data in guiding the pricing of insurance. However, the knowledge gained from climate model experiments in combination with other sources of climate knowledge, such as climate analogues and remote sensing data, can add value to the decision making process and strengthen the channels by which science is utilised in the insurance industry.

6.7 Discussion of Results

6.7.1 Using climate model output to inform insurance strategies

In this chapter, the use of climate model output as a source of information to guide insurance decisions has been investigated. Section 6.2.3 presents the planning time horizons associated with ten strategic insurance issues. As articulated in this chapter, there is a desire to provide relevant climate model information to guide the management of strategic decisions but the specific information requirements of (re)insurers varies depending on the business activities and perils of interest. The underlying commonalities are the need for transparency in the assumptions made by climate modellers and the need for information which spans the range of plausible uncertainty in future climate states.

In using climate model forecasts to inform insurance decisions, it is important to understand how the climate system and climate models behave in order to gain confidence in quantitative projections. Chapter five showed the existence of regimes and almost intransitive behaviour for a model with subsystems operating on different time scales. Abrupt shifts in climate are therefore not to be unexpected and identifying the risks of such occurrences for regions of interest can have profound effects for insurance decisions. Whilst the analysis presented in this chapter utilised single model realisations to estimate changes in return periods, a more useful approach would utilise IC ensemble projections which can highlight the transient nature of climate under climate change. Embedding large IC ensembles within model forecasts to rigorously explore uncertainty and establish the differences between model climate distributions is therefore important in providing useful climate model information to the insurance industry.

6.7.2 Lessons from the BN case study

As emphasized by Cain (2001), "a BN should be used as a 'tool for thinking' not as an automatic answer provider". In the case study the BN approach provides a framework for combining climate model information with observational data to inform a specific decision problem subject to many competing decision factors. The existence of model errors, possible uncertainties in the observations and the reliance on the ergodic assumption mean that the assessment of utility of a particular index insurance pricing structure for Kolhapur is unlikely to be accurate. However the BN tool does allow an insurer to test system assumptions and sensitivities in a transparent manner. The primary aim of building the BN is not to provide an optimal pricing structure but to demonstrate how one might assess the sensitivity of various pricing structures to the input climate data. For example, in section 6.6.2 it is shown that a premium of 27% is required to yield the policy structure profitable for the supply-side under the assumptions embedded in the BN design. Determining such values and sensitivities could be of a real use in guiding the provision of index-based microinsurance under current and future climate scenarios.

The case study presented in this chapter focuses on the viability of index insurance for the rice

crop in Kolhapur, India. The methodology outlined could be easily extended to other weather index-insurance products covering a number of climate-related perils. The BN tool demonstrates how insurers might utilise climate model output in combination with observed data to inform themselves about potential return periods and threshold exceedance probabilities for variables of interest. Four sources of quantitative information are used in the case study. Preliminary data analysis presented in section 6.5.3 shows that the model precipitation output is associated with large model biases. The results in sections 6.6.3 and 6.6.4 show how these biases can be accounted for but the methodology is purely demonstrative and there are a number of reasons for urging caution in bias correcting precipitation data. Given the possibility of nonlinear changes in the climate variable distributions of chaotic systems, explored rigorously in this thesis, care should be taken when utilising imperfect model projections to inform return periods. Manipulating data to remove biases can compromise the value of model forecast distributions which can contain information about the dynamics of the climate within the model.

The BN is designed so that each data source can be individually selected or assigned a weight (relative probability). The result in figure 6.14 (and in figures D-1 and D-2 in the appendix) show the effect of weighting the sources in the network. However the decision to weight different model projections is contentious and depends on appropriate estimates of a model's ability to represent the climate system; a topic discussed in more detail by Tebaldi and Knutti (2007). Numerous methods have been developed to establish different metrics and measures of skill to weight models. Tebaldi et al. (2005) uses climatological mean temperatures to evaluate model skill whilst Greene et al. (2006) focuses on the ability of models to capture trend behaviour. However, the decision to weight models based on their ability to capture observations or key climatic processes has been questioned in a study by Weigel et al. (2010) which states:

> "When internal variability is large, more information may be lost by inappropriate weighting than could potentially be gained by optimum weighting...results indicate that for many applications equal weighting may be the safer and more transparent way to combine models".

The BN approach has the potential to add transparency to the decision-making process. The tool can distil complex information into a usable format and perform what-if scenarios to ensure that decisions are robust. There is clearly more work to be done in order to better align the approach with existing insurance decision structures but the research presented in this chapter represents an important step in improving the handling of climate model information in the insurance decision making process.

6.7.3 Limitations

The focus of the case study is on the burgeoning index insurance sector. The BN developed cannot be easily adjusted to address traditional insurance practices. The primary reason for the lack of a generalisation is the different nature of the payout process for index insurance and

traditional claims based insurance. Traditional insurance payouts are impacted by many risk factors as opposed to a single proxy measure. This impacts the determination of estimates for return periods and threshold exceedances for individual policy premiums. For weather index insurance, the maximum payouts for policies occur once a threshold has been surpassed while the maximum payouts for claims-based insurance are a function of the precise magnitude of the hazard. Using climate model output to inform traditional insurance therefore carries additional uncertainties and requires a more complex analysis.

The success of the BN approach in quantifying and communicating the risks of climate variability and climate change to the index insurance sector is dependant on a number of factors. Perhaps most importantly, there needs to be a decision (or set of decisions) which are sensitive to uncertain climate information. Whilst this seems to be an obvious consideration for policies designed to address weather- and climate-related perils, the regulatory and societal constraints (especially for microinsurance in developing economies) may deem the use of alternative sources of climate information irrelevant for policy design and loss estimates. For example, an insurer needs to be able to communicate what the insurance is based on and users may not be willing to accept premiums based on forecasts. Additionally, the user of the BN (in this case the insurer) must be willing and able to interpret probabilistic information conditional on a number of assumptions. In the case study explored in this chapter, the absence of reliable quantitative model projection data means that choices considered optimal based on the BN expected utility values will potentially lead to maladaptation and risk significant losses to insurers. In a climate change context, the tool ought therefore be used to examine preconceptions and guide decision makers rather than to optimise decisions.

The factors considered in the case study are not exhaustive and other potential factors which affect the viability of insurance could be included. For example, additional nodes could represent a detailed breakdown of expenses and administration cost options, the volatility in the price of the crop yields, the willingness of consumers to pay and/or alternative coverage periods. Inevitably, the number of nodes and data requirements could become very large. Without a specific user involved in the construction process, the content of the BN and the application of the approach is therefore limited.

An important additional uncertainty not considered in this study is the impact of emissions scenario uncertainty. For estimates of the change in climate risk in the 2030s the emissions scenario is unlikely to be a major factor but by the 2080s the emissions scenario used to drive model projections is likely to be a critical consideration. The BN approach would also allow for a comparison of model results under alternative emissions scenarios.

6.7.4 Further work

Research could be extended to further examine the use of climate model information to guide the pricing and policy structures of index insurance. An area which has been acknowledged

but not explored in detail is the potential to utilise BNs with climate model forecasts to inform premiums on an annual or seasonal basis. There is an element of seasonal to inter-annual predictability of the Indian monsoon, largely due to the El Niño Southern Oscillation (ENSO) phenomena. Droughts (floods) during the Indian monsoon are often accompanied by developing El Niño (La Niña) events in the Pacific Ocean (Krishnamurthy and Goswami (2000)). Selvaraju (2003) shows that the phase of ENSO has a significant correlation with food production in India. Comparing different model projections on seasonal forecast time scales using the BN approach could be beneficial to insurers who are interested in pricing insurance premiums to reflect seasonal forecast information.

If the pricing structure of an index based product is risk-based (employing actuarial assessments), the pricing signal can also be used to communicate risk to the policyholder. Carriquiry and Osgood (2008) state:

> "Insurance prices may communicate forecast information when farmers do not have direct access to the forecast. Studies exploring the potential of insurance prices as aggregators of forecast information would be valuable."

The work presented in this chapter could therefore be extended to consider the demand-side perspective. How climate model projections can be utilised to communicate the changing nature of weather risks under climate change through an index insurance product would be a valuable extension of the work presented here. Moreover, the BN approach could be developed to include different assumptions about socio-economic variables, such as *willingness to pay* which is a critical factor in the successful provision of index insurance.

Chapter 7

Discussion

7.1 Introduction

> **"We perceive the world, both as theoreticians and as citizens of the universe, according to our experiences and expectations, not always, perhaps even never, according to how the world actually is."**
>
> *Daniel Everett: Don't Sleep, There are Snakes (2008)*

Our expectations of weather and climate in the future are conditioned on what we perceive to be both plausible and likely given our experiences of weather and climate in the past. Daniel Everett's supposition of human perception in the discipline of linguistics is therefore applicable to the field of climate modelling. In using models to predict future climate change, scientists are attempting to predict the future evolution of the climate system, based on limited knowledge of how the climate has responded in the past and information on how the system evolves in computer simulations under current and future forcing conditions.

Given the societal relevance of climate science, it is vital that climate model experiments are designed appropriately to provide credible, robust and relevant information for the decision-making community. The work presented in this thesis has been focused on addressing the needs of the user community and particularly the insurance industry by exploring what climate model information is relevant and useful given the chaotic, nonlinear and highly complex nature of the climate system. In this final chapter, the themes of the research are discussed with reference to the analysis presented in the core chapters of this thesis. In section 7.2, the definition of climate under climate change is re-examined in light of the experiments conducted with the L63, L84 and LS84 models. Section 7.3 highlights the value of these experiments for gaining insight into the predictability of the climate system. The relevance of exploring transitivity in simple models to inform understanding of the behaviour of the climate system is discussed in section 7.4. The design of IC ensemble experiments, advocated throughout the thesis, is outlined in section 7.5. Section 7.6 discusses the links between the core thesis chapters, outlining the implications

of the research for the insurance industry. The limitations and difficulties experienced while conducting research are discussed in section 7.7. Section 7.8 details possible future research areas. Finally, section 7.9 reconsiders the thesis aims and presents final conclusions based on the experimental evidence and the analysis of the results.

7.2 Defining Climate Under Climate Change

7.2.1 The concept of climate

The climate system is deterministic (von Storch and Zwiers (1999)) so given a perfect model and perfect initial observations of the system, one would be able to produce an entirely accurate prediction of the system's evolution. Of course we are not fortunate enough to know the exact state of the system and we do not (and never will) possess a perfect model. Numerical models of the climate system are therefore inherently limited in their predictive capabilities. Over time scales longer than a few weeks, knowledge of *typical* atmospheric and oceanic conditions are therefore relevant to society and the notion of *climate* becomes a useful concept.

7.2.2 Competing definitions for climate

One of the recurring themes that has shaped the experiments presented in the preceding chapters, is the notion of climate under climate change. Defining climate is necessary to form an understanding of climate change, yet the definition of climate remains contested and has led to confusion in both the public and scientific discourse surrounding global warming and climate change. As discussed in section 2.1.1, there are broadly two classes of definition for the term climate. Firstly, *temporal* definitions have been widely adopted where climate is defined as a set of statistical quantities that can be derived from the evolution of the atmosphere (as well as other sub-systems) over a period of time (e.g Dymnikov and Gritsoun (2001), Burroughs (2003)). Secondly, *nonlinear dynamical* definitions exist where climate is expressed as a distribution of physical states consistent with the underlying boundary and forcing conditions, as dictated by the composition of the atmosphere and ocean as well as the radiative properties acting on the atmosphere-ocean system (e.g. Fraedrich (1986), Smith (2002)).

When using a temporal definition of climate, it is challenging to disentangle internally produced climate variability from externally driven climatic changes. Modes of short-term internal variability (such as ENSO) and longer-term variability (such as the AMO) have to be taken into account when deciding the length of time over which to define climate. Whilst all modes of variability are intrinsically related to the dynamic motions in the atmosphere-ocean system, we may wish to define some of the longer term modes, such as the glacial-interglacial cycle, as climatic changes. The statistics of climate will inevitably be influenced by sampling length; even in the absence of changes in the external forcings on the climate, climate change between two periods is inevitable.

It is argued here that the nonlinear dynamical definition of climate as a distribution of system states is more appropriate for climate change adaptation purposes. The definition utilises the concept of a climate attractor, or pseudo-attractor, which is useful in generating a thorough conceptual understanding of what climate is for a nonlinear dynamic system. Furthermore, investigating how changes in the system forcings affect the geometry of the attractor (pseudo-

attractor) can provide a basis for understanding what constitutes climate change.

7.2.3 Climate as a distribution

To clarify what is meant by climate defined as a distribution, it is important to note that the word *distribution* has (at least) three different uses within climate science discourse. Firstly, climate is spatially distributed as different regions on Earth experience different climatic conditions. The Köppen, or Köppen-Geiger, climate classification map (and variations thereof) illustrates the spatial distribution of classified climate-types across the world (Wilcock (1968))[1]. The spatial distribution of climate model output, and observational data, is commonly communicated using colour-coded maps. For example, figure 7.1 shows the spatial distribution of mean air temperature over Europe in winter and summer, using data from the Climatic Research Unit (CRU) CL 2.0 data bank (New et al. (2002)) at a horizontal resolution of 10' lat/long (approximately 18 km × 18 km at the equator). The graphics are compiled using observed temperature data for the period 1961 to 1990.

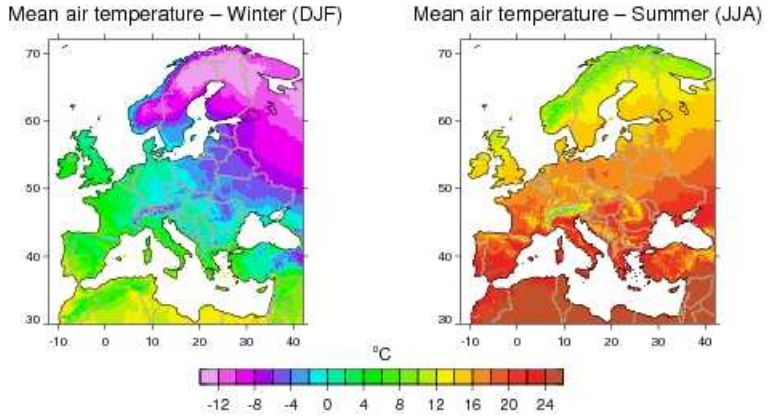

Figure 7.1: CRU CL 2.0 mean observed climate for Europe and N. Africa (1961 - 1990). Reproduced from CRU Ecochange climate data website: available at http://www.cru.uea.ac.uk/projects /ecochange/climatedata/desc.

The word *distribution* is also commonly used within the climate science community to refer to a multi-model or perturbed parameter ensemble (PPE) distribution. A PPE is simply a special case of the multi-model ensemble where each PPE member can be thought of as a different model version with the same underlying model structure. The use of multi-model ensembles and PPEs was discussed in more detail in section 2.2.3. Figure 7.2 shows the distribution of climate sensitivity from the PPE used in the climate*prediction*.net experiment (Stainforth et al. (2005)). The frequency distribution illustrates a range of model results and provides a quantified uncertainty assessment of the climate sensitivity within a single GCM (HadCM3), subject to substantial assumptions, particularly regarding parameter space sampling. The

[1] A recent version of the map by Kottek et al. (2006) presents an updated spatial distribution of climate-types to account for climatic conditions in the latter half of the twentieth century.

spatial distribution of climate will be different in each model version so for each PPE member, it would be possible to determine alternative versions of the plots shown in figure 7.1.

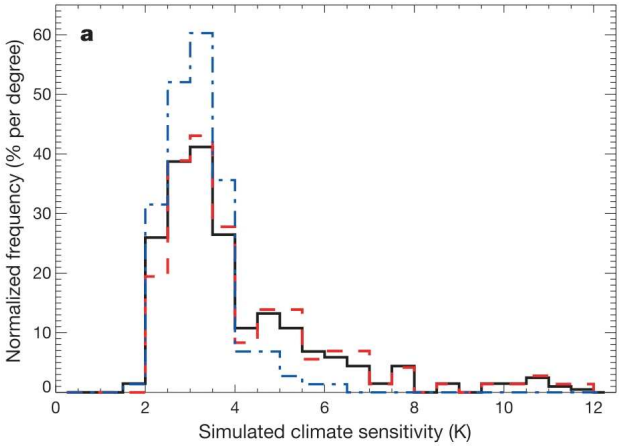

Figure 7.2: Frequency distribution of simulated climate sensitivity using all model versions (black), all model versions except those with perturbations to the cloud-to-rain conversion threshold (red), and all model versions except those with perturbations to the entrainment coefficient (blue). Reproduced from Stainforth et al. (2005).

The final use of the word *distribution* is that used in the nonlinear dynamical definition of climate. This form of the word is central to the proposed definition of climate suitable for climate change adaptation applications (highlighted in the conclusions in section 7.9.1) and is utilised in previous chapters in relation to the simple model experiments. In this context, climate is the distribution of states consistent with the system's forcings, conditioned on the uncertainty in the initial state of the climate system. The conditioning on the initial state of the system is crucial as not all states consistent with the system's attractor(s) or pseudo-attractor(s) will be possible given long-term variability and IC memory. The distribution of states is therefore intrinsically related to internal climate variability. An example IC ensemble distribution, shown in figure 7.3, is a reproduction of figure 3.5(a) and shows the distribution of states, as projected onto the X variable, for the L63 attractor with conventional parameters. In climate modelling, an IC ensemble is necessary to generate a frequency distribution of the form shown in figure 7.3, for some variable of interest under transient changes in the climate forcings; if the forcing isn't changing and the system is not intransitive, then a sufficiently long control run will suffice (see discussion in section 7.4). It follows that each PPE member used to generate the plot in figure 7.2 can be run with an associated IC ensemble to reveal the frequency distributions of climate variables at a given spatial resolution.

7.2.4 Determining climate variable distributions

In analysing historical climates and projecting future climates, scientists often use time series data to estimate the climate distributions for variables of interest. In order to illustrate the spatial inhomogeneity of mean temperatures across Europe and north Africa, shown in figure 7.1,

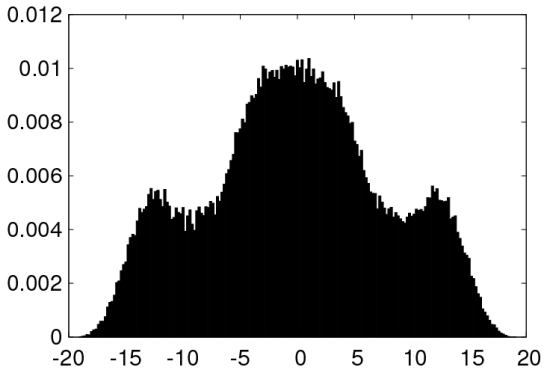

Figure 7.3: Normalised frequency distribution for the X variables in the L63 model, from a 100,000 member IC ensemble with ICs spread evenly along a transect from $(X_l, Y_l, Z_l) = (-20, -25, 1)$ to $(X_h, Y_h, Z_h) = (20, 25, 40)$ after a simulation period of 1,000 LTUs. The y-axis corresponds to the frequency of ensemble members per occupied bin; bin width = 0.2. (Reproduced from figure 3.5(a))

the mean of observed temperatures over the 1961 to 1990 interval were extracted and plotted. One could also use the thirty years of data to plot the distribution of observed temperatures for each grid-box as a set of frequency distribution plots. Crucially, the forcings on the climate system in 1990 were different to the forcings in 1961. In the PMS, an IC ensemble forced with 1961 conditions is therefore likely to yield different model PDFs compared to an IC ensemble forced with 1990 conditions. Furthermore, one would not expect the temperature in the year 1975 (the mid-point of the time series) to have a 50% probability of exceeding the median value from the 1961 to 1990 period, unless one assumes that the climate changed linearly between 1961 and 1990; a highly questionable assumption given known nonlinearities in the climate system. In a non-stationary climate the use of temporally averaged data can therefore be misleading.

In reality there is no perfect model with which to estimate the actual climate variable distributions for past years using large IC ensemble simulations. It is therefore inevitable that scientists and analysts use observational time series data to determine the statistics of climate in the past. In predicting future climate distributions however, it is important to find ways to extract useful information from imperfect models. Consequently, estimating and understanding the reliability of imperfect model projections is crucial.

In order to assess the reliability of climate models, modellers have traditionally opted to compare model realisations against observations (Annan and Hargreaves (2010)). Knutti (2008) states, "If the model and data do not agree, the scientist should be worried (assuming the model was designed to reproduce the data), because it implies that the model (or the data) is in error". However, this notion is potentially misleading. Owing to the complexity of the climate system, the presence of various modes of internal variability, and the possibility of almost intransitive behaviour, the observed trajectory of climate may exhibit long-term dependence on the initial state of the system. In order to have confidence in a particular model (over a specified time scale) it is only necessary that one IC ensemble member, from a sufficiently large model ensemble simulation, tracks or "shadows" the observations (Gilmour (1998), Judd

et al. (2004)). Disqualifying or down-weighting a climate model based on the ability of a limited sample of single model trajectories to reproduce observed data is flawed. Whilst observations are crucial for model development and process understanding, successfully reproducing an observed time series from a limited IC ensemble size is not a necessary condition in determining model reliability.

In the context of climate change adaptation, climate is best defined as a distribution and comparing distributions from different climate models is a way to establish confidence in model projections. The use of climate distribution statistics to evaluate model reliability is common in climate science but evaluations are typically reliant on the problematic, and often implicit, ergodic assumption (e.g. Perkins et al. (2007)). Boer (2000) and later Räisänen (2007) comment that model evaluation ought to be based on comparisons with real world data, presenting three broad categories for comparison. Räisänen (2007) states, "the first is morphology of climate as given by the spatial distribution and structure of means, variances, covariances and possibly other statistics of basic climate parameters." In practice this means assuming ergodicity and determining statistical measures from time series data. Moreover, comparisons are limited to specific properties of the distributions such as means and variances rather than the full distribution. The distributions of the L63, L84 and LS84 models show that nonlinear chaotic systems are often associated with irregular variable distributions so statistical properties which assume Gaussian distributions are limited. In the next section, further insights from the exploration of these models are identified.

7.3 Insights from Simple Models

The experiments conducted on the L63, L84 and LS84 models have been central to the development of the thesis conclusions. In this section, the specific insights gained from using each model are presented.

7.3.1 L63 model

The much studied L63 model has been a valuable tool in developing hypotheses relating to the predictability of the atmosphere. It is therefore a natural starting point to address the research theme of climate predictability under climate change. In section 3.3.1, the climate of the autonomous L63 model is defined as the distribution of states across all model variables consistent with the model attractor for fixed parameter values. A change in climate is therefore observed when the geometric properties of the model attractor change in response to a perturbation in one (or more) of the model parameters. The climate distributions of the L63 model (estimated using a 100,000 member IC ensemble in section 3.5) are governed by the values of the parameters, ρ, β and σ. For conventional parameter values, IC ensemble distributions are shown to converge to the model climate distributions over a time scale of approximately 50 LTUs, irrespective of the original location of the ensemble in model state space. This is illustrated in figure 3.10 using the KS test. The relatively short-lived memory of ICs in the L63 model is related to the transitive nature of the model.

For fixed parameters it is shown that the L63 model is ergodic; the single trajectory distributions converge to the IC ensemble distributions illustrated in figure 3.5. The time scale for convergence for the single model realisation selected is approximately 150 LTUs. The ergodic assumption is therefore valid in estimating the climate of the L63 model and computationally more efficient than the IC ensemble method (for fixed parameters). Ergodicity is observed because the model is transitive and a single trajectory is able to visit all regions of the attractor. In the absence of parameter changes, and assuming the climate system is a transitive system, the results support the conceptual model of viewing trajectories which orbit the attractor as "weather" (noise), whilst viewing the climate as the statistical properties of the fixed attractor determined from a single trajectory or an IC ensemble distribution.

Understanding the L63 climate under climate change requires an exploration of the model under altered parameter conditions. Sections 3.5 to 3.8 focus on the impact of varying the model parameter ρ. Considered as an analogy to the GHG forcing, periodic and nonperiodic fluctuations in ρ are introduced into the L63 model. Figure 3.12 shows how periodic fluctuations in ρ, varying on a time scale comparable to the time scale for regime orbits, influence the IC ensemble distributions. The altered distributions occur as a result of the changing geometry of the model attractor. The dependence on the frequency of the periodicity in ρ suggests evidence of resonant model behaviour. Yet even in the presence of resonance the model continues to be ergodic as described in section 3.6.1.

Experiments with nonperiodic fluctuations in ρ reveal evidence of hysteresis in the L63 model as the IC ensemble distributions are dependent on the pathway of the parameter ρ. The ergodic assumption fails when the model is subject to fluctuating frequencies in ρ which induce model resonance because the ensemble distributions are path-dependent as well as time-dependent. IC ensembles are therefore required to determine the model PDFs at particular time instants. Interestingly, figure 3.22 shows that the IC ensembles from different locations on the pseudo-attractor[2] converge to the climate distributions of the model when subject to nonperiodic fluctuations in ρ. This result is useful as it tells us that even if the ergodic assumption is no longer valid, transitive behaviour of the model ensures that the memory of IC uncertainty is finite. Furthermore, the convergence of ensembles to the model climate distributions is more rapid under nonperiodic parameter changes, as shown in section 3.7.5.

If the climate system were subject to resonance induced by a nonperiodic fluctuating forcing, then the results shown in this chapter would have far-reaching implications for the way climate model experiments are designed to explore uncertainty. When predicting future climate changes with a unique set of forcings that has not existed throughout Earths history (Dessai and Hulme (2004)), it would be unwise to rule out the potential impact of fluctuating radiative forcing frequencies on the global climate system simply because the relevant results presented in chapter three are confined to a low-dimensional model. Further experiments on more complex climate models would yield additional insights to inform the possibility of observing this phenomena in the real climate system.

Perhaps of more immediate interest to climate modellers is the path dependence, or hysteresis, exhibited in the model ensemble distributions for nonperiodic fluctuations in ρ. The implication for the climate system is that climate variable distributions might be dependent on the pathway of a particular forcing scenario. In the context of twenty-first century anthropogenic climate change, the resulting hypothesis is that the response of the climate system is not only dependent on the cumulative build-up of GHG concentrations (Allen et al. (2009)) but also on the *pathway* of the build-up in GHG concentrations. The hypothesis is consistent with the Epstein and McCarthy (2004) study which postulates that the stability of the climate system is a function of the system's forcings. In relating the impact of GHG concentrations to the variability and stability of the climate system, Epstein and McCarthy (2004) state:

> "Stabilization of CO_2 at 450 or 550 ppm may possibly avoid some critical adverse thresholds; but, there is no assurance that the rate of change of greenhouse gas build-up in the interim will not force the system to oscillate erratically and yield significant and punishing surprises, or even force the system to jump into another equilibrium state."

Running large IC ensembles with multiple forcing scenarios in a number of climate models would help address both the hypothesis regarding climate system hysteresis and the stability of

[2]The term pseudo-attractor is introduced in chapter four.

climate for different rates of GHG build-up.

The definition of an attractor as a region in state space to which trajectories evolve loses its precise meaning when the properties of the attractor become time-dependent. The introduction of the term pseudo-attractor in chapter four is an attempt to be consistent with nonlinear dynamics theory in developing an understanding of the climate for non-autonomous systems. In any case, the notion of an attractor and the associated geometric properties that denote the climate of the system has value in creating a conceptual model of the nonlinear chaotic climate system under climate change.

The main message that emerges from the work conducted on the L63 model is that large IC ensemble experiments are likely to be a vital ingredient in aiding understanding of the dynamic behaviour associated the climate system under climate change. Using the L84 and LS84 models, further experiments were conducted to refine this message and gain additional insight into potential future areas of focus.

7.3.2 L84 model

Employing a definition of climate as a distribution consistent with the system's attractor has its limitations; not least because of the potential coexistence of multiple attractors. The main advantage of analysing the behaviour of the L84 model in addition to the L63 model, is that large regions of parameter space have more than one coexisting attractor (Lorenz (1984), Freire et al. (2008)). Given the complex interactions in the climate system, and the fact that the system is constantly adjusting to time-dependent forcings, it is difficult to assess the existence of multiple coexisting attractors. However, as described in section 4.6.1, Budyko (1969) explains that the present configuration of continents and oceans could support two climatic regimes. In addition, observed abrupt shifts in climate over the past millennia suggest that the climate system consists of multiple equilibria (Schneider (2004)), which suggests the possibility of coexisting attractors.

Utilising the definitions of summer and winter, adapted in the Lorenz (1990) study, the model climate distributions are determined in section 4.3.2. For experiments in the permanent summer configuration, in which more than one attractor coexist, the ergodic assumption is shown to be invalid (see section 4.3.3). The two periodic attractors identified for the summer configuration of the L84 model are associated with intransitive behaviour. Figure 4.6 displays the basins of attraction for the X-Y plane illustrating the foliated nature of the basins dictating the evolution of model trajectories from different ICs. For an initial state with uncertainty that spans the basins of attraction, the attractor to which the model trajectory evolves is also uncertain.

The climate of the L84 model is investigated with a seasonal cycle in which F (equator-to-pole temperature difference) varies as a sinusoid with a wavelength equal to one model year. The ergodic assumption is tested for mid-winter and mid-summer where F returns to $F = 8$ and $F = 6$ respectively. Figure 4.22 shows the time scale at which single trajectory distributions converge towards the ensemble climate distributions. The ergodic assumption is shown to

be valid over a simulation period of many thousands of model years. The long simulation period is necessary because only one data point is selected each year at mid-winter and mid-summer. Including more data points, from the months of January and July, in the single trajectory distributions to speed up the convergence time is shown to be problematic (see section 4.4.4). In this case, the single trajectory distributions do not entirely converge towards the ensemble distributions. Including data points from the model under different parameter conditions distorts the single trajectory distributions. In the analogy to the climate system, the result suggests that in estimating a climate distribution at a specific time instant, inclusion of data points that are associated with alternative forcing and/or boundary conditions could potentially lead to the creation of misrepresentative PDFs.

The L84 model is also used to explore transient climate change (see section 4.5). The value of F is decreased over time in a transition to more summer-like conditions as an analogy to a possible future climate and the ergodic assumption is again investigated. Despite a linear change in F_m, the changes in the geometric properties of the climate distributions are not smooth over time and the ergodic assumption is shown to be invalid. Additionally, the memory of ICs is investigated in the transient phase between two fixed climates. The results presented in section 4.5.3 show multi-decadal memory exists as model trajectories propagate according to the unstable pseudo-attractor (PA2) before transitioning to the stable pseudo-attractor (PA1). The rate at which trajectories transition to PA1 reveals an exponential-like decay function, illustrated in figure 4.33. The results suggest that under transient climatic conditions, the memory of the system can be affected.

7.3.3 LS84 model

In the L84 model, the climate change analogy considers a transition from a transitive region of parameter space to an intransitive region of parameter space. To extend the analogy, the LS84 model is investigated, in which the L84 model is coupled to the S61 ocean-box model creating almost intransitive dynamic behaviour for certain parameter values.

The extent to which long-term climate change is dependent on the current state of the climate system is an area which divides opinion. Whilst is has become widely acknowledged that initialising the ocean is important for improving the accuracy of decadal forecasts, the impact of IC uncertainty on multi-decadal and longer time scales is largely ignored in the climate modelling community. Experiments with the LS84 model are therefore driven by an interest in system IC memory. With the addition of an ocean component the interaction of two sub-systems evolving with different time scales is investigated. The goal is to generate further insight into the interactions between nonlinear chaotic behaviour and long-term internal variability.

The coupling of the L84 model and the S61 model is based on the study by Van Veen et al. (2001). Two sets of coupling parameters, referred to as "active" and "passive", are explored and figure 5.2 illustrates the behaviour of the ocean variables T and S, associated with the different

coupling parameters. The terms *active* and *passive*, coined by Van Veen et al. (2001), lose their literal meanings when subject to a seasonal cycle in F_0 but for continuity with the Van Veen et al. (2001) study, the terms continue to be used in the analysis presented in chapter five. Under passive coupling parameters, the model exhibits two distinct regimes referred to as the LT and HT regimes. Figure 5.4(b) shows the centennial scale variability in the T and S variables. In T the transitions are abrupt and the residence time in each regime lasts from tens to hundreds of years. The long residence times in each regime convey almost intransitive behaviour which is of particular interest in the analogy to climate under climate change. The figure also shows the resemblance between T and f, denoting the strength of the THC, highlighting that the model is temperature driven under the parameter conditions chosen.

Section 5.2.5 explains the logic for focussing analysis on the ocean variables. In the LS84 model, the phase of the ocean is a major controlling factor in the annual variability in the atmosphere. By analogy to the climate system, large-scale oscillations in the oceans, such as the South Pacific and the North Atlantic, can dominate the atmospheric circulation in many regions across the world. The analysis of model memory and ergodicity is therefore presented for the ocean variables but the results extend to the long-term predictability of the atmosphere.

The ensemble climate distributions and ergodicity of the seasonally driven LS84 model are determined in section 5.3. The results show that a model simulation of thousands of years is required to demonstrate the convergence of single trajectory distributions. The convergence is slower under passive coupling because of the long residence periods spent in each regime. Figure 5.11 illustrates the convergence of single trajectory distributions to the model "climate" distributions (estimated from a 100,000 member ensemble) showing that the model is in fact ergodic under both forms of coupling but very long simulations (thousands of years) are needed before the single trajectory distributions converge to the ensemble climate distributions. Furthermore, the convergence is not smooth and over some periods, particularly under passive coupling, increasing the simulation length for a single trajectory might not improve the estimates of the underlying climate distributions. The results suggest that almost intransitivity limits the use of the ergodic assumption. Even under fixed parameter conditions (albeit with a seasonal cycle in F_0) a large IC ensemble is more appropriate in estimating the climate distributions.

The size of IC ensembles required to accurately estimate model PDFs is investigated in section 5.4. A simple experiment is devised to determine the proportion of ensemble members in each regime as a function of ensemble size. The results indicate that an ensemble size of 2,000 to 4,000 members is necessary to provide robust probability estimates regarding the probability of a transition between the two specified regimes. To improve tail estimates, more ensemble members may be required but the result highlights a minimum IC ensemble size requirement to provide robust estimates of some climate variable distribution properties. It would be interesting to pursue this result further by extending the experiment to higher-order climate models.

The experiment is also inverted to provide a measure of the IC memory in the LS84 model under passive coupling. The IC ensemble distributions are found to be dependent on ICs for a

period of up to 200 model years. In section 5.5, the memory of the ensemble distributions is further investigated for ensembles originating in different regimes. The results show that the initial values of T are more important than those of S in determining the convergence rates between ensembles. Crucially, the findings suggest that IC uncertainty limits predictability more significantly when the variables have an important role in the dynamic evolution of the system.

Finally, the LS84 model under passive coupling is used to investigate climate change in the LS84 model by introducing a linear trend in F_0. The model is forced from a region of parameter space associated with transitive behaviour, where $F_m = 8$, to the previously identified almost intransitive region of parameter space, where $F_m = 7$. Three single model realisations with slightly different ICs are shown which expose differences in the evolution of the T variable over the 2,000 year simulation period. In the original parameter configuration, the internal variability exhibited by the model trajectories is similar. After a linear decrease in F_0, two of the trajectories, labelled *IC 1* and *IC 2*, show relatively frequent transitions between the LT and HT regimes whilst the trajectory labelled *IC 3* spends more time in the LT regime (see figure 5.20). The KS test is used to quantify the differences between single trajectory distributions under the initial transitive climate and in the altered climate associated with almost intransitive behaviour. The results imply that skill in the ability of a single model realisation to capture the statistics of climate should not necessarily lead to confidence in the ability of a single trajectory to provide reliable estimates of the climate variable distributions under altered parameter conditions. In the next section, the issue of the transitivity of the climate system and the implications for climate prediction are discussed in greater detail.

7.4 The Transitivity Debate

The extent to which the climate system can be considered transitive under current and altered forcing conditions underlies much of the research presented in this thesis. Lorenz (1990) reasons that the "atmosphere-ocean-earth system" is unlikely to be intransitive. The conclusion was based on experiments with the seasonally driven L84 model (explored in chapter four) in which the winter evolution is chaotic and a single attractor exists whilst in the summer the model behaviour is periodic and multiple attractors coexist. The presence of chaos in the winter ultimately yields transitive model behaviour as the attractor to which a trajectory propagates in the succeeding summer is a "virtually randomly chosen circulation pattern". However, the L84 model was only investigated in a stationary mode and with periodic changes to F. The real climate system is non-stationary and includes modes of variability on all time scales. The research presented in chapter five shows that when the L84 model (representing the rapidly evolving atmosphere) is coupled to the S61 model (representing the slowly evolving ocean component) the evolution of the atmosphere in the summer parameter configuration is no longer "randomly" chosen as the probability of an *active* or *inactive* summer is affected by the underlying state of the ocean (see section 5.2.5). This dependence on the slowly evolving ocean means that statistics of the atmosphere taken over *long* finite periods, in which the ocean is displaying one type of behaviour, will be different from the infinite-term statistics; a property referred to as almost intransitivity (Lorenz (1968)). The conclusion of Lorenz (1990) that the climate system is unlikely to be intransitive does not rule out the possibility of almost intransitive behaviour and the model results shown in chapter five reveal the presence of this behaviour in an idealised coupled atmosphere-ocean model.

Considering the possibility of almost intransitivity in the climate system raises important questions for how climate is defined and how GCMs are run to explore climate under climate change. In section 2.1.4, the work of Schneider and Dickinson (2000) is discussed. Schneider and Dickinson (2000) state that because the climate system may not be transitive, a time-averaged definition of climate is more appropriate than a definition which includes all states consistent with the forcing and boundary conditions. The implied logic behind this assertion is that in studying past climates, it is more useful to analyse the observed behaviour of the system rather than speculate about theoretically possible states that haven't been experienced. Whilst this reasoning may be appropriate for specific analyses of the past *observed* behaviour of the climate system, applying the same reasoning to advocate a temporal definition of climate when considering future climate change adaptation is flawed.

Under transient climate change, even if the climate system is transitive not all possible system states will be realised as the climate distributions change in time with the underlying modulations to the system attractor/pseudo-attractor(s), in response to the altered forcings. In the PMS, a sufficiently large IC ensemble will elucidate the range of possible states for a particular forcing scenario. The additional possibility of almost intransitive system behaviour means that conditioning the IC ensemble on the current uncertainty in the initial state is crucial.

For an almost intransitive system, the range of possible future states will be constrained as certain states, which may be consistent with the underlying boundary and forcing conditions, may not necessarily be possible given constrained IC uncertainty. Moreover, the time-mean climate for each IC ensemble member trajectory is likely to be different over a finite interval given almost intransitive behaviour yet the distribution of future states (for a specific forcing scenario) will represent the full range of uncertainty conditioned on uncertainty in the initial state. It is this distribution of states which is relevant to climate change adaptation. The most suitable definition of climate under climate change is therefore the distribution of states consistent with the system's forcings, *conditioned* on the uncertainty in the initial state of the system.

For altered system behaviour under climate change, not only might we expect a shift in variable distributions (changes in the mean statistics) but also significant changes in the shape of the distributions such as altered modal properties. Observing these changes in climate model simulations using single model trajectories is problematic. In the *climate change* experiments conducted with the LS84 model the results show that a shift from transitive to almost intransitive conditions can have significant impacts on the model dynamics. Single model realisations are unable to fully represent the model climate distributions associated with the different dynamic regimes.

In relation to climate change adaptation decisions, particularly within the insurance industry, establishing reliable probability estimates for possible future climate states is the ultimate objective. In order to meet this challenge, the evidence provided in the model results shows that incorporating IC uncertainty into the design of climate model experiments is a critical ingredient. Given the possibility for almost intransitive behaviour, resulting from the interaction of subsystems operating on different dynamic time scales, it is also vitally important to condition IC ensembles on the current uncertainty in the initial state of the climate system.

7.5 IC Ensembles in Climate Model Experiments

Climate model output is used to estimate changes in climate variable statistics at a number of prediction lead times. Using past observations (e.g. 1961 to 1990), time series data is often multiplied by a change factor derived from the mean statistics of individual model projections. This transformation is being done, albeit with crude adjustments for changes in variability, to provide guidance to certain sectors that are interested in climate change adaptation (e.g. the construction sector, Belcher et al. (2005), CIBSE (2006)). However, if the future variability of climate is subject to nonlinear changes, such that the shape and range of the distribution of climate variables are altered, then a transformation reliant solely on past observations is inappropriate. Utilising large IC model ensembles would be preferable to avoid crude assumptions in guiding climate change adaptation.

The experimental results from the study of the L63, L84 and LS84 models suggest that large IC ensemble simulations will benefit climate prediction, and remove reliance on the ergodic assumption. Adopting this approach will ultimately have value for decision makers wishing to be robust to climate uncertainties, for at least four reasons. Firstly, even in the absence of changes in external forcings conditions (such as the GHG forcing and solar forcing) the climate system is subject to a number of modes of internal variability on spatial and temporal scales of interest for climate change adaptation. As a consequence, even armed with a perfect model, single model trajectory frequency distributions could fail to converge to the system climate distributions over a relevant time scale. Secondly, if the climate system contains multiple coexisting attractors or pseudo-attractors, then a single trajectory will not capture the range of possible futures consistent with the ICs, if indeed the IC uncertainty spans more than one basin of attraction. Thirdly, because all climate models are imperfect, IC ensemble distributions from different models subjected to the same boundary and forcing conditions could reveal discrepancies between the model climates. Finally, abrupt changes in the model climate, in response to altered/transient forcing conditions, will be more easily observed in IC ensemble results as the climate change signal can be distinguished from internal variability exhibited by an individual model realisation.

Listed below are a number of steps, guided by the results obtained using simple models, which need to be considered in designing IC ensemble experiments to produce climate variable distributions relevant for climate change adaptation applications:

- Establish the extent of observational uncertainty in the initial state of the atmosphere, ocean and other subsystems included in the climate model.
- Determine the necessary IC ensemble size required to generate robust quantitative information for the variables of interest.
- Select models, model versions (from a PPE) and forcing scenarios to be explored.

- Choose an appropriate sampling methodology for each variable in the IC ensemble[3] (e.g. Monte Carlo techniques).
- Test the sensitivity of model climate distributions to IC selection/sampling method for a sub-sample of the model versions being investigated by examining the rate of convergence between the distributions.

An inevitable criticism of advocating large IC ensemble experiments with AOGCMs is that IC ensemble simulations will increase computational costs and be time-consuming. For each step listed, the modelling resource required is indeed potentially very significant. Scientifically, this argument is irrelevant but on a practical level such a consideration needs to be addressed. There are methods that can cope with increasing ensemble size requirements. The use of distributed computing, utilised by Stainforth et al. (2005), is a vast resource that has the capacity to run large numbers of individual model realisations. In addition, the emergence of cloud computing offers a potentially valuable avenue for running large ensembles with coupled AOGCMs (Evangelinos and Hill (2008), Vecchiola et al. (2009)). Ultimately, compromises will need to be made between achieving an appropriate level of model complexity and spatial resolution whilst preserving the ability to sample uncertainty. However, in providing quantitative information to decision makers, under-sampling of (IC) uncertainty risks undermining the value and trust placed in the provision of climate model information. The choices and compromises climate scientists make in designing climate model experiments will benefit from knowledge of how users understand and interpret the model output.

In order for quantitative information from climate model output to be considered robust across models, the information should be insensitive to model choice. Comparing IC ensembles for multiple *imperfect* models may show that information regarding certain variables of interest is highly dependent on the model used and the parameters chosen. Therefore, the value of model information for influencing decisions may come from the range of possible behaviour across multiple models and PPEs. Model output can be useful in bounding uncertainty and providing a range of future climate states, at a number of spatial and temporal scales, within which adaptation decisions can be assessed. In the absence of robust information from climate models, confident statements about future climate will be more qualitative than quantitative (Stainforth et al. (2007a).

[3] A detailed discussion of sampling methods for ensemble forecasting in relation to numerical weather prediction is given by Leutbecher and Palmer (2008).

7.6 Implications for Insurance

7.6.1 Informing insurance strategy

In a strategic analysis of insurance activity, Ernst & Young (2008) identified an "over-reliance on model-based risk management" as a major threat to the insurance industry, given the inability of various modelling approaches to deal with extreme volatility. In relation to climate change, the lack of formal uptake of climate model information within the industry means that the threat of an over-reliance on climate model output is small at present. However, in the future as insurers work more closely with climate scientists and climate modellers, it is important to avoid the situation where insurers become reliant on climate model projections which are not fit for purpose. Ignoring the issues of model inadequacy and directly using highly conditional climate model output in pricing and strategic decision making could exacerbate the risks faced by insurers.

In section 6.2, ten strategic insurance issues are identified which are likely to be affected by climate variability and climate change. Figure 6.1 illustrates the time scales over which climate model information may be useful in guiding general (non-life) insurance decisions. Whilst the majority of business practices within the insurance and reinsurance sectors are typically dictated by short time scale considerations (with a lead time of up to one year), section 6.2.3 explains how climate information can be relevant for strategic planning on time scales of greater than five years. The impacts of climate change on issues such as *risks to reputation* and *liability* may be viewed as largely negative for the insurance industry but the impact of climate change on other strategic considerations such as *emerging markets* and *investments* present significant opportunities for insurers. If insurers are proactive in utilising climate model information and can form strategies which are robust to climatic uncertainties, the industry can become resilient and aid society in adapting to the impacts of climate change.

7.6.2 What climate model information is relevant?

Stainforth et al. (2007a) state that climate change adaptation decisions are sensitive to more than just the mean of the distribution. This assertion is particularly relevant to the insurance industry which exists primarily to mitigate extreme risk associated with tail events. Risk-based pricing requires knowledge of return periods and recurrence probabilities that are typically estimated using available meteorological observations and loss datasets. In a non-stationary climate, insurers cannot rely on probability estimates derived purely from past observations. In addition, nonlinearities in the climate system and abrupt transitions between climatic regimes mean that assuming ergodicity to estimate climate variable distributions from single model realisations in the future is inappropriate.

Insurance decisions are typically made at regional and local scales so high resolution information from climate models appears desirable. In addition, climate models currently operate with

parameterisation schemes at subgrid-scales and moving to higher resolution models might enable some subgrid-scale processes to be better resolved. It would therefore appear that developing higher resolution models would be beneficial to both scientists wishing to understand the behaviour of the climate system and in providing valuable information to insurers. The arguments articulated in relation to experimental design do not refute the value of high resolution models in climate science. Used in a research mode, high resolution models have the potential to generate useful insights to increase scientific understanding of key climate processes. However, high resolution models require additional computational capacity and the number of possible model runs is decreased. The ability to run large IC ensembles would be diminished and the problems associated with relying on single model realisations to project future climate change would remain. Therefore, extending the use of high resolution model information into the public domain could be hazardous. Precise information in the absence of an adequate uncertainty analysis is both scientifically naive and potentially misleading for the user community.

It is valuable to make a distinction between need and desire. The needs of insurers represents the minimum information required from climate projections to justify any changes to policy structures, strategies and/or premium prices. The desires of insurers relate to information that would enable insurers to make robust, accurate and timely adjustments to climate-related policies and business lines. The desire for ever higher resolution information is likely to remain because insurers are often interested in assessing risk at high resolutions, particularly in areas with major concentrations of exposure as noted by Ranger et al. (2009). However, the needs of insurers are diverse and it is likely that climate model output cannot satisfy the needs of all insurers interested in adapting policy and strategy in the face of climate change. This does not mean that coarse scale climate model information is irrelevant but it suggests that quantitative output from climate models cannot be directly used in all areas of the insurance industry.

Qualitative information from climate model projections can be valuable in the absence of robust quantitative information. Inherently, climate prediction under climate change is conditional on assumptions about GHG emissions and changes to other system forcings (such as solar and volcanic influences). Quantitative output from climate models is therefore scenario dependent. For strategic insurance decisions, knowledge about the possible and plausible impacts of climate change is potentially of more value than highly conditional "best" estimates. Ultimately, for insurers to remain solvent and ensure resilience to climate change, awareness of the capacity of climate model projections to explore uncertainty is beneficial. If climate model experiments are to be useful in providing information to guide strategic, and perhaps operational insurance decisions, it is important that all sources of uncertainty, including IC uncertainty, are appropriately acknowledged in the design of ensemble based experiments.

7.6.3 Insights from case study

One sub-sector of insurance that could directly benefit from the appropriate use and interpretation of climate model output is the burgeoning index insurance sector. The case study presented in chapter six, sections 6.3 to 6.6, demonstrates the use of climate model information in determining the pricing and viability of index insurance for crop cover in India, under climate change. The focus on index weather insurance allows the socio-economic considerations affecting insurance losses to be side-stepped as payouts are triggered according to meteorological proxy measurements. The case study highlights the interest of insurers in thresholds and threshold exceedance probabilities. In the design of index insurance products, estimates of exceedance probabilities are currently based on the observational record assuming both stationarity and ergodicity in the climate system. The dangers of assuming stationarity are well acknowledged by insurers and scientists alike (Wunsch (1999), Dlugolecki (2008)). However, as discussed throughout this thesis, under climate variability and climate change the ergodic assumption can be misleading; this assumption is however rarely stated in the use of climate information to inform policy.

In designing index insurance products, insurers need to account for imperfect and incomplete climate information whilst dealing with significant uncertainty and ambiguity. The climate model information from the regional HadRM3 model runs are only available in the form of single model realisations. Inevitably, the user community if forced to assume ergodicity in using the information to estimate exceedance probabilities. The case study also shows how reliance on only one source of information (i.e. one model) can create false confidence and potentially lead to maladaptation. The output of the HadRM3 model is strongly dependent on the driving data. The figures presented in section 6.6 illustrate the differences in the model output when driven by the HadCM3 model, the ECHAM5 model and the ERA-interim reanalysis data. When the data is ingested into the BN, the viability of the index insurance design is shown to be highly sensitive to model choice, as described in section 6.6.2. Introducing bias corrections, as described in section 6.6.3, is problematic and requires careful consideration regarding the physical interpretation of bias corrected model data. Diagnosing the reasons for the differences in the model output is of course a challenging task and not something that the user community is likely to be able to accomplish alone. Therefore insurers and the adaptation community more generally are likely to benefit from making decisions that are insensitive to model choice. Robust decisions are therefore likely to be associated with low-regret options, such as diversifying portfolios, but the risk appetite of different insurers is variable and certain companies may accept less robust policy options.

The strength of BNs to support climate change decision problems is also discussed in relation to the case study. In section 6.6.5, it is noted that the BN tool is useful not only to provide quantitative decision support but also to reveal node and state dependencies which have a large impact on the decision outcome. The tool aims to be transparent and enables users to see the effects of node choices on the probabilities throughout the network. However, the BN approach

is limited and despite aiming to be exhaustive, the decision tool requires quantitative input for all variables, either in the form of continuous data or subjective probabilistic choices, which may not always be possible and/or appropriate. A more detailed discussion of the value of BNs and the success and limitation of the case study is provided in section 6.7. In communicating climate model information to users, BNs provide a useful framework enabling diverse information sources to be combined while tailoring information to a specific decision problem. Nonetheless, a variety of tools and approaches are likely to be needed to address the different types of decisions being made by insurers wishing to utilise climate model output.

7.6.4 The balance of quantitative versus qualitative information

Climate models are not only used in an operational setting to provide climate information to policy-makers but can also be valuable tools with which to test hypotheses and develop understanding of the complex interactions of particular physical processes in the climate system. The distinction between a model which is being used to advance research and a model which is being used to inform societal decision-making is crucial. Currently, climate modelling centres appear to be creating ever more complex climate models in an attempt to become user-relevant. A recent study by Pope et al. (2007) begins with the statement:

> "Useful climate predictions depend on having the most comprehensive and accurate available models of the climate system."

However, as noted by Pope et al. (2007), in order to create a comprehensive climate model compromises must be struck between model complexity, model resolution and the ability of the model to deal with uncertainty. A climate model prediction for adaptation decisions in general, and insurance decisions in particular, requires a comprehensive assessment of uncertainty if it is to be deemed "useful". Ultimately, it is the uncertainty rather than the best estimate, that really drives decisions related to climate variability and climate change. This is especially true in the insurance industry where uncertainty is intrinsically related to risk.

It is crucial to be able to communicate the uncertainty arising from climate model experiments and develop a modelling framework to allow for further exploration of key uncertainties. The notion that relatively low resolution model output is irrelevant for policy making is misinformed as the scales at which many insurance decisions are made can often deal with coarse resolutions. Insurance and reinsurance decisions are applied at a variety of spatial scales, and examining the uncertainty more thoroughly at coarser scales can be of use to the industry. In focussing model experiments on the exploration of uncertainty, it is of course possible to increase the uncertainty associated with climate projections. Pidgeon and Fischhoff (2011) argue that climate modellers need to confront such an apparent contradiction and find ways to carefully explain the results of more rigorous experiments to decision makers and the public. Given the existence of known unknowns in climate model experiments, finding the appropriate balance between quantified results and qualitative guidance to decision makers is therefore of utmost importance.

7.7 Limitations and Difficulties Experienced

7.7.1 Modelling by analogy

The models used in this thesis are highly idealised representations of physical systems. All models used to inform us about the evolution of the climate system are imperfect but only high-dimensional GCMs and AOGCMs can claim to be sufficiently complex to replicate the dynamic behaviour of the climate system. That said, the increased complexity and computational capacity required to run operational climate models prevents comprehensive exploration of model dependencies and makes the interpretation of model results conceptually challenging. There is enormous value in running experiments with simple models where model dependencies and sensitivities can more easily be explored and understood. The results of the model experiments are useful in providing a theoretical grounding to guide the design of GCM and AOGCM experiments to better explore uncertainty. However, the results cannot be expected to scale directly to the climate system and inform projections of future climate change. As noted by Smith (2002), identifying issues in simpler models is a first step in developing testable hypotheses. Yet to test a hypothesis in an operational model, a collaborative effort and an understanding of the intricacies of individual models is required.

7.7.2 The challenge of interdisciplinary research

In any field of applied science, trade-offs must inevitably be made between achieving a depth of research and enabling the findings to be translated into meaningful results for users. In relation to applied climate change research, it has long been acknowledged that studies confined to single disciplines cannot appropriately address the needs of those who have to consider a multitude of factors in the decision making process (Schneider (1977)). By examining both the role of nonlinear dynamics in climate prediction and the adaptation decisions needs of insurers, the research presented attempts to bridge climate science with the policy considerations of the insurance industry. However, as evident in the limitations of using climate model output to inform index insurance decisions, the results show that there is a significant disconnect between the information desired by insurers and the capabilities of modelling groups.

The added complexity of a policy dimension to the research places the work in the realm of post-normal science (PNS). Funtowicz and Ravetz (1993) describes PNS as "inquiries that occur at the interfaces of science and policy where uncertainties and value-loadings are critical". Clearly, this description is befitting to the work presented in this thesis and it is hoped that the implications of the research have relevance to both a scientific readership and those involved in making policy decisions sensitive to climate change.

7.7.3 Engaging with insurers

As stated in section 1.6, a key aim of the research is to determine the extent to which climate model output can be utilised by insurers. Within the industry, decisions are taken at a variety of organisational levels and risk calculations are often aggregated across entire portfolios. It is therefore challenging to illuminate the channels by which climate model information can directly influence decisions, with the possible exception of catastrophe modelling. Climate change, as a *problem* to be managed, is embedded within many other issues faced by insurers. The decision process is therefore dilute and the potential use of climate model information in guiding insurance decisions is unlikely to be similar for different insurers and different insurance sub-sectors.

In designing climate model experiments to be more relevant to insurers and reinsurers, one of the key obstacles facing the both scientists and the insurance industry is finding ways to improve communication channels. The relatively recent initiatives such as ClimateWise[4], the Willis Research Network[5] and the Munich Re Climate Change Initiative[6] are likely to play a central role in steering the future of applied climate research and the provision of climate information, at least within Europe. For the global insurance industry, the creation of climate services at different national modelling centres is likely to provide opportunities for further collaboration between insurers and scientists.

[4] http://www.climatewise.org.uk
[5] http://www.willisresearchnetwork.com
[6] http://www.climate-insurance.org

7.8 Further Research

7.8.1 Abrupt climate change and feedbacks

In the climate system, changes in the system's forcings are rarely, if ever, linear. Pulse emissions from volcanoes or feedback mechanisms, such as methane release in permafrost regions and ocean sediments, can and have disrupted the climate system over relatively short time scales (e.g. MacDonald (1990)). With respect to anthropogenic emissions of GHGs, in a palaeoclimate context at least, the increase in concentrations over the past one hundred years can be likened to an abrupt shift in the system's forcing. In developing the analogy to the climate system, it would be useful to extend analysis to consider rapid and nonlinear trends in the forcing parameters of the L84 and LS84 models. Experiments in the uncoupled L84 model could be performed to establish whether or not the increased memory of the IC location, evident in section 4.5.3 under a smooth linear change in the L84 model forcing, is increased further when subject to abrupt changes in the forcing. Additionally, introducing abrupt shifts in the parameter F in the LS84 model would be useful to investigate the effects of hysteresis in an almost intransitive system.

Further experiments could be conducted to incorporate feedback mechanisms, which are prevalent in the climate system. In the LS84 model, a positive feedback between T and F could be introduced so that as F decreases, the rate of change in T increases disproportionately. In section 5.5.2, it is shown that the convergence of IC ensembles is strongly controlled by the initial value of T under passive coupling; ensembles with similar initial values of T converge more quickly. If under a particular climate change scenario with a positive feedback, IC ensemble distributions from different locations on the original pseudo-attractor converge less rapidly, then the results would strengthen the case for running large IC ensembles conditioned on present IC uncertainty as the memory of the initial ensemble location becomes more important.

7.8.2 The imperfect model scenario

Understanding the role that model inadequacy has in capturing the statistics of climate is an essential component of the climate change prediction problem. The experiments presented have been conducted in the PMS but the issues considered could be further addressed in the imperfect model scenario (IMS). In section 3.9.3, discussion was directed towards the possible extension of the L63 model experiments to consider the IMS. Understanding how the climate distributions are affected under fixed, periodic and nonperiodic variations in ρ for various imperfect L63 models (using approximations to model variables/parameters) would reveal the extent to which model inadequacy limits the ability to capture the climate of the L63 system. As the L63 model demonstrates convergence in transitive regions of parameter space, it would be relatively straight-forward to compare the rate and extent of convergence for different imperfect L63 model climate distributions to the actual L63 climate distributions estimated in figure 3.5. Determining the time scales over which imperfect models continue to contain useful information about the

climate of the L63 model would provide an interesting analogy to the inadequate modelling of the climate system.

Similarly, the IMS could also be investigated in the L84 and LS84 models. Exploring the impact of model error on the climate distributions of the model variables could provide additional insight regarding the value of IC ensemble experiments in addition to single model realisations.

7.8.3 Extension to EMICs

Consideration could also be given to the role of IC uncertainty in the dynamic behaviour of Earth System Models of Intermediate Complexity (EMICs, Claussen et al. (2002)). The decreased level of complexity when compared to GCMs affords users the ability to run EMICs numerous times under different scenarios and model assumptions. In a comparison of eight EMICs, Petoukhov et al. (2005) conclude that "EMICs could be successfully employed as a useful and highly efficient, in terms of the running time, tool for the assessment of the long-term surface air temperature, precipitation and sea level changes, under a variety of future and past climate scenarios". For particular model variables of interest, the ergodic assumption could therefore be investigated with EMICs under a number of climate forcing scenarios utilising a large IC ensemble experimental design. In demonstrating the sensitivity of decisions to IC ensemble distributions as opposed to single model trajectory distributions, EMICs could provide a valuable platform to bridge the results from simple models explored here to inform the design of experiments in GCMs.

EMICs are not only used to explore scientific hypotheses but have also been adopted in studies to address societal decision-making. For example, the MAGICC climate model (Wigley and Raper (1992), Hulme et al. (1995)) has been used to study the impact of GHG emissions scenarios on the increase in global temperatures in relation to a number of policy-related questions (Calvin and Thomson (2010), Pielke (2009)). Working with the user community, EMIC IC ensemble experiments could be run to further understand how model uncertainty can best be communicated to guide adaptation policy.

7.8.4 Further engagement with index insurers

The index insurance case study developed in chapter six would benefit from direct collaboration with practitioners in the index insurance sector. There are two research aspects which could be further explored in collaboration with a specific index insurer. Firstly, the value of imperfect climate model output in guiding index insurance pricing decisions and strategic concerns could be investigated with direct input from practitioners using model output within existing decision frameworks. A pilot project in which climate model information was utilised to inform pricing strategy could be established to analyse the impact of such additional information on decisions and to learn how model output might be interpreted in an operational setting. Secondly, the value of the BN tool as a decision aid could be further analysed by working with a specific

insurer on a one or more focussed decision problems to highlight the practical benefits and limitations of the tool.

7.9 Conclusions

7.9.1 Addressing the thesis aims

In section 1.6, five key aims are listed in the form of research questions. In this section, the extent to which the thesis has been successful in answering each question is discussed in sequence.

What are the climate model information needs for strategic decision-making within the insurance industry and are the current generation of climate model experiments capable of providing such information?

Ten strategic issues that are likely to be impacted directly or indirectly by climate change are identified in section 6.2.3. The climate model information needs of insurers vary considerably across different business sectors. Decisions usually require estimates of return periods for damaging meteorological events such as tropical and convective storms. Probability exceedance curves are required for the appropriate pricing of insurance policies and in developing strategies to address changing degrees of exposure. Insurers typically rely on observational data despite acknowledging the limitations in the stationarity assumption. It is perceived that climate modellers ought to strive to provide information which can directly substitute for observational data to estimate current and future risk. Many insurers therefore support the efforts of climate modelling centres towards the provision of high spatial resolution climate model information. However, the findings presented in this thesis highlight some problems associated with generating high resolution model data in the absence of a thorough exploration of epistemic and aleatoric uncertainty. Furthermore, insurers have a genuine interest in incorporating the uncertainties in the estimates of exceedance probabilities and return periods into the decision-making process. The insurance industry exists to help individuals and businesses manage financial risk so insurers have both a responsibility and a vested interest in pricing contracts to accurately reflect the underlying uncertainties. This research suggests that large IC ensemble model experiments could improve both the quantification and reliability of climate model uncertainty estimates and remove reliance on the ergodic assumption.

It is clear from analysis of the literature and engagement with insurers that the relationship between climate modellers and the insurance industry is still in its infancy. Developing reliable climate model projections at the multiple temporal and spatial scales of interest for insurers places enormous demands on climate modelling centres to tailor model output and provide information which is both useful and usable by insurers. The increased level of formal engagement between insurers and climate modelling centres (at least in Europe) provides an opportunity to improve the accessibility and communication of model output. However, there is a real danger that in focussing on the provision of model output, climate modelling centres will over-simplify what is a hugely complex and uncertain prediction problem. Climate change projections will, for the foreseeable future, be subject to large uncertainties and communicating the uncertainty is as important, if not more important, than providing model output at a spatial and temporal scale of immediate use to insurers.

How should climate be defined to best address the needs of the climate change adaptation community?

There is no single definition of climate which is universal and can be considered useful for all applications. Both temporal and dynamical systems-based definitions have value in different contexts. However, in providing climate model information to decision makers concerned with robust adaptation to plausible future climate scenarios, the following definition is considered to be the most appropriate:

> Climate is the distribution of states consistent with the system's forcings, conditioned on the uncertainty in the initial state[7] of the system.

There are a number of reasons why this definition is appropriate for climate change adaptation. Firstly, the definition focusses on the possible states consistent with the climate system's forcings. In adapting to climate change it is important to know the range and distribution of states in order to enact robust solutions. By using a temporal definition, the assumption is that the forcing conditions are fixed, or linearly changing, over time which is an incorrect assumption given the known occurrence of nonlinear changes in climate forcings. Secondly, the definition is conditioned on IC uncertainty. Uncertainty in the initial state of the system is inevitable given observational uncertainties and the sparsity of observing networks in certain regions of the world. It is important to try and reduce IC uncertainty but in making adaptation decisions, decision makers need to ensure that policy responses consider the range of future model states consistent with the current level of uncertainty. Finally, the definition is compatible with nonlinear dynamical systems theory. Conceptually, climate variable probability distributions provide a measure of the system's climate for each individual system variable. These distributions can be thought of in relation to the attractor or pseudo-attractor of the climate system. This can aid the interpretation of climate under climate change as it is no longer necessary to consider time series data spanning two sets of forcing conditions.

Is the ergodic assumption valid for a climate system subject to altered forcings?

The use of the ergodic assumption in climate modelling has been challenged using numerical simulations of simple models analogous to the climate system. Three conditions under which the ergodic assumption has been shown to fail are listed below:

1. Hysteresis induced by nonlinear interactions in the presence of nonperiodic fluctuations in system forcings.
2. Coexistence of attractors (or pseudo-attractors) in which the evolution of a system trajectory is dependent on the initial state of the system.
3. Transient climate change where the attractor (or pseudo-attractor) changes nonlinearly in the presence of a trend in the forcings.

[7] where the initial state refers to the values of the system variables at time $t = 0$ in the model forecast simulation

Is the climate dependent on the pathway of the forcing?

The model results shown in chapters three to five come with the inevitable caveat that the models are highly idealised and cannot be directly related to the behaviour of the climate system. Nonetheless, each model exhibits nonlinear chaotic behaviour and displays many of the properties associated with the climate system. Experiments using the L63 model with nonperiodic fluctuations in ρ demonstrate the existence of hysteresis in the climate distributions. In response to time-varying parameters, trajectories evolve according to the changes in the underlying attractor. The IC ensemble distributions reveal the dependence of the model's climate to the pathway of the parameter. In addition, the L84 model distributions show evidence of hysteresis when subject to a seasonal cycle in F. In section 4.4.2, the model climate distributions when F returns to $F = 8$ at the maximum of the sinusoidal variation, are shown to be different to the model climate distributions when F is fixed at $F = 8$. The memory of previous model states affects the climate of the model.

The implication is that for a system as complex as the climate system, the response of the climate attractor/pseudo-attractor is unlikely to be decoupled to the pathway of the system forcings. Evidence of hysteresis in the climate is difficult to observe given only one trajectory of past climate so exploring hysteresis effects with climate models requires large IC ensembles experiments.

How should climate model experiments be designed to explore the full range of climate change uncertainties?

Predicting the range of climate states under transient climate change relies on the intelligent design of modelling experiments. It is argued here that large IC ensembles are required to provide such information from climate models. Whilst the use of large IC ensembles will not guarantee the capacity to provide decision relevant information to the user community, it is a necessary and important step in attempting to bridge the gap between climate model output and user needs.

In section 7.5, a number of steps are presented to guide the development of IC ensemble experiments using complex climate models. It is important to note that accounting for the memory of the initial state in the climate system using IC ensembles is only part of the climate change prediction problem and the uncertainties associated with physical parameterisations, model structural inadequacies and forcing scenario assumptions also require considerable attention. In order to advocate the use of climate models to inform robust decision making and to provide useful quantitative support to the insurance industry, a significant component of computational effort should be devoted to running ensembles with multiple models, multiple model versions (PPEs), many ICs and a number of forcing scenarios. Moreover, it is important that experiments explore uncertainty at the time scales of interest to decision makers. Given the value of uncertainty information to insurance decisions, the spatial scale with which models are run should be largely driven by the ability to explore uncertainty. Without an adequate exploration of uncertainty, high resolution model information is unfit for guiding decisions within

the insurance industry and the adaptation community.

7.9.2 Final remarks

In the climate modelling community and the insurance industry, the use of the ergodic assumption is not justified in a changing climate. Relying on single model simulations to assess climate under climate change is therefore misguided and IC ensembles are required to detail the evolution of climate variable distributions over time. Without varying ICs it is not possible to reliably estimate the entire distribution of climate at times of interest within a model simulation. In developing model experiments to inform the user community, it is therefore vital to provide an honest appraisal of how uncertainty has been incorporated in the experimental design.

Uncertainty is the real driver of decisions regarding climate change adaptation, particularly within the insurance industry, and it is important to acknowledge this reality. Given the desire of the insurance sector for increasingly detailed knowledge of climate change impacts to guide decisions, climate modellers need to be wary of providing projections which are highly conditional on implicit assumptions. Addressing all sources of climate uncertainty thoroughly is vital if model projections are to be used wisely in quantitative climate impacts assessments. Acknowledging potential nonlinear interactions between the different sources of uncertainty is critical in improving the relevance of climate model experiments for guiding adaptation decisions. In order for the adaptation community to make sensible decisions in the face of climate change, the climate modelling community needs to provide ensemble-based model projections which are consistent with the definition of climate as a distribution of states conditioned on IC uncertainty. Useful climate predictions do not depend simply on having the most comprehensive and accurate available models of the climate system. Rather, useful climate predictions will incorporate an ensemble design that accounts for the diverse range of climate change uncertainties.

Appendices

Appendix A: L63 Results

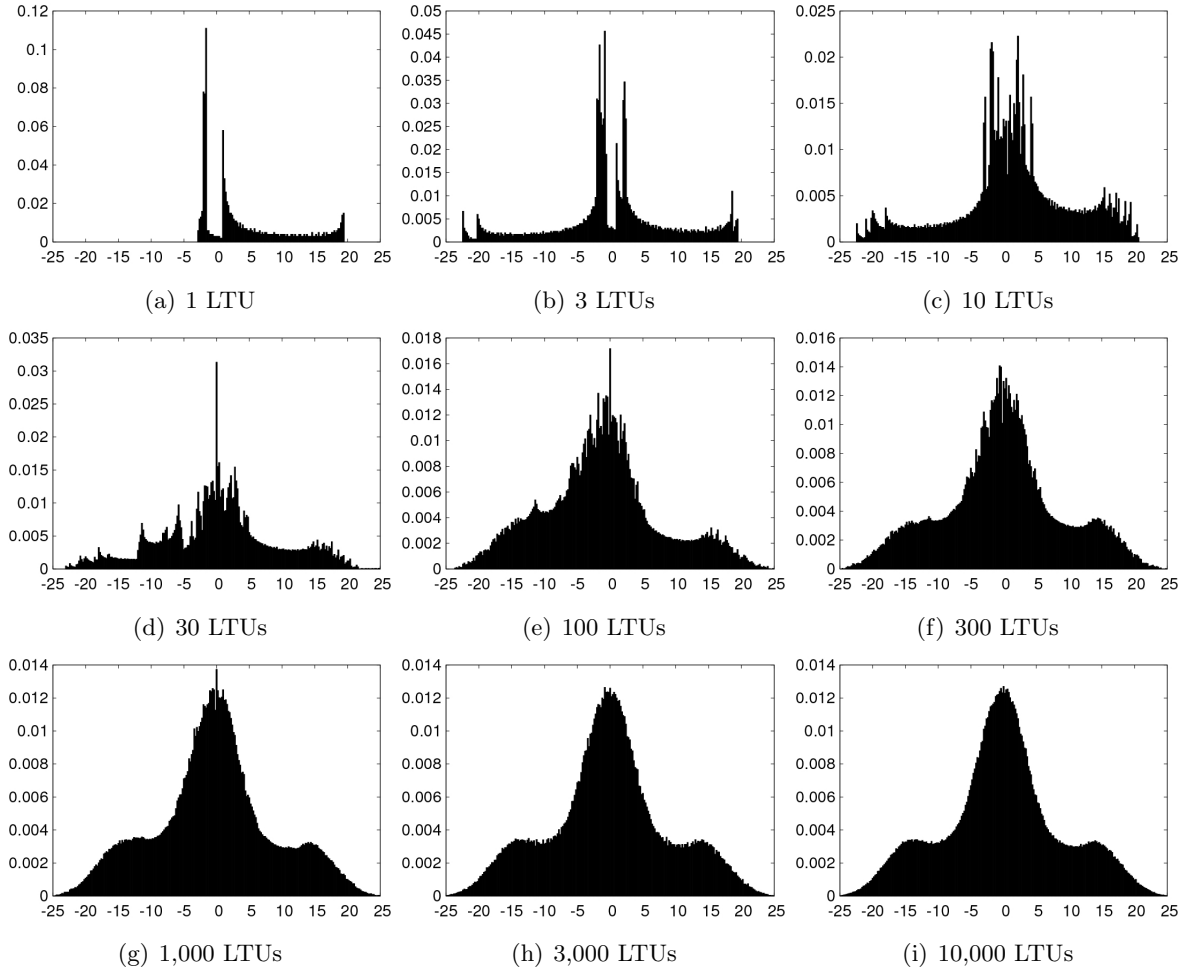

(a) 1 LTU (b) 3 LTUs (c) 10 LTUs

(d) 30 LTUs (e) 100 LTUs (f) 300 LTUs

(g) 1,000 LTUs (h) 3,000 LTUs (i) 10,000 LTUs

Figure A-1: Normalised frequency distributions of the Y variable from a single trajectory of the L63 model with ICs $(X, Y, Z) = (1.0, 1.0, 25.0)$, over increasing time periods. In each plot, the x-axis corresponds to the Y variable and the y-axis corresponds to the frequency per occupuied bin; bin width = 0.2.

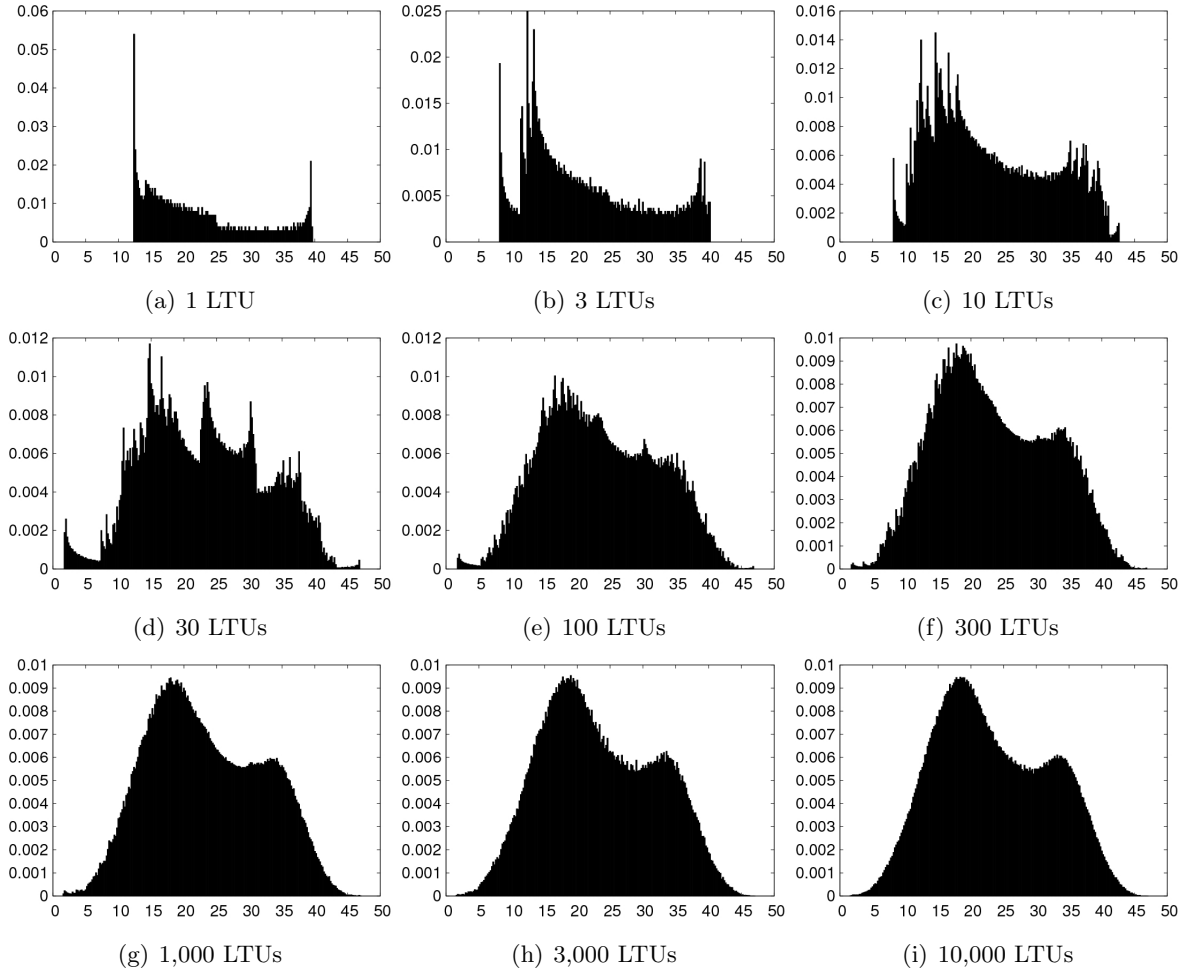

(a) 1 LTU (b) 3 LTUs (c) 10 LTUs

(d) 30 LTUs (e) 100 LTUs (f) 300 LTUs

(g) 1,000 LTUs (h) 3,000 LTUs (i) 10,000 LTUs

Figure A-2: Normalised frequency distributions of the Z variable from a single trajectory of the L63 model with ICs $(X, Y, Z) = (1.0, 1.0, 25.0)$, over increasing time periods. In each plot, the x-axis corresponds to the Z variable and the y-axis corresponds to the frequency per occupuied bin; bin width = 0.2.

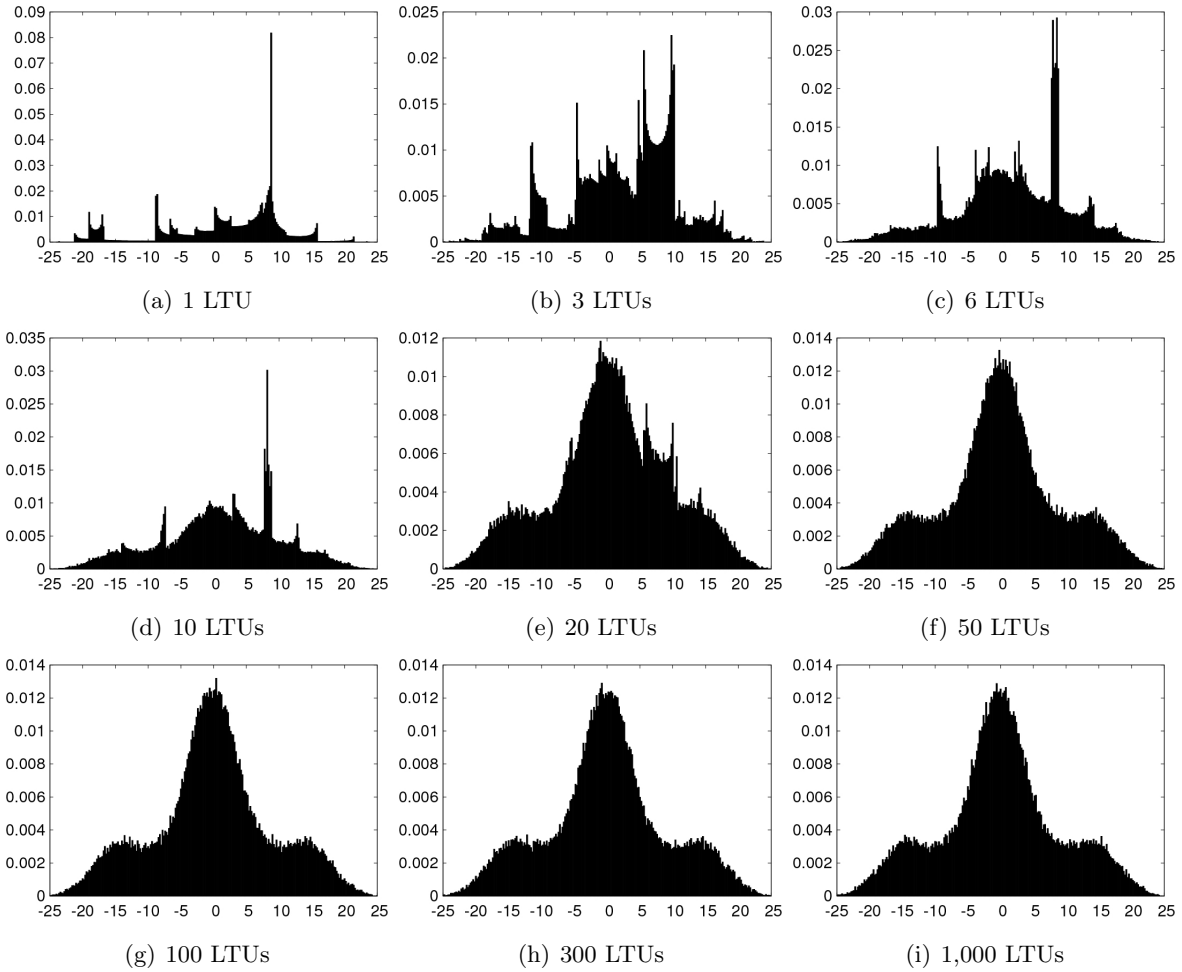

(a) 1 LTU (b) 3 LTUs (c) 6 LTUs

(d) 10 LTUs (e) 20 LTUs (f) 50 LTUs

(g) 100 LTUs (h) 300 LTUs (i) 1,000 LTUs

Figure A-3: Normalised frequency distributions of the Y variable for the L63 model, from a 100,000 member IC ensemble with ICs spread evenly along a transect from $(X_l, Y_l, Z_l) = (-20, -25, 1)$ to $(X_h, Y_h, Z_h) = (20, 25, 40.0)$. The distributions show the states of each ensemble member at the given time instant in the simulation period. In each plot, the x-axis corresponds to the Y variable and the y-axis corresponds to the frequency of ensemble members per occupuied bin; bin width = 0.2.

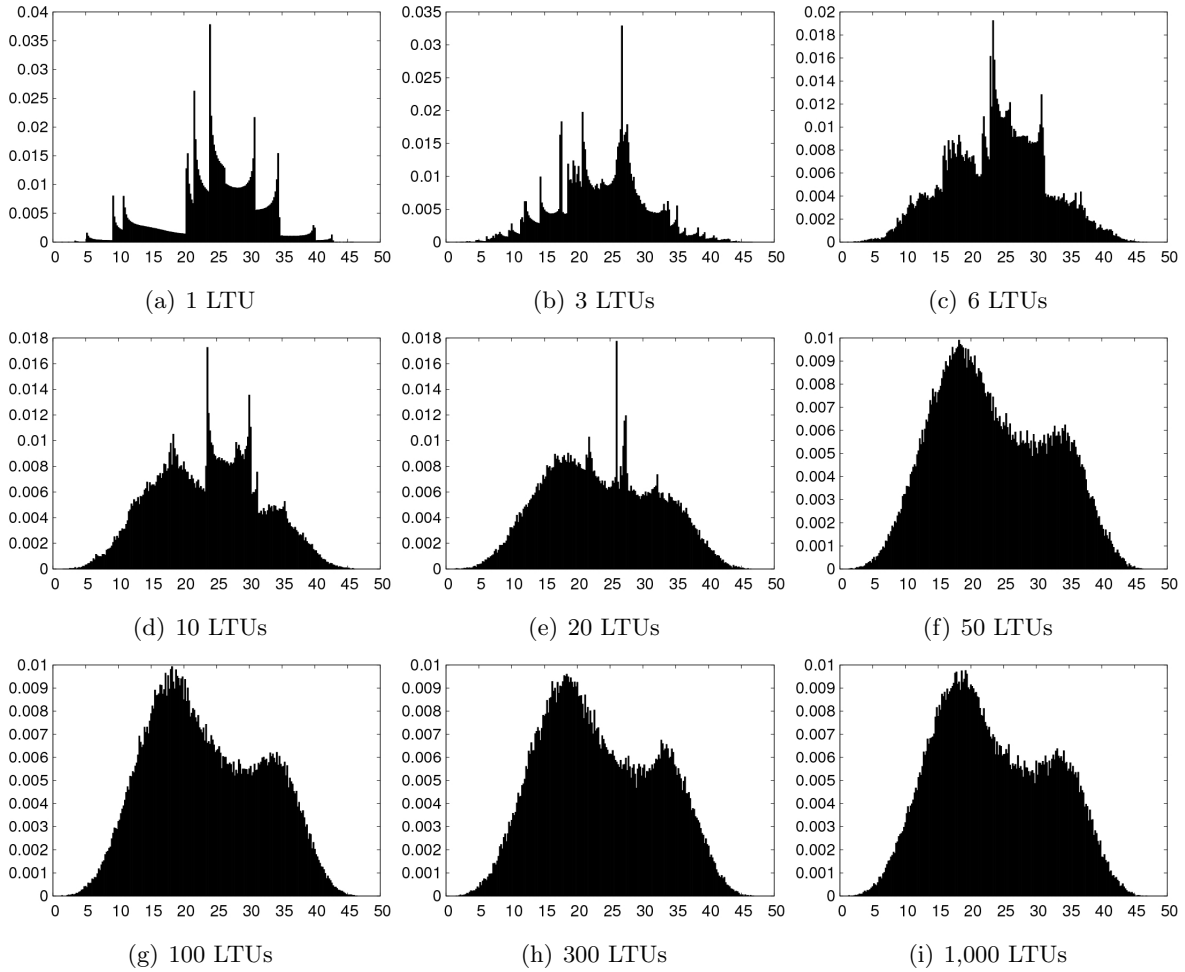

(a) 1 LTU (b) 3 LTUs (c) 6 LTUs

(d) 10 LTUs (e) 20 LTUs (f) 50 LTUs

(g) 100 LTUs (h) 300 LTUs (i) 1,000 LTUs

Figure A-4: Normalised frequency distributions of the Z variable for the L63 model, from a 100,000 member IC ensemble with ICs spread evenly along a transect from $(X_l, Y_l, Z_l) = (-20, -25, 1)$ to $(X_h, Y_h, Z_h) = (20, 25, 40.0)$. The distributions show the states of each ensemble member at the given time instant in the simulation period. In each plot, the x-axis corresponds to the Z variable and the y-axis corresponds to the frequency of ensemble members per occupuied bin; bin width = 0.2.

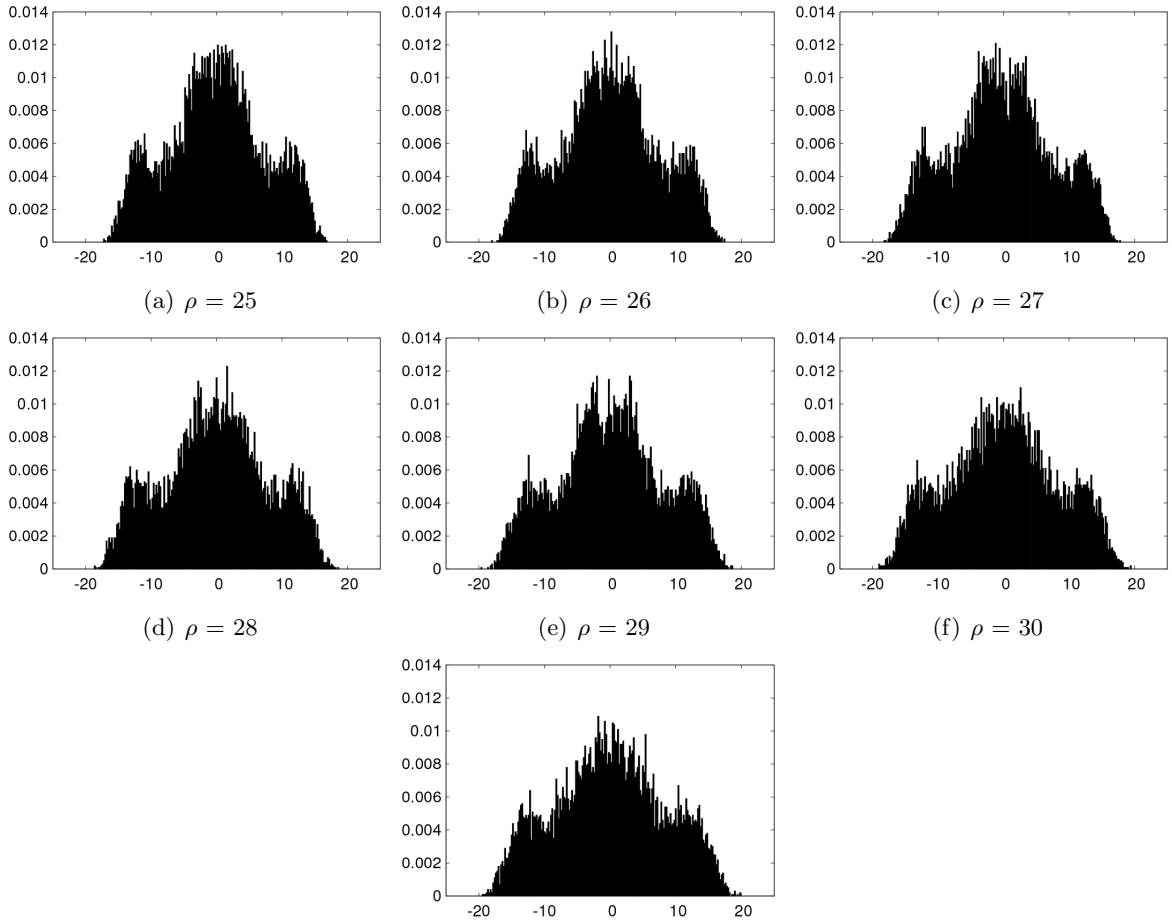

(a) $\rho = 25$ (b) $\rho = 26$ (c) $\rho = 27$

(d) $\rho = 28$ (e) $\rho = 29$ (f) $\rho = 30$

(g) $\rho = 31$

Figure A-5: Normalised frequency distributions for a 10,000 member IC ensemble after 100 LTUs for different values of ρ for the X variable. The IC ensembles were initiated with ICs taken from the first 10,000 members of the equilbirium climate distributions for $\rho = 28$, shown in figure 3.5. In each plot, the x-axis corresponds to the X variable and the y-axis corresponds to the frequency of ensemble members per occupuied bin; bin width = 0.2.

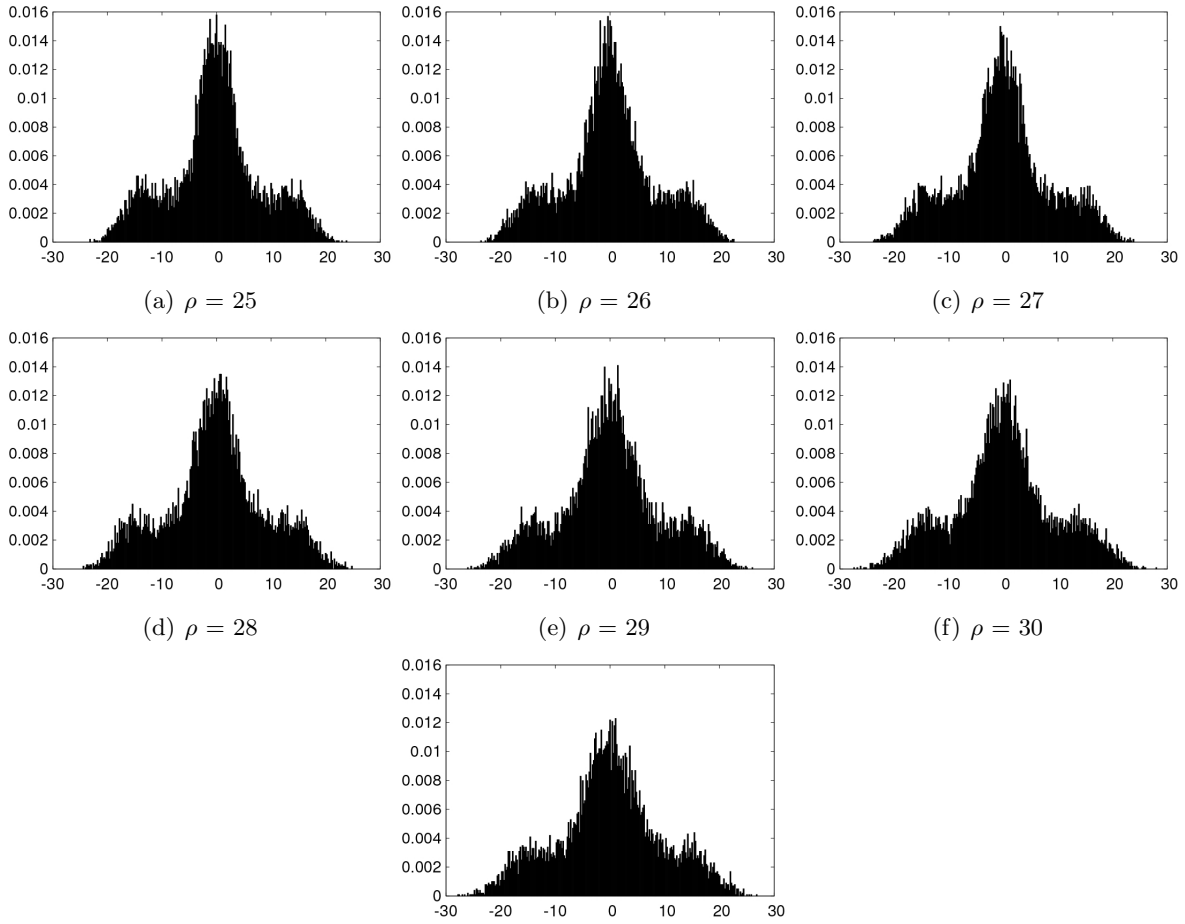

(a) $\rho = 25$ (b) $\rho = 26$ (c) $\rho = 27$

(d) $\rho = 28$ (e) $\rho = 29$ (f) $\rho = 30$

(g) $\rho = 31$

Figure A-6: Normalised frequency distributions for a 10,000 member IC ensemble after 100 LTUs for different values of ρ for the Y variable. The IC ensembles were initiated with ICs taken from the first 10,000 members of the equilbirium climate distributions for $\rho = 28$, shown in figure 3.5. In each plot, the x-axis corresponds to the Y variable and the y-axis corresponds to the frequency of ensemble members per occupuied bin; bin width = 0.2.

Appendix B: L84 Results

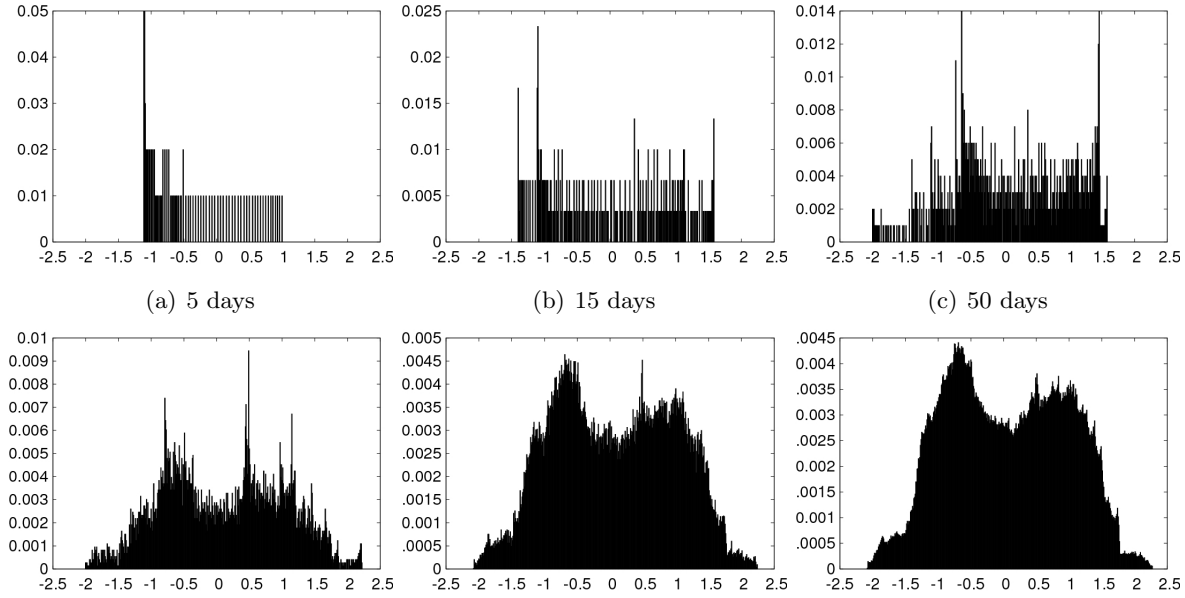

(a) 5 days (b) 15 days (c) 50 days

(d) 1 year (e) 10 years (f) 100 years

Figure B-1: Normalised frequency distributions for the Y variable of a single trajectory in the L84 model when $F = 8$ after given simulation periods, with ICs: $(X, Y, Z) = (1.0, 1.0, 1.0)$. In each plot, the x-axis denotes the Y variable and the y-axis corresponds to the frequency per occupied bin; bin width = 0.01.

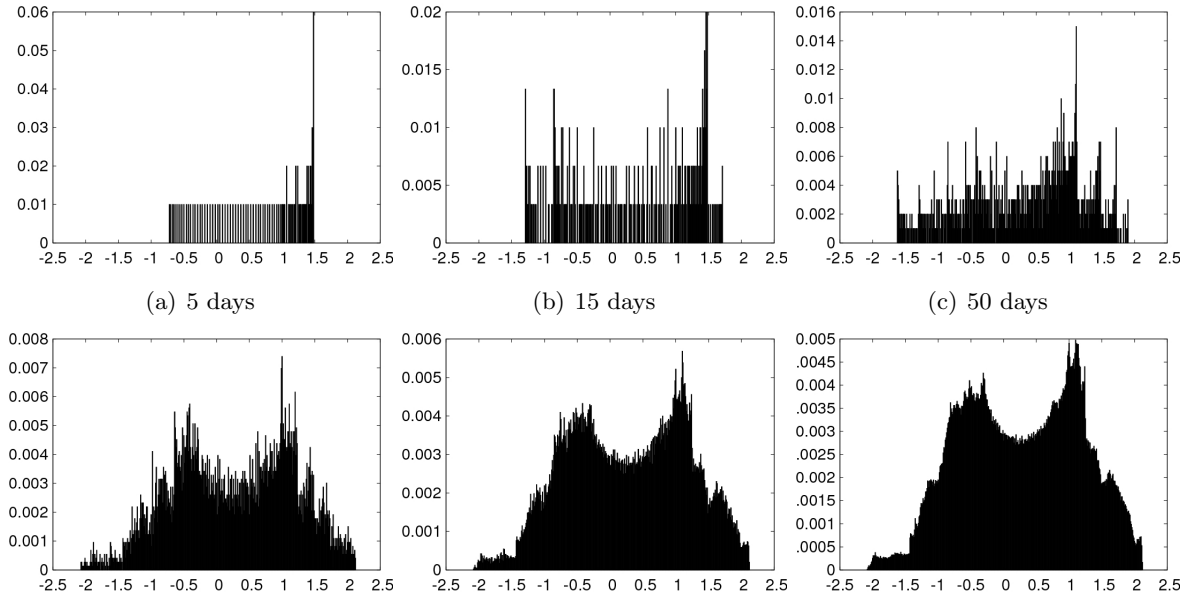

(a) 5 days (b) 15 days (c) 50 days

(d) 1 year (e) 10 years (f) 100 years

Figure B-2: Normalised frequency distributions for the Z variable of a single trajectory in the L84 model when $F = 8$ after given simulation periods, with ICs: $(X, Y, Z) = (1.0, 1.0, 1.0)$. In each plot, the x-axis denotes the Z variable and the y-axis corresponds to the frequency per occupied bin; bin width = 0.01.

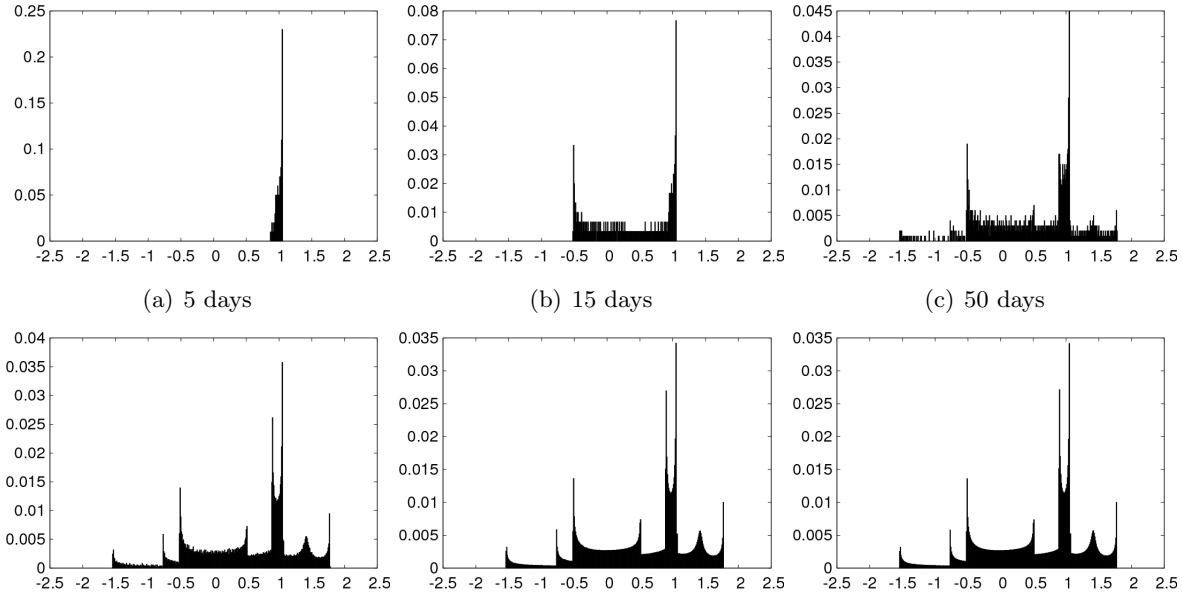

(a) 5 days (b) 15 days (c) 50 days

(d) 1 year (e) 10 years (f) 100 years

Figure B-3: Normalised frequency distributions for the Y variable of a single trajectory in the L84 model when $F = 6$ after given simulation periods, with ICs: $(X, Y, Z) = (0.12, 0.95, -0.26)$. In each plot, the x-axis denotes the Y variable and the y-axis corresponds to the frequency per occupied bin; bin width $= 0.01$.

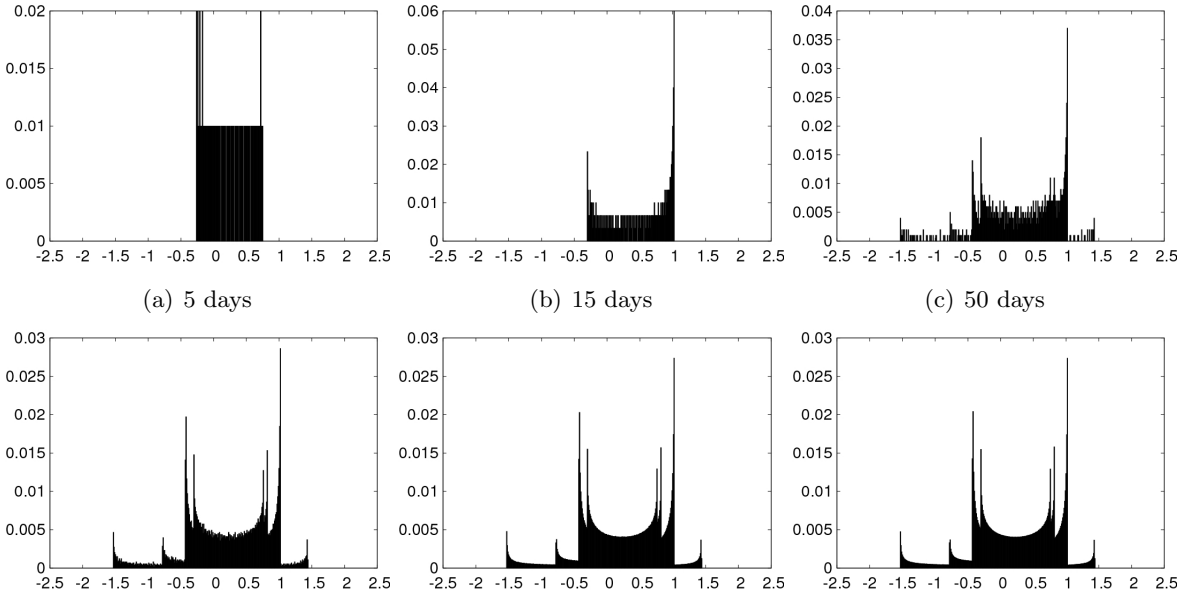

(a) 5 days (b) 15 days (c) 50 days

(d) 1 year (e) 10 years (f) 100 years

Figure B-4: Normalised frequency distributions for the Z variable of a single trajectory in the L84 model when $F = 6$ after given simulation periods, with ICs: $(X, Y, Z) = (0.12, 0.95, -0.26)$. In each plot, the x-axis denotes the Z variable and the y-axis corresponds to the frequency per occupied bin; bin width $= 0.01$.

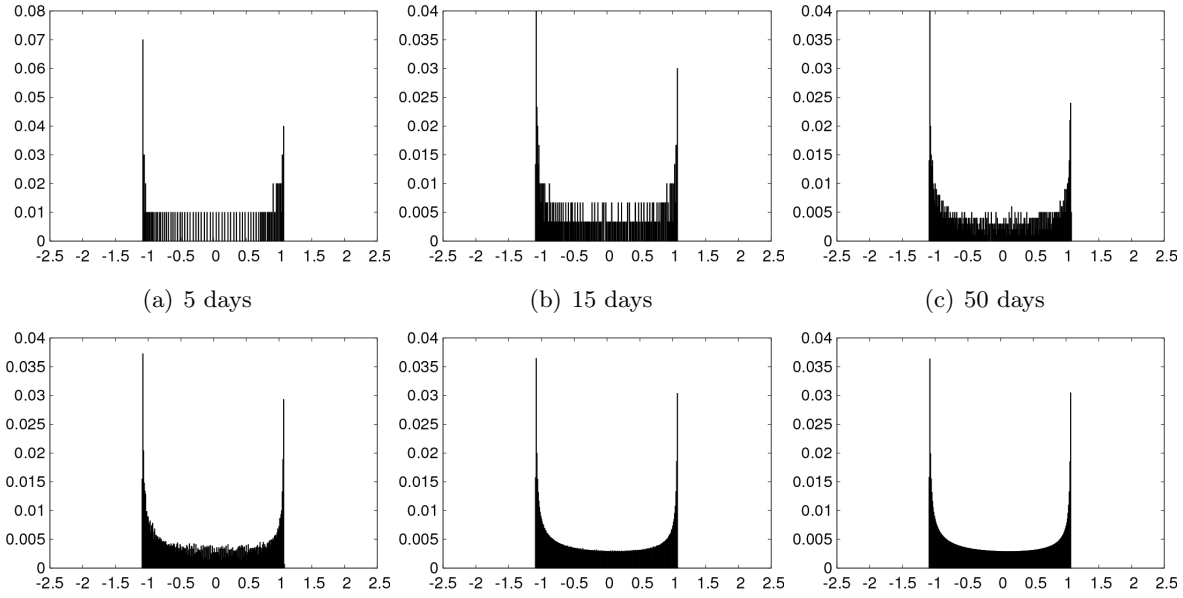

(a) 5 days (b) 15 days (c) 50 days

(d) 1 year (e) 10 years (f) 100 years

Figure B-5: Normalised frequency distributions for the Y variable of a single trajectory in the L84 model when $F = 6$ after given simulation periods, with ICs: $(X, Y, Z) = (0.93, -1.04, 0.58)$. In each plot, the x-axis denotes the Y variable and the y-axis corresponds to the frequency per occupied bin; bin width $= 0.01$.

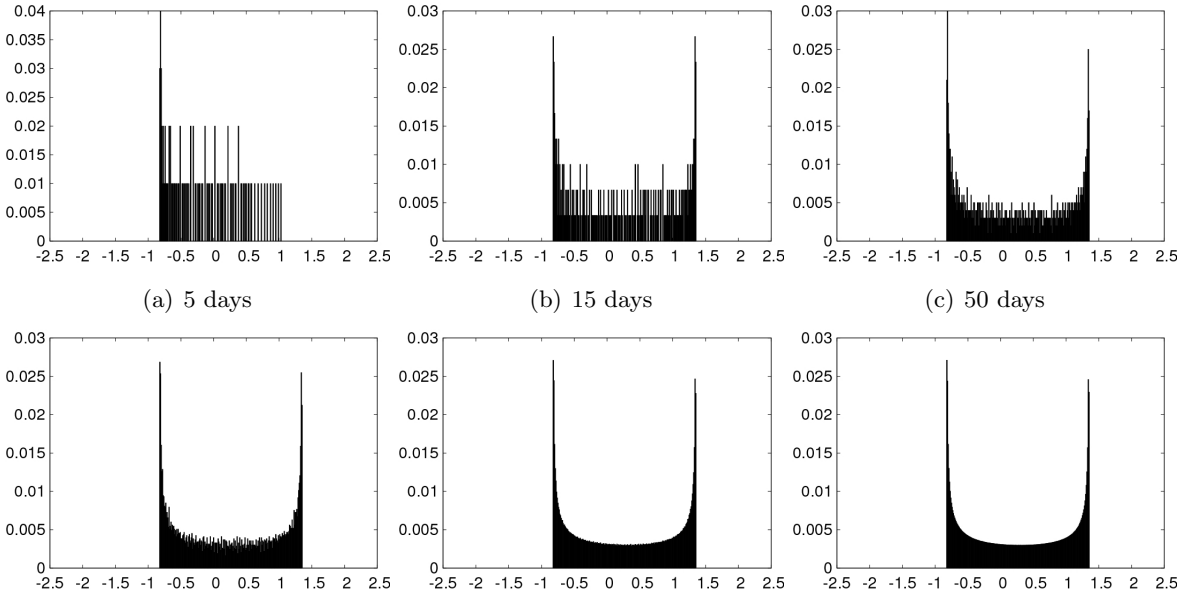

(a) 5 days (b) 15 days (c) 50 days

(d) 1 year (e) 10 years (f) 100 years

Figure B-6: Normalised frequency distributions for the Z variable of a single trajectory in the L84 model when $F = 6$ after given simulation periods, with ICs: $(X, Y, Z) = (0.93, -1.04, 0.58)$. In each plot, the x-axis denotes the Z variable and the y-axis corresponds to the frequency per occupied bin; bin width $= 0.01$.

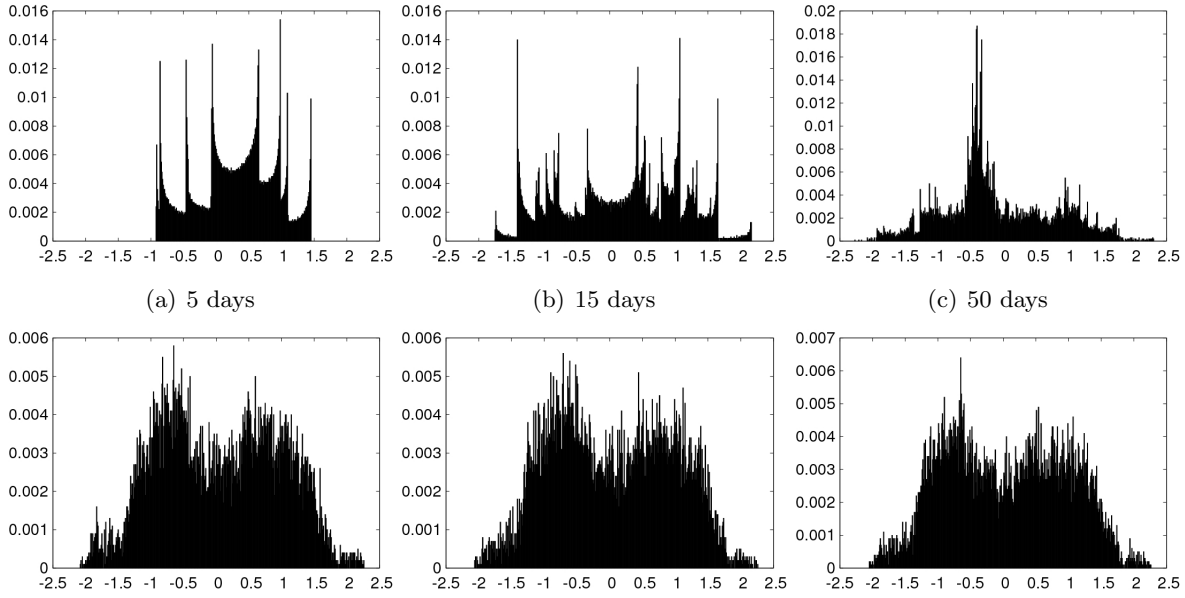

(a) 5 days (b) 15 days (c) 50 days

(d) 1 year (e) 10 years (f) 100 years

Figure B-7: Normalised frequency distributions for a 10,000 member IC ensemble of the L84 model when $F = 8$ after given simulation periods with ICs spread along a transect from $(-1, -2.5, -2.5)$ to $(2.5, 2.5, 2.5)$. In each plot, the x-axis denotes the Y variable and the y-axis corresponds to the frequency per occupied bin; bin width = 0.01.

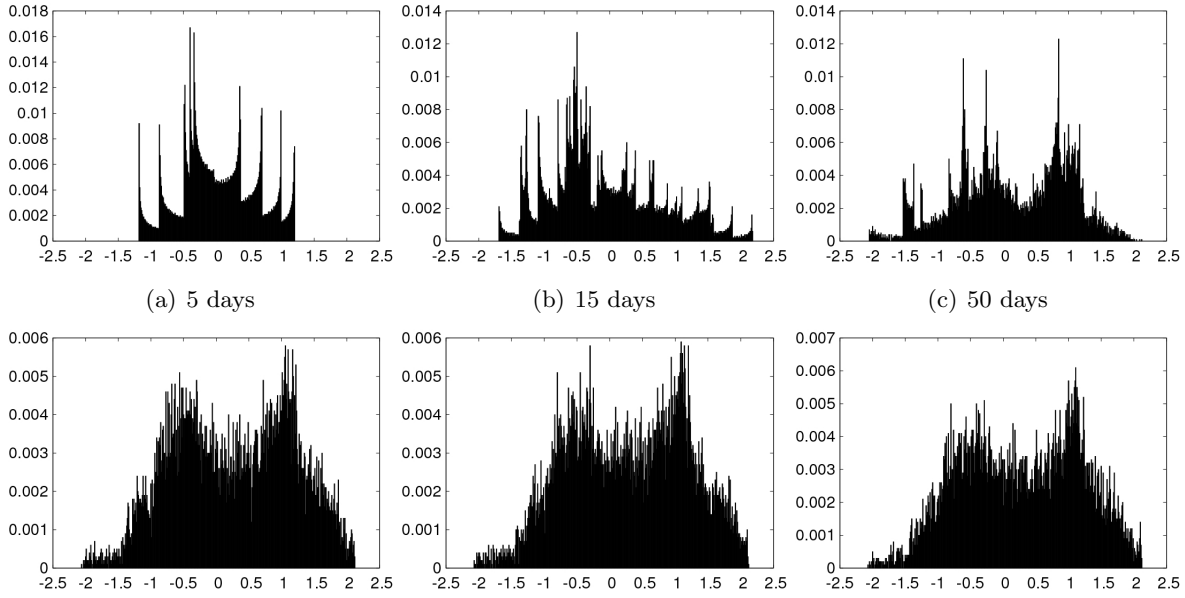

(a) 5 days (b) 15 days (c) 50 days

(d) 1 year (e) 10 years (f) 100 years

Figure B-8: Normalised frequency distributions for a 10,000 member IC ensemble of the L84 model when $F = 8$ after given simulation periods with ICs spread along a transect from $(-1, -2.5, -2.5)$ to $(2.5, 2.5, 2.5)$. In each plot, the x-axis denotes the Z variable and the y-axis corresponds to the frequency per occupied bin; bin width = 0.01.

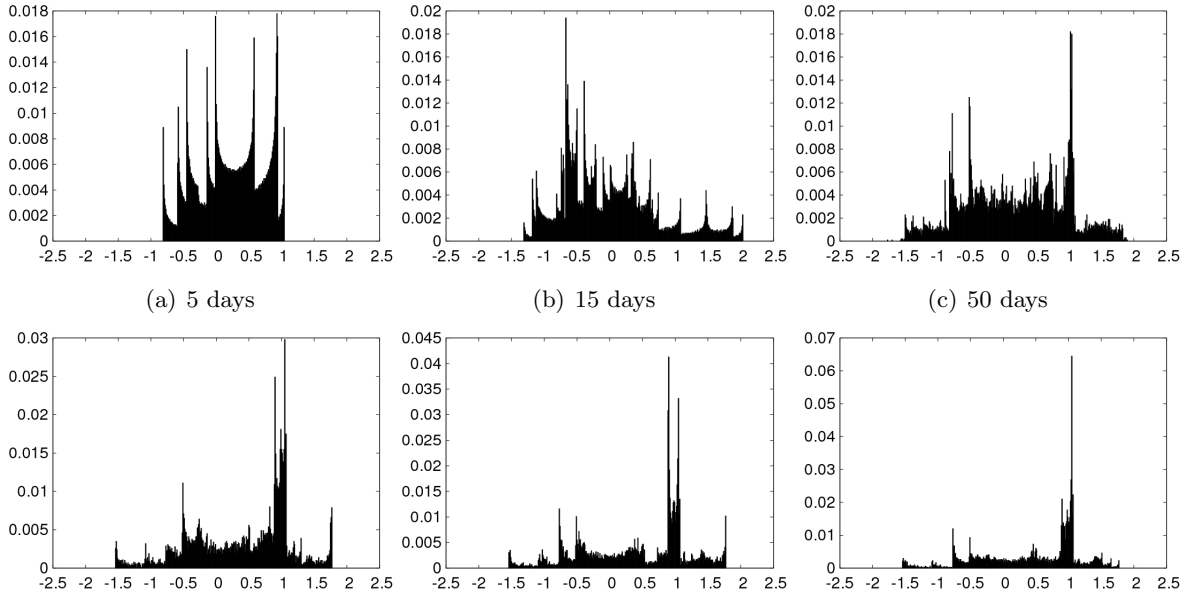

(a) 5 days (b) 15 days (c) 50 days

(d) 1 year (e) 10 years (f) 100 years

Figure B-9: Normalised frequency distributions for a 10,000 member IC ensemble of the L84 model when $F = 6$ after given simulation periods with ICs spread along a transect from $(-1, -2.5, -2.5)$ to $(2.5, 2.5, 2.5)$. In each plot, the x-axis denotes the Y variable and the y-axis corresponds to the frequency per occupied bin; bin width = 0.01.

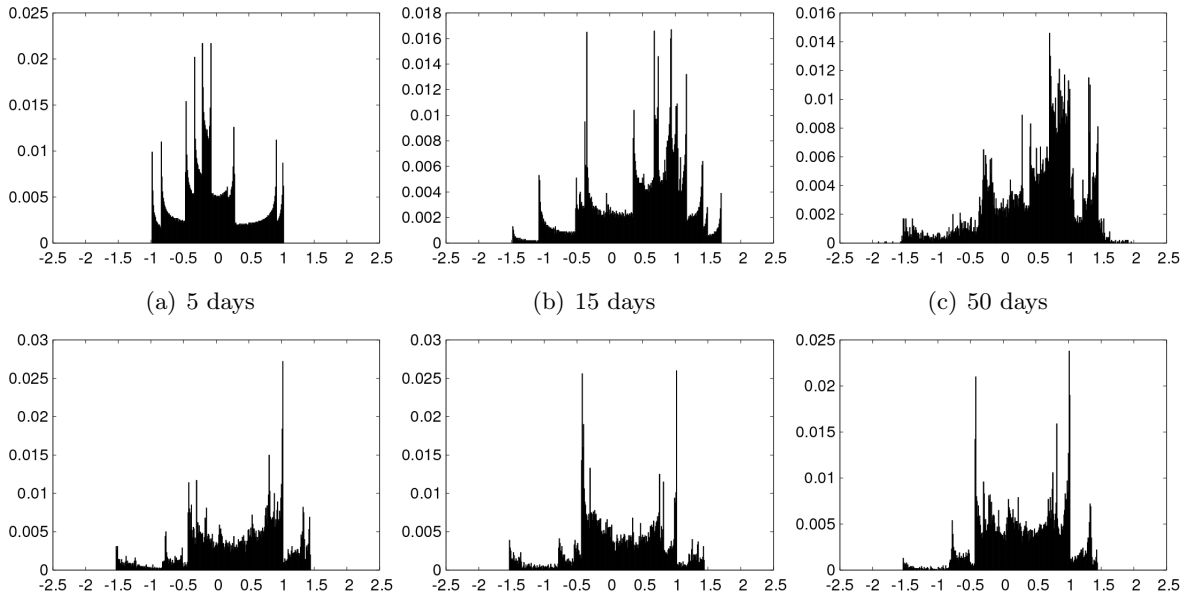

(a) 5 days (b) 15 days (c) 50 days

(d) 1 year (e) 10 years (f) 100 years

Figure B-10: Normalised frequency distributions for a 10,000 member IC ensemble of the L84 model when $F = 6$ after given simulation periods with ICs spread along a transect from $(-1, -2.5, -2.5)$ to $(2.5, 2.5, 2.5)$. In each plot, the x-axis denotes the Z variable and the y-axis corresponds to the frequency per occupied bin; bin width = 0.01.

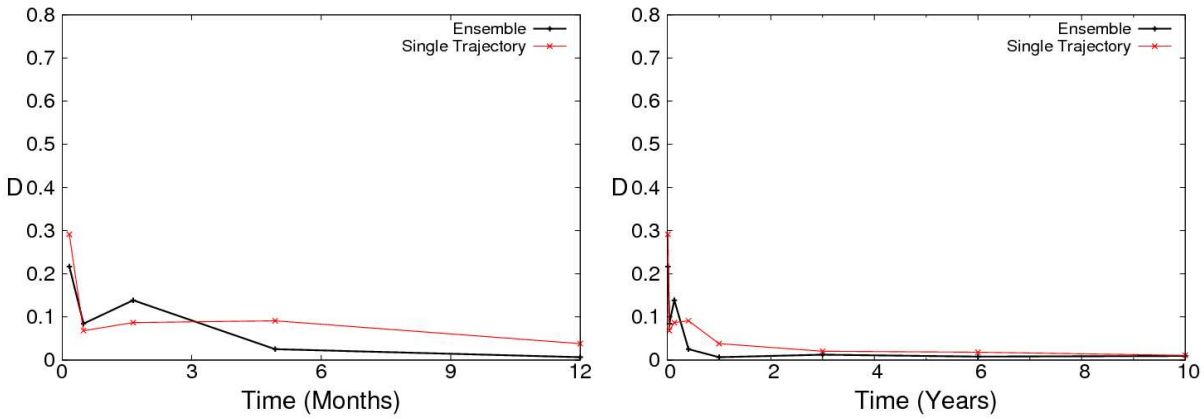

(a) 1 year (b) 10 years

Figure B-11: KS comparisons for the Y variable in the L84 model with $F = 8$ between the 100,000 member IC ensemble distributions shown in figure 4.15 and: (i) the 10,000 member IC ensemble distributions shown in figure B-7; and (ii) the single trajectory distributions shown in figure B-1.

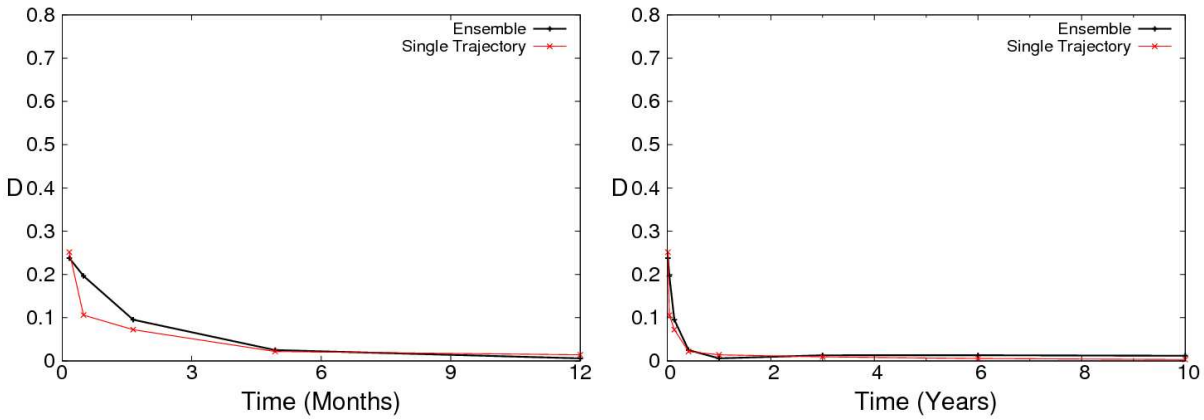

(a) 1 year (b) 10 years

Figure B-12: KS comparisons for the Z variable in the L84 model with $F = 8$ between the 100,000 member IC ensemble distributions shown in figure 4.15 and: (i) the 10,000 member IC ensemble distributions shown in figure B-8; and (ii) the single trajectory distributions shown in figure B-2.

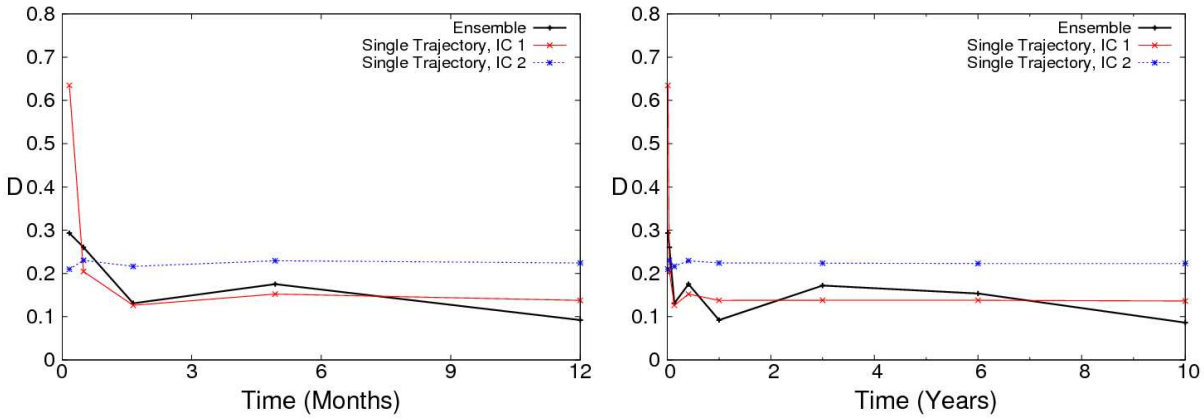

(a) 1 year (b) 10 years

Figure B-13: KS comparisons for the Y variable in the L84 model with $F = 6$ between the 100,000 member IC ensemble distributions shown in figure 4.15 and: (i) the 10,000 member IC ensemble distributions shown in figure B-9; (ii) the single trajectory distributions shown in figure B-3 from $IC1$ (associated with attractor $A1$); and (iii) the single trajectory distributions shown in figure B-5 from $IC2$ (associated with attractor $A2$).

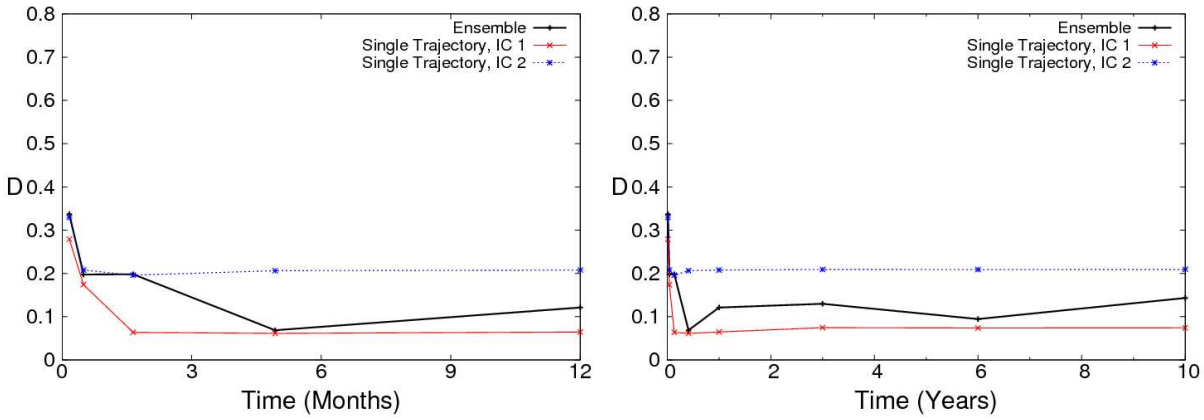

(a) 1 year (b) 10 years

Figure B-14: KS comparisons for the Z variable in the L84 model with $F = 6$ between the 100,000 member IC ensemble distributions shown in figure 4.15 and: (i) the 10,000 member IC ensemble distributions shown in figure B-10; (ii) the single trajectory distributions shown in figure B-4 from $IC1$ (associated with attractor $A1$); and (iii) the single trajectory distributions shown in figure B-6 from $IC2$ (associated with attractor $A2$).

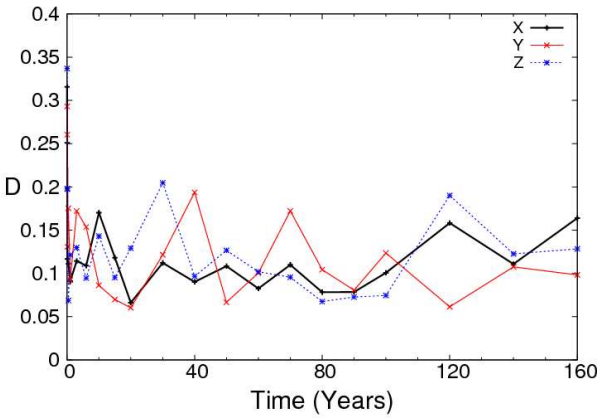

Figure B-15: KS comparisons for all variables in the L84 model with $F = 6$ between the 100,000 member IC ensemble distributions shown in figure 4.15 and the 10,000 member IC ensemble distributions shown in figure 4.11 over a simulation period of 160 years.

Appendix C: LS84 Results

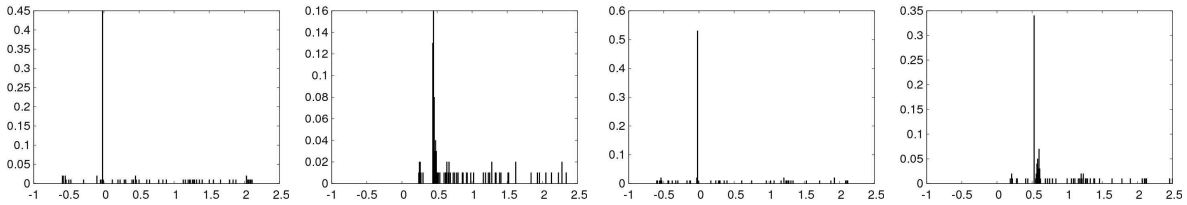

(a) 100 yrs, Active, Su (b) 100 yrs, Active, W (c) 100 yrs, Passive, Su (d) 100 yrs, Passive, W

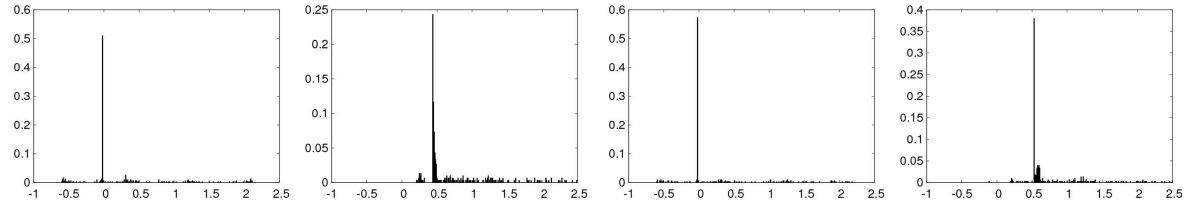

(e) 300 yrs, Active, Su (f) 300 yrs, Active, W (g) 300 yrs, Passive, Su (h) 300 yrs, Passive, W

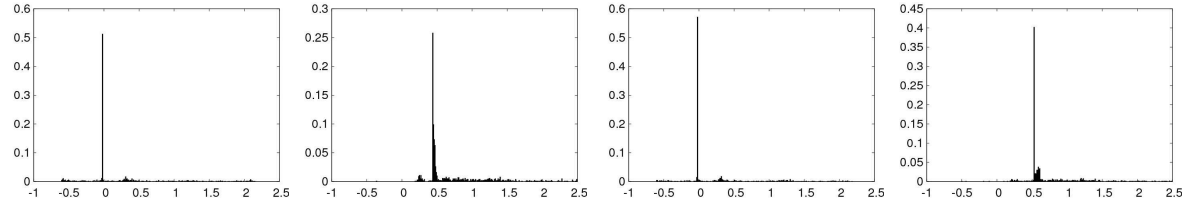

(i) 1,000 yrs, Active, Su (j) 1,000 yrs, Active, W (k) 1,000 yrs, Passive, Su (l) 1,000 yrs, Passive, W

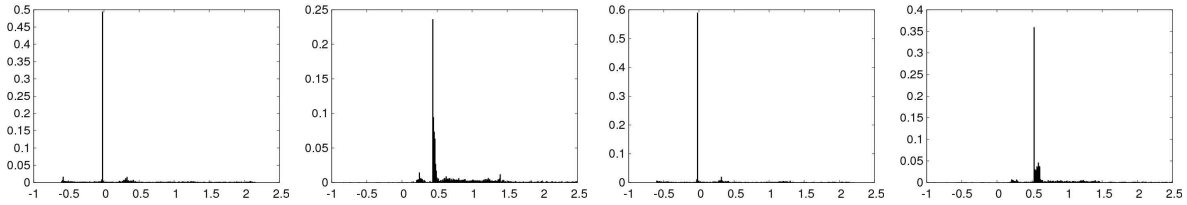

(m) 3,000 yrs, Active, Su (n) 3,000 yrs, Active, W (o) 3,000 yrs, Passive, Su (p) 3,000 yrs, Passive, W

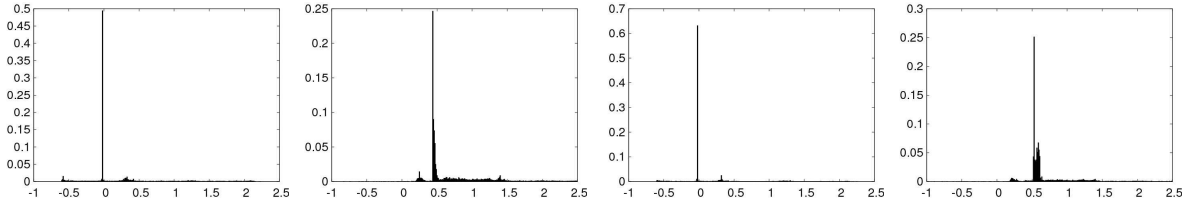

(q) 10,000 yrs, Active, Su (r) 10,000 yrs, Active, W (s) 10,000 yrs, Passive, Su (t) 10,000 yrs, Passive, W

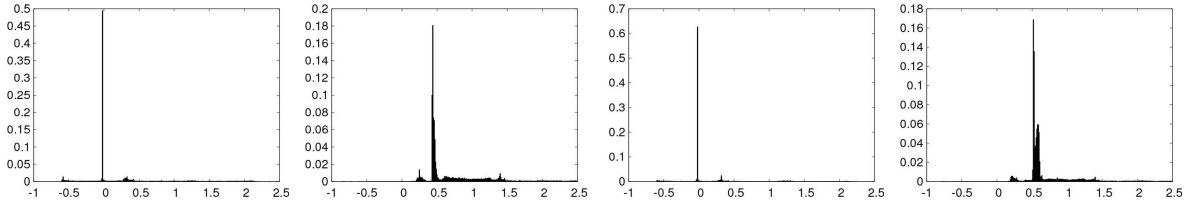

(u) 30,000 yrs, Active, Su (v) 30,000 yrs, Active, W (w) 30,000 yrs, Passive, Su (x) 30,000 yrs, Passive, W

Figure C-1: Normalised frequency distributions for a single trajectory of the LS84 model variable X over increasing time periods. The method of coupling is given as active or passive and the respective ICs are given in table 5.7. *Su* denotes mid-summer and W denotes mid-winter. In each plot, the x-axis corresponds to the atmosphere variable X and the y-axis corresponds to the frequency per occupuied bin; bin width = 0.01.

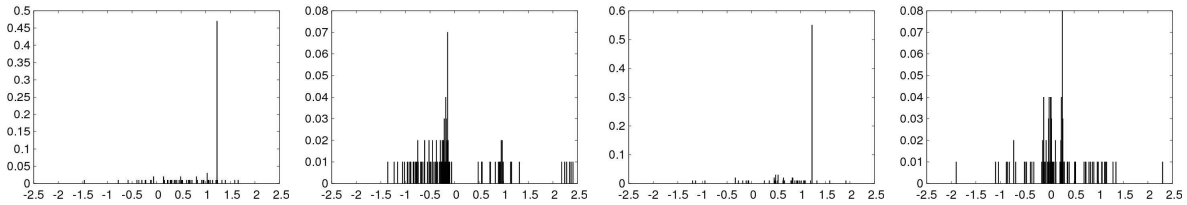

(a) 100 yrs, Active, Su (b) 100 yrs, Active, W (c) 100 yrs, Passive, Su (d) 100 yrs, Passive, W

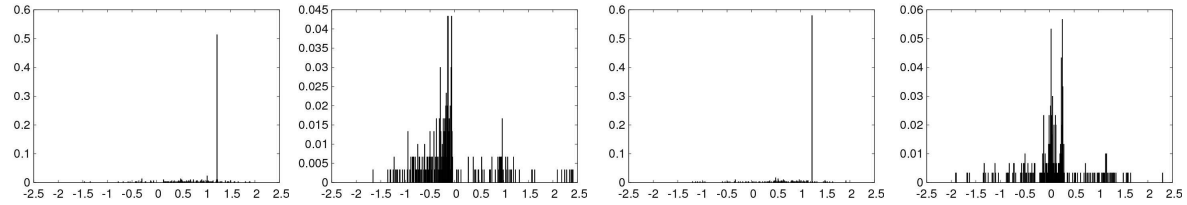

(e) 300 yrs, Active, Su (f) 300 yrs, Active, W (g) 300 yrs, Passive, Su (h) 300 yrs, Passive, W

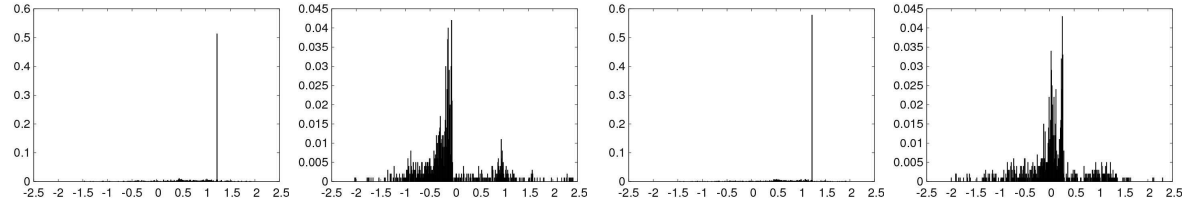

(i) 1,000 yrs, Active, Su (j) 1,000 yrs, Active, W (k) 1,000 yrs, Passive, Su (l) 1,000 yrs, Passive, W

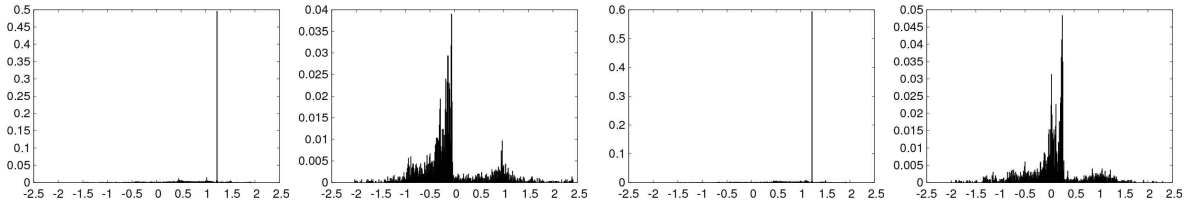

(m) 3,000 yrs, Active, Su (n) 3,000 yrs, Active, W (o) 3,000 yrs, Passive, Su (p) 3,000 yrs, Passive, W

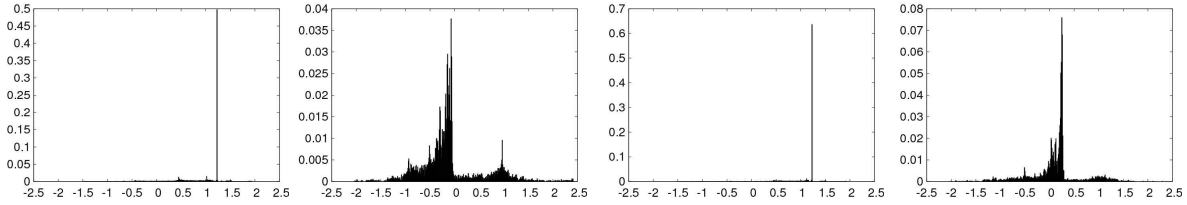

(q) 10,000 yrs, Active, Su (r) 10,000 yrs, Active, W (s) 10,000 yrs, Passive, Su (t) 10,000 yrs, Passive, W

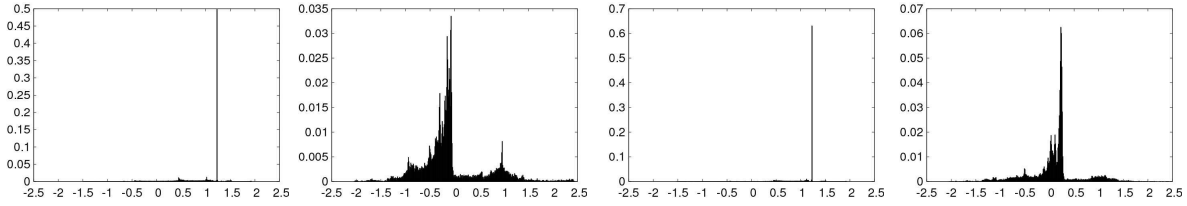

(u) 30,000 yrs, Active, Su (v) 30,000 yrs, Active, W (w) 30,000 yrs, Passive, Su (x) 30,000 yrs, Passive, W

frequency distributions for a single trajectory of the LS84 model variable Y over increasing time periods]Normalised frequency distributions for a single trajectory of the LS84 model variable Y over increasing time periods. The method of coupling is given as active or passive and the respective ICs are given in table 5.7. *Su* denotes mid-summer and *W* denotes mid-winter. In each plot, the x-axis corresponds to the atmosphere variable Y and the y-axis corresponds to the frequency per occupuied bin; bin width = 0.01.

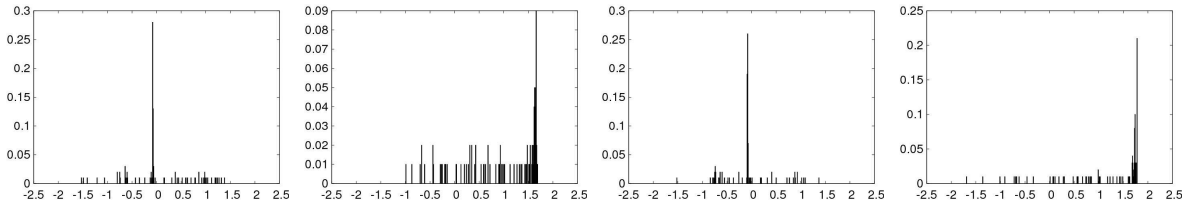

(y) 100 yrs, Active, Su (z) 100 yrs, Active, W () 100 yrs, Passive, Su () 100 yrs, Passive, W

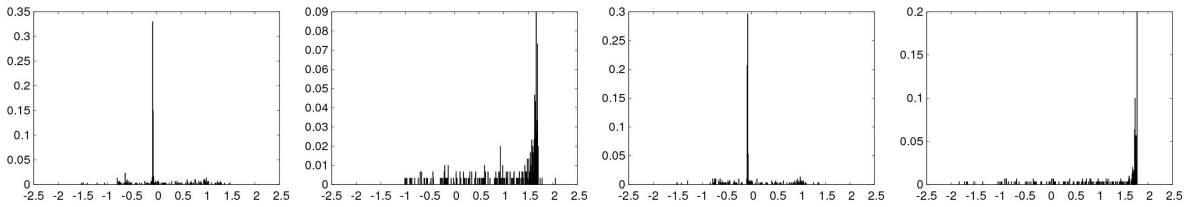

() 300 yrs, Active, Su () 300 yrs, Active, W () 300 yrs, Passive, Su () 300 yrs, Passive, W

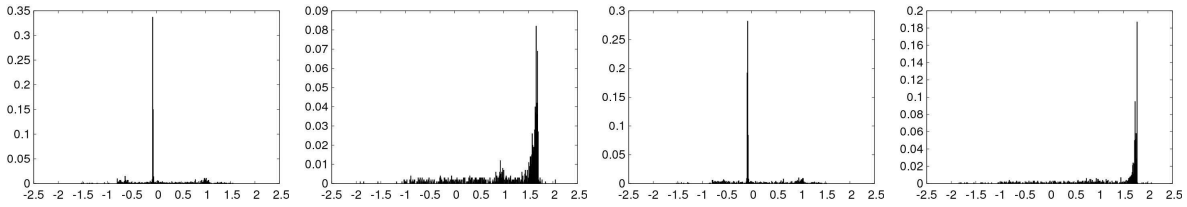

() 1,000 yrs, Active, Su () 1,000 yrs, Active, W () 1,000 yrs, Passive, Su () 1,000 yrs, Passive, W

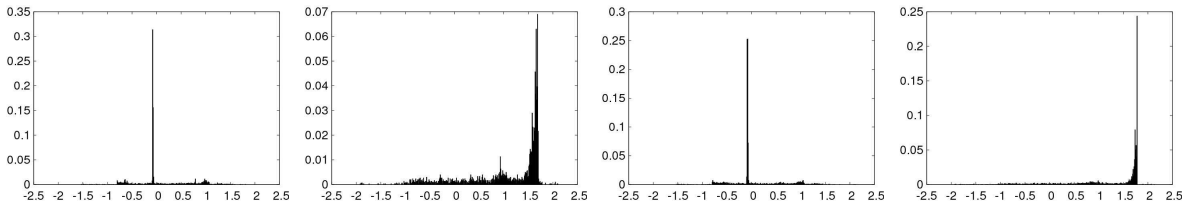

() 3,000 yrs, Active, Su () 3,000 yrs, Active, W () 3,000 yrs, Passive, Su () 3,000 yrs, Passive, W

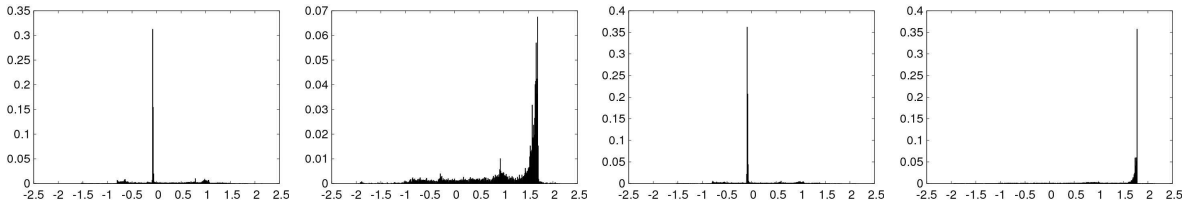

() 10,000 yrs, Active, Su () 10,000 yrs, Active, W () 10,000 yrs, Passive, Su () 10,000 yrs, Passive, W

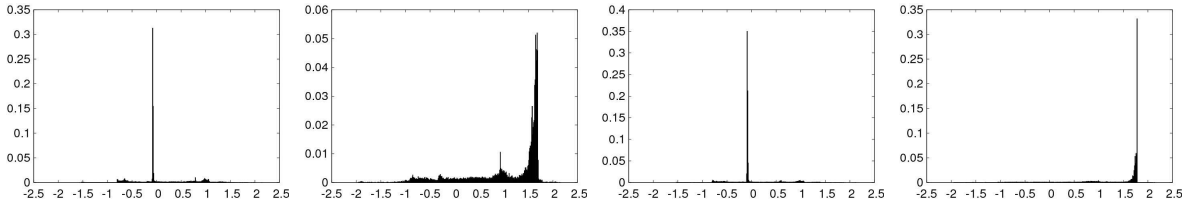

() 30,000 yrs, Active, Su () 30,000 yrs, Active, W () 30,000 yrs, Passive, Su () 30,000 yrs, Passive, W

frequency distributions for a single trajectory of the LS84 model variable Z over increasing time periods]Normalised frequency distributions for a single trajectory of the LS84 model variable S over increasing time periods. The method of coupling is given as active or passive and the respective ICs are given in table 5.7. *Su* denotes mid-summer and *W* denotes mid-winter. In each plot, the x-axis corresponds to the atmosphere variable Z and the y-axis corresponds to the frequency per occupuied bin; bin width = 0.01.

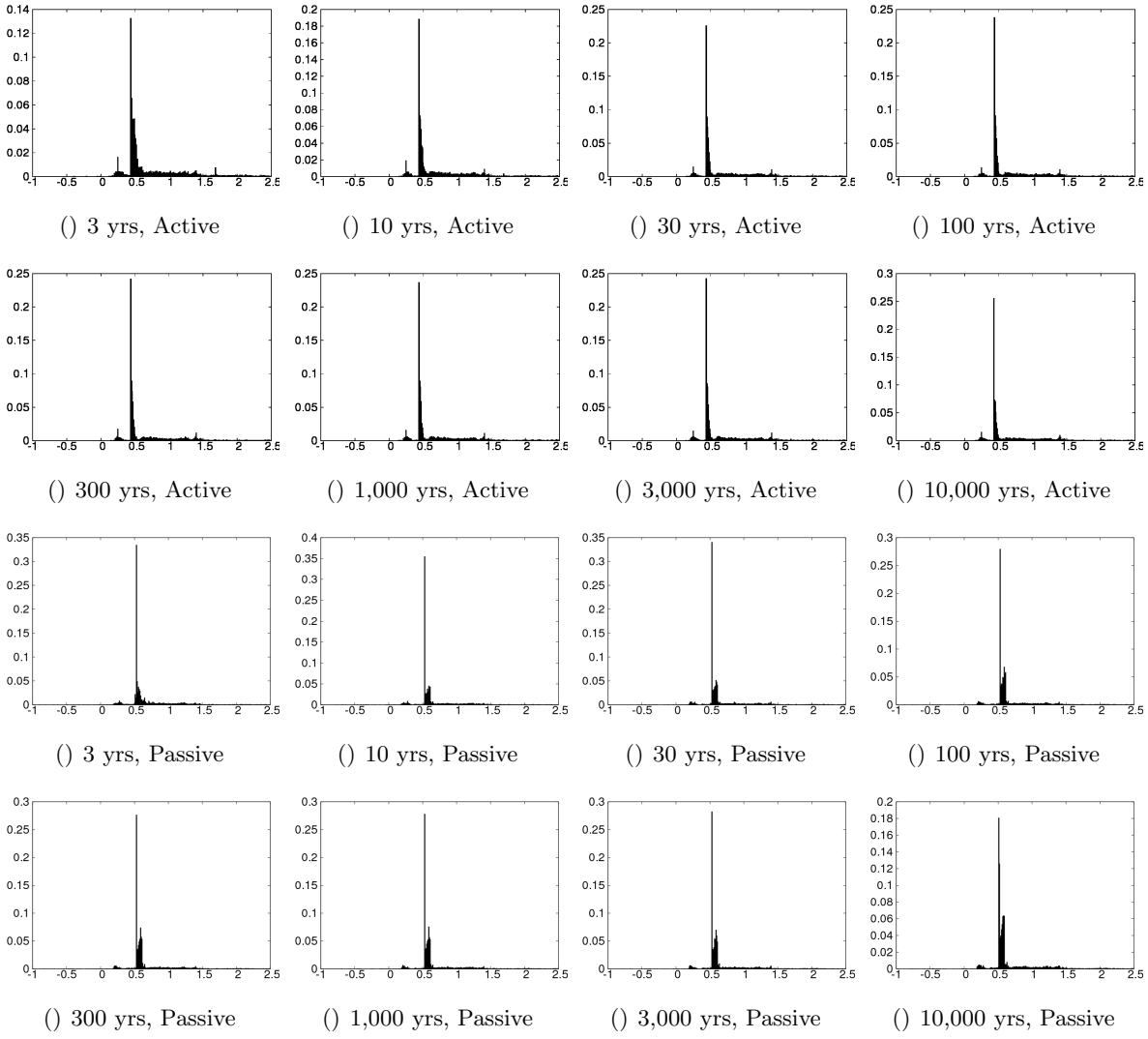

Figure C-2: Normalised frequency distributions for the atmosphere variable X from a 10,000 member IC ensemble of the LS84 model in mid-winter at given instants in time. The method of coupling is given as active or passive and ICs are spread evenly along a transect spanning the range from $(X_1, Y_1, Z_1, T_1, S_1) = (-1.0, -2.5, -2.5, 3.8, 1.45 \times 10^{-3})$ to $(X_{10000}, Y_{10000}, Z_{10000}, T_{10000}, S_{10000}) = (2.5, 2.5, 2.5, 5.0, 1.8 \times 10^{-3})$. In all plots, the x-axis corresponds to X and the y-axis corresponds to the frequency of ensemble members per occupuied bin; bin width = 0.01.

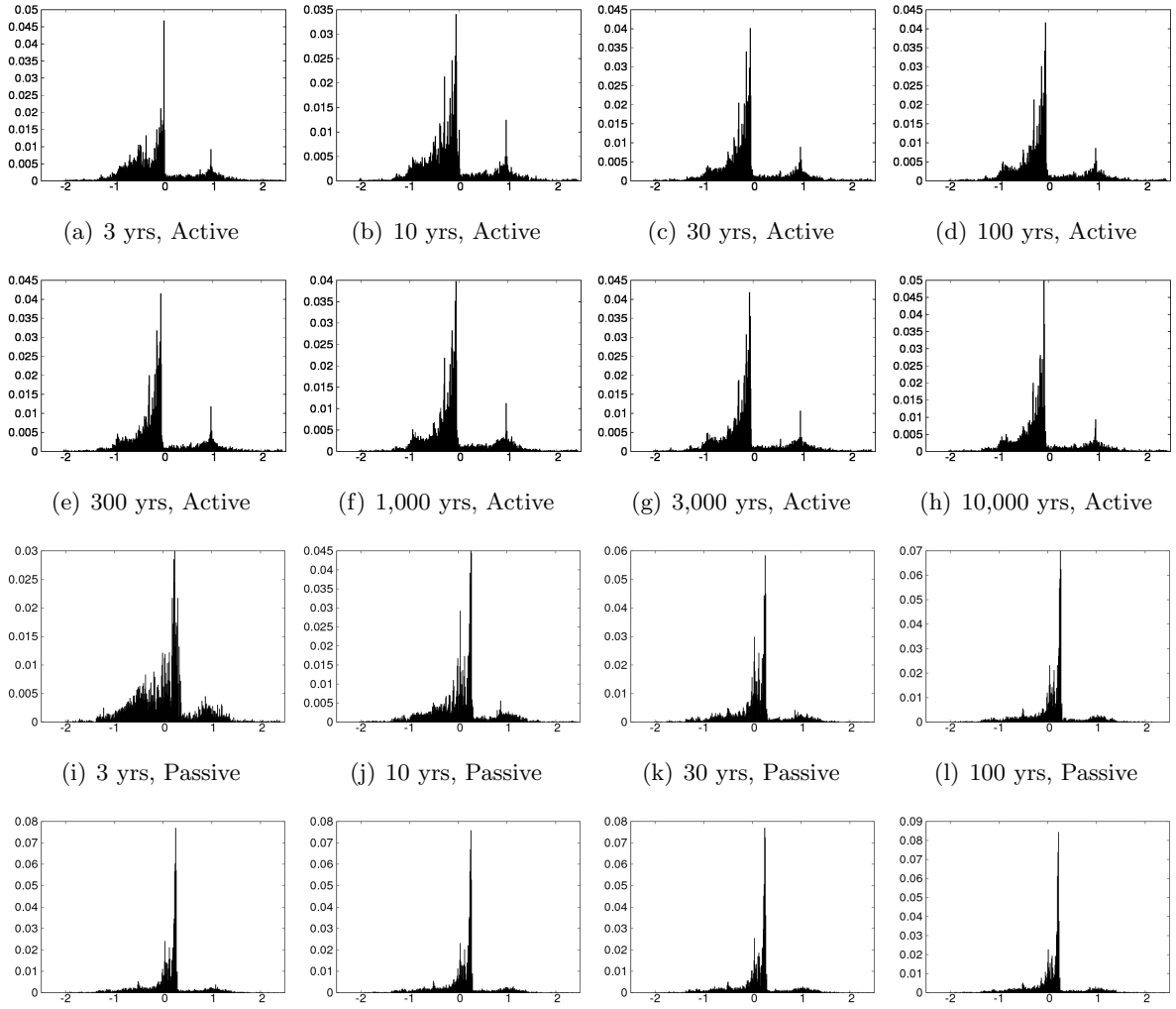

(a) 3 yrs, Active (b) 10 yrs, Active (c) 30 yrs, Active (d) 100 yrs, Active

(e) 300 yrs, Active (f) 1,000 yrs, Active (g) 3,000 yrs, Active (h) 10,000 yrs, Active

(i) 3 yrs, Passive (j) 10 yrs, Passive (k) 30 yrs, Passive (l) 100 yrs, Passive

(m) 300 yrs, Passive (n) 1,000 yrs, Passive (o) 3,000 yrs, Passive (p) 10,000 yrs, Passive

Figure C-3: Normalised frequency distributions for the atmosphere variable Y from a 10,000 member IC ensemble of the LS84 model in mid-winter at given instants in time. The method of coupling is given as active or passive and ICs are spread evenly along a transect spanning the range from $(X_1, Y_1, Z_1, T_1, S_1) = (-1.0, -2.5, -2.5, 3.8, 1.45 \times 10^{-3})$ to $(X_{10000}, Y_{10000}, Z_{10000}, T_{10000}, S_{10000}) = (2.5, 2.5, 2.5, 5.0, 1.8 \times 10^{-3})$. In all plots, the x-axis corresponds to Y and the y-axis corresponds to the frequency of ensemble members per occupuied bin; bin width = 0.01.

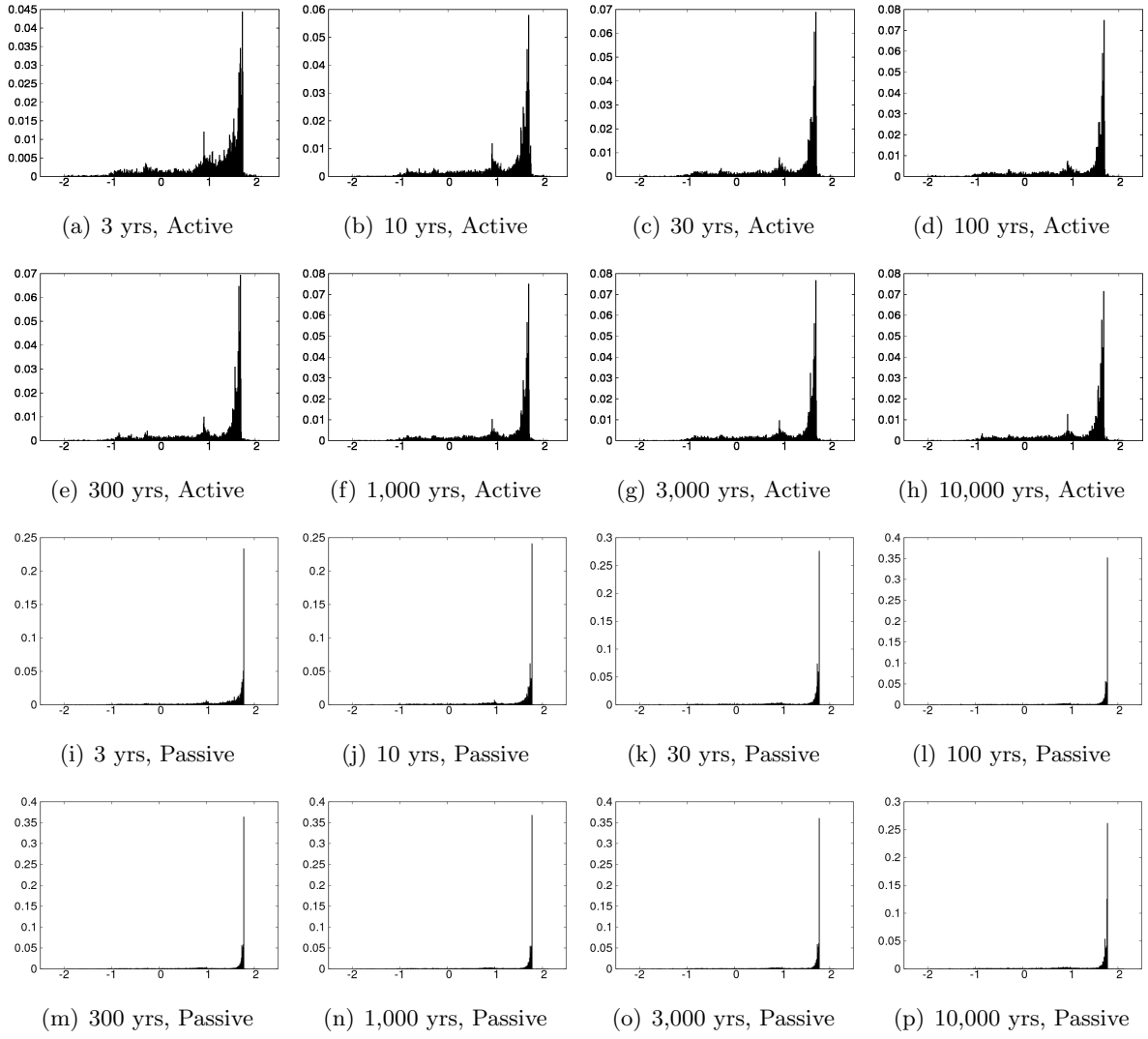

(a) 3 yrs, Active (b) 10 yrs, Active (c) 30 yrs, Active (d) 100 yrs, Active

(e) 300 yrs, Active (f) 1,000 yrs, Active (g) 3,000 yrs, Active (h) 10,000 yrs, Active

(i) 3 yrs, Passive (j) 10 yrs, Passive (k) 30 yrs, Passive (l) 100 yrs, Passive

(m) 300 yrs, Passive (n) 1,000 yrs, Passive (o) 3,000 yrs, Passive (p) 10,000 yrs, Passive

Figure C-4: Normalised frequency distributions for the atmosphere variable Z from a 10,000 member IC ensemble of the LS84 model in mid-winter at given instants in time. The method of coupling is given as active or passive and ICs are spread evenly along a transect spanning the range from $(X_1, Y_1, Z_1, T_1, S_1) = (-1.0, -2.5, -2.5, 3.8, 1.45 \times 10^{-3})$ to $(X_{10000}, Y_{10000}, Z_{10000}, T_{10000}, S_{10000}) = (2.5, 2.5, 2.5, 5.0, 1.8 \times 10^{-3})$. In all plots, the x-axis corresponds to Z and the y-axis corresponds to the frequency of ensemble members per occupuied bin; bin width = 0.01.

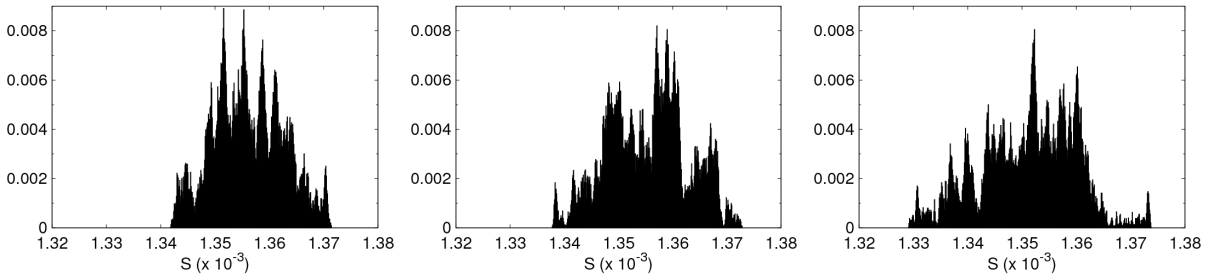

(a) IC 1 (b) IC 2 (c) IC 3

Figure C-5: Normalised frequency distributions from three single trajectories of S from the LS84 model with passive coupling and a fixed value of $F_m = 8$, with different initial values in T. The three ICs correspond to: *IC 1* $= (0.167, 1.045, -0.547, 5.248, 1.352 \times 10^{-3})$; *IC 2* $= (0.167, 1.045, -0.547, 5.348, 1.352 \times 10^{-3})$; *IC 3* $= (0.167, 1.045, -0.547, 5.448, 1.352 \times 10^{-3})$. In each plot, the y-axis corresponds to the frequency of ensemble members per occupuied bin; bin width $= 1 \times 10^{-7}$.

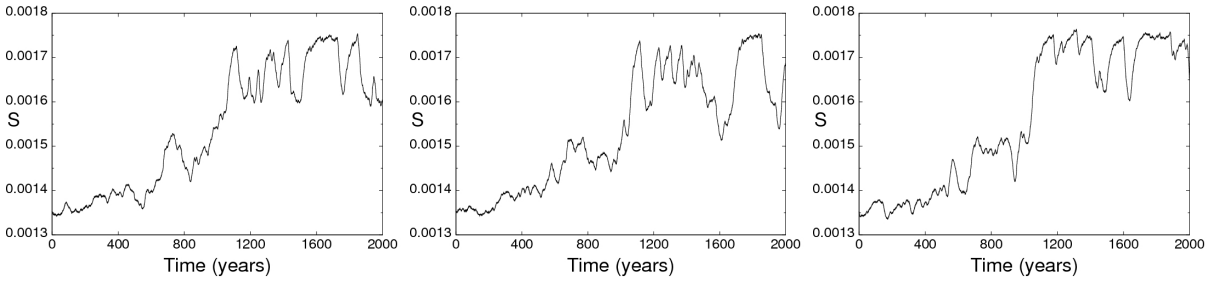

(a) IC 1 (b) IC 2 (c) IC 3

Figure C-6: Evolution of three single trajectories of S from the LS84 model with passive coupling under climate change, with different initial values in T. The mean value of F decreases from $F_m = 8$ to $F_m = 7$ over the first 1,000 years and then remains constant at $F_m = 7$ for the following 1,000 years. The three ICs correspond to: *IC 1* $= (0.167, 1.045, -0.547, 5.248, 1.352 \times 10^{-3})$; *IC 2* $= (0.167, 1.045, -0.547, 5.348, 1.352 \times 10^{-3})$; *IC 3* $= (0.167, 1.045, -0.547, 5.448, 1.352 \times 10^{-3})$.

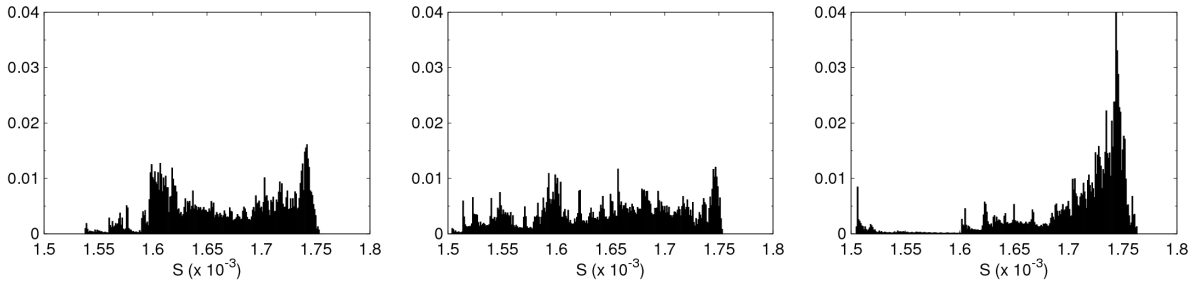

(a) IC 1 (b) IC 2 (c) IC 3

Figure C-7: Normalised frequency distributions from three single trajectories of S from the LS84 model over a 1,000 year period following a linear change in F_m from $F_m = 8$ to $F_m = 7$ over the previous 1,000 years (as in fig. 5.20). The three ICs correspond to: *IC 1* $= (0.167, 1.045, -0.547, 5.248, 1.352 \times 10^{-3})$; *IC 2* $= (0.167, 1.045, -0.547, 5.348, 1.352 \times 10^{-3})$; *IC 3* $= (0.167, 1.045, -0.547, 5.448, 1.352 \times 10^{-3})$. In each plot, the y-axis corresponds to the frequency of ensemble members per occupuied bin; bin width $= 1 \times 10^{-6}$.

Appendix D

Preparatory questions for informal discussions with insurance practitioners

- What are the main strategic issues being considered by insurers that may be influenced by knowledge of climate change?
- Can you identify any insurance issues that are relevant on time scales greater than one year?
- How is climate change factored into existing insurance decisions?
- Over what time scales is climate change information considered relevant to insurance strategies?
- In what specific areas of insurance activity is climate model information being utilised?
- How might climate model information on multi-decadal time scales be relevant for strategic planning with the insurance industry?

BNs combining observational and model data

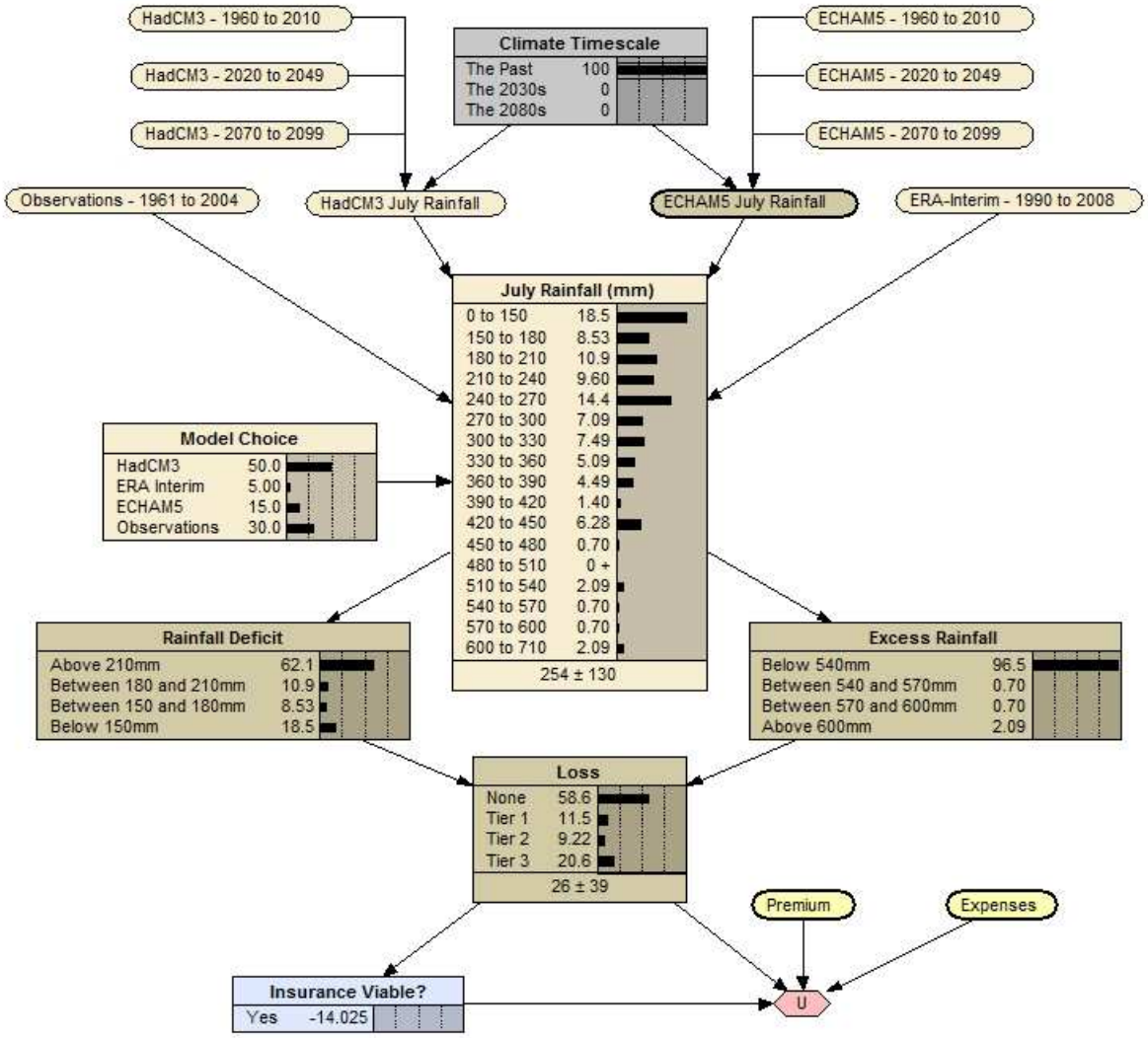

Figure D-1: BN to inform viability of weather index insurance for rice production in Kolhapur, India. The relative weights of the states in the *Model Choice* node have been arbitrarily selected and the *Climate Timescale* set to the past. Constants are given the values: premium = 15% of maximum indemnity and expenses = 3% of maximum indemnity.

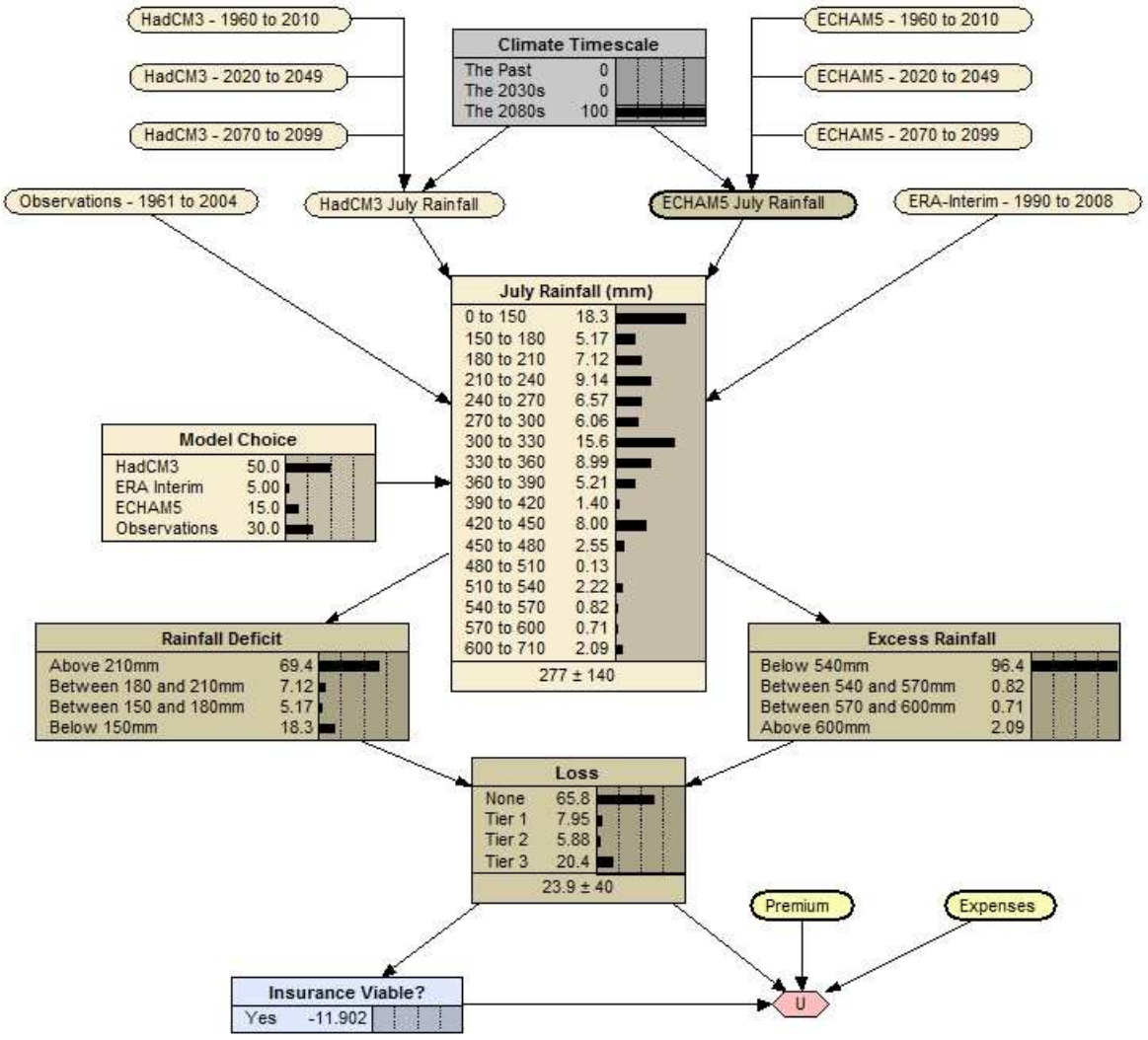

Figure D-2: BN to inform viability of weather index insurance for rice production in Kolhapur, India. The relative weights of the states in the *Model Choice* node have been arbitrarily selected and the *Climate Timescale* set to the 2080s. Constants are given the values: premium = 15% of maximum indemnity and expenses = 3% of maximum indemnity.

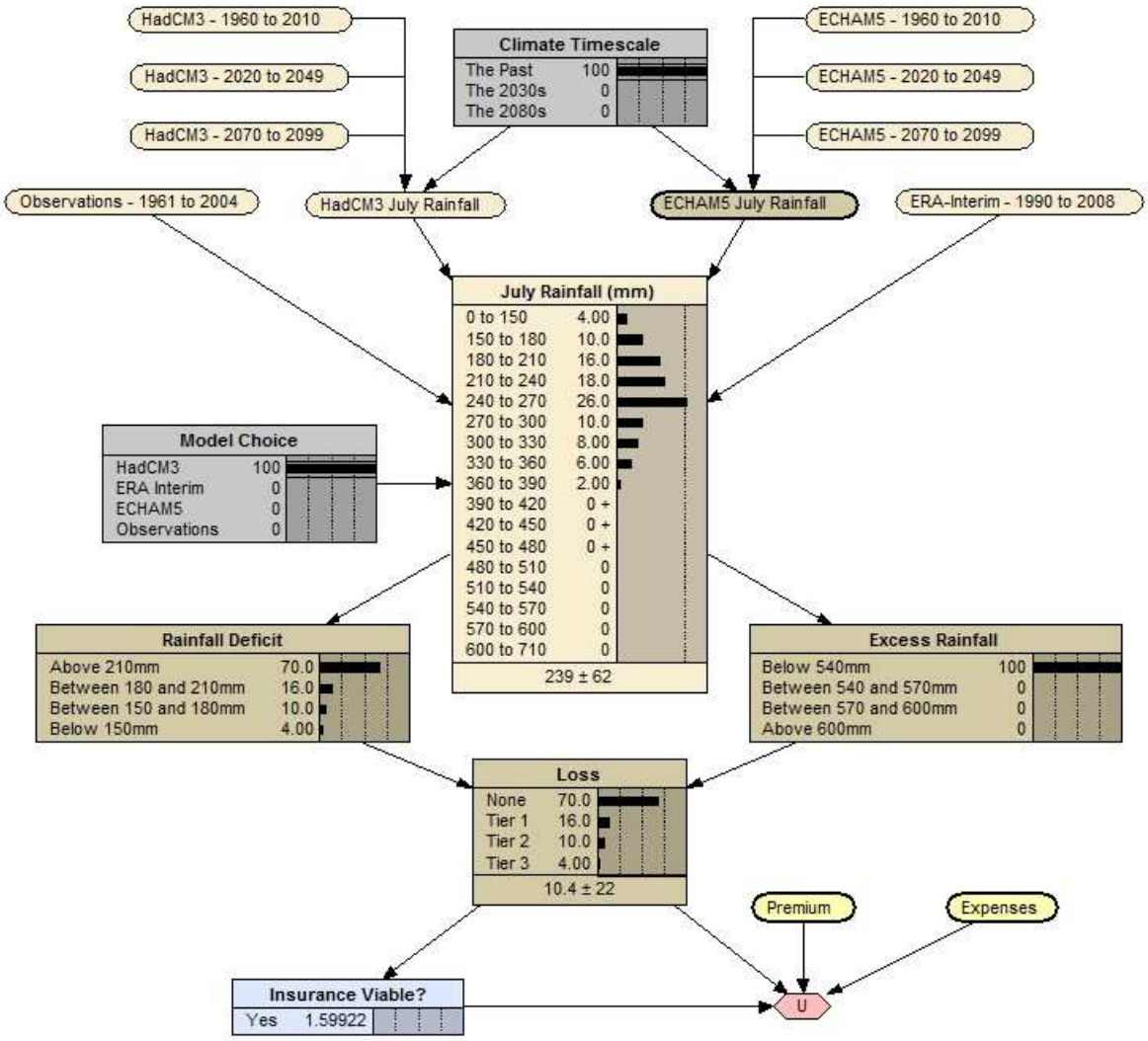

Figure D-3: BN to inform viability of weather index insurance for rice production in Kolhapur, India. The HadCM3 model has been selected in the *Model Choice* node and the *Climate Timescale* set to the past. Constants are given the values: premium = 15% of maximum indemnity and expenses = 3% of maximum indemnity.

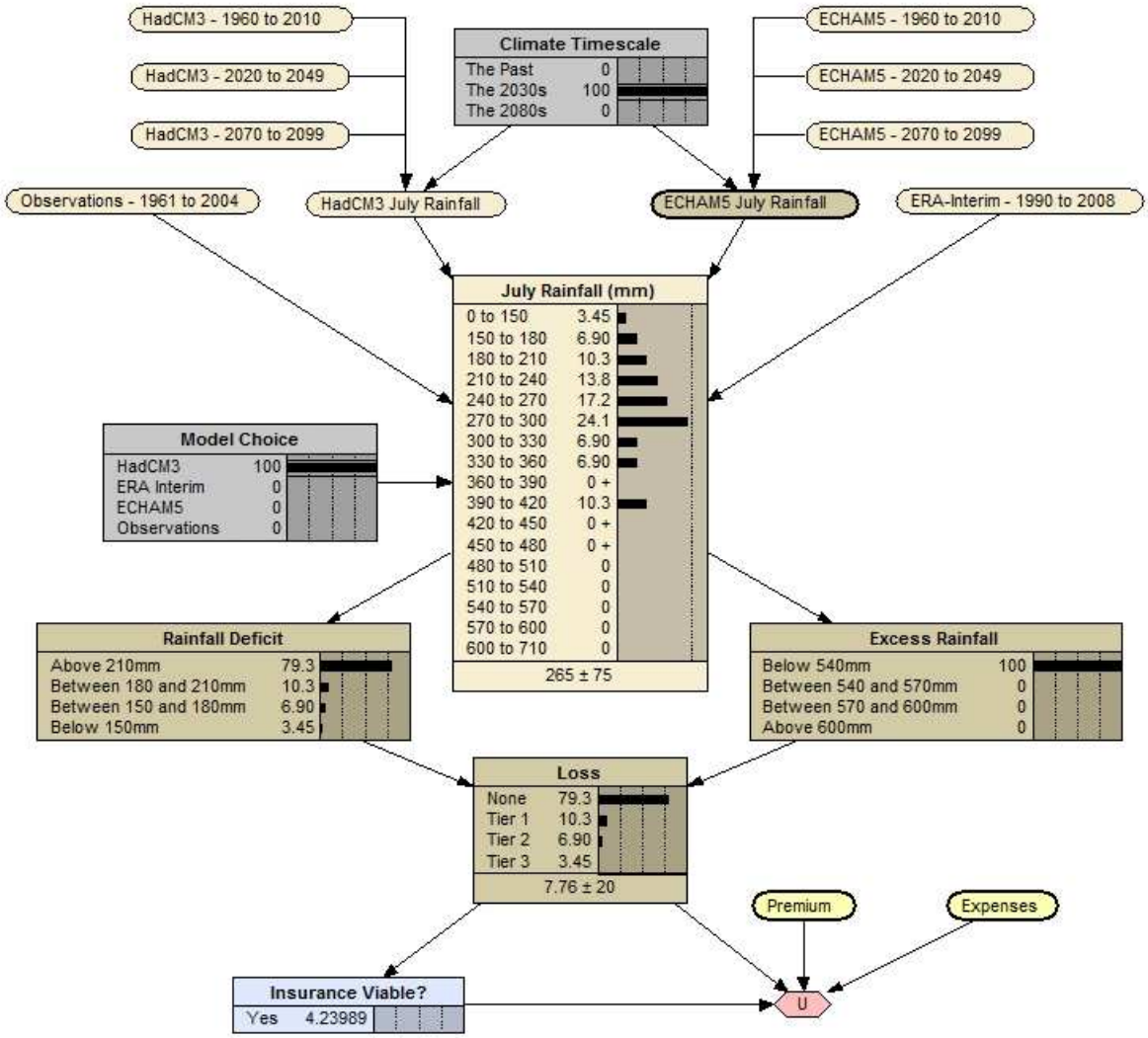

Figure D-4: BN to inform viability of weather index insurance for rice production in Kolhapur, India. The HadCM3 model has been selected in the *Model Choice* node and the *Climate Timescale* set to the 2030s. Constants are given the values: premium = 15% of maximum indemnity and expenses = 3% of maximum indemnity.

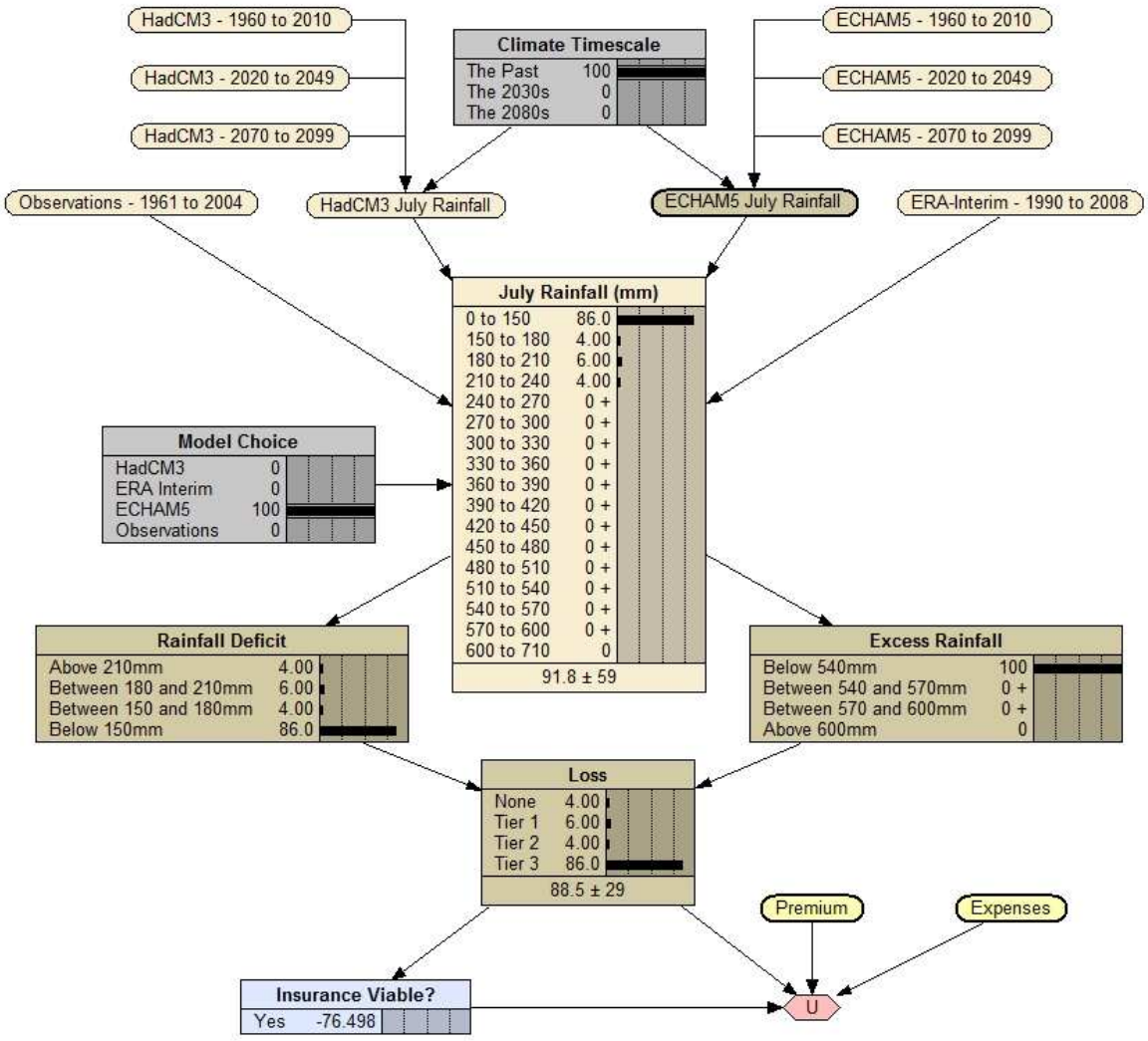

Figure D-5: BN to inform viability of weather index insurance for rice production in Kolhapur, India. The ECHAM5 model has been selected in the *Model Choice* node and the *Climate Timescale* set to the past. Constants are given the values: premium = 15% of maximum indemnity and expenses = 3% of maximum indemnity.

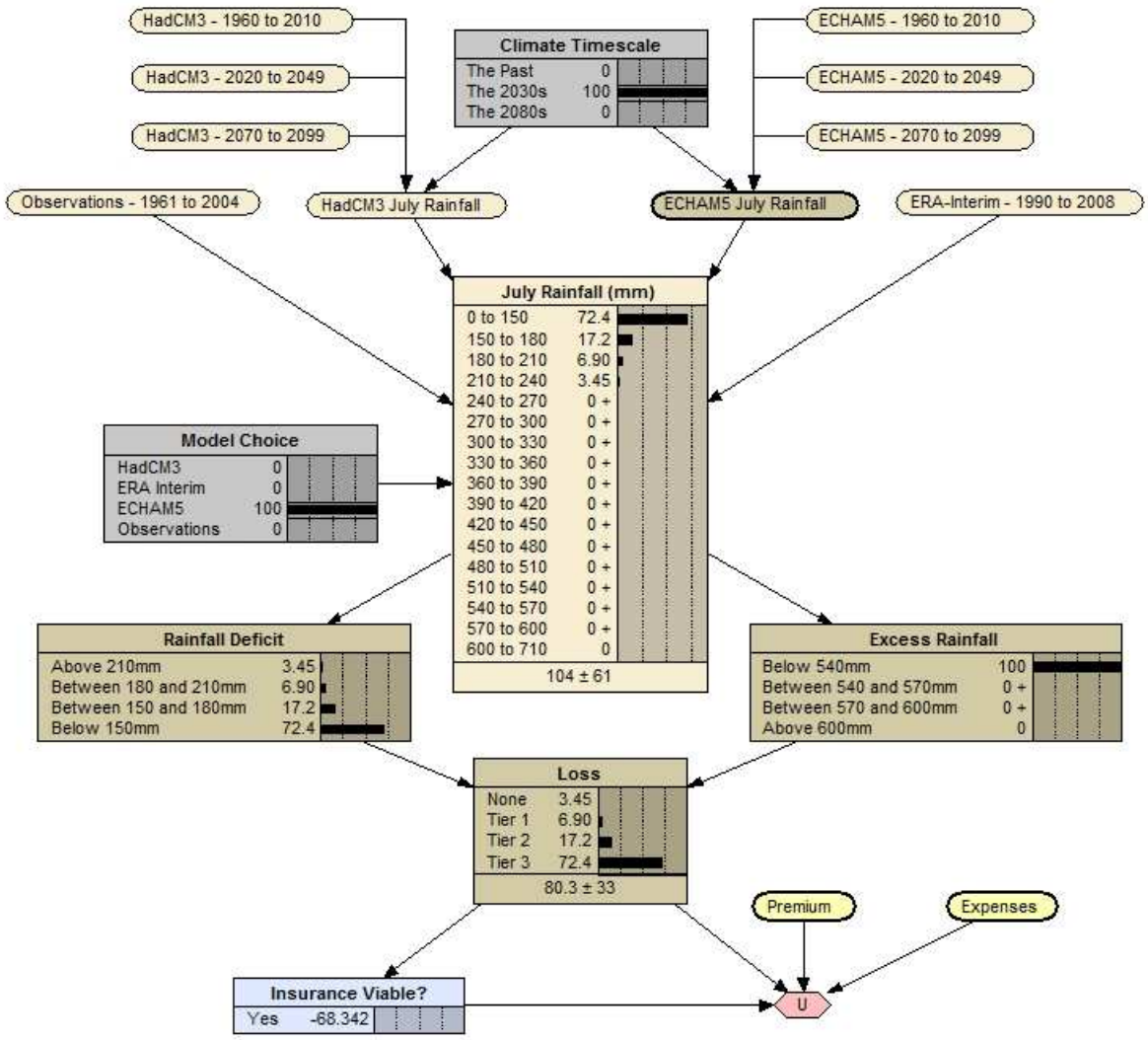

Figure D-6: BN to inform viability of weather index insurance for rice production in Kolhapur, India. The ECHAM5 model has been selected in the *Model Choice* node and the *Climate Timescale* set to the 2030s. Constants are given the values: premium = 15% of maximum indemnity and expenses = 3% of maximum indemnity.

BNs incorporating bias corrected model data

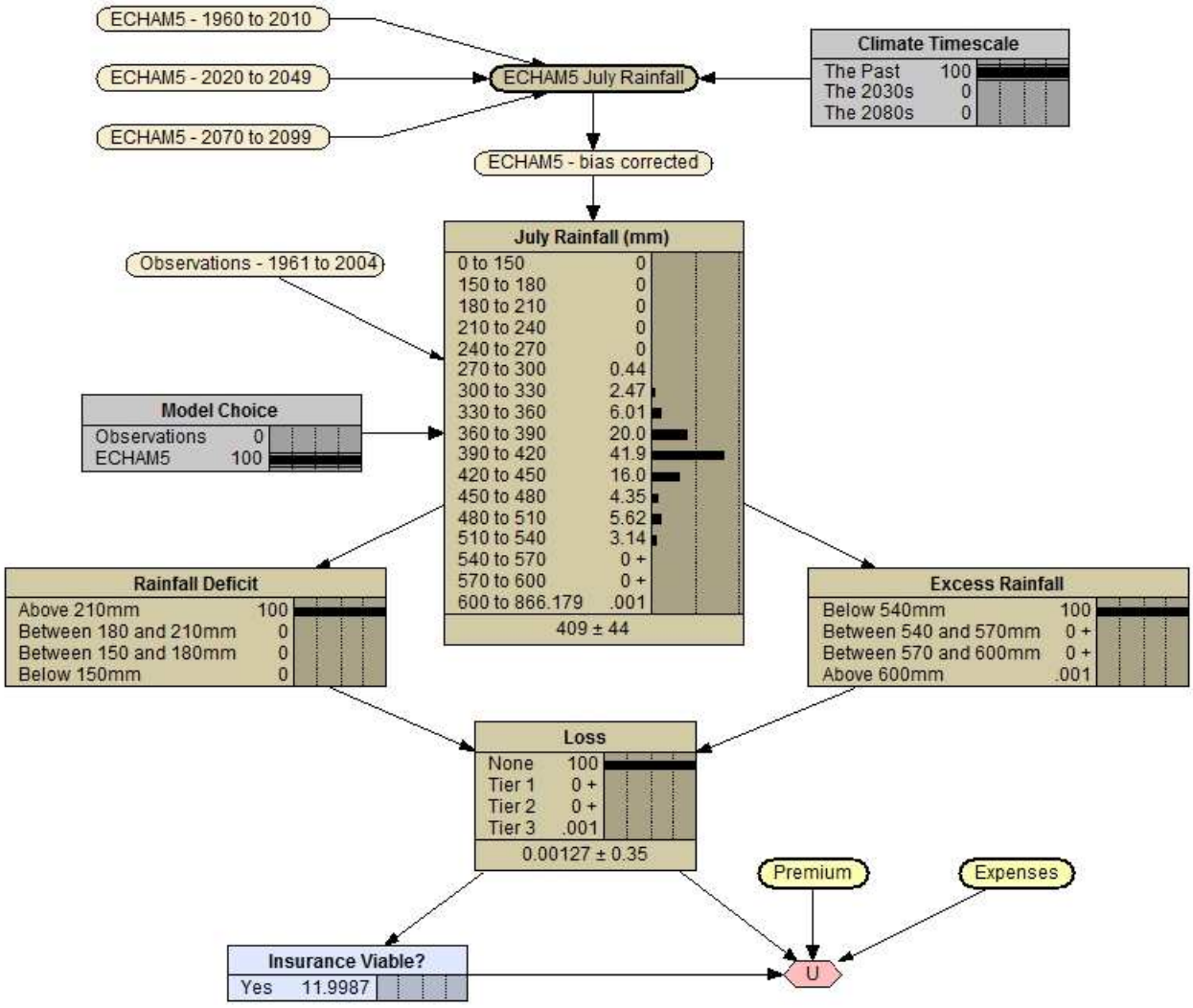

Figure D-7: BN to inform viability of weather index insurance for rice production in Kolhapur, India. The ECHAM5 model has been selected in the *Model Choice* node and a bias correction has been applied according to table 6.6. The *Climate Timescale* is set to the past. Constants are given the values: premium = 15% of maximum indemnity and expenses = 3% of maximum indemnity.

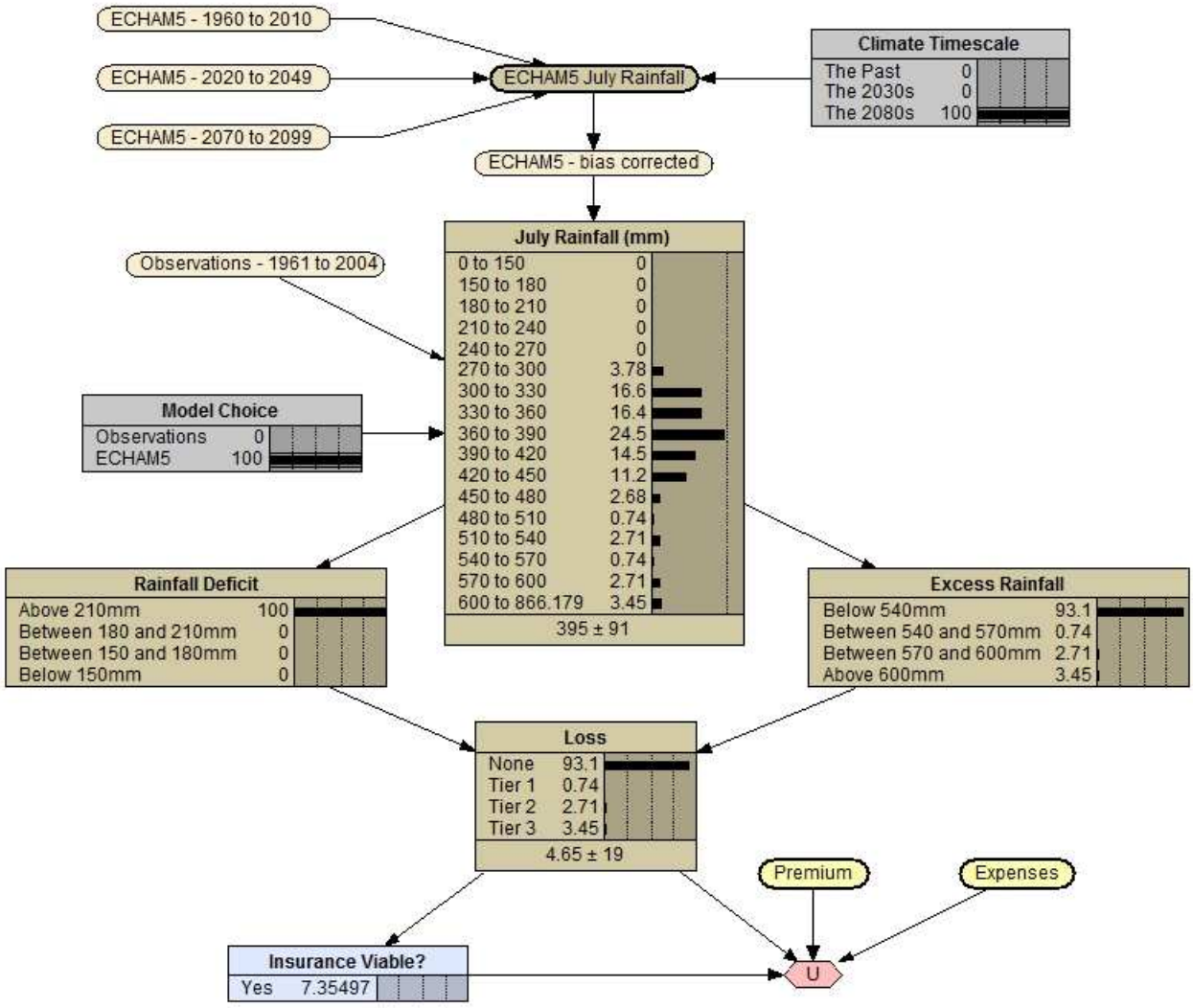

Figure D-8: BN to inform viability of weather index insurance for rice production in Kolhapur, India. The ECHAM5 model has been selected in the *Model Choice* node and a bias correction has been applied according to table 6.6. The *Climate Timescale* is set to the 2080s. Constants are given the values: premium = 15% of maximum indemnity and expenses = 3% of maximum indemnity.

BNs with observational data altered using model output anomalies

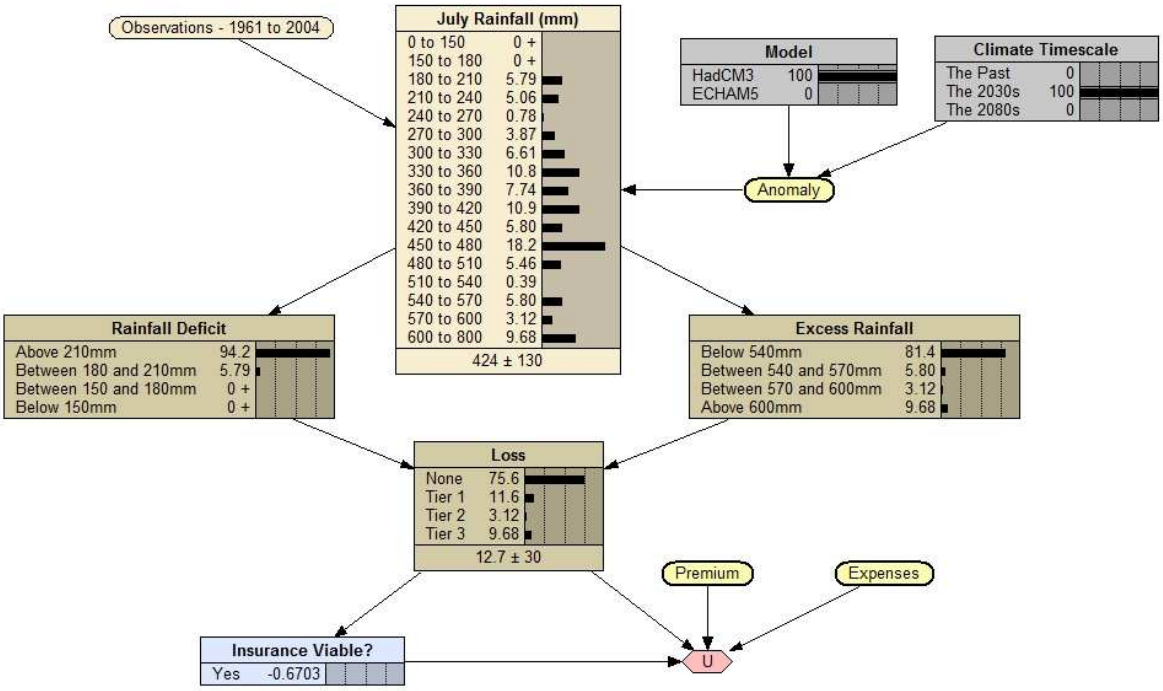

Figure D-9: BN to inform viability of weather index insurance for rice production in Kolhapur, India. Observational data is altered using anomaly information from the HadCM3 model projections according to table 6.7. The *Climate Timescale* is set to the 2030s. Constants are given the values: premium = 15% of maximum indemnity and expenses = 3% of maximum indemnity.

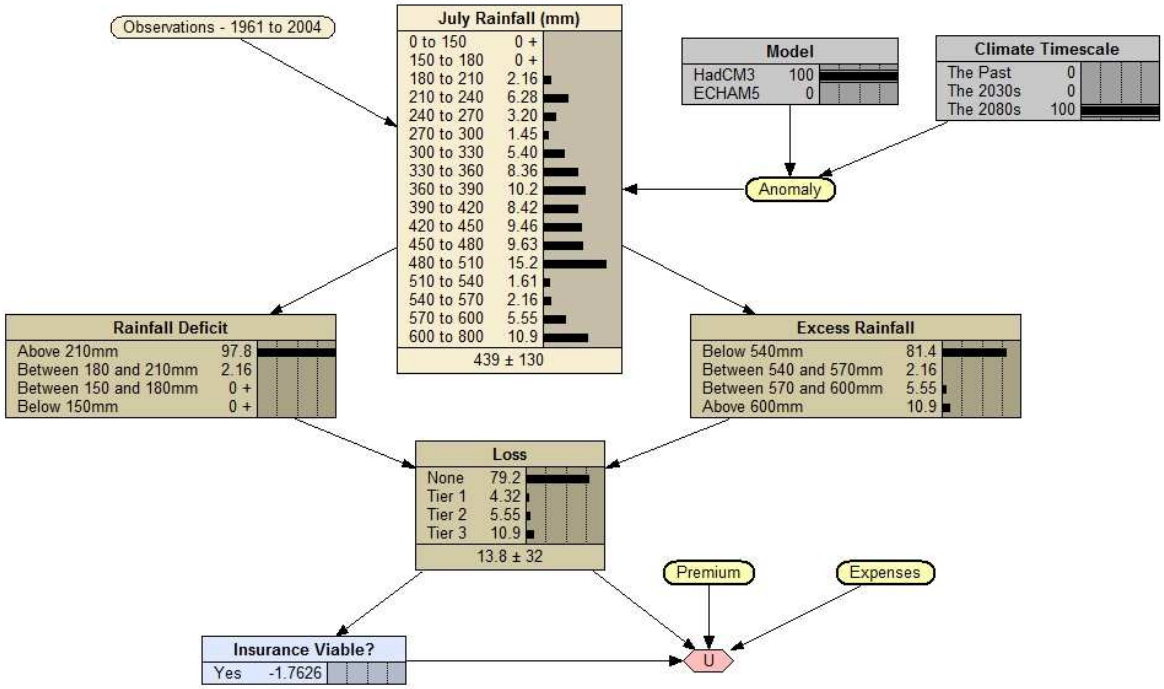

Figure D-10: BN to inform viability of weather index insurance for rice production in Kolhapur, India. Observational data is altered using anomaly information from the HadCM3 model projections according to table 6.7. The *Climate Timescale* is set to the 2080s. Constants are given the values: premium = 15% of maximum indemnity and expenses = 3% of maximum indemnity.

Glossary

Transitivity	A transitive system is one in which a trajectory can pass through all of the possible system states.
Intransivity	An intransitive system is one in which a trajectory will only pass through a subset of all possible system states; the subset is determined by the initial state and once established, will persist forever.
Almost intransitivity	A system displays almost intransitivity if the statistics of a single trajectory taken over infinitely long time intervals are independent of initial conditions, but the statistics of a single trajectory taken over very long but finite intervals depend very much upon initial conditions.
Ergodic hypothesis	The assertion that the probability distribution derived from many iterations of a single orbit is the same as the probability distribution derived from a high-order iteration of many orbits with a range of different initial conditions.
Hysteresis	Exhibited by a system whose current state is a function of the past evolution of the system.
Psuedo-attractor	The set of states towards which a trajectory evolves for a dynamical system subject to time-periodic forcings.

Bibliography

ABI. A Changing Climate for Insurance: A Summary Report for Cheif Executives and Policymakers, June 2004. Association of British Insurers, www.abi.org.uk/climatechange.

ABI. Insuring Our Future Climate: Thinking for Tomorrow, Today, September 2007. Association of British Insurers, www.abi.org.uk/climatechange.

ABI. Long-term Retail General Insurance: The Potential for Long-term Home Insurance Contracts in the Context of Flood Risk, 2010. ABI Research Paper No 21 by R. Goss and D. O'Neill.

J. Aguirre, J. C. Vallejo, and M. A. F. Sanjuan. Wada basins and unpredictability in hamiltonian and dissipative systems. *International Journal of Modern Physics B*, 17:4171–4175, 2003.

H. Alderman and T. Haque. *Insurance Against Covariate Shocks: The Role of Index-Based Insurance in Social Protection in Low-Income Countries of Africa*. Africa Human Development Series. World Bank Working Paper no. 95, Washington, D.C., 2007.

K. Allen. *Vulnerability reduction and the community-based approach*, pages 170–184. In: Pelling (ed.), Natural Disasters and Development in a Globalising World, 2003.

M. R. Allen. Do-it-yourself climate prediction. *Nature*, 401:627, 1999.

M. R. Allen and W. J. Ingram. Constraints on future changes in climate and the hydrologic cycle. *Nature*, 419:224–232, 2002.

M. R. Allen, P. A. Stott, J. F. B. Mitchell, R. Schnur, and T. L. Delworth. Quantifying the uncertainty in forecasts of anthropogenic climate change. *Nature*, 407:617–620, 2000.

M. R. Allen, J. A. Kettleborough, and D. A. Stainforth. Model error in weather and climate forecasting, 2002. Paper presented at 2002 ECMWF Predictability Seminar, Eur. Cent. for Medium Range Weather Forecasting, Reading, UK.

M. R. Allen, D. J. Frame, C. Huntingford, C. D. Jones, J. A. Lowe, M. Meinshausen, and N. Meinshausen. Warming caused by cumulative carbon emissions towards the trillionth tonne. *Nature*, 458:1163–1166, 2009.

D. P. Ames, Neilson B. T., Stevens D. K., and U. Lall. Using bayesian networks to model watershed management decisions: an east canyon creek case study. *Journal of Hydroinformatics*, 7(4):267–282, 2005.

D. L. T. Anderson and J. Willebrand. volume 44 of *Global Environmental Change*. Springer-Verlag Berlin Heidelberg, Germany, 1996.

J. L. Anderson and V. Hubeny. A re-examination of methods for evaluating the predictability of the atmosphere. *Nonlinear Processes in Geophysics*, 4:157–165, 1997.

J. D. Annan and J. C. Hargreaves. Reliability of the CMIP3 ensemble. *Geophys. Res. Lett.*, 37: L02703, 2010.

J. D. Annan, J. C. Hargreaves, R. Ohgaito, A. Abe-Ouchi, and S. Emori. Efficiently constraining climate sensitivity with ensembles of Paleoclimate simulations. *Sci. On-line Lett. Atmos.*, 1: 181–184, 2005.

S. Arrhenius. On the Influence of Carbonic Acid in the Air upon the Temperature of the Ground. *Phil. Mag.*, 41(251):237–276, 1896.

AXA. Preparing for Climate Change: A practical guide for small businesses, 2006. Available at http://www.cea.eu/uploads/Modules/Publications/Climate%20Change%20report%20final.pdf.

D. N. Barnett, S. J. Brown, J. M. Murphy, D. M. H. Sexton, and M. J. Webb. Quantifying uncertainty in changes in extreme event frequency in response to doubled CO_2 using a large ensemble of GCM simulations. *Clim. Dyn.*, 26:489–511, 2006.

F. Barthel and E. Neumayer. A Trend Analysis of Normalized Insured Damage from Natural Disasters (May 4, 2011). *Climatic Change*, 2012. Available at SSRN: http://ssrn.com/abstract=1831633.

D. S. Battisti and R. L Naylor. Historical warnings of future food insecurity with unprecedented seasonal heat. *Science*, 323:240–244, 2009.

S. E. Belcher, J. N. Hacker, and D. S. Powell. Constructing design weather data for future climates. *Building Serv. Eng. Res. Technol.*, 26(1):49–61, 2005.

R. Benzi. Stochastic resonance: from climate to biology. *Nonlin. Processes Geophys.*, 17: 431–441, 2010.

R. Benzi, A. Sutera, and A. Vulpiani. The mechanism of stochastic resonance. *J. Phys. A*, 14: L453, 1981.

R. Benzi, G. Parisi, A. Sutera, and A. Vulpiani. Stochastic resonance in climatic change. *Tellus*, 34:10–16, 1982.

G. A. Berz. Catastrophes and climate change: concerns and possible countermeasures of the insurance industry. *Mitigation and Adaptation Strategies for Global Change*, 4:283–293, 1999.

R. A. Betts, Y. Malhi, and J. T. Roberts. The future of the amazon: new perspectives from climate, ecosystem and social sciences. *Phil. Trans. R. Soc. B*, 363(1498):1729–1735, 2008.

A. Bhattacharya. The climate attractor. *Proc. Indian Acad. Sci. (Earth Planet Sci.)*, 102(1): 113–120, 1993.

S. I. Bhuiyan. Water management in relation to crop production: Case study on rice. *Outlook on Agriculture*, 21:293–299, 1992.

G. D. Birkhoff. Proof of the Ergodic Theorem. *Proc. Nat. Acad. Sci. USA*, 17:656–660, 1931.

G. J. Boer. Analysis and verification of model climate. In P. Mote and A. O'Neill, editors, *Numerical Modeling of the Global Atmosphere in the Climate System*, pages 59–82. Kluwer Academic Publishers, Dordrecht, 2000.

L. Boltzmann. Einige allgemeine Sätze über Wärmegleichgewicht. *Wien. Ber.*, 63:679–711, 1871.

L. Boltzmann. Weitere Studien über das Wärmegleichgewicht unter Gasmolekülen. *Wien. Ber.*, 66:265–370, 1872.

A. Bostrom, M. Granger Morgan, B. Fischhoff, and D. Reade. What do people know about global climate change? *Risk Anal.*, 14(6):959–970, 1994.

W. Bourke, B. Mcavaney, K. Puri, and R. Thurling. *Global Modeling of Atmospheric Flow by Spectral Methods*, pages 267–324. In: General Circulation Models of the Atmosphere. New York, Academic Press Inc, 1977.

N. L. Bowers, H. U. Gerber, J. C. Hickman, D. A. Jones, and C. J. Nesbitt. *Actuarial Mathematics*, chapter 1. The Society of Actuaries, Schaumburg, Illinois, 1986.

W. S. Broecker. Climatic Change: Are We on the Brink of a Pronounced Global Warming? *Science*, 189(4201):460–463, 1975.

H. Broer and R. Vitolo. Dynamical systems modeling of low-frequency variability in low-order atmospheric models. *Discrete and Continuous Dynamical Systems Series B*, 10:401–419, 2008.

H. Broer, C. Simo, and R. Vitolo. Bifurcations and strange attractors in the lorenz-84 climate model with seasonal forcing. *Nonlinearity*, 15:1205—-1267, 2002.

H. Broer, C. Simo, and R. Vitolo. Quasi-periodic hénon-like attractors in the lorenz-84 climate model with seasonal forcing. *Proceedings Equadiff*, 15:601–607, 2003.

M. I. Budyko. The effect of solar radiation variations on the climate of the earth. *Tellus*, 5: 611–619, 1969.

H. Bühlmann. *Mathematical Methods in Risk Theory*, chapter 4. Springer-Verlag Berlin Heidelberg, second edition, 2005.

J. E. Burns, M. G. Gouda, and R. E. Miller. Stabilization and pseudo-stabilization. *Distributed Computing*, 7(1):35–42, 1993.

W. Burroughs. *Climate: Into the 21st Century*. World Meteorological Organisation, Cambridge University Press, 2003.

I. Burton, S. Huq, B. Lim, O. Pilifosova, and E. L. Schipper. From impacts assessment to adaptation priorities: the shaping of adaptation policy. *Climate Policy*, 2:145–159, 2002.

J. Cain. Planning improvements in natural resources management: guidelines for using bayesian networks to support the planning and management of development programmes in the water sector and beyond. Technical report, Centre for Ecology and Hydrology, Wallingford, UK, 2001. ISBN: 0903741009.

K. V. Calvin and A. M. Thomson. Impact of Heavy Duty Vehicle Emissions Reductions on Global Climate, August 2010. Prepared for the U.S. Department of Energy.

M. A. Carriquiry and D. E. Osgood. Index Insurance, Probabilistic Climate Forecasts, and Production, March 2008. Center for Agricultural and Rural Development, Working Paper 08-WP 465.

CEA. Reducing the Social and Economic Impact of Climate Change and Natural Catastrophes: Insurance Solutions and Public-Private Partnerships, June 2007. CEA Insurers of Europe, Brussels.

S. A. Changnon, R. A. Pielke Jr., D. Changnon, R. T. Sylves, and R. S. Pulwarty. Human Factors Explain the Increased Losses from Weather and Climate Extremes. *Bull. Am. Meteorol. Soc.*, 81(3):437–442, 2000.

M. Chekroun, I. Zaliapin, and M. Ghil. Pullback attractors in nonautonomous dynamical systems with delay: Applications to an enso model with seasonal forcing. volume 12 of *Geophysical Research Abstracts*. EGU General Assembly, 2010a.

M. D. Chekroun, E. Simonnet, and M. Ghil. Stochastic climate dynamics: random attractors and time-independent invariant measures. *Physica D, accepted*, 2010b.

J. H. Christensen, T. R. Carter, M. Rummukainen, and G. Amanatidis. Evaluating the performance and utility of regional climate models: the PRUDENCE project. *Climatic Change*, 81(1):1–6, 2007a.

J. H. Christensen, B. Hewitson, A. Busuioc, A. Chen, X. Gao, I. Held, R. Jones, R.K. Kolli, W.-T. Kwon, R. Laprise, V. Magaña Rueda, L. Mearns, C.G. Menéndez, J. Räisänen, A. Rinke, A. Sarr, and P. Whetton. *Climate Change 2007: The Physical Science Basis, Contribution of Working Group 1 to the Fourth Assessment Report of the Intergovernmental Panel on Climate Change*, chapter Regional Climate Projections. Cambridge University Press, United Kingdom and New York, NY, USA, 2007b. [Solomon, S., D. Qin, M. Manning, Z. Chen, M. Marquis, K.B. Averyt, M. Tignor and H.L. Miller (eds.)].

P. C. Chu. Two Kinds of Predictability in the Lorenz System. *J. Atmos. Sci.*, 56:1427–1432, 1999.

CIBSE. Guide a environmental design. Technical report, Chartered Institution of Building Service Engineers, 2006. ISBN: 978190387668.

M. P. Clark and R. S. Pulwarty. Devising resilient responses to potential climate change impacts. *Ogmius - Newsletter of the Center for Science and Technology Policy Research*, 5:2–3, 2003.

M. Claussen, L. A. Mysak, A. J. Weaver, M. Crucifix, T. Fichefet, M. F. Loutre, S. L. Weber, J. Alcamo, V. A. Alexeev, A. Berger, R. Calov, A. Ganopolski, H. Goosse, G. Lohmann, F. Lunkeit, Mokhov II, V. Petoukhov, P. Stone, and Z. Wang. Earth system models of intermediate complexity: closing the gap in the spectrum of climate system models. *Clim. Dyn.*, 18:579–586, 2002.

B. F. Clegg, R. Kelly, G. H. Clarke, I. R. Walker, and F. S. Hu. Nonlinear response of summer temperature to Holocene insolation forcing in Alaska. *Proc. Natl. Acad. Sci.*, 108(48):19299–19304, 2011.

Climate Etc. Spatio-temporal chaos, February 2011. Posted on 10/02/2011 by Thomas Milanovic. Available at http://judithcurry.com/2011/02/10/spatio-temporal-chaos/.

ClimateWise. ClimateWise Initiative: Reduding the Risk for Tomorrow, 2011. Accessed on 03/03/2011, available at http://www.climatewise.org.uk.

Collector Office, Kolhapur, 2009. Available at http://kolhapur.gov.in/new. Accessed 19/04/2011.

M. Collins. Climatic predictability on interannual to decadal time scales: the initial value problem. *Climate Dynamics*, 19(8):671–292, 2002.

M. Collins and M. R. Allen. Assessing the Relative Roles of Initial and Boundary Conditions in Interannual to Decadal Climate Predictability. *J. Climate*, 15:3104–3109, 2002.

M. Collins and C. Senior. Projections of future climate change. *Weather*, 57:283–287, 2002.

M. Collins, S. F. B. Tett, and C. Cooper. The internal climate variability of HadCM3, a version of the Hadley Centre coupled model without flux adjustments. *Clim. Dyn.*, 17:61–81, 2001.

M. Collins, M. Botzet, A. F. Carril, H. Drange, A. Jouzeau, M. Latif, S. Masina, O. H. Otteraa, H. Pohlmann, A. Sorteberg, R. Sutton, and L. Terray. Interannual to Decadal Climate Predictability in the North Atlantic: A Multimodel-Ensemble Study. *J. Climate*, 19:1195–1203, 2006.

M. Collins, B. B. Booth, B. Bhaskaran, G. R. Harris, J. M. Murphy, D. M. H. Sexton, and M. J. Webb. Climate model errors, feedbacks and forcings: a comparison of perturbed physics and multi-model ensembles. *Clim. Dyn.*, 36(9-10):1737–1766, 2010.

U. Confalonieri, B. Menne, R. Akhtar, K. L. Ebi, M. Hauengue, R.S. Kovats, B. Revich, and A. Woodward. *Climate change 2007: Impacts, Adaptation and Vulnerability. Contribution of Working Group II to the Fourth Assessment Report of the Intergovernmental Panel on Climate Change.* (eds M. L. Parry, O.F. Canziani, J.P. Palutikof, P.J. van der Linden and C.E. Hanson), Cambridge University Press, Cambridge, UK, 2007.

P. Cox and D. Stephenson. A changing climate for prediction. *Science*, 317:207–208, 2007.

A. Crisanti, M. Falcioni, G. Paladin, and A. Vulpiani. Stochastic resonance in deterministic chaotic systems. *J. Phys. A.*, 27:L597–L603, 1994.

P. Dailey, M. Huddleston, S. Brown, and D. Fasking. The financial risks of climate change, 2009. Association of British Insurers, Research Paper No 19. Report by AIR Worldwide Corp. and the Met Office.

A. R. Daneshkhah. Uncertainty in Probabilistic Risk Assessment: A Review, August 2004. Available at www.shef.ac.uk/content/1/c6/03/09/33/risk.pdf.

J. D. Daron and D. McNeall. Using Bayesian Networks to inform climate risk: A case study on the resilience of the UK health infrastructure to increased temperatures. *In Preparation.*

Defra. UK Climate Projections: What is meant by probability in UKCP09?, 2009. Accessed 29/11/2009, available at http://ukclimateprojections.defra.gov.uk/content/view/1205/531/.

T. L. Delworth, R. Zhang, and M. E. Mann. Decadal to centennial variability of the atlantic from observations and models. *Ocean Circulation: Mechanisms and Impacts, Geophysical Monograph Series 173, Washington, DC, American Geophysical Union*, pages 131–148, 2007.

S. Dessai. *Robust adaptation decisions amid climate change uncertainties.* PhD thesis, School of Environmental Sciences, University of East Anglia, Norwich, UK, November 2004.

S. Dessai and M. Hulme. Does climate adaptation policy need probabilities? *Climate Policy*, 4:107–128, 2004.

S. Dessai and R. Wilby. How can developing country decision makers incorporate uncertainty about climate risks into existing planning and policymaking processes? *World Resources Report Uncertainty Series*, 2011. Available at http://www.worldresourcesreport.org/.

A. E. Dessler and E. A. Parson. *The Science and Politics of Global Climate Change.* Cambridge University Press, Cambridge, United Kingdom, 2006.

R. Dettmer. Chaos and engineering. *IEE Review*, 39(5):199–203, 1993.

W. L. Ditto. Applications of chaos in biology and medicine. *AIP Conf. Proc.*, 376:175–201, 1996.

A. Dlugolecki. An overview of the impact of climate change on the insurance industry. In H. F. Diaz and R. J. Murnane, editors, *Climate Extremes and Society*, chapter 13, pages 249–278. Cambridge University Press, 2008.

A. Dlugolecki and S. Lafeld. Climate Change and the Financial Sector: An Agenda for Action, 2005. A publication of Allianz Group and WWF, 59pp.

A. Dlugolecki, P. Bolster, A. Couchman, M. Agnew, C. Goodess, P. Jones, T. Osborn, K. Bermingham, C. Crerar, M. Docrill, N. Ford, J. Harpum, D. Crichton, D. Clark, M. Johnson, N. S. Lambert, A. Milroy, D. Martin, S. aslett-Jones aslett-Jones aslett Jones, J. Walden, I. Coates, C. Hall, J. Bean, A. Perry, D. Rochester, N. Silver, J. Richardson, and W. Buist. Coping with climate change: Risks and opportunites for insurers. Technical report, Chartered Insurance Institute, London, 2009.

M. Donald, A. Cook, and K. Mengersen. Bayesian network for risk of diarrhea associated with the use of recycled water. *Risk Analysis*, 29(12):1672–1685, 2009.

H. Du, F. Niehoerster, and L. A. Smith. Robust measure of predictive skill and ensemble design. 2011. In the first Conference of EQUIP, Leeds, UK.

V. P. Dymnikov and A. S. Gritsoun. Climate model attractors: chaos, quasi-regularity and sensitivity to small perturbations of external forcing. *Nonlinear Processes in Geophysics*, 8: 201–209, 2001.

J. P. Eckmann and D. Ruelle. Ergodic theory of chaos and strange attractors. *Rev. Mod. Phys*, 57(3):617–656, 1985.

P. N. Edwards. *A Vast Machine: Computer Models, Climate Data and the Politics of Global Warming*. The MIT Press, Cambridge, Massachusetts; London England, 2010.

P. Embrechts, C. Klüppelberg, and T. Mikosch. *Modelling Extreme Events for Insurance and Finance*. Springer-Verlag Berlin Heidelberg New York, 2003.

P. R. Epstein and J. J. McCarthy. Assessing climate stability. *Bull. Amer. Meteor. Soc.*, 85 (12):1863–1870, 2004.

Ernst & Young. Strategic Business Risk: Insurance 2008. In collaboration with Oxford Analytica. Technical report, 2008.

R. Essery, M. Best, and P. Cox. Moses 2.2 Technical Documentation, 2001. Hadley Centre Technical Note 30. Available at http://www.metoffice.gov.uk/publications/HCTN /HCTN_30.pdf.

European Commission. The 2°C target: Information reference document, 2008. Prepared and adopted by EU Climate Change Expert Group 'EG Science'. Available at ec.europa.eu/clima/policies/international/docs/brochure_2c.pdf.

C. Evangelinos and C. N. Hill. Cloud Computing for Parallel Scientific HPC Applications: Feasibility of Running Coupled Atmosphere-Ocean Climate Models on Amazon's EC2, October 2008.

N. E. Fenton. Bayesian net references: a comprehensive listing, 2007. Available at http://www.agenarisk.com/resources.

N. E. Fenton and M. Neil. Combining evidence in risk analysis using Bayesian Networks. Agena White Paper W0704/01, AgenaRisk, 2004. Available at http://www.agenarisk.com/resources.

N. E. Fenton and M. Neil. Managing Risk in the Modern World. Knowledge transfer report, London Mathematical Society, 2007. Available at http://www.lms.ac.uk/activities.

H. J. Fowler, S. Blenkinsop, and C. Tebaldi. Linking climate change modelling to impacts studies: recent advances in downscaling techniques for hydrological modelling. *Int. J. Climatol.*, 27:1547–1578, 2007.

K. Fraedrich. Estimating the dimensions of weather and climate attractors. *J. Atmos. Sci*, 43: 419–432, 1986.

J. G. Freire, C. Bonatto, C. C. DaCamarra, and J. A. Gallas. Multistability, phase diagrams, and intransitivity in the lorenz-84 low-order atmospheric circulation model. *Chaos*, 18(6): 1705–1717, 2008.

S. O. Funtowicz and J. R. Ravetz. Science for the Post-Normal Age. *Futures*, 25:739–755, 1993.

H. M. Füssel and R. J. T. Klein. Climate change vulnerability assessments: an evolution of conceptual thinking. *Climatic Change*, 75(3):301–329, 2006.

S. Gadgil and K. Rupa Kumar. *The Asian Monsoon*, chapter 18: Agriculture and economy, pages 651–683. Springer Praxis Books, 2006.

L. Gammaitoni, P. Hanggi, P. Jung, and F. Marchesoni. Stochastic resonance. *Rev. Mod. Phys.*, 70(1):223–287, 1998.

M. Gawith, R. Street, R. Westaway, and A. Steynor. Application of the UKCIP02 climate change scenarios: Reflections and lessons learnt. *Global Environmental Change*, 19:113–121, 2009.

M. Ghil. Hilbert problems for the geosciences in the 21st century. In *Nonlinear Processes in Geophysics*, volume 8, pages 211–222, 2001.

M. Ghil. chapter Natural Climate Variability, pages 544–549. John Wiley and Sons, Ltd, Chichester, 2002.

I. Gilmour. *Nonlinear model evaluation: iota-shadowing, probabilistic prediction and weather forecasting.* PhD thesis, Mathematical Institute, Oxford University, 1998.

F. Giorgi. Climatic Change Prediction. *Climatic Change*, 73:239–265, 2005.

F. Giorgi and L. O. Mearns. Approaches to the simulation of regional climate change: A review. *Reviews of Geophysics*, 29(2):191–216, 1991.

J. Gleick. *Chaos: The amazing science of the unpredictable*. Vintage, The Random House Group Ltd, London, 1988.

N. Goldenfeld and L. P. Kadanoff. Simple Lessons from Complexity. *Science*, 284(5411):87–89, 1999.

C. Gordon, C. Cooper, C. A. Senior, Banks H. T., J. M. Gregory, T. C. Johns, J. F. B. Mitchell, and R. A. Wood. The simulation of SST, sea ice extents and ocean heat transports in a version of the Hadley Centre coupled model without flux adjustments. *Clim. Dynam.*, 16:147–168, 2000.

P. Grassberger. Do climate attractors exist? *Nature*, 323:339–368, 1986.

C. Grebogi, E. Ott, S. Pelikan, and J. A. Yorke. Strange attractors that are not chaotic. *Physica D: Nonlinear Phenomena*, 13:261–268, 1984.

A. Greene, L. Goddard, and U. Lall. Probabilistic multimodel regional temperature change projections. *J. Clim.*, 19:4326–4343, 2006.

P. Grossi, H. Kunreuther, and D. Windeler. Chapter 2: An Introduction to Catastrophe Models and Insurance. *Catastrophe Modeling: A new Approach to Managing Risk*, 25(1):23–42, 2005.

J. O. Haerter, S. Hagemann, C. Moseley, and C. Piani. Climate model bias correction and the role of timescales. *Hydrol. Earth Syst. Sci.*, 15:1065–1079, 2011.

R. Hagedorn, F. J. Doblas-Reyes, and T. N. Palmer. The rationale behind the success of multi-model ensembles in seasonal forecasting. *Tellus A*, 57(3):219–233, 2005.

S. Hagemann, K. Arpe, and E. Roeckner. Evaluation of the hydrological cycle in the ECHAM5 model. *J. Climate*, 19:3810–3827, 2006.

Y. Y. Haimes. *Risk Modeling, Assessment, and Management*. John Wiley and Sons, 2009.

J. Hall, C. Twyman, and A. Kay. Influence diagrams for represneting uncertainty in climate-related propositions. *Clim. Change*, 69:343–365, 2005.

J. W. Hall. Probabilistic climate scenarios may misrepresent uncertainty and lead to bad adaptation decisions. *Hydrological Processes*, 21(8):1127–1129, 2007.

S. Hallegate. Strategies to adapt to an uncertain climate change. *Global Environmental Change*, 19(2):240–247, 2009.

J. Hansen, M. Sato, R. Ruedy, A. Lacis, K. Asamoah, K. Beckford, S. Borenstein, E. Brown, B. Cairns, B. Carlson, B. Curran, S. de Castro, L. Druyan, P. Etwarrow, T. Ferede, M. Fox, D. Gaffen, J. Glascoe, H. Gordon, S. Hollandsworth, X. Jiang, C. Johnson, N. Lawrence, J. Lean, J. Lerner, K. Lo, J. Logan, A. Luckett, M. P. McCormick, R. McPeters, R. Miller, P. Minnis, I. Ramberran, G. Russell, P. Russell, P. Stone, I. Tegen, S. Thomas, L. Thomason, A. Thompson, J. Wilder, R. Willson, and J. Zawodny. Forcings and chaos in interannual to decadal climate change. *J. Geophys. Res.*, 102(D22):25679–25720, 1997.

S. Harrison. Predicting future climate change: lessons from palaeoclimatology, July 2007. Environmental research group. Available at http://www.actuaries.org.uk/research-and-resources/documents/predicting-future-climate-change-lessons-palaeoclimatology.

K. Hasselmann. Stochastic climate models: Part i. theory. *Tellus*, 6:473–485, 1976.

E. Hawkins and R. Sutton. The Potential to Narrow Uncertainty in Regional Climate Predictions. *Bull. Am. Meteorol. Soc.*, 90:1095–1107, 2009.

P. Hazell, J. Anderson, N. Balzer, A. H. Clemmensen, U. Hess, and F. Rispoli. The potential for scale and sustainability in weather index insurance for agriculture and rural livelihoods, March 2010. International Fund for Agricultural Development and World Food Programme.

C. J. Hearn. Application of the stommel model to shallow mediterranean estuaries and their characterization. *J. Geophys. Res.*, 103:391–404, 1998.

D. Heckerman, A. Mamdani, and M. Wellman. Real-world applications of bayesian networks. *Comm ACM*, 38:25–26, 1995.

G. C. Hegerl, F. W. Zwiers, P. Braconnot, N. P. Gillett, Y. Luo, J. A. Marengo Orsini, N. Nicholls, J. E. Penner, and P. A. Stott. *Understanding and Attributing Climate Change*. 2007. In: Climate Change 2007: The Physical Science Basis. Contribution of Working Group I to the Fourth Assessment Report of the Intergovernmental Panel on Climate Change. [Solomon, S.,D. Qin, M. Manning, Z. Chen, M. Marquis, K.B. Averyt, M. Tignor and H.L. Miller (eds.)]. Cambridge University Press, Cambridge, United Kingdom and New York, NY, USA.

C. Herweijer, N. Ranger, and R. E. T. Ward. Adaptation to Climate Change: Threats and Opportunities for the Insurance Industry. *The Geneva Papers on Risk and Insurance - Issues and Practice*, 34:360–380, 2009.

H. Heyen, E. Zorita, and H. von Storch. Statistical downscaling of monthly mean North-Atlantic air-pressure to sea level anomalies in the Baltic Sea. *Tellus*, 48A:312–323, 1996.

HighNoon. Adaptation to changing water resources availability in northern India with respect to Himalayan glacier retreat and changing monsoon pattern, 2009. European Comission, Seventh Framework Programme. Available at http://www.eu-highnoon.org.

HM Treasury. Vision for the insurance industry in 2020: a report from the insurance idustry working group, July 2009. Available at www.hm-treasury.gov.uk/d/fin_insuranceindustry270709.pdf.

B. F. Hobbs, P. T. Chao, and B. N. Venkatesh. Using decision analysis to include climate change in water resources decision making. *Climatic Change*, 37:177–202, 1997.

S. Hochrainer, R. Mechler, G. Pflug, and A. Lotsch. Investigating the Impact of Climate Change on the Robustness of Index-based Microinsurance in Malawi. *Policy Research Working Paper, World Bank*, WPS4631, 2008.

P. L. Houtekamer, L. Lefaivre, J. Derome, H Ritchie, and H. L. Mitchell. A System Simulation Approach to Ensemble Prediction. *Mon. Wea. Rev.*, 124:1225–1242, 1996.

B. Huang, P. S. Schopf, and J. Shukla. Intrinsic ocean-atmosphere variability of the tropical atlantic ocean. *J. Climate*, 17:2058–2077, 2004.

D. A. Hudson and R. G. Jones. Regional climate model simulations of present-day and future climates of Southern Africa. Technical report, UK Met Office, August 2002. Hadley Centre technical note 39.

M. Hulme, S. C. B. Raper, and T. M. L. Wigley. An integrated framework to address climate change (ESCAPE) and further developments of the global and regional climate modules (MAGICC). *Energy Policy*, 23(4-5):347–355, 1995.

M. Hulme, G. J. Jenkins, X. Lu, J. R. Turnpenny, T. D. Mitchell, R. G. Jones, J. Lowe, J. M. Murphy, D. Hassell, P. Boorman, R. McDonald, and S. Hill. *Climate Change Scenarios for the UK: The UKCIP02 Scientific Report.* Tyndall Centre for Climate Change Research, School of Environmental Sciences, University of East Anglia, Norwich, UK, 2002.

R. A. Humble. Deterministic Chaos within a Forced Boundary Layer. In *37th AIAA Fluid Dynamics Conference and Exhibit, 25-28 June 2007, Miami, FL*, 2007.

R. Huth. Statistical downscaling in central Europe: evaluation of methods and potential predictors. *Climate Research*, 13:91–101, 1999.

IIASA. Climate Change: What Role for Insurance?, December 2008. International Institute for Applied Systems Analysis Policy Brief No. 4. Available at www.iiasa.ac.at.

IITM. Indian institute of tropical meteorology, 2011. available at http://www.tropmet.res.in, accessed 24/02/2011.

IPCC. Emissions Scenarios, 2000. A Special Report of Working Group III of the Intergovernmental Panel on Climate Change. Cambridge University Press, Cambridge, United Kingdom.

IPCC. *Climate change 2001: the scientific basis. Contribution of Working Group I to the third assessment report of the Intergovernmental Panel on Climate Change*. (eds J. T. Houghton, Y. Ding, D. J. Griggs, M. Noguer, P. J. van der Linden, D. Xiaosu, X. Dai, K. Maskell and C. A. Johnson), p. 881. Cambridge University Press, Cambridge, UK, 2001.

IPCC. *Appendix I: Glossary*, pages 869–883. In: Climate Change 2007: Impacts, Adaptation and Vulnerability. Contribution of Working Group II to the Fourth Assessment Report of the Intergovernmental Panel on Climate Change [M. L. Parry, O. F. Canziani, J. P. Palutikof, P. J. van der Linden and C.E. Hanson (eds)]. Cambridge University Press, Cambridge, UK and New York, NY, 2007a.

IPCC. *Summary for Policy Makers*. 2007b. In: Climate Change 2007: The Physical Science Basis. Contribution of Working Group I to the Fourth Assessment Report of the Intergovernmental Panel on Climate Change. [Solomon, S.,D. Qin, M. Manning, Z. Chen, M. Marquis, K.B. Averyt, M. Tignor and H.L. Miller (eds.)]. Cambridge University Press, Cambridge, United Kingdom and New York, NY, USA.

IPCC. Scoping Paper - IPCC Special Report: Managing the Risks of Extreme Events and Disasters to Advance Climate Change Adaptation, 2009. Submitted by V. Barros, C. Field, Co-chairs of Working Group 2 and J. P. van Ypersele, Vice-chair IPCC.

IPCC. Organization, 2011. Available at http://www.ipcc.ch/organization/organization.shtml. Accessed on 17/05/2011.

H. M. Ito. Ergodicity of randomly perturbed Lorenz model. *J. Stat. Phys.*, 35(1,2):151–158, 1984.

D. Jaffee, H.Kunreuther, and E. Michel-Kerjan. Long-Term Property Insurance. *Journal of Insurance Regulation, in press*, 2011. Working Paper no. 2010-04-19, The Wharton School, University of Pennsylvania.

M. Jametti and T. von Ungern-Sternberg. Hurricane Insurance in Florida. *CESIFO Working Paper no. 2768*, 2009.

G. Jenkins and J. Lowe. Handling uncertainties in the UKCIP02 scenarios of climate change. Technical report, November 2003. Hadley Centre technical note 44.

R. Jones, M. Noguer, D. Hassell, D. Hudson, S. Wilson, G. Jenkins, and J. Mitchell. Generating high resolution climate change scenarios using Precis, 2004. Available at http://precis.metoffice.com/docs.

K. Judd, L. Smith, and A. Weisheimer. Gradient free descent: shadowing, and state estimation using limited derivative information. *Physica D*, 190:153–166, 2004.

T. R. Karl and K. E. Trenberth. Modern Global Climate Change. *Science*, 302:1719–1723, 2003.

N. S. Keenlyside, M. Latif, J. Jungclaus, L. Kornblueh, and E. Roeckner. Advancing decadal-scale climate prediction in the North Atlantic sector. *Nature*, 453:84–88, 2008.

E. J. Kendon, R. G. Jones, E. Kjellström, and J. M. Murphy. Using and Designing GCM-RCM Ensemble Regional Climate Projections. *J. Climate*, 23:6485–6503, 2010.

A. S. Kitoh, A. N. Yukimoto, and T. Motoi. Simulated changes in the Asian summer monsoon at time of increased C02. *J. Meteor. Soc. Japan*, 75:1019–1031, 1997.

C. G. Knight, S. H. E. Knight, N. Massey, T. Aina, C. Christensen, D. J. Frame, J. A. Kettleborough, A. Martin, B. Sanderson, S. Pascoe, D. A. Stainforth, and M. R. Allen. Association of parameter, software and hardware variation with large scale behavior across 57,000 climate models. *PNAS*, July 2007.

R. Knutti. Should we believe model predictions of future climate change? *Phil. Trans. R. Soc. A*, 366:4647–4664, 2008.

R. Knutti, G. A. Meehl, M. R. Allen, and D. A. Stainforth. Constraining climate sensitivity from the seasonal cycle in surface temperature. *J. Climate*, 19:4224–4233, 2006.

R. Knutti, R. Furrer, C. Tebaldi, J. Cermak, and G. A. Meehl. Challenges in Combining Projections from Multiple Climate Models. *J. Climate*, 23:2739–2758, 2010.

R. W. Kock. Routes to chaos in the preiodically driven Lorenz-84 system. Master's thesis, 1998.

M. Kottek, J. Grieser, C. Beck, B. Rudolf, and F. Rubel. World Map of the Köppen-Geiger climate classification updated. *Meteorologische Zeitschrift*, 15(3):259–263, June 2006.

V. Krishnamurthy and B. N. Goswami. Indian Monsoon–ENSO Relationship on Interdecadal Timescale. *J. Climate*, 13:579–595, 2000.

T. N. Krishnamurti, C. M. Kishtawal, Z. Zhang, T. LaRow, D. Bachiochi, and E. Williford. Multimodel ensemble forecasts for weather and seasonal climate. *J. Climate*, 13:4196–4216, 2000.

S. Kuikka and O. Varis. Uncertainties of climatic change impacts in Finnish watersheds: a Bayesian network analysis of expert knowledge. *Boreal environment research*, 2(1):109–128, 1997.

Z. W. Kundzewicz, M. Radziejewski, and I. Pińskwar. Precipitation extremes in the changing climate of Europe. *Climate Research*, 31:51–58, 2006.

H. Kunreuther. Reducing Losses from Catastrophic Risks through Long-Term Insurance and Mitigation. *Social Research*, 75(3):905–930, 2008.

H. Kunreuther, R. Meyer, and E. Michel-Kerjan. Strategies for Better Protection against Catastrophic Risks, September 2007. Working Paper # 2007-09-14.

M. Lakshmanan and S. Rajasekar. *Nonlinear Dynamics: Integrability, Chaos and Patterns*, chapter 3, pages 32–34. Springer-Verlag Berlin Heidelberg, 2003.

M. Lal, T. Nozawa, S. Emori, H. Harasawa, K. Takahashi, M. Kimoto, A. Abe-Ouchi, T. Takemura, and A. Numaguti. Future climate change: Implications for Indian summer monsoon and its variability. *Current Science*, 81(9):1196–1207, 2001.

S. L. Lauritzen and D. J. Spiegelhalter. Local computations with probabilities on graphical structures and their application to expert systems (with discussion). *J. Roy Stat Soc B*, 50: 157–224, 1988.

D. J. Lea, M. R. Allen, and T. W. N. Haine. Sensitivity analysis of the climate of a chaotic system. *Tellus*, 52A:523–532, 2000.

R. Lester. Introduction to the Insurance Industry, March 2009. World Bank. Primer series on insurance, issue 1.

M. Leutbecher and T. N. Palmer. Ensemble forecasting. *J. Comp. Phys.*, 227:3515–3539, 2008.

T. Y. Li and J. A Yorke. Period three implies chaos. *American Mathematical Monthly*, 82: 985–992, 1975.

J. W. B. Lin and J. D. Neelin. Toward stochastic deep convective parameterization in general circulation models. *Geophys. Res. Lett.*, 30(4):1162–1165, 2003.

Lloyd's. Climate Change: Adapt or Bust, 2006a. 360 Risk Project. Available at www.lloyds.com/360.

Lloyd's. Rapid Climate Change, November 2006b. 360 Risk Project. Available at www.lloyds.com/360.

Lloyd's. Coastal Communities and Climate Change: Maintaining Future Insurability, 2008. 360 Risk Project. Available at www.lloyds.com/360.

Lloyd's. Forecasting Risk: The value of long-range forecasting for the insurance industry, 2011a. In collaboration with the UK Meteorological Office.

Lloyd's. Risk Index 2011, 2011b. Available at http://www.lloyds.com/News-and-Insight/Risk-Insight.

G. Lohmann and J. Scheider. Dynamics and predictability of stommel's box model: A phase space perspective with implications for decadal climate variability. *Tellus A*, 51(2):326–336, 1998.

E. N. Lorenz. Deterministic nonperiodic flow. *J. Atmos. Sci.*, 20:130–141, 1963.

E. N. Lorenz. Climatic determinism. *Meteor. Monographs*, 8(30):1–3, 1968.

E. N. Lorenz. Climatic change as a mathematical problem. *J. App. Meteor.*, 9(3):325–329, 1970.

E. N. Lorenz. Nondeterministic theories of climatic change. *Quaternary Research*, 6:495–506, 1976.

E. N. Lorenz. Irregularity: a fundamental property of the atmosphere. *Tellus*, 36A:98–110, 1984.

E. N. Lorenz. Can chaos and intransitivity lead to interannual variability? *Tellus*, 42A:378–389, 1990.

E. N. Lorenz. Chaos, spontaneous climatic variations and detection of the greenhouse effect. In *Greenhouse-Gas-Induced Climate Change: A critical appraisal of simulations and Observations*, pages 445–453. M. E. Schlesinger, Elsevier, Amsterdam, 1991a.

E. N. Lorenz. Dimension of weather and climate attractors. *Nature*, 353:241–244, 1991b.

E. N. Lorenz. Climate is what you expect. *Prepared for publication by NCAR; unknown if actually printed*, pages 1–33, 1997.

V. Lucarini. Towards a definition of climate science. *Int. J. Environment and Pollution*, 18(5): 413–422, 2002.

P. Lucas-Picher, J. H. Christensen, F. Saeed, P. Kumar, S. Asharaf, B. Ahrens, A. Wiltshire, D. Jacob, and S. Hagemann. Can regional climate models represent the Indian monsoon? *Journal of Hydrometeorology*, 2011. Available at http://journals.ametsoc.org /doi/abs/10.1175/2011JHM1327.1.

L. R. M. Maas. A simple model for the three-dimensional, thermally and wind-driven ocean circulation. *Tellus*, 46A:671–680, 1994.

G. J. MacDonald. Role of methane clathrates in past and future climates. *Climatic Change*, 16 (3):247–281, 1990.

S. Manabe and K. Bryan. Climate calculations with a combined ocean-atmosphere model. *J. Atmos. Sci*, 26:786–789, 1969.

S. Manabe and R. J. Stouffer. Low-frequency variability of surface air temperature in a 1000-year integration of a coupled atmosphere-ocean-land surface model. *J. Climate*, 9:376–393, 1996.

S. Manabe and R. T. Wetherald. The Effects of Doubling the CO_2 Concentration in Air on the Radiation Balance of the Earth's Surface and on the Climate. *J. Atmos. Sci.*, 32(1):3–15, 1975.

S. Manabe, K. Bryan, and M. J. Spelman. A Global Ocean-Atmosphere Climate Model: Part I. The Atmospheric Circulation. *J. Phys. Ocean.*, 5(1):3–29, 1975.

P. Manneville and Y. Pomeau. Intermittency and the Lorenz model. *Physics Letters*, 75A(1,2): 1–2, 1979.

V. Masson-Delmotte, M. Kageyama, P. Braconnot, S. Charbit, G. Krinner, C. Ritz, E. Guilyardi, J. Jouzel, A. Abe-Ouchi, M. Crucifix, R. M. Gladstone, C. D. Hewitt, A. Kitoh, A. N. LeGrande, O. Marti, U. Merkel, T. Motoi, R. Ohgaito, B. Otto-Bliesner, W. R. Peltier, I. Ross, P. J. Valdes, G. Vettoretti, S. L. Weber, F. Wolk, and Y. YU. Past and future polar amplification of climate change: climate model intercomparisons and ice-core constraints. *Climate Dynamics*, 26(5):513–529, 2006.

T. Maynard. The impact of climate change on non-life insurance. Technical report, Climate change working party, 2007.

T. Maynard and N. Ranger. Long term insurance - premium investigations, May 2010. Technical note, to be submitted.

K. McGuffie and A. Henderson-Sellers. *A climate modelling primer*, chapter 2, page 70. Wiley-Blackwell, 2005.

L. O. Mearns, I. Bogardi, F. Giorgi, I. Matyasovszky, and M. Palecki. Comparison of climate change scenarios generated from regional climate model experiments and statistical downscaling. *J. Geophys. Res.*, 104(D6):6603–6621, 1999.

G. A. Meehl and W. M. Washington. South Asian summer monsoon variability in a model with doubled atmospheric carbon dioxide. *Science*, 260:1101–1104, 1993.

G. A. Meehl, G. J. Bovey, C. Covey, M. Latif, and R. J. Stouffer. The Coupled Model Intercomparison Project (CMIP). *Bull. Am. Meteorol. Soc.*, 81(2):313–318, 2000a.

G. A. Meehl, T. Karl, D. R. Easterling, S. Changnon, R. Pielke Jr., D. Changnon, J. Evans P. Ya. Groisman, T. R. Knutson, K. E. Kunkel, L. O. Mearns, C. Parmesan, R. Pulwarty, T. Root, R. T. Sylves, P. Whetton, and F. Zwiers. An introduction to trends in extreme weather and climate events: Observations, socioeconomic impacts, terrestrial ecological impacts, and model projections. *Bull. Am. Meteorol. Soc.*, 81(3):413–416, 2000b.

G. A. Meehl, F. Zwiers, J. Evans, T. Knutson, L. Mearns, and P. Whetton. Trends in Extreme Weather and Climate Events: Issues Related to Modeling Extremes in Projections of Future Climate Change. *Bull. Am. Meteor. Soc.*, 81(3):427–437, 2000c.

G. A. Meehl, C. Covey, T. Delworth, M. Latif, B. McAvaney, J. F. B. Mitchell, R. J. Stouffer, and K. E. Taylor. The WCRP CMIP3 Multimodel Dataset: A New Era in Climate Change Research. *Bull. Am. Meteorol. Soc.*, 88:1383–1394, 2007a.

G. A. Meehl, T. F. Stocker, W. D. Collins, P. Friedlingstein, A. T. Gaye, J. M. Gregory, A. Kitoh, R. Knutti, J. M. Murphy, A. Noda, S. C. B. Raper, I. G. Watterson, A. J. Weaver, and Z. C. Zhao. *Global Climate Projections.* 2007b. In: Climate Change 2007: The Physical

Science Basis. Contribution of Working Group I to the Fourth Assessment Report of the Intergovernmental Panel on Climate Change. [Solomon, S.,D. Qin, M. Manning, Z. Chen, M. Marquis, K.B. Averyt, M. Tignor and H.L. Miller (eds.)]. Cambridge University Press, Cambridge, United Kingdom and New York, NY, USA.

H. E. M. Meier. Baltic Sea climate in the late twenty-first century : a dynamical downscaling approach using two global models and two emission scenarios. *Clim. Dyn.*, 27(1):29–68, 2006.

MicroEnsure. Weather Index Crop Insurance. Available at http://www.microensure.com /products-weather.asp, Accessed 02/12/2010. 2010.

E. Mills. Insurance as an adaptation strategy for extreme weather events in developing countries and economies in transition. June 2004. Prepared for the Agency for International Development Bureau for Economic Growth, Agriculture and Trade Office of Environment and Science Policy Climate Change Team. Available at http://eetd.lbl.gov/emills/PUBS/Insurance_Emerging_Markets.html.

E. Mills. Insurance in a Climate of Change. *Science*, 309(5737):1040–1044, 2005.

E. Mills. From Risk to Opportunity: Insurer Responses to Climate Change. October 2007. Published by Ceres, http://www.ceres.org.

E. Mills. A Global Review of Insurance Industry Responses to Climate Change. *The Geneva Papers*, 34:323–359, 2009.

J. Milnor. On the Concept of Attractor. *Commun. Math. Phys.*, 99:177–195, 1985.

A. S. Monin. *An introduction to the theory of climate.* D. Reidel Publishing Company, Dordrecht, Holland, 1986.

D. A. Mooley and B. Parthasarathy. Fluctuations in All-India summer monsoon rainfall during 1871–1978. *Climatic Change*, 6:287–301, 1984.

Munich Re. Topics. Annual Review: Natural Catastrophes 2002. Technical report, Geo Risks Research Dept, 2003.

Munich Re. Knowledge Series: Weather Catastrophes and Climate Change - is there still hope for us?, June 2005. ABI Financial Risks of Climate Change.

J. M. Murphy. An Evaluation of Statistical and Dynamical Techniques for Downscaling Local Climate. *J. Climate*, 12:2256–2284, 1999.

J. M. Murphy, D. Sexton, D. Barnett, G. Jones, M. Webb, and M Collins. Quantification of modelling uncertainties in a large ensemble of climate change simulations. *Nature*, 430: 768–772, 2004.

J. M. Murphy, D. M. H. Sexton, G. J. Jenkins, B. B. B. Booth, C. C. Brown, R. T. Clark, M. Collins, G. R. Harris, E. J. Kendon, R. A. Betts, S. J. Brown, P. Boorman, T. P. Howard, K. A. Humphrey, M. P. McCarthy, R. E. McDonald, A. Stephens, C. Wallace, R. Warren, R. Wilby, and R. A. Wood. UK Climate Projections Science Report: Climate change projections. 2009. Met Office Hadley Centre, Exeter.

J. K. Musango and C. Peter. A Bayesian approach towards facilitating climate change adaptation research on the South African agricultural sector. *Agrekon*, 46(2):245–259, 2007.

N. Nakićenović, J. Alcamo, G. Davis, B. de Vries, J. Fenhann, S. Gaffin, K. Gregory, A. Grübler, T. Yong Jung, T. Kram, E. Lebre La Rovere, L. Michaelis, S. Mori, T. Morita, W. Pepper, H. Pitcher, L. Price, K. Riahi, A. Roehrl, H. H. Rogner, A. Sankovski, M. Schlesinger, P. Shukla, S. Smith, R. Swart, S. van Rooijen, N. Victor, and Z. Dadi. IPCC Special report on emissions scenarios, November 2000. Published to web by GRID-Arendal. Available at http://www.grida.no/publications.

NASA. 2009: Second Warmest Year on Record; End of Warmest Decade, January 2010. National Aeronautics and Space Administration, Goddard Institute for Space Studies, Research News. Available at http://www.giss.nasa.gov/research/news/20100121/.

E. Neumayer and F. Barthel. Normalizing economic loss from natural disasters: A global analysis. *Glob. Env. Change*, 21(1):13–24, 2011.

M. New and M. Hulme. Representing uncertainty in climate change scenarios: a Monte-Carlo approach . *Integrated Assessment*, 1:203–213, 2000.

M. New, M. Hulme, and P. Jones. Representing Twentieth-Century Space-Time Climate Variability. Part I: Development of a 1961–90 Mean Monthly Terrestrial Climatology. *J. Climate*, 12:829–856, 1999.

M. New, D. Lister, M. Hulme, and I. Makin. A high-resolution data set of surface climate over global land areas. *Clim. Res.*, 21:1–25, 2002.

C. Nicolis and G. Nicolis. Is there a climatic attractor? *Nature*, 311:529–532, 1984.

F. Niehörster, T. Spangehl, I. Fast, and U. Cubasch. Quantification of model uncertainties: parameter sensitivities of the coupled model ECHO-G with middle atmosphere. In *Geophys Res Abs 8, EGU06-A-08526*, 2006.

S. Nissan and J. Williams. Insurance and the climate change challenge, 2009.

NIST/SEMATECH. Kolmogorov Smirnov Goodness-of-Fit Test, 1.3.5.16 Engineering Statistics Handbook, 2008. Available at http://www.itl.nist.gov/div898/handbook/eda /section3/eda35g.htm. Accessed on 06/08/2008.

G. R. North, R. F. Cahalan, and J. A. Coakley Jr. Energy Balance Climate Models. *Reviews of Geophysics and Space Physics*, 19(1):91–121, 1981.

N. Oreskes, D. A. Stainforth, and L. A. Smith. Adaptation to Global Warming: Do Climate Models Tell Us What We Need to Know? *Philosophy of Science*, 77:1012–1028, 2010.

W. Ouerdane and A. Tsoukias. Argumentation and decision aiding. In *Proceedings of the 2nd Meeting of the Decision Analysis Special Interest Group*, London, England, December 2009.

J. Overpeck and R. Webb. Nonglacial rapid climate events: Past and future. *Proc. Natl. Acad. Sci.*, 97(4):1335–1338, 2000.

R. C. Pacanowski and S. G. H. Philander. Parameterization of vertical mixing in numerical models of tropical oceans. *J. Phys. Ocean.*, 11:1443–1451, 1981.

J. A. Pagaran. Thermohaline circulation box models. pages 1–9, 2010. Accessed 11/11/2010, available at http://www.awi.de.

T. N. Palmer. Extended-range atmospheric prediction and the lorenz model. *Bull. Am. Meteorol. Soc.*, 74:49–65, 1993.

T. N. Palmer. A nonlinear dynamical perspective on climate prediction. *J. Climate*, 12:575–591, 1999.

T. N. Palmer and P. D. Williams. *Stochastic physics and climate modelling*. Cambridge University Press, 2009.

T. N. Palmer, U. Anderson, P. Cantelaube, M. Davey, M. Deque, F. J. Doblas-Reyes, H. Feddersen, R. Graham, S. Gualdi, J. F. Gueremy, R. Hagedorn, M. Hoshen, N. Keenlyside, M. Latif, A. Lazar, E. Maisonnave, V. Marletto, A. P. Morse, B. Orfila, P. Rogel, J. M. Terres, and M. C. Thomsen. Development of a European multi-model ensemble system for seasonal to inter-annual prediction (DEMETER). *Bull. Am. Meteorol. Soc.*, 85(6):853–872, 2004.

PCMDI. CMIP - Coupled Model Intercomparison Project - Overview, 2011. Program For Climate Model Diagnosis and Intercomparison. Accessed on 07/04/2011, available at http://cmip-pcmdi.llnl.gov/.

A. Peara and E. Mills. Global climate change and its implications for life insurance and health organizations, 1999. Available at http://eande.lbl.gov/ea/EMills/PUBS/PDF/CC-and-Life-Health.pdf.

J. Pearl. Fusion, propagation, and structuring in belief networks. *Artif. Intelligence J.*, 29: 241–288, 1986.

Y. Peicai, B. Jianchun, W. Geli, and Z. Xiuji. Hierarchy and nonstationarity in climate systems: Exploring the prediction of complex systems. *Chinese Science Bulletin*, 48(48):2148–2154, 2003.

J. P. Peixoto, A. F. Oort, and P. D. Williams. *Physics of Climate*. American Institute of Physics, New York, 520 pp, 1992.

J. D. Pelletier. Analysis and Modeling of the Natural Variability of Climate. *J. Climate*, 10: 1331–1342, 1997.

S. E. Perkins, A. J. Pitman, N. J. Holbrook, and J. Mcaneney. Evaluation of the AR4 climate models simulated daily maximum temperature, minimum temperature, and precipitation over Australia using Probability Density Functions. *J. Climate*, 20:4356–4376, 2007.

J. R. Petit, J. Jouzel, D. Raynaud, N. I. Barkov, J.-M. Barnola, I. Basile, M. Bender, J. Chappellaz, M. Davis, G. Delaygue, M. Delmotte, V. M. Kotlyakov, M. Legrand, V. Y. Lipenkov, C. Lorius, L. Pepin, C. Ritz, E. Saltzman, and M. Stievenard. Climate and atmospheric history of the past 420,000 years from the Vostok ice core, Antarctica. *Nature*, 399:429–436, 1999.

V. Petoukhov, M. Claussen, A. Berger, M. Crucifix, M. Eby, A. V. Eliseev, T. Fichefet, A. Ganopolski, H. Goosse, I. Kamenkovich, I. I. Mokhov, M. Montoya, L. A. Mysak, A. Sokolov, P. Stone, Z. Wang, and A. J. Weaver. EMIC Intercomparison Project (EMIP–CO_2): comparative analysis of EMIC simulations of climate, and of equilibrium and transient responses to atmospheric CO_2 doubling. *Clim. Dyn.*, 25:363–385, 2005.

C. Piani, D. J. Frame, D. A. Stainforth, and M. R. Allen. Constraints on climate change from a multi-thousand member ensemble of simulations. *Geophys. Res. Lett.*, 32:L23825, 2005.

N. Pidgeon and B. Fischhoff. The role of social and decision sciences in communicating uncertain climate risks. *Nature Climate Change*, 1:35–41, 2011.

R. A. Pielke. Climate prediction as an initial value problem. *Bull. Am. Meteorol. Soc.*, 79: 2743–2746, 1998.

R. A. Pielke. An idealized assessment of the economics of air capture of carbon dioxide in mitigation policy. *Environ. Sci. Policy*, 12(3):216–225, 2009.

R. A. Pielke and X. Zeng. Long-Term Variability of Climate. *Am. Meteor. Soc.*, 51(1):155–159, 1994.

A. B. Pittock, R. N. Jones, and C. Mitchell. Probabilities will help us plan for climate change - without estimate, engineers and planners will have to delay decision or take a gamble. *Nature*, 413:249–249, 2001.

V. D. Pope, M. Gallani, P. R. Rowntree, and R. A. Stratton. The impact of new physical parameterisations in the Hadley Centre climate model - HadAM3. *Clim. Dyn.*, 16:123–146, 2000.

V. D. Pope, S. Brown, R. Clark, M. Collins, W. Collins, C. Dearden, J. Gunson, G. Harris, C. Jones, A. Keen, J. Lowe, M. Ringer, C. Senior, S. Sitch, M. Webb, and S. Woodward. The met office hadley centre climate modelling capability: the competing requirements for improved resolution, complexity and dealing with uncertainty. *Phil. Trans. R. Soc. A*, 365: 2635–2657, 2007.

M. Prange, V. Romanova, and G. Lohmann. The glacial thermohaline circulation: Stable or unstable? *Geophys. Res. Lett.*, 29(21):2028, 2002.

W. H. Press, B. P. Flannery, S. A. Teukolsky, and W. T. Vetterling. *Numerical Recipes in FORTRAN: The Art of Scientific Computing, 2nd ed.*, pages 617–620. Cambridge University Press, 1992.

J. Räisänen. How reliable are climate models? *Tellus*, 59A:2–29, 2007.

B. Rajagopalan. Risk Assessment and Forecasting of Indian Summer Monsoon for Agricultural Drought Impact Planning, June 2009. Colorado Water Institute, Completion Report No. 215.

N. Ranger and S. L. Garbett-Shiels. How can decision-makers in developing countries incorporate uncertainty about future climate risks into existing planning and policy-making processes?, March 2011. Policy paper. Centre for Climate Change Economics and Policy and the Grantham Research Institute on Climate Change and the Environment in collaboration with the World Resources Report.

N. Ranger and R. Ward. Aiming for a 2°C Goal: What does it mean for the insurance industry?, May 2010. Insurance Industry Brief. The Munich Re Programme of the Centre for Climate Change Economics and Policy.

N. Ranger, R. Muir-Wood, and S. Priya. Assessing extreme climate hazards and options for risk mitigation and adaptation in the developing world, February 2009. World Development Report: Development and Climate Change, Background Note.

N. Ranger, A. Millner, S. Dietz, S. Fankhauser, A. Lopez, and G. Ruta. Adaptation in the UK: a decision-making process, September 2010. Policy Brief. Grantham Research Institute on Climate Change and the Environment and the Centre for Climate Change Economics and Policy.

J. A. Rial. Abrupt climate change: chaos and order at orbital and millennial scales. *Global and Planetary Change*, 41(2):95–109, 2004.

J. A. Rial, R. A Pielke Sr., M. Beniston, M. Claussen, J. Candell, P. Cox, H. Held, N. De Noblet-Ducoudre, R. Prinn, J. F. Reynolds, and J. D Salas. Nonlinearities, feedbacks and critical thresholds within the Earth's climate system. *Climatic Change*, 65:11–38, 2004.

D. Rind. Complexity and Climate. *Science*, 284:105–107, 1999.

D. Rind. The Sun's role in climate variations. *Science*, 296:673–678, 2002.

P. J. Roebber. Climate variability in a low-order coupled atmosphere-ocean model. *Tellus*, 47A (4):473–494, 1995.

E. Roeckner, G. Bauml, L. Bonaventura, R. Brokopf, M. Esch, M. Giorgetta, S. Hagemann, I. Kirchner, L. Kornblueh, E. Manzini, A. Rhodin, U. Schlese, U. Schulzweida, and

A. Tompkins. The Atmospheric Circulation model ECHAM 5 Part 1: model description, November 2003. Max Plank Institute for Meteorology Report 349. Available at http://www.mpimet.mpg.de/fileadmin/models/echam.

A. P. Rothmayer and D. W. Black. Ensembles of the Lorenz Attractor. *Proceedings: Mathematical and Physical Sciences*, 441(1912):291–312, 1993.

J. C. Rougier, D. M. H. Sexton, J. M. Murphy, and D. A. Stainforth. Analysing the climate sensitivity of the HadSM3 climate model using ensembles from different but related experiments. *J. Climate*, 22:3540–3557, 2009.

D. Ruelle. A measure associated with axiom-a attractors. *Am. J. Math.*, 98(3):137–151, 1976.

D. Ruelle. Small random perturbations of dynamical systems and the definition of attractors. *Comm. Math. Phys.*, 82(1):619–654, 1981.

A. Sahay and K. R. Sreenivasan. The search for a low-dimensional characterization of a local climate system. *Phil. Trans. R. Soc. A.*, 354:1715–1750, 1996.

J. Schmidli, C. Frei, and P. L. Vidale. Downscaling from GCM precipitation: A benchmark for dynamical and statistical downscaling methods. *Int. J. Climatol.*, 26:679–689, 2006.

E. K. Schneider and J. L Kinter III. An examination of internally generated variability in long climate simulations. *Clim. Dyn.*, 10:181–204, 1994.

S. H. Schneider. Climate change and the world predicament: A case study for interdisciplinary research. *Climatic Change*, 1(1):21–43, 1977.

S. H. Schneider. What is dangerous climate change? *Nature*, 411:17–19, 2001.

S. H. Schneider. Abrupt non-linear climate change, irreversibility and surprise. *Global Environmental Change Part A*, 14(3):245–258, 2004.

S. H. Schneider and R. E. Dickinson. Climate Modeling. *Climatic Change*, 45:203–221, 2000.

S. H. Schneider, W. E. Easterling, and L. O. Mearns. Adaptation: Sensitivity to natural variability, agent assumptions and dynamic climate changes. *Climatic Change*, 45:203–221, 2000.

S. Schubert and A. Henderson-Sellers. A statistical model to downscale daily temperature extremes from synoptic-scale atmospheric circulation patterns in the Australian region. *Clim. Dyn.*, 13:223–234, 1997.

H. G. Schuster and W. Just. *Deterministic Chaos: An Introduction.* WILEY-VCH Verlag GmbH and Co. KGaA, 2005.

S. Scott. Clocks and Chaos in Chemistry. *New Scientist*, 124(1693):53–53, 1989.

R. Selvaraju. Impact of El Niño–southern oscillation on Indian foodgrain production. *Int. J. Climatol.*, 23(2):187–206, 2003.

J. Seo and O. Mahul. The Impact of Climate Change on Catastrophe Risk Models: Implications for Catastrophe Risk Markets in Developing Countries, 2009. World Bank Policy Research Working Paper 4959.

J. Shulka. Predictability in the Midst of Chaos: A Scientific Basis for Climate Forecasting. *Science*, 282(5389):728–731, 1998.

A. J. Simmons, K. M. Willett, P. D. Jones, P. W. Thorne, and D. P. Dee. Low-frequency variations in surface atmospheric humidity, temperature and precipitation: Inferences from reanalyses and monthly gridded observational datasets. *J. Geophys. Res.*, 115, 2010.

J. R. Skees. Challenges for use of index-based weather insurance in lower income countries. *Agricultural Finance Review*, 68:197–217, 2008.

J. R. Skees, P. Hazell, and M. Miranda. New approaches to crop yield insurance in developing countries, November 1999. Environment and Production Technology Division, Discussion Paper no. 55.

J. R. Skees, A. Murphy, B. Collier, M. J. McCord, and J. Roth. Scaling up index insurance. Microinsurance Centre, LLC. 2007.

B. Smit, I. Burton, R. J. T. Klein, and R. Street. The science of adaptation: A framework for assessment. *Mitigation and Adaptation Strategies for Global Change*, 4(3-4):199–213, 1999.

B. Smit et al. *Adaptation to Climate Change in the Context of Sustainable Development and Equity*, chapter 18, pages 877–912. 2001. In McCarthy, J.J., Canziani, O., Leary, N.A., Dokken, D.J. and White, K.S., editors, Climate change 2001: impacts, adaptation and vulnerability. IPCC Working Group II. Cambridge: Cambridge University Press.

D. M. Smith, S. Cusack, A. W. Colman, C. K. Folland, G. R. Harris, and J. M. Murphy. Improved Surface Temperature Prediction for the Coming Decade from a Global Climate Model. *Science*, 317(5839):796–799, 2007.

L. Smith. *Chaos: A Very Short Intoduction*, chapter 3, pages 54–56. Oxford University Press, 2007.

L. A. Smith. *Disentangling Uncertainty and Error: On the Predictability of Nonlinear Systems*, chapter 2, pages 31–64. 2000. In: Nonlinear Dynamics and Statistics, A. Mees (ed.), Birkhauser.

L. A. Smith. What might we learn from climate forecasts? *Proc. Natl Acad. Sci.*, 99:2487–2492, 2002.

L. A. Smith, A. Lopez, D. Stainforth, N. Ranger, and F. Niehörster. Toward decision-relevant probability distributions: Communicating ignorance, uncertainty and model-noise, 2009. Presented at the 2009 Royal Meteorological Scoiety Conference, Reading UK.

Norsys Software Corp. Netica 4.09, 1998. Available at http://www.norsys.com/, Accessed 07/09/2009.

S. Solomon, D. Qin, M. Manning, Z. Chen, M. Marquis, K. B. Averyt, M. Tignor, and H. L. Miller. Climate Change 2007: The Physical Science Basis, Contribution of Working Group 1 to the Fourth Assessment Report of the Intergovernmental Panel on Climate Change, Cambridge University Press, Cambridge, United Kingdom and New York, NY, USA. 2007.

C. Sparrow. *The Lorenz Equations: Bifurcations, Chaos and Strange Attractors*, volume 41 of *Applied Mathematical Sciences*. Springer-Verlag New York Inc., 1982.

J. C. Sprott. *Chaos and Time-Series Analysis*. Oxford University Press, 2003.

D. A. Stainforth, J. Kettleborough, M. Allen, M. Collins, A. Heaps, and J. Murphy. Distributed computing for public-interest climate modeling research. *Comput. Sci. Eng.*, 4:82–89, 2002.

D. A. Stainforth, T. Ania, C. Christensen, M. Collins, N. Faull, D. J. Frame, J. A Kettleborough, S. Knight, A. Martin, J. M. Murphy, C. Piani, D. Sexton, L. A. Smith, R. A. Spicer, A. J. Thorpe, and M. R. Allen. Uncertainty in predictions of the climate response to rising levels of greenhouse gases. *Nature*, 433:403–406, 2005.

D. A. Stainforth, M. R. Allen, E. R. Tredger, and L. A. Smith. Confidence, uncertainty and decision-support relevance in climate predictions. *Phil. Trans. R. Soc. A*, 365:2145–2161, 2007a.

D. A. Stainforth, T. E. Downing, R. Washington, A. Lopez, and M. New. Issues in the interpretation of climate model ensembles to inform decisions. *Phil. Trans. R. Soc. A*, 365: 2163–2177, 2007b.

J. Sterman and L. Sweeney. Understanding public complacency about climate change: adults mental models of climate change violate conservation of matter. *Climatic Change*, 80(3): 213–238, 2007.

I. Stewart. *Does God Play Dice? The New Mathematics of Chaos*. Penguin Group, Penguin Books Ltd, London, second edition, 2009.

H. Stommel. Thermohaline convection with two stable regimes of flow. *Tellus*, 13(2):224–230, 1961.

J. Strachan. Science in the city. *Panet Earth*, pages 24–25, 2007a. Autumn edition.

J. Strachan. The use of high-resolution global climate models for climate risk assessment, October 2007b. Catastrophe Modelling Forum, New York City, Extended Abstract.

J. Strachan, P. L. Vidale, R. Vitolo, and D. Stephenson. Utilising climate research to inform the insurance industry: Can we use dynamically simulated storms for risk assessment? In *Geophysical Research Abstracts*, volume 12, EGU General Assembly, 2010.

A. Sutera. Stochastic perturbation of a pure convectie motion. *J. Atmos. Sci*, 37:245–249, 1980.

Swiss Re. Sigma study, catastrophe report 2005, March 2005. No 1/2005. Available at http://www.swissre.com/media.

Swiss Re. Sigma study, catastrophe report 2006, February 2006. No 2/2006. Available at http://www.swissre.com/media.

M. Tabor. *Chaos and Integrability in Nonlinear Dynamics: An Introduction*, page 206. Wiley: New York, 1989.

K. E. Taylor, R. J. Stouffer, and G. A. Meehl. A Summary of the CMIP5 Experiment Design, December 2009. World Climate Research Programme. Available at http://cmip-pcmdi.llnl.gov/cmip5/experiment
_design.html.

C. Tebaldi and R. Knutti. The use of multi-model ensembles in probabilistic climate projections. *Phil Trans R Soc A*, 365(1857):2053–2075, 2007.

C. Tebaldi, R. L. Smith, D. Nychka, and L. O. Mearns. Quantifying uncertainty in projections of regional climate change: A Bayesian approach to the analysis of multi-model ensembles. *J. Climate*, 18:1524–1540, 2005.

J. Teixeira and A. Carolyn. Stochastic nature of physical parameterizations in ensemble prediction: A stochastic convection approach. *Mon. Wea. Rev.*, 136:483–496, 2008.

J. Teixeira, C. A. Reynolds, and K. Judd. Time step sensitivity of nonlinear atmospheric models: numerical convergence, truncation error growth, and ensemble design. *J. Atmos. Sci.*, 64:175–189, 2007.

TheCityUK. Insurance 2010. Available at www.TheCityUK.com, Basinghall Street, London. 2010.

S. M. Tobias and N. O. Weiss. Resonant interations between solar activity and climate. *J. Climate*, 13:3745–3759, 2000.

R. S. J. Tol. Climate change and insurance: a critical appraisal. *Energy Policy*, 26(3):257–262, 1998.

Z. Toth and E. Kalnay. Ensemble Forecasting at NMC: The Generation of Perturbations. *Bull. Am. Meteorol. Soc.*, 74(12):2317–2330, 1993.

UKCP09. Use of UKCP09, FAQ, 2011. Accessed 10/05/2011. Available at http://ukclimate projections.defra.gov.uk/content/view/1380/500.

UNDESA. Developing Index-Based Insurance for Agriculture in Developing Countries, 2007. Innovation Briefs No. 2. United Nations – Department of Economics and Social Affairs, New York, NY. Available at http://www.un.org/esa/sustdev/publications /innovationbriefs/no2.pdf.

USAID. Index insurance for weather risk in lower-income countries, November 2006. United States Agency International Development. Prepared by GlobalAgRisk, Inc., Lexington, Kentucky.

L. J. Valverde and M. W. Andrews. Global Climate Change and Extreme Weather: An Exploration of Scientific Uncertainty and the Economics of Insurance. *Insurance Information Institute Working Paper Series*, June 2006.

L. A. van den Berge, F. M. Selten, W. Wiegerinck, and G. S. Duane. A multi-model ensemble method that combines imperfect models through learning. *Earth Syst. Dynam. Dicuss.*, 1: 247–296, 2010.

L. Van Veen. Overturning and wind-driven circulation in a low-order ocean–atmosphere model. *Dyn. Atm. Ocean*, 37:197–221, 2003.

L. Van Veen, T. Opsteegh, and F. Verhulst. Active and passive ocean regimes in a low-order climate model. *Tellus*, 53A:616–628, 2001.

E. J. Vaughan and T. M. Vaughan. *Fundamentals of Risk and Insurance.* John Wiley and Sons, Inc., New York, 2003.

C. Vecchiola, S. Pandey, and R. Buyya. High-Performance Cloud Computing: A View of Scientific Applications. *International Symposium on Pervasive Systems, Algorithms, and Networks*, pages 4–16, 2009. doi: http://doi.ieeecomputersociety.org/10.1109/I-SPAN.2009.150.

V. N. Veeramani, L. J. Maynard, and J. R. Skees. Assessment of the Risk Management Potential of a Rainfall Based Insurance Index and Rainfall Options in Andhra Pradesh, India. *Indian Journal of Economics and Business*, 4(1):195–208, 2005.

R. L. Viana, S. Camargo, R. F. Pereira, M. C. Verges, S. R. Lopes, and S. E. S. Pinto. Riddled basins in complex physical and biological systems. *Journal of Computational Interdisciplinary Sciences*, 1(2):73–82, 2009.

R. Vitolo, J. Strachan, P. L. Vidale, D. Stephenson, I. Cook, S. Flay, and M. Foote. A Global Climate Model based event set for tropical cyclone risk assessment in the West Pacific. In *Geophysical Research Abstracts*, volume 12, EGU General Assembly, 2010.

J. von Neumann. Beweis des Ergodensatzes und des H-Theorems in der neuen Mechanik. *Zeitschrift für Physik*, 57:30–70, 1929.

H. von Storch and F. W. Zwiers. *Statistical Analysis in Climate Research*. Cambridge University Press, Cambridge, UK and New York, 1999.

R. E. T. Ward, C. Herweijer, N. Patmore, and R. Muir-Wood. The Role of Insurers in Promoting Adaptation to the Impacts of Climate Change. *The Geneva Papers*, 33:133–139, 2008.

A. P. Weigel, R. Knutti, M. A. Liniger, and C. Appenzeller. Risks of model weighting in multimodel climate projections. *J. Climate*, 23(15):4175–4191, 2010.

R. White and D. Etkin. Climate Change, Extreme Events and the Canadian Insurance Industry. *Natural Hazards*, 16(2-3):135–163, 1997.

T. M. L. Wigley and S. C. B. Raper. Implications for climate and sea level of revised IPCC emissions scenarios. *Nature*, 357:293–300, 1992.

T. J. Wilbanks, P. Romero Lankao, M. Bao, F. Berkhout, S. Cairncross, J. P. Ceron, M. Kapshe, R. Muir-Wood, and R. Zapata-Marti. *Industry, settlement and society. Climate Change 2007: Impacts, Adaptation and Vulnerability. Contribution of Working Group II to the Fourth Assessment Report of the Intergovernmental Panel on Climate Change*, pages 357–390. M. L. Parry, O. F. Canziani, J. P. Palutikof, P. J. van der Linden and C.E. Hanson (eds). Cambridge University Press, Cambridge, UK, 2007.

R. L. Wilby and S. Dessai. Robust adaptation to climate change. *Weather*, 65(7):180–185, 2010.

R. L. Wilby, S. P. Charles, E. Zorita, B. Timbal, P. Whetton, and L. O. Mearns. Guidelines for Use of Climate Scenarios Developed from Statistical Downscaling Methods. *Supporting material of the Intergovernmental Panel on Climate Change*, 2004. Available from the DDC of IPCC TGCIA, 27.

A. A. Wilcock. Köppen after fifty years. *Ann. Assoc. Am. Geog*, 58(1):12–28, 1968.

A. Wiltshire, C. Mathison, J. Ridley, C. Witham, C. McSweeny, P. Kumar, and D. Jacob. HighNoon Delivery Report: analysis of climate uncertainty. Technical report, November 2010. Available at http://www.eu-highnoon.org/publications/delivery-reports.

R. A. Winter. The Dynamics of Competitive Insurance Markets. *J. Financial Intermediation*, 3:379–415, 1994.

WMO. Climatological normals (CLINO) for the period 1961-1990, 1996. WMO/OMM 847, 768 pp. Available from World Meteorological Organisation, Geneva, Switzerland.

A. Wolf. *Quantifying chaos with Lyapunov exponents*. In: Chaos. A. V. Holden. Manchester University Press, Oxford Road, Manchester, UK, 1986.

S. A. Wooldridge, T. J. Done, R. Berkelmans, R. Jones, and P. Marshall. Precursors for resilience in coral communities in a warming climate: a belief network approach. *Mar Ecol Prog Ser*, 295:157–169, 2005.

World Bank. Weather index insurance for agriculture: Guidance for Development Practitioners, November 2011. Agriculture and rural development discussion paper 50.

C. Wunsch. The interpretation of short climate records, with comments on the North Atlantic and Southern Oscillations. *Bull. Am. Meteorol. Soc.*, 80(2):245–255, 1999.

C. Wunsch. Thermohaline loops, Stommel box models, and the Sandström theorem. *Tellus A*, 57(1):84–99, 2005.

J. I. Yano, J. Quass, T. M. Wagner, and R. S. Plant. Toward statistical descriptions of convective cloud dynamics. *EOS, Trans. Am. Geophys. Union*, 88(23):212, 2008.

L. S. Yao. Computed Chaos or Numerical Errors. 2005.

A. Yatagai, P. Xie, and P. Alpert. Development of a daily gridded precipitation data set for the Middle East. *Adv. in Geosci.*, 12:165–170, 2008.

A. Yatagai, O. Arakawa, K. Kamiguchi, H. Kawamoto, M. I. Nodzu, and A. Hamada. A 44-year daily gridded precipitation dataset for Asia based on a dense network of rain gauges. *SOLA*, 5:137–140, 2009.

J. A. Yorke and E. D. Yorke. Metastable Chaos: The Transition to Sustained Chaotic Behavior in the Lorenz Model. *J. Stat. Phys.*, 21(3):263–277, 1979.

X. Zeng, R. A. Pielke, and R. Ekyholt. Estimating the fractal dimension and the predictability of the atmosphere. *J. Atmos. Sci.*, 49:649–659, 1992.